UNCLASSIFIED

AD 262 200

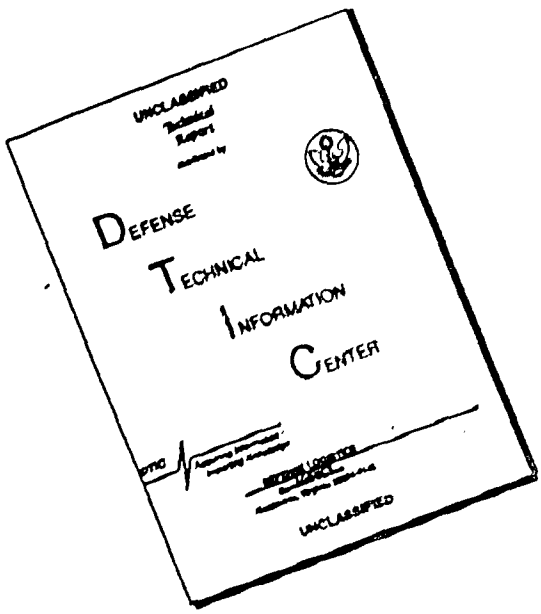
Reproduced
by the

ARMED SERVICES TECHNICAL INFORMATION AGENCY
ARLINGTON HALL STATION
ARLINGTON 12, VIRGINIA



UNCLASSIFIED

DISCLAIMER NOTICE



THIS DOCUMENT IS BEST QUALITY AVAILABLE. THE COPY FURNISHED TO DTIC CONTAINED A SIGNIFICANT NUMBER OF PAGES WHICH DO NOT REPRODUCE LEGIBLY.

NOTICE: When government or other drawings, specifications or other data are used for any purpose other than in connection with a definitely related government procurement operation, the U. S. Government thereby incurs no responsibility, nor any obligation whatsoever; and the fact that the Government may have formulated, furnished, or in any way supplied the said drawings, specifications, or other data is not to be regarded by implication or otherwise as in any manner licensing the holder or any other person or corporation, or conveying any rights or permission to manufacture, use or sell any patented invention that may in any way be related thereto.

26220

U. S. ARMY
TRANSPORTATION RESEARCH COMMAND
FORT EUSTIS, VIRGINIA

USAREC TECHNICAL REPORT 61-43

HIGH PERFORMANCE TANDEM HELICOPTER STUDY

VOL. 2 - DESIGN ANALYSIS

Task 9R38-13-014-01

Contract DA44-177-TC-686

April 1961

prepared by :

VERTOL DIVISION
BOEING AIRPLANE COMPANY
Morton, Pennsylvania

XEROX

ASTIA
AUG 30 1961

DISCLAIMER NOTICE

When Government drawings, specifications, or other data are used for any purpose other than in connection with a definitely related Government procurement operation, the United States Government thereby incurs no responsibility nor any obligation whatsoever; and the fact that the Government may have formulated, furnished, or in any way supplied the said drawings, specifications, or other data is not to be regarded by implication or otherwise as in any manner licensing the holder or any other person or corporation, or conveying any rights or permission, to manufacture, use, or sell any patented invention that may in any way be related thereto.

* * *

ASTIA AVAILABILITY NOTICE

Qualified requestors may obtain copies of this report from

Armed Services Technical Information Agency
Arlington Hall Station
Arlington 12, Virginia

* * *

This report has been released to the Office of Technical Services, U. S. Department of Commerce, Washington 25, D. C., for sale to the general public.

* * *

The information contained herein will not be used for advertising purposes.

* * *

This report is exempt from the provisions of USATRECOM Circular 715-10 which prohibit the use of more than one color in a report, since the preparation of this report will be at no cost to the Government.

ABSTRACT

TREC 61-43

Vertol Division, The Boeing Company, Morton, Pennsylvania, High Performance Tandem Helicopter Study, Volume II - Design Analysis, January 1961.316 pp. including illustrations, tables. Contract DA44-177-TC-686.

Unclassified Report

A preliminary design study has been conducted to establish a tandem helicopter configuration capable of the following minimum performance: (1) 1600 nautical miles ferry range at zero headwind with 1 hour fuel reserve. (2) 200 miles per hour speed with a minimum payload of 800 pounds. (3) Flying qualities to meet MIL-H-8501. Detailed aerodynamic and design layout studies are presented for the High Performance 107-II. The major design areas covered are rotor blades, hub, and controls; mechanical instability, drive system, fuselage changes, flight controls, and weight. Both performance and flying qualities are thoroughly investigated. Overall feasibility of a high performance helicopter is assured. Studies of an Advanced 107 and Advanced YHC-1B (Chinook) indicate that operational high performance helicopters are obtained if the ratio of payload to empty weight is maintained in going to the high performance configuration.

DESIGN ANALYSIS REPORT

HIGH PERFORMANCE HELICOPTER STUDY

TRECOM CONTRACT
DA-44-177-TC-686

VERTOL DIVISION
MORTON PENNSYLVANIA
BOEING

R 234

ACKNOWLEDGEMENTS

This study was accomplished by the Research and Preliminary Design Staff of the Vertol Division of The Boeing Company. Notable contributions were made by the following personnel:

F. D. Harris - Project Aerodynamicist
N. Jeffrey - Aerodynamicist
F. Lentine - Aerodynamicist
G. Holcombe - Aerodynamicist
G. Donovan - Aerodynamicist
R. Swan - Weights
P. Leone - Aero-Elasticity
D. Hoffstedt - Rotor Design
F. Pallone - Rotor Design
C. Albrecht - Rotor Stress
R. Gable - Dynamics
J. Mayer - Rotor Controls

HEADQUARTERS
U. S. ARMY TRANSPORTATION RESEARCH COMMAND
Fort Eustis, Virginia

FOREWARD

The data presented in the following pages represent the detailed calculations, methods and results of the design analysis conducted by Vertol Division, Boeing Airplane Company, in their high performance tandem helicopter study. This program was sponsored by the U. S. Army Transportation Research Command at Fort Eustis, Virginia.

This report, which is volume two of a two volume final report, supports the conclusions presented in volume one - Summary Report. Volume I which has been published, presented a summary of the gains in performance, i.e. range, productivity and speed, that can be obtained through modification of current helicopters or in the design of future helicopters wherein the latest advanced design techniques are utilized.

This design analysis report also presents limited preliminary data regarding growth versions of the high performance design, that is, further increases in performance that can be obtained through the addition of auxiliary propulsion and/or wings.

The data presented in this design analysis report have been reviewed by this Command and are concurred with.

FOR THE COMMANDER:

APPROVED BY:

Robert D. Powell Jr

ROBERT D. POWELL, JR.
USATRECOM, Project Engineer

Earl A. Wirth

EARL A. WIRTH
CWO-4 USA
Adjutant

TABLE OF CONTENTS

	Page
TABLE OF CONTENTS	v
List of Figures	vii
List of Tables	xiii
List of Drawings	xv
List of Symbols	xvii
SUMMARY	xxiii
CONCLUSIONS	xxvii
RECOMMENDATIONS	xxix
AERODYNAMIC DATA	
PARAMETRIC STUDY - PHASE I	
Summary	1-1
Methodology	2-1
Configuration Study	3-1
Detailed Rotor Study	4-1
Rotor Environment	5-1
PRELIMINARY DESIGN - PHASE II	
Summary	6-1
Performance	7-1
Flying Qualities	8-1
Wind Tunnel Tests	9-1
DESIGN DATA	
Summary	10-1
Fuselage Changes	11-1
Mechanical Instability	12-1
Rotor Blades	13-1
Rotor Hub	14-1
Rotor Controls	15-1
Rotor Hub Fairing	16-1
Drive System	17-1
Flight Controls	18-1
Weight Studies	19-1
PERFORMANCE POTENTIALS	
Fundamentals	20-1
Growth Versions	21-1
Unloaded Rotor Versions	22-1
BIBLIOGRAPHY	23-1
APPENDICES	
I. "Chinook" Study	24-1
II. ASR-3 Study	25-1
III. Rotor Stress Study	26-1

LIST OF FIGURES

Figure No.	Title	Page No.
1	Comparison of Present Power Required Calculations With Flight Test	2-1
2	NACA 0012 Section Aerodynamic Characteristics - C_l and C_d as a function of α and M	2-3
3	Comparison of Extended Power Required Method With Flight Test	2-4
4	Definition of Extended Performance Method Rotor Terms	2-4
5	Typical Performance Data from Extended Performance Method	2-5
6 - 17	Optimum L/D_E and C_t'/σ vs. Twist at Selected Forward Speeds and Advancing Tip Mach Numbers	3-2 to 3-13
18	Graphical Form of Configuration Study Solution	3-17
19 - 29	Configuration Study - Gross Weight vs. Rotor Blade Radius	3-18 to 3-28
30	Summary Curves of High Performance 107-II Rotor Sizing Study - Payload vs. Rotor Radius	4-2
31 - 45	Detailed High Performance 107-II Rotor Study - Gross Weight and Payload vs. Forward Speed	4-3 to 4-17
46	NACA 0012 Section Aerodynamic Characteristics - C_l and C_d as a Function of α and M	5-2
47	NACA 0009.5 Section Aerodynamic Characteristics - C_l and C_d as a Function of α and M	5-3
48	Effect of Root Collective Pitch on Total Performance Coefficients of L/D_E, C_t'/σ, X/L, C_p/σ and C_{po}/σ	5-5
49	Component Terms of L/D_E Equation vs. Root Collective Pitch	5-6
50	Growth of Stall and Compressibility with Increasing Collective Pitch	5-8
51	Mach Number as an Analytical Variable	5-11

LIST OF FIGURES

Figure No.	Title	Page No.
52	Mach Number Distribution	5-13
53	Stall and Drag Divergence Angles of Attack as a Function of Mach Number for the NACA 0012 and NACA 0009.5 Airfoils	5-14
54	Regions of Stall and Compressibility - Effect of Advance Ratio	5-16
55	Regions of Stall and Compressibility - Effect of Inflow Ratio	5-19
56	Regions of Stall and Compressibility - Effect of Blade Twist	5-21
57	Comparison of Regions of Stall and Compressibility between the NACA 0012 and NACA 0009.5 Rotors	5-23
58	Polar Data for NACA 0012 Ref. Case 1	5-24
59	Polar Data for NACA 0009.5 Ref. Case 9	5-25
60	Lift Coefficient Along the Stall Limit Boundary	5-26
61a-d	Effect of Mach Number on Rotor Performance	5-28 to 5-29
62a-d	Effect of Advance Ratio on Rotor Performance	5-30 to 5-31
63a-d	Effect of Inflow Ratio on Rotor Performance	5-32 to 5-33
64a-d	Effect of Blade Twist on Rotor Performance	5-34 to 5-35
65	Altitude vs. Power Available T58-GE-8 Shaft Turbine Engine	7-5
66	Fuel Flow vs. Power Available T58-GE-8 Shaft Turbine Engine	7-6
67	Lift, Drag, and Pitching Moment vs. Angle of Attack - High Performance 107-II	7-8
68	Drive System Schematic - Transmission Losses	7-10
69	Hover Performance - Altitude vs. Gross Weight, Standard Day	7-12

LIST OF FIGURES

Figure No.	Title	Page No.
70	Hover Performance - Altitude vs. Gross Weight, 95°F Day	7-13
71	Shaft Horsepower Required vs. Forward Speed	7-14
72	Shaft Horsepower Required vs. Rate of Climb	7-15
73	Rate of Climb vs. Gross Weight	7-16
74	Service Ceiling vs. Gross Weight	7-17
75	Specific Range vs. Rate of Climb	7-18
76	Normal Cruise Performance	7-19
77	Maximum Forward Speed Cruise Performance	7-20
78	Maximum Forward Speed vs. Gross Weight	7-21
79	Payload Range at Sea Level and 10,000 Feet	7-23
80	Productivity and Maintainability vs. Forward Speed	7-24
81	Body Axes Co-ordinate System	8-3
82a,b	Longitudinal Stability - High Performance 107-II and Boeing-Vertol 107-II Aerodynamic Fuselage Characteristics	8-4 to 8-5
83a,b	Longitudinal Stability Derivatives vs. True Air Speed in Level Flight	8-7 to 8-8
84	Longitudinal Control Power vs. True Air Speed in Level Flight	8-9
85	Longitudinal Cyclic Pitch Schedule	8-10
86	Differential Collective Pitch Schedule	8-11
87a,b	Lateral-Directional Stability Derivatives vs. True Air Speed in Level Flight	8-12 to 8-13
88	Lateral - Directional Stability Control Powers vs. True Air Speed in Level Flight	8-14
89	Boeing-Vertol Model 107 SAS	8-17

LIST OF FIGURES

Figure No.	Title	Page No.
90	Boeing-Vertol Model 107 Control System Schematic Showing Typical SAS Installation	8-18
91	Speed Stability Comparison	8-20
92	Static Directional Stability and Effective Dihedral	8-21
93a-d	Dynamic Stability - SAS Off	8-26 to 8-29
94a-h	Dynamic Stability SAS On	8-30 to 8-37
95	Wind Tunnel Test of the High Performance 107-II	9-1
96	Wetted Area Drag Coefficient vs. Reynold's Number	9-2
97	Lift, Drag, and Pitching Moment vs. Angle of Attack, Fuselage Alone	9-3
98	Luminescent Oil Photographs - Forward Pylon	9-4
99	Luminescent Oil Photographs - Stub Tanks	9-6
100	Lift, Drag, and Pitching Moment vs. Angle of Attack, Fuselage with Aft Stub Tanks	9-7
101	Lift, Drag, and Pitching Moment vs. Angle of Attack, High Performance 107-II	9-8
102	Side Force, Rolling Moment, and Yawing Moment vs. Yaw Angle, High Performance 107-II	9-9
103	Comparison of 107-II and High Performance 107-II in Yaw	9-10
104	Luminescent Oil Photograph - Final Configuration in Yaw	9-11
105	Static Directional Stability Derivative vs. Angle of Attack - High Performance 107-II	9-12
106a-c	Ground Instability Analysis	12-6 to 12-8
107	Flight Stresses	13-10
108	Spanwise Weight Distribution	13-15

LIST OF FIGURES

Figure No.	Title	Page No.
109	Flapwise Stiffness Distribution	13-16
110	Chordwise Stiffness Distribution	13-17
111	Chordwise Neutral Axis and CG Location	13-18
112	Static Moment Diagram	13-19
113	Centrifugal Force @ 262 Rotor RPM	13-20
114a-c	Flap Bending Moments in a Vacuum	13-21
115	Chord Bending Moments in a Vacuum	13-22
116	Constant Flap Bending Moment	13-23
117	Average Flap Vibratory Bending Moment	13-24
118	Constant Chord Bending Moment	13-25
119	Average Chord Vibratory Bending Moment	13-26
120a-f	Alternating Flap Bending Moment	13-27 to 13-28
121	Nondimensional Pitching Moment vs. Rotor Advance Ratio	15-5
122	Rotor Controls	18-1
123a	Ferry Range versus % Decrease in SFC	20-1
123b	Maximum Speed versus % Increase in Shaft Horsepower	20-1
124	Ferry Range and Maximum Speed versus Equivalent Flat Plate Area	20-2
125	Ferry Range, 107 Series	21-1
126	Payload-Range at Sea Level and 10,000 ft., 107 Series	21-3
127	Productivity/Weight Empty versus Forward Speed, 107 Series	21-4
128	Maintainability versus Forward Speed, 107 Series	21-5
129	Comparison of Ferry Range	22-3

LIST OF FIGURES

Figure No.	Title	Page No.
130	Comparison of Maximum Speed	22-3
131	Ferry Range, Chinook Series	24-1
132	Payload-Range @ S.L. and 10,000 ft., Chinook Series	24-3
133	Productivity/Weight Empty versus Forward Speed, Chinook Series	24-4
134	Maintainability versus Forward Speed, Chinook Series	24-5
135	Number of Aircraft Required	25-1

LIST OF TABLES

Table	Title	Page
I.	Results of Parametric Study	3-17
II.	Rotor Parameters for High Performance 107-II Study	4-1
III.	Polar Data Investigation	5-4
IV.	Aerodynamic Airfoil Characteristics	5-22
V.	Comparison of Rotor Performance	5-27
VI.	Performance Data for the High Performance 107-II	7-1
VII.	Dimensions and General Data - High Performance 107-II	7-2
VIII.	Weight Breakdown - High Performance 107-II	7-3
IX.	Drag Breakdown High Performance 107-II	7-7
X.	Summary of Accessory Losses	7-9
XI.	Physical Data for the High Performance 107-II	8-2
XII.	Flight Conditions for Stability Derivatives	8-6
XIII.	Longitudinal Pitch Accelerations Available	8-22
XIV.	Roll Acceleration Available	8-23
XV.	Summary of Analog Studies	8-24
XVI.	Comparison of Afterbodies	9-2
XVII.	Comparison of Fuselage Drag	9-4
XVIII.	Summary of Blades Examined for Dynamic Properties	13-2
XIX.	Comparison of Boeing-Vertol 107 and High Performance 107 Blade Dynamic Properties	13-4
XX.	Cases Considered in Blade Moment and Stress Study	13-7
XXI.	Summary of Blade Moment and Stress Study	13-8

LIST OF TABLES

Table	Title	Page
XXII.	Blade Second Mode Amplification Factors	13-11
XXIII.	Section Properties of Blade at Various Sections	13-12
XXIV.	Steady Flapwise Stresses	13-12
XXV.	Vibratory Flapwise Stresses and Moments	13-13
XXVI.	Steady Chordwise Stresses	13-14
XXVII.	Vibratory Chordwise Stresses	13-14
XXVIII.	Flight Conditions for Rotor Hub Analysis	14-3
XXIX.	Centrifugal Force Loads	14-3
XXX.	In Plane Hub Loads	14-4
XXXI.	Table of Control Ranges	18-4
XXXII.	Summary Weight Statement	19-4
XXXIII.	Summary of Weights and Performance, Boeing-Vertol 107 Series	21-2
XXXIV.	Summary of Weights and Performance, Unloaded Rotor Versions	22-2
XXXV.	Summary of Weights and Performance, Chinook Series	24-2

LIST OF DRAWINGS

No.	Title	Page
SK-10321	High Performance	11-3
SK-10249	Main Gear Retraction	11-5
SK-10333	Nose Gear Retraction	11-7
SK-10340	Aft Fuselage Modifications	11-9
SK-10327	Cockpit Glass Installation	11-11
SK-9892	25 Ft. Metal Rotor Blade 0009.5 Airfoil	13-5
SK-10307	Rotor Hub	14-5
SK-10242	Rotor Controls	15-7
SK-10319	Rotor Hub Fairing	16-3
L107C2021	Flight Controls	18-5
SK-10315	Advanced 107-II	21-7
SK-10314	Advanced YHC-1B	24-7

LIST OF SYMBOLS

A.C.	Aerodynamic Center
a	Speed of Sound, ft/sec
a_o	Lift Curve Slope
B, b	Number of Blades per Rotor
$B_y B_\zeta$	Damping Product Required for Neutral Stability
C, C_o, c	Rotor Blade Chord, ft
C_D wet	Drag Coefficient Based on Wetted Area, $\frac{D}{\frac{1}{2}\rho V^2 S \text{ wet}}$
C_d	Two Dimensional Drag Coefficient, $\frac{D}{\frac{1}{2}\rho V^2 S}$
C.F.	Centrifugal Force, lbs
C.G.	Center of Gravity
C.P.	Center of Pressure
C.P.M.	Cycles per Minute
C_ζ	Damping Produced by Each Blade Lag Damper
C	Effective Damping at the Rotor Hub
C_l	Two Dimensional Lift Coefficient, $\frac{L}{\frac{1}{2}\rho V^2 S^2}$
C_L/σ	Rotor Lift Coefficient - Solidity Ratio, $\frac{L}{\frac{1}{2}\rho \pi R^2 V^2 \sigma}$
C_p/σ	Total Rotor Power Coefficient - Solidity Ratio, $\frac{P}{\rho \pi R^2 (\Omega R)^3 \sigma}$
C_{po}/σ	Profile Power Coefficient - Solidity Ratio, $\frac{P_o}{\rho \pi R^2 (\Omega R)^3 \sigma}$
C_T/σ	Thrust Coefficient - Solidity Ratio, $\frac{T}{\rho \pi R^2 (\Omega R)^2 \sigma}$
C_T'/σ	Vertical Force Coefficient - Solidity Ratio, $\frac{L}{\rho \pi R^2 (\Omega R)^2 \sigma}$
C_H/σ	Longitudinal Force Coefficient, $\frac{H}{\rho \pi R^2 (\Omega R)^2 \sigma}$
D	Drag, lbs
D/q	Drag-Dynamic Pressure Ratio, ft^2, Positive to Right

LIST OF SYMBOLS, (Continued)

D_E	Effective Drag, lbs, - X + P/V
D_e	Rotor Power - Forward Speed Ratio, P/V
D.C.P.	Differential Collective Pitch, deg.
f_e	Equivalent Flat Plate Area, ft^2
G.W.	Gross Weight, lbs
GW/f_e	Gross Weight - Equivalent Flat Plate Area Ratio
H	Rotor Drag Force, lbs, in the Plane-Of-No-Feathering
HP	Horizontal Pin, Horsepower
HP_{acc}	Accessory Horsepower
HPHD	High Performance Helicopter Design
I/C	Section Modulus, $in.^3$
L	Rotor Lift, lbs; Distance Between Rotors, ft
L/D_E	Lift - Effective Drag Ratio
L/q	Lift - Dynamic Pressure Ratio, ft^2, Positive Upwards
$\mathcal{L}/q$	Rolling Moment - Dynamic Pressure Ratio, Positive to the Right
$\mathcal{L}_\beta$	Rolling Moment Due to Side Slip, ft-lb/rad
$\mathcal{L}_{\dot{\phi}}$	Rolling Moment Due To Roll Rate, ft-lb-sec/rad
$\mathcal{L}_{\dot{\psi}}$	Rolling Moment Due To Yaw Rate, ft-lb-sec/rad
$\mathcal{L}_{\delta_S}$	Rolling Moment Due To Lateral Stick, ft-lb/in.
$\mathcal{L}_{\delta_R}$	Rolling Moment Due To Rudder Pedal, ft-lb/in.
M, M_t	Advancing Blade Tip Mach Number
M/q	Pitching Moment - Dynamic Pressure Ratio, ft^3, Positive Nose Up
M_{B_1}	Blade Bending Moment, ft-lb
MFCG	Most Forward Center of Gravity
MRP	Military Rated Power
M_α	Pitching Moment Due To Fuselage Angle of Attack, ft-lb/rad

LIST OF SYMBOLS, (Continued)

M_{μ}	Pitching Moment Due To Advance Ratio, ft-lbs
$M_{\dot{\theta}}$	Pitching Moment Due To Pitch Rate, ft-lb-sec/rad
M_{θ_c}	Pitching Moment Due To Collective Pitch, ft-lb/rad
M_{δ}	Pitching Moment Due To Longitudinal Stick Position, ft-lb/in.
NRP	Normal Rated Power
N_r	Rotor Speed at Take-Off, rpm
N/q	Yawing Moment - Dynamic Pressure Ratio, ft^3, Positive Nose Right
N_{β}	Yawing Moment Due To Sideslip, ft-lb/rad
$N_{\dot{\phi}}$	Yawing Moment Due To Roll Rate, ft-lb-sec/rad
$N_{\dot{\psi}}$	Yawing Moment Due To Yaw Rate, ft-lb-sec/rad
N_{δ_S}	Yawing Moment Due To Lateral Stick, ft-lb/in.
N_{δ_R}	Yawing Moment Due To Rudder Pedal, ft-lb/in.
$(N/q)_{\beta}$	Static Directional Stability Derivative, ft^3/deg
O.G.E.	Out of Ground Effect
P	Power, lb-ft/sec
PV/E	Productivity, The Product of Payload and Forward Speed Divided by the Weight Empty, Knots
Q/b	Torque per Rotor Blade, lb-ft
q	Dynamic Pressure, lb/ft^2; Oleo Strut Displacement, in.
$\dot{q}$	Oleo Strut Velocity, in/sec
R	Rotor Radius, ft
RHP	Rotor Horsepower
RN_e	Effective Reynold's Number, $\frac{\rho V \text{ (Characteristic Length)} \times \left(\text{Turbulence Factor}\right)}{\mu}$
RPM	Revolutions per Minute
r	Local Rotor Radius, ft; Distance from Centerline of Rotation to Blade Attaching Bolt, ft
S	Area, ft^2
S.A.S.	Stability Augmentation System
S.F.C.	Specific Fuel Consumption, lb/HP-hr

LIST OF SYMBOLS, (Continued)

SHP	Shaft Horsepower
S.L.	Sea Level
T	Thrust, lb
TOGW	Take-Off Gross Weight, lb
V	Forward Velocity, Knots or mph
V_t	Rotor Tip Speed, ($R\Omega$), ft/sec
VP	Vertical Pin
V_{max}	Maximum Forward Velocity, Knots or mph
W_B	Body Weight, lb
W_d	Drive System Weight, lb
W_e	Installed Engine Weight, lb
W_{fc}	Flight Controls Weight, lb
W_r	Rotor Weight, lb
X	Longitudinal Propulsive Force, lb
X/L	Propulsive Force-Lift Ratio
X_μ	Longitudinal Force Due To Advance Ratio, lbs
X_α	Longitudinal Force Due To Fuselage Angle of Attack, lb/rad
$X_{\dot{\theta}}$	Longitudinal Force Due To Pitch Rate, lb-sec/rad
X_{θ_c}	Longitudinal Force Due To Collective Pitch, lb/rad
X_δ	Longitudinal Force Due To Longitudinal Stick Position, lb/in.
Y/q	Side Force - Dynamic Pressure Ratio, ft^2
Y_β	Side Force Due To Sideslip, lb/rad
$Y_{\dot{\phi}}$	Side Force Due To Roll Rate, lb-sec/rad
$Y_{\dot{\psi}}$	Side Force Due To Yaw Rate, lb-sec/rad
Y_{δ_S}	Side Force Due To Lateral Stick, lb/in.
Y_{δ_R}	Side Force Due To Rudder Pedal, lb/in.
y	Lateral Displacement at the Rotor Hub, in.

$\dot{y}$	Lateral Velocity at the Rotor Hub, in./sec
z_μ	Vertical Force Due To Advance Ratio, lbs
z_α	Vertical Force Due To Fuselage Angle of Attack, lb/rad
$z_{\dot{\theta}}$	Vertical Force Due To Pitch Rate, lb-sec/rad
z_{θ_t}	Vertical Force Due To Collective Pitch, lb/rad
z_δ	Vertical Force Due To Longitudinal Stick Position, lb/in.
α	Fuselage Angle of Attack, rad or deg; Rotor Angle of Attack to the Plane-Of-No-Feathering, rad

$$\alpha = \text{Tan}^{-1}\left[\frac{\lambda}{\mu} + \frac{C_T}{2\mu\sqrt{\mu^2 + \lambda^2}}\right]$$

β	Sideslip Angle, rad
σ	Rotor Solidity, $\frac{bc}{\pi R}$
μ	Damping Ratio; Kinematic Viscosity of Air, lb-sec^2/ft^4; Rotor Advance Ratio, $\frac{V\cos\alpha}{V_t}$
ϵ	Distance From Aerodynamic Center To Pitch Axis, ft
λ	Inflow Ratio, $\frac{V\sin\alpha - v}{V_t}$
λ_v	Nondimensional Pitching Moment Coefficient
θ_o	Root Collective Pitch, rad or deg
θ_t	Blade Twist Angle, deg
θ_{TF}	Front Rotor Collective Pitch, rad
θ_{TR}	Rear Rotor Collective Pitch, rad
η_T	Transmission Efficiency
ψ	Rotor Blade Azimuth Position, deg; Yaw Angle, rad or deg
ω, Ω	Angular Velocity, rad/sec
ξ	Nondimensional Rotor Hinge Offset
ρ	Mass Density of Air, Slugs/ft^3
γ	Lock Number, $\frac{\rho\, acR^4}{2I_f}$

SUMMARY

In June 1960, the Vertol Division of The Boeing Company received a contract from TRECOM to undertake a preliminary design study of a high performance helicopter. The primary performance requirements for this helicopter were extended ferry range capability (1600 n.mi.) and speed (200 mph). Furthermore, the design should employ existing components which would not require further design, development, or extensive modification in order to minimize cost and elapsed time.

In the conceptual phase, the goal of this design study was to be a research helicopter intended to demonstrate in-flight feasibility of the high performance capability. The original approach, as envisaged in the proposal, considered as examples either the use of the Boeing-Vertol 107 with cut-down Chinook blades or the use of the H-25 dynamic components with a new specially designed fuselage and cut-down H-21 blades.

The controlling item with respect to utilization of existing components is the selection of rotor blades. The performance requirements dictate the use of high blade area (low blade loading) which may be achieved by either using large-chord blades cut-down in radius, or, for a given existing helicopter, to extend the radius and chord by modest amounts. Either of these means offer the advantage of proven structure and use of existing tooling.

To gain insight into the applicability of existing blades, a parametric study was undertaken, varying blade radius for a number of existing Vertol blades. To these families of blades was applied a forward flight criterion to determine allowable gross weights. Thus, a wide spectrum of high performance helicopters was examined and the best possible configurations were delineated. Blades utilizing the basic chord, airfoil and twist distribution of the H-25, H-21 and YHC-1A Vertol-designed Army-funded helicopters were investigated.

YHC-1A (Boeing-Vertol 107) Study

The parametric study confirmed the validity of the use of existing oversized blades to provide the lower blade loading requirement to demonstrate high speed capability. As the parametric study progressed, it became apparent that application of reduced radius YHC-1B Chinook blades to the Boeing-Vertol 107 (YHC-1A) helicopter could fulfill the requirements of high performance. Furthermore, it was considered desirable to demonstrate the required high performance capability with an existing operational Army production type helicopter in order to avoid development cost of a single purpose research aircraft. Consequently, recommendations were made to discontinue further parametric investigation and proceed immediately to the preliminary design phase of the Boeing-Vertol 107 equipped with cut-down Chinook blades. The YHC-1B was not considered in the parametric study since there were no larger chord blades available.

The parametric study indicated that the High Performance 107-II with reduced-radius Chinook blades would provide the desired ferry range requirement (1600 n.mi.) and, at reduced gross weight, the high speed capability (200 mph).

High Performance 107-II

In parallel to the development of the performance parametric studies was a thorough investigation of rotor environment at high forward speeds. The effects of blade twist, compressibility, stall and reverse flow were examined in the range of advance ratios characteristic of the High Performance 107-II. Both the parametric and rotor environment studies indicated substantial performance increases could be obtained from thinner airfoil sections and more twisted blades. It was concluded that the NACA 0009.5 airfoil section and blade twist of -14 degrees offered superior aerodynamic properties for the High Performance 107-II rotor.

Preliminary design, aerodynamic and design studies were begun in December 1960 to more clearly define the High Performance 107-II. As the design progressed it became apparent that the reduced radius Chinook blades were overly heavy causing a "chain reaction" in weight penalty because of over sized rotor hub, upper controls, etc. The best solution, under the requirement to use existing blades, was to increase the chord of the present Boeing-Vertol 107-II blades to 23 inches. This decision was well suited to the aerodynamic requirements for a thinner section, since the 107-II blade has an NACA 0012 airfoil section and a constant chord of 18 inches. The blade radius was held constant at 25 feet. This blade proved to have acceptable dynamic properties and a theoretical study was therefore begun to determine the effects of various flight parameters on blade bending moments and blade stresses.

A static wind tunnel test was conducted at the University of Maryland to support the drag reduction required for high performance. By retracting the landing gear, reducing aft pylon - hub interference drag with a rooftop fairing and extended chord pylon, reshaping the after body - rear ramp volume, and fairing the rotor hubs, the parasite drag area of the Boeing-Vertol 107-II was reduced from 30.2 square feet to 20.5 square feet. Other Boeing-Vertol test programs were completely reviewed to obtain supporting data to the overall study.

These modifications to the 107-II were submitted to the respective design sections. The overall design was governed by the requirement to use existing 107-II components wherever possible.

Retraction of the main landing gear completely into the stub wing was accomplished using the present attachment points and rotating the gear forward. The stub wing span was increased by 18 inches to insure that the fuel volume was not decreased. The nose gear is rotated aft and partially retracted. The exposed portions are faired. The wheels, tires, and oleos of the 107-II are retained.

A detailed review of ground instability characteristics at gross weights of 14,300 pounds, 19,130 pounds, and 23,000 pounds indicated that the above alighting gear design was acceptable.

The rotor hub was selected primarily from aerodynamic considerations, giving the smallest possible hub radius and a minimum total frontal area. Wire ply tension-torsion straps, now under development at Vertol Division, permitted a further shortening of the hub arm. The rotor hub is basically of the same configuration as the YHC-1B, with the pitch bearings located inboard of the vertical pin. A light-weight fiberglas rotor hub fairing, permitting full kinematic freedom, was designed to aid in the drag reduction program.

The present 107-II drive system was found to be satisfactory for the High Performance 107-II and only minor changes were required in the flight controls and upper rotor controls to establish the control kinematics required by increased performance.

The design feasibility of the High Performance 107-II was paralleled with detailed performance and flying qualities investigations. The studies of aircraft flying qualities demonstrated that the increased performance is not accompanied by detrimental static and dynamic stability effects. The increased aft pylon area along with the Boeing-Vertol designed stability augmentation system insures flying qualities characteristic of the present 107 helicopter series.

The detailed performance studies of the High Performance 107-II indicated that this configuration would meet the performance requirements of ferry range (1600 n.mi.) and speed (200 mph). This configuration, though commensurate with the early conceptual phase of the contract (a research helicopter intended to demonstrate in-flight feasibility of high performance), was not regarded as an acceptable operational helicopter design, due to the reduced short-range payload characteristics caused by empty weight increases. The additional solidity required for reduced blade loadings in high speed forward flight, when achieved only by increased chord, severely penalizes the hover performance leading to a further reduction in payload.

Advanced 107 Study

The most effective means for increasing the payload was found to be optimizing the blade radius and chord for the mission requirements. Introducing the Army hovering requirement of 6,000 feet on a 95°F day along with the 100 n.mile mission, an advanced 107 was defined with the overall forward flight performance of the High Performance 107-II and complete operational suitability. By increasing the radius from 25 feet to 26.25 feet and reducing the chord from 23 inches to 21 inches, the present 107-II useful load was maintained. The merit of this design over the intermediate High Performance 107-II Helicopter and present Boeing-Vertol 107 Model II is clearly demonstrated. The design feasibility of the High Performance 107-II, established in this report, is directly applicable to the advanced 107.

YHC-1B Study

To determine the performance potential of the YHC-1B, a brief study leading to an advanced YHC-1B was completed. By increasing the radius from 29.5 feet for the YHC-1B to 30.8 feet and increasing the chord from 23 inches to 26 inches, both operational improvements and high performance are achieved.

Compound High Performance Helicopter Study

Finally, two compound versions of the advanced 107 received a small percentage of attention. These were (1) unloading of propulsive force only on to a pusher propeller and (2) unloading both propulsive force and lift to propeller and wing respectively. Improvements in speed were characteristic of both versions, but significant ferry range increases required the unloading of rotor lift onto the wings. The addition of a third engine was found necessary to insure operational feasibility.

The high performance helicopter has been found to be technically feasible through modest advances in the state of the art. It has been shown that either the advanced 107 or the advanced YHC-1B is capable of the performance requirements and could be used to demonstrate the feasibility of high performance. The concept, however, is certain to be applied mainly to production helicopters of the YHC-1B type for which the Army has a long term program. Cost studies indicate the overall high performance program costs would be significantly lower if the advanced YHC-1B is selected for development. IT IS THEREFORE RECOMMENDED THAT THE ADVANCED YHC-1B CONFIGURATION BE ADOPTED AS THE DESIGN HIGH PERFORMANCE HELICOPTER.

CONCLUSIONS

A preliminary design study establishing the feasibility of high performance using operational aircraft is concluded. Substantial increases in helicopter performance in terms of range, speed and productivity are assured through modest advances in the state of the art.

The following specific conclusions are made based on the results of this preliminary design study:

1. Both drag reduction and reduced blade loading are mandatory to efficient high forward speed flight.

2. Wind tunnel tests confirm the parasite drag area of 20.5 sq. ft. for the high performance 107 series.

3. Both parametric and rotor environment studies indicate the desirability of thinner blade airfoil sections having higher drag divergence Mach number characteristics. Allowable blade loading may be increased through more negatively twisted blades.

4. Flying qualities are not detrimentally effected by increased performance because of the Boeing-Vertol designed stability augmentation system and increased aft pylon area.

5. Increasing the blade chord without optimizing rotor radius or increasing installed power severely penalizes the short range payload characteristics.

It is concluded therefore, that the next generation of transport helicopters may be efficiently achieved through the normal evolution process concomitant to aircraft growth with accruing advantages in lead time and unit cost. The next step, amplifying these studies toward the realization of the high performance helicopter, would be the detailed design phase preparatory to actual fabrication.

RECOMMENDATIONS

Based on the results of this study phase, the following recommendations concerning a continuation of this program are summarized below:

1. Establish a detailed design phase for the Advanced YHC-1B

2. Review compound versions of the YHC-1B

SUMMARY OF PHASE I

During the first two and one-half months of this contract, the Vertol Aerodynamics Group applied and extended its overall knowledge of high speed helicopter design with the High Performance Helicopter Study (Contract DA44-177-TC-686). The results of these efforts will be the development of a helicopter capable of the following minimum performance.

1. Payload - 800 lbs. with items 2 and 4 below.
2. Speed - 200 miles per hour with items 1 and 4.
3. Ferry range - 1600 natucial miles with item 4 at zero headwind and 1 hour reserve fuel.
4. Satisfactory flying and handling requirements (MIL-SPEC 8501).

To insure accurate calculations of rotor performance data which would reflect both stall and compressibility, the analytical techniques of References 3 and 4 were developed on the IBM 704 at Boeing Aero-Space Division, Seattle, Washington. This program was used to investigate performance of isolated rotors at high advance ratios and advancing tip Mach numbers. Calculations were performed for blades having linear twists from -4 to -14 degrees. The effects of Mach number, advance ratio, twist and inflow ratio are summarized as performance charts.

The initial parametric study investigated various configurations capable of at least 210 miles per hour maximum speed at sea level standard day using normal rated power and carrying a minimum payload of 800 pounds. The weight trend data indicated that this payload would be higher when considering the more practical configurations.

Despite the fact that the parametric study indicated many configurations that would meet the design requirements, itwas felt that those configurations derived from the present Vertol 107 aircraft offered the most potential for a minimum of cost. These feelings were related to the contracting agency and mutual agreement permitted further emphasis on the High Performance 107.

The primary variable at the high speed condition was payload capability greater than 800 pounds. To examine this variable in a more parametric manner with the High Performance 107 an investigation was conducted into the potential of both modified YHC-1A and YHC-1B rotor systems, as well as an optimum rotor system. The rotors under consideration were:

1. Modified YHC-1A blade
   a. Chord = 18 inches
   b. Twist = .333 degrees per foot
   c. Three blades per rotor
   d. Radii = 25, 27, 29 feet
2. Modified YHC-1B blade
   a. Chord = 23 inches
   b. Twist = .305 degrees per foot
   c. Three blades per rotor
   d. Radii = 25, 27, 29 feet

3. Optimum rotor derived from
   a. Chord = 23, 20.5, 18 inches
   b. Total twist = -14 degrees
   c. Three blades per rotor
   d. Radii = 25, 27, 29 feet

The blades were of constant chord and linear twist.

The overall effects of increased fuselage length, et cetera, to accommodate the extended radius blades were considered in the weight empty.

The qualitative investigation of stall, compressibility and reverse flow provided increased understanding of rotor characteristics at high advance ratio. The magnitude of drag divergence on the retreating blade as well as the shifting of stall to blade azimuth angles between 270 and 360 degrees indicated the need for a definitive criteria of rotor stall to avoid vibration increases.

The aerodynamic considerations of the high performance helicopter obtained during the first two and one-half month study period progressed through the following four (4) phases:

1. Methodology (development of preliminary design performance charts)

2. Configuration Study (initial parametric study)

3. Detailed Rotor Study (detailed study of rotor parameters for the High Performance 107-II)

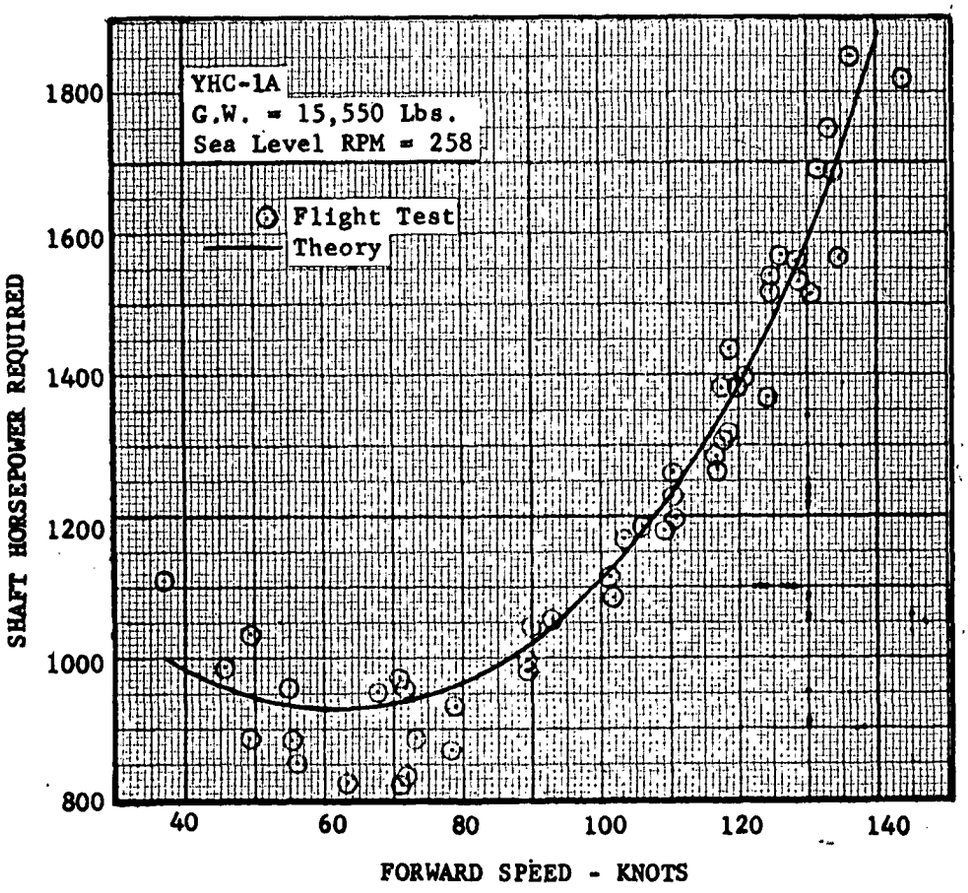
4. Rotor Environment (an investigation of stall, compressibility and reverse flow characteristics)

METHODOLOGY

The detailed design work required in investigating the performance characteristics of the high performance helicopter necessitated an advancement in techniques for calculating rotor performance. The high forward speed potential required accurate evaluation of compressibility, stall and reverse flow effects on rotor performance. Present performance techniques correlate well with flight test data (see Figure 1, below), but extrapolation into regions of higher advance ratio and compressibility appeared unsatisfactory.

FIGURE 1

COMPARISON OF PRESENT POWER REQUIRED CALCULATIONS WITH FLIGHT TEST



To make available rotor performance data which would include the effects of stall, compressibility and reverse flow, the numerical equations and procedures for calculating the aerodynamic characteristics of lifting rotors, discussed in Reference 3 and 4, have been programmed for the IBM Model 704 at the Applied Mathematics Section, Aero-Space Division, Boeing Company in Seattle, Washington.

The method of analysis consists of calculating the individual force contributions of a specific number of blade sections at various points on the rotor disk, averaging the values around the disk at a particular radial station, and then radially integrating these averages along the blade to obtain the rotor characteristics of thrust, power, drag and flapping motion of a blade.

Since the method is essentially a blade element analysis, the numerical results are a direct function of the airfoil section properties included in the program. These properties of section lift and drag coefficient as a function of Mach No. and angle of attack are shown in Figure 2 for the NACA 0012 airfoil.

Using the above performance program, a voluminous amount of data was collected to cover the range of forward speeds and tip speeds contemplated in the design. Data was obtained for linear twists from -4 degrees to -14 degrees, advance ratios from .3 to .5, and advancing tip Mach No. from .7 to .9.

To insure that this more extensive performance technique was valid, a comparison to the flight test data was made. The results, shown in Figure 3, indicate correlation as satisfactory as the presently used performance method.

For preliminary design work during this phase it was found more meaningful to work with the performance parameters of lift-effective drag ratio, vertical force coefficient, and longitudinal force-lift ratio rather than the usual thrust, power, and drag coefficients. Figure 4 shows clearly the derivation of these performance parameters.

It is seen that the longitudinal force-lift ratio (X/L) represents the useful propulsive force component of the resultant rotor thrust and drag forces; that is, what is available in the rotor to overcome aircraft drag.

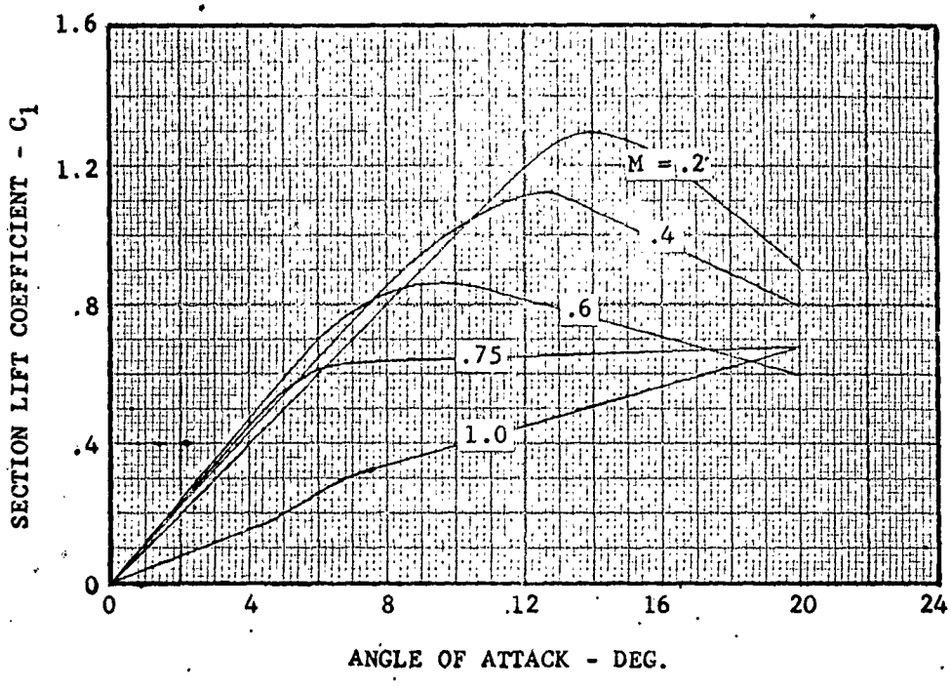
The vertical force coefficient (C_T'/σ) is the net lift component of the resultant force in the nondimensional form characteristic of a thrust coefficient-solidity ratio.

The lift-effective drag ratio (L/D_E) expresses the true "L/D" of the lifting rotor since the effective drag represents the total power expressed as a drag minus the propulsive force component which leaves only the induced and profile components due to the rotor.

The output data from this extensive performance program was first plotted in the form shown in Figure 5.

FIGURE 2

NACA 0012 SECTION AERODYNAMIC CHARACTERISTICS - C_l and C_d AS A FUNCTION OF α AND M



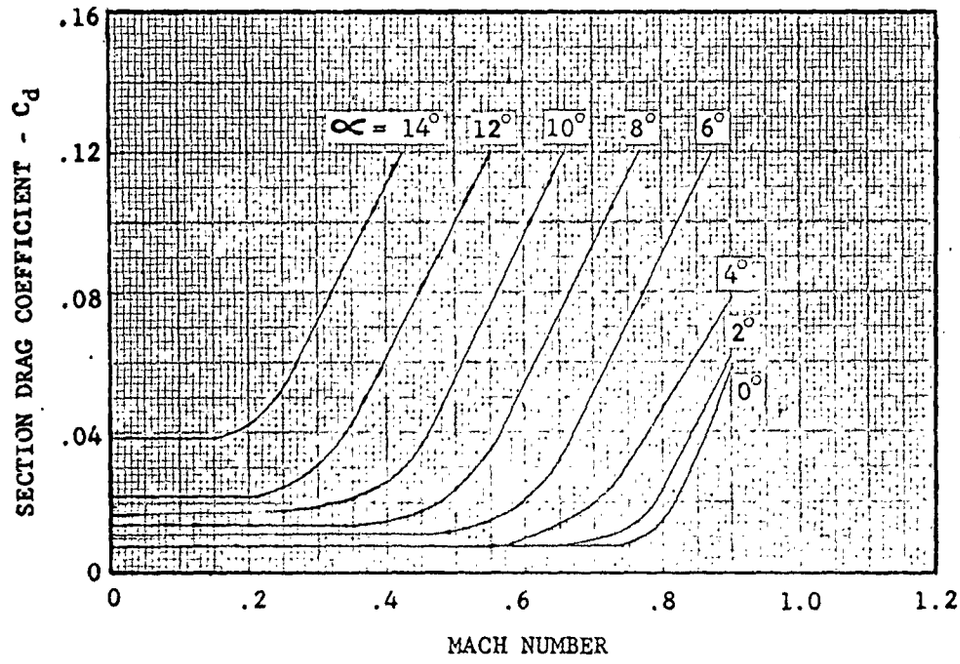


FIGURE 3

COMPARISON OF EXTENDED POWER REQUIRED METHOD WITH FLIGHT TEST

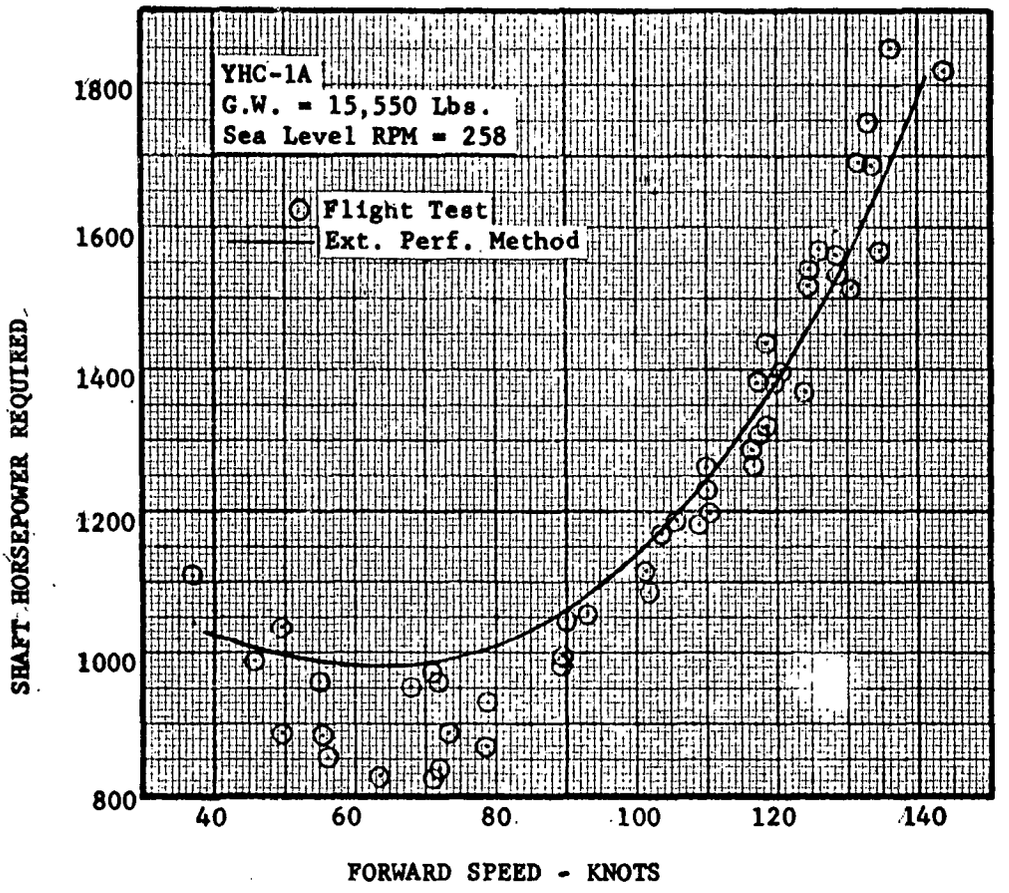
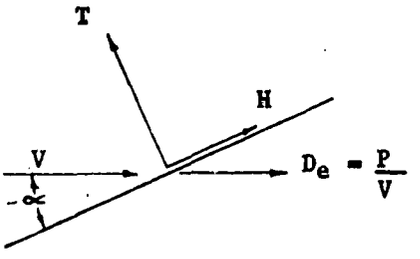


FIGURE 4

DEFINITION OF EXTENDED PERFORMANCE METHOD ROTOR TERMS

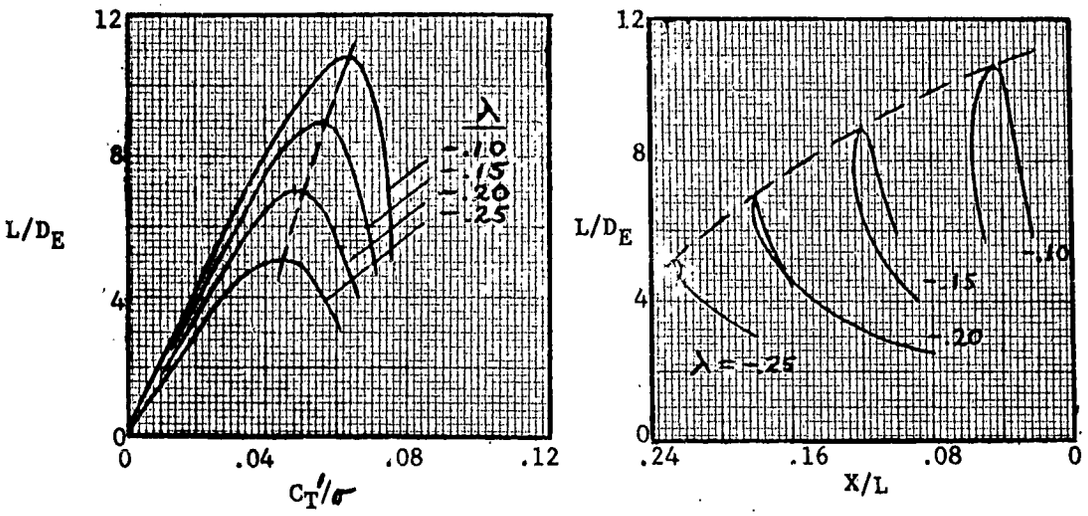


1. $L = T\cos\alpha - H\sin\alpha$
2. $D_E = -X + D_e = -X + P/V$
3. $X = -T\sin\alpha - H\cos\alpha$
4. $L/D_E = ①/②$
5. $X/L = ③/①$
6. $C_T'/\sigma = ①/\rho\pi R^2(\Omega R)^2\sigma$
7. $C_L/\sigma = ①/\frac{1}{2}\rho\pi R^2 v^2\sigma$
8. $\alpha = \text{TAN}^{-1}\left[\frac{\lambda}{\mu} + \frac{C_T}{2\mu\sqrt{\mu^2+\lambda^2}}\right]$

FIGURE 5

TYPICAL PERFORMANCE DATA FROM EXTENDED PERFORMANCE METHOD

$\mu = .45$ $M_t = .85$ $\theta_t = -9^\circ$



The independent variable along any constant inflow ratio line is root collective pitch. The major variables of advance ratio, advancing tip Mach No., and twist were held constant for each plot. These typical performance plots each showed a peak lift-effective drag ratio and associated vertical force coefficient and longitudinal force-lift ratio. Since the optimum aerodynamic configuration should be designed to fly at the peak L/D_E, cross plots of peak L/D_E and associated C_T'/σ versus associated X/L were made for the various Mach numbers and twists under consideration. These plots as well as plots of X/L @ $L/D_{E\ MAX}$ versus inflow ratio are presented in Appendix II of Reference 2.

These summary charts of peak L/D_E and associated C_T'/σ and X/L established the over-all performance data for the parametric studies.

Configuration Study

To establish design gross weights as well as select the basic rotor parameters which would define a group of aircraft capable of the required performance, the Phase I Plan for performance of this contract suggested a configuration study to determine the gross weight variation with blade chord, number of blades and blade radius at a design point of 200 MPH subject to the comfort stall limit and a Mach number range for rotor power divergence of .75 to .90 at the advancing tip. At least three existing blades, which may be cut down in radius, will be considered. These are the HUP-4, H-21, and HC-1B blades which have chords of 13, 18 and 23 inches, respectively. The analysis will be performed for gross weight to flat plate area loadings of 500, 750, 1000, and 1250 PSF for both three and four blades per rotor. The results will be plotted as gross weight versus blade radius for the three chords and two sets of blades. There will be twenty-four of these curves. On each curve will be marked power available limits for (1) T-53, (1) T-58, (1) T-55 and (2) T-58's.

Similar graphs will be developed showing empty weight variation and from this will be derived useful load and thence range performance.

From these plots, a number of possible configurations in the gross weight range from 6000 to 18,000 pounds will be selected for more detailed design and analytical study

The range performance was not completed since it was agreed on the basis of the preliminary work that the Vertol 107 would, over-all, be the best configuration to proceed with in the preliminary design phase.

To determine the particular performance charts for the selected gross weight to equivalent flat plate area ratios (GW/f_e), the relationship between advance ratio (μ), inflow ratio (λ), and advancing tip Mach number (M_t) for speeds of 150, 170, 190, and 210 miles per hour was established. Since the frequently used small angle assumption on advance ratio (i.e., $\mu = V\cos\alpha/V_t \approx V/V_t$) is not valid when the required inflow ratio (λ) becomes large, the following assumptions, in equation form, were made.

$$M_t = \frac{V + V_t}{a} \quad (3\text{-}1) \qquad \mu = \frac{V\cos\alpha}{V_t} \quad (3\text{-}2) \qquad \lambda = \frac{V\sin\alpha}{V_t} \quad (3\text{-}3)$$

The resulting relationship between μ, λ, and M_t becomes

$$\mu = \frac{V}{aM_t - V}\cos\left\{\sin^{-1}\left[\frac{\lambda}{V}(aM_t - V)\right]\right\} \quad (3\text{-}4)$$

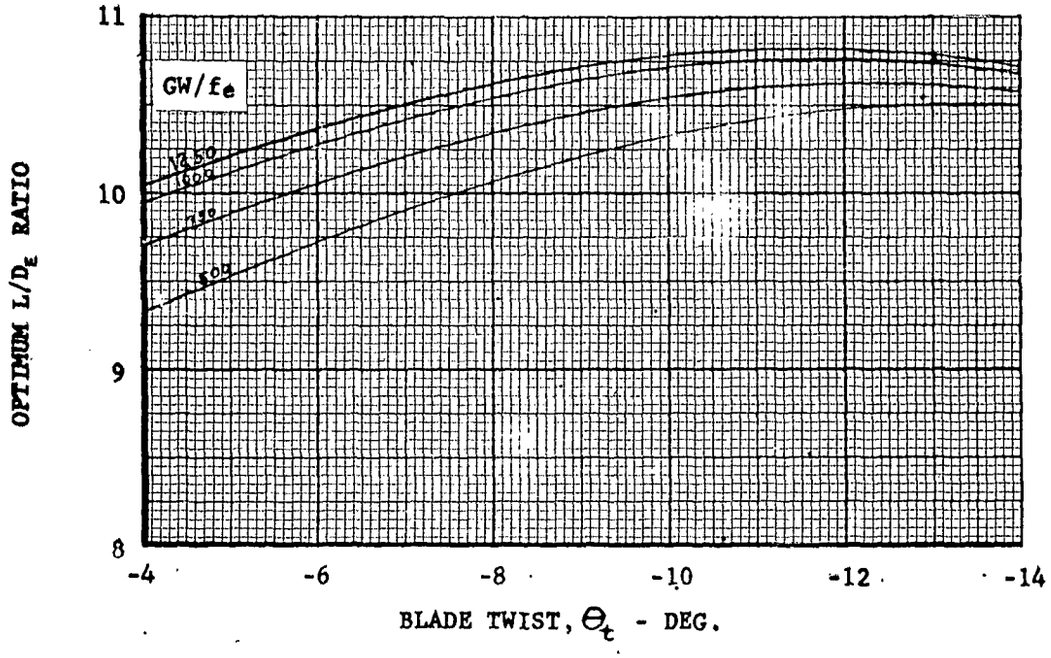
Utilizing this relationship and the plots of X/L versus λ for various advance ratios and advancing tip Mach numbers, the μ and λ for GW/f_e values of 1250, 1000, 750, and 500 at speeds of 150, 170, 190, and 210 miles per hour at sea level were determined. The values of L/D_E and C_T/σ versus twist for Mach numbers of .80, .85, and .90 at speeds of 150, 170, 190, and 210 miles per hour are presented on Figures 6 through 17.

FIGURE 6

OPTIMUM L/D_E AND C_T'/σ VS TWIST

FORWARD SPEED, V = 130.2 KNOTS = 150 MPH

ADVANCING TIP MACH NUMBER, M_t = 0.80



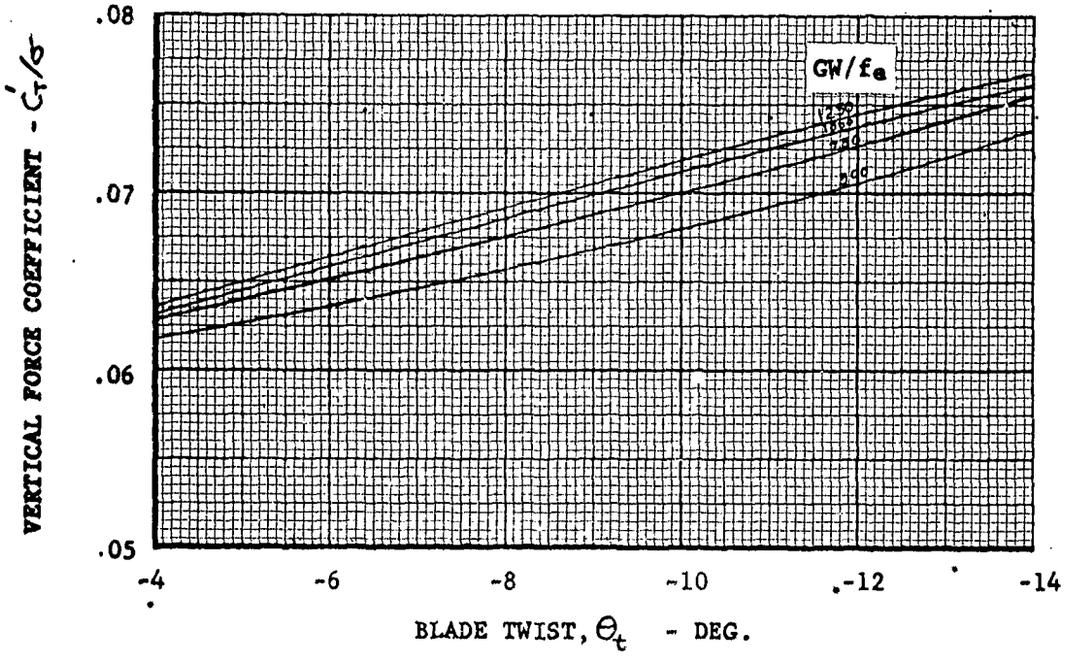
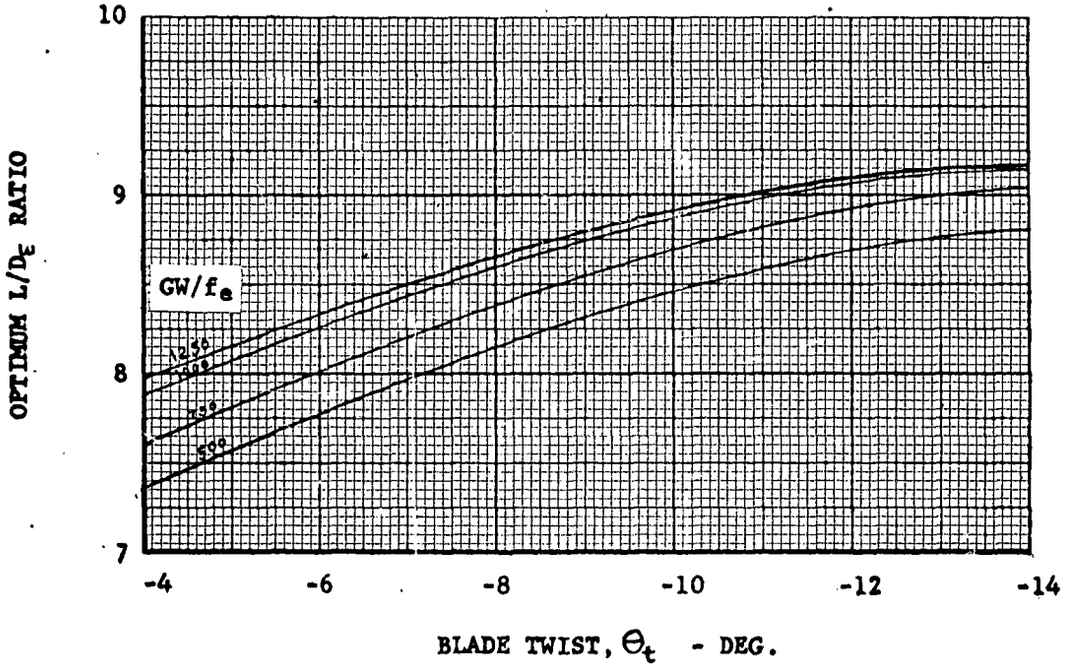


FIGURE 7

OPTIMUM L/D_E AND C_T'/σ VS TWIST

FORWARD SPEED, V = 130.2 KNOTS = 150 MPH

ADVANCING TIP MACH NUMBER, M_t = 0.85



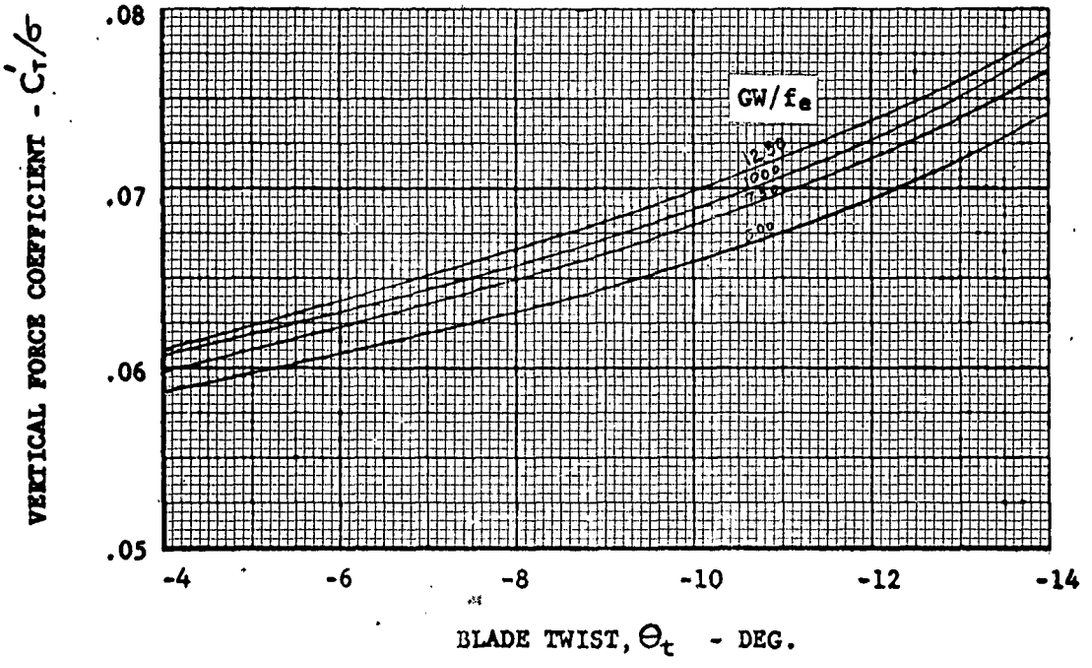
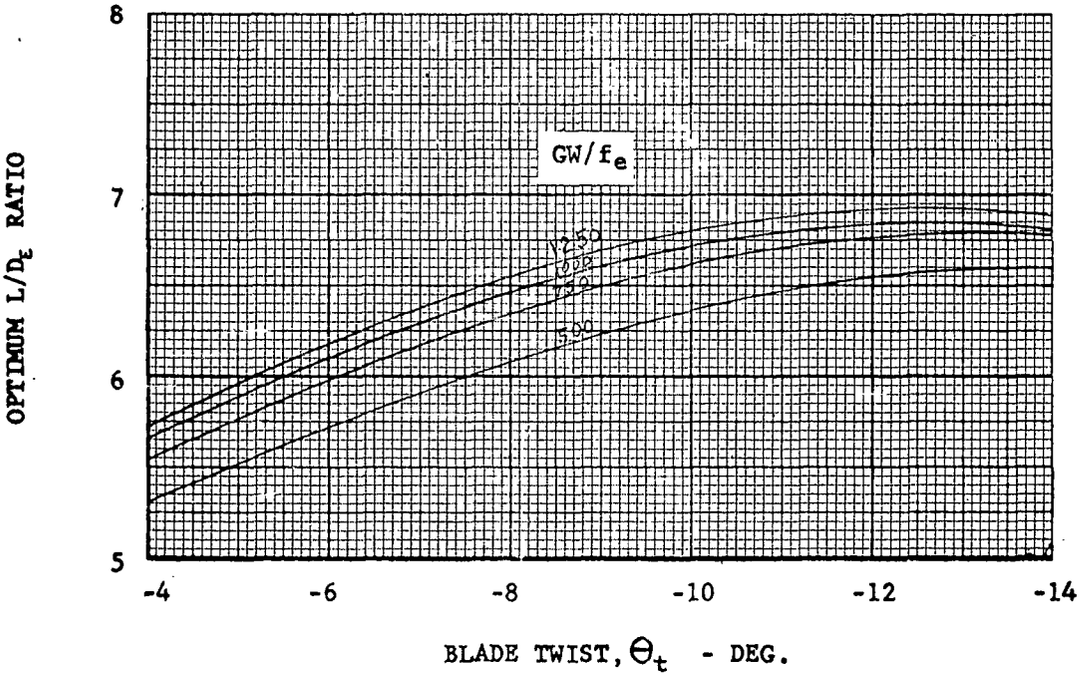


FIGURE 8

OPTIMUM L/D_E AND C_T'/σ VS TWIST

FORWARD SPEED V = 130.2 KNOTS = 150 MPH

ADVANCING TIP MACH NUMBER, M_t = 0.90



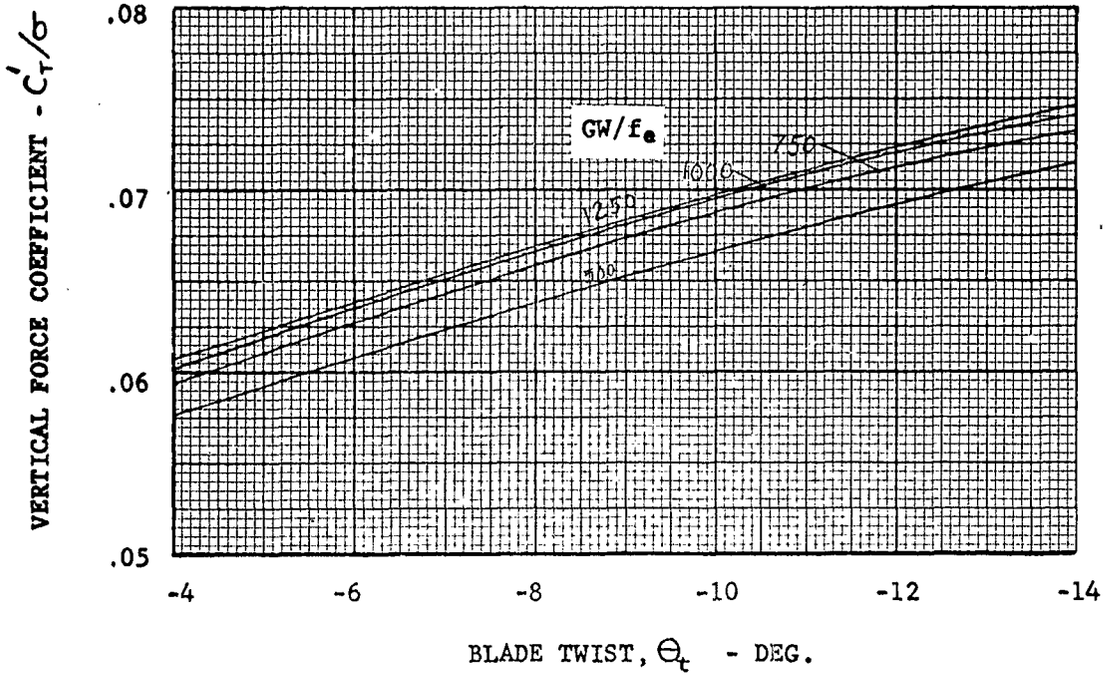
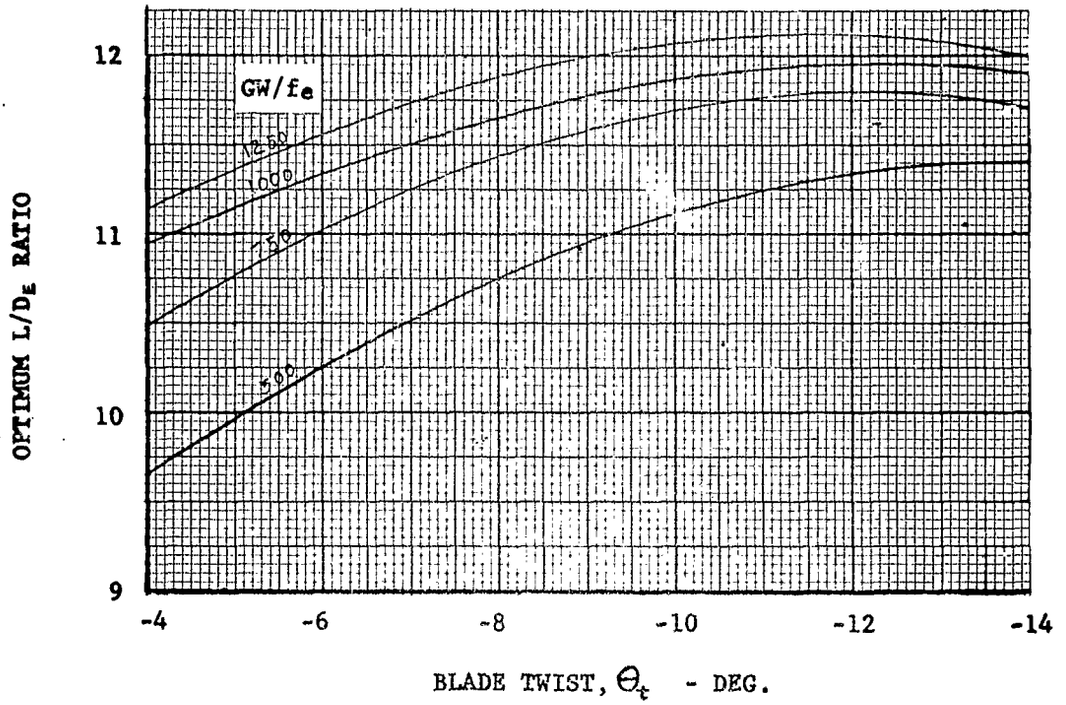


FIGURE 9

OPTIMUM L/D_E AND C_T'/σ VS TWIST

FORWARD SPEED, V = 147.7 KNOTS = 170 MPH

ADVANCING TIP MACH NUMBER, M_t = 0.80



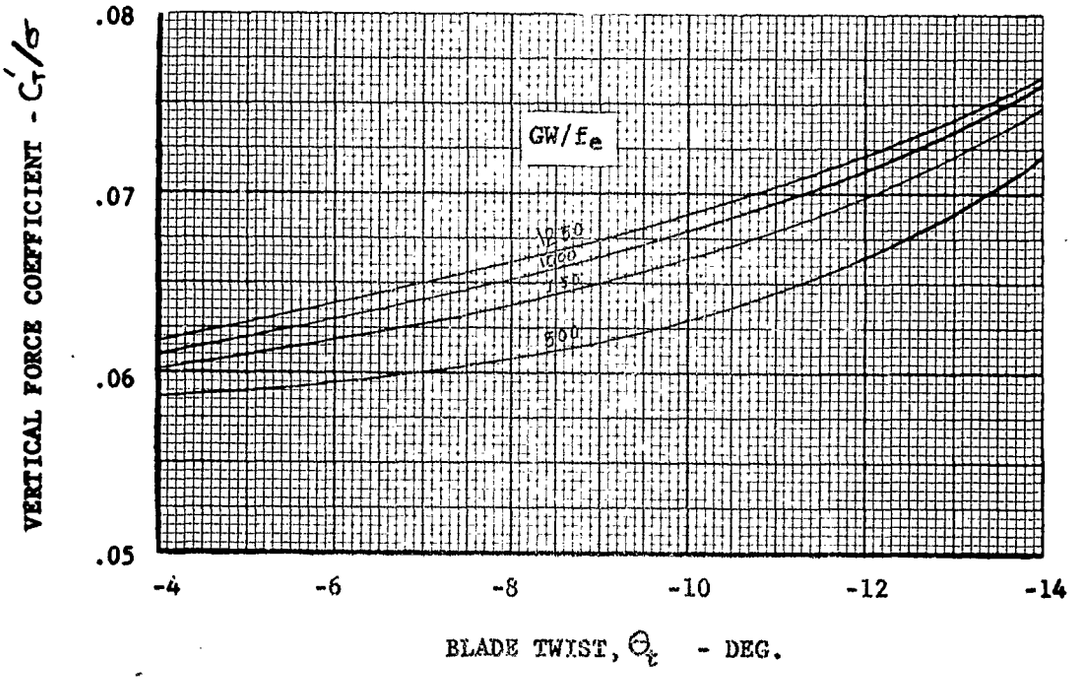
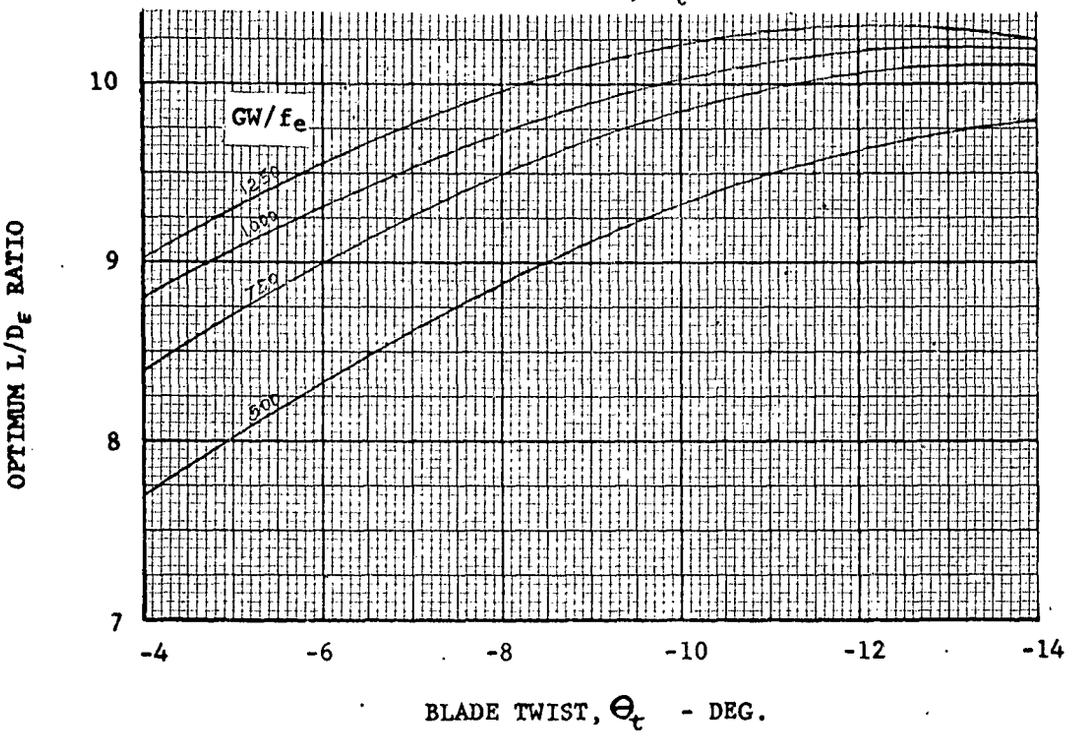


FIGURE 10

OPTIMUM L/D_ϵ AND C_T'/σ VS TWIST

FORWARD SPEED, V = 147.7 KNOTS = 170 MPH

ADVANCING TIP MACH NUMBER, M_t = 0.85



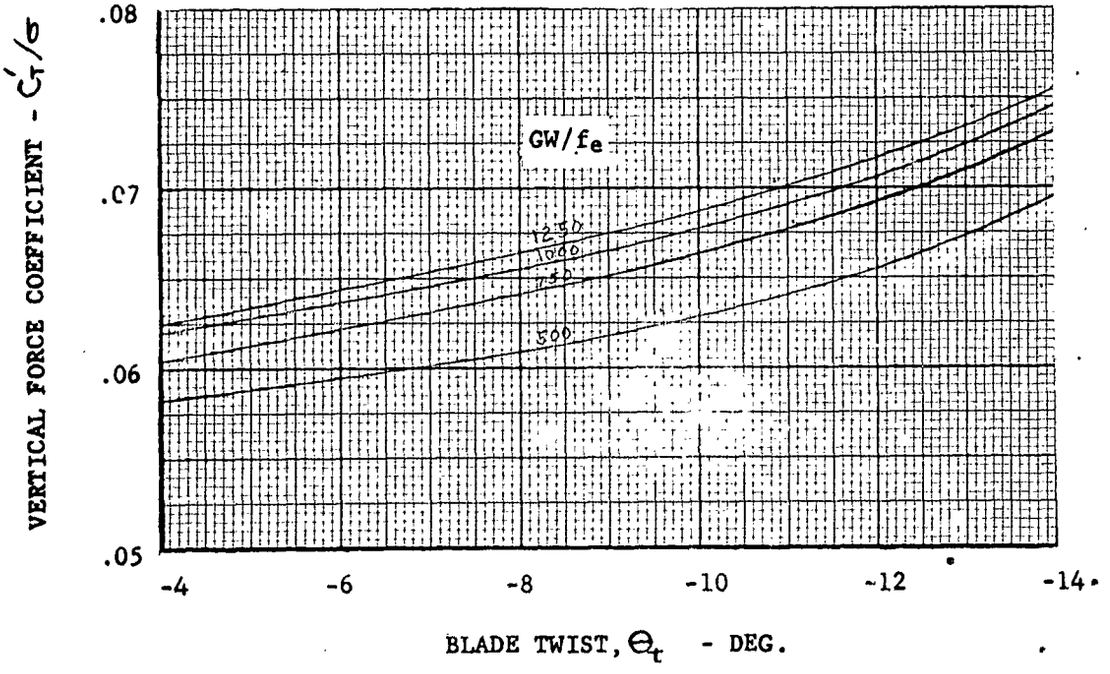
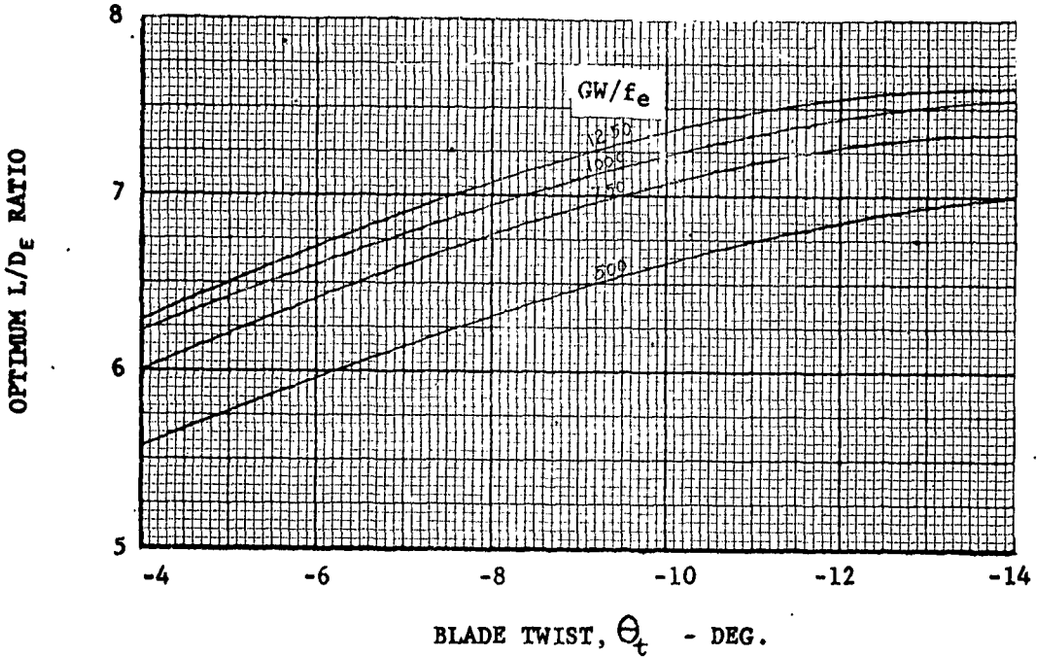


FIGURE 11

OPTIMUM L/D_E AND C_T'/σ VS TWIST

FORWARD SPEED, V = 147.7 KNOTS = 170 MPH

ADVANCING TIP MACH NUMBER, M_t = 0.90



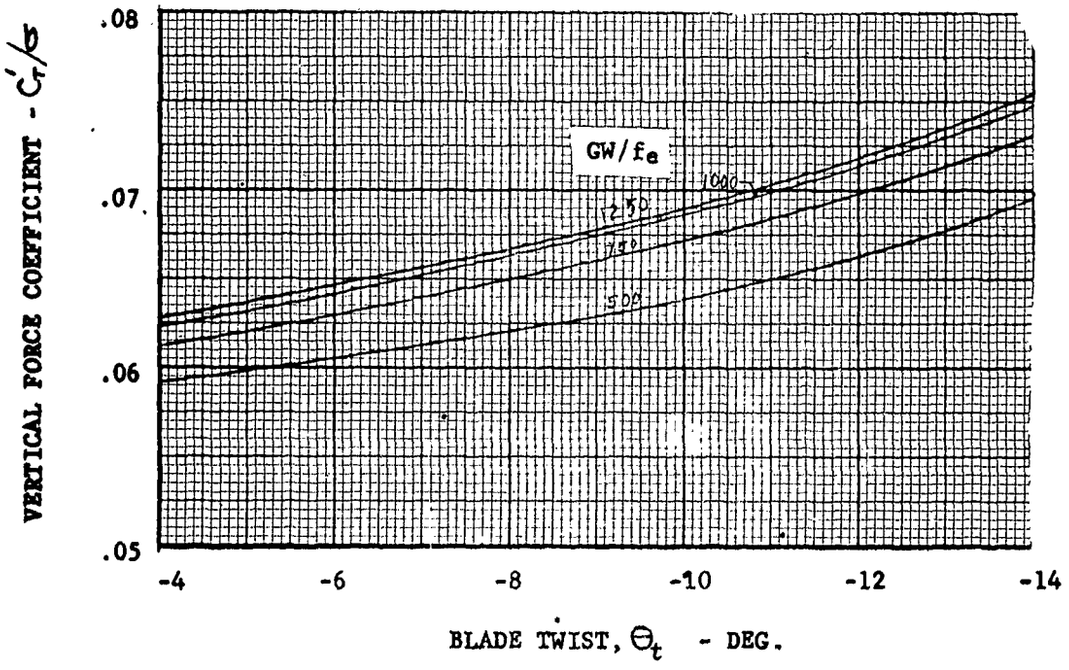
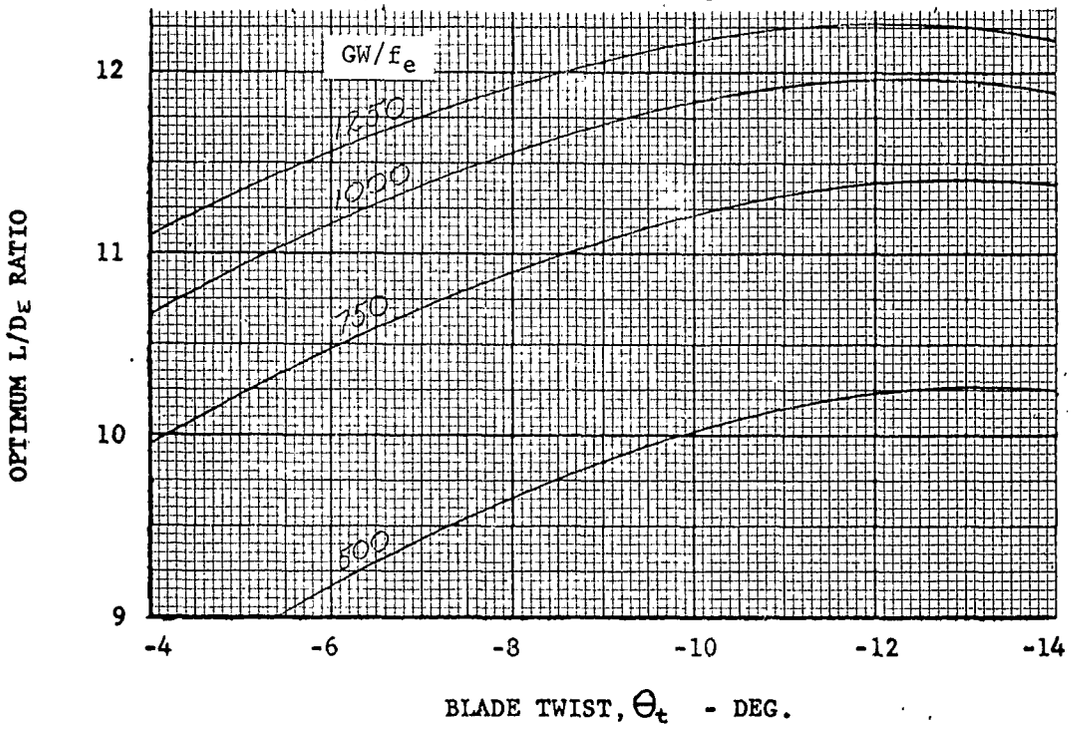


FIGURE 12

OPTIMUM L/D_ϵ AND C_T'/σ VS TWIST

FORWARD SPEED, V = 165 KNOTS = 190 MPH

ADVANCING TIP MACH NUMBER, M_t = 0.80



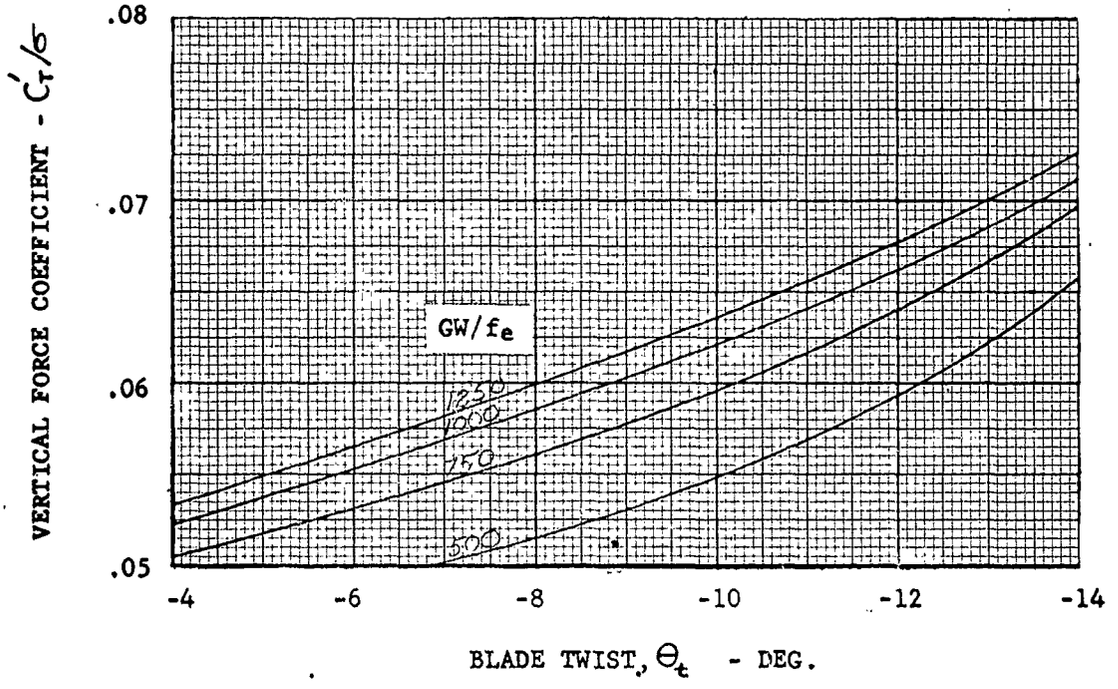
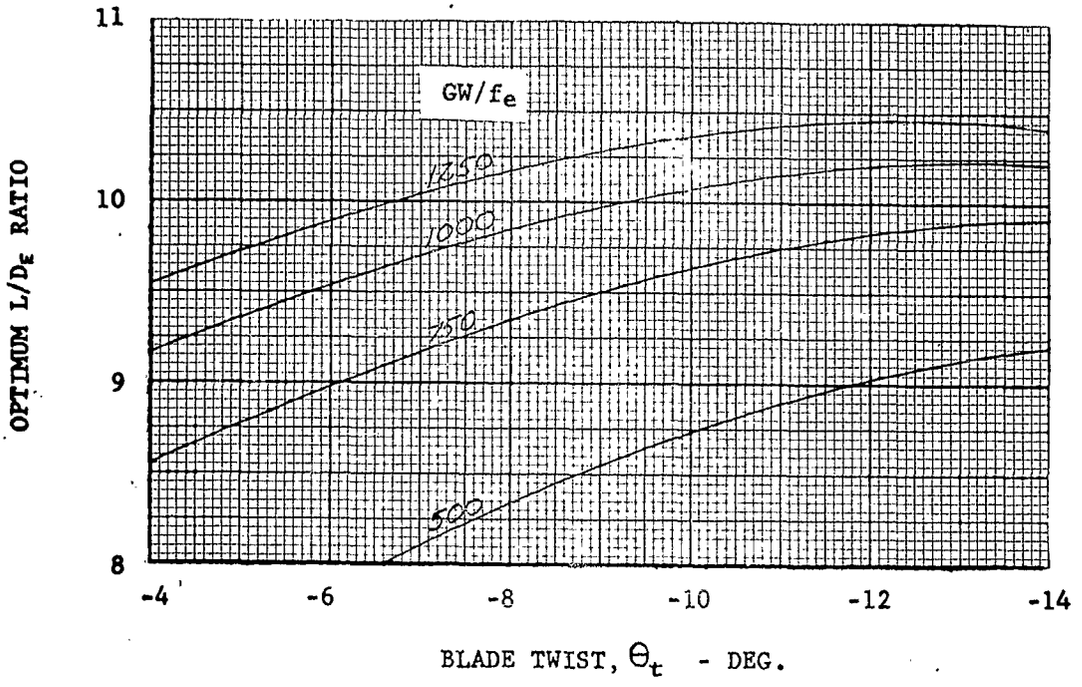


FIGURE 13

OPTIMUM L/D_E AND C_T'/σ VS TWIST

FORWARD SPEED, V = 165 KNOTS = 190 MPH

ADVANCING TIP MACH NUMBER, M_t = 0.85



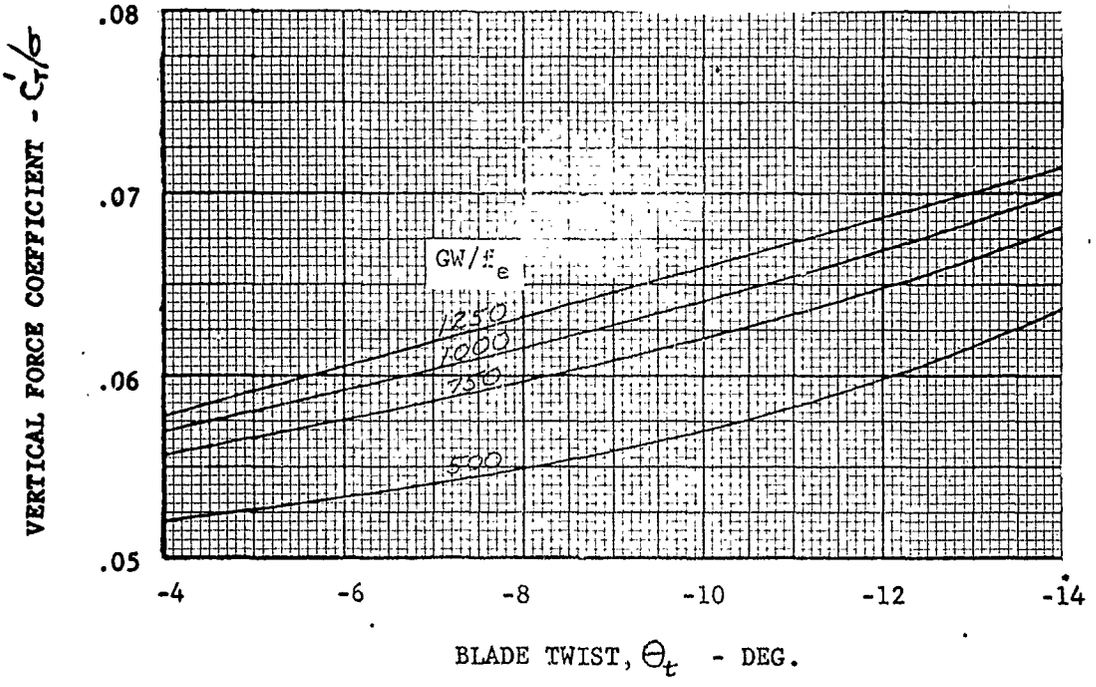
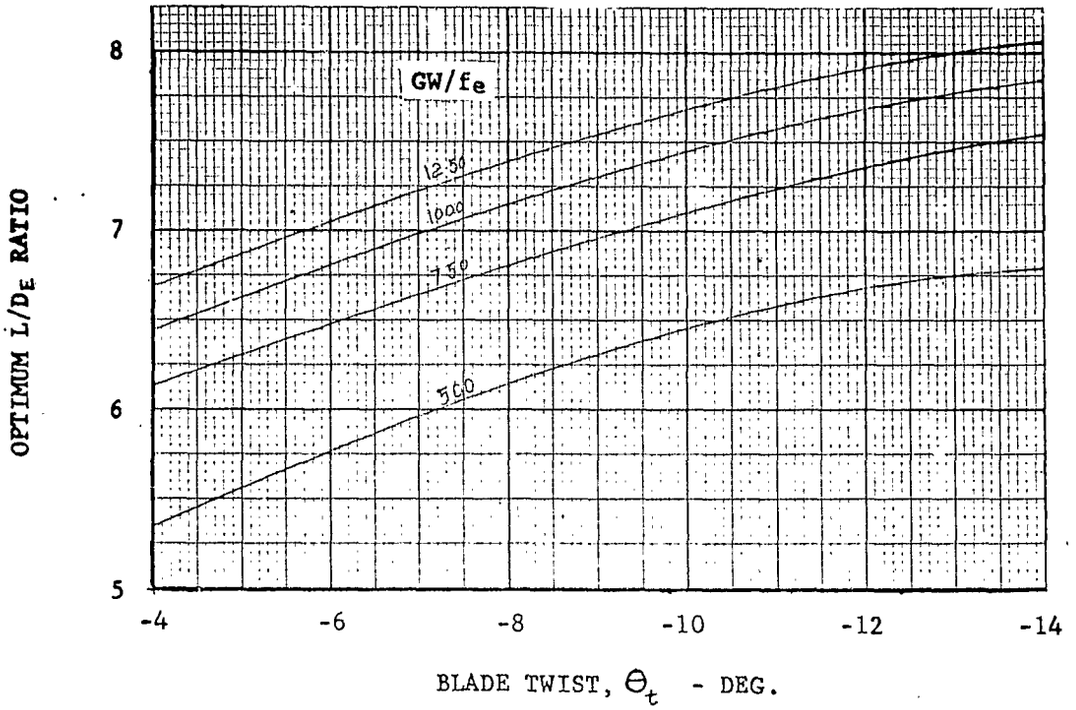


FIGURE 14

OPTIMUM L/D_E AND C_T'/σ VS TWIST

FORWARD SPEED, V = 165 KNOTS = 190 MPH

ADVANCING TIP MACH NUMBER, M_t = 0.90



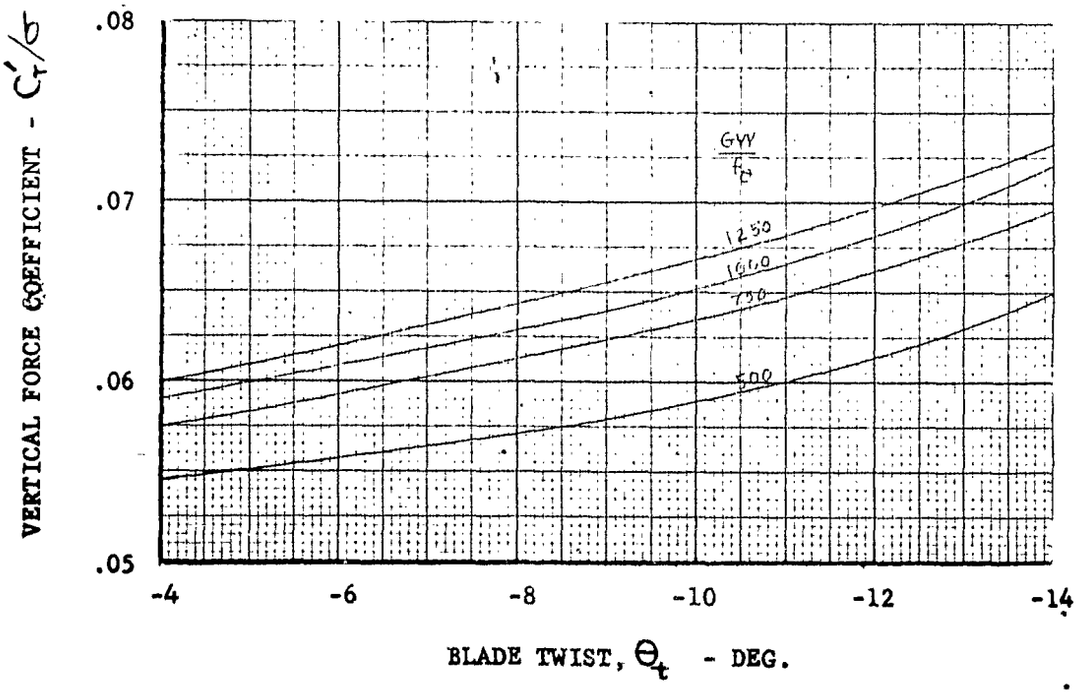
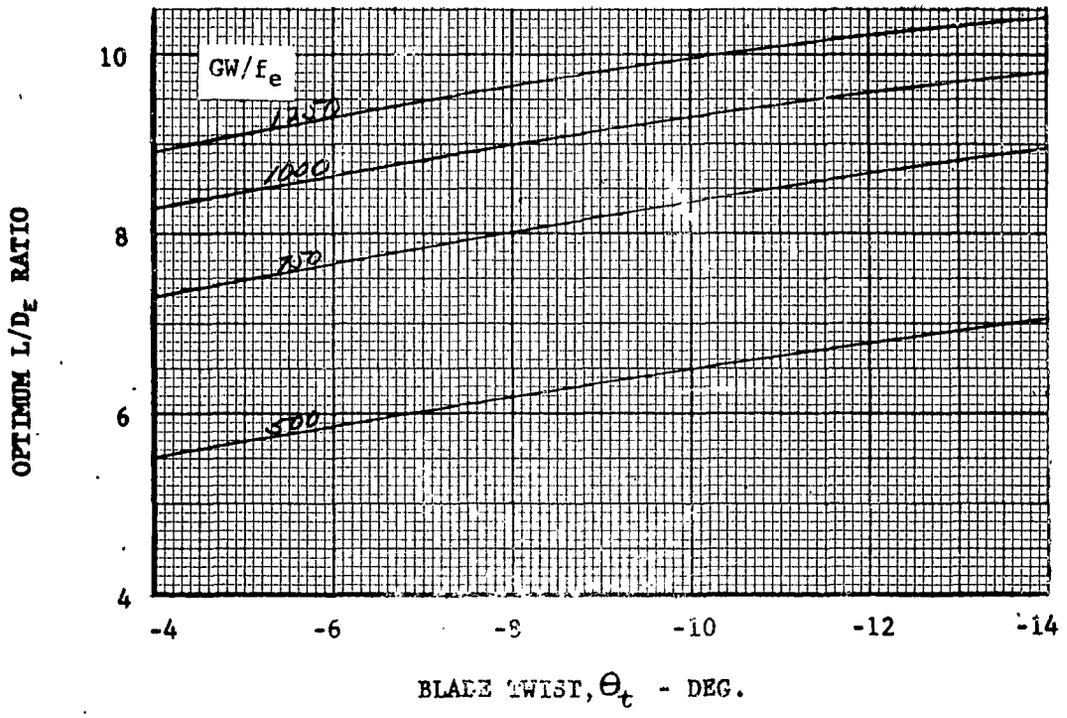


FIGURE 15

OPTIMUM L/D_e AND C_T'/σ VS TWIST

FORWARD SPEED, V = 182.3 KNOTS = 210 MPH

ADVANCING TIP MACH NUMBER, M_t = 0.80



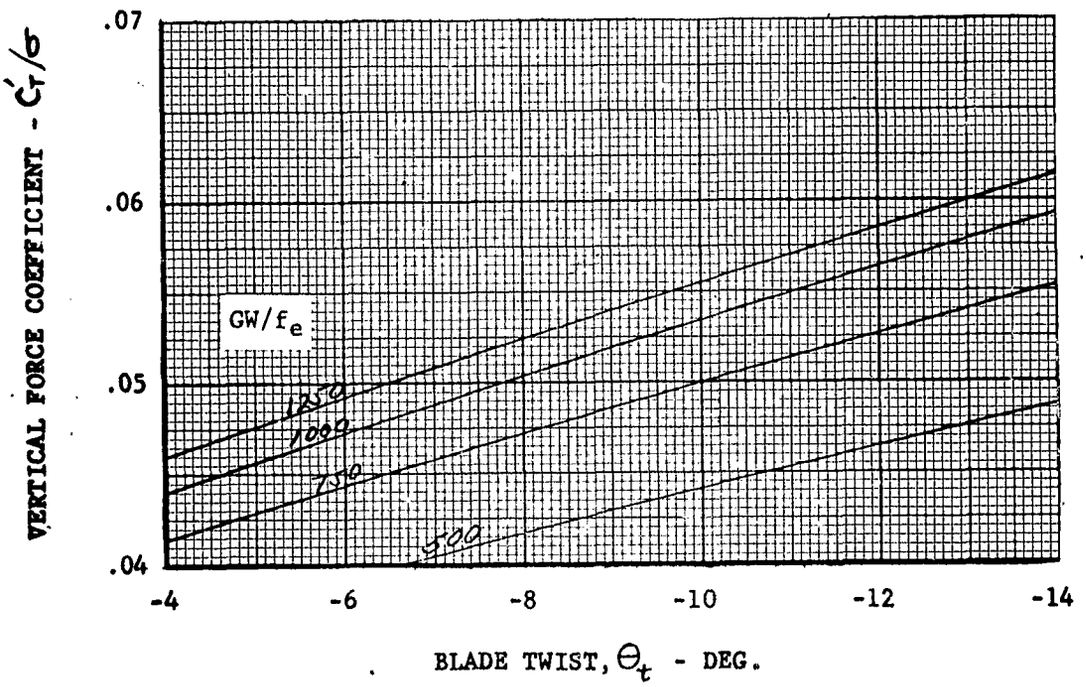
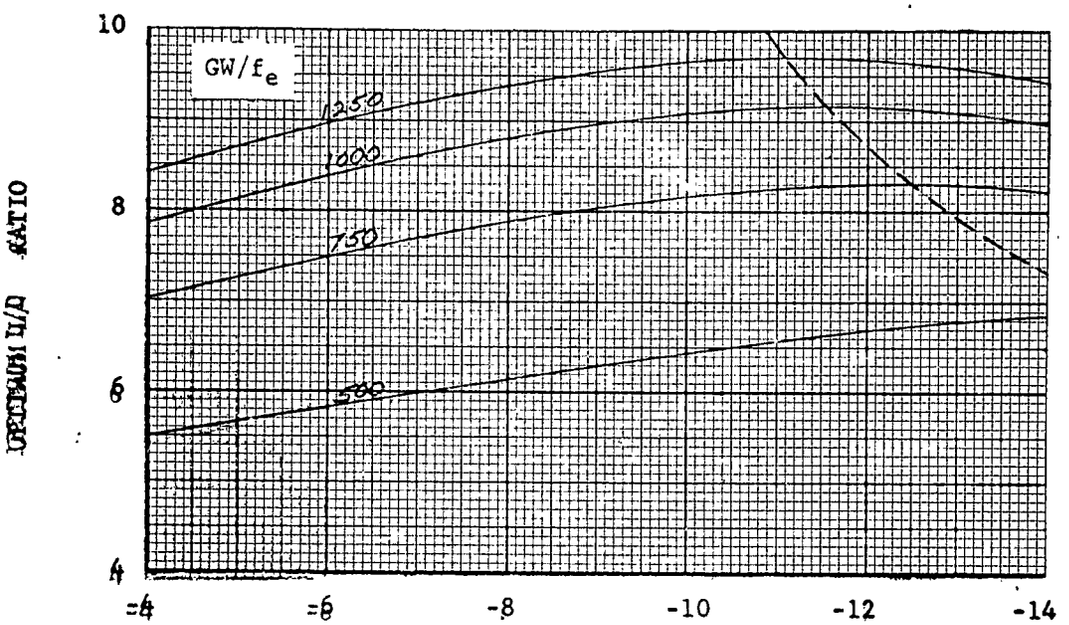


FIGURE 16

OPTIMUM L/D_E AND C_T/σ VS TWIST

FORWARD SPEED, V = 182.3 KNOTS = 210 MPH

ADVANCING TIP MACH NUMBER, M_t = 0.85



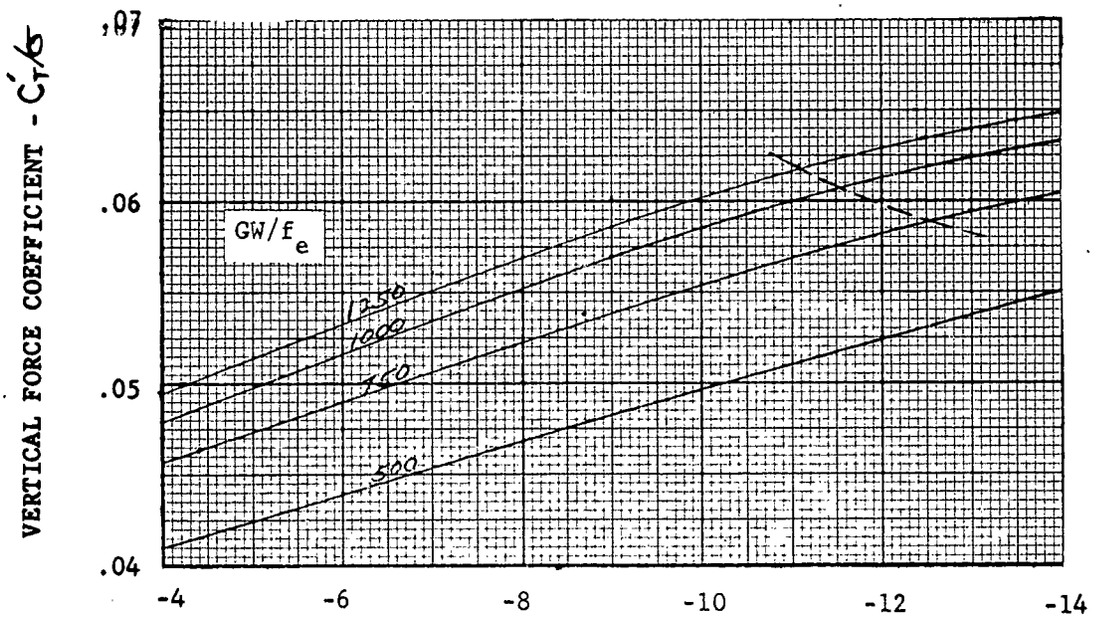
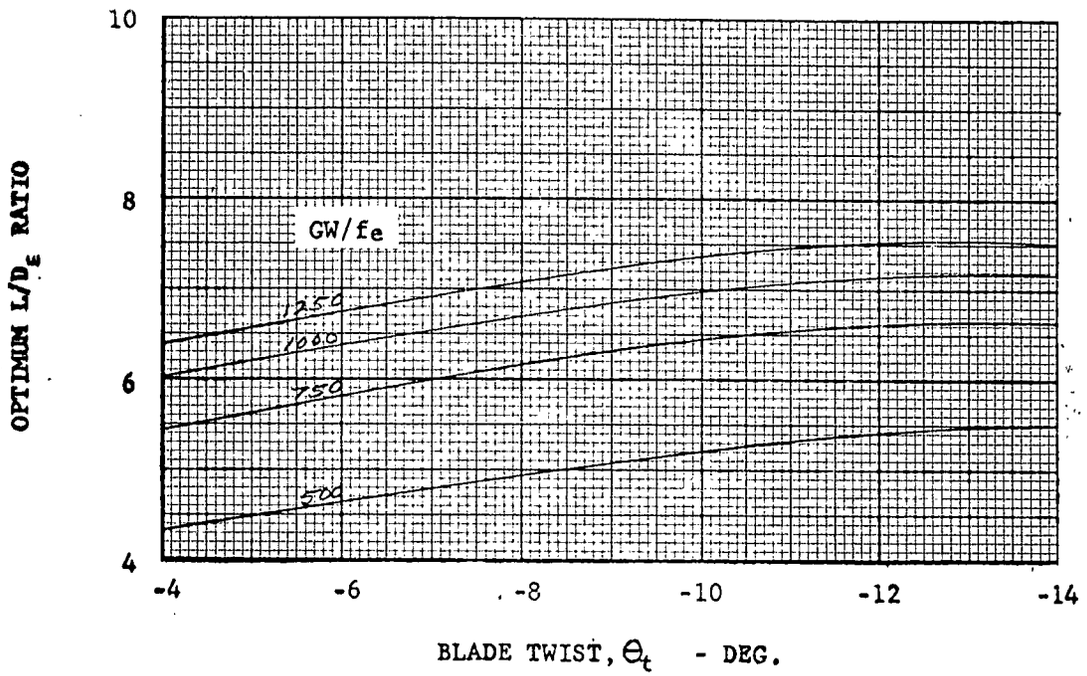


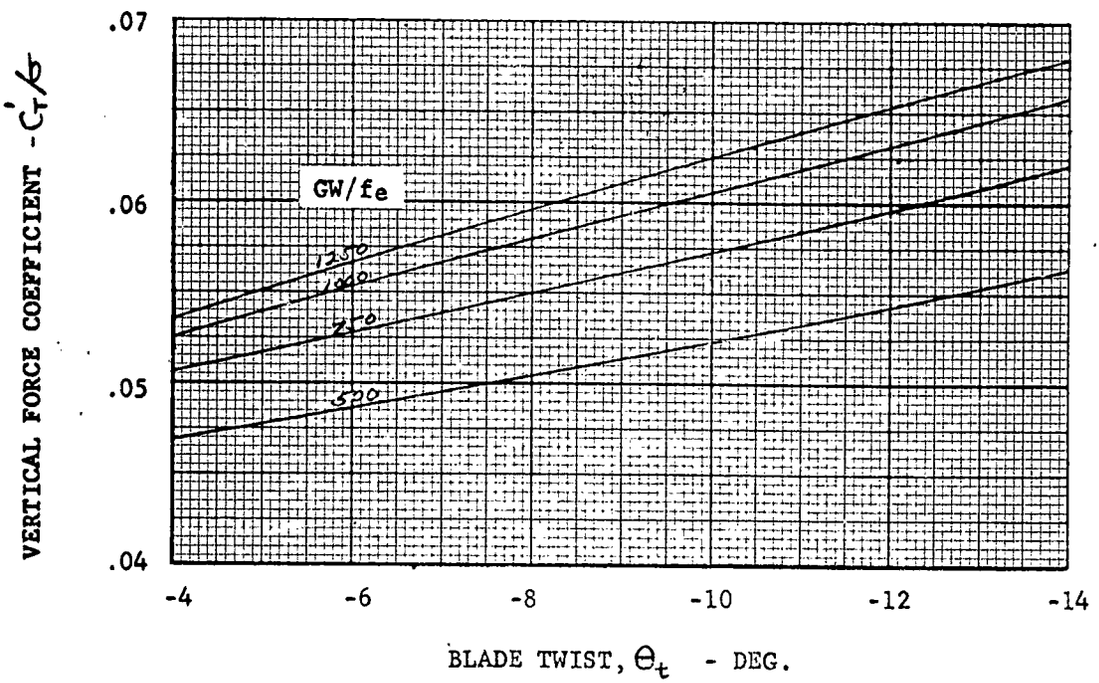
FIGURE 17

OPTIMUM L/D_e AND C_T'/σ VS TWIST

FORWARD SPEED, V = 182.3 KNOTS = 210 MPH

ADVANCING TIP MACH NUMBER, M_t = 0.90





This initial parametric study was used to establish configurations in the gross weight range of 6000 pounds to 18,000 pounds capable of carrying a minimum payload of 800 pounds at a design speed of 210 miles per hour, using normal power of installed engines. The configurations were investigated from both aerodynamic and weight points and emcompassed the variables of gross weight, blade radius, blade chord, number of blades per rotor and gross weight - equivalent flat plate area ratio.

The aerodynamic study was based upon performance characteristics of rotor blades that could be obtained through modification to blades having a good deal of design, test, and/or operational background. This selection consisted of:

1) The HUP type blade modified by practical reduction of extension of radius, but with constant chord of 13 inches.

2) The H-21 through YHC-1A blade of constant chord of 18 inches, again with practical radius modifications.

3) The YHC-1B blade of constant chord equal to 23 inches.

In this initial study, it was felt that holding total linear twist constant at -9 degrees would not substantially change the characteristic trend data. Some additional simplification was introduced by holding constant advancing tip Mach number of .85. The aerodynamic fuselage characteristics were varied through the gross weight-equivalent flat plate area ratio which ranged between 500 and 1250 pounds per square foot.

Since the modification to blade radius required to meet the design conditions was the key variable, the presentation of parametric data is in the form of gross weight versus blade radius plots at the design speed of 210 miles per hour. The nondimensional performance data at a twist of -9 degrees and advancing tip Mach number of .85 is obtained from Figure 16 and summarized below:

GW/f_e	$L/D_{E\ opt}$	C_T'/σ
500	6.3	.04775
750	8.05	.0539
1000	8.98	.0570
1250	9.52	.05855

The variation of gross weight with radius for each gross weight-equivalent flat plate area ratio is derived from its corresponding value of C_T'/σ

Since,

$$C_T'/\sigma = \frac{L}{\rho \pi R^2 V_t^2 \sigma} \qquad (3\text{-}5)$$

and, $L = \frac{GW}{2}$ (3-6) $\sigma = \frac{bc}{\pi R}$ (3-7)

The equation for gross weight becomes:

$$GW = 2 \quad C_t'/\sigma \rho \; V_t^2 \; bcR \tag{3-8}$$

This equation expresses the gross weight at which L/D_E optimum will be realized. The study was conducted for both three and four blades per rotor.

Referring to Figure 18 page 3-17, this aerodynamic relationship (Equation 3-8) is shown as the line noted AERO. Any gross weight above this line will lead to an excessive amount of blade stall while gross weights below the line are conservative.

The value of L/D_E optimum and corresponding value of GW/f_e along with the available power may be used to determine the maximum gross weight potential for each configuration.

Since

$$L/D_E = \frac{L}{-X + P/V} \tag{3-9}$$

the expression for rotor horsepower required is

$$RHP = \frac{LV}{550} \left(\frac{1}{L/D_E} + \frac{X}{L} \right) \tag{3-10}$$

But X/L is the propulsive force ratio and must equal the drag to gross weight ratio of the aircraft; hence,

$$X/L = \frac{\frac{1}{2} \rho V^2 f_e}{GW} \tag{3-11}$$

Thus rotor horsepower required becomes

$$RHP_{Req'd} = \frac{GW\ V}{500} \left(\frac{1}{L/D_E} + \frac{1}{2} \rho \frac{V^2 f_e}{GW} \right) \tag{3-12}$$

The T-58-GE-8 turbo shaft engine was chosen for power available having 1050 SHP at sea level normal rated power as noted in Reference 5. Values of over-all transmission efficiency and accessory horsepower are noted on the next page.

No. of Engines	Type	Transmission Efficiency	Accessory Horsepower
(1)	T58-GE-8	$\eta_t = .955$	$HP_{acc} = 20$
(2)	T58-GE-8	$\eta_t = .945$	$HP_{acc} = 30$

Thus the shaft horsepower required becomes

$$SHP_{Req'd} = \frac{RHP_{Req'd}}{\eta_t} + HP_{acc} \qquad (3\text{-}13)$$

The maximum gross weight for each configuration is obtained by equating SHP required to SHP available and may be expressed as:

$$GW_{max} = \frac{550\,\eta_t\,(SHP_{avail} - HP_{acc})}{V\left[\frac{1}{L/D_E} + \frac{1}{2}\,\rho\,V^2\,(f_e/GW)\right]} \qquad (3\text{-}14)$$

Referring again to Figure 18, this maximum gross weight is shown as the line noted NRP ( ) T-58-8.

To establish the line noted WEIGHTS on Figure 18, the basic weight empty as predicted by Vertol Division weight trend data and the gross weight variation with radius as determined by aerodynamics (line noted AERO) was obtained. To this was added:

1) 1-1/2 hours of fuel consumption at NRP of the T-58-8
2) 2 minutes of warm up at NRP
3) 10 percent reserve fuel
4) 800 pounds of payload

Thus, the WEIGHT line represents the variation of gross weight that will meet the high speed design mission. Any gross weight below this line will include a payload less than 800 pounds.

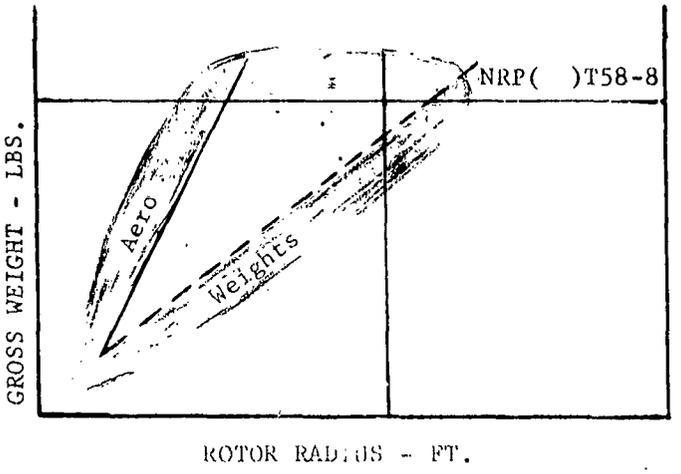
The aerodynamic and weight limitations defining a configuration may be summarized as:

1) A line noted AERO along which optimum L/D_E is realized.
2) A line noted NRP ( ) T-58-8 which defines the maximum gross weight that may be flown with this power available at the optimum L/D_E and design conditions.
3) A line noted WEIGHTS which defines the minimum gross weight to do the mission.
4) A vertical line noted by aircraft designation defining the present design radius with the particular chord.

Thus, the parametric study in graphical form becomes:

FIGURE 18

GRAPHICAL FORM OF CONFIGURATION STUDY SOLUTION



and the practical configuration falls within the unshaded triangle. The optimum configuration lies at the intersection of the AERO and NRP ( ) T-58-8, provided the radius modification is practical.

No configurations having a $GW/f_e = 500$ were practical.

Figures 19 through 29 illustrate the results of this parametric study to define configurations in the gross weight range of 6000 to 18,000 pounds, all of which meet the design requirement of at least 200 mile per hour speed with an 800 pound payload.

Table I below summarizes the practical configurations, derived from this investigation, which appeared worthy of further study.

TABLE I

RESULTS OF PARAMETRIC STUDY

Config.	GW/f_e	Blade Type	No. of Engines	No. of Blades	Radius Ft.	Gross Weight	Payload
A	750	YHC-1B	2	3	21.1	12,750	900
B	750	107	2	4	20.2	12,750	1000
C	1000	107	1	3	16.0	8,000	920
D	1000	HUP	1	4	16.7	8,000	870
E	1000	YHC-1B	2	3	24.4	15,600	2675
F	1000	107	2	4	23.3	15,600	2700
G	1250	107	1	3	17.1	9,200	1800
H	1250	HUP	1	4	17.9	9,200	2000
I	1250	YHC-1B	2	3	25.9	17,850	4200
J	1250	107	2	4	24.7	17,850	4300

This table illustrates a requirement for GW/f_e ratios approaching 1000 to obtain other than a marginal aircraft. To avoid the development of an entirely new fuselage (consistent with the requirement to "emphasize the use of existing components"), a radius consistent with presently available types (possibly HUP or Vertol 107) would be the most advantageous. Similarly the use of a three-bladed rotor system would be more feasible than the development of a four-bladed system. Configurations C and E appeared the most practical for further study under the above assumptions.

Because it was considered desirable to demonstrate the required high performance capability with an existing operational Army production type helicopter, in order to avoid development cost of a single purpose research aircraft, recommendations were made to discontinue further parametric investigation and proceed immediately to the preliminary design phase of the Vertol 107 equipped with cut-down Chinook blades. The YHC-1B was not considered in the parametric study since there were no larger chord blades available.

FIGURE 19

GROSS WEIGHT VS ROTOR BLADE RADIUS

NUMBER OF BLADES = 3

GW/f_e = 750

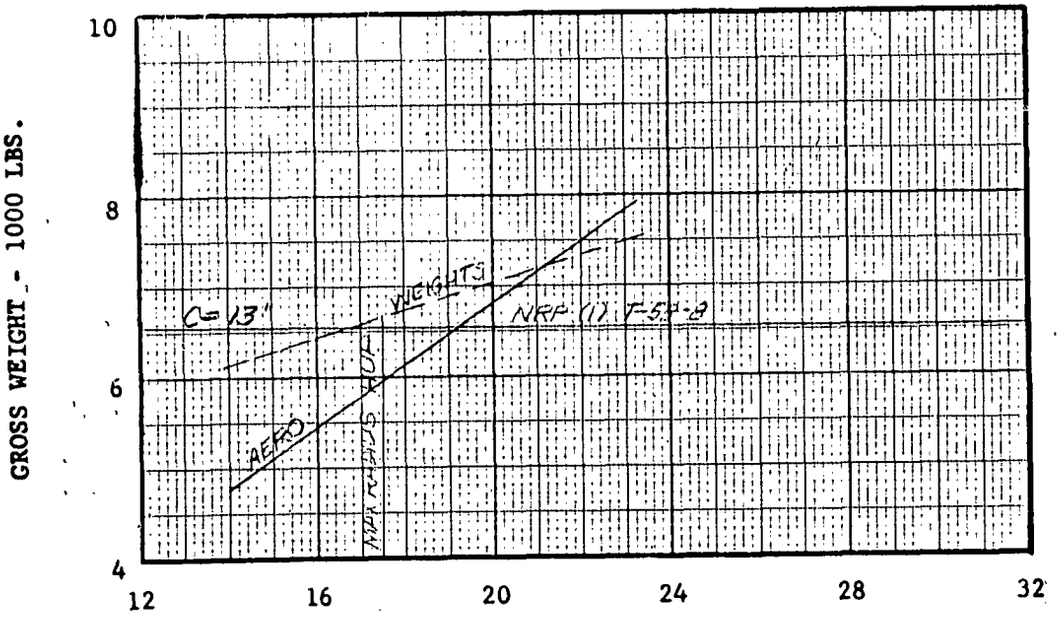


FIGURE 20

GROSS WEIGHT VS ROTOR BLADE RADIUS

NUMBER OF BLADES = 3

GW/f_e = 750

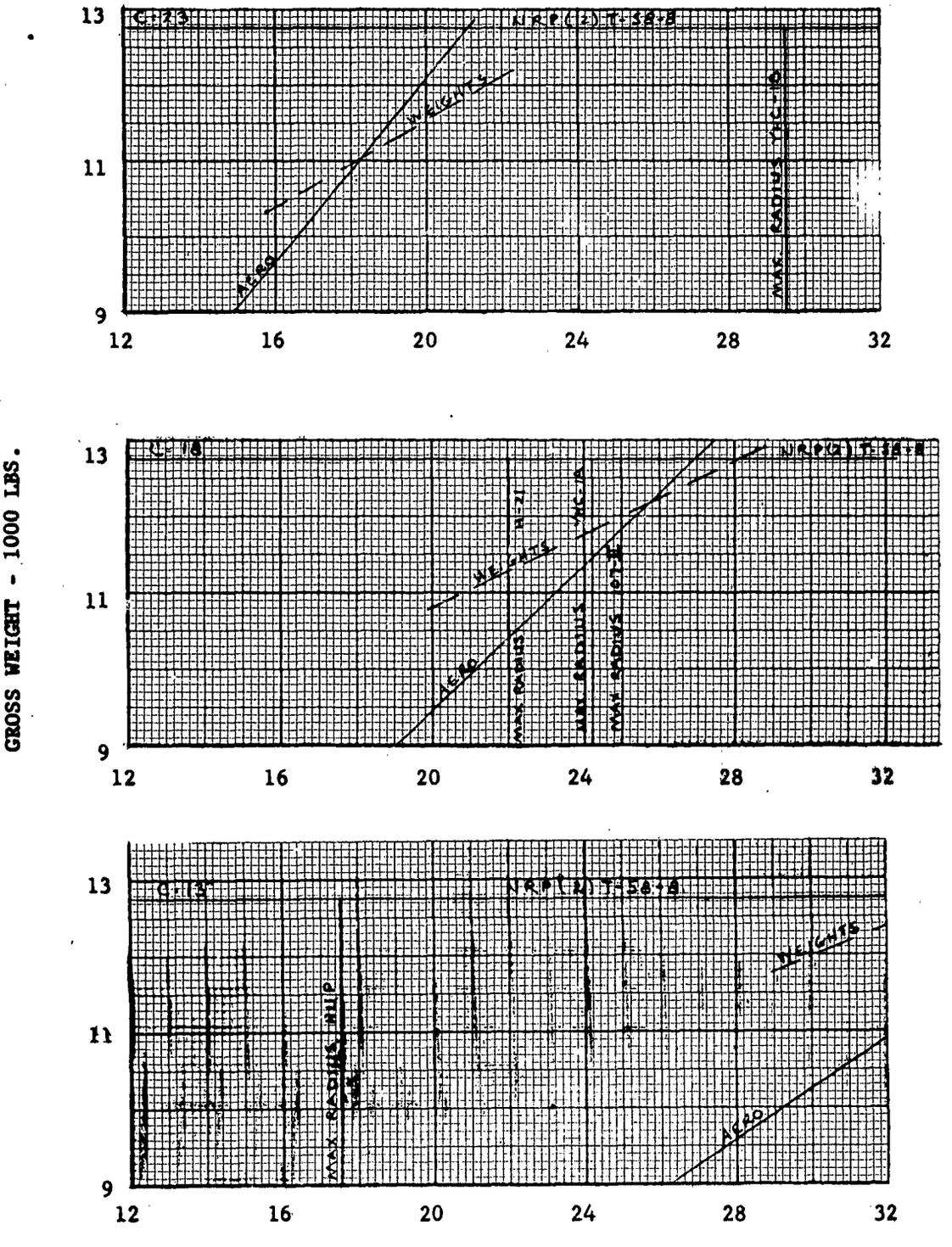


FIGURE 21

GROSS WEIGHT VS ROTOR BLADE RADIUS

NUMBER OF BLADES = 4

GW/f_e = 750

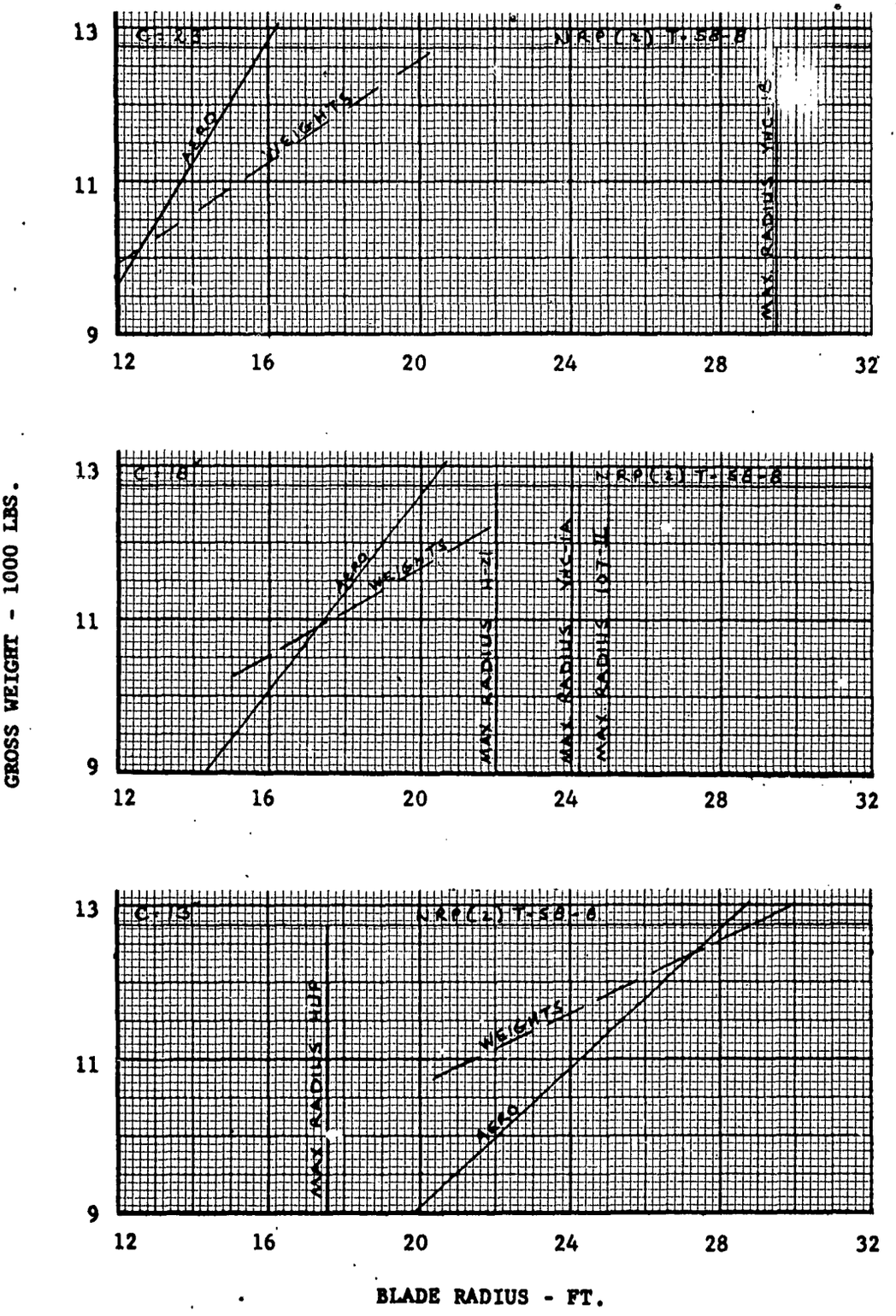


FIGURE 22

GROSS WEIGHT VS ROTOR BLADE RADIUS

GW/f_e = 1000

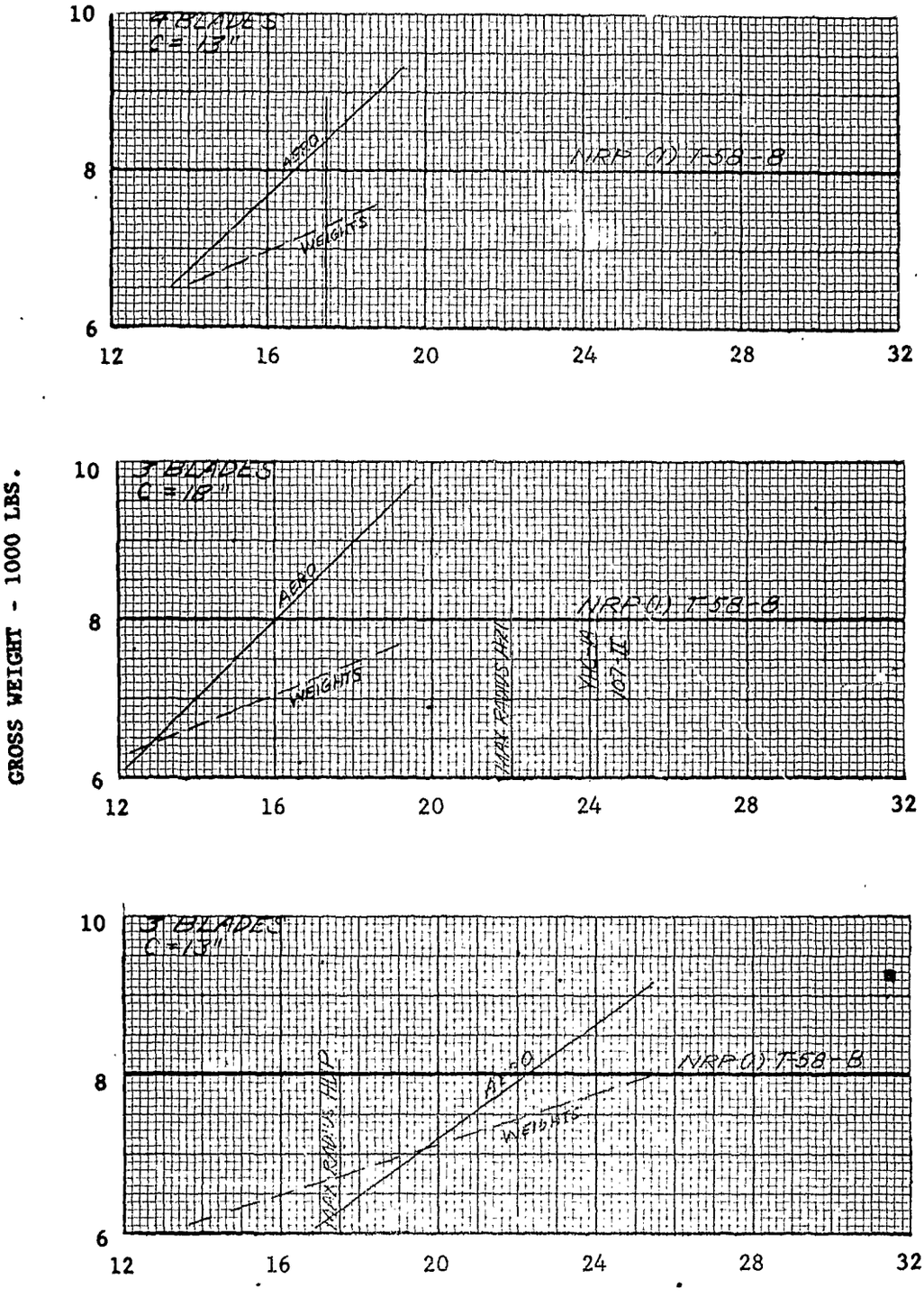


FIGURE 23

GROSS WEIGHT VS ROTOR BLADE RADIUS

NUMBER OF BLADES = 3

GW/f_e = 1000

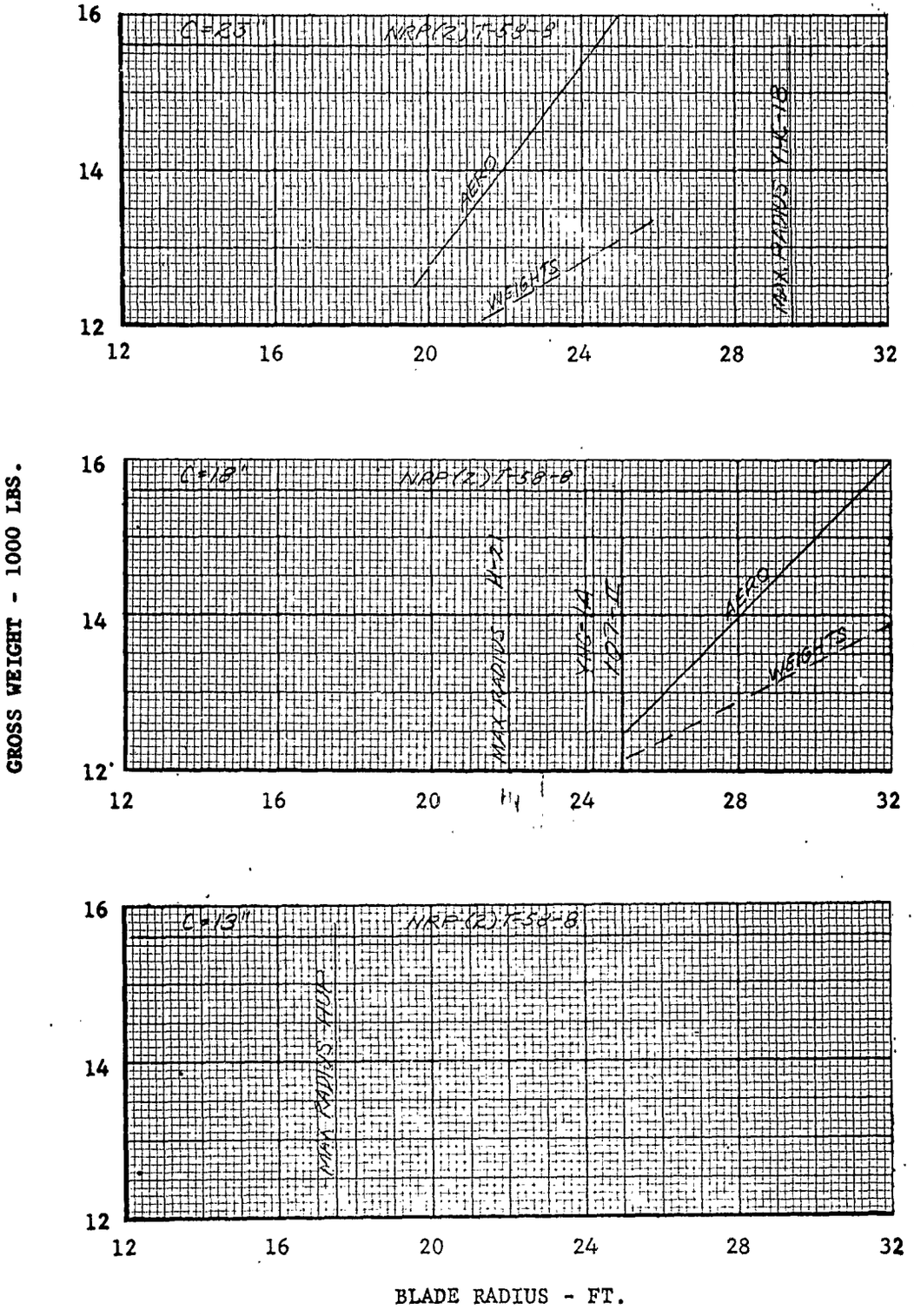


FIGURE 24

GROSS WEIGHT VS ROTOR BLADE RADIUS

NUMBER OF BLADES = 4

GW/f_e = 1000

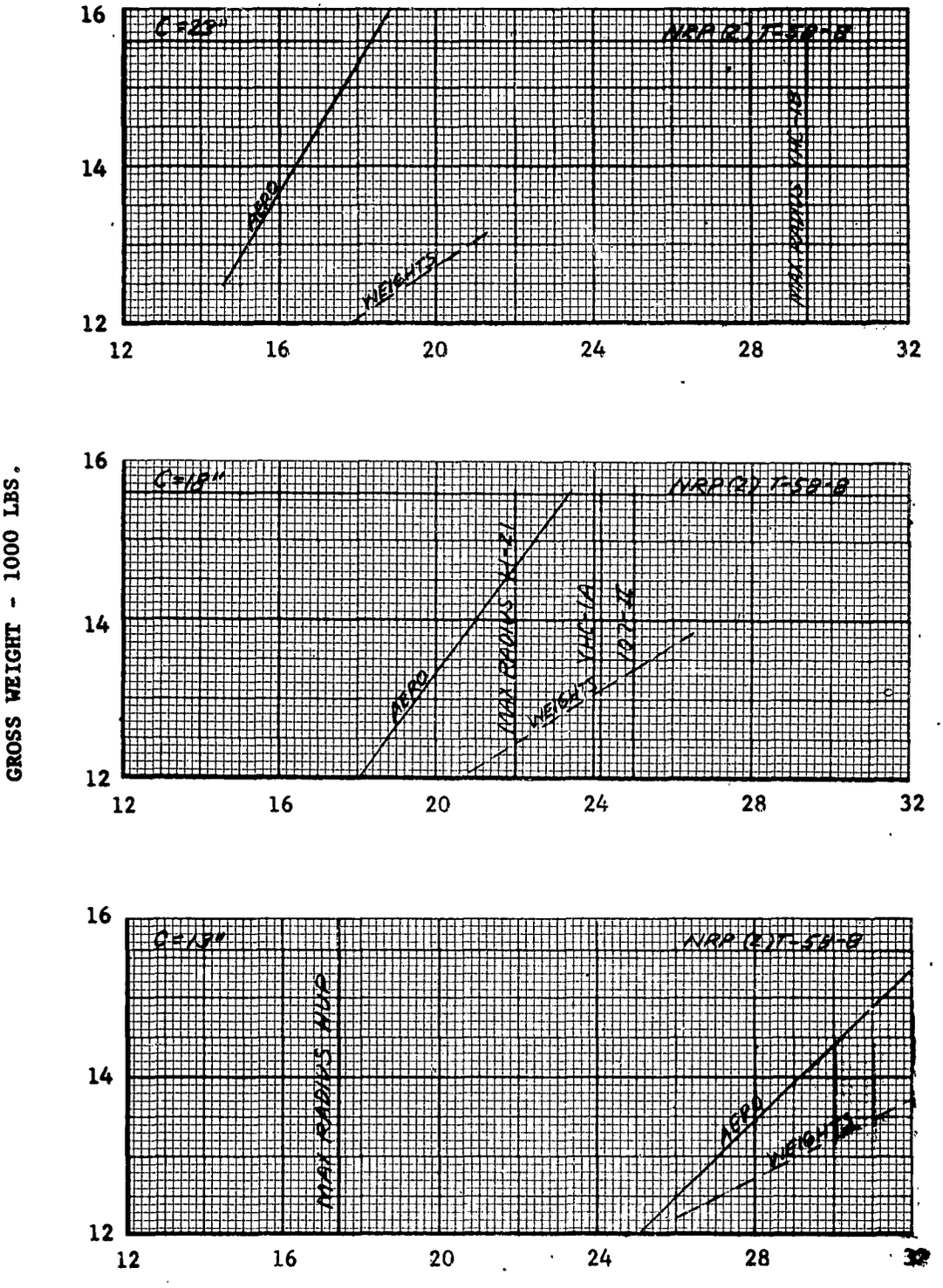


FIGURE 25

GROSS WEIGHT VS ROTOR BLADE RADIUS

NUMBER OF BLADES = 3

GW/f_e = 1250

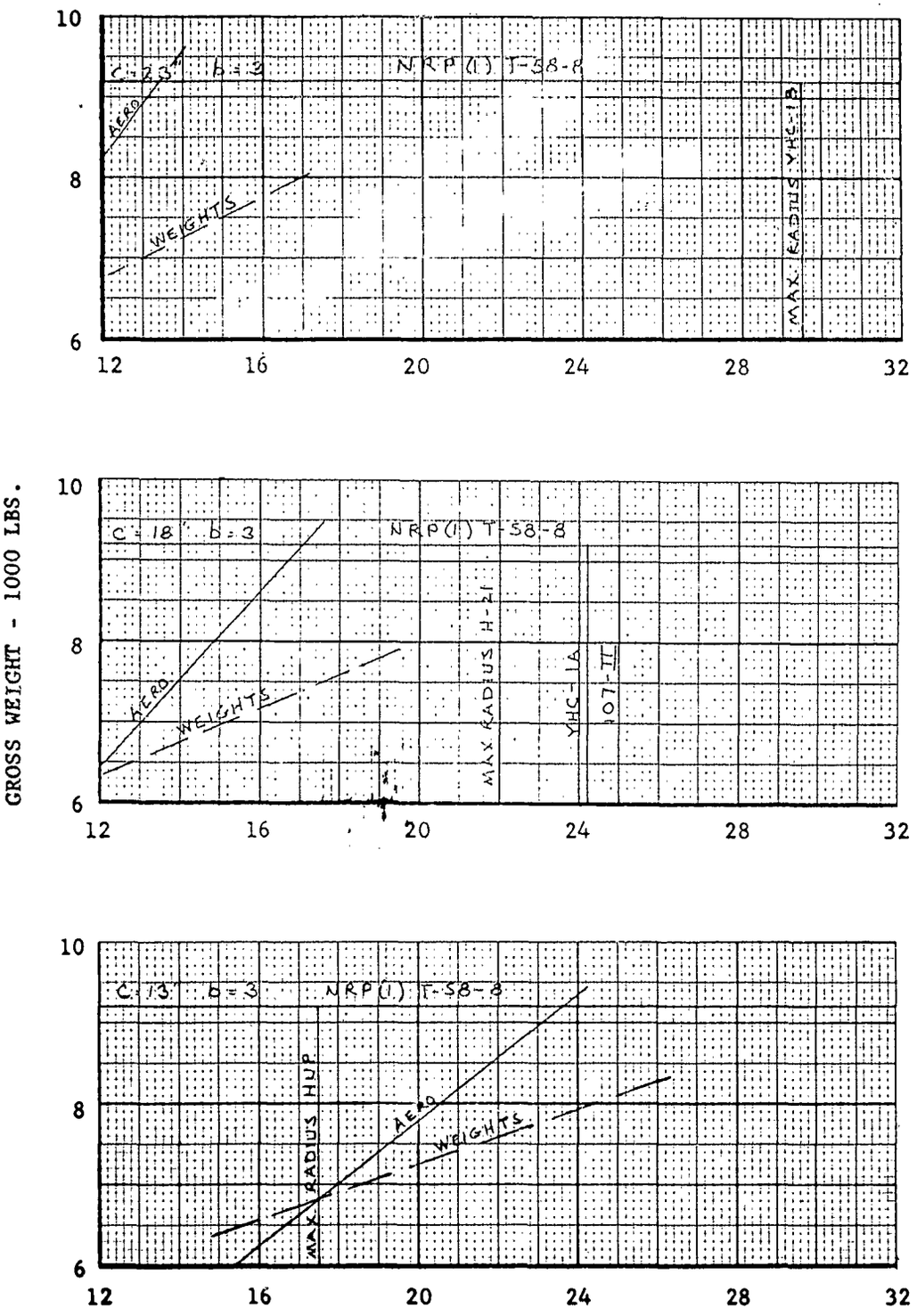


FIGURE 26

GROSS WEIGHT VS ROTOR BLADE RADIUS

NUMBER OF BLADES = 4

GW/f_e = 1250

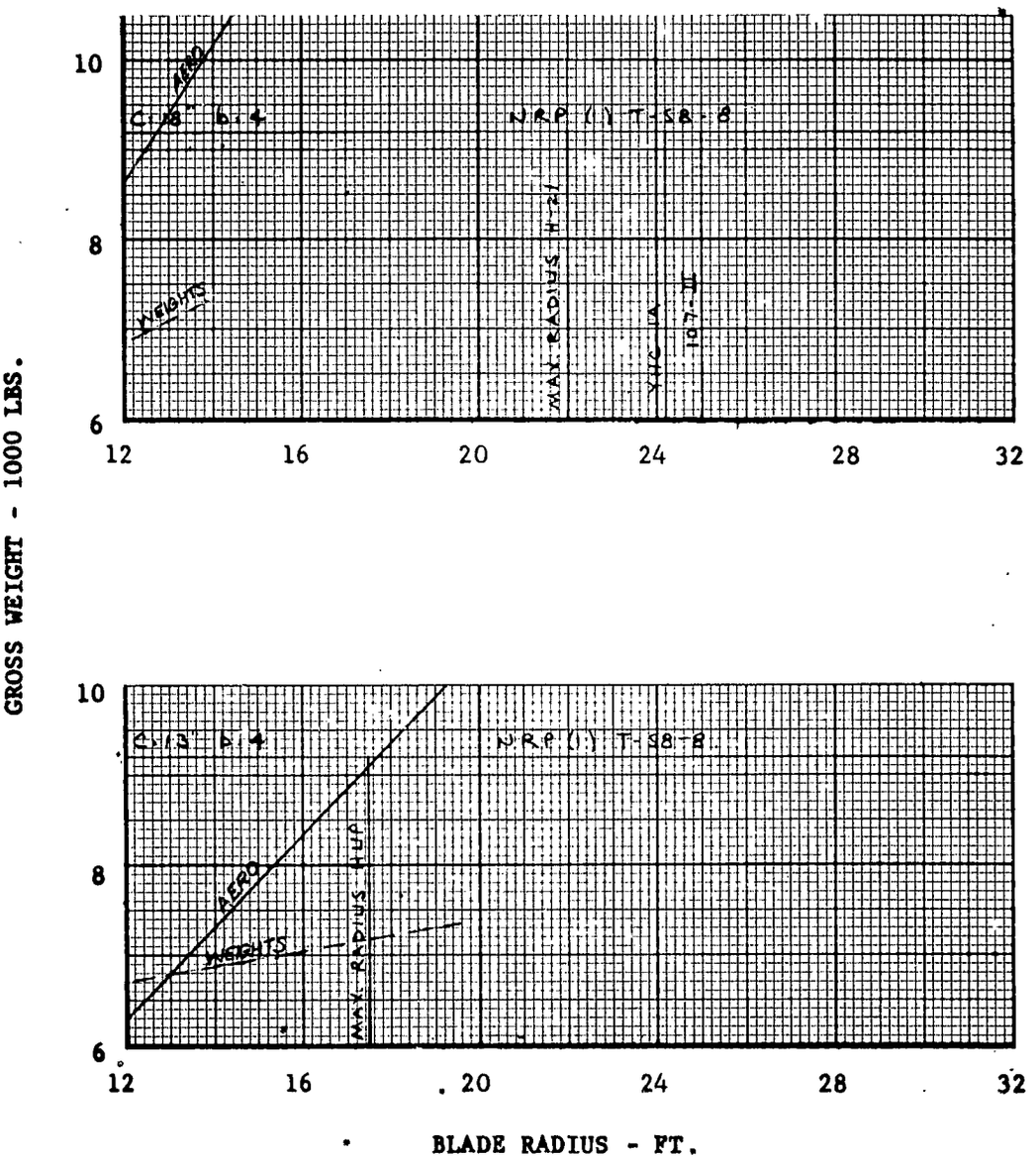


FIGURE 27

GROSS WEIGHT VS ROTOR BLADE RADIUS

NUMBER OF BLADES = 3

GW/f_e = 1250

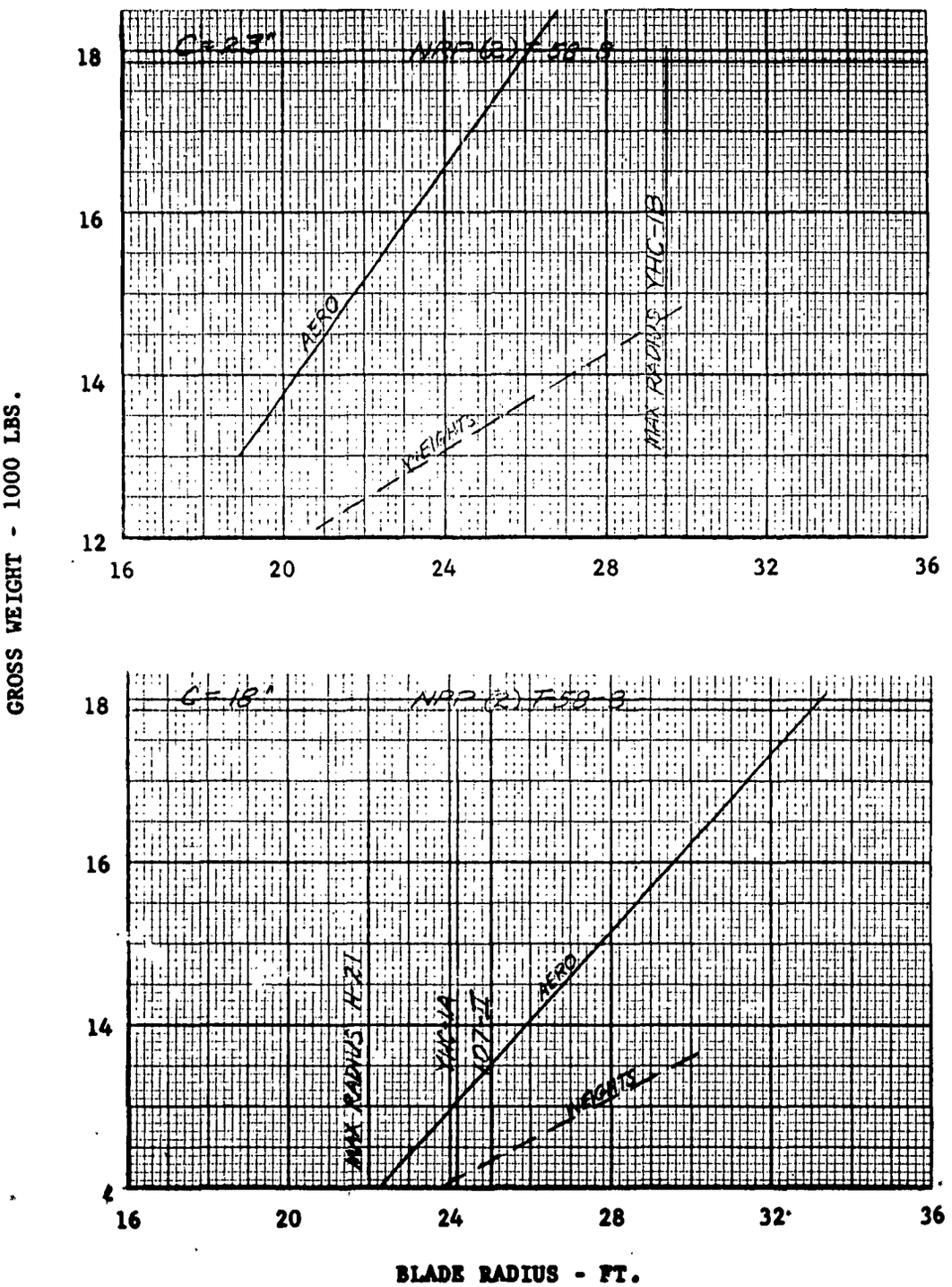


FIGURE 28

GROSS WEIGHT VS ROTOR BLADE RADIUS

NUMBER OF BLADES = 4

GW/f_e = 1250

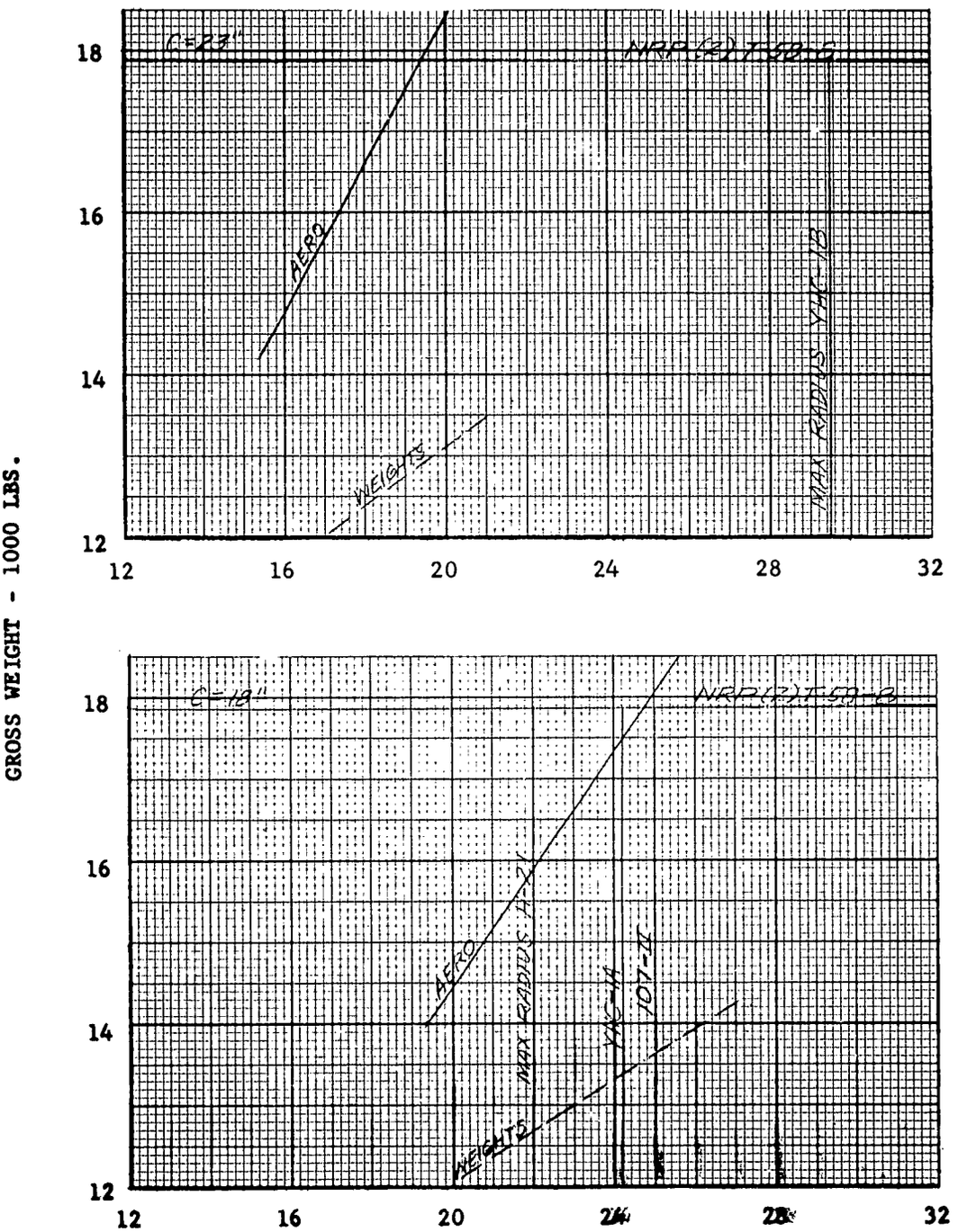
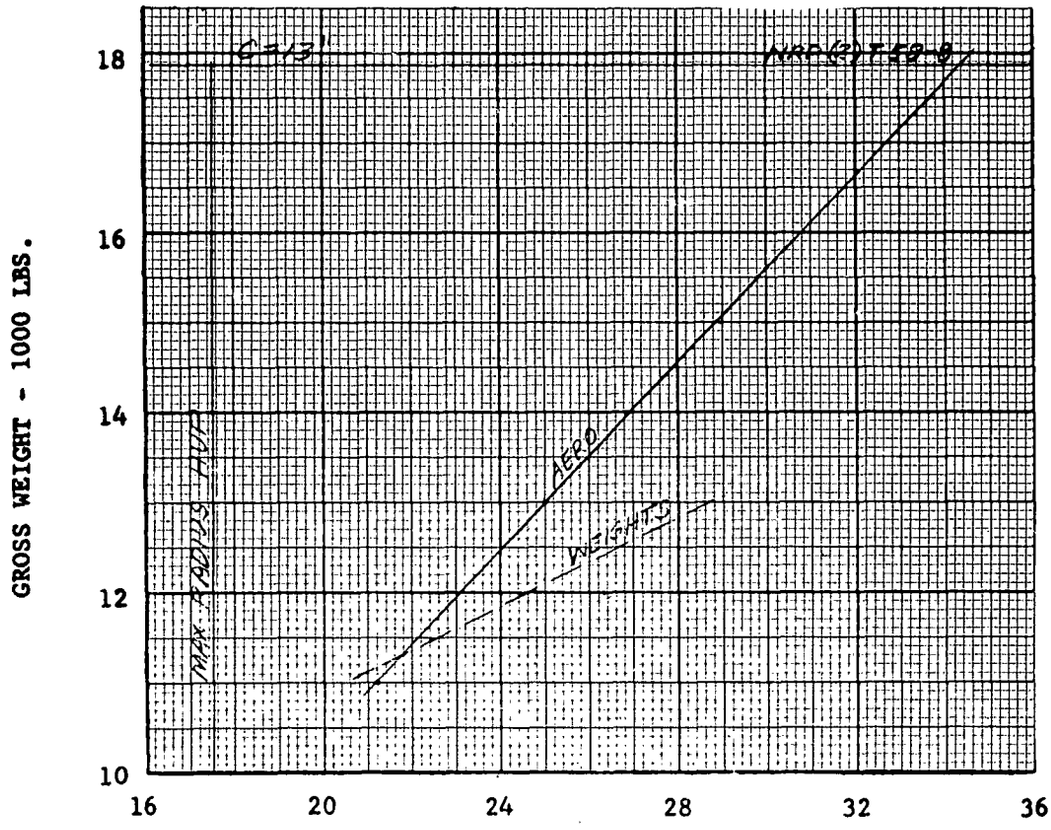


FIGURE 29

GROSS WEIGHT VS ROTOR BLADE RADIUS

NUMBER OF BLADES = 4

GW/f_e = 1250



Detailed Study of Rotor Parameters for the High Performance 107-II

The Vertol 107 is a desirable aircraft for the high performance helicopter not only for reasons of mission versatility, but also for production economy. The magnitude of versatility becomes apparent when consideration is given to payload capabilities, cargo space, and cleanliness of basic design. The fuselage drag characteristics are of prime concern. The present flat plate area of the 107 is approximately 30 square feet. It has been conservatively estimated that a general drag clean-up can produce an equivalent area of less than 20 feet. This will be accomplished by fairing the rotor hub assemblies, fuselage fairing and streamlining, and landing gear retraction.

A preliminary study has been made to determine the control system requirements which include the requirements for longitudinal stick, longitudinal DCP speed trim for forward speed and C.G. variation, cyclic speed trim, lateral-directional control, collective pitch control, directional control, and SAS requirements.

The rotor study was divided into two general parts. The first portion was an evaluation of modified production rotors with the normal linear twist resulting from blade radius variance. The second part assumed the same blades, but with constant linear twist of -14 degrees. An intermediate chord of 20.5 inches was included.

Using the performance charts presented on Figures 6 through 17, power required plots for an aircraft drag of 20 square feet were obtained. These power plots were presented in terms of shaft horsepower required versus gross weight, at various speeds and advancing tip Mach number. By using the fixed values for NRP and MRP for the T-58-8 engine, the plots of gross weight versus velocity were obtained. These curves are presented on Figures 31 through 45. The blades considered for these studies are listed as:

TABLE II

Rotor Parameters for High Performance 107-II Study

Part I			Part II		
R	C	θ_t	R	C	θ_t
25 feet	18 inches	-8.33 degrees	25 feet	18 inches	-14 degrees
27 feet	18 inches	-9.00 degrees	27 feet	18 inches	-14 degrees
29 feet	18 inches	-9.67 degrees	29 feet	18 inches	-14 degrees
25 feet	23 inches	-7.63 degrees	25 feet	20.5 inches	-14 degrees
27 feet	23 inches	-8.23 degrees	27 feet	20.5 inches	-14 degrees
29 feet	23 inches	-8.85 degrees	29 feet	20.5 inches	-14 degrees
			25 feet	23 inches	-14 degrees
			27 feet	23 inches	-14 degrees
			29 feet	23 inches	-14 degrees

The basic weight empty has been derived from the weight study for the Utility Version of the Vertol Model 107 with a design horsepower of 2500 horsepower. Weight trend data was used to reflect changes in rotor radius and afterbody fairing, general drag clean-up, and retractable gear. Fuel weight was based on full internal tanks (2280 pounds) which results in approximately 1-1/2 hours endurance at NRP of two T-58-GE-8 engines.

Detailed summary curves of the rotor sizing study for the High Performance 107 is presented below. Over-all, roughly the same performance trades are obtained from chord, radius, or twist. The reduced radius YHC-1B blade of chord 23", -18.3 min./ft. of twist, and 25 foot radius meets the performance requirements; the improvement in payload through increased twist is outstanding.

FIGURE 30

SUMMARY CURVES OF HIGH PERFORMANCE 107-II ROTOR SIZING STUDY - PAYLOAD VS. ROTOR RADIUS

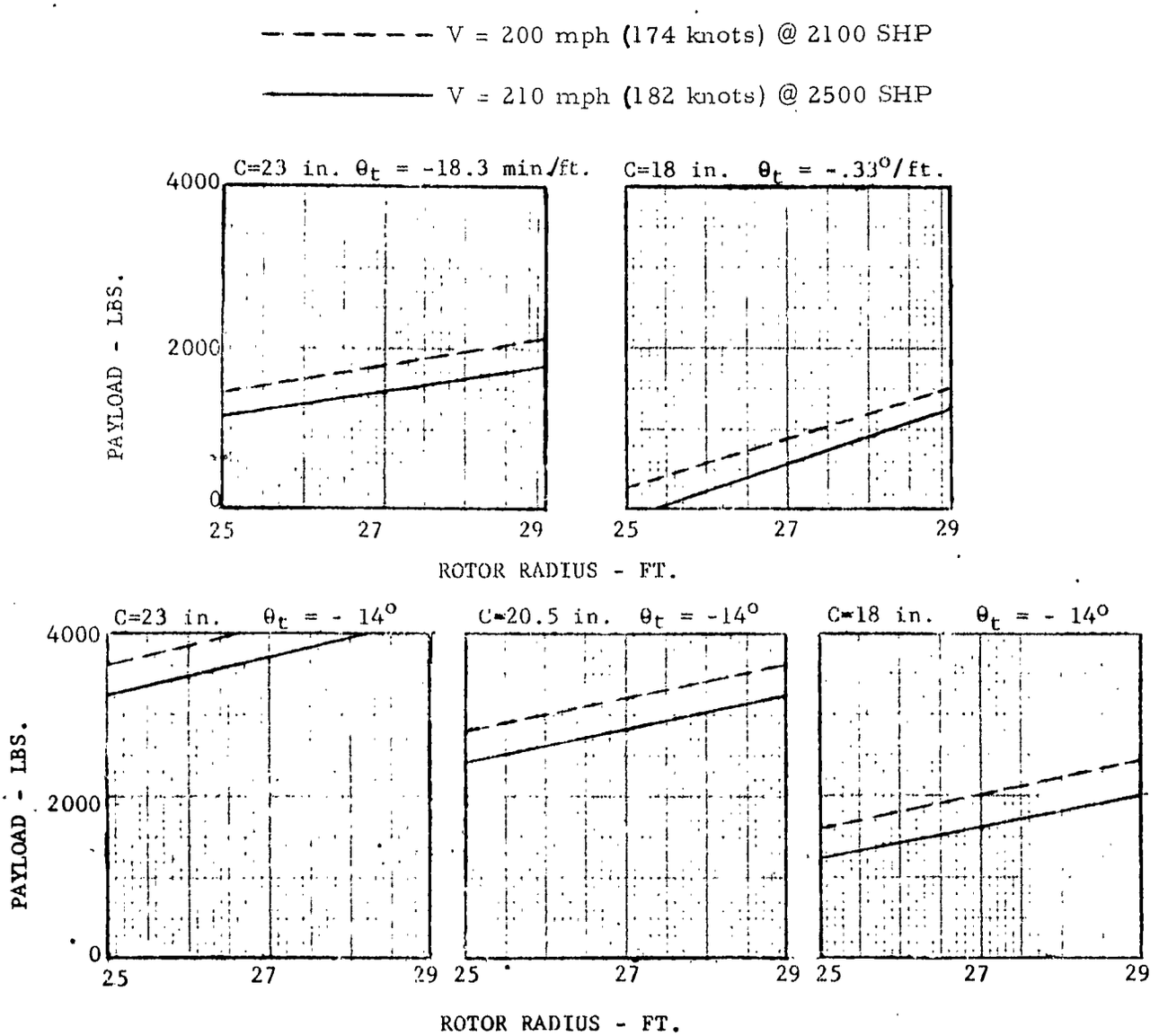


FIGURE 31

GROSS WEIGHT AND PAYLOAD VS. FORWARD SPEED

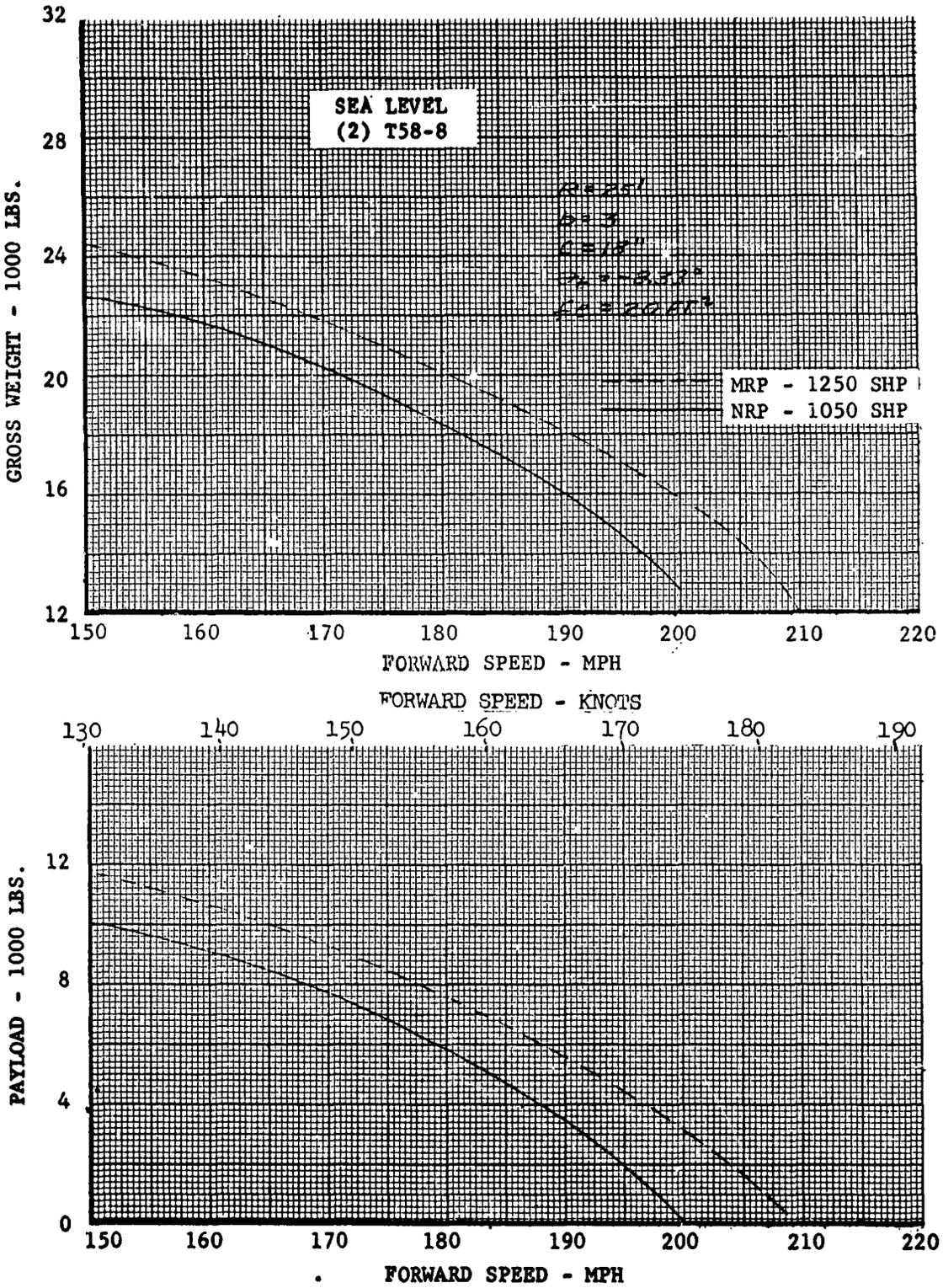


FIGURE 32

GROSS WEIGHT AND PAYLOAD VS. FORWARD SPEED

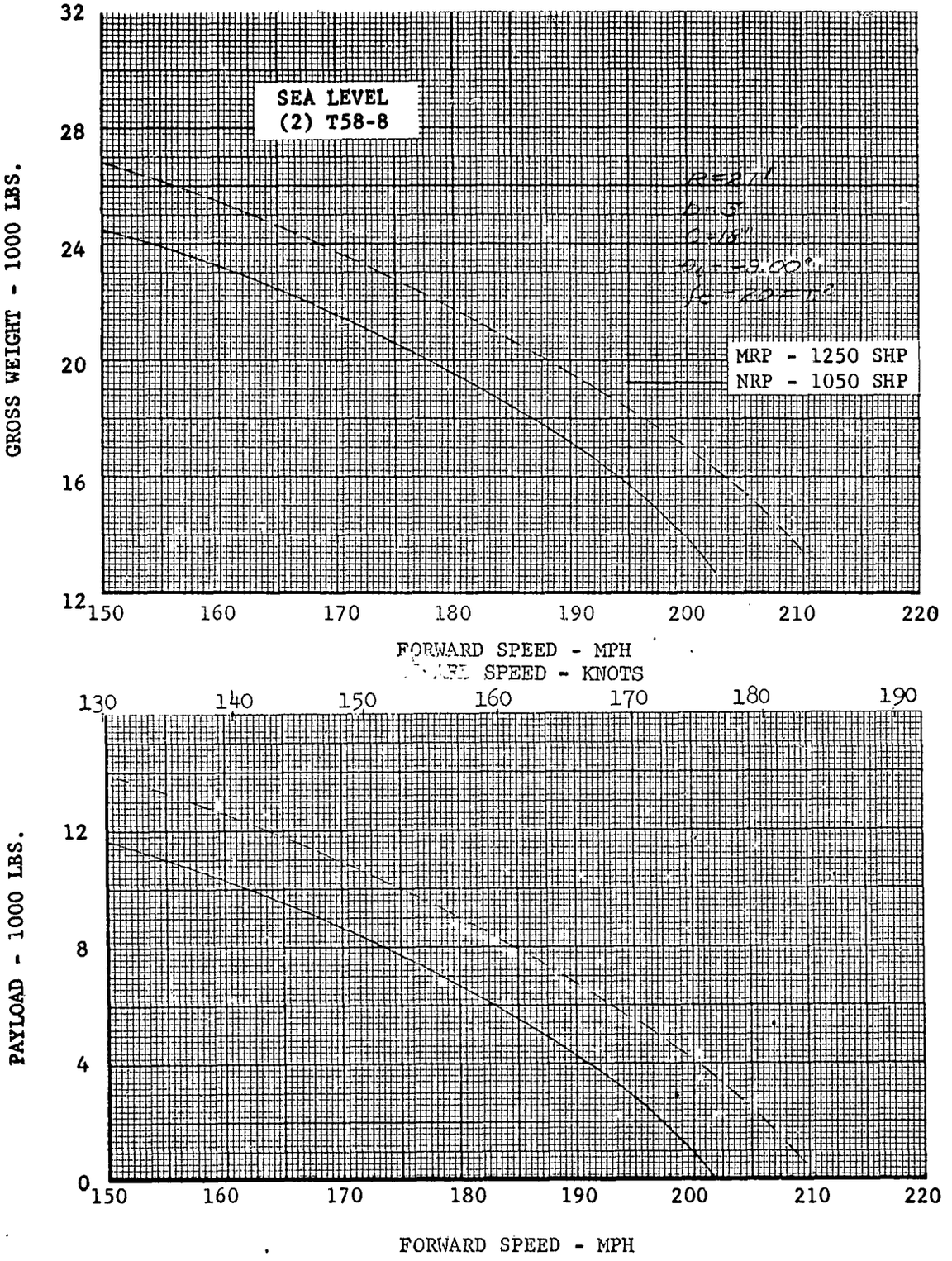


FIGURE 33

GROSS WEIGHT AND PAYLOAD VS. FORWARD SPEED

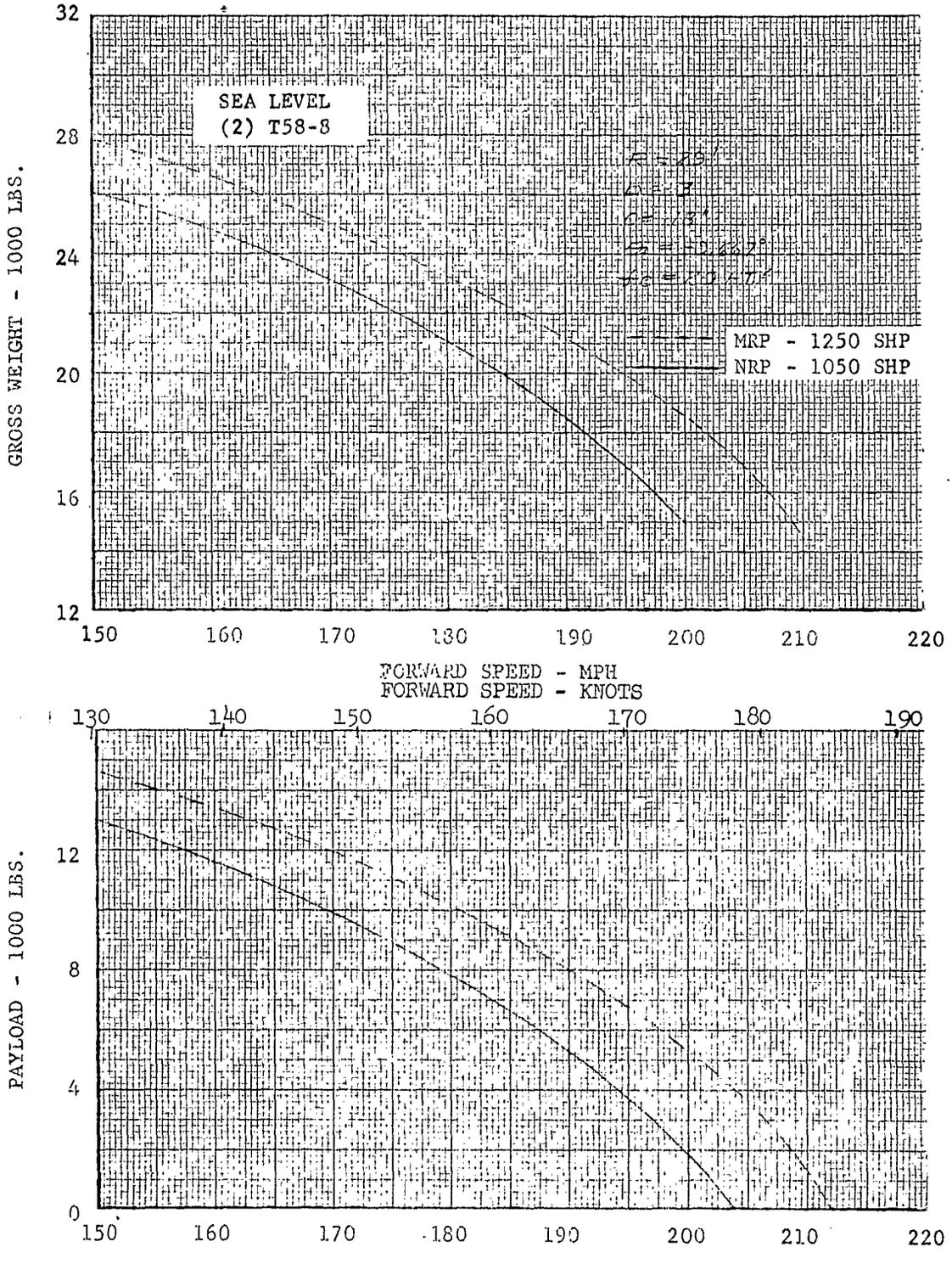


FIGURE 34

GROSS WEIGHT AND PAYLOAD VS. FORWARD SPEED

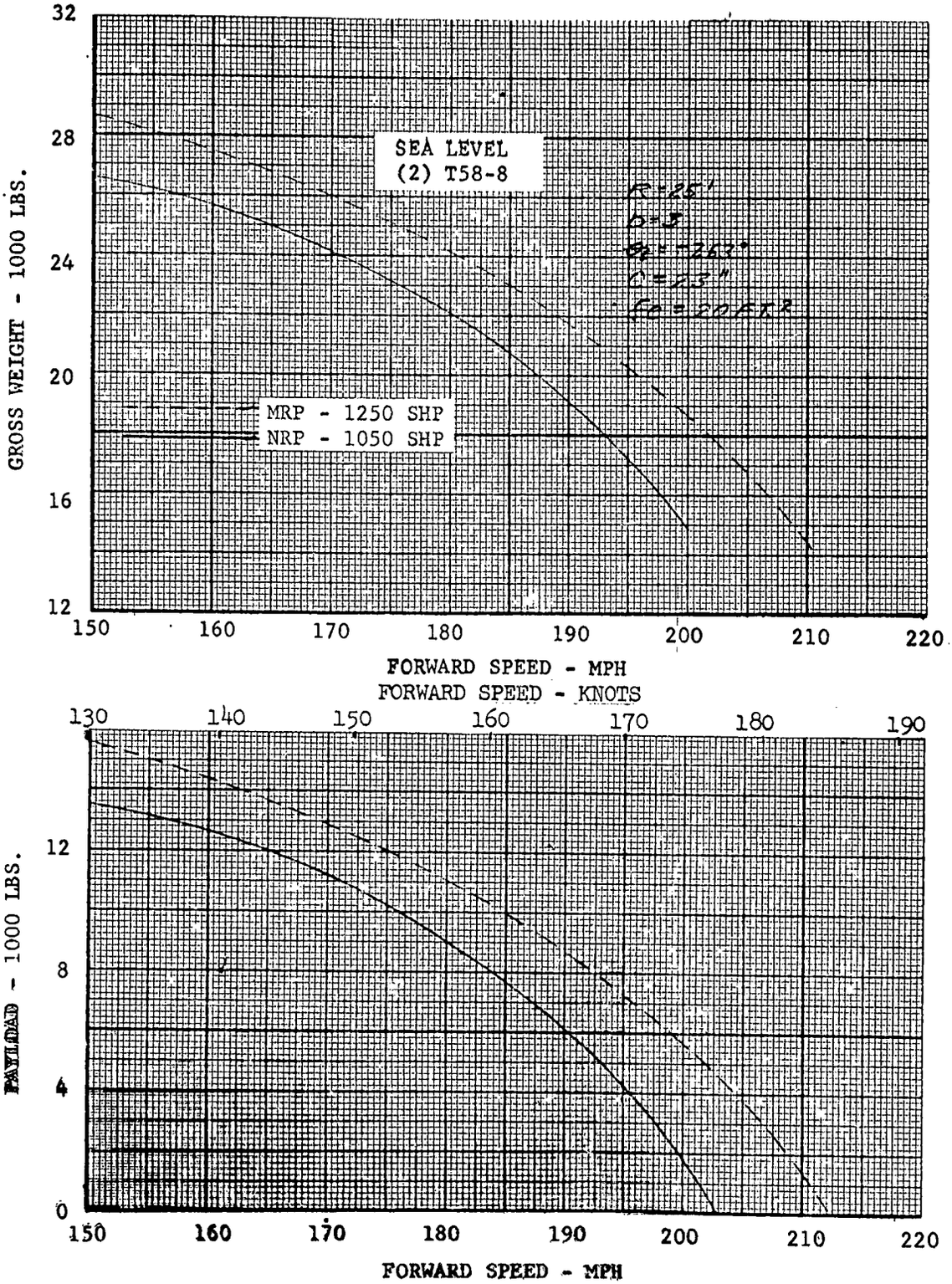


FIGURE 35

GROSS WEIGHT AND PAYLOAD VS. FORWARD SPEED

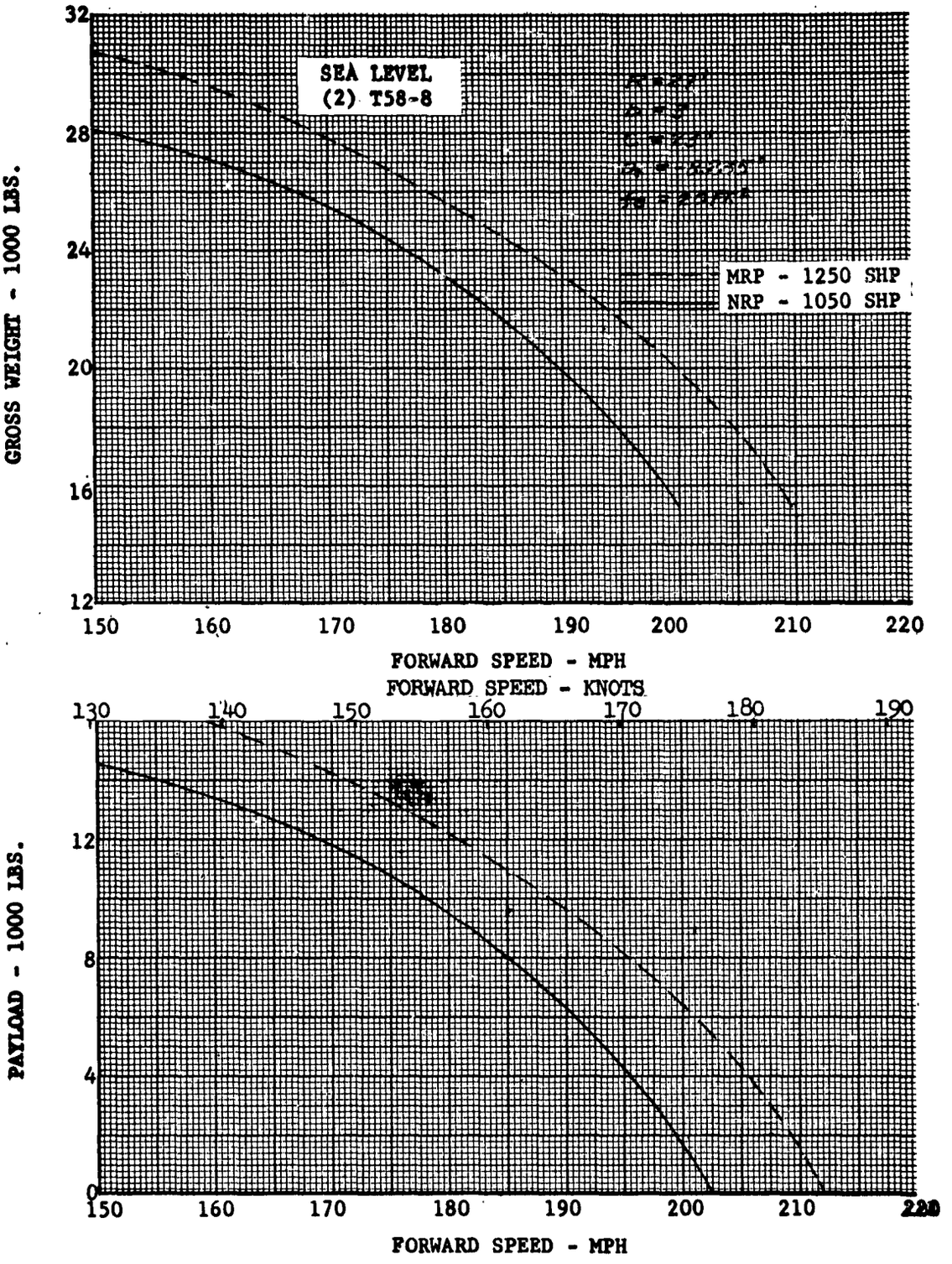


FIGURE 36

GROSS WEIGHT AND PAYLOAD VS. FORWARD SPEED

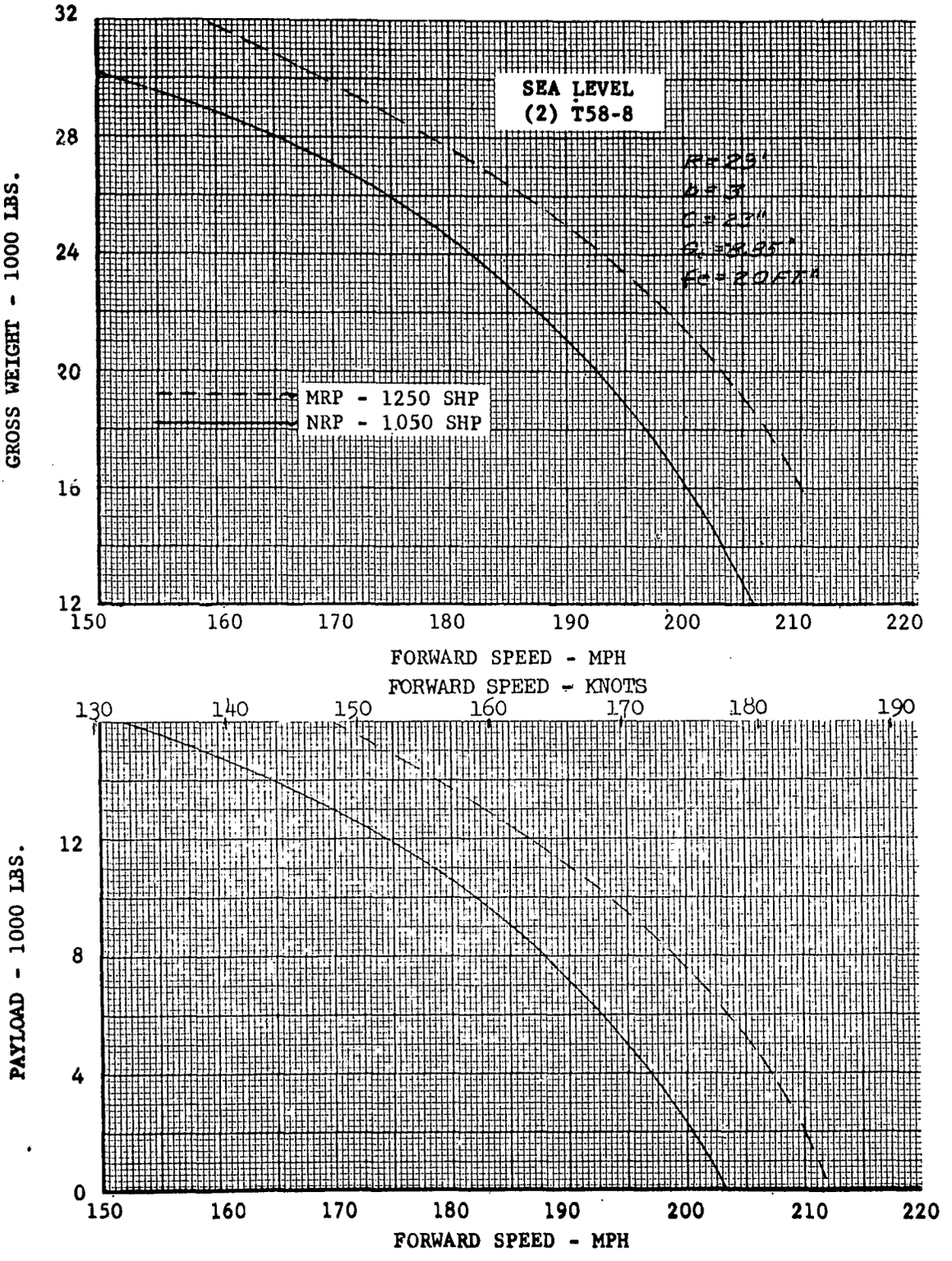


FIGURE 37

GROSS WEIGHT AND PAYLOAD VS. FORWARD SPEED

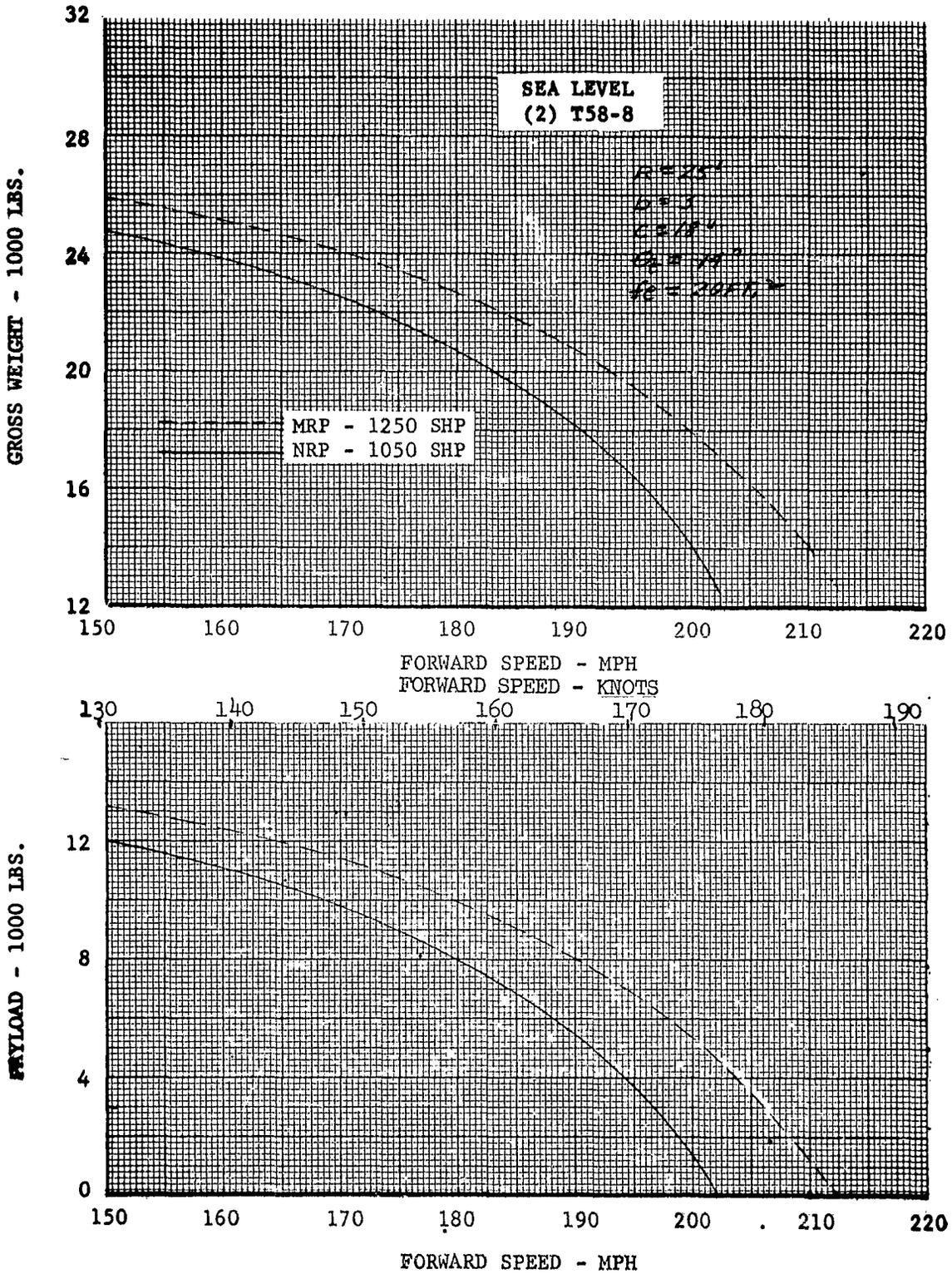


FIGURE 38

GROSS WEIGHT AND PAYLOAD VS. FORWARD SPEED

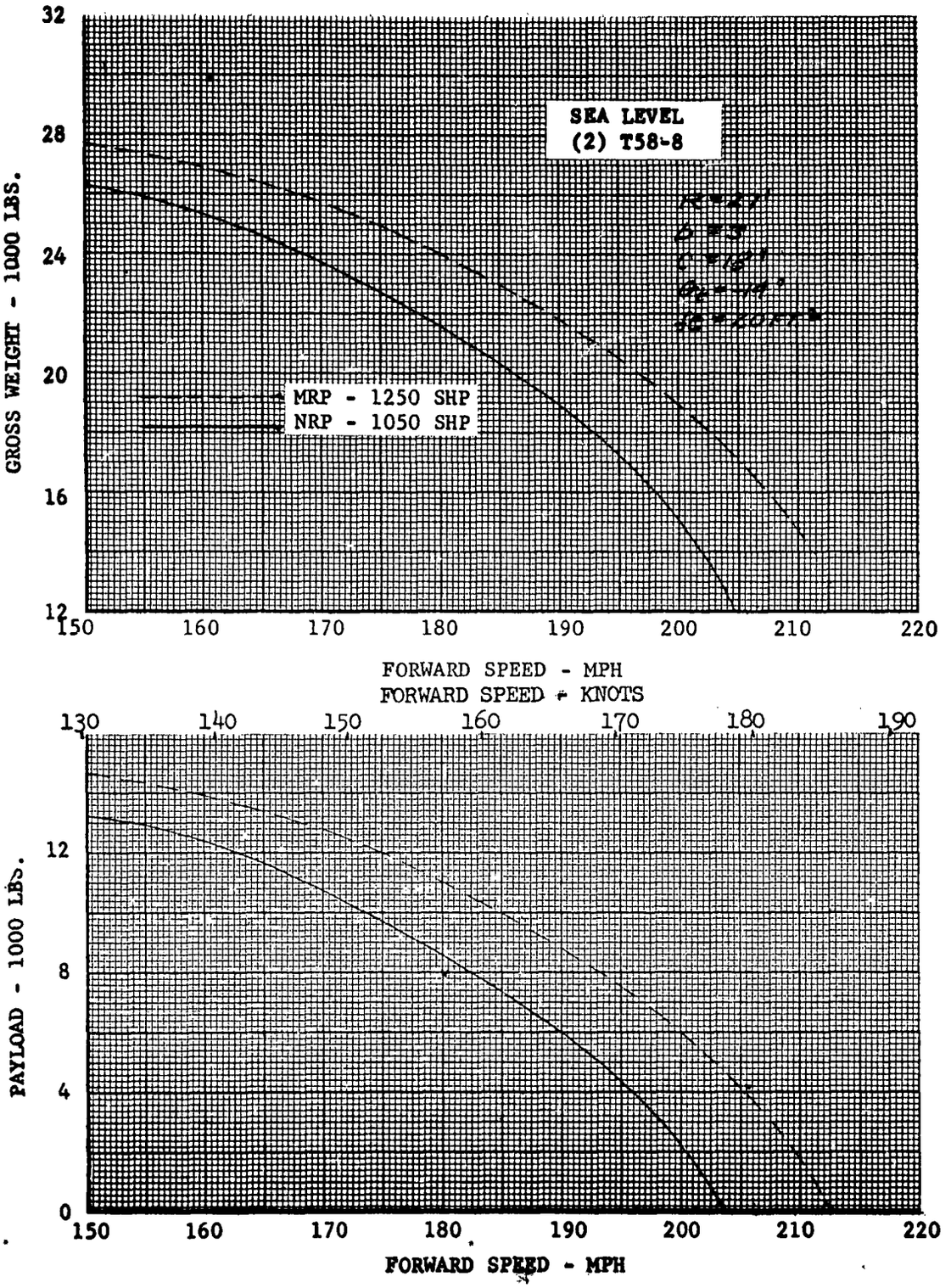


FIGURE 39

GROSS WEIGHT AND PAYLOAD VS. FORWARD SPEED

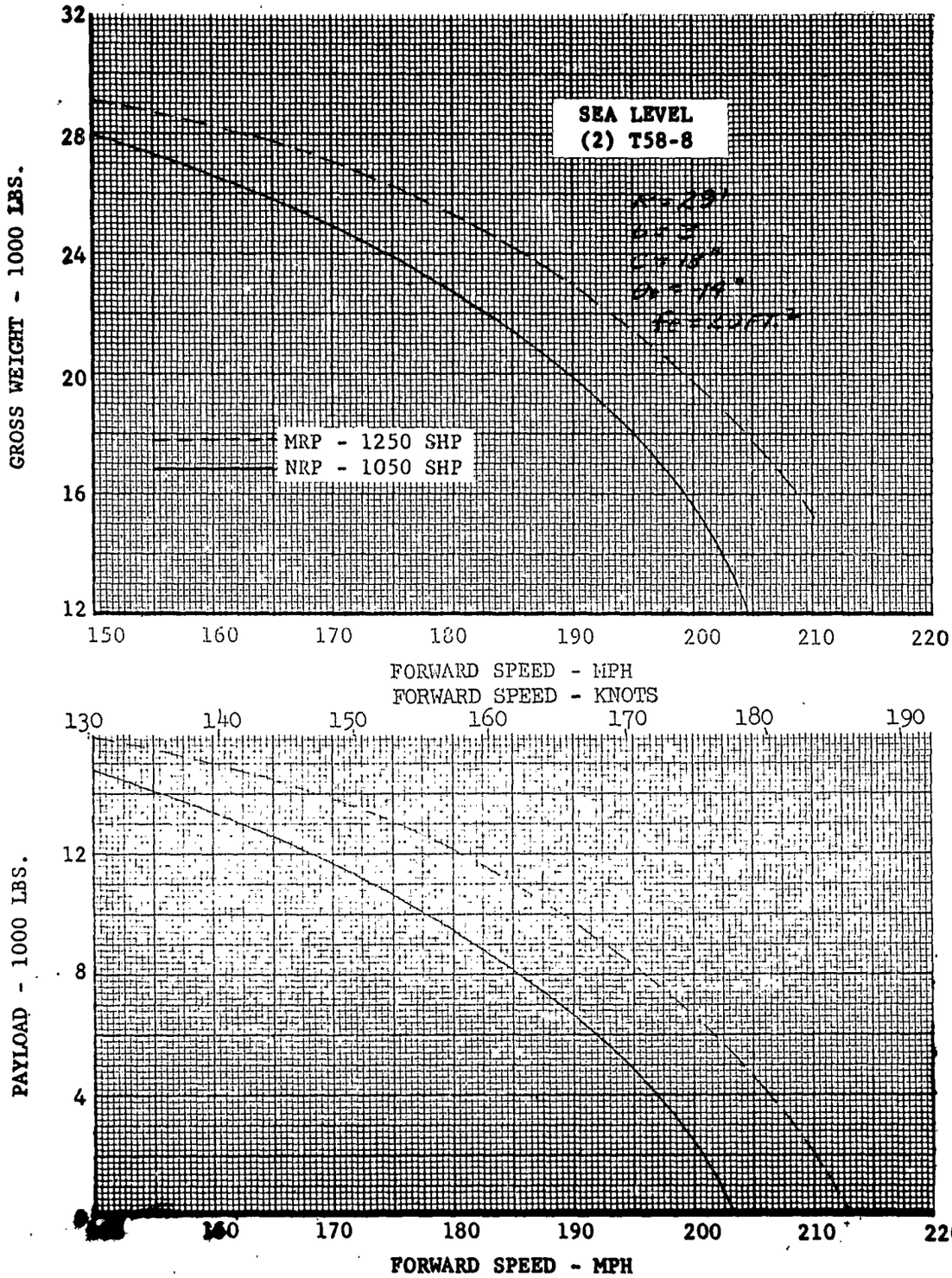


FIGURE 40

GROSS WEIGHT AND PAYLOAD VS. FORWARD SPEED

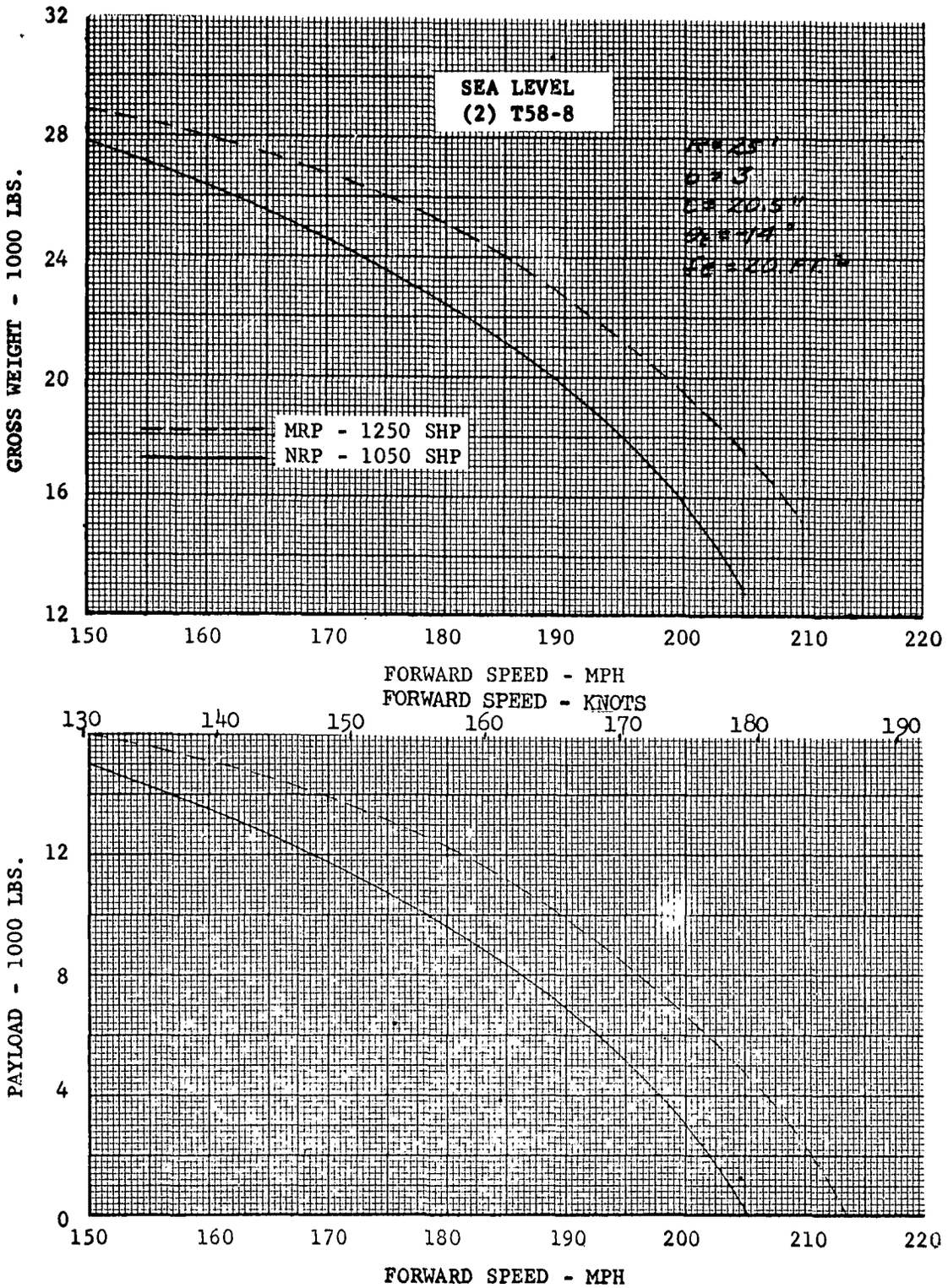


FIGURE 41

GROSS WEIGHT AND PAYLOAD VS. FORWARD SPEED

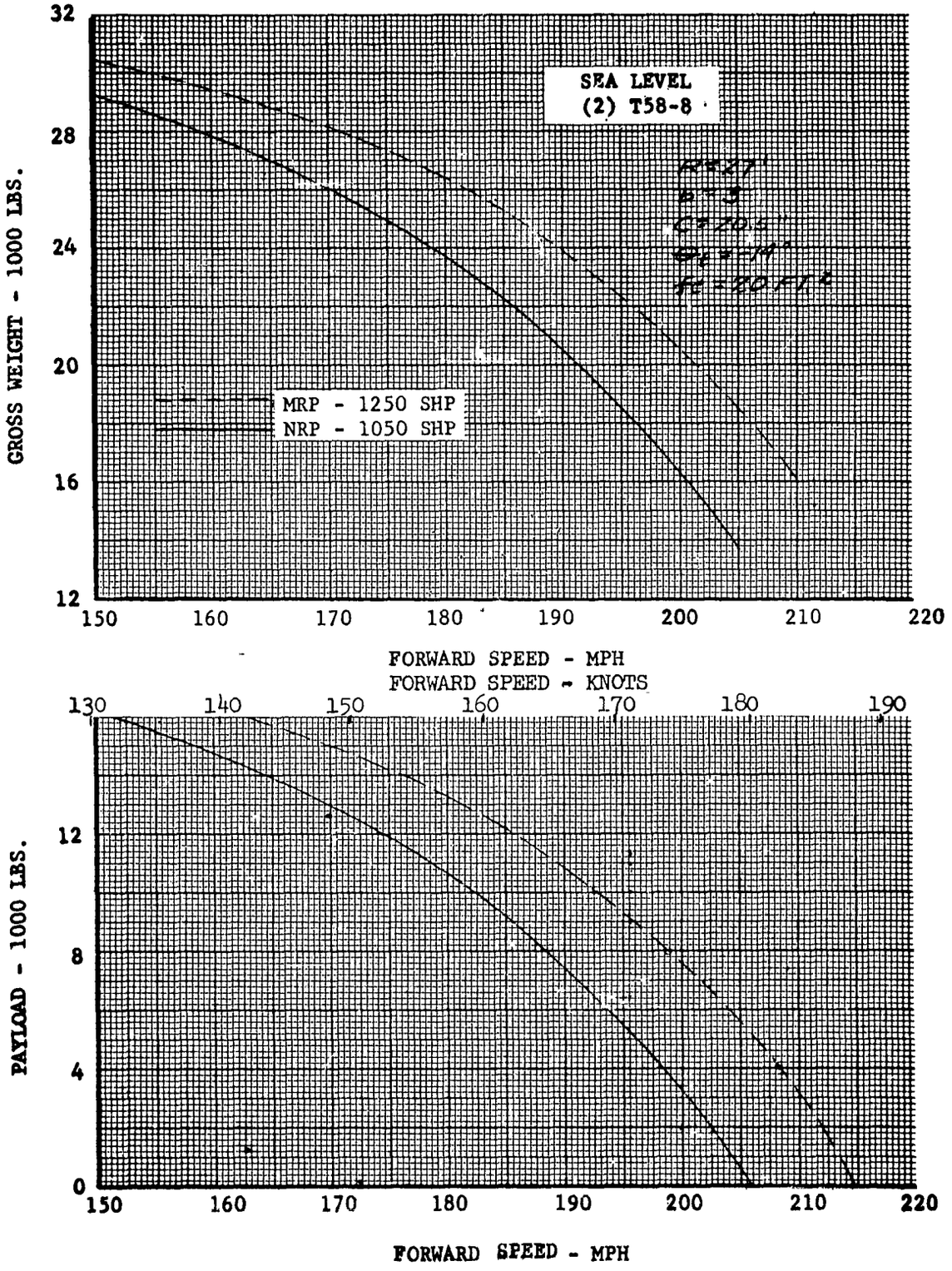


FIGURE 42

GROSS WEIGHT AND PAYLOAD VS. FORWARD SPEED

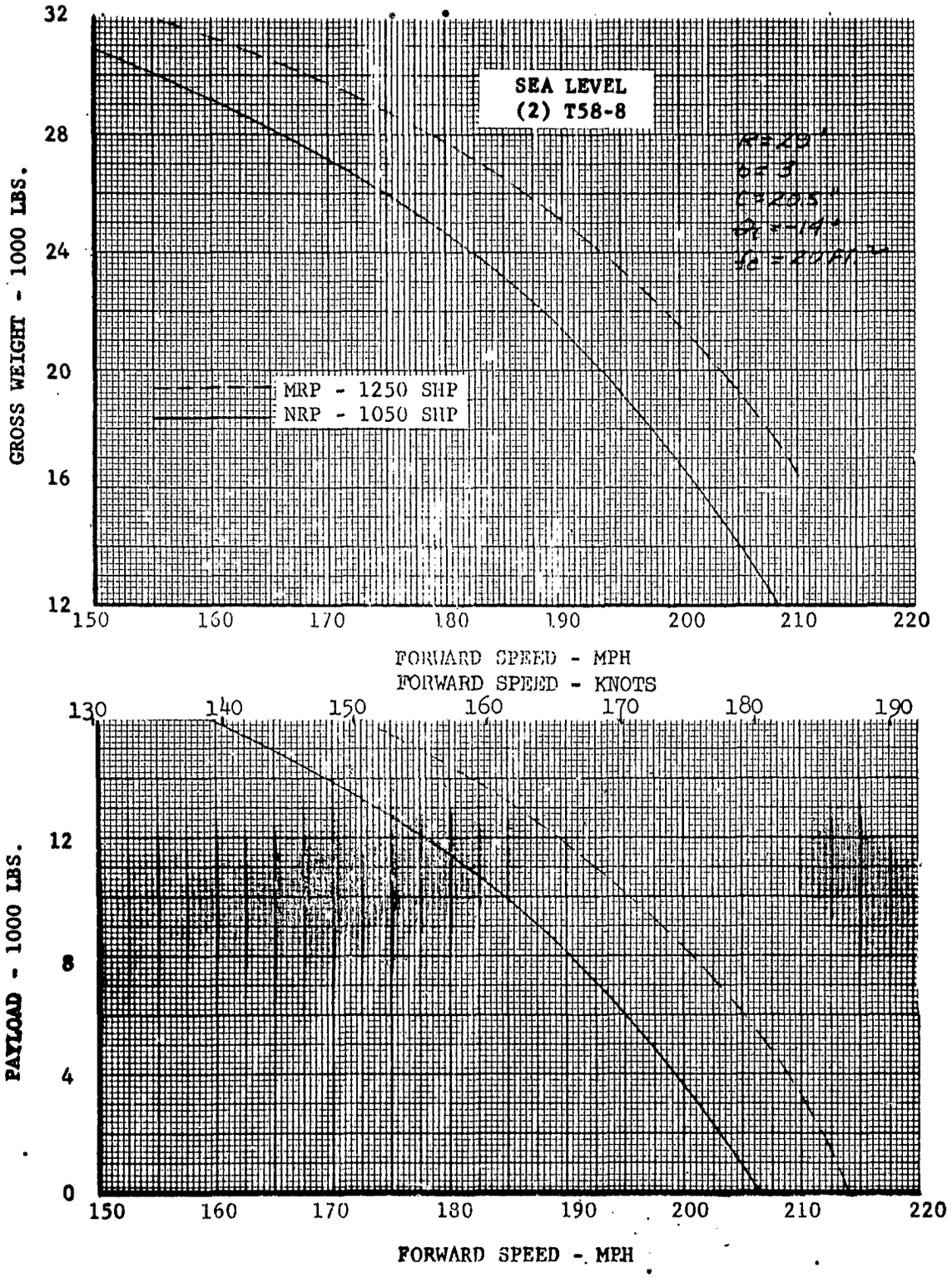


FIGURE 43

GROSS WEIGHT AND PAYLOAD VS. FORWARD SPEED

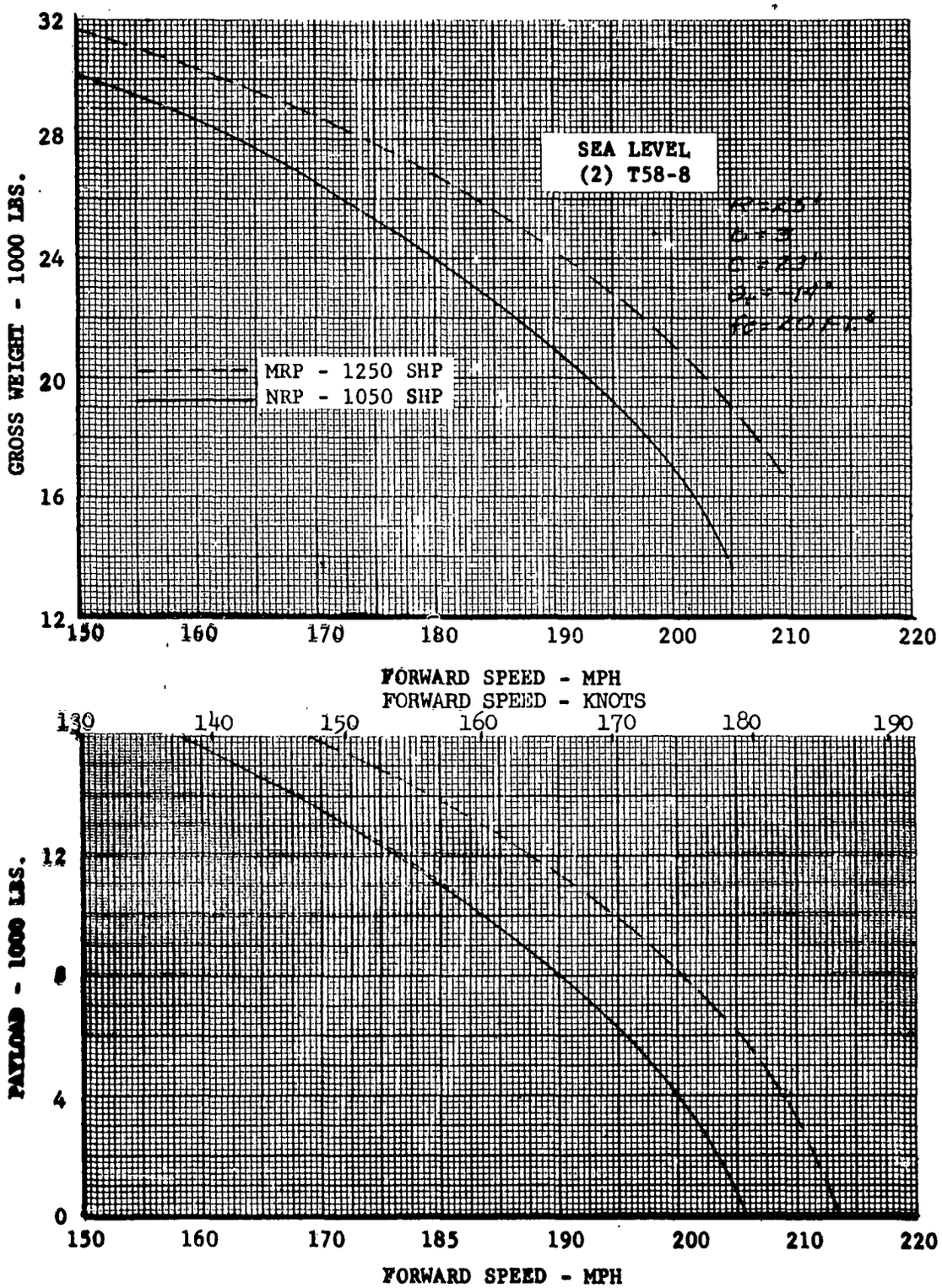


FIGURE 44

GROSS WEIGHT AND PAYLOAD VS. FORWARD SPEED

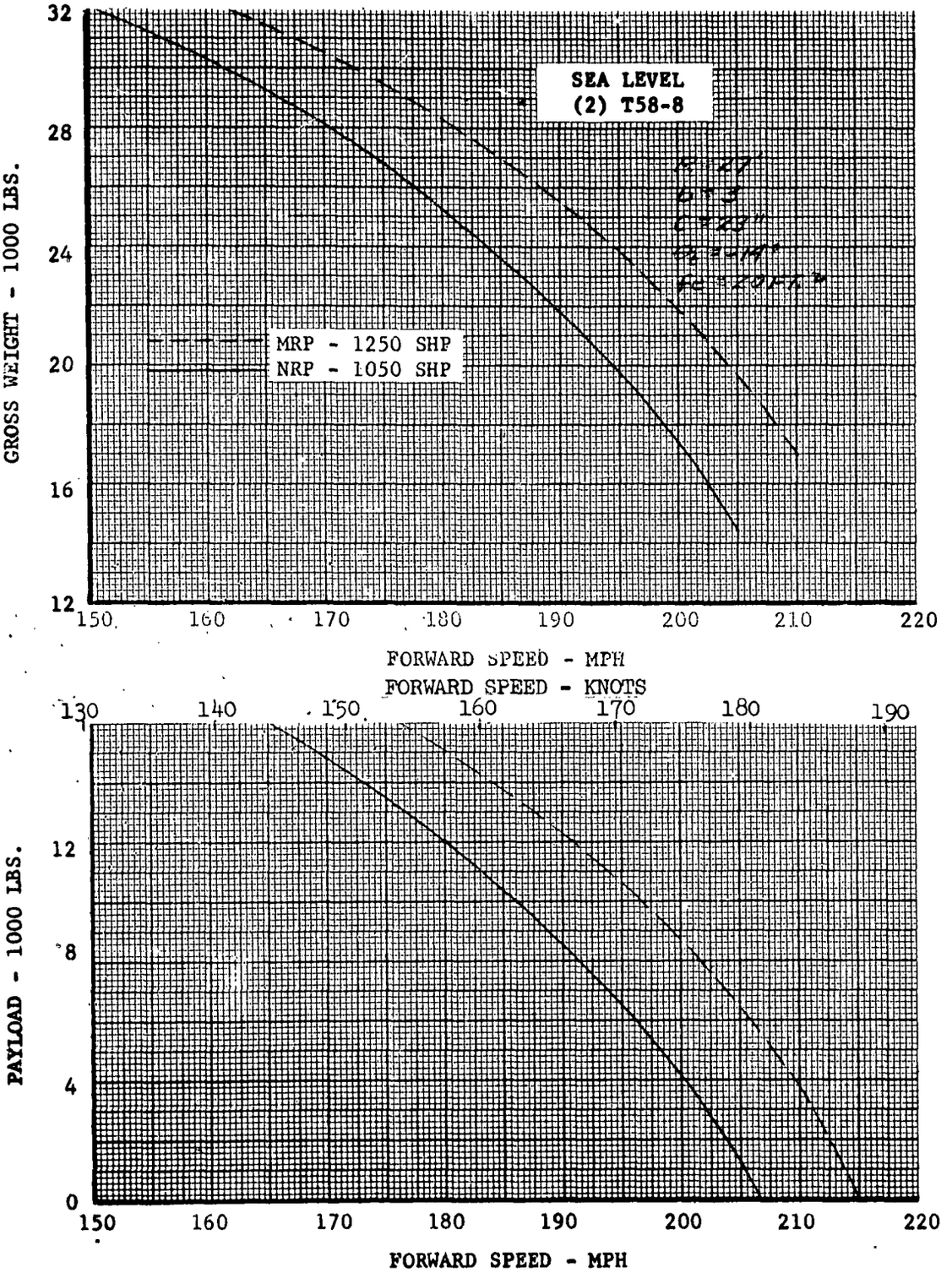
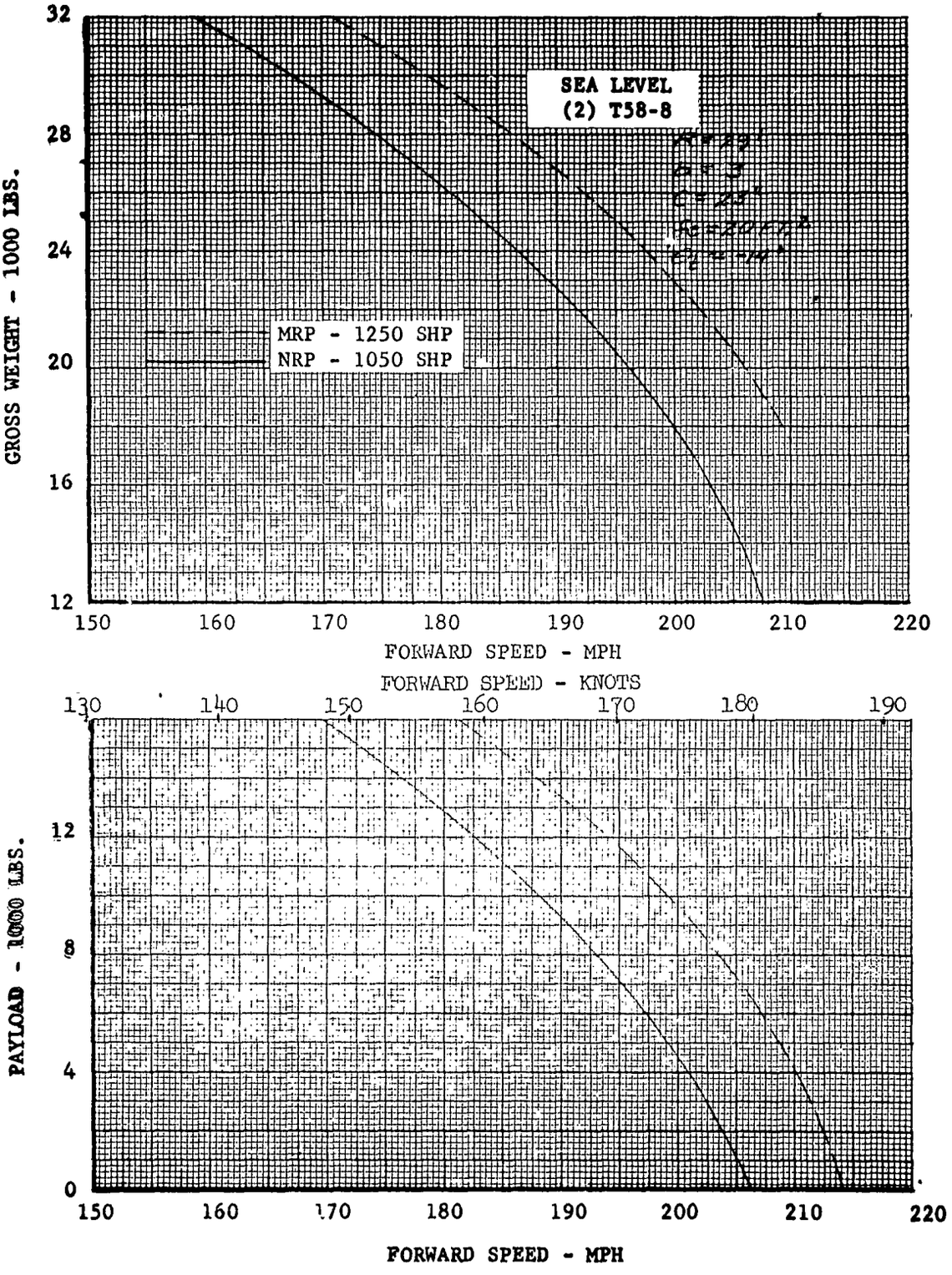


FIGURE 45

GROSS WEIGHT AND PAYLOAD VS. FORWARD SPEED



Rotor Environment

To obtain a better understanding of the requirements for a high performance helicopter, an investigation was initiated, prior to the inception of this contract, to study the stall, compressibility, and reverse flow characteristics of a lifting rotor at high forward speeds.

Since the overall rotor performance is greatly affected by the extent these flow conditions have "invaded" the rotor disc, with regard to power, lift, and propulsive force as well as vibration, the investigation was formed about the major independent variables leading to stall, compressibility and reverse flow. The four operating conditions and two physical properties investigated were:

A. Operating Conditions

1. Root Collective pitch - θ_0
2. Advancing tip Mach Number - M_t
3. Advance ratio - μ
4. Inflow ratio - λ

B. Physical Properties

1. Total blade twist - θ_t
2. Blade airfoil section properties

The study was conducted through the use of the IBM Model 704 Computer at the Applied Mathematics Section, Aero Space Division, The Boeing Company, Seattle, Washington. Numerical equations and procedures for calculating the aerodynamic characteristics of lifting rotors, discussed in Reference 3 and 4, were programmed on this digital computer. The method consists of calculating the individual force contributions of a specific number of blade stations at various points on the rotor disc, averaging the values around the disc at a particular radial station, and then radially integrating these averages along the blade to obtain the rotor characteristics of thrust, power, drag, and flapping motion of a blade. Tables of the airfoil section properties, C_l and C_d, as a function of Mach number, as well as angle of attack, were included in the analysis for two airfoils. Figures 46 and 47 present the section aerodynamic characteristics for the NACA 0012 and NACA 0009.5 as a function of angle of attack and Mach number.

Although the total rotor performance coefficients of C_T/σ , C'_T/σ , C_P/σ , C_{PO}/σ , L/D_E, etc. formed the major required output, selected cases, necessary to this rotor environment study, had the additional output of elemental data at specific radial and azimuthal stations. These data are:

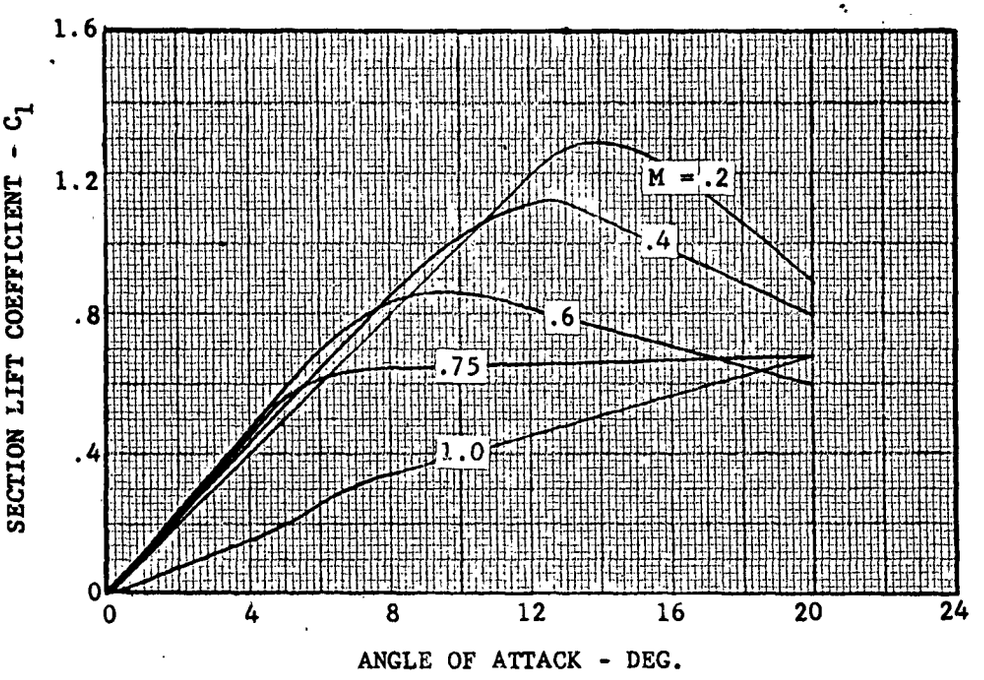
α_X - local station angle of attack

M_X - local station Mach number

$\frac{\partial C_T/\sigma}{\partial X}$ - elemental non-dimensional thrust coefficient

FIGURE 46

NACA 0012 SECTION AERODYNAMIC CHARACTERISTICS -
C_l AND C_d AS A FUNCTION OF α AND M



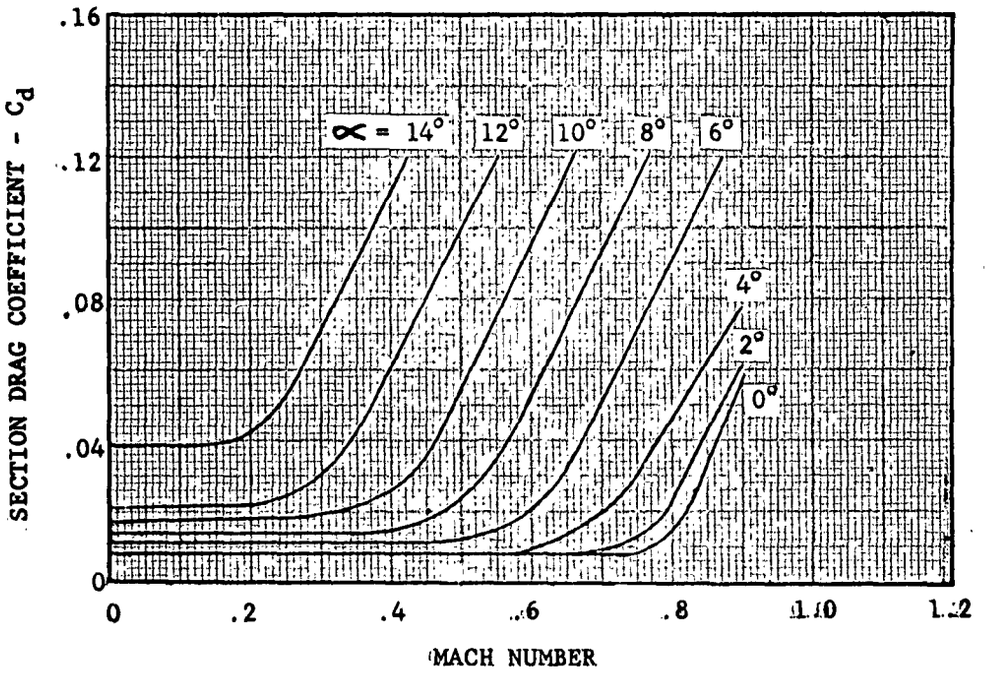
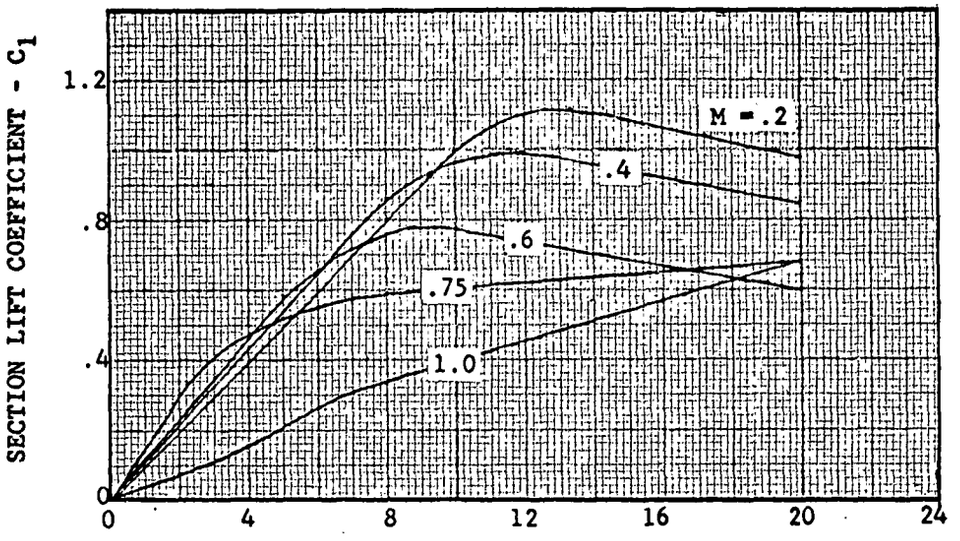
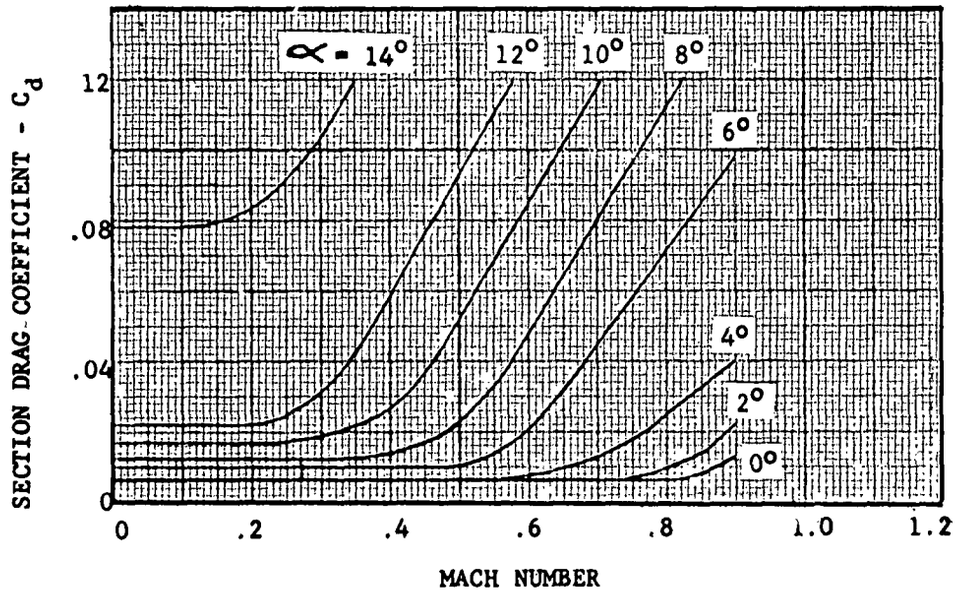


FIGURE 47

NACA 0009.5 SECTION AERODYNAMIC CHARACTERISTICS -
C_l AND C_d AS A FUNCTION OF α AND M





$\frac{\partial C_p/\sigma}{\partial X}$ - elemental non-dimensional power coefficient

$\frac{\partial C_{po}/\sigma}{\partial X}$ - elemental non-dimensional profile power coefficient

Using the planform of the lifting rotor as a boundary, lines of constant elemental coefficient, local angle of attack, or Mach number were drawn for one given operating condition. These data are hereafter referred to as Polar Data. The total rotor performance of L/D_E, C_T'/σ, and X/L was also plotted to establish the overall trend with respect to the variable under investigation. Although the total performance data is presented for a wide range of the particular independent variable, the Polar Data was only obtained a small increment away from the reference condition. The table below summarizes points at which Polar Data has been obtained.

TABLE III

Polar Data Investigation

Airfoil - NACA 0012

Variable	Case	μ	λ	M_t	θ_t	θ_o
Ref. Case	1	.45	-.15	.85	-9^o	Fixed at Peak L/D_E, 19.255^o
θ_o	2,3,4	.45	-.15	.85	-9^o	19.0^o, 19.5^o, 20.5^o
M_t	5	.45	-.15	.90	-9^o	Fixed at Peak L/D_E, $\theta_o = 19.23^o$
μ	6	.50	-.15	.85	-9^o	Fixed at Peak L/D_E, $\theta_o = 18.55^o$
λ	7	.45	-.20	.85	-9^o	Fixed at Peak L/D_E, $\theta_o = 22.23^o$
θ_t	8	.45	-.15	.85	-14^o	Fixed at Peak L/D_E, $\theta_o = 23.00^o$

Airfoil - NACA 0009.5

Variable	Case	μ	λ	M_t	θ_t	θ_o
Ref. Case	9	.45	-.15	.85	-9^o	Fixed at Peak L/D_E, $\theta_o = 19.07^o$
M_t	10	.45	-.15	.90	-9^o	Fixed at Peak L/D_E, $\theta_o = 19.03^o$

All Polar Data is removable from the inside back cover of this report.

The rotor blade considered in the analysis had the following physical properties:

A. Lock Number - $\gamma = \frac{\rho acR^4}{2I_f} = 5.46$

B. Non-dimensional flapping hinge offset station - $\xi = \frac{r}{R} = .01978$

C. Initial airfoil section station - $X_c = .15$

D. Solidity - $\sigma = \frac{bc}{\pi R} = .1$

E. No cyclic input

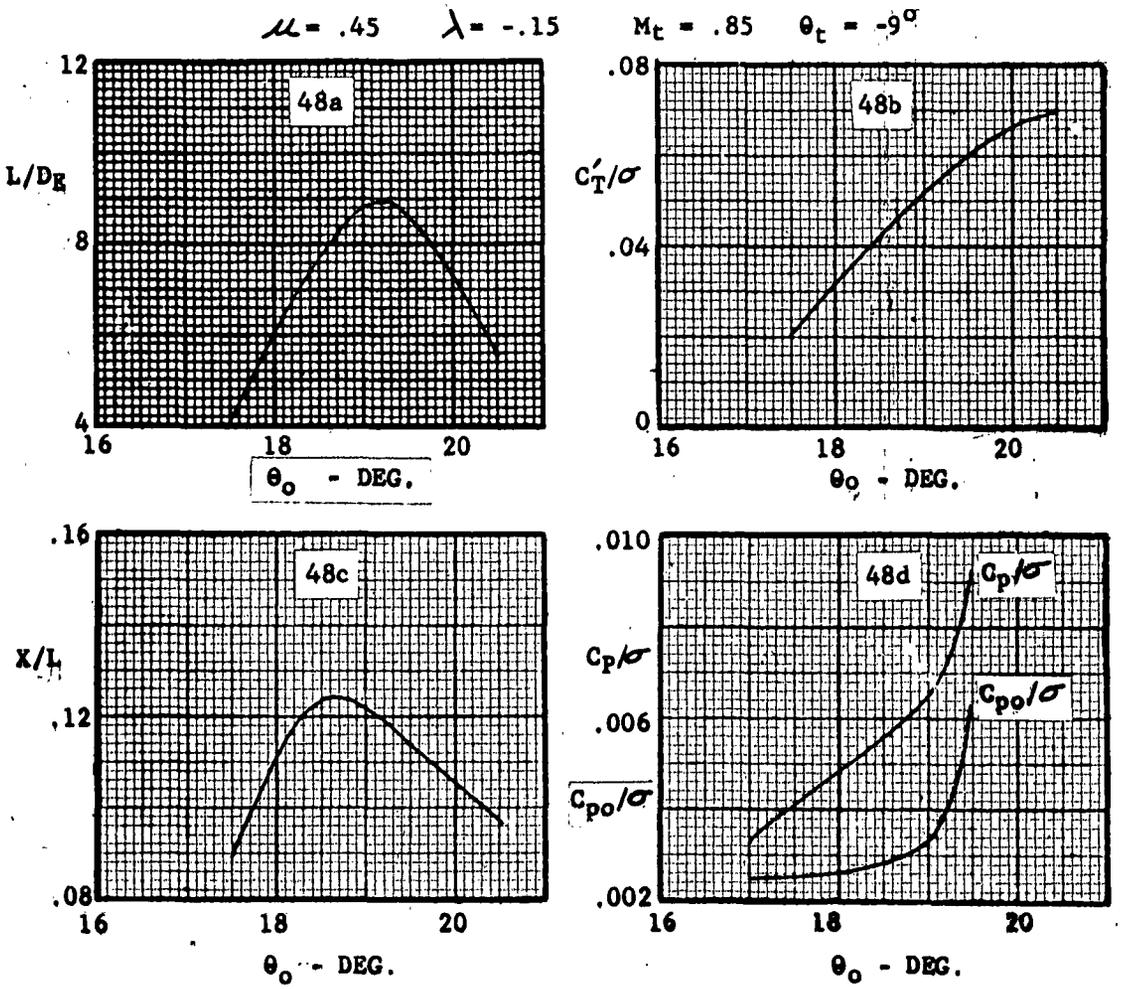
Effect of Root Collective Pitch - θ_o

The majority of performances computed in the Phase I portion of this contract was derived from data summarizing the variation of L/D_E MAX (peak value) with the trim conditions of advancing tip Mach number and advance ratio. As was noted previously, exact values of C_T'/σ and X/L, associated with L/D_E MAX, completed the performance data. The use of L/D_E MAX was predicated upon the fact that little retreating blade stall existed.

To establish a complete understanding of why L/D_E reaches a peak, as well as the growth of stall and compressibility with the collective pitch control, Polar Data at three values of θ_o, surrounding θ_o = 19.255 degrees (L/D_E MAX), were obtained. The total performance coefficients L/D_E, C_T'/σ, X/L versus root collective pitch and C_T'/σ versus both C_p/σ and C_{po}/σ are shown below.

FIGURE 48

EFFECT OF ROOT COLLECTIVE PITCH ON TOTAL PERFORMANCE COEFFICIENTS OF L/D_E, C_T'/σ, X/L, C_p/σ, AND C_{po}/σ



The mathematical argument for peak L/D_E is immediately observed from the figures above and the equational expression for L/D_E below:

$$L/D_E = \frac{1}{-X/L + \frac{C_P/\sigma}{\mu C_T'/\sigma}} \qquad (5\text{-}1)$$

The positive increase in X/L at the lower values of collective pitch reduces the numerical value of the denominator which tends to increase L/D_E. The second term, $\frac{C_P/\sigma}{\mu C_T'/\sigma}$, initially decreases with collective pitch tending to also increase L/D_E. Both terms reach a maximum and the slope reverses.

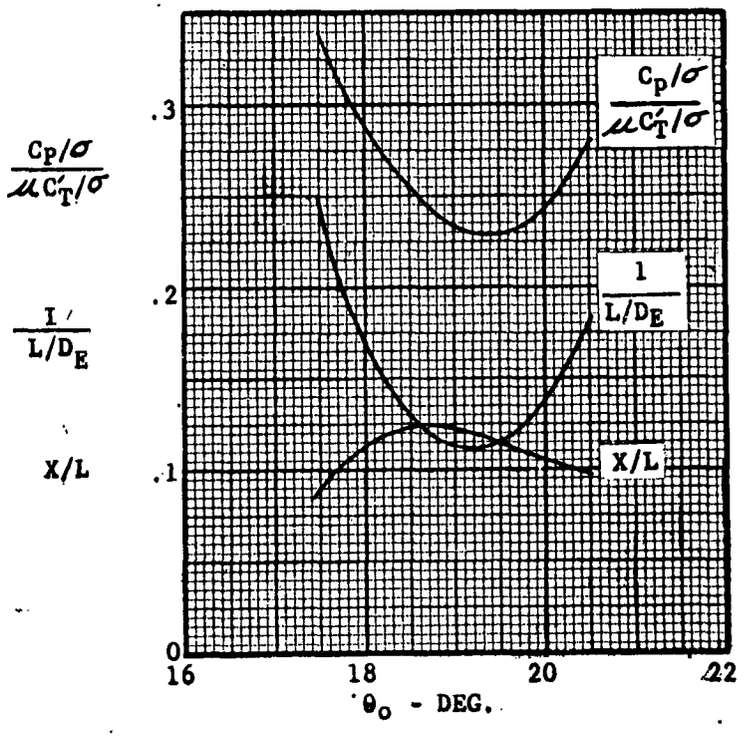
As θ_o approaches the value for maximum L/D_E, the L/D_E curve becomes increasingly concave down. However, when X/L peaks, L/D_E does not. (θ_o for X/L MAX = 18.7°, while θ_o for L/D_E MAX = 19.26°)

<u>The figure below clearly indicates that the predominate term in the L/D_E equation is $\frac{C_P/\sigma}{\mu C_T'/\sigma}$.</u>

FIGURE 49

COMPONENT TERMS OF L/D_E EQUATION VS. ROOT COLLECTIVE PITCH

$\mu = .45 \quad \lambda = -.15 \quad M_t = .85 \quad \theta_t = -9°$



This figure expresses the terms of the reciprocal of the L/D_E equation below:

$$\frac{1}{L/D_E} = -\frac{X}{L} + \frac{C_p/\sigma}{\mu C_T'/\sigma} \qquad (5\text{-}2)$$

Because X/L changes very little over the collective pitch range, the reciprocal of L/D_E arrears nearly equal to a constant plus the $\frac{C_p/\sigma}{\mu C_T'/\sigma}$ term.

Having established the dominant term in the L/D_E equation, it is readily seen that the power coefficient C_p/σ produces the major change, since C_T'/σ is acceptably linear over the collective pitch range (Figure 48b). C_p/σ itself is remarkably linear up to a C_T'/σ value of approximately 0.06 ($\theta_o = 19.5^o$). At higher values, the sharp rise in the profile power coefficient, C_{po}/σ , increases total power, $\frac{C_p/\sigma}{\mu C_T'/\sigma}$ rises rapidly and L/D_E immediately decreases.

The slope $\frac{d\ C_{po}/\sigma}{d\ C_T'/\sigma}$ is noted to be approximately 0.0786.

The details of the rise of profile power with collective pitch may be reviewed from the Polar Data; Cases (in sequence of increasing collective pitch) 2,1,3, and 4.

The Regions of Stall and Compressibility in Figure 50 illustrates a slow progression of drag divergence ($\frac{dCd}{dM} = .1$) into the fourth quadrant of the disc (appearing first near an azimuth angle of 330°). The stall limit, as established by $C_{l\ MAX}$, appears first at a 315° azimuth station.

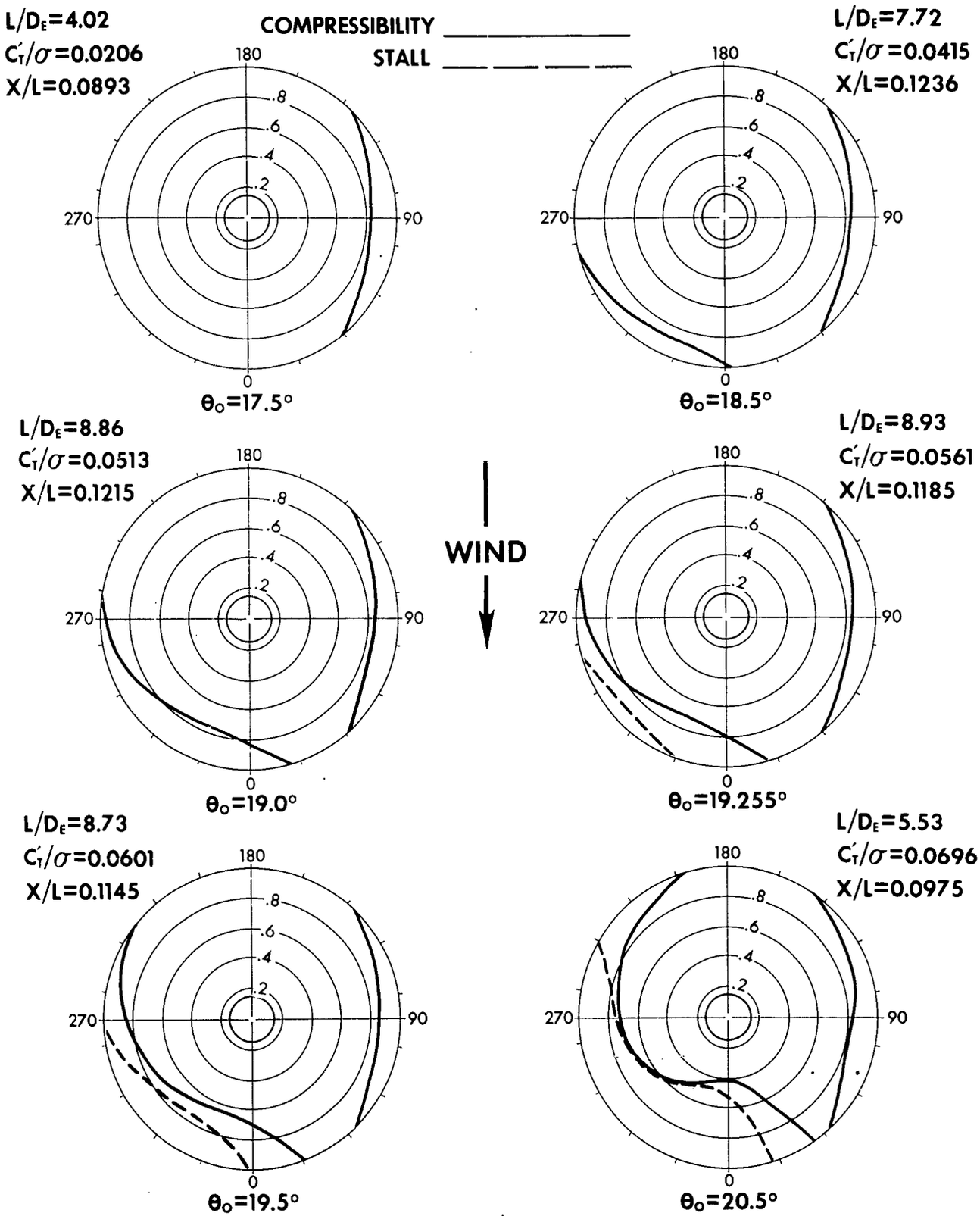
Inception of drag divergence on the advancing side varies little with collective pitch. From the profile power Polar Data, however, the gradient of $\frac{\partial C_{Po}/\sigma}{\partial X}$ from the radial station for drag divergence to the tip increases markedly with collective pitch for the retreating portions of the disc. As the additional drag due to stall appears the radial profile power gradient increases even more. It is concluded that the profile power due to advancing tip drag divergence (both magnitude and inception) is relatively independent of collective pitch and, hence, C_T'/σ .

The small amount of disc area operating above the stall limit at maximum L/D_E points out the significance of retreating blade stall. As drag divergence progresses inboard, the slope of L/D_E versus θ_o slowly drops off, but comparatively little stall is tolerated before this slope reverses entirely.

ROTOR AERODYNAMIC ENVIRONMENT

FIGURE 50 NACA 0012: GROWTH OF STALL AND COMPRESSIBILITY WITH INCREASING COLLECTIVE PITCH

μ =0.45 λ=−0.15 M_t=0.85 θ_t=−9°



It may be concluded, therefore, that retreating blade stall accounts for the peak in the L/D_E curve; drag divergence due to Mach number is established as the secondary factor in the magnitude of L/D_E MAX. .

The angle of attack Polar Data establishes the secondary effect of collective pitch - blade flapping motion, due primarily to variations of thrust around the disc. Since a phase angle of approximately 90° exists for the fully articulated rotor blade, a corollary between the effect of collective pitch on elemental thrust coefficient and the resulting angle of attack nearly 90° later is clearly brought to light. If increases in collective pitch cause a reduction in elemental thrust, the angle of attack approximately 90° later will reduce with increasing collective pitch. The converse also appears true. At the azimuth station of 340° the elemental thrust Polar Data reflects the loss in C_l with stall (yet at this station, angle of attack increases linearly with collective pitch.) The angle of attack near azimuth station 80° drops off with increasing collective pitch. The positive increase in angle of attack with θ_o at $\psi = 340^\circ$ is assured since the elemental thrust increases (though not linearly) with θ_o near $\psi = 240^\circ$.

The growth of stall, then, reduces the elemental thrust in the stall region while producing blade flapping motion which creates higher negative angles of attack in the advancing portion of the disc. The latter effect, as indicated from the thrust polar plot at $\theta_o = 20.5^\circ$, is so severe that a large negative thrust region on the advancing portion of the disc is quite apparent. Note that the total area of negative thrust as well as magnitude remains essentially constant for collective pitches up to and including $\theta_o = 19.5^\circ$. The collective pitch of 20.5° leads to severe stall and large reductions in L/D_E.

The effect of the negative angle of attack on the advancing tip is shown in the elemental total power Polar Data where a component of C_l is produced forward, i.e. pulling the blade, which offsets the large C_d aft. This effect is quite pronounced at $\psi = 60^\circ$ where the total power coefficient is "pocketed" with negative (reducing total power) values. The major power quadrant is from $\psi = 90^\circ$ to $\psi = 180^\circ$. The portion of the blade operating around stall has remarkably low elemental power coefficients.

At this point in the discussion it is well to point out that techniques for empirically establishing a "stall criterion" can be derived from this analysis.

Suffice it to say, the following points have been noted:

A. L/D_E MAX (with an associated C_T'/σ) occurs prior to a significant growth of stall. (Figures 48a and 48d)

B. A marked divergence in profile power (both elemental values in the stall region and total integrated value) with collective pitch as stall progresses. (Figure 48d and Polar Data cases 2, 1, 3, 4)

C. A distinct association of stall limit with angle attack in the fourth quadrant of the disc (growing inboard as a chord line of a circle and beginning near $\psi = 315^{\circ}$. Note that angle of attack for C_l MAX varies with Mach Number. (Polar Data)

The following conclusions regarding the effect of collective pitch on rotor performance as well as stall, compressibility and reverse flow are noted:

A. The predominate term in the L/D_E equation is $\frac{C_P/\sigma}{\mu C_T'/\sigma}$

B. Maximum L/D_E is determined first by retreating blade stall and secondarily by drag divergence associated with both advancing and retreating portions of the disc.

C. Profile power due to compressibility on the advancing portions of the disc is nearly independent of total thrust. As would be expected, and seen later, the operating conditions of advance ratio and advancing tip Mach number establish advancing blade compressiblity power.

D. A significant amount of profile power is absorbed in retreating blade compressibility.

E. Total rotor lift still increases with collective pitch even with large amounts of local blade stall.

F. The propulsive force - lift ratio begins to diminish with increasing collective pitch as retreating blade compressibility "invades" the disc.

Effect of Advancing Tip Mach Number

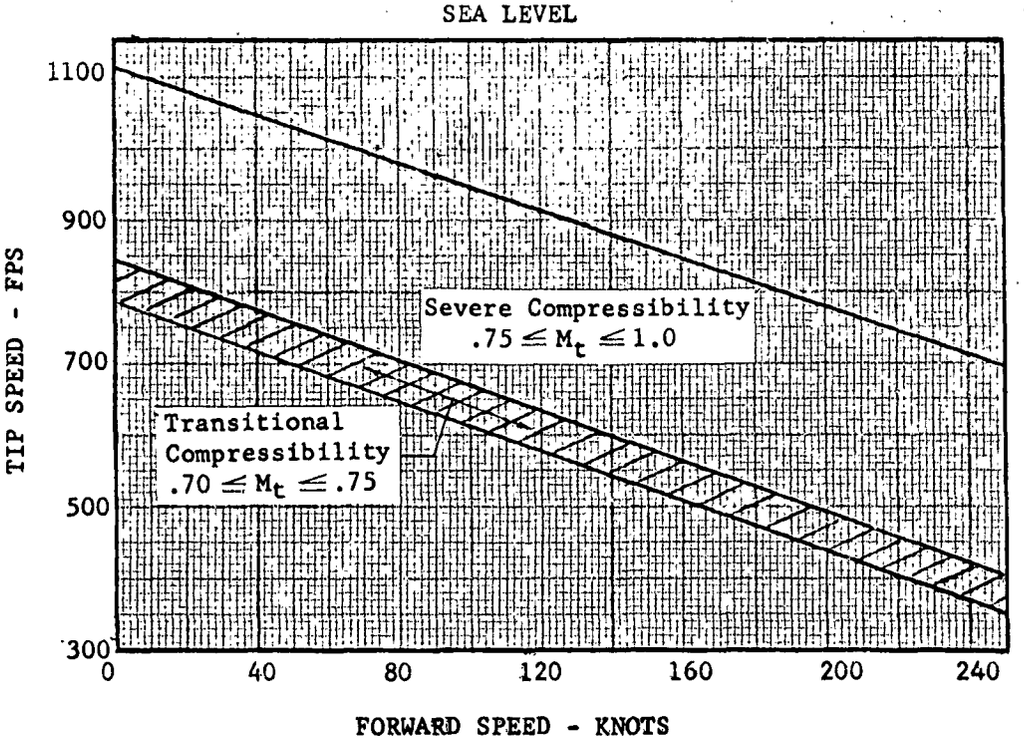
The total rotor performance associated with L/D_E MAX, as effected by advancing tip Mach number, is shown on Figure 61, page 5-28. Maximum L/D_E associated C_T'/σ and X/L for the NACA 0012 and NACA 0009.5 are plotted versus advancing tip Mach number. Note that all other variables, advance ratio (μ), inflow ratio (λ) and twist (θ_t) remain constant. The Polar Data required for this discussion are: NACA 0012 - Ref. Case 1 (M_t = .85), overlaid on Case 5 (M_t = .90) and NACA 0009.5 - Ref. Case 9 (M_t = .85), overlaid on Case 10 (M_t = .90).

The total rotor performance data illustrates the marked reduction in L/D_E MAX at high Mach numbers. The NACA 0012 experiences almost a 45% loss in L/D_E between M_t = .70 and M_t = .90, while the NACA 0009.5 loss is less than 16%. The vertical force coefficient C_T'/σ remains constant with Mach number, but L/D_E MAX is attained at a lower C_T'/σ (.051) with the NACA 0009.5 then the NACA 0012 (.056), approximately 9% loss in C_T'/σ. Note how flat X/L is with Mach number for the NACA 0009.5, while Mach number reduces the NACA 0012 available propulsive force-lift ratio by over 13%.

Below an advancing tip Mach number of .70 the effects of compressibility may be neglected. Above M_t = .75 Mach number must become a variable. The suggested limits with regard to the inclusion of Mach number as an analytical variable in rotor performance calculations are shown below.

FIGURE 51

MACH NUMBER AS AN ANALYTICAL VARIABLE



In Figure 52 the regions of Stall and Compressibility are super-imposed on Polar Data of constant Mach number lines for both the NACA 0012 and NACA 0009.5 at $M_t = .85$ and $M_t = .90$.

The stall and retreating drag divergence are relatively insensitive to Mach number increases, while a large growth in advancing drag divergence is apparent. This is the primary cause for deterioration in L/D_E MAX.

The limits of stall and drag divergence are established from both angle of attack and Mach number. Figure 53 illustrates the combinations of local flow α_x and M_x which lead to C_l MAX and $\frac{dCd}{dM} = .1$ (drag divergence) values derived from the airfoil section characteristics used in the computer program.

The Polar Data of angle of attack shows that the angle of attack distribution is essentially unchanged with Mach number which explains why C_T'/σ is relatively uneffected by Mach number. The negative angle of attack, with resulting negative thrust, in the advancing portion of the disc remains characteristic of L/D_E MAX.

A slight growth of stall and retreating blade drag divergence with Mach number is seen. This is not really surprising since, for a given Mach number, L/D_E MAX occurs at a collective pitch which permits only a small "invasion" of stall on the retreating side. The growth of stall with collective pitch is insensitive to Mach number.

The Polar Data of profile power clearly established the reason for the L/D_E loss with increasing Mach number. Not only has the advancing tip drag divergence area increased, but the radial gradient of profile power has increased slightly. Advancing tip drag divergence for the NACA 0012 is closely associated with $\frac{\partial C_{Po}/\sigma}{\partial X} = .01$, while $\frac{\partial C_{Po}/\sigma}{\partial X} = .0125$ more closely approximates the NACA 0009.5. Note also that the improved compressibility characteristics of the thinner airfoil reduce the total advancing portion of the disc operating above drag divergence, but exhibits the same boundary change with increasing Mach number.

The efficiency of the NACA 0009.5 is illustrated by the higher L/D_E MAX and associated X/L, but shows lower angles of attack on the retreating quadrant ($270^\circ \leq \Psi \leq 360^\circ$) consistent with the lower maximum lift coefficient.

The efficiency of the NACA 0012 for operation up to advancing tip Mach numbers of .75 is well established. Its use, in preference to the thinner section, could be derived from the increased C_T'/σ available associated with higher maximum lift coefficients. Losses in L/D_E MAX and X/L at higher Mach numbers, however, are extremely unattractive.

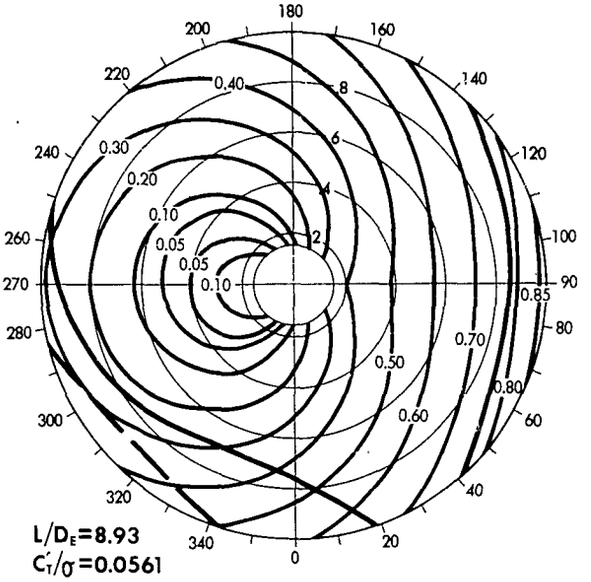
ROTOR AERODYNAMIC ENVIRONMENT

FIGURE 52 MACH NUMBER DISTRIBUTION

μ =0.45 λ=−0.15 θ_1=−9°

COMPRESSIBILITY ——— STALL — — —

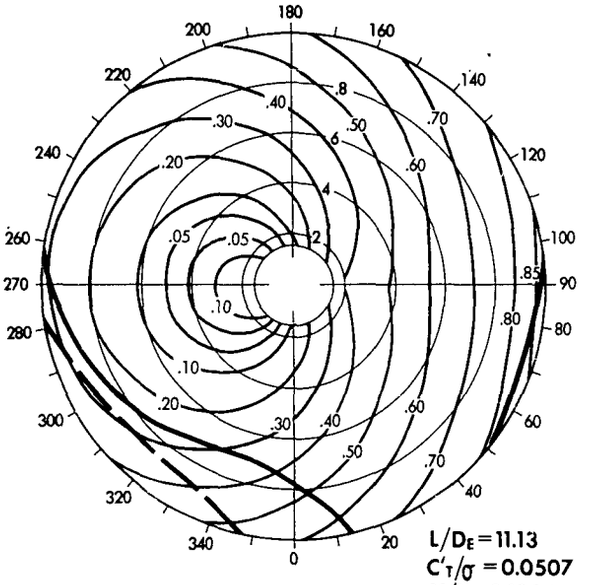
NACA 0012



L/D_E=8.93
C_T'/σ=0.0561
X/L=0.1185
θ_o=19.255°

M_t=0.85

NACA 0009.5

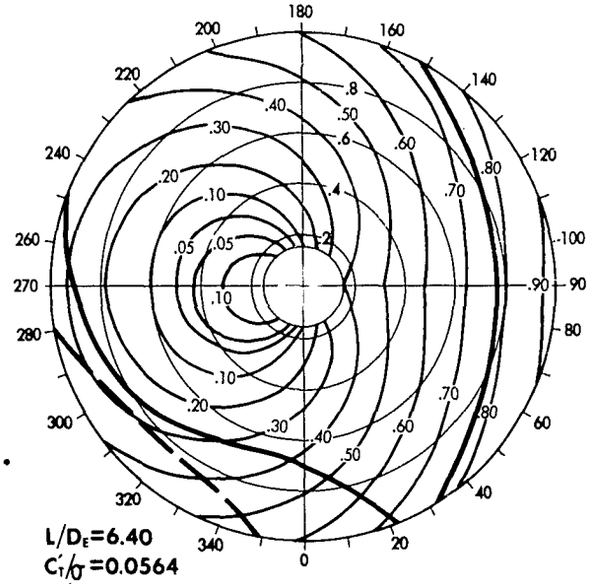


L/D_E=11.13
C_T'/σ=0.0507
X/L=0.1284
θ_o=19.07°

M_t=0.85

WIND

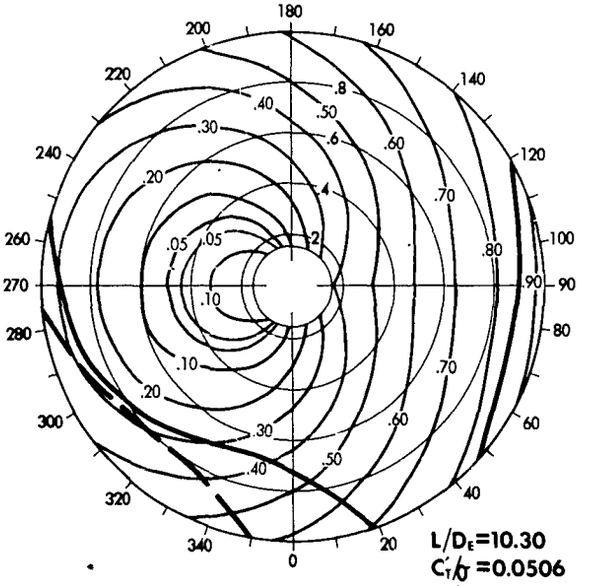
NACA 0012



L/D_E=6.40
C_T'/σ=0.0564
X/L=0.1058
θ_o=19.23°

M_t=0.90

NACA 0009.5

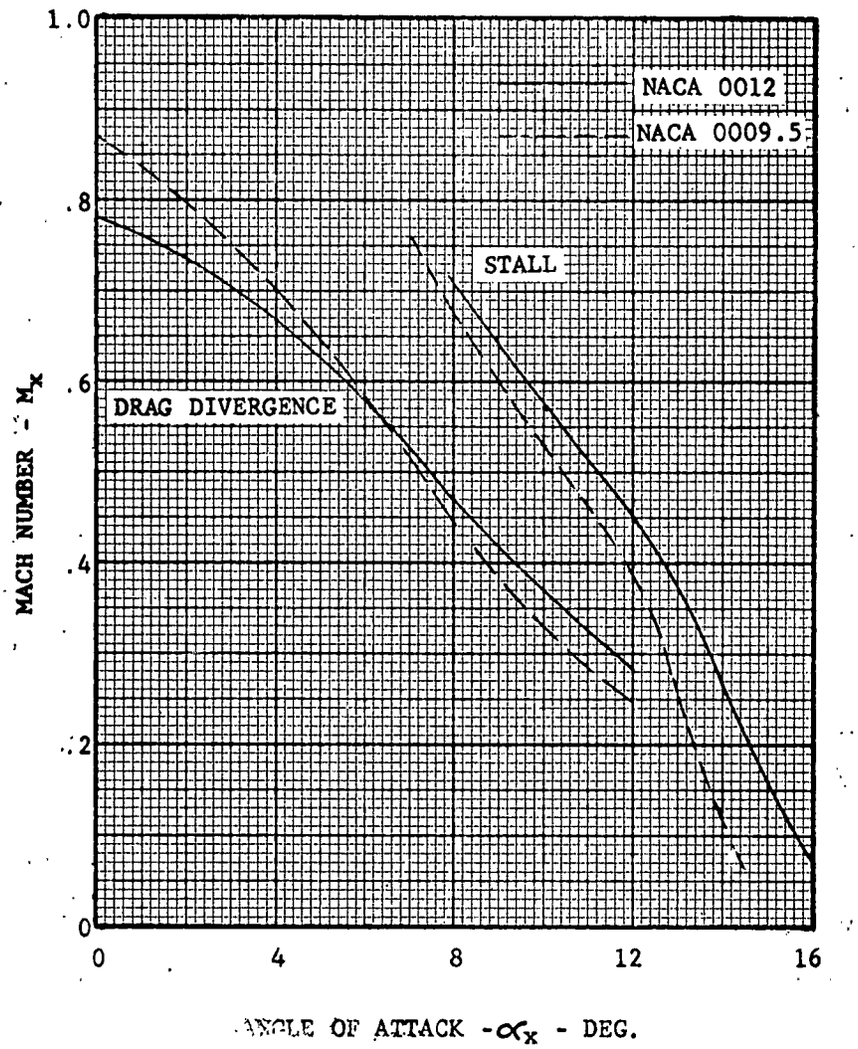


L/D_E=10.30
C_T'/σ=0.0506
X/L=0.1276
θ_o=19.03°

M_t=0.90

FIGURE 53

STALL AND DRAG DIVERGENCE ANGLES OF ATTACK AS A FUNCTION OF MACH NUMBER FOR THE NACA 0012 AND NACA 0009.5 AIRFOILS



Effect of Advance Ratio

Figure 62, page 5-30 shows the variation of maximum L/D_E and associated C_T'/σ and X/L with advance ratio (μ) for constant λ, θ_t, and M_t. Polar Data for the discussion are NACA 0012 - Ref. Case 1 ($\mu = .45$) overlaid on Case 6 ($\mu = .50$). The NACA 0009.5 Polar Data has been deleted from the analysis because of the similarity in total rotor performance trends.

The optimizing of both L/D_E MAX and C_T'/σ with advance ratio is clearly indicated; however, the optimum μ is entirely dependent on inflow ratio, advancing tip Mach number and twist; although the optimum L/D_E MAX does appear to fall in the range $.40 \leq \mu \leq .50$ (in powered flight) regardless of the above variables.

The loss in the propulsive force-lift ratio X/L, with advance ratio is extreme. This loss is recoverable, of course, with a forward (nose down) inclination in the rotor plane of no-feathering which will, however, be seen later to produce about the same extreme loss in <u>both</u> L/D_E MAX and C_T'/σ. At high speeds, a real blow to efficiency is in store for the rotor atop a "dirty" fuselage.

A review of the Regions of Stall and Compressibility, in Figure 54, for both the NACA 0012 and NACA 0009.5 indicated no change in the advancing drag divergence boundary in going to the higher advance ratio and only subtle changes in retreating drag divergence. The stall limit boundary has moved further into the disc sector of $280^\circ \leq \psi \leq 360^\circ$. This is particularly true of the NACA 0009.5.

The Polar Data comparison expresses the overall slight changes that were characteristic of the increase in the collective pitch study first discussed in this section. The increase in μ from .45 to .5 results in comparable changes associated with a collective pitch range of $\theta_o = 19.225$ (Ref. Case 1) to $\theta_o = 19.50^\circ$ (Case 3); perhaps a little more severe.

The loss in propulsive force is clearly a function of an increase in total rotor induced drag with only slight increase in profile drag. From Figure 4, page 2-4, the expression for propulsive force-lift ratio is

$$X/L = \frac{-T \sin\alpha - H \cos\alpha}{T \cos\alpha - H \sin\alpha} \qquad (5\text{-}3)$$

where the angle of attack of the plane of no feathering is

$$\tan \quad = \frac{\lambda}{\mu} + \frac{C_T}{2\mu\sqrt{\mu^2 + \lambda^2}} \qquad (5\text{-}4)$$

The X/L equation may be manipulated so that

$$X/L = -\tan(\alpha + a') \quad \text{where,} \quad \frac{H}{T} = \tan a' \qquad (5\text{-}5)$$

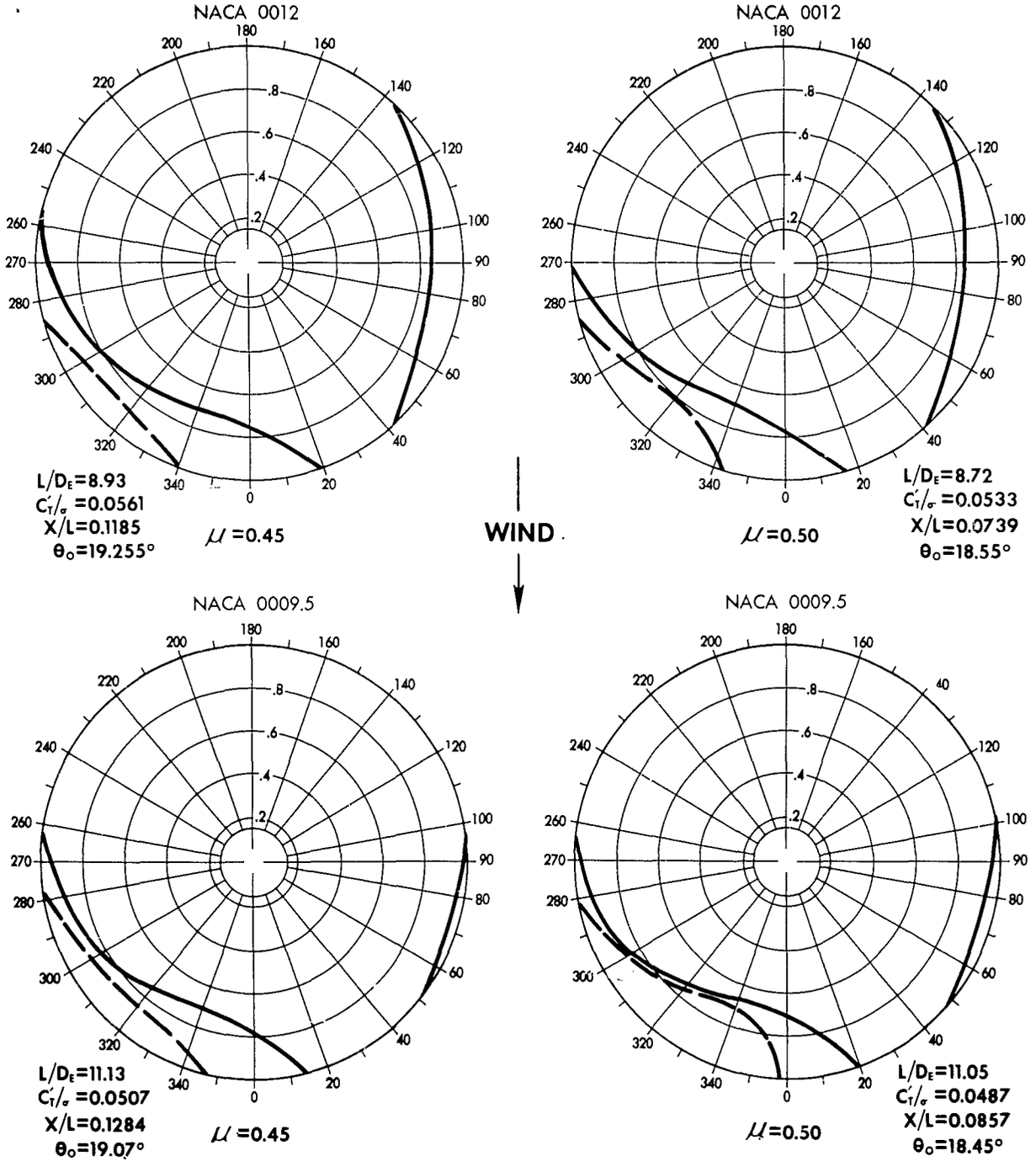
ROTOR AERODYNAMIC ENVIRONMENT

FIGURE 54 REGIONS OF STALL AND COMPRESSIBILITY

-EFFECT OF ADVANCE RATIO-

$\lambda = -0.15$ $M_t = 0.85$ $\theta_1 = -9°$

COMPRESSIBILITY ——— STALL — — — —



The effect of μ is seen to reduce both the $\frac{\lambda}{\mu}$ and $\frac{C_T}{2\mu\sqrt{\mu^2+\lambda^2}}$ terms of the angle of attack equation. Since λ in powered flight is negative, the effect is a nose up increase in α which rotates the thrust ($T \sin\alpha$) aft, an induced drag effect. Alternately, from the expression $X/L = -\tan(\alpha + a')$ this angle of attack change rotates the rotor resultant force aft.

An advance ratio may be established for each λ, M_t and θ_t, where the total propulsive force is reduced to zero. This, in effect, provides an analytical limit to forward speed for the powered rotor as required for a pure helicopter. This limit was roughly established at 250 knots with L/D_E MAX reduced to the 2 to 4 range.

Effect of Inflow Ratio

The variation of maximum L/D_E and associated C_T'/σ and X/L with inflow ratio (λ) for constant μ, θ_t and M_t is presented on Figure 63, Page 5-32. Polar Data for the discussions are NACA 0012 Reference Case 1 ($\lambda = -.15$) overlaid on Case 7 ($\lambda = -.20$). Because of the similarity in total rotor performance trands, the NACA 0009.5 has been deleted from the discussion.

The increase in propulsive force-lift ratio, X/L, with a forward inclination of the plane of no feathering is immediately reflected in the reduced maximum L/D_E. Significantly, the reduction in the vertical force coefficient, C_T'/σ, with decreasing λ produces approximately 50% of the total loss in the L/D_E ratio.

In Figure 55 below, the stall limit boundary has grown considerably with the forward inclination of the plane of no feathering. A slight increase in the drag divergence boundary, both advancing and retreating, is also significant.

The Polar Data of thrust distribution and angle-of-attack explain the basic lift loss. The major thrust reduction occurs in the inboard section of the blade and appears consistent at nearly all azimuth stations. In the reverse flow region there is a marked down load increase. The advancing tip angle of attack is consistent with $L/D_{E\ max}$, (slightly negative angles of attack), while the retreating quadrant stall region is greater.

This increase in retreating blade stall reduces $L/D_{E\ max}$ through the C_P/σ increase. Note, also, the rise of elemental profile power coefficient in the reverse flow region.

Thus, any requirement for additional propulsive force and, hence, forward inclination of the plane of no feathering will precipitate increased stall, loss in available thrust and significant increase in rotor profile drag and profile power.

A secondary increase in total aircraft L/D therefore exists for a "clean" configuration, since the rotor becomes inherently more efficient.

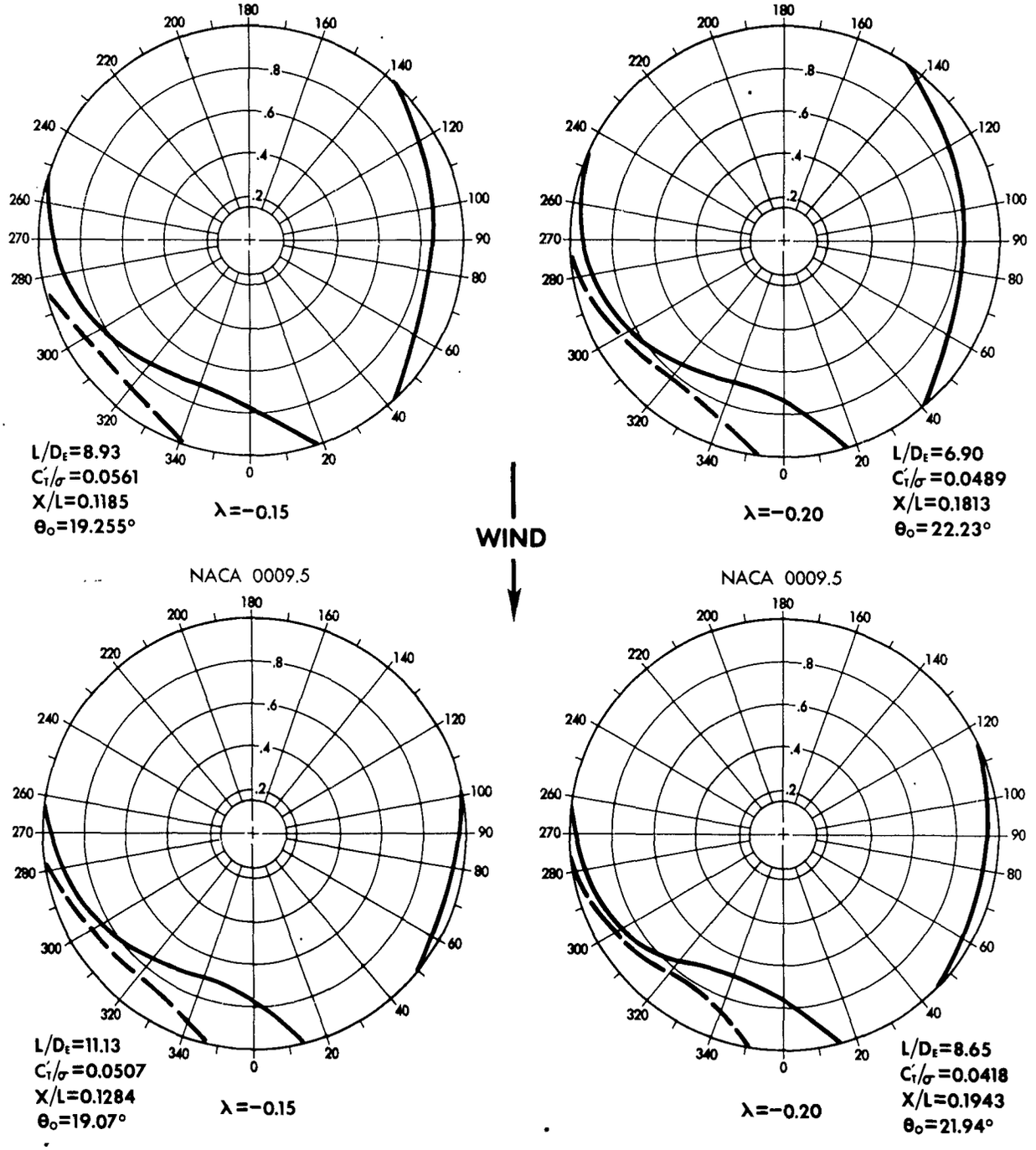
ROTOR AERODYNAMIC ENVIRONMENT

FIGURE 55 REGIONS OF STALL AND COMPRESSIBILITY

-EFFECT OF INFLOW RATIO-

μ =0.45 M_t=0.85 θ_t=-9°

COMPRESSIBILITY ——— STALL — — —



Effect of Blade Twist

During the initial periods of this contract, the increasing amount of analyzed data continued to indicate benefits in twists higher than those presently characteristic of operational helicopters. Preliminary performance data of L/D_E, C_T'/σ, and X/L was obtained for a blade twist of -9 degrees, while a minimal of data investigated the effects of twist. As shown on Figure 64, page 5-34, the advance ratio and inflow ratio under consideration ($\mu = .45$, $\lambda = -.15$) established an optimum twist (-12° to -14°) for best $L/D_{E\ max}$. Increasing twist significantly improved the C_T'/σ associated with $L/D_{E\ max}$, while the propulsive force-lift ratio decreased. Using the data from Figure 64, the increase of twist from -9 degrees to -14 degrees allows an 8 percent increase in the thrust per horsepower at constant speed and aircraft equivalent flat plate area. It is important to note that despite the loss in X/L with increasing twist, the net available propulsive remains nearly constant due to the increase in available lift as measured by C_T'/σ.

Figure 56 illustrates the effect of twist on the stall and compressibility boundaries for both the NACA 0012 and NACA 0009.5 sections, clearly establish a marked reduction in blade stall in the retreating quadrant with increasing blade twist as well as a minor reduction in retreating blade compressibility. The advancing blade compressibility boundary for the NACA 0012 appears constant with twist while the NACA 0009.5 boundary becomes more severe.

The Polar Data for this discussion are: NACA 0012 - Ref. Case 1 ($\theta_t = -9^\circ$), overlaid on Case 8 ($\theta_t = -14^\circ$).

The angle of attack distribution points out an increase in the radial gradient of section, with increasing twist. Also the movement of higher angles of attack toward the root. A reduction of approximately one degree in blade tip angle of attack along both the advancing and retreating quadrants is apparent.

The thrust distribution shows how amazingly similar - both in magnitude and station - the two twists are for the azimuth stations from $\psi = 180^\circ$ to $\psi = 360^\circ$. The net vertical force coefficient, C_T'/σ increase (from .056 at $\theta_t = -9^\circ$ to .0628 at $\theta_t = -14^\circ$) comes from the "pocket" of elemental thrust in the azimuth range $\psi = 90^\circ$ to $\psi = 180^\circ$.

Despite the increase in elemental profile power along the advancing portion of the disc (recall now that the inception of advancing blade compressibility appeared unchanged with twist and that the radial gradient of angle of attack was higher in this region), an increase in accelerating torque due to the increased negative thrust in this region is available to offset the profile drag effect. The elemental profile power in the stalled region is slightly lower reflecting the lower angle of attack.

It is seen, then, that the increase in twist reduces blade stall, moves the average radial thrust load somewhat inboard, redistributes the elemental total power, increases advancing blade elemental profile power in the compressibility region and offers approximately an 8 percent increase in available power loading.

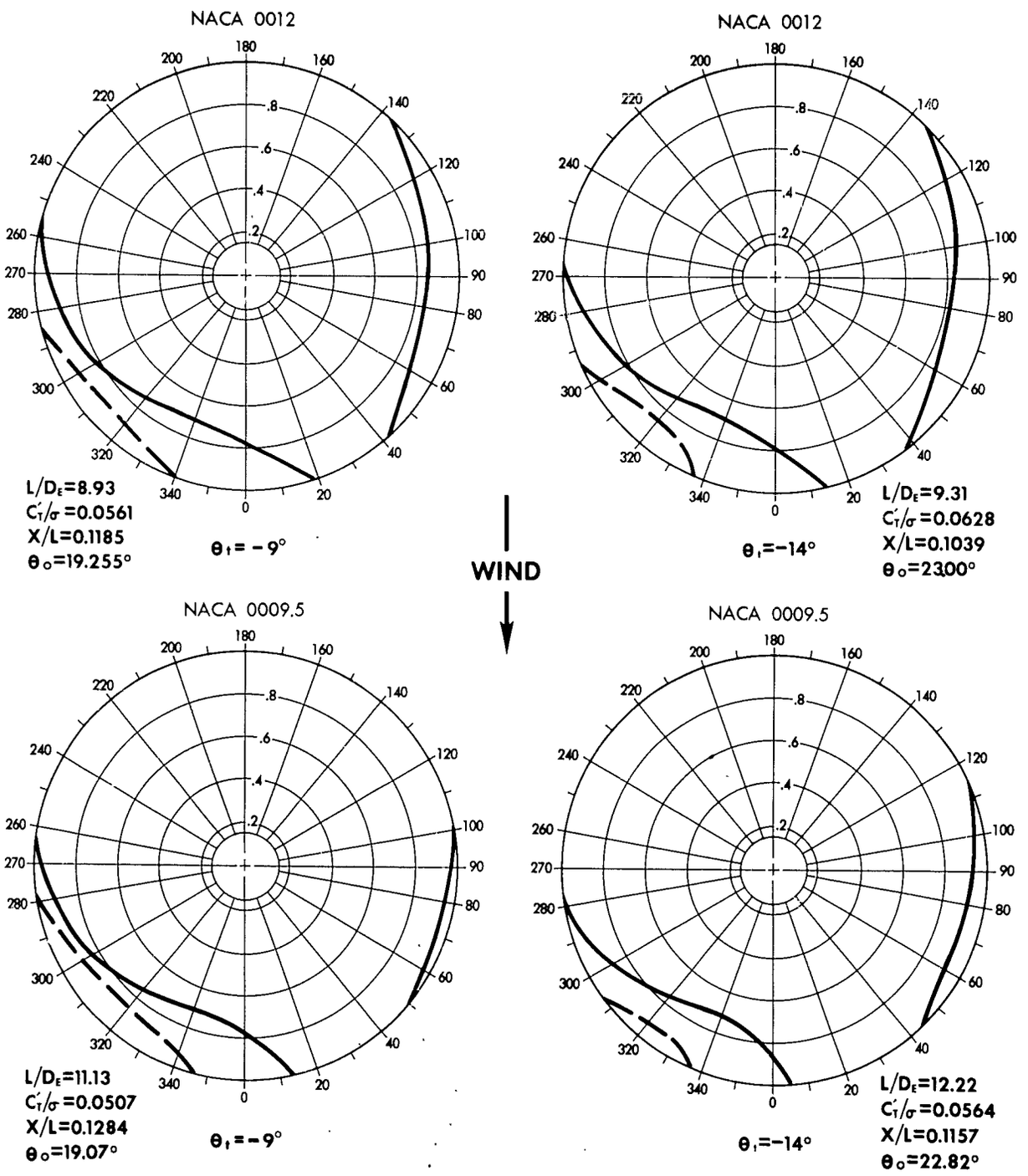
ROTOR AERODYNAMIC ENVIRONMENT

FIGURE 56 REGIONS OF STALL AND COMPRESSIBILITY

-EFFECT OF BLADE TWIST-

$\mu = 0.45$ $\lambda = -0.15$ $M_t = 0.85$

COMPRESSIBILITY ——— STALL — — — —



Effect of Airfoil Properties

One of the major aspects of the rotor performance is the nature of the airfoil section in terms of minimum drag coefficient at low Mach number, the drag divergence Mach number, the maximum lift coefficient at the moderate Mach numbers of the retreating blade and the drag rise as stall is approached.

The NACA 0012 section was considered first, consistent with the original intention of using a cut-down existing YHC-1B blade which incorporated that section. The 0009.5 airfoil was subsequently employed when design studies indicatedthe need for a lower thickness ratio to obtain acceptable blade dynamic characteristics. As will be shown, the use of that section also provided better matching to the aerodynamic environment.

From Figures 46 and 47, the NACA 0009.5 is suspected of having a lower minimum drag coefficient at low Mach number, superior drag characteristics (Prior to stall) at high Mach number, but a lower maximum lift coefficient. The table below summarizes significant aerodynamic properties of both airfoil sections as they were used in the analytical program.

TABLE IV

Aerodynamic Airfoil Characteristics

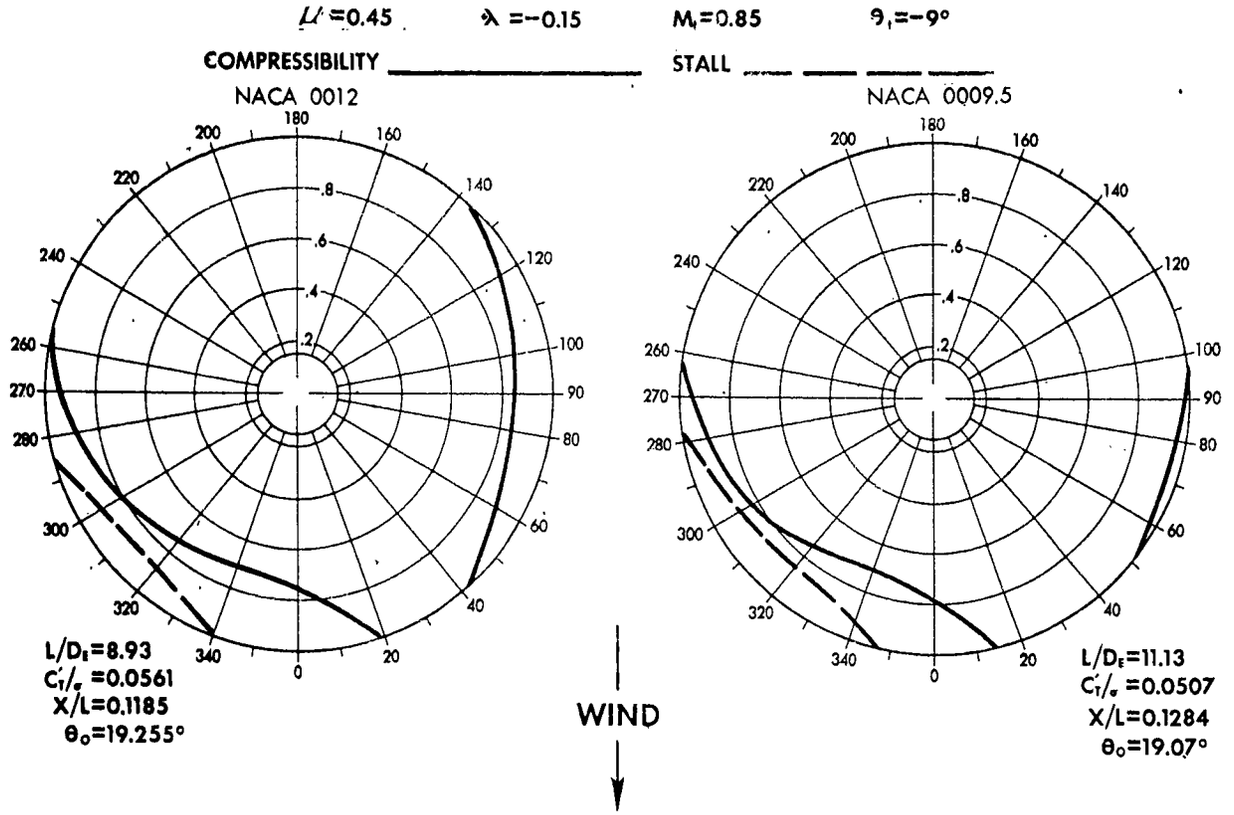
Property		NACA 0012	NACA 0009.5
Min. Drag Coefficient	@ $\alpha = 0^\circ$, $M = .3$	.0078	.0068
Drag Divergence Mach No.	@ $\alpha = 0^\circ$	.78	.87
Drag Coefficient at	@ $\alpha = -2^\circ$, $M = .85$	.042	.015
Angle of Attack for Max. Lift Coefficient	$M = .45$	12.0°	11.2°
Max. Lift Coefficient	$M = .45$	1.05	.95

As may be seen in Figure 61 both L/D_E and X/L for the NACA 0009.5 are superior to the NACA 0012. The cost of this performance increase apparent in the loss of available C_T'/σ (from .056 for the NACA 0012 to .051 with the NACA 0009.5).

The Regions of Stall and Compressibility in Figure 57 clearly establishes the desirability of the higher drag divergence Mach number characteristics of the NACA 0009.5. Both advancing and retreating drag divergence boundaries for the thinner section are markedly reduced. The stall limit boundary, consistent with the lower stall characteristics of the NACA 0009.5, is sharply increased.

FIGURE 57

COMPARISON OF REGIONS OF STALL AND COMPRESSIBILITY BETWEEN THE NACA 0012 AND NACA 0009.5 ROTORS



A comparison of the Polar Data is presented on the following two pages for the NACA 0012 and NACA 0009.5 sections.

ROTOR AERODYNAMIC ENVIRONMENT

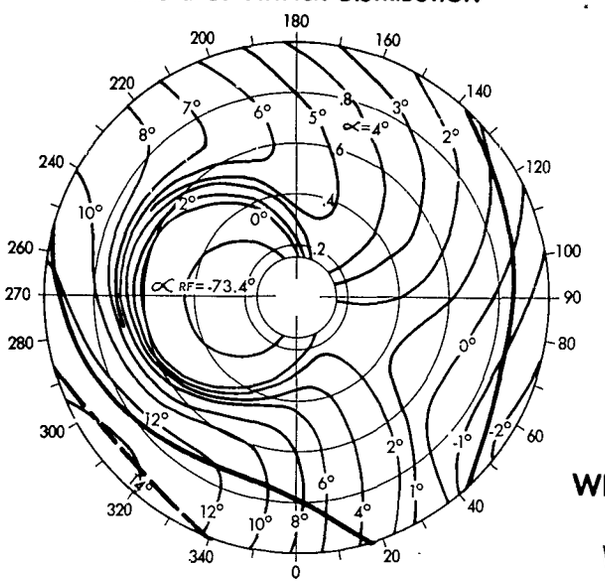
CASE 1.—NACA 0012 : BASE REFERENCE CASE

μ=0.45 λ=−0.15 M_t=0.85 θ_t=−9° θ_o=19.255° σ=0.10

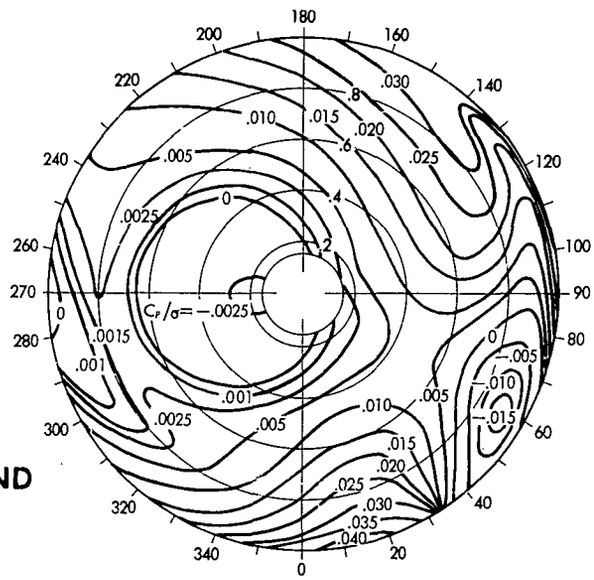
COMPRESSIBILITY ——————

STALL —— — —— — ——

ANGLE OF ATTACK DISTRIBUTION

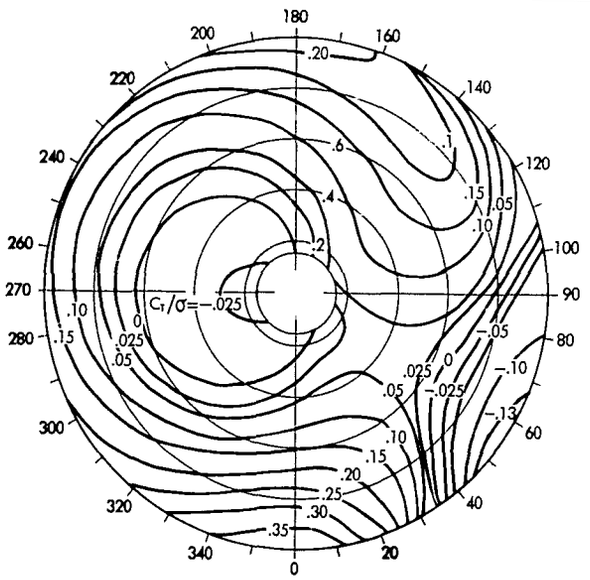


TOTAL POWER DISTRIBUTION

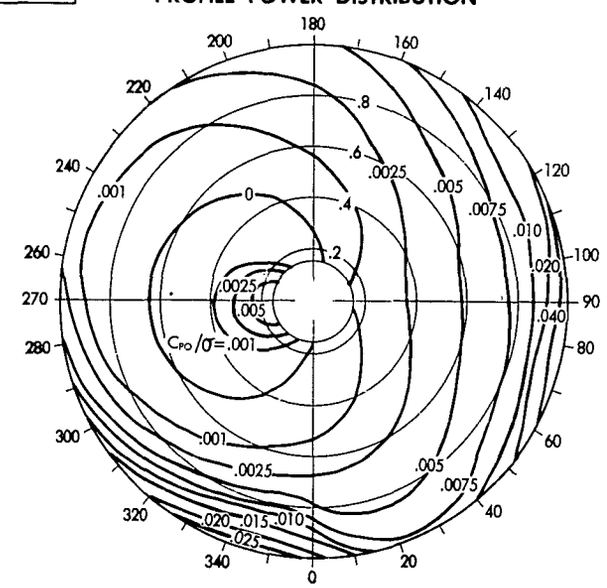


L/D_E=8.93
C_T/σ=0.0561
X/L=0.1185

THRUST DISTRIBUTION



PROFILE POWER DISTRIBUTION



ROTOR AERODYNAMIC ENVIRONMENT

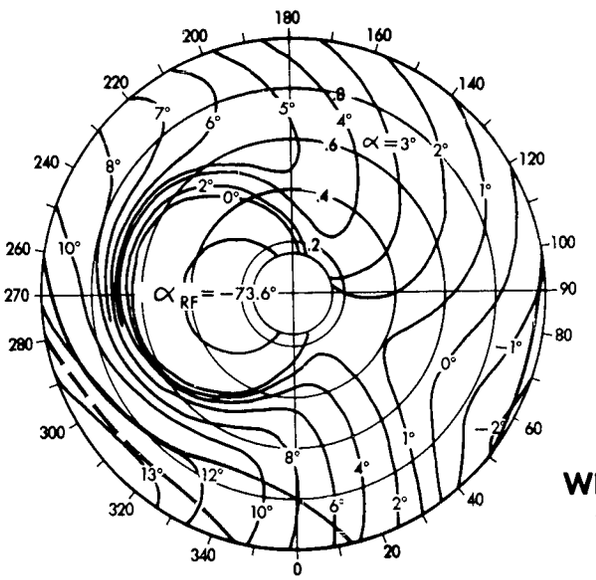
CASE 9 NACA 0009.5 REFERENCE CASE

$\mu = 0.45$	$\lambda = -0.15$	$M_t = 0.85$	$\theta_t = -9°$	$\theta_o = 19.07°$	$\sigma = 0.10$

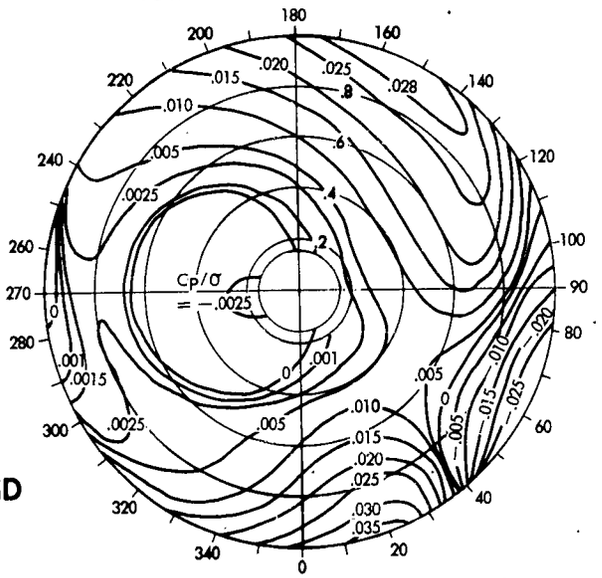
COMPRESSIBILITY ————————

STALL ———— ———— ————

ANGLE OF ATTACK DISTRIBUTION



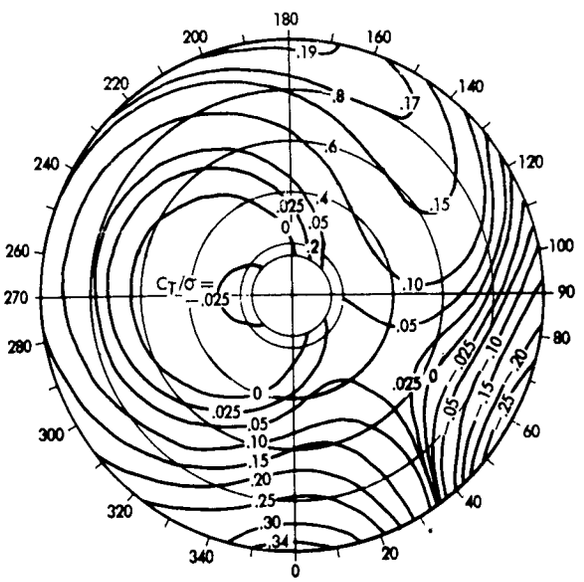
TOTAL POWER DISTRIBUTION



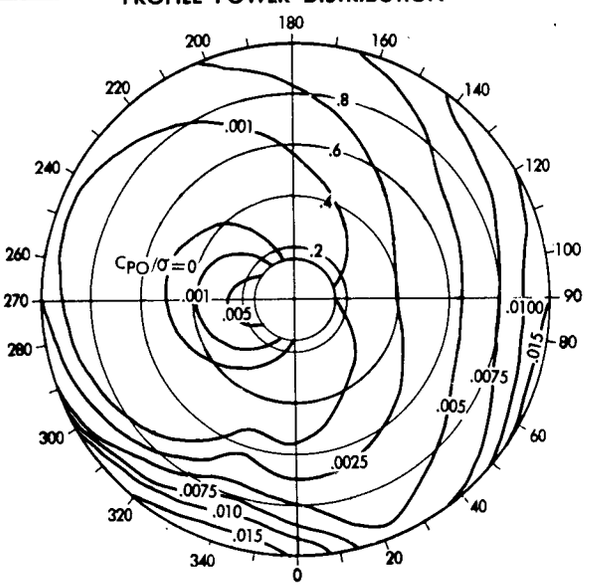
WIND

$L/D_E = 11.13$
$C^T/\sigma = 0.0507$
$X/L = 0.1284$

THRUST DISTRIBUTION



PROFILE POWER DISTRIBUTION

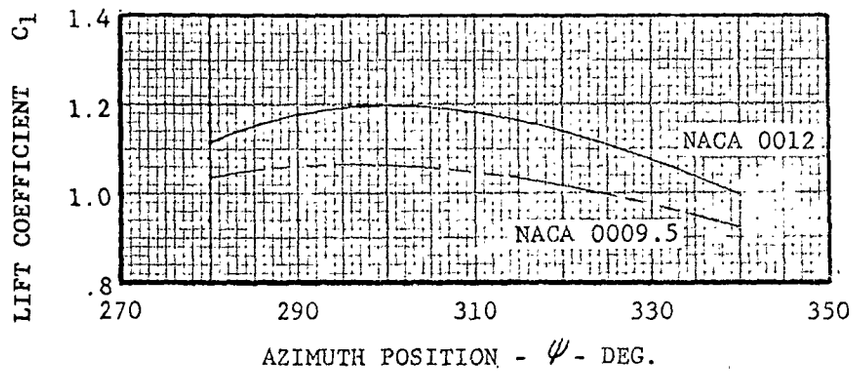


The angle of attack Polar Data is quite similar for the two cases with slight negative values along the advancing disc. Maximum L/D_E for both rotors is attained with minimal stall in the retreating quadrant, the lower $C_{l_{MAX}}$ for the NACA 0009.5 apparent from the lower angles of attack in this region.

Figure 60 below shows the variation of section lift coefficient along the stall limit boundary for both rotors. It can be seen that the stall limits represent nearly a constant C_l line.

FIGURE 60

LIFT COEFFICIENT ALONG THE STALL LIMIT BOUNDARY



The thrust distribution along the retreating quadrant for the NACA 0009.5 is only slight lower than the NACA 0012. Apparently the lower net vertical force coefficient, C_T'/σ, of the thinner section results from the large negative thrust load on the advancing portion of the disc. Blade tip loads for the NACA 0009.5 reach -.25, while the NACA 0012 is hardly above -.13. Differences of only -.01 exist in the retreating quadrant. This large download difference on the advancing disc is due to the higher lift curve slope of the thinner section.

Thus, the C_T'/σ associated with $L/D_{E\ MAX}$ for the NACA 0009.5 is lower than that for the NACA 0012, not because of its lower stall lift coefficient, but because of its higher lift curve slope in the compressibility region which leads to advancing blade download due to the negative angles of attack in this region.

The elemental profile power coefficient distribution illustrates the effect of reduced section drag characteristics. The advancing blade C_{P_O}/σ values do not significantly suggest compressibility and distinct differences in the reverse flow between the two rotors are not evident. In fact, the profile power associated with the stalled area of the NACA 0012 is higher than the NACA 0009.5

It is apparent from the total elemental power coefficient distribution that both airfoils contribute equally to stall and retreating blade compressibility. The major difference in total power appears due to the C_p/σ distribution in the azimuth range from $\psi = 40$ degrees to $\psi = 90$ degrees where the negative thrust load of the NACA 0009.5 yields a significant accelerating power.

Since the NACA 0009.5 must operate at a slightly lower C_T'/σ to achieve its higher L/D_E, it is imperative that superiority of the thinner section be established for the higher tip speed which would be used at equal gross weight.

If the design conditions of equal rotor lift (L), rotor area (bcR), aircraft equivalent flat plate area (f_e), and forward speed remain for a rotor having NACA 0012 section and one with NACA 0009.5 section, the thinner section tip speed must be:

$$V_{t0009.5} = V_{t0012} \sqrt{\frac{(C_T'/\sigma)_{0012}}{(C_T'/\sigma)_{0009.5}}}$$

The table below summarizes a comparison of these two rotors

TABLE V

Comparison of Rotor Performance

Item		NACA 0012 Ref. Case 1	NACA 0009.5 Ref. Case 9	Adjusted Tip Speed NACA 00009.5
		.45	.45	.4295
M_t		.85	.85	.8786
C_T'/σ		.05611	.05071	.05071
		-.15	-.15	-.128
X/L		.1185	.1284	.1185
L/D_E		8.931	11.13	11.6
V_t	fps	653	653	685
V	knots	174	174	174
Blade Area	ft^2	143.8	143.8	143.8
Rotor Lift	lbs	8200	7400	8200
f_e	ft^2	9.48	9.28	9.48
R HP	hp	1011	865	897
Power Loading	lbs/hp	8.1	8.55	9.14

It is apparent then, that despite the fact the NACA 0009.5 has a lower $C_{l\ MAX}$ its compensating lower drag leads to an excellent propulsive force and L/D_E, even if operated at a slightly higher tip speed to insure a lower C_T'/σ. Stalling on the retreating blade should be no more of a problem with the NACA 0009.5 than with the NACA 0012.

EFFECT OF MACH NUMBER ON ROTOR PERFORMANCE

$\mu = 0.45$ $\lambda = -0.15$ $\theta_z = -9°$

FIGURE 61a

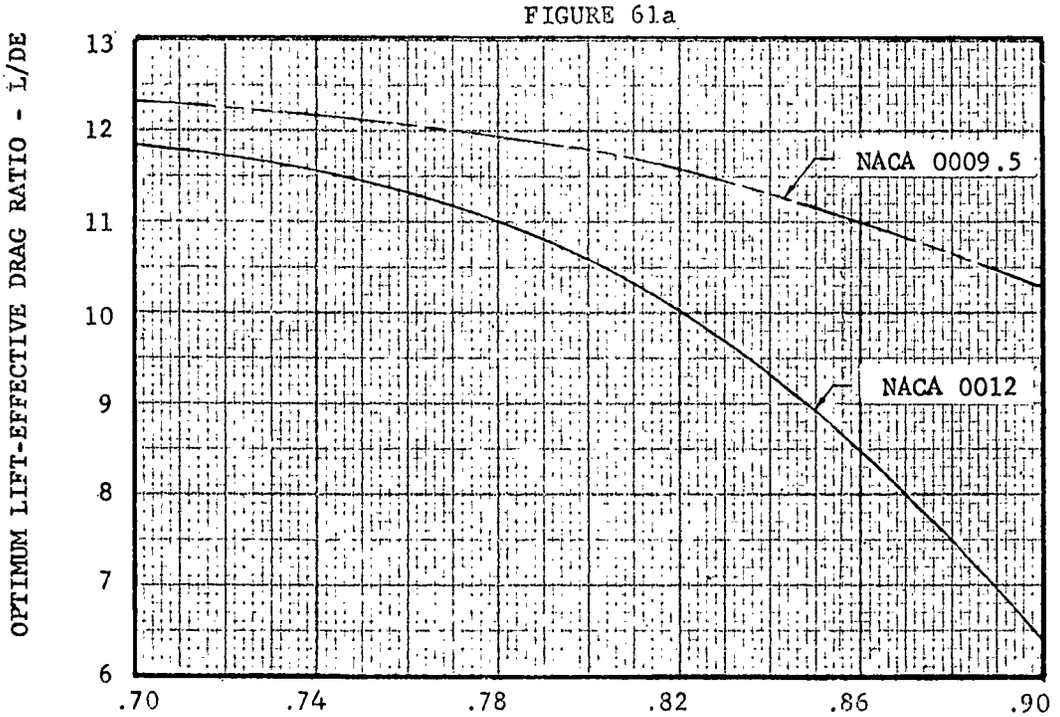
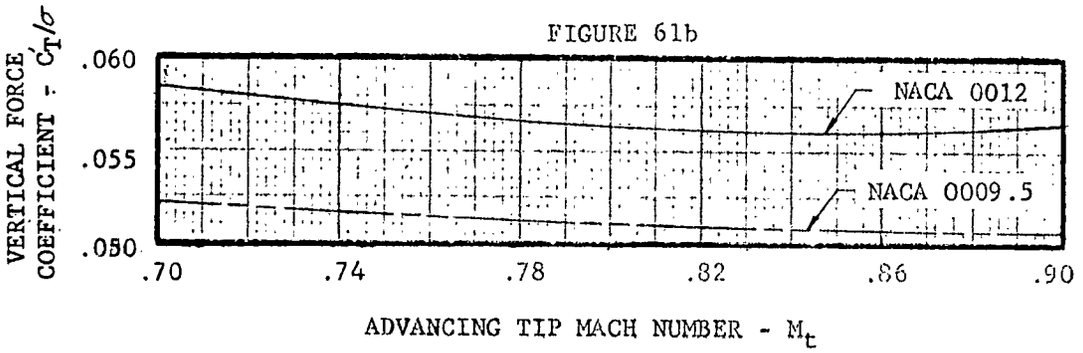


FIGURE 61b



EFFECT OF MACH NUMBER ON ROTOR PERFORMANCE

$\mu = 0.45 \quad \lambda = -0.15 \quad \theta_t = -9°$

FIGURE 61c

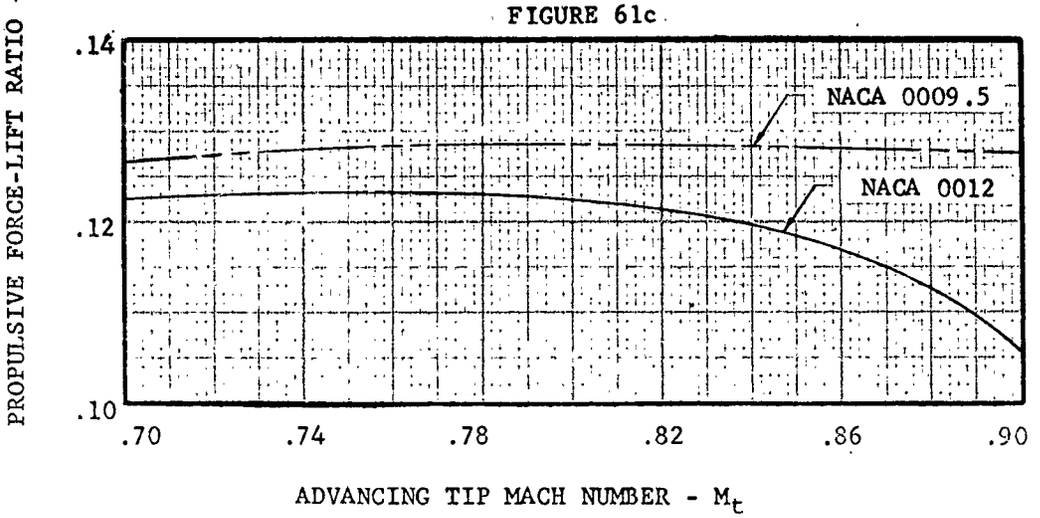
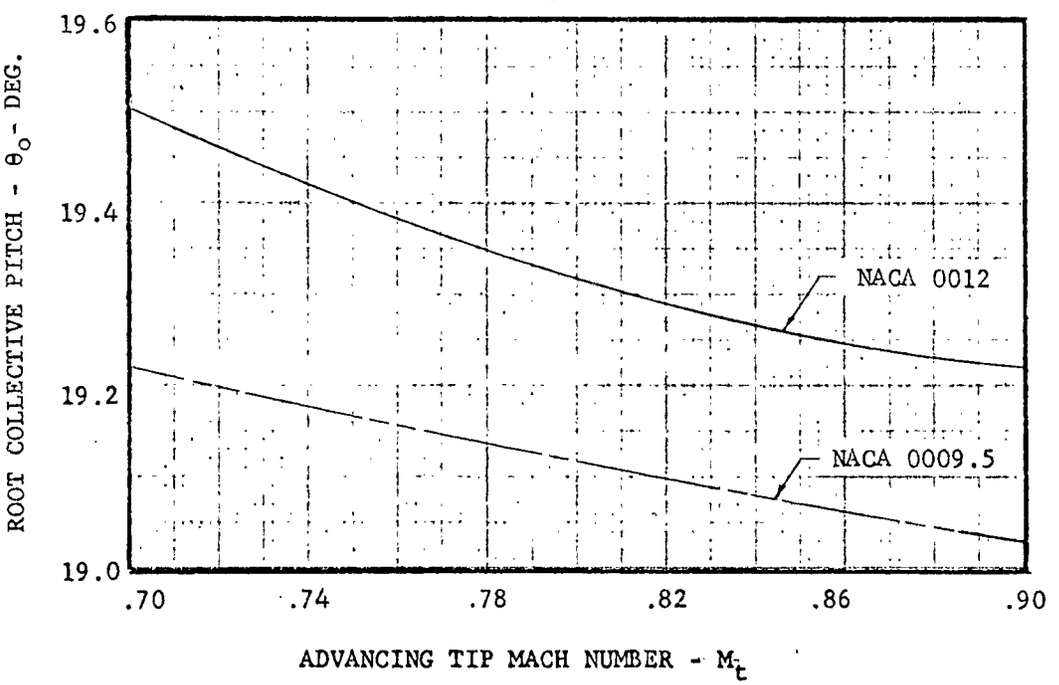


FIGURE 61d



EFFECT OF ADVANCE RATIO ON ROTOR PERFORMANCE

$\lambda = -0.15$ $M_t = 0.85$ $\theta_t = -9^\circ$

FIGURE 62a

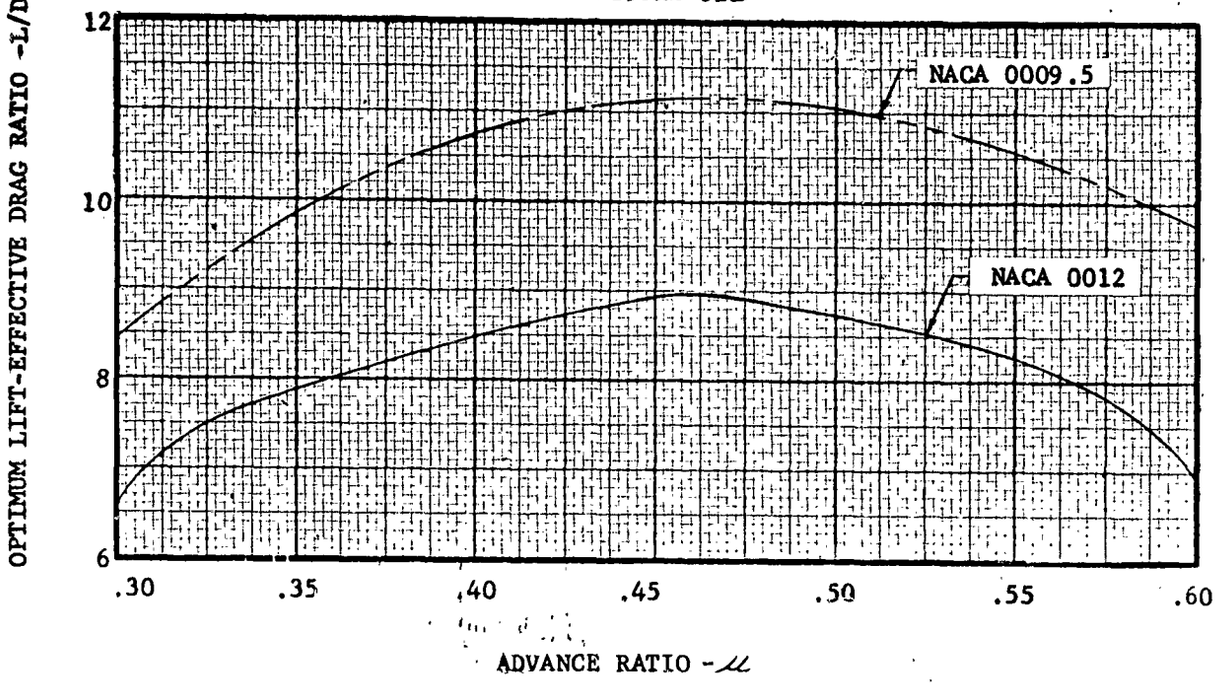
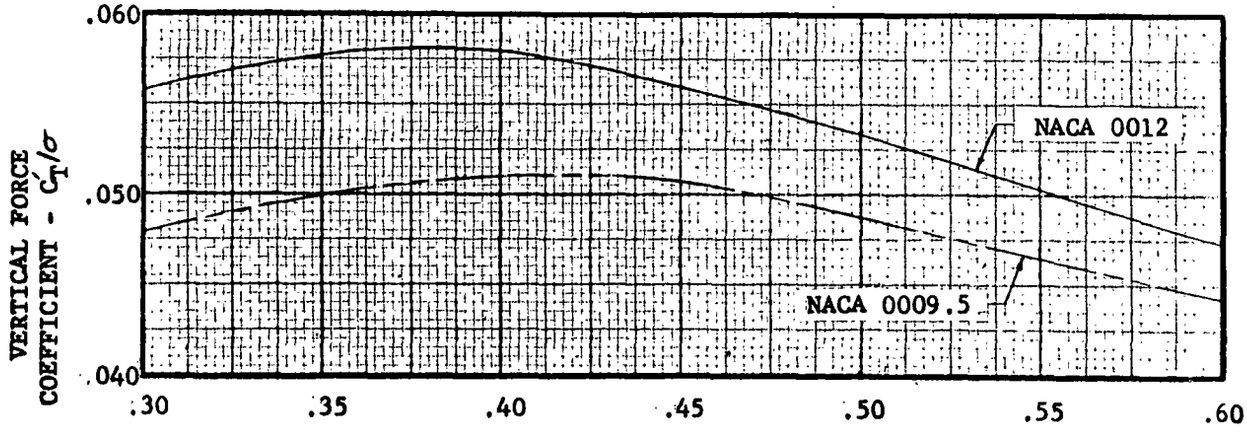


FIGURE 62b



EFFECT OF ADVANCE RATIO ON ROTOR PERFORMANCE

λ = - 0.15 M_t = 0.85 θ_t = -9°

FIGURE 62c

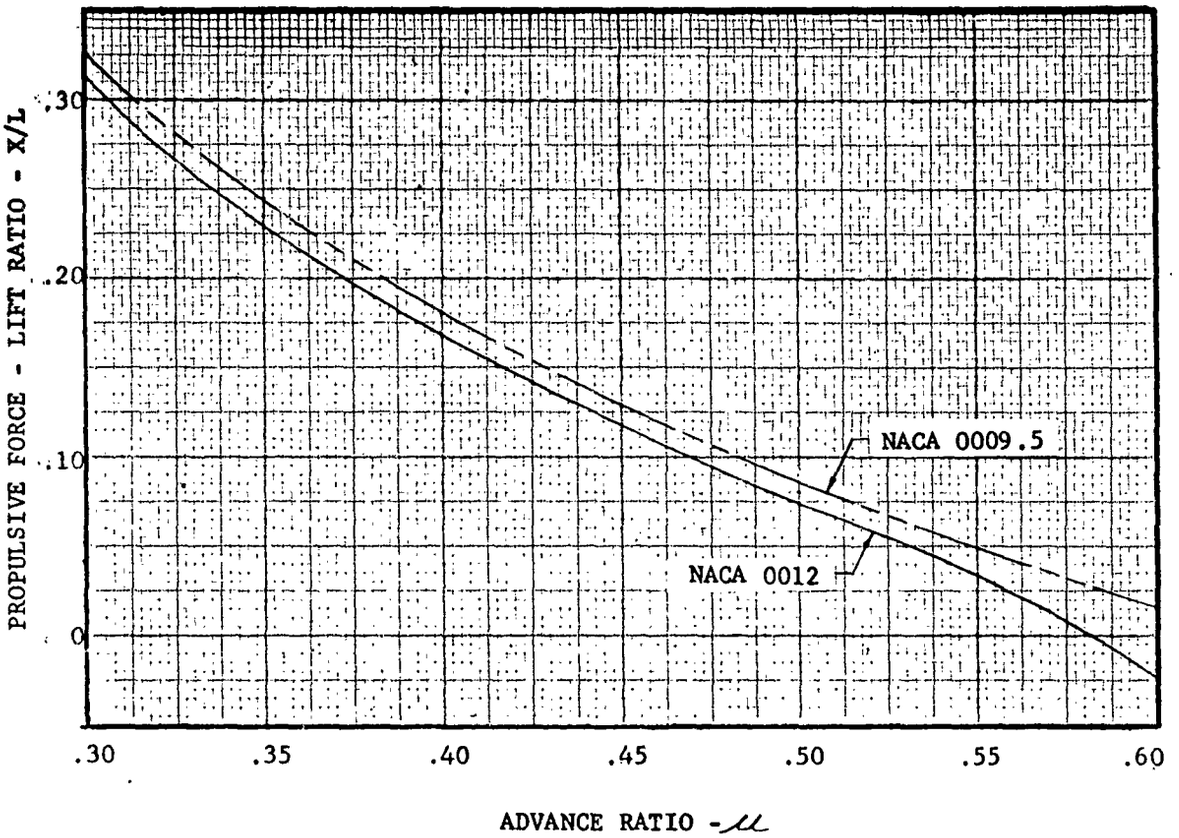
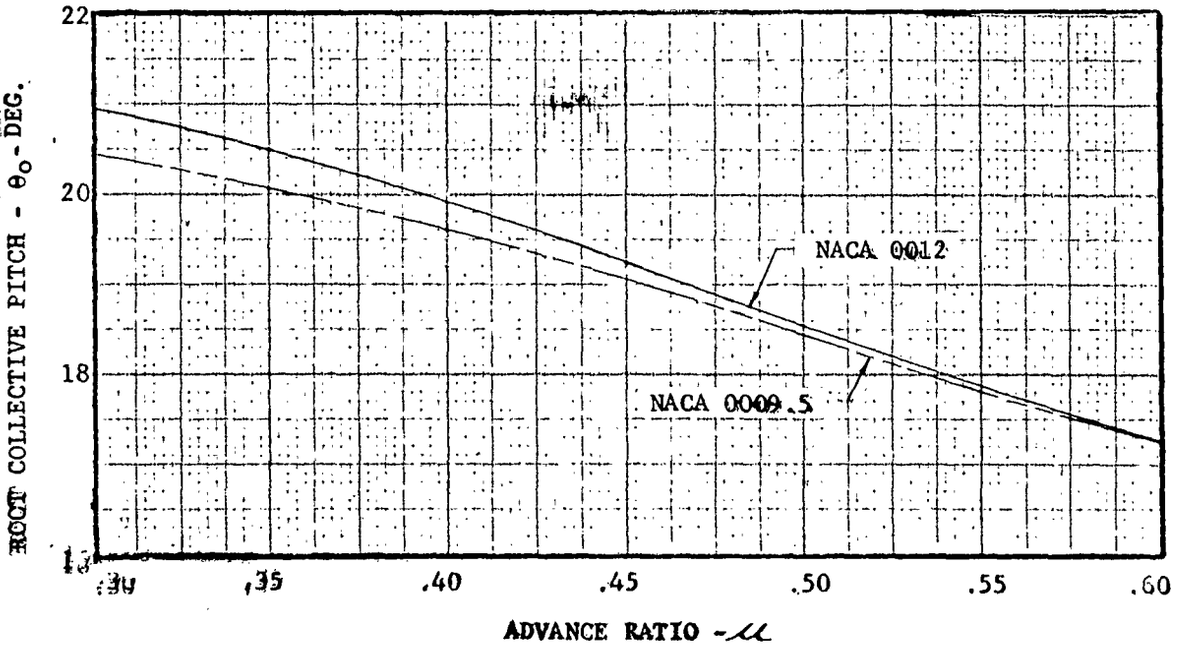


FIGURE 62d



EFFECT OF INFLOW RATIO ON ROTOR PERFORMANCE

$\mu = 0.45$ $M_t = 0.85$ $\theta_t = -9^\circ$

FIGURE 63a

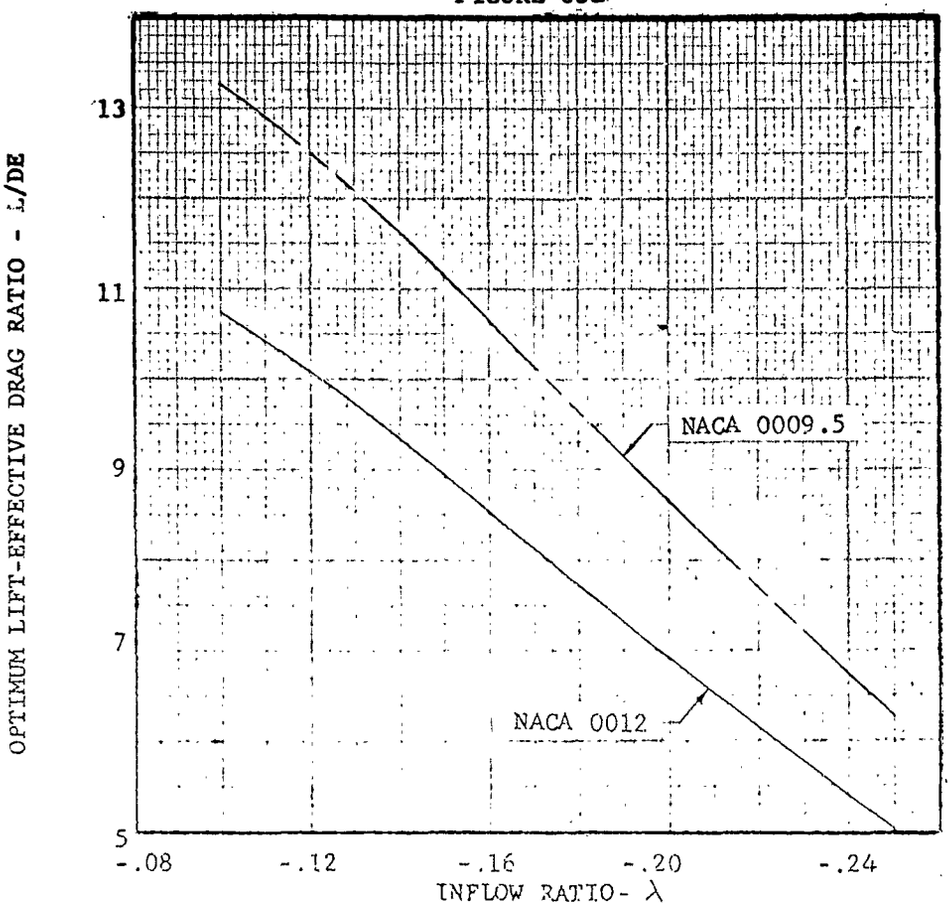
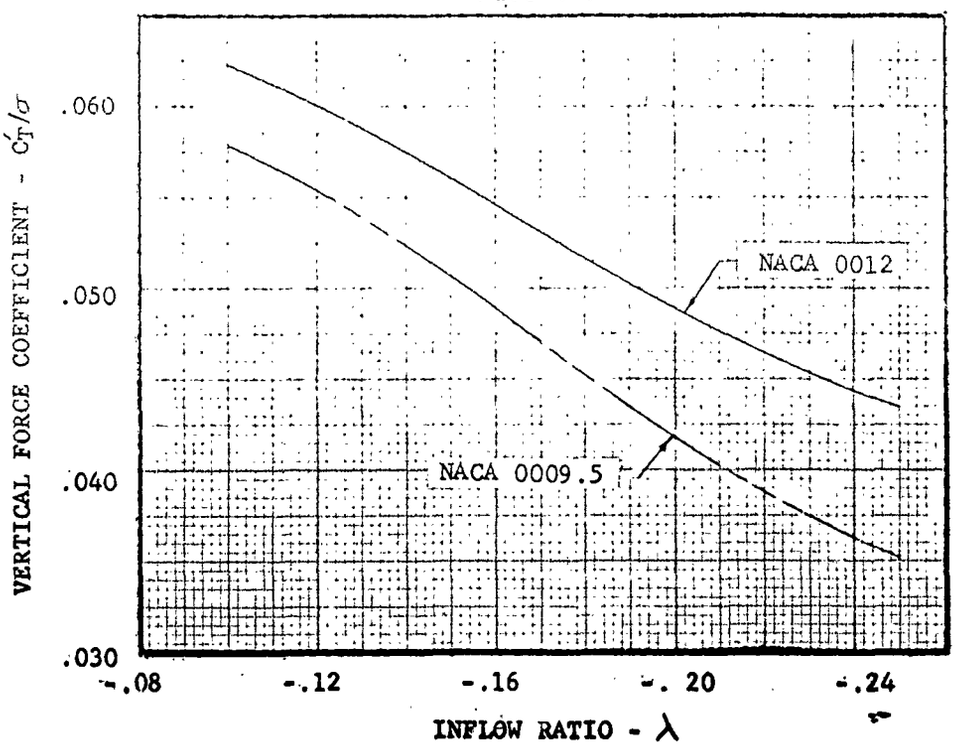


FIGURE 63b



EFFECT OF INFLOW RATIO ON ROTOR PERFORMANCE

μ = 0.45 M_t = 0.85 α_s = -9°

FIGURE 63c

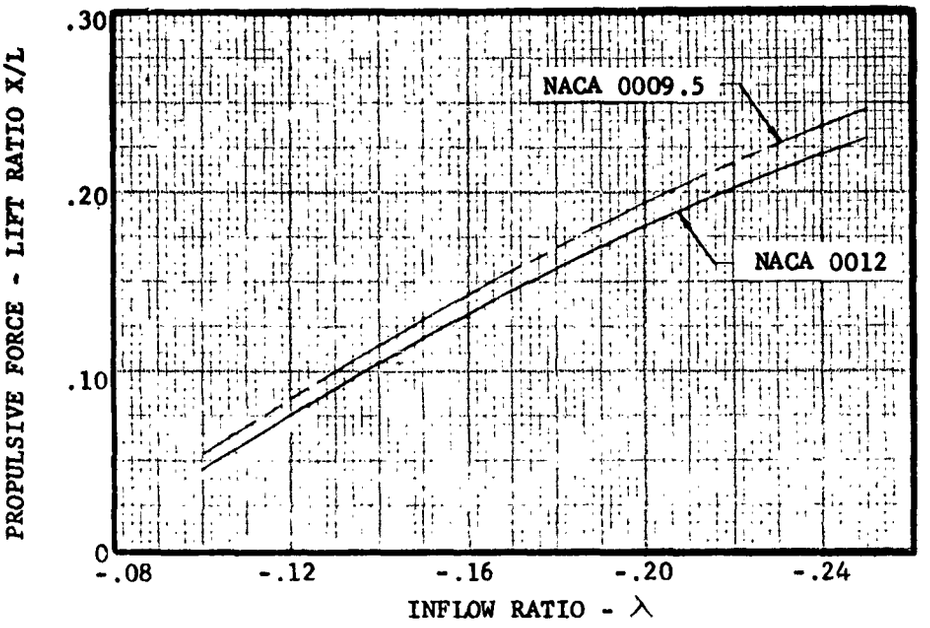
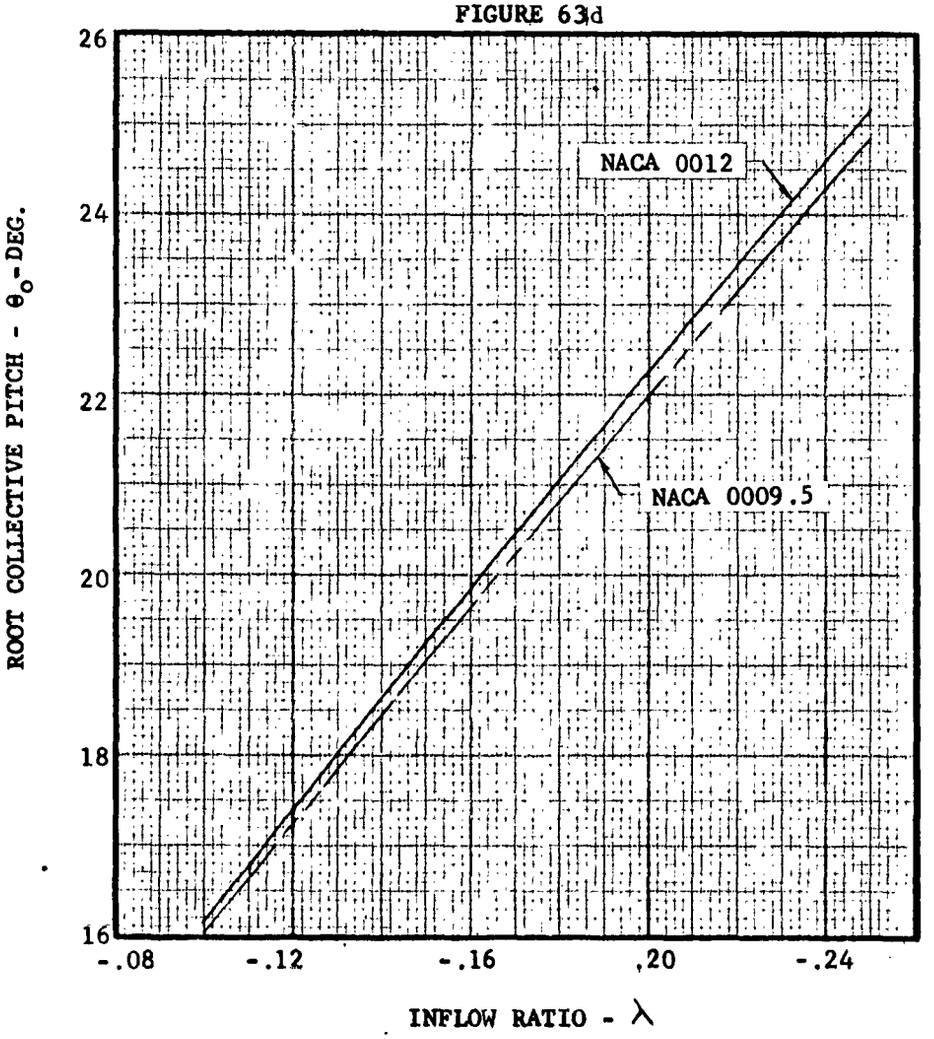


FIGURE 63d



EFFECT OF BLADE TWIST ON ROTOR PERFORMANCE

μ = 0.45 λ = -0.15 M_t = 0.85

FIGURE 64a

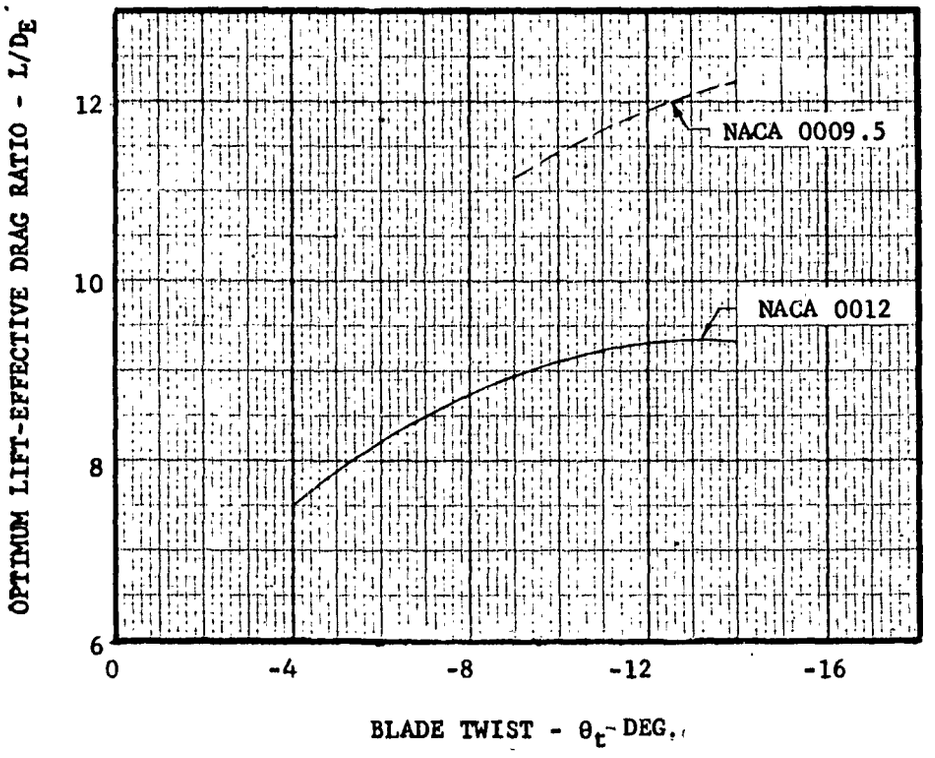
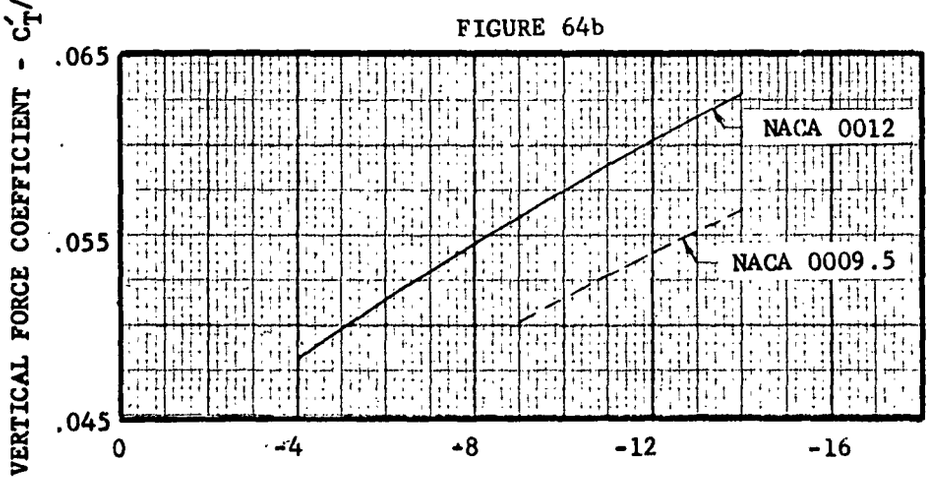


FIGURE 64b



EFFECT OF BLADE TWIST ON ROTOR PERFORMANCE

μ = 0.45 λ = -0.15 M_t = 0.85

FIGURE 64c

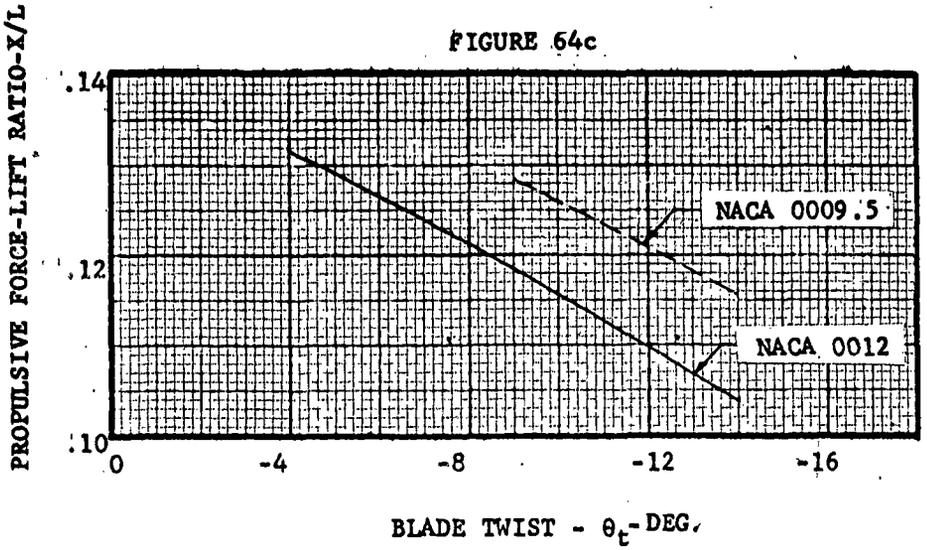
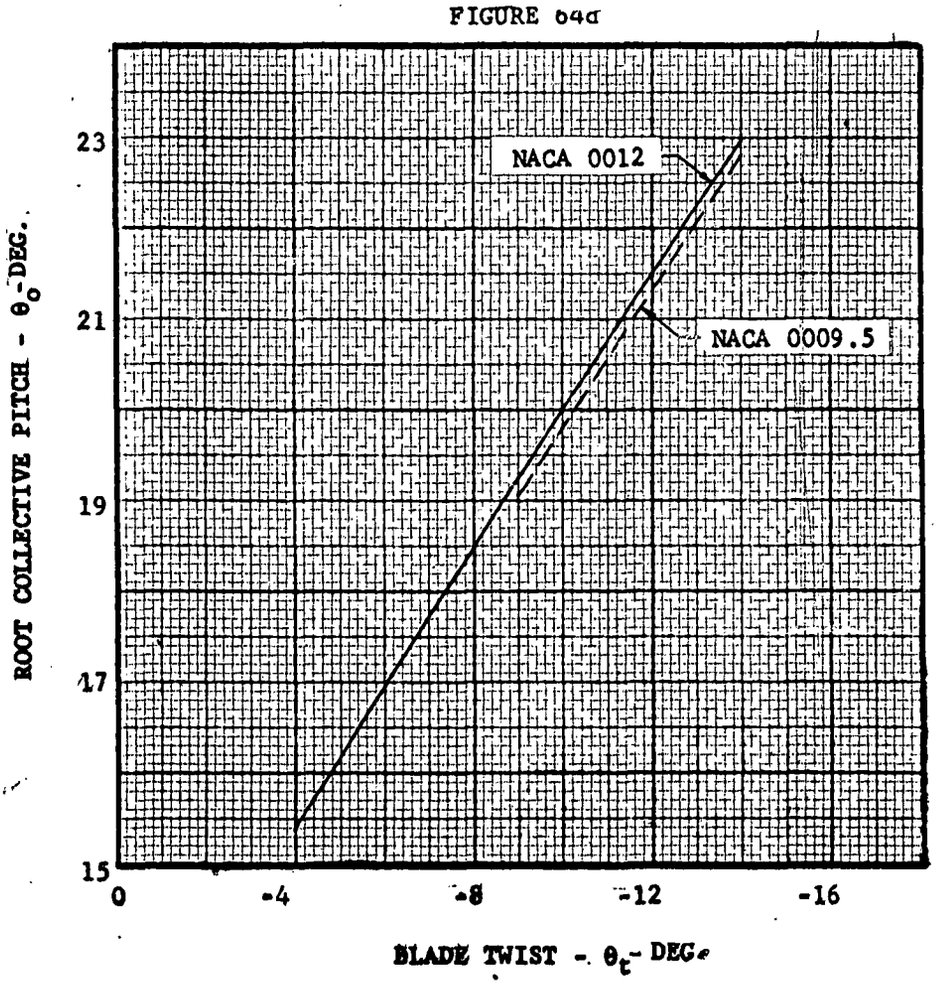


FIGURE 64d



SUMMARY

Aerodynamic preliminary design was begun on the High Performance 107-II during the Phase II portion of this contract. Detailed performance characteristics and flying qualities were established, wind tunnel tests were made, and a review of all supporting programs which might reflect into the design was accomplished.

The performance studies indicated that the High Performance 107-II will meet the contractual requirements of range (1600 n. miles) and speed 200 mph (174 knots), but because of the reduced short-range payload characterictics caused by empty weight increases, this configuration is not regarded as an acceptable operational aircraft.

The studies of aircraft flying qualities demonstrate that the increased performance is achieved without detrimental static and dynamic stability effects. The increased aft pylon area along with the Boeing-Vertol designed stability augmentation system insures flying qualities characteristic of the present 107 YHC-1A helicopter series.

The static wind tunnel tests conducted at the University of Maryland supported the drag reduction required for high performance. The 107-II parasite area of 30.2 sq. ft. was reduced to 20.5 sq. ft.

Boeing-Vertol test programs which offered supporting data to the overall study included:

1. blade specimen tests to compare aerodynamic characteristics of production blades versus ideally contoured smooth specimens at Mach numbers up to .9 and through a complete angle of attack range

2. a parasite drag reduction program on both the 107 and YHC-1B helicopters

3. hub fairing studies using a 1/3 scale powered model of the YHC-1B hub

Substantial performance increases through modest advances in the state of the art are adequately insured by these studies.

PERFORMANCE SUMMARY

Performance analysis of the High Performance 107 is necessary to demonstrate compliance with the specified minimum requirements.

These requirements were:

Ferry Range	1600 n.mi.
Maximum Speed (Sea Level)	200 mph (174 Knots)
Payload	800 lbs.

Analytical results presented in this section are summarized in the following table and clearly indicate that all requirements will be met or exceeded.

TABLE VI

PERFORMANCE DATA FOR THE HIGH PERFORMANCE 107-II

Gross Weight*	15,165 lbs.
Weight Empty	9,988 lbs.
Useful Load	5,177 lbs.
Fixed Useful Load	459 lbs.
Fuel (100 n.mi. radius @ S.L.)	1,842 lbs.
Payload (outbound only)	2,876 lbs.
Hover Ceiling @ 95°F, O.G.E.	6,000 ft.
Service Ceiling (std day @ gross wt.1 eng. @ mil power)	7,300 ft.
Max. Speed, Mil. Power @ S.L.	174 kts.
Max. Speed, NRP @ S.L.	168 kts.
Speed for Best Range, S.L.	158 kts.
Forward Rate of Climb @ NRP @ S.L.	2,200 fpm
Ferry Range	2,015 n.mi.
Ferry Range Gross Weight **	26,250 lbs.

*Hover Ceiling 6,000 ft., 95°F
**500 fpm Rate of Climb @ NRP @ S.L.

TABLE VII

DIMENSIONS & GENERAL DATA - HIGH PERFORMANCE 107-II

OVER-ALL DIMENSIONS:	
Length	44.62 ft.
Width	15.02 ft.
Height	16.71 ft.
Distance Between Rotors	33.333 ft.
POWER PLANT:	
Designation	(2) T58-GE-8
Military Rated Power	1250 SHP
Normal Rated Power	1050 SHP
ROTOR;	
Number of Blades	3
Radius	25.0 ft.
Chord	23.0 in.
Solidity	.07321
Airfoil Section	NACA 0009.5
Blade Twist	-14.0 deg.
Swept Disc Area	3925 ft^2
WEIGHTS:	
Mission Design Gross Weight	18,450 lbs.
Gross Weight	15,165 lbs.
Maximum Alternate Gross Weight	26,250 lbs.
Empty Weight	9,988 lbs.
Fixed Useful Load	459 lbs.
Normal Fuel Capacity	2,275 lbs.
LOADINGS:	
Normal Disc Loading	3.864 lbs/ft^2
Power Loading (Normal G.W. @ Mil. Power)	8.466 lbs/SHP

TABLE VIII

WEIGHT BREAKDOWN - HIGH PERFORMANCE 107-II

Rotor Group		1,964 lbs.
Body Group		2,366
Alighting Gear		667
Flight Controls		758
Engine Section		68
Propulsion Group		2,807
Instr. and Nav.		135
Electrical Group		436
Electronics Group		300
Furn. and Equipment Group		266
Air Cond. and De-Icing		164
Auxiliary Gear		44
Mfg. Variation		13
Weight Empty		9,988 lbs.
Fixed Useful Load		459 lbs.
Crew	400	
Trapped Liquids	28	
Engine Oil	31	
Gross Weight (1)		15,165 lbs.
Ferry Range Gross Weight (2)		26,250 lbs.

NOTE: (1) Hover Ceiling @ 95°F, O.G.E. = 6,000 ft.

(2) 500 fpm. Rate of Climb @ S.L., @ N.R.P., Std. NASA Atmos.

ENGINE POWER AVAILABLE AND FUEL CONSUMPTION

Two (2) General Electric T58-GE-8 engines are installed. Power ratings at sea level are 1250 SHP at Military (MIL.) .Power and 1050 SHP at Normal Rated Power (NRP).

Reference 5 describes the engine characteristics in detail.

Figure 65 presents the variation of power available with pressure altitude at MIL. and NRP ratings for various rotor tip speeds.

Figure 66 shows fuel flow variation with available power and tip speed at sea level.

FIGURE 65

ALTITUDE VS POWER AVAILABLE PER ENGINE
T58-GE-8 SHAFT TURBINE ENGINE
STANDARD ATMOSPHERE

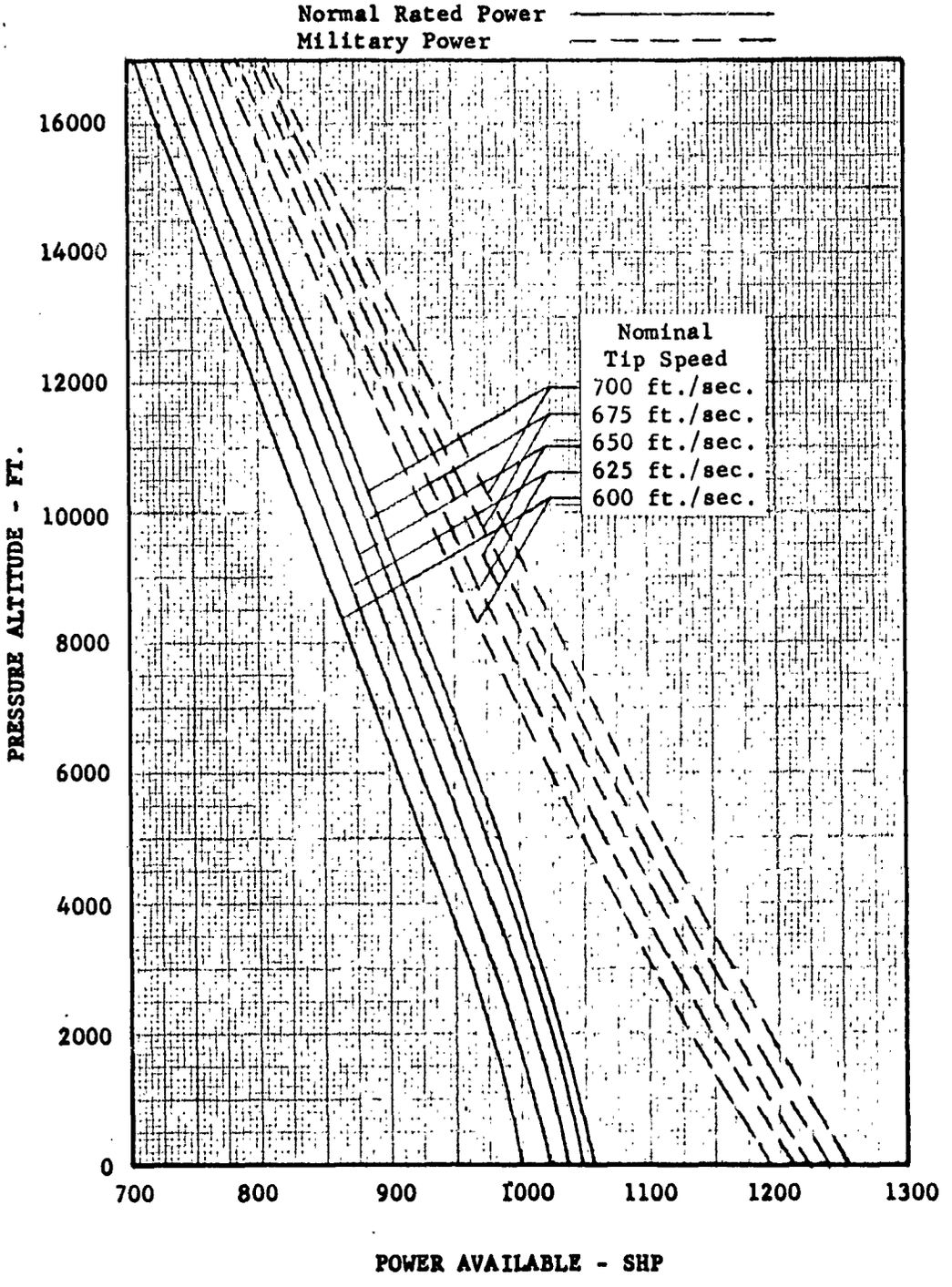
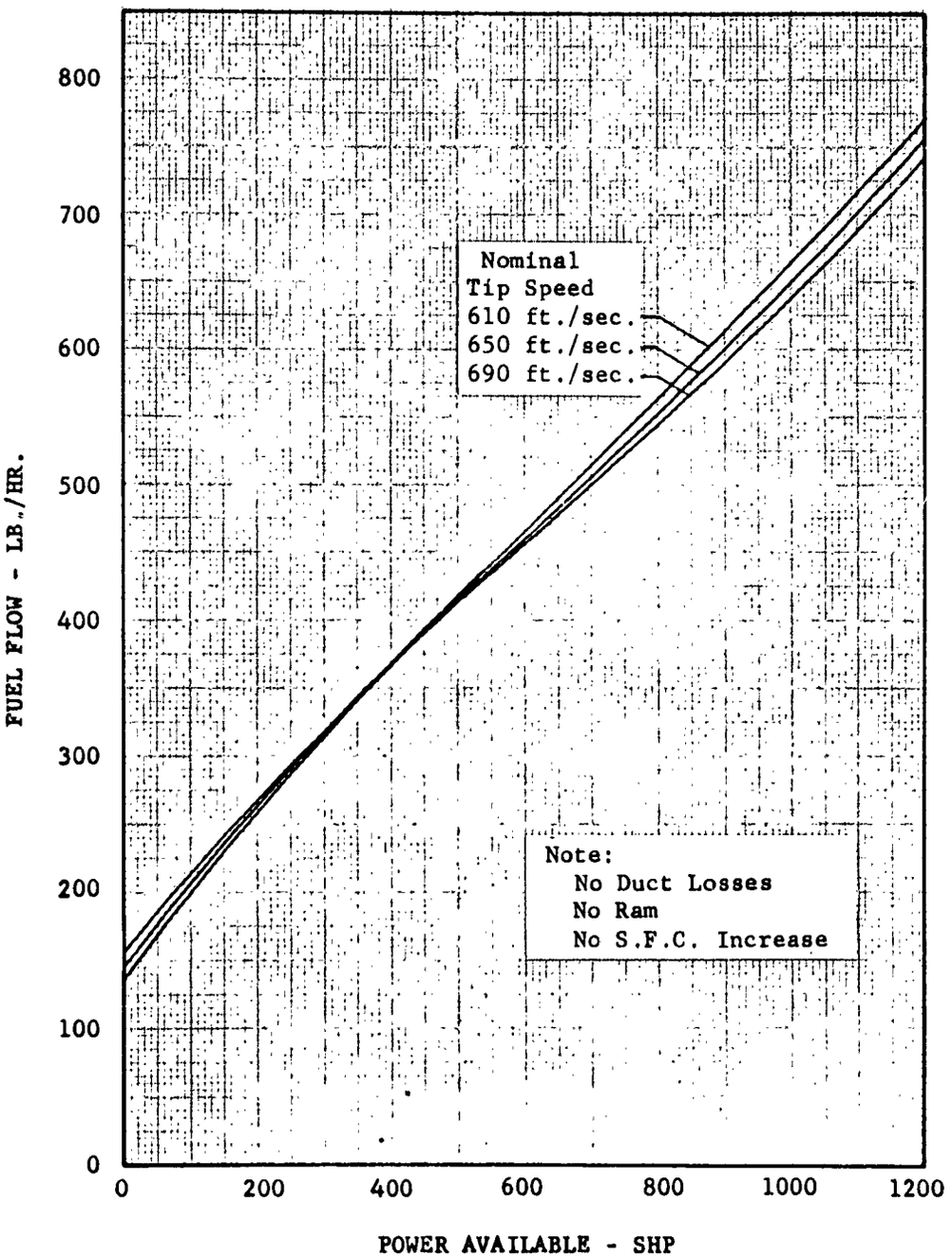


FIGURE 66

FUEL FLOW PER ENGINE VS POWER AVAILABLE
T58-GE-8 SHAFT TURBINE ENGINE
SEA LEVEL STANDARD ATMOSPHERE



AERODYNAMIC DATA

(1) Drag Analysis

Extensive wind tunnel testing backed up by flight test data on existing Vertol helicopters has facilitated drag analysis of the configuration.

The following table summarizes the equivalent flat plate drag area contributions by components.

TABLE IX

DRAG BREAKDOWN

COMPONENT	DRAG AREA
Fuselage	9.7
Wing Stubs	2.8
Rotor Hubs	5.0
Landing Gear	0
Air Inlets	1.5
Protuberances	.5
Roughness (5%)	1.0
Total (ft^2)	20.5

(2) Fuselage Lift Drag and Pitching Moment

Basic fuselage characteristics of the configuration have been obtained from extensive wind tunnel test data.

Figure 67 shows typical characteristics at zero sideslip angle as obtained from this data.

(3) Hover Download

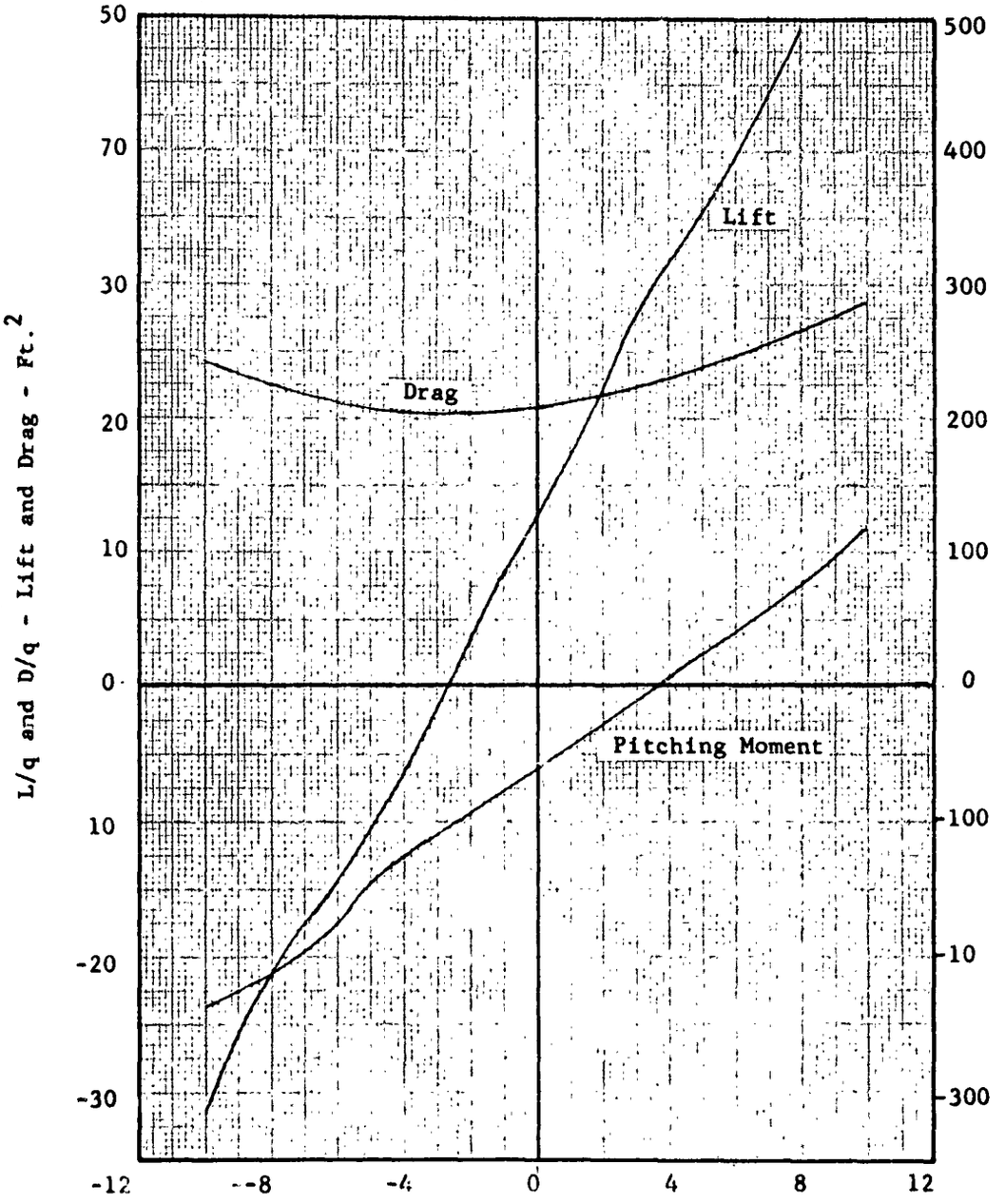
Additional power required to hover due to vertical drag or download on the fuselage has been included. This correction to hover power required is based on wind tunnel tests of the fuselage and flight test data from the Model 107 prototype and amounts to approximately a 5 percent increase in total thrust required. Rotor overlap corrections, applied to the available rotor thrust-power characteristics, further reduce total available hovering thrust.

(4) Rotor Airfoil Characteristics

A NACA 0009.5 rotor blade airfoil section is employed. This section was chosen as the result of extensive analysis which indicates that superior drag characteristics at high Mach number and acceptable blade dynamic characteristics may be obtained with a small sacrifice in maximum lift coefficient.

FIGURE 67

LIFT, DRAG, AND PITCHING MOMENT VS ANGLE OF ATTACK
HIGH PERFORMANCE 107-II
$R.N._e$ = 10,910,000



POWER AVAILABLE

(1) Transmission Losses

The drive system consists of two (2) General Electric T-58-8 gas turbine engines driving through a herringbone and spur idler gear to a common spur gear on the interconnect shaft. The interconnect shaft drives the forward and aft rotors through spiral bevel gears and planetary systems. Assuming a loss of 1% of the transmitted power for herringbone, spur, and spiral bevel gears and 1-1/2% for the planetary systems, the transmission system is estimated as 95.5% efficient.

A schematic drawing of the drive system is presented in Figure 68.

It should be noted that an increase of 2% in forward flight and 3% in hover has been included to provide a margin of conservatism in resultant performance calculations. This approach has been demonstrated to be conservative through YHC-1A and Vertol 107 prototype testing.

(2) Accessory Losses

There are five (5) groups of power driven accessories. The groups are: electrical system, flight control hydraulic system, utility hydraulic system, transmission cooling system and engine accessories.

Table X summarizes the power losses due to accessories.

TABLE X

SUMMARY OF ACCESSORY LOSSES

Electrical System	13.8 HP
Flight Control Hydraulic System	6.0 HP
Utility Hydraulic System	2.8 HP
Transmission Cooling System	6.0 HP
Engine Accessories	1.6 HP
Total	30.2 HP

(3) Transmission Torque Limit

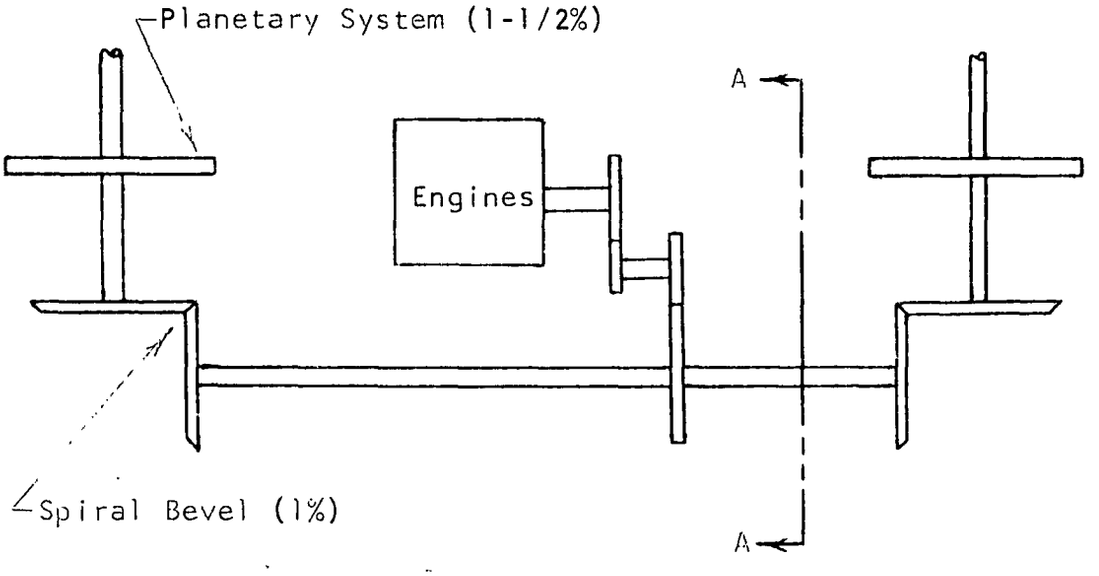
The standard versions of the Vertol 107 series have a design transmission torque limit. As a result, Military Power availability is affected under certain operating conditions. Performance calculations have been based upon transmission torque limited power.

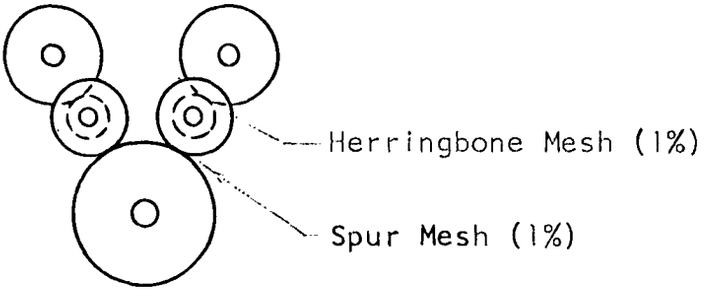
(4) **Induction and Exhaust Losses**

Theoretical analysis substantiated by flight tests on the YHC-1A and Vertol 107 prototype indicates that zero loss may be conservatively assumed in forward flight. The loss of power resulting from duct pressure loss which exists at hover is offset by ram pressure at even moderate forward speeds. A 0.6% loss is used for hover.

FIGURE 68

TRANSMISSION LOSSES





A - A

TOTAL LOSS = 4.5% OF TRANSMITTED POWER

METHODS OF PERFORMANCE CALCULATION

(1) Hover Power Analysis

A conventional method of calculating hover power required is used based on Goldstein's Vortex Theory of propellers using Prandtl's tip loss factor in place of Goldstein's Kappa Factor. Corrections for fuselage download, tandem rotor overlap, ground effect and compressibility are included.

Good agreement with whirl test and flight test data has been obtained with this method.

(2) Low Speed Forward Flight Power Requirements

At forward speeds up to approximately 140 knots, power required has been determined by means of a combined longitudinal trim analysis and power calculation programmed on the IBM 650 digital computer. The power calculation is based on an adaptation of NASA TN 2656.

This method of analysis has produced predicted results which are in very good agreement with flight test data on Vertol Models 44, 107 Prototype, and YHC-1A.

(3) High Speed Forward Flight Power Requirement

Extensive modifications are incorporated in the existing trim analysis and power required calculation of the IBM 650 computer. These modifications consist of empirical corrections for stall and compressibility based on detailed analysis of rotor performance incorporating NACA 0009.5 airfoil section properties with an IBM 704 digital computer program method. The IBM 704 program, based on the numerical equations and procedures for calculating the aerodynamic characteristics of lifting rotors from NASA TN's 3366 and 3747, calculates power required at high forward speeds far more accurately than the unmodified IBM 650 method.

Comparison of power calculations by the modified IBM 650 and the IBM 704 programs shows good agreement for rotors with NACA 0012 sections. Similar empirical correction procedures have been used for NACA 0009.5 section data.

FIGURE 69

ALTITUDE VS. GROSS WEIGHT
HOVER PERFORMANCE
STANDARD ATMOSPHERE

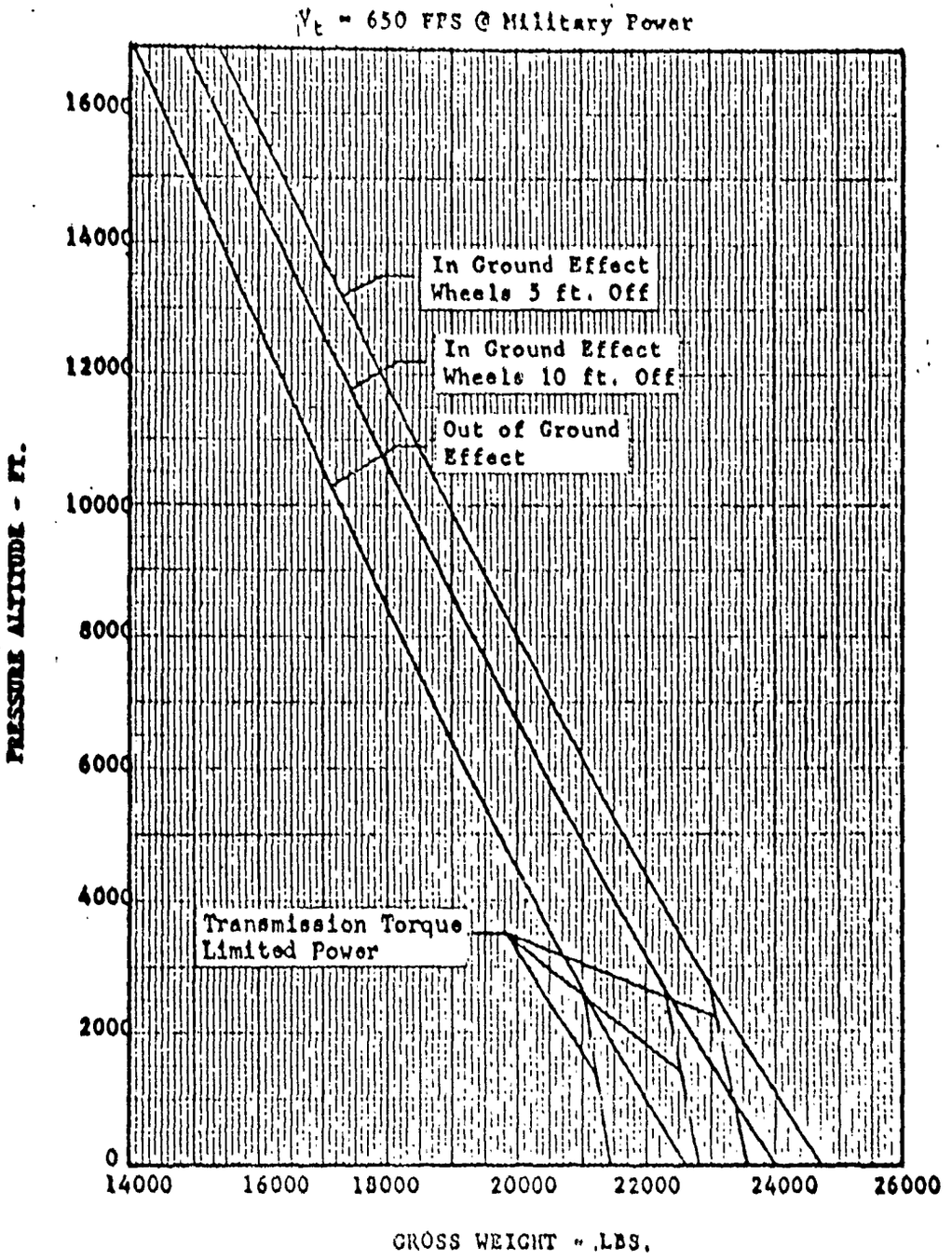


FIGURE 70

ALTITUDE VS GROSS WEIGHT
HOVER PERFORMANCE
95°F DAY

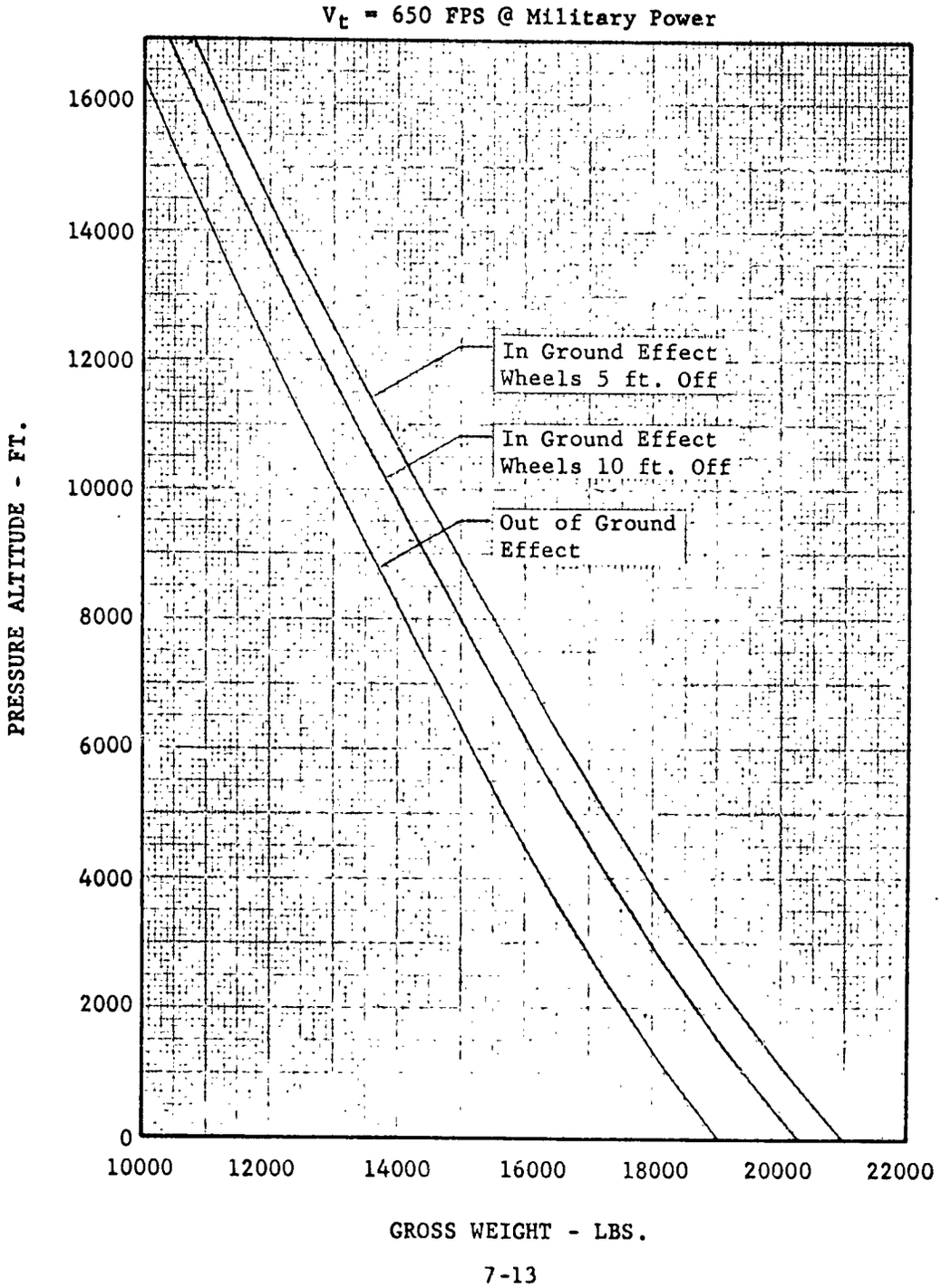


FIGURE 71

SHAFT HORSEPOWER VS. FORWARD SPEED
SEA LEVEL STANDARD ATMOSPHERE

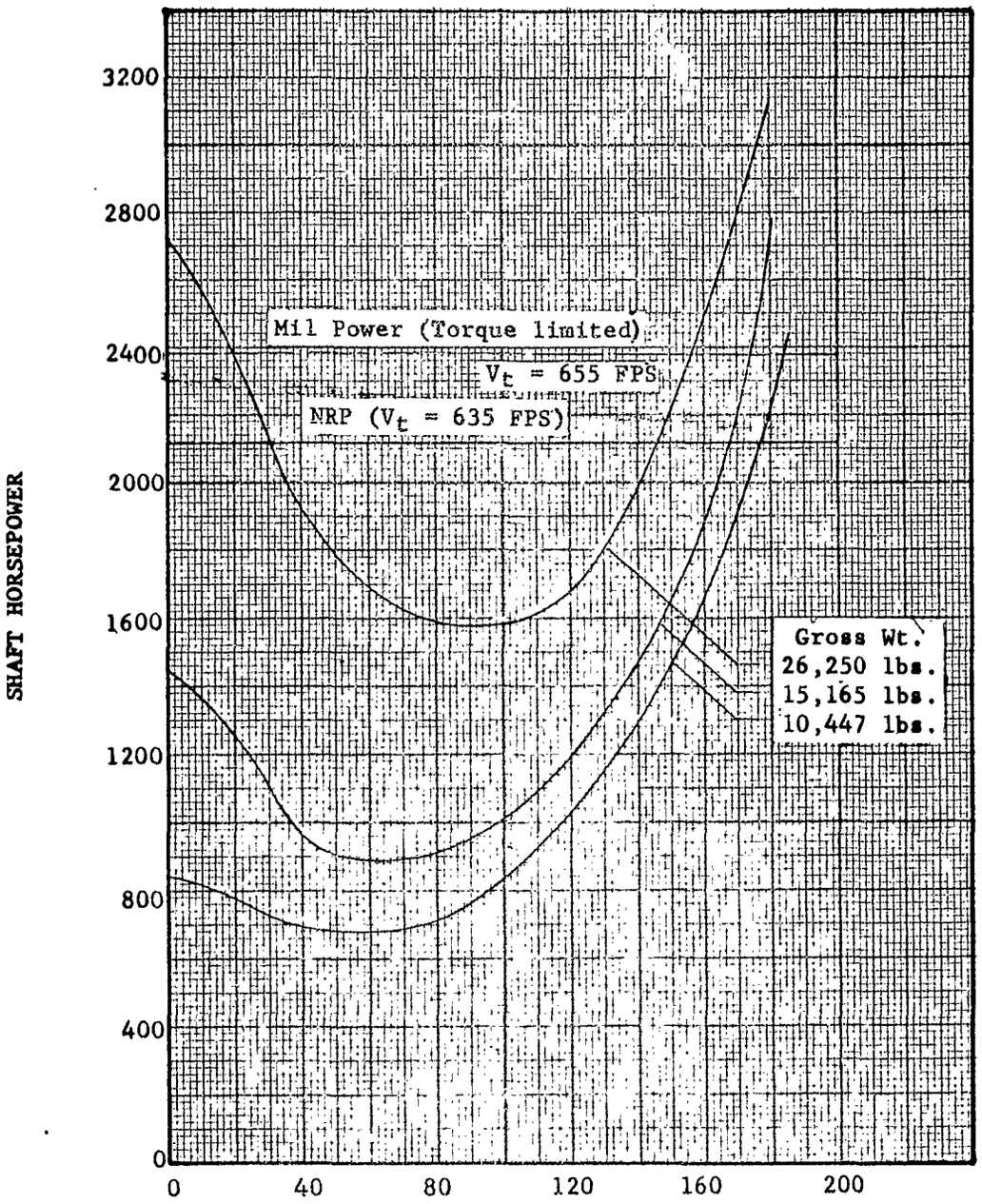


FIGURE 72

SHAFT HORSEPOWER VS RATE OF CLIMB
SEA LEVEL - STANDARD ATMOSPHERE
TIP SPEED = 625 FT./SEC.
(2) T58-8

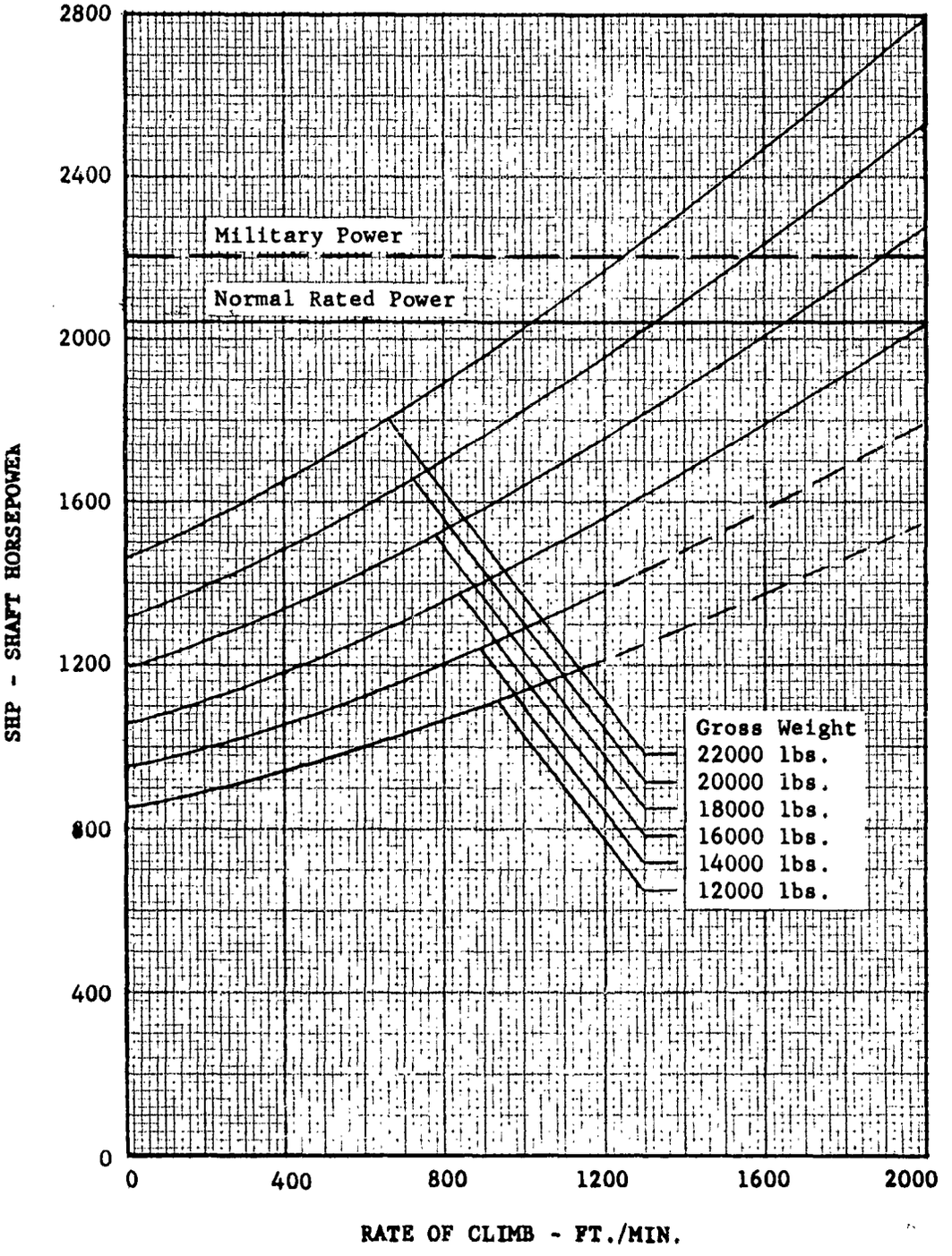


FIGURE 73

RATE OF CLIMB VS GROSS WEIGHT
SEA LEVEL STANDARD ATMOSPHERE
NORMAL RATED POWER
(2) T-58-8 ENGINES
V_k = 70 KNOTS

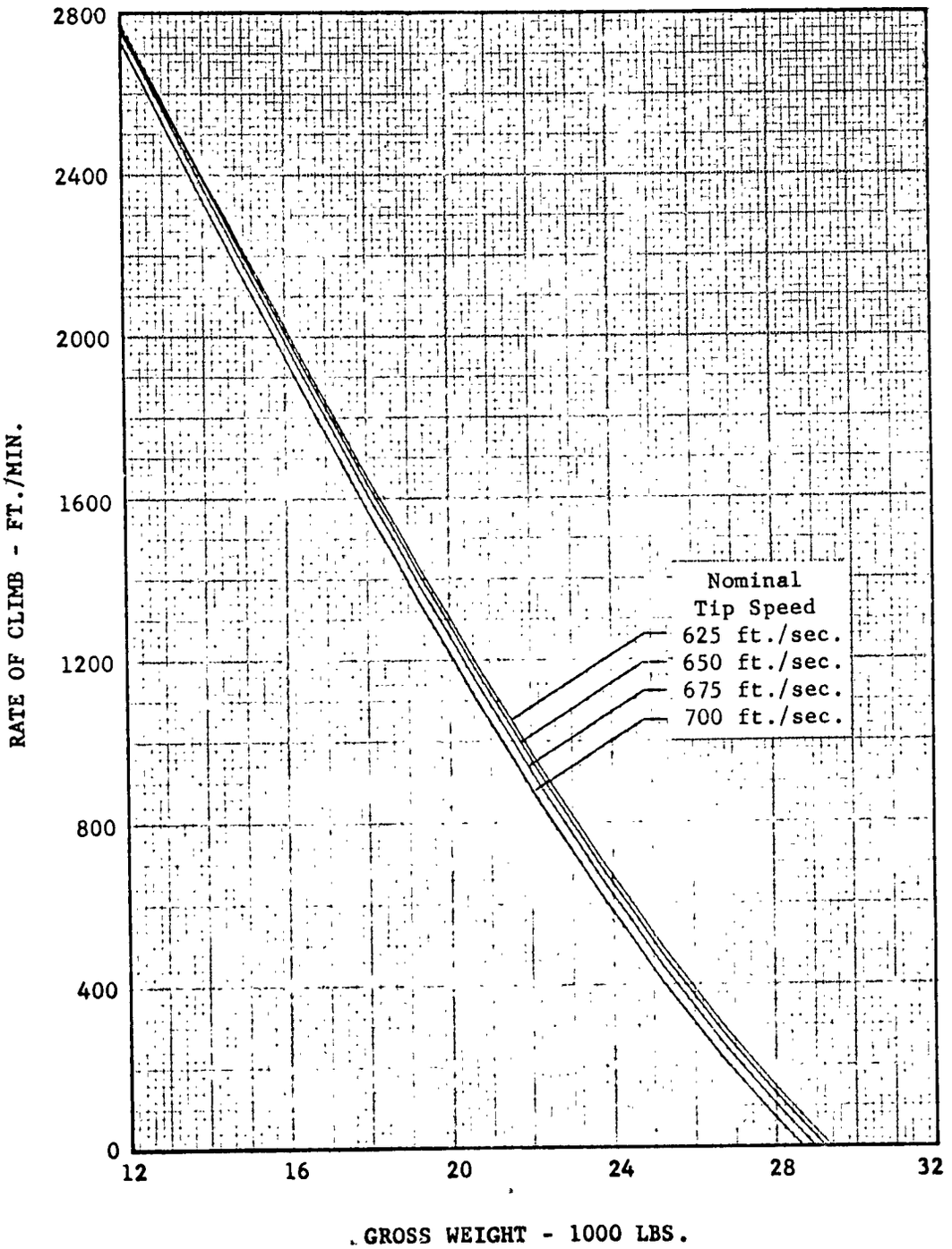


FIGURE 74

SERVICE CEILING VS GROSS WEIGHT
STANDARD ATMOSPHERE
OPTIMUM TIP SPEED

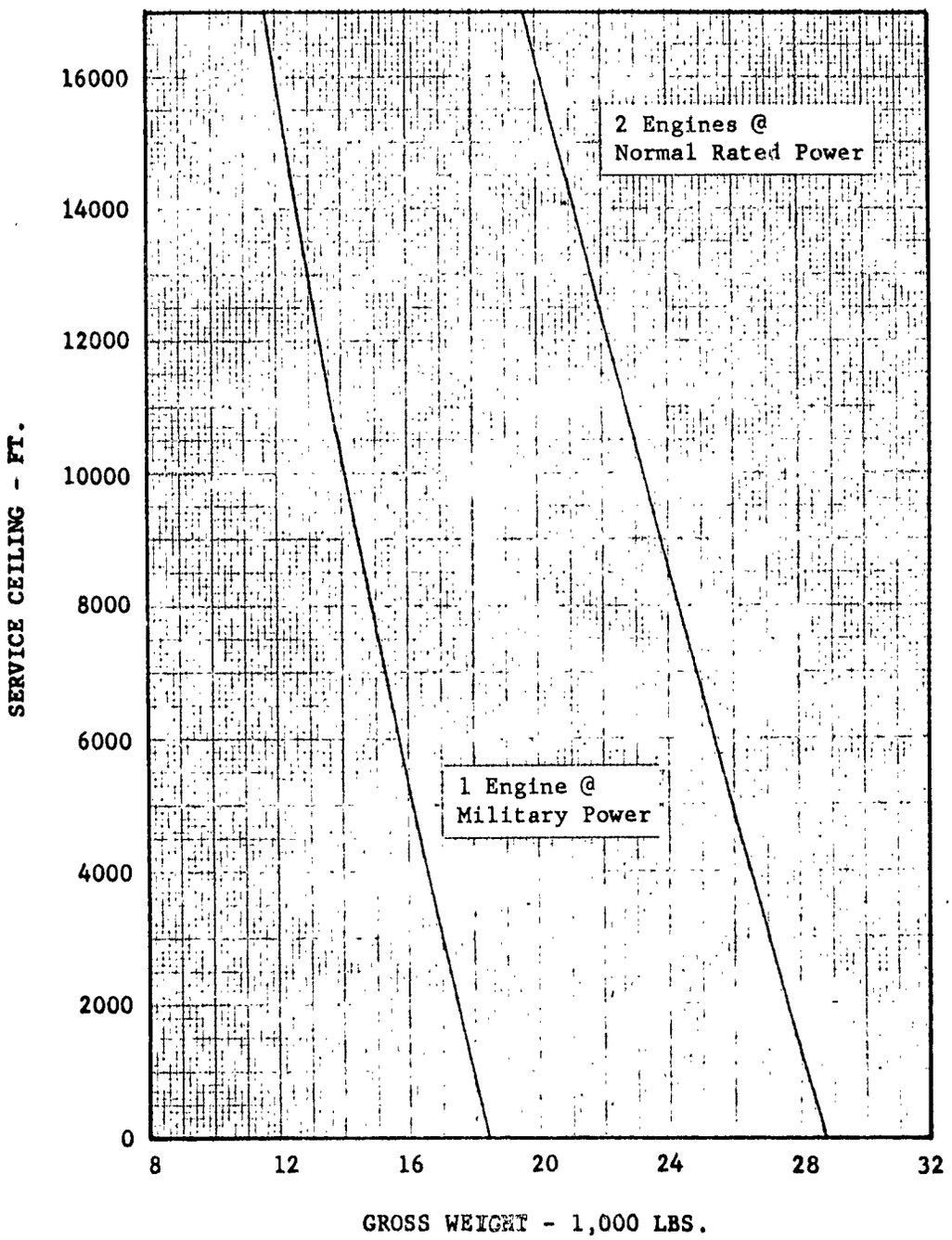


FIGURE 75

NAUTICAL MILES PER POUND VS RATE OF CLIMB
SEA LEVEL STANDARD ATMOSPHERE
TIP SPEED = 625 FT./SEC.
(2) T58-8
V_k = 70 KNOTS

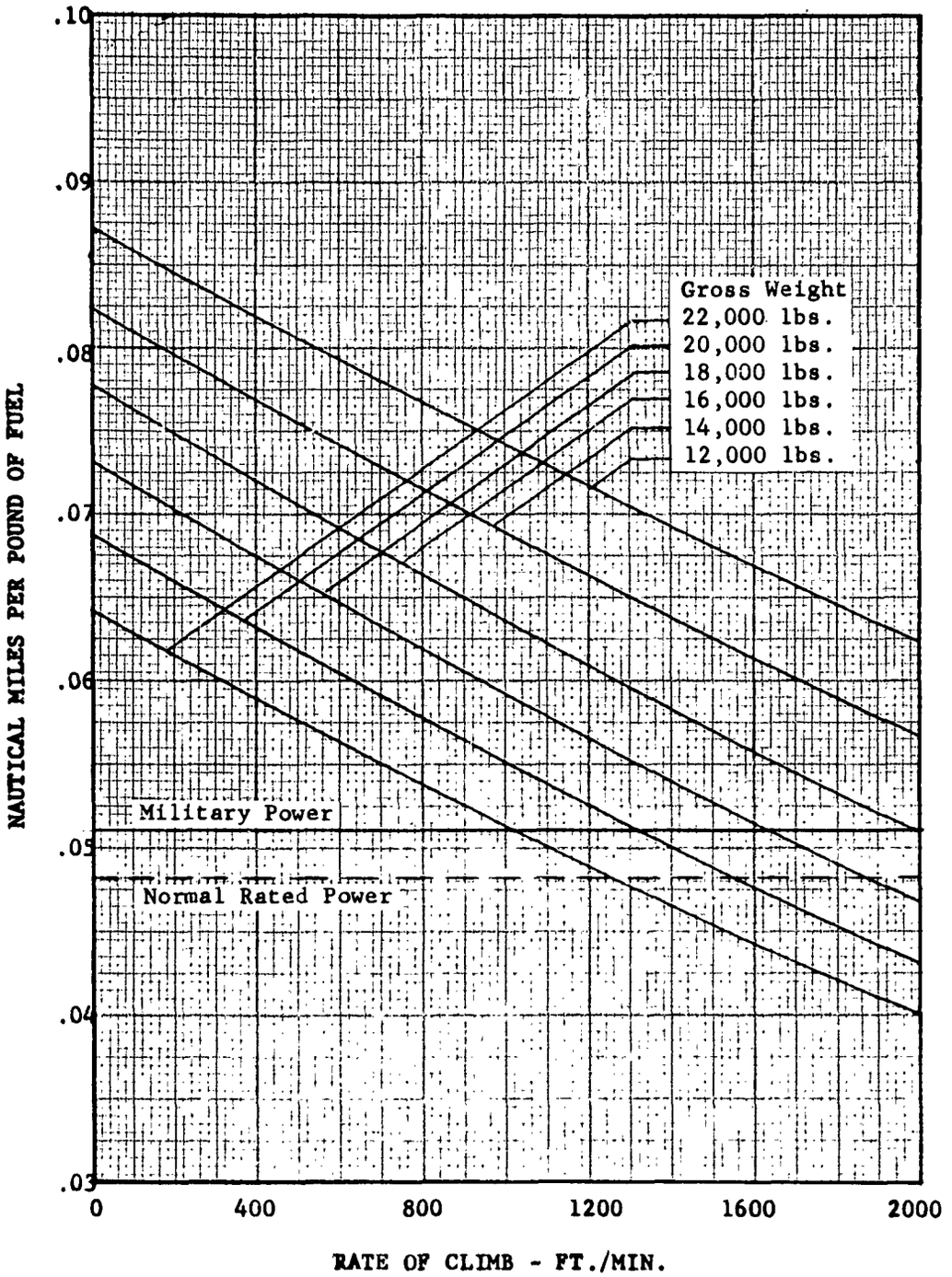
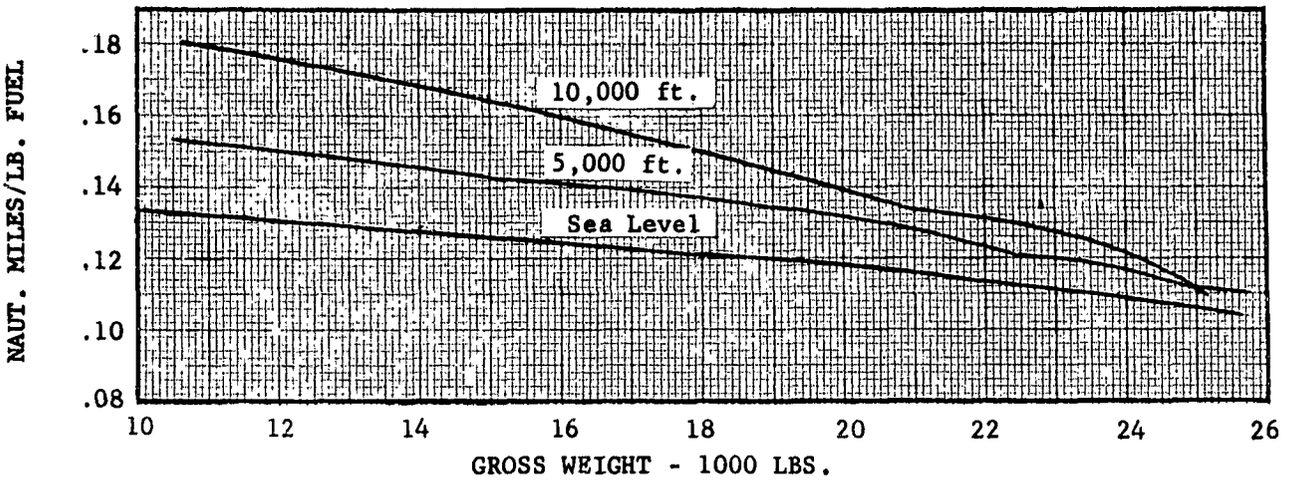
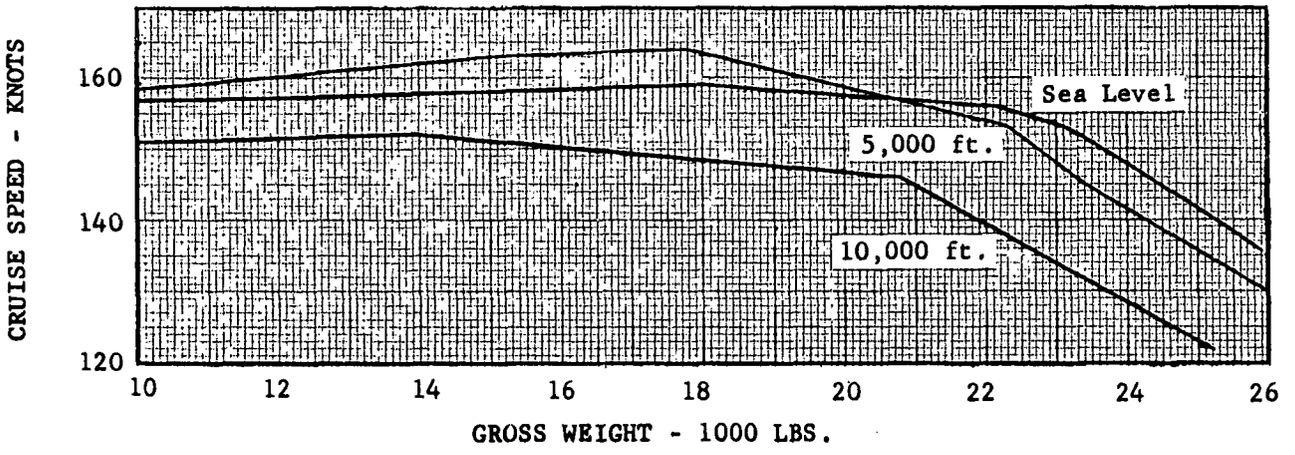


FIGURE 76

NORMAL CRUISE PERFORMANCE
STANDARD ATMOSPHERE





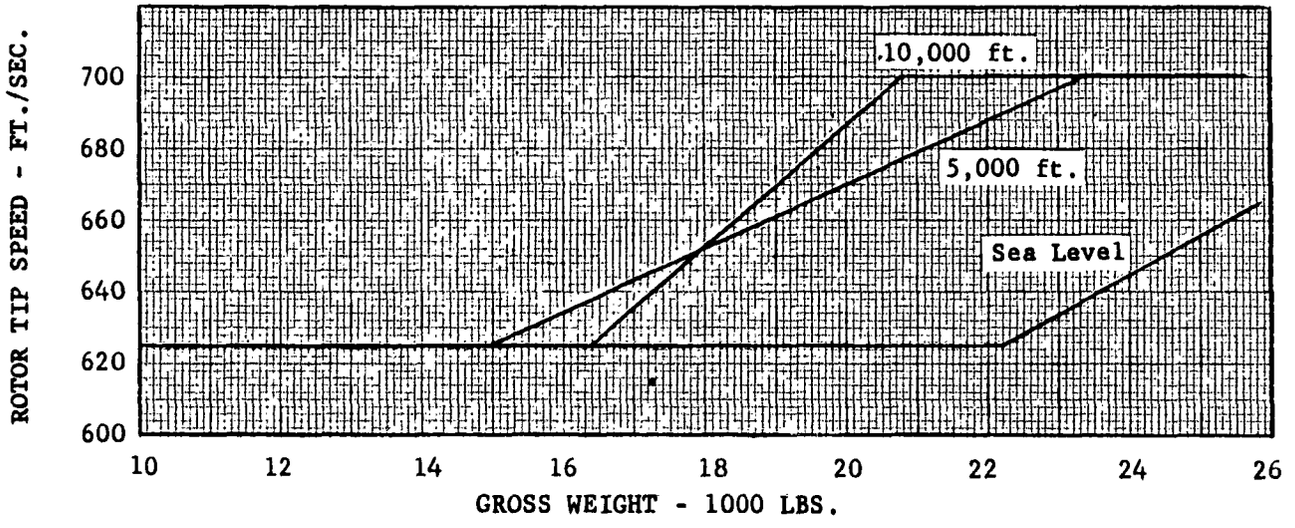
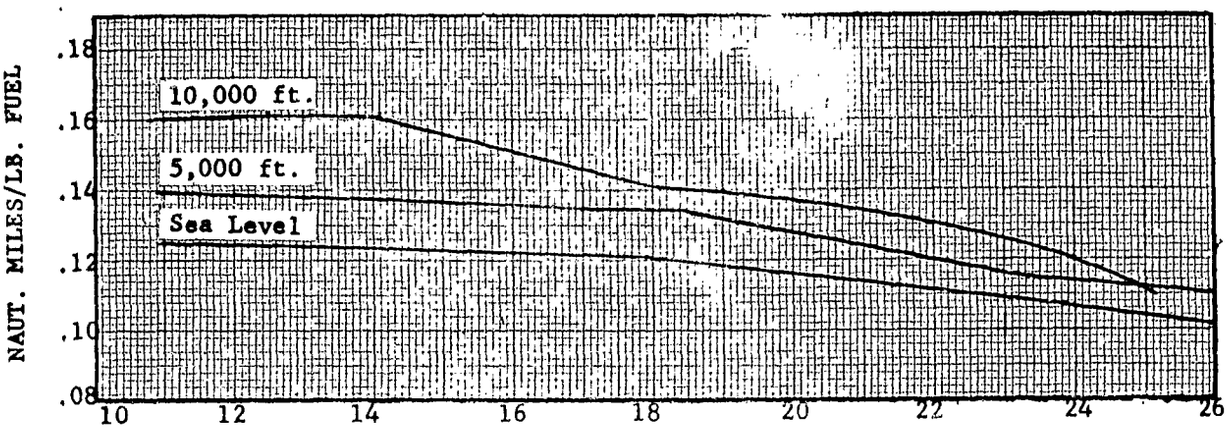
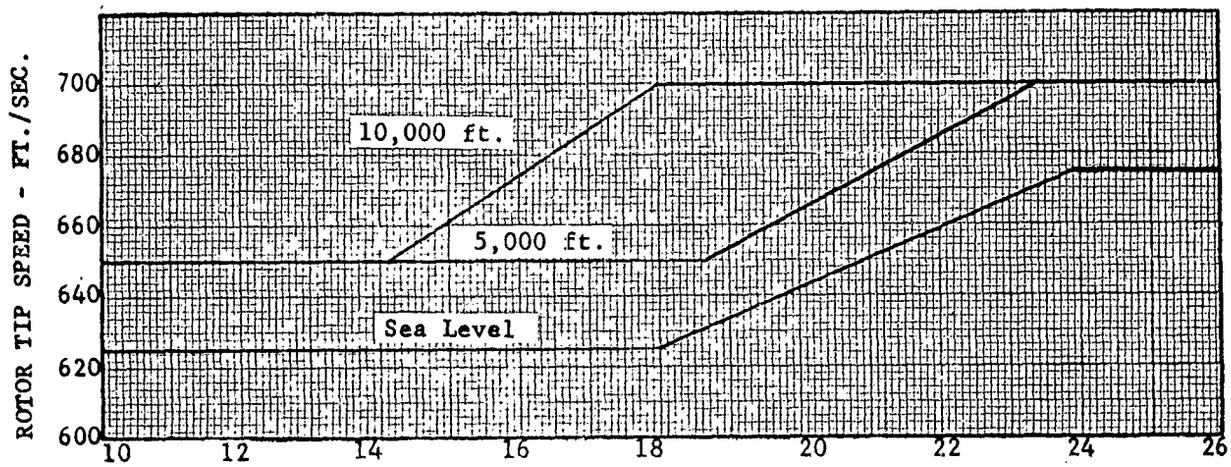


FIGURE 7.7

MAXIMUM FORWARD SPEED CRUISE
STANDARD ATMOSPHERE





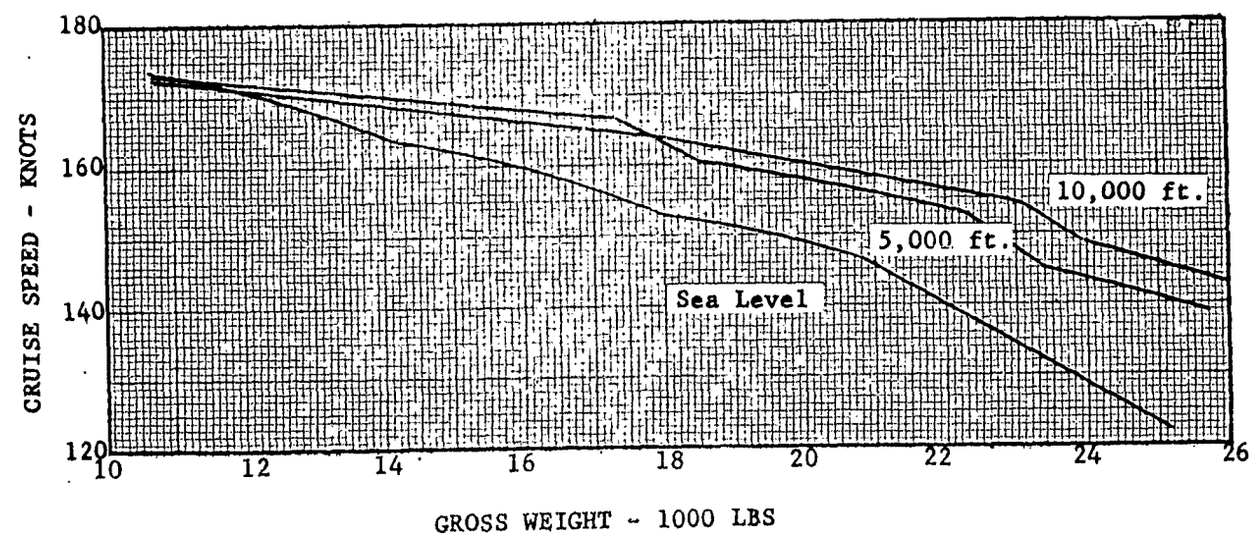
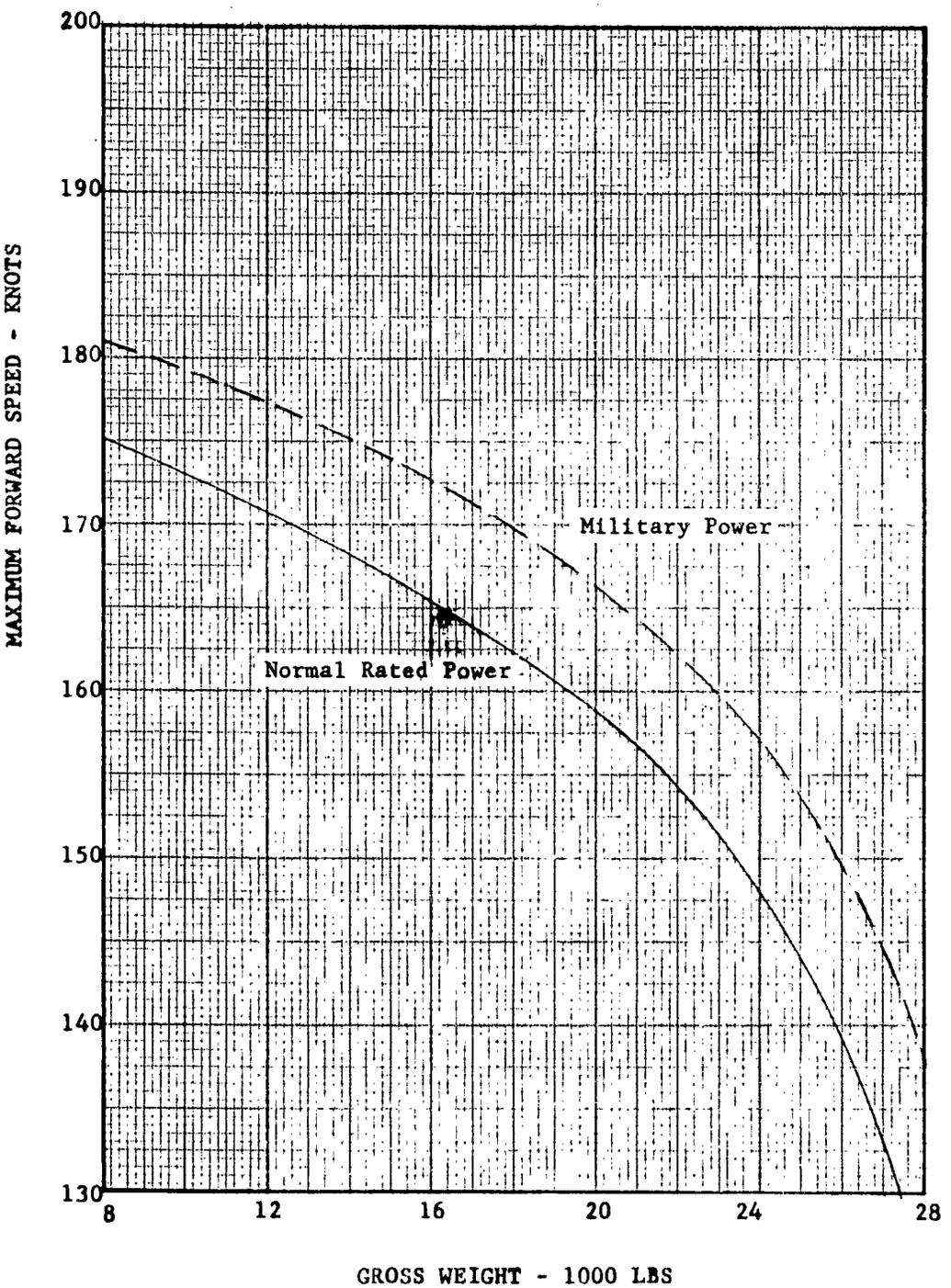


FIGURE 78

MAXIMUM FORWARD SPEED VS. GROSS WEIGHT
SEA LEVEL STANDARD ATMOSPHERE
(2) T58-8 ENGINES



PAYLOAD - RANGE

The following criteria were used to establish payload-range characteristics for sea level cruise:

(1) Initial gross weight for sea level cruise defined by hover at 6,000 ft. on a 95°F day out of ground effect = 15,165 lbs.

(2) Weight empty = 9,988 lbs.

(3) Fixed useful load = 459 lbs.

(4) Warm-up for 2 minutes at Normal Rated Power at sea level on 2 engines = 47 lbs. fuel.

(5) Main tank fuel capacity = 2275 lbs.

(6) Reserves for sea level cruise are 10% of fuel used to cruise

The additional criteria for ferry range are:

(7) Initial gross weight for 10,000 ft. altitude cruise defined by 500 ft./min. rate-of-climb at sea level on a standard day = 26250 lbs.

(8) Fuel required in addition to main tank fuel has an associated additional tankage weight of 0.5 lbs. per gallon.

(9) Reserve for 10,000 ft. altitude cruise is fuel for one hour cruise at speed for best range.

PRODUCTIVITY

The product of payload in pounds and cruise speed in miles per hour divided by empty weight in pounds has been calculated for various cruise speeds at sea level.

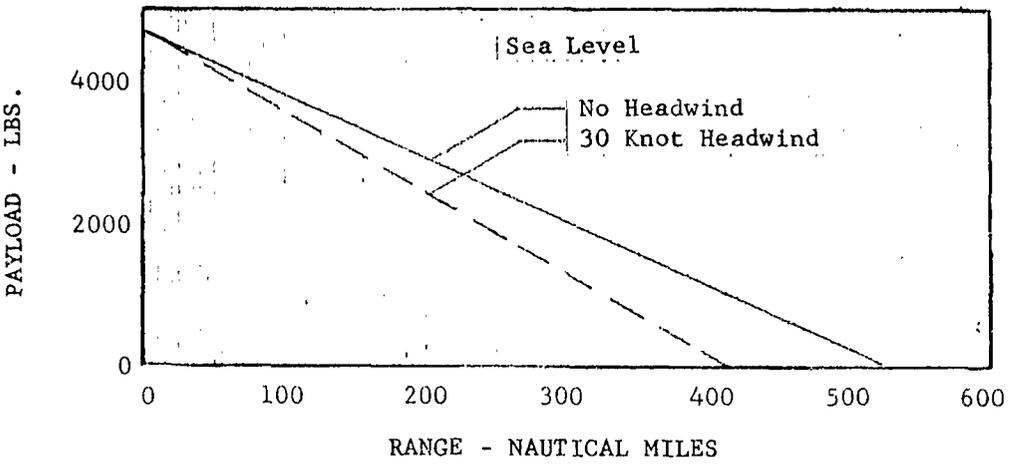
Criteria used to calculate payload are similar to those for the sea level payload-range calculation with the following exceptions: Full payload is carried out to a drop point at a distance equal to half the total range. Engines are presumed shut down and then warmed up for an additional two (2) minutes. The helicopter is then flown back at sea level to the starting point with zero payload.

MAINTAINABILITY

Maintenance costs in dollars per ton mile have been calculated for several fixed cruise speeds at sea level. Statistical data indicates a cost of $106.43 per flight hour for the helicopter at an empty weight of 9,988 lbs. Cost per flight hour is divided by the weight empty in tons and the productivity at each forward speed to obtain cost per ton mile presented as Figure 80.

FIGURE 79

PAYLOAD-RANGE
STANDARD ATMOSPHERE
(2) T58-8



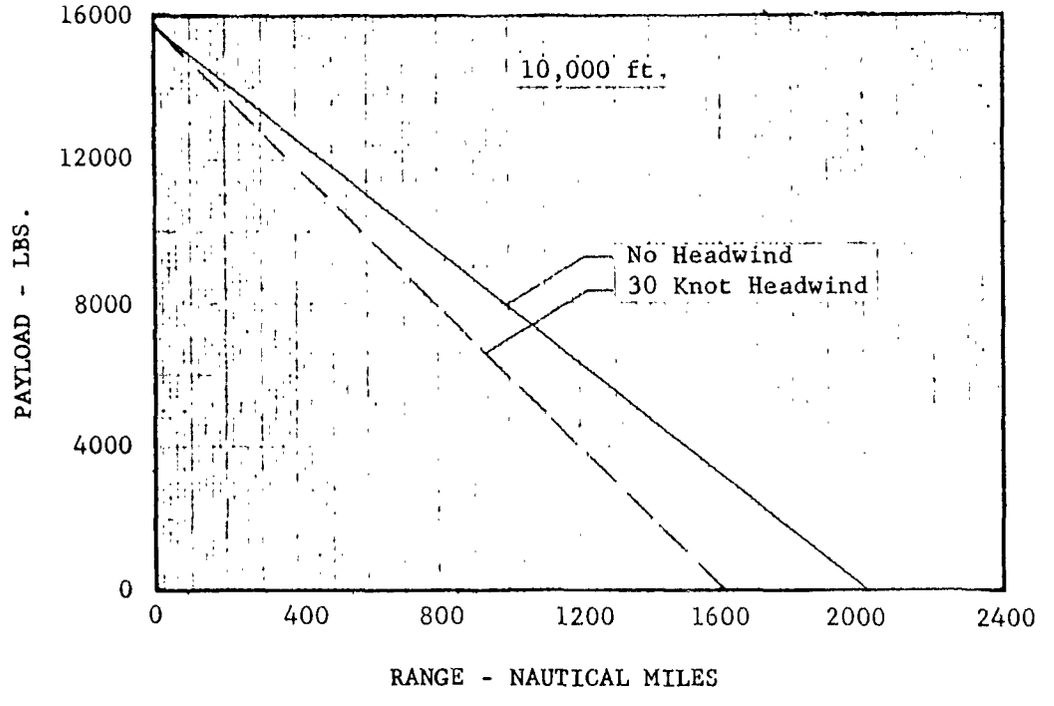
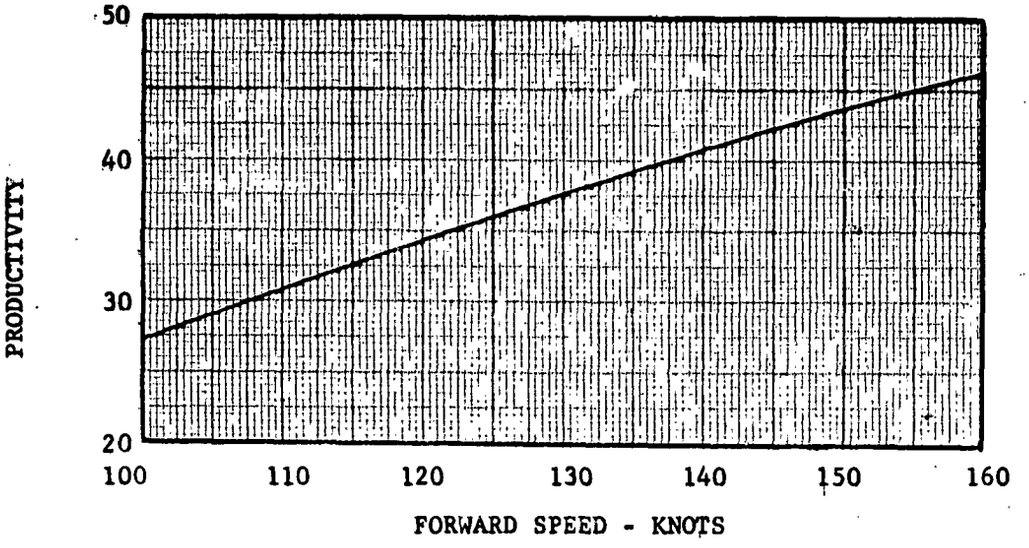


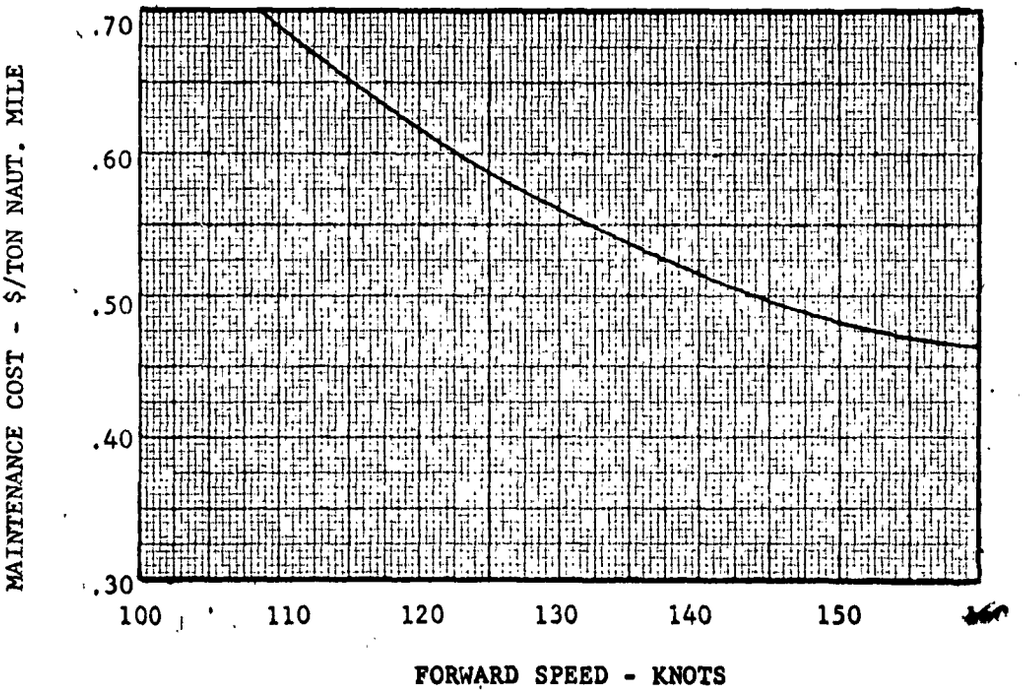
FIGURE 80

PRODUCTIVITY AND MAINTAINABILITY VS. FORWARD SPEED

SEA LEVEL - STANDARD ATMOSPHERE

(2) T-58-8 ENGINES





FLYING QUALITIES

The Boeing-Vertol High Performance 107-II embodies the basic flying qualities proven in the preceding aircraft of the Boeing-Vertol 107 series. The basic configuration, including the rotor, fuselage and control system has been refined so that performance necessary for high speed is attained. This section demonstrates that this increased performance is achieved without detrimental static and dynamic stability effects.

The marked similarity of the stability and control parameters within the 107 series aircraft indicate that the High Performance 107-II will exhibit the same outstanding flying qualities as the 107 series aircraft.

The High Performance 107-II control system incorporates the stability augmentation system which has been tested and proven in the YHC-1A and 107-II aircraft. This S.A.S. system tends to modify the basic dynamic stability characteristics of the aircraft so that the flying qualities are greatly improved.

Table XII lists the flight conditions which have been investigated in order that effects of the increase in maximum forward speed of the High Performance 107-II may be evaluated.

Fuselage Characteristics

Extensive wind tunnel data is available from tests on 1/8th scale models of both the 107-II and High Performance 107-II.

Figures 82a and 82b present the fuselage characteristics with angle-of-attack at zero sideslip and with sideslip at zero angle-of-attack for both models. These figures illustrate the general similarity of aerodynamic characteristics. The most notable difference between the two occurs in the plot of directional stability, N/q versus ψ. The greater directional stability of the High Performance version, particularly at negative yaw angles, may be partly attributed to increased rear pylon side area relative to the front pylon. Large discontinuities in slopes at yaw angles of approximately ± 5 degrees are due to the effects of cross bleed on the front pylon.

These fuselage stability characteristics are superimposed on those obtained from an analysis of the rotor to obtain overall vehicle stability and performance.

The rotor parameters and control kinematics of the High Performance 107-II are presented below.

TABLE XI

PHYSICAL DATA FOR THE HIGH PERFORMANCE 107-II

A. ROTOR PARAMETERS

Rotor Radius	25.	ft.
Blade Chord	1.16	ft.
Solidity	.074	
Disc Area	1,963	ft^2
Front Shaft Incidence	3.5	deg.
Rear Shaft Incidence	7.0	deg.
Hinge Offset	0.0	% R
Blade Twist	-12.	deg.
Rotor Airfoil Section	0009.5	

B. CONTROL KINEMATICS

Collective Trim

Collective Stick Length - Travel	7.0 in.
Blade Travel at .75 Radius	-4° to 16°

(a) Longitudinal Control

Longitudinal Stick Travel	±9.75 in.
D.C.P. Blade Travel Due to Stick	±4.5°
D.C.P. Blade Travel Due to 'e' Sensor	
Front Rotor	0° to 5°
Rear Rotor	0° to 5°
Cyclic Trim Due to 'q' Sensor	
Front Rotor	0° to -1.5°
Rear Rotor	-1.5° to +1.5°

Stick Positioner

Stick Rate	±1.0 in./sec
Blade Travel	±1.0°

(b) Lateral Control

Lateral Stick Travel	±9.0 in.
Cyclic Blade Travel	
Front Rotor	±7.0°
Rear Rotor	±7.0°

(c) Directional Control

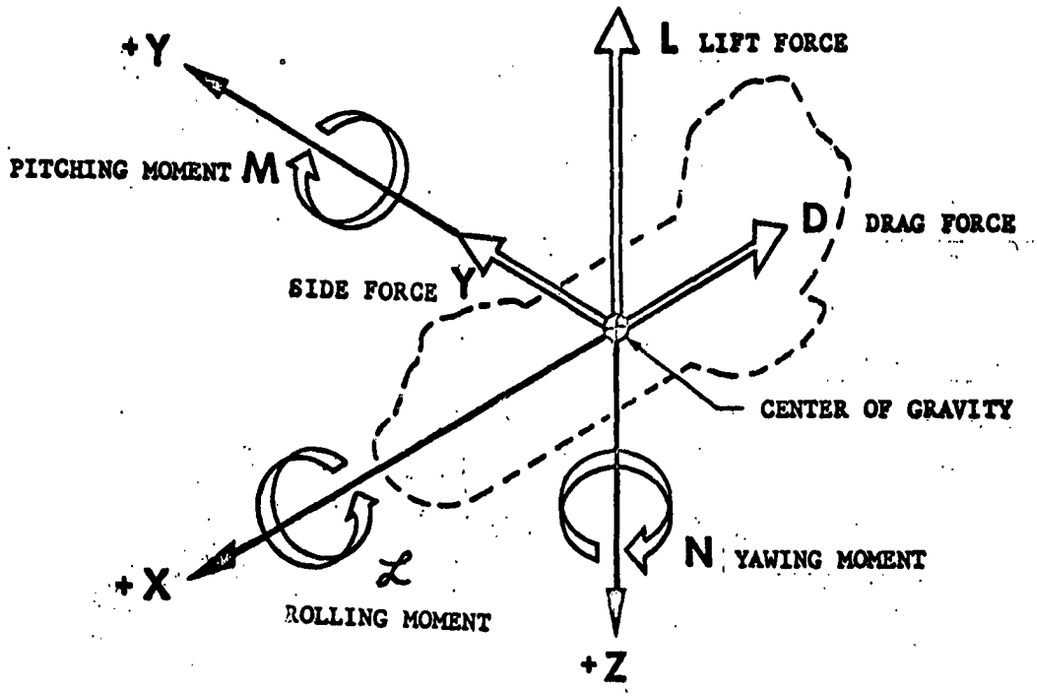
Rudder Pedal Travel	±2.3"
Lateral Cyclic Blade Travel	
Front Rotor	±9.85°
Rear Rotor	±8.85°

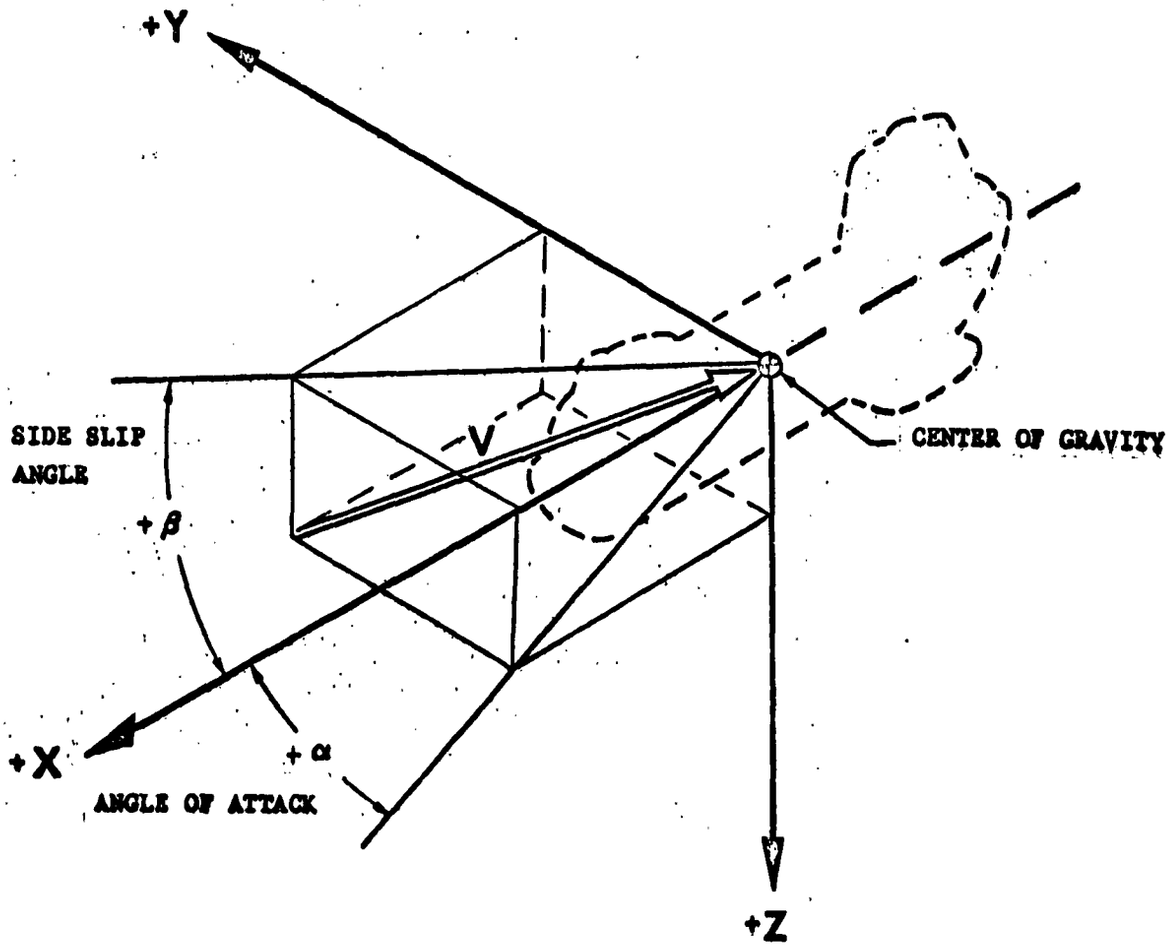
(d) Lateral - Directional

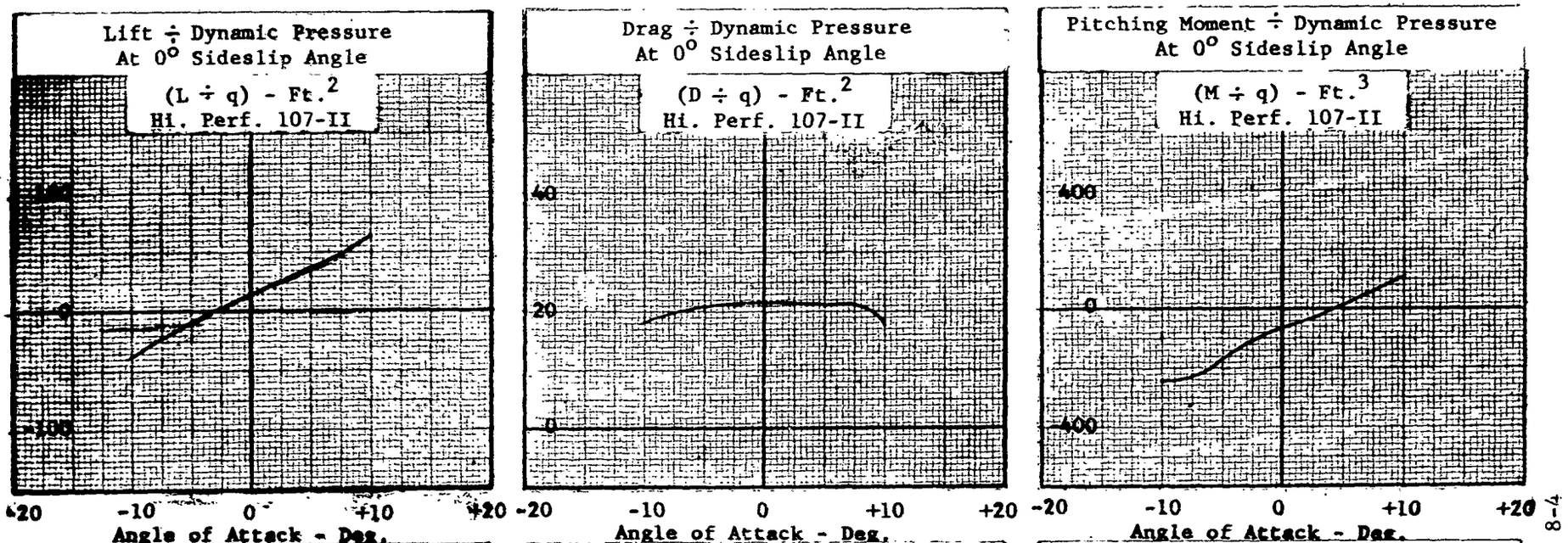
Design Total

Front Rotor	±10.5°
Rear Rotor	±10.5°

FIGURE 81 BODY AXIS CO-ORDINATE SYSTEM







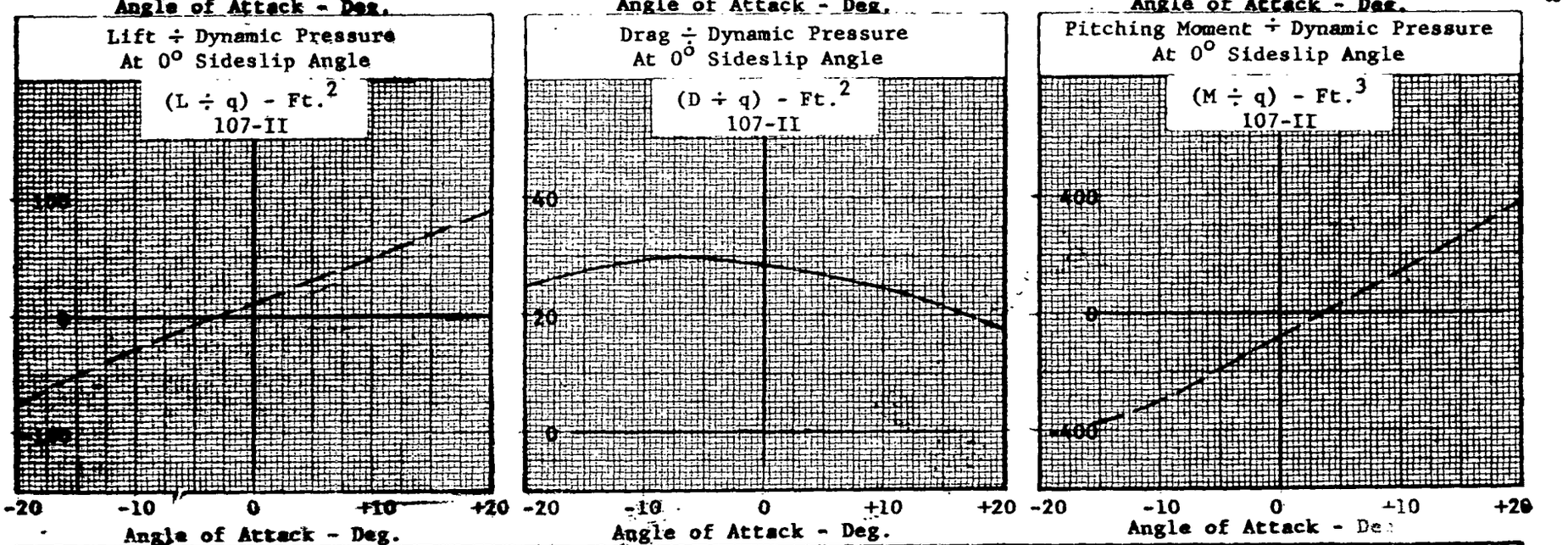


Fig. 82a High Performance 107-II & 107-II Fuselage Characteristics Referred to Body Axis System

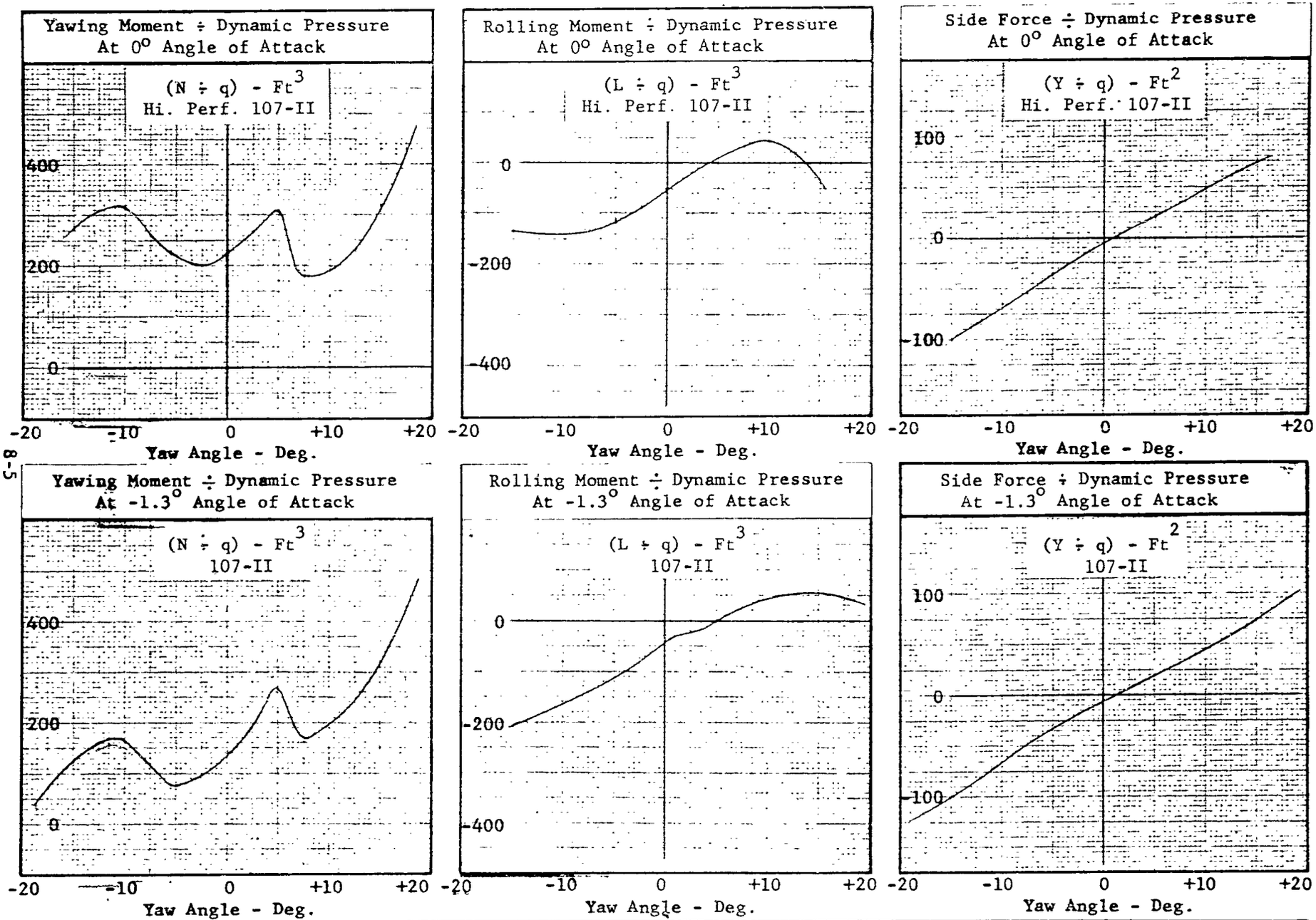


Fig. 82b High Performance 107-II & 107-II Fuselage Characteristics Referred to Body Axis System

Rotor Aerodynamic Characteristics

Rotor longitudinal stability derivatives are determined by the solution of the longitudinal equations of motion for the steady case; i.e. with the acceleration terms set equal to zero. Derivatives have been obtained for the High Performance 107-II through use of an IBM 650 digital computer program and are presented in Figures 83 and 84.

Lateral-directional derivatives have been obtained in a similar way and results are plotted in Figures 87 through 88.

Table XII specifies the flight conditions for which stability derivatives were obtained.

TABLE XII

FLIGHT CONDITIONS FOR STABILITY DERIVATIVES

Gross Weight (lbs.)	Center of Gravity	Altitude (ft)	Tip Speed (fps)	Case	Level Flight Forward Speed (knots)
Normal 15,165	Normal	0	650	long. lat.	50, 70, 90, 110, 130, 150, 170, 174 40, 100, 174
Ferry Mission 26,250	Normal	0	650	long. lat.	40, 135 40, 100, 135
		10,000	650	long. lat.	130 130

The longitudinal cyclic pitch and differential collective pitch schedules are shown in Figures 85 and 86 respectively. The longitudinal cyclic pitch varies with the dynamic pressure. The differential collective pitch has been designed to vary with the cyclic pitch schedule. These schedules have been chosen to optimize performance and provide superior flying qualities at all calibrated airspeeds.

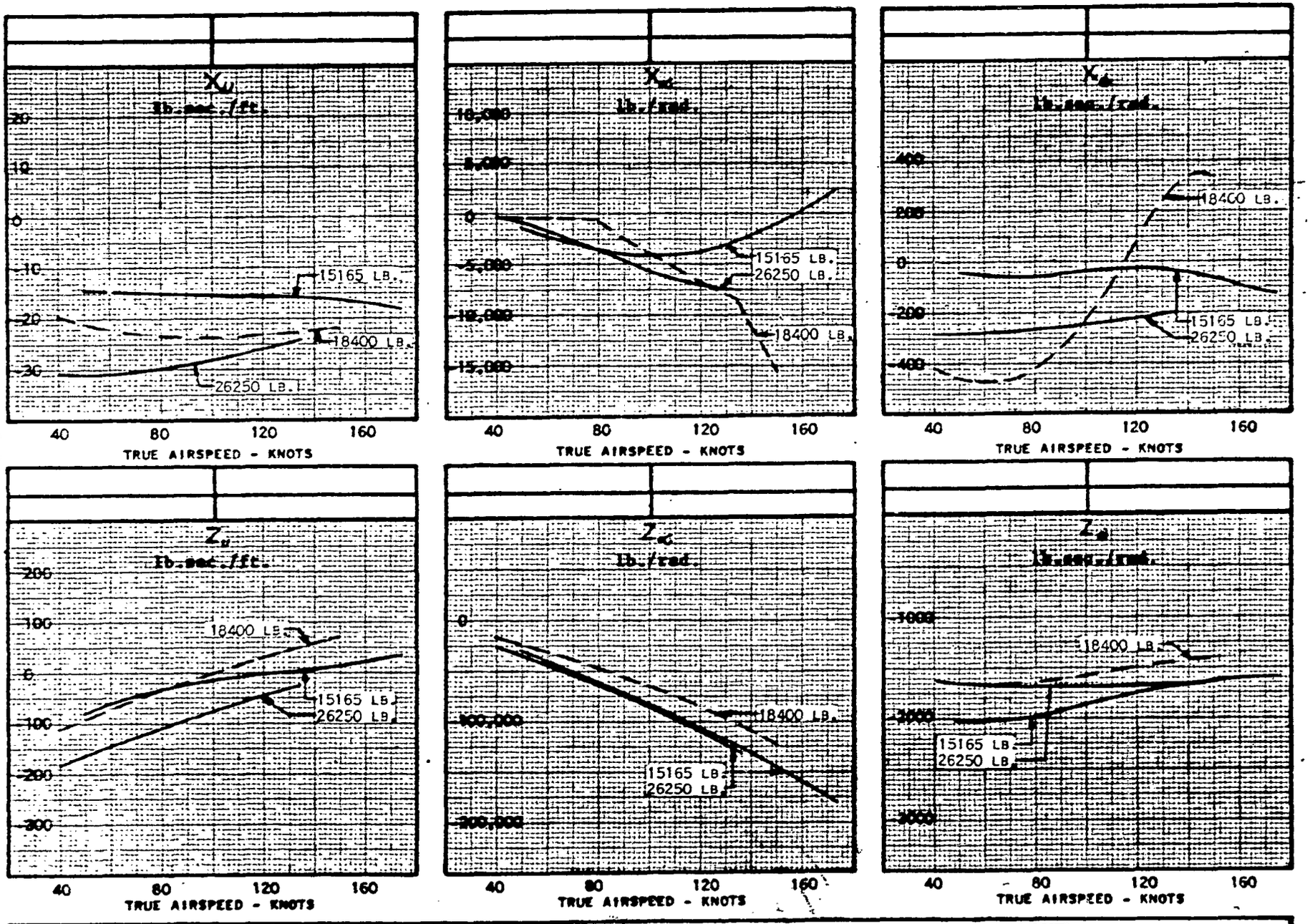


FIG. 83a - LONGITUDINAL STABILITY DERIVATIVES VS TRUE AIR SPEED IN LEVEL FLIGHT

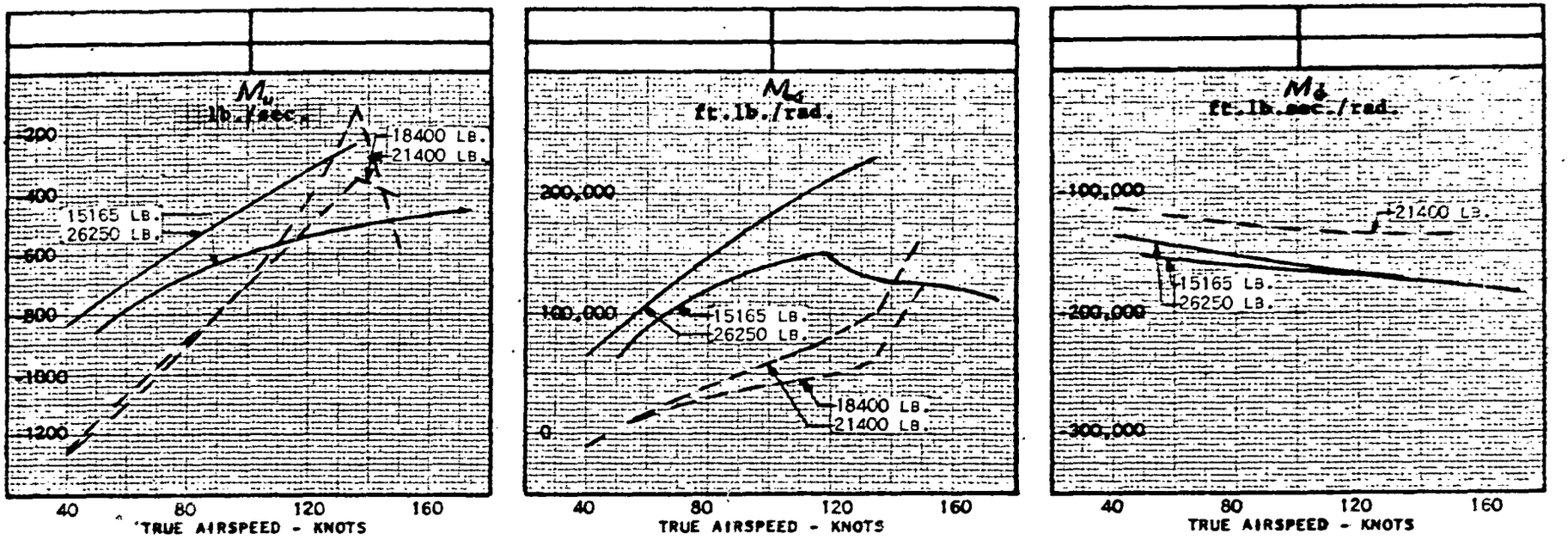


FIG.83b - LONGITUDINAL STABILITY DERIVATIVES VS TRUE AIR SPEED IN LEVEL FLIGHT

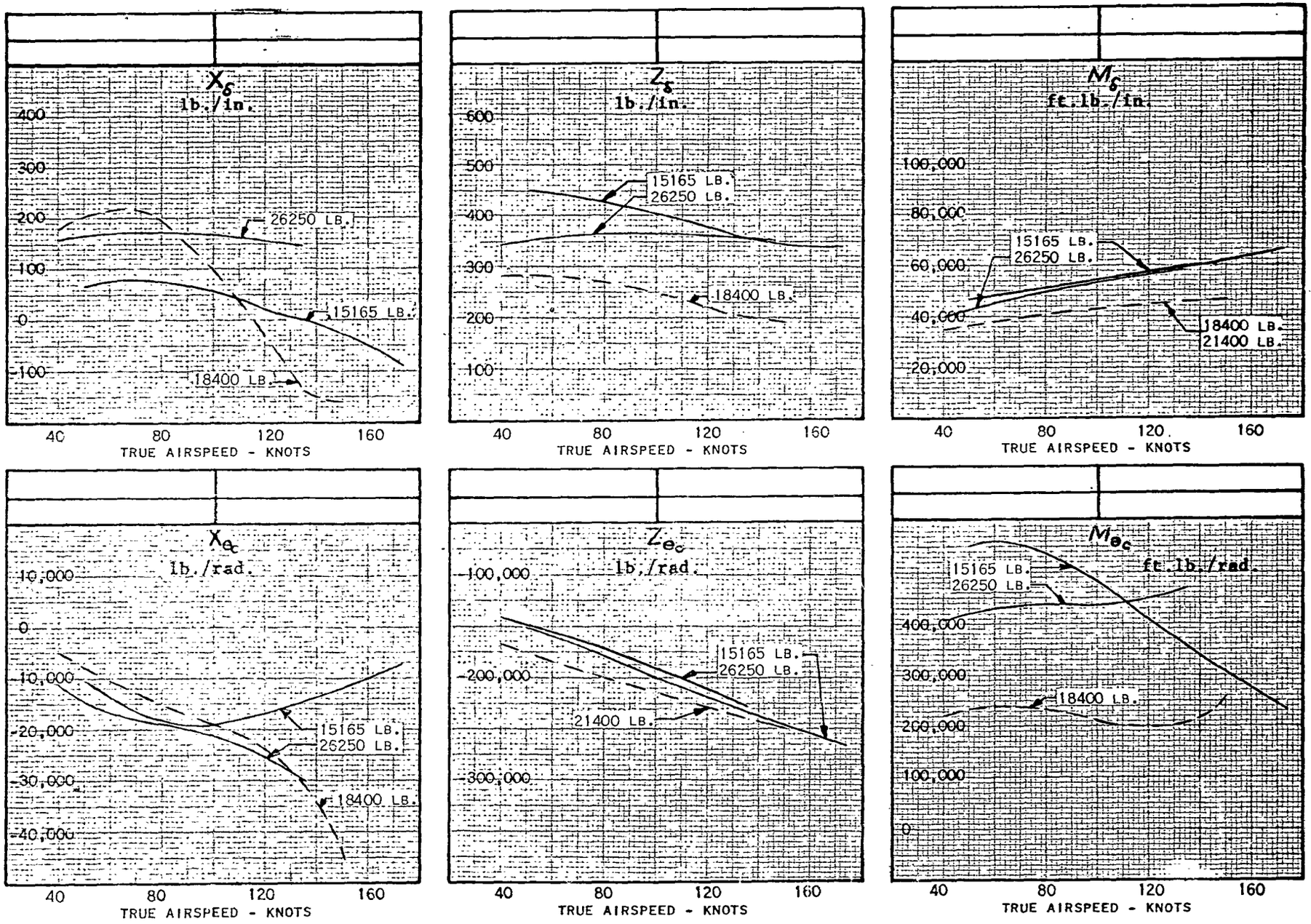


FIG. 84 - LONGITUDINAL CONTROL POWERS VS TRUE AIR SPEED IN LEVEL FLIGHT

NOTE: Sea Level Standard Day

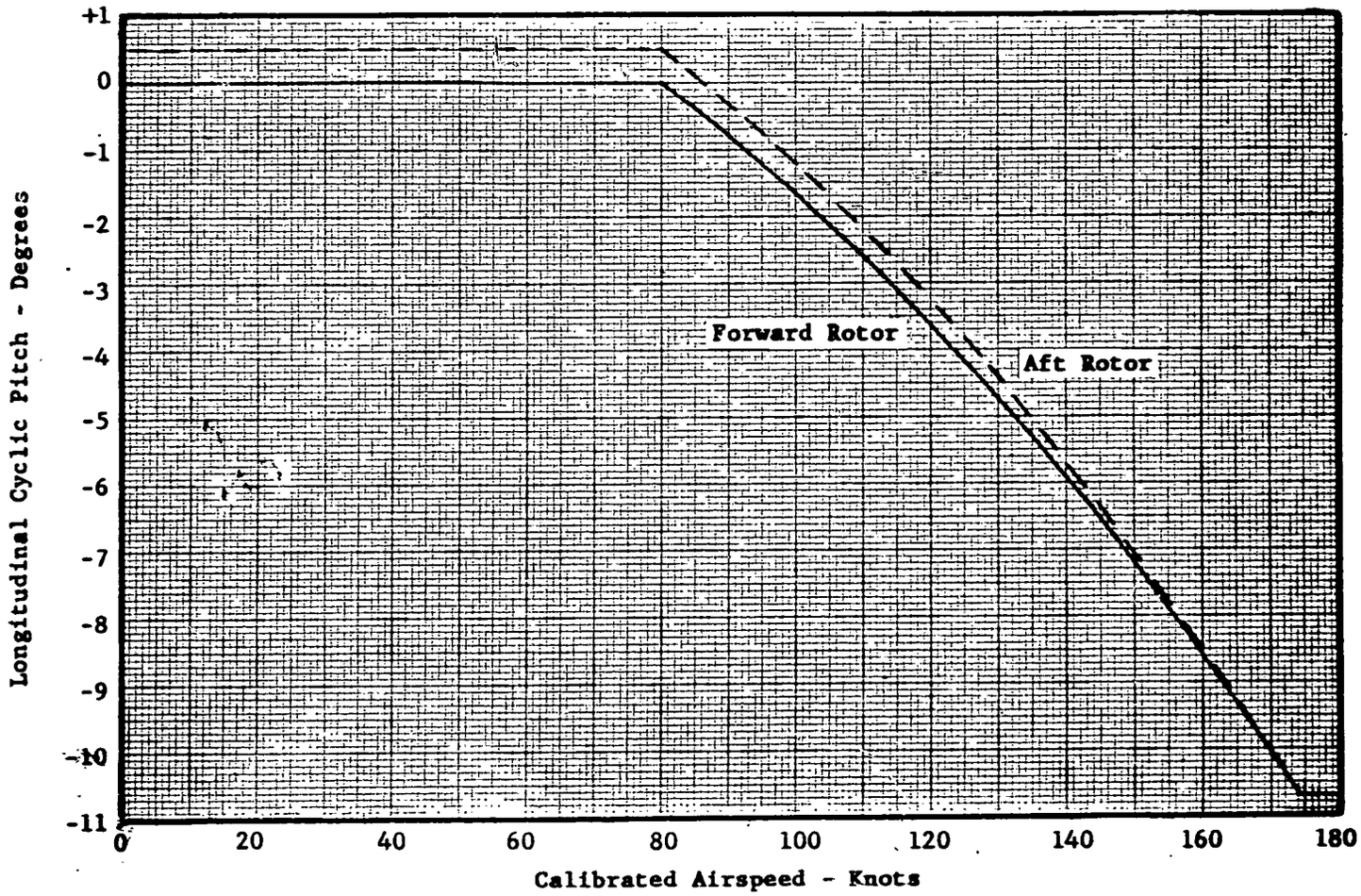


FIGURE 85 - LONGITUDINAL CYCLIC PITCH SCHEDULE

NOTE: Sea Level Standard Day

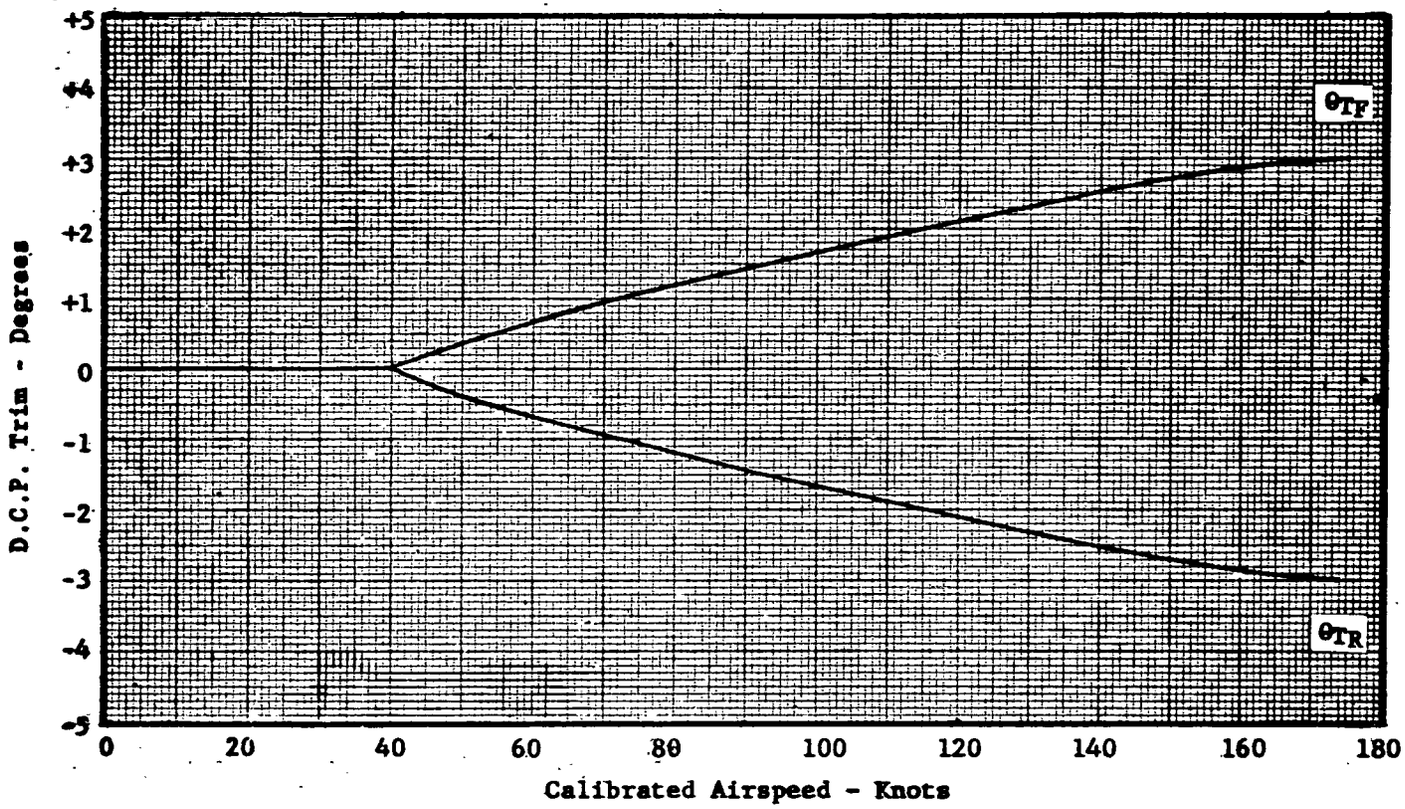


FIGURE 86 - DIFFERENTIAL COLLECTIVE PITCH SCHEDULE

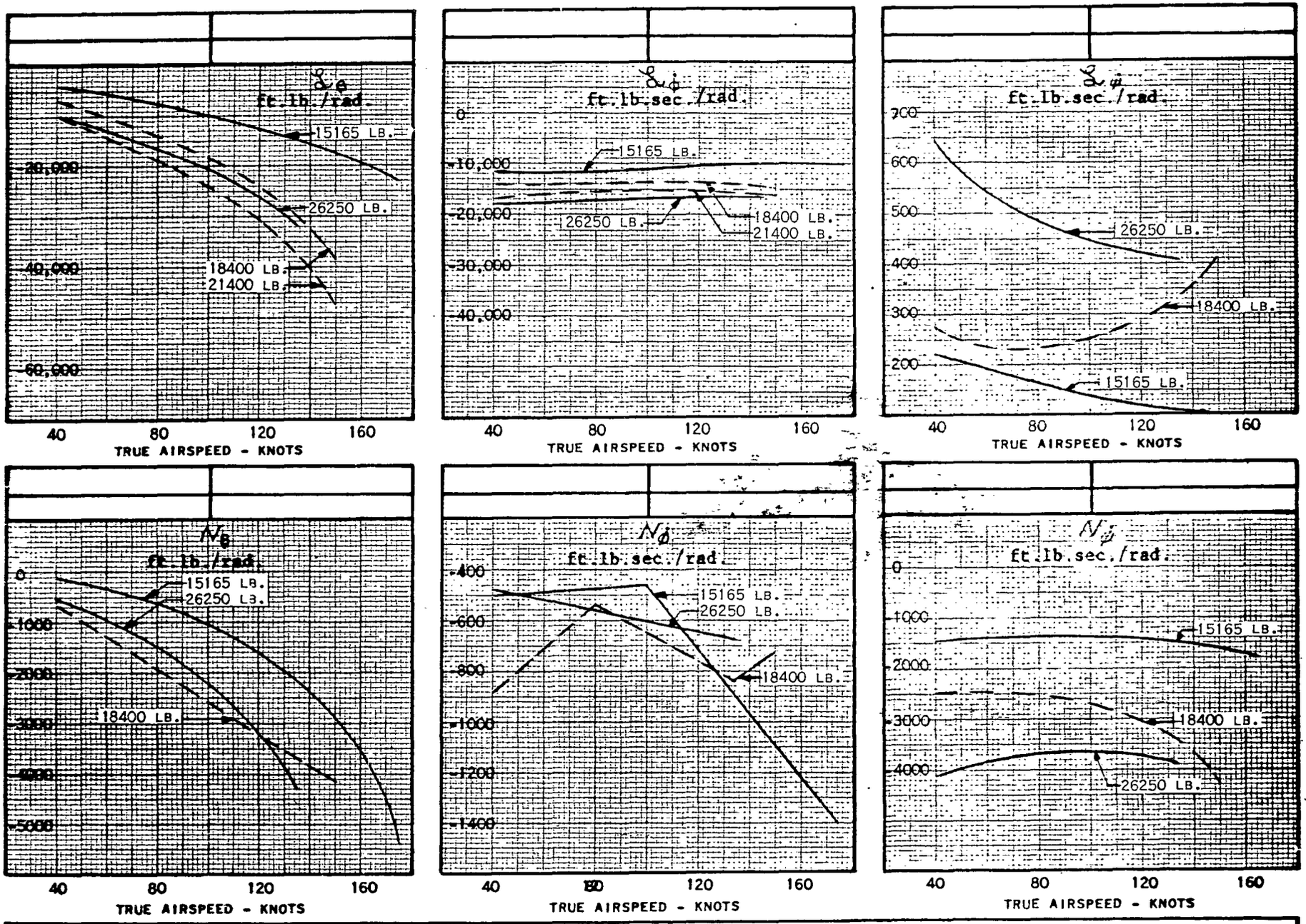


FIG.87a. - LATERAL DIRECTIONAL STABILITY DERIVATIVES VS TRUE AIR SPEED IN LEVEL FLIGHT

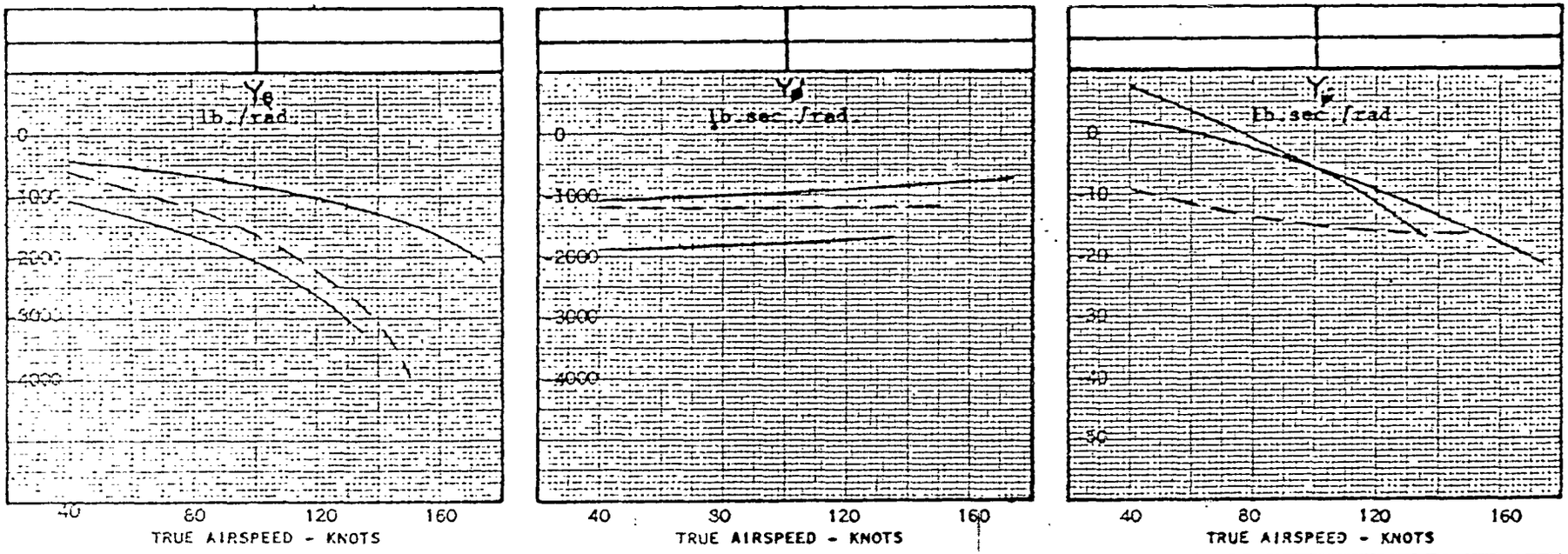


FIG. 8.6b - LATERAL DIRECTIONAL STABILITY DERIVATIVES VS TRUE AIR SPEED IN LEVEL FLIGHT

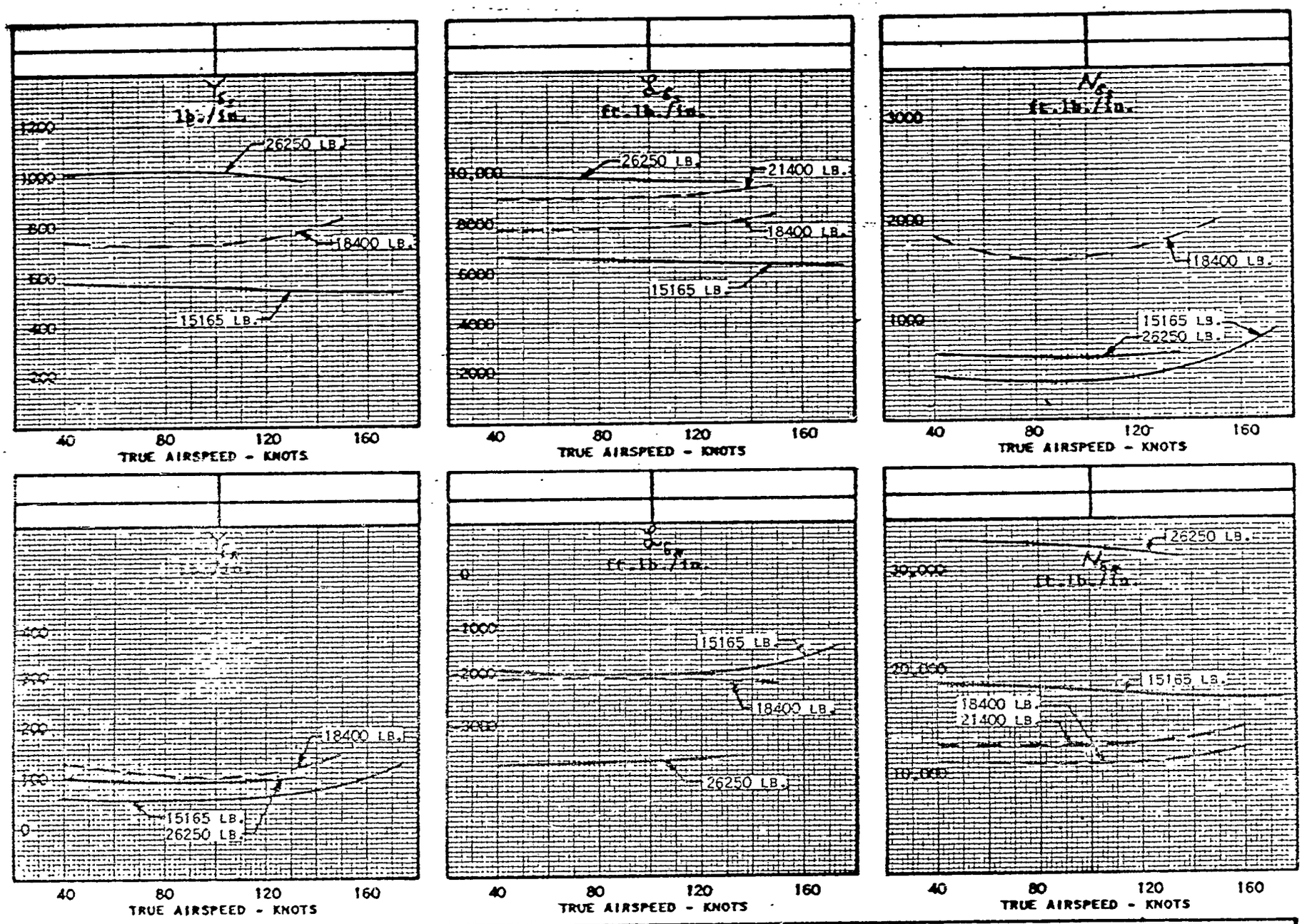


FIG. 88 - LATERAL-DIRECTIONAL CONTROL POWERS VS TRUE AIR SPEED IN LEVEL FLIGHT

VERTOL 107 STABILITY AUGMENTATION SYSTEM

The Vertol Division of The Boeing Company has developed a Stability Augmentation System (SAS) to provide helicopters with flying qualities equivalent to those of a fixed wing aircraft. With a SAS equipped helicopter it is now possible to fly "hands off" for several minutes at a time and to make well-coordinated "stick" turns over a wide range of forward speeds.

The following paragraphs provide a brief description of the general principles of SAS, and a detailed explanation, with block diagrams, of a typical system for the 107 series of helicopters.

PRINCIPLES OF VERTOL SAS

The Vertol SAS system consists of a sensor in each axis to detect helicopter motion and feed a corrective signal into the control system. The signals from the sensor are fed into the control system differentially, i.e., the controls at the rotor heads are moved without any motion of the pilot's controls. The differential system offers two basic advantages. First, it eliminates undesirable forces and motions from the pilot's controls and second, it permits the use of limited authority so that the SAS can never move the controls by more than a fixed percentage of their total travel. This means that even in the event of a malfunction resulting in a hardover signal, there would be no large sudden motions of the aircraft and the pilot can easily override the SAS. In addition, the control system stops are arranged on the output side of the SAS actuators so that in the event of a hardover signal normal full control plus a sufficient overtravel to counteract the full SAS signal is available.

DESCRIPTION OF THE VERTOL 107 SAS

The Vertol 107 SAS is a dual system with the following features:

a. Transistor amplifiers for reliability.
b. Lightweight - 5.5 pounds for the electronic unit.
c. Plug-in, printed circuit amplifiers for quick and easy maintenance.
d. Self-checking without test equipment.
e. Low power consumption (less than 30 watts total).

The system function may be explained as follows:

Servo Amplifier - The servo amplifier is identical for roll, pitch and yaw. It consists of a transistor amplifier, the output of which drives the torque motor of a differential hydraulic actuator. The actuator motion is sensed with a differential transformer causing a proportional voltage to be fed back to the amplifier to cancel out the input voltage. This results in actuator displacement proportional to input signal voltage applied to the amplifier. Since an AC amplifier is used, DC signals going into the amplifier must be modulated. The amplifier output must be demodulated to provide the required DC driving signal to the hydraulic actuator torque motor.

Roll Axis - The signal applied to the roll amplifier is roll rate from the roll rate gyro. It provides the necessary roll damping

Pitch Axis - The pitch axis is identical to the roll axis except for a network which performs a lag-lead on the demodulated rate. gyro signal. This particular shaping is optimum for a tandem helicopter.

Yaw Axis - Four signals feed the yaw axis amplifier. They are as follows:

1. A yaw rate signal generated by the rate gyro. The signal passes through an electronic "washout" network before reaching the amplifier, which eliminates any steady state yaw rate gyro signal. This allows steady turns to be made without bottoming the yaw SAS actuators.

2. A roll rate signal from the roll rate gyro, passing through an electronic lag network. This lagged roll rate signal tends to speed up turn entry. Rapid, well coordinated turns are then possible.

3. A sideslip signal, which is detected by a differential pressure transducer. The transducer is fed by a pair of static ports symmetrically located on the extreme forward part of the fuselage. For optimum directional stability at all airspeeds, the gain of this transducer is programmed as a function of airspeed by means of a second airspeed sensing, differential pressure transducer. Precise turn coordination and stick trim capability is obtained between the speeds of 60 knots and V_{max}.

4. A rudder pedal pickoff signal, which tends to cancel the yaw rate gyro signal in hovering turns. This is needed in order to retain optimum control in hover

In the 107-II the system is completely duplicated so that no single failure, whether it be the actuator, the electronics unit, the electrical supply system or the hydraulic system, can cause a loss of stability augmentation. The dual system is designed so that either SAS can be used independently or the two can be used in conjunction, with each operating at half gain. In the normal mode of operation, both are operating and hence a single failure will be of little consequence to the pilot since the unfailed SAS will continue to stabilize the helicopter

A block diagram showing the systems which stabilize the roll, pitch, and yaw axes is presented in Figure 89 A schematic of the control system, including dual SAS installation, is shown in Figure 90. The single axis presented is typical for roll, pitch and yaw control.

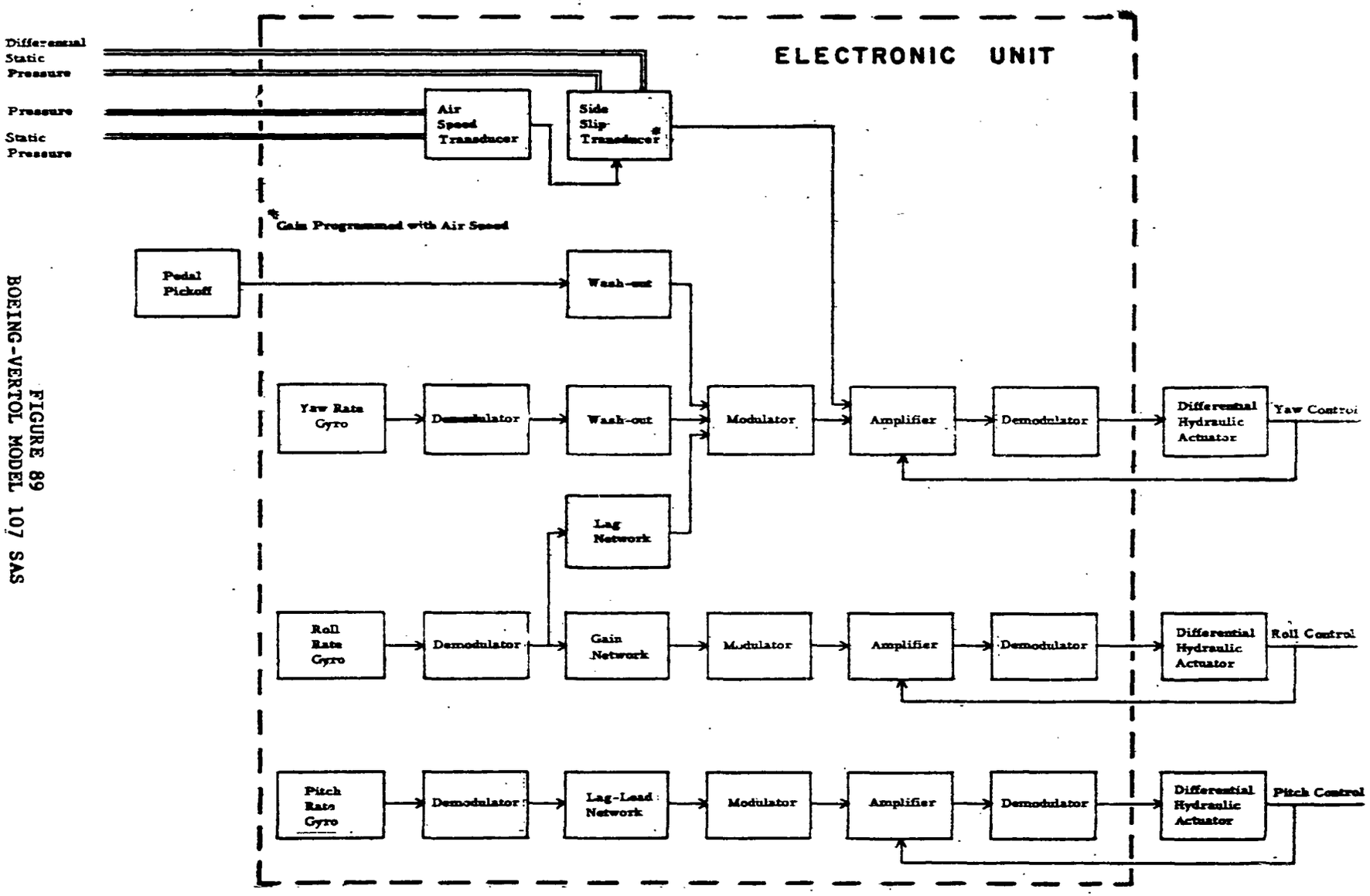


FIGURE 89
BOEING-VERTOL MODEL 107 SAS

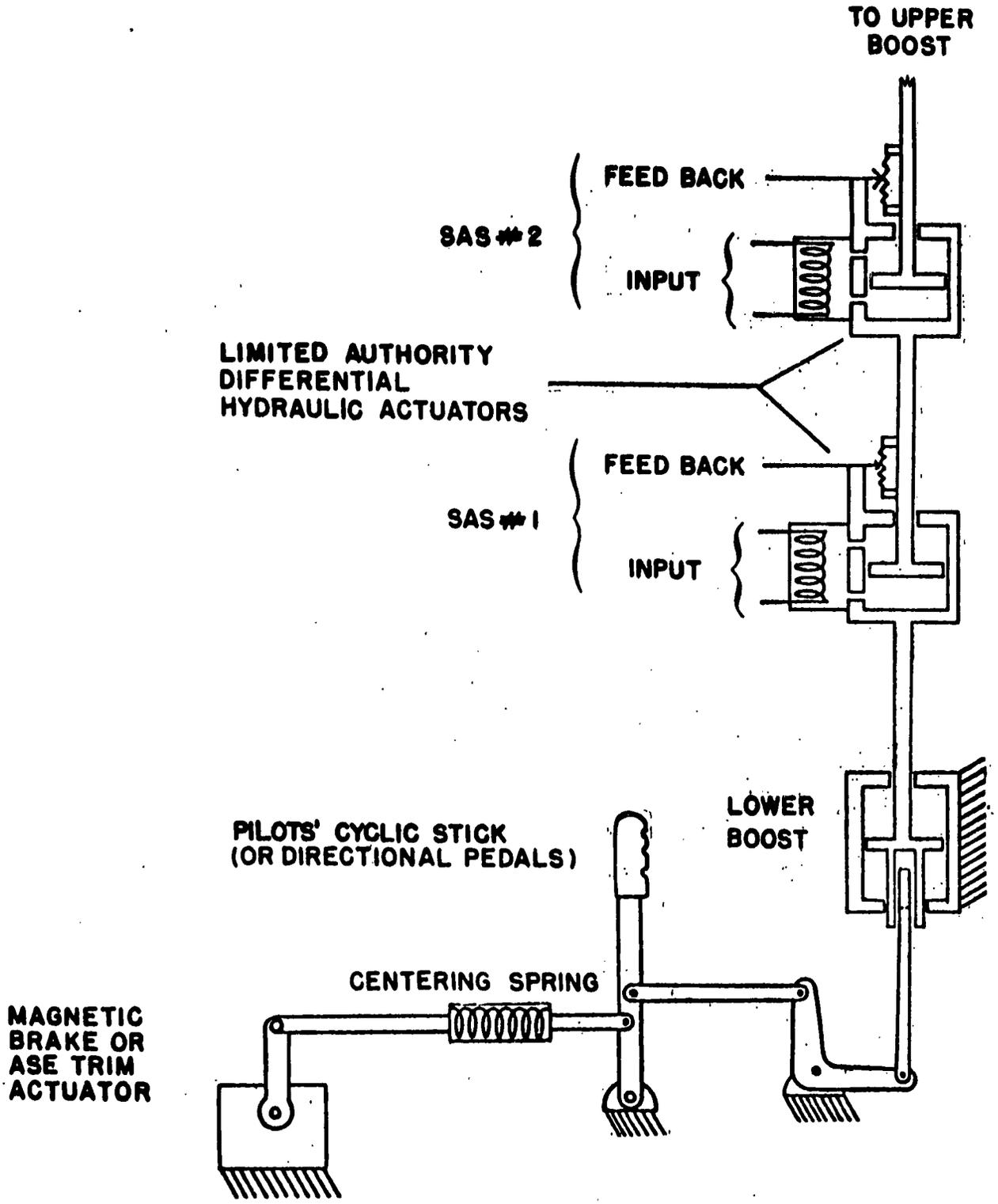


FIG. 90 BOEING-VERTOL MODEL 107 CONTROL SYSTEM SCHEMATIC SHOWING TYPICAL SAS INSTALLATION.

STATIC LONGITUDINAL STABILITY

The degree of static longitudinal stability of the High Performance 107-II is evaluated by considering the M_{α} of the aircraft and the speed stability of the aircraft. If the aircraft exhibits longitudinal static stability the M_{α} derivative is negative. In the case of the 107-II and the High Performance 107-II the M_{α} derivative is positive thus indicating that the aircraft does not have inherent longitudinal static stability.

The aforementioned derivative is composed of M_{α} fuselage and M_{α} rotor. A comparison of the fuselage pitching moment versus angle of attack for the two aircraft indicate that the slope of the curves is similar for a range of angles of attack corresponding to the trim α's associated with the normal gross weights of each model. Thus the fuselage pitching moment contribution of the High Performance 107-II is equivalent to that of the 107-II.

The M_{α} derivative of the High Performance 107-II, at the maximum forward speed is less than that of the 107-II at its maximum forward speed. The trend of the M_{α} with speed is an increasing destabilizing moment up to a velocity of approximately 40 knots. At this point the High Performance 107-II exhibits a decreasing M_{α} up to its maximum forward velocity. This effect is pronounced at the normal G.W. of 15,165 pounds. The M_{α} derivative of the 107-II tends to become nondestabilizing with forward speed although the High Performance 107-II has higher initial values for all gross weights through the 150 knots region.

In light of this data, it is concluded that the High Performance 107-II exhibits static longitudinal stability similar to that demonstrated by the 107-II. At the respective maximum forward speeds of both models, the High Performance 107-II appears to have a smaller destabilizing pitching moment. At gross weights greater than normal this small margin becomes less apparent and the aircraft tend to exhibit similar longitudinal behavior.

Speed Stability

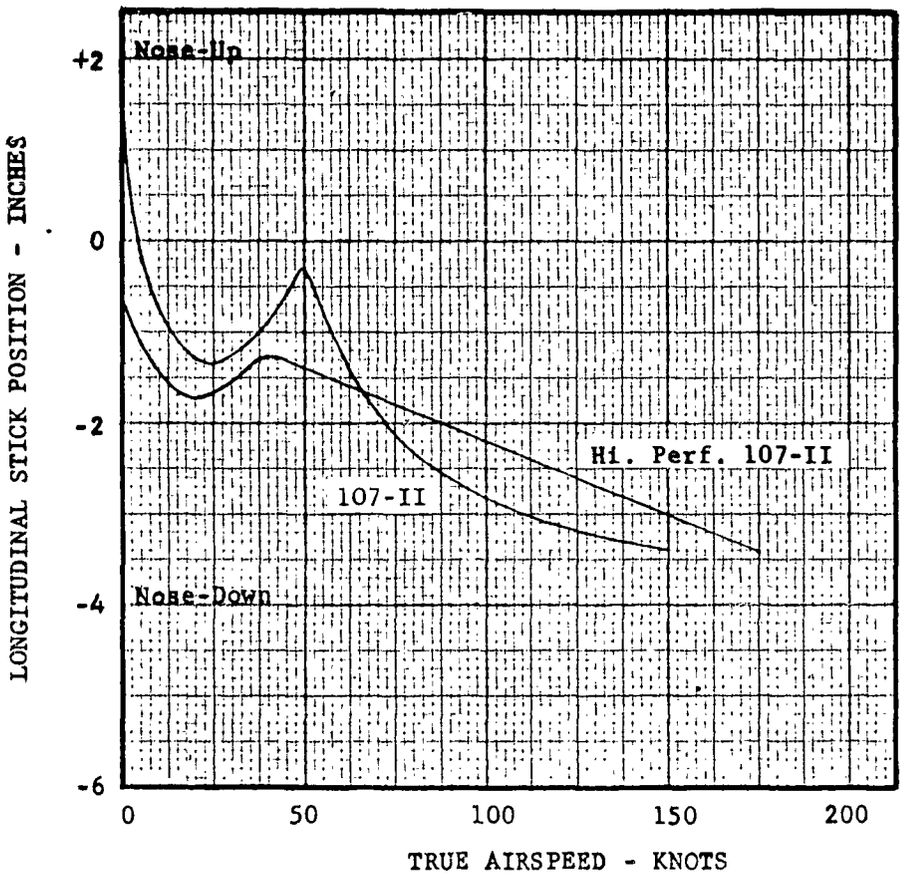
The introduction of the differential collective trim device into the control system insures that the variation of stick position with speed is stable. Figure 91 graphically demonstrates that both the High Performance 107-II and 107-II exhibit no adverse stick position gradients above 40 knots At speeds below 40 knots, a moderate amount of instability exists.

The conditions for which these particular gradients were determined are:

	High Performance 107-II	107-II
Gross Weight	15,165 lb.	15,500
Center of Gravity	18 in. Forward	23 in. Forward
Altitude	Sea Level	Sea Level
Tip Speed	650 fps	650 fps

FIGURE 91

SPEED STABILITY COMPARISON



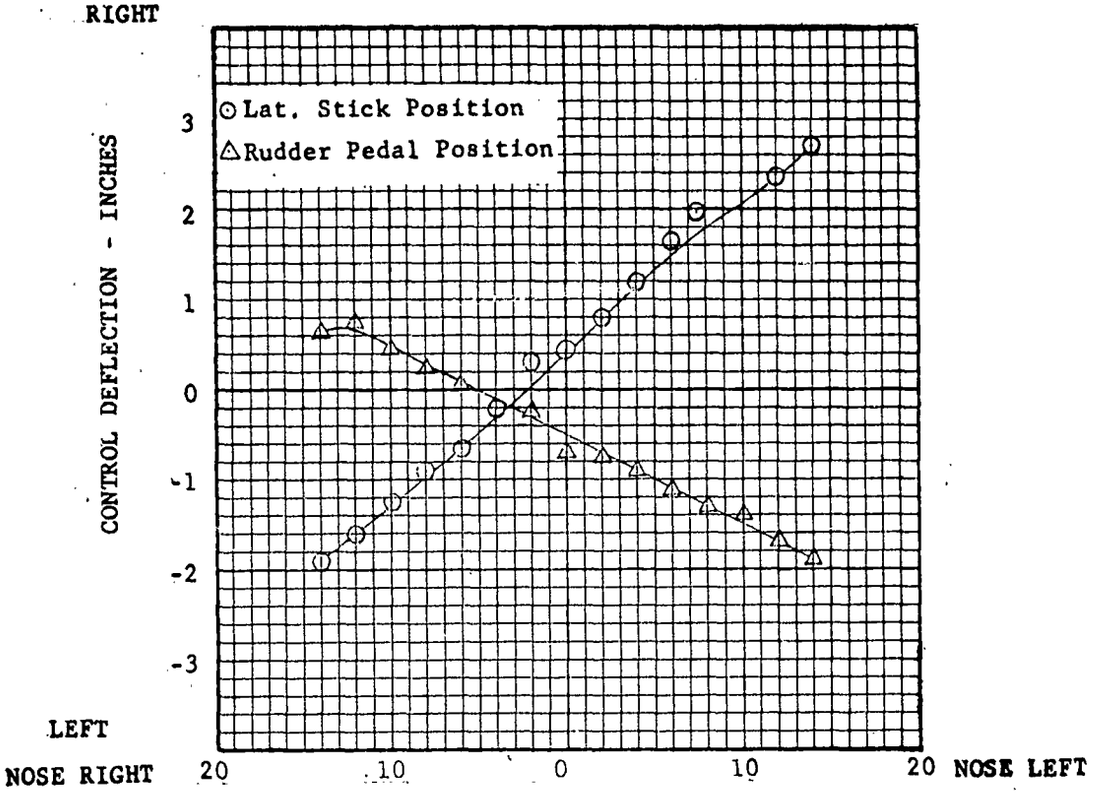
Static Directional Stability and Effective Dihedral

Figure 92 presents flight test data from the YHC-1A for lateral stick and rudder pedal positions required to trim for varying degrees of sideslip. The data indicates that this version of the 107 has positive directional stability and effective dihedral in addition to virtually linear control displacement variation with sideslip.

Comparison of 107-II rotor and fuselage stability derivatives and control powers with those of the High Performance version shows that the latter will have characteristics equal or superior to the 107-II over the entire speed range.

FIGURE 92

STATIC DIRECTIONAL STABILITY AND EFFECTIVE DIHEDRAL



Control Power and Controllability

The High Performance 107-II has sufficient control power to permit effective operation over the entire flight envelope. In particular, there is a large amount of inherent pitch control available due to the tandem rotor configuration.

IBM 650 digital computer programs were used to obtain longitudinal, lateral and directional control powers under the same flight conditions as those listed in Table VIII. These calculated control powers are presented for longitudinal cases in Figure 84. The corresponding lateral directional cases are shown in Figure 88.

Comparison with similar data for the 107-II reveals that, at the same flight condition, the High Performance 107-II can produce a larger control moment for an identical amount of stick or pedal deflection. This increased control effectiveness is primarily due to a 28% increase in blade chord over that used for the 107-II.

Pitch accelerations attainable, SAS off, at sea level maximum forward speed by moving the stick from its trim position to the nearest control stop are tabulated in Table XIII below. MIL-H-8501A (Section 3.2.1) dictates that helicopters shall be capable of at least 10% of the pitch acceleration obtainable in hover assuming movement of the control stick equal to its total throw. As the table indicates, the High Performance 107-II exceeds this requirement by an excellent margin.

TABLE XIII

LONGITUDINAL PITCH ACCELERATION AVAILABLE (DEG./SEC.^{2})

Gross Weight (Lbs.)	Center of Gravity	Altitude (Ft.)	Tip Speed (FPS)	MIL-H-8501A	Level Flight (173.6 Knots)
Normal 15,165	Normal	0	650	29.3	131.9
Ferry Mission 26,250	Normal	0	650	29.2	158.5

Flight testing has demonstrated that the 107 series has good control characteristics with SAS operative.

Table XIV presents the rolling accelerations produced by a lateral stick movement from the trim position to the nearest stop. Using the MIL-H-8501A (Section 3.3.4) of 10% of the maximum attainable rolling acceleration in hover, the 107 series exhibits a large margin at forward speedsof 135 and 173.6 knots.

TABLE XIV

ROLL ACCELERATION AVAILABLE (DEG./SEC.^{2})

Gross Weight (Lbs.)	Center of Gravity	Altitude (Ft.)	Tip Speed (F.P.S.)	MIL-H-8501A	Level Flight Speed 173.6 Kts.	135 Kts.
Normal 15,165	Normal	0	650	28.8	134.8	-
Ferry Mission 26,250	Normal	0	650	34.4	-	157.5

Effects of SAS on these accelerations are, in general, the same as on longitudinal characteristics.

Dynamic Response Characteristics

Studies of dynamic response to control input pulses have been carried out on the Vertol Pace 16-31R Real Time Analog computers. Behavior of the High Performance 107 was analyzed for the operating conditions summarized below in Table XV.

TABLE XV

SUMMARY OF ANALOG STUDIES

Model	Gross Weight(lbs.)	Velocity (knots)	Altitude (ft)	SAS	Data Presented
107-II	18,400	147.0	S.L.	off	Longitudinal
Hi. Perf. 107-II	15,165	174.0	S.L.	off	Longitudinal
107-II	18,400	147.0	S.L.	off	Lateral-Directional
Hi. Perf. 107-II	15,165	174.0	S.L.	off	Lateral-Directional
107-II	18,400	147.0	S.L.	on	Longitudinal
Hi. Perf. 107-II	15,165	174.0	S.L.	on	Longitudinal
107-II	18,400	147.0	S.L.	on	Lateral-Directional
Hi. Perf. 107-II	15,165	174.0	S.L.	on	Lateral-Directional
Hi. Perf. 107-II	26,250	135.0	S.L.	on	Longitudinal Lateral-Directional
Hi. Perf. 107-II	26,250	130.0	10,000	on	Longitudinal Lateral-Directional

Investigation has been limited to the maximum forward speed that can be attained at the gross weights and altitudes indicated. Response to other operating conditions within the normal flight envelope should reflect the same satisfactory tendencies as existing versions of the 107 series.

The Stability Augmentation System of the 107-II was applied to the High Performance 107 for purposes of this analysis. In reality, a developed version of this sytem would be used for optimum performance. The effect of this system upon the helicopter's behavior is representative of the dynamic responses which would be demonstrated if a SAS system tailored to the unique requirements of this aircraft were installed.

Analog traces presented are comparable to those obtained for the 107-II and YHC-1A flight test data. Reactions of the aircraft to a stick input pulse indicate that the required rates are of comparable magnitude and in the required direction. The damping displayed is more than adequate to insure smooth and comfortable flight at high forward speeds.

Figures 93a through 93d represent the responses of the Boeing-Vertol 107-II and the High Performance 107 at their respective maximum forward speeds, SAS off. The data indicates that both aircraft are dynamically unstable and they diverge rapidly. A comparison of data does indicate, however, that the High Performance 107 is less divergent than the 107-II but the aircraft does not exhibit sufficient dynamic stability to meet the requirements of MIL-H-8501.

The addition of a Stability Augmentation System alters the dynamic responses of the aircraft such that both are well within the MIL-H-8501 requirements. Figures 94a and 94b are representative of the responses resulting from a 1" =1 second pulse with a SAS incorporated in the control system. The data presented tends to confirm that the High Performance 107-II is superior to the prototype but that a SAS is required in order to provide desirable flying qualities during high speed flight.

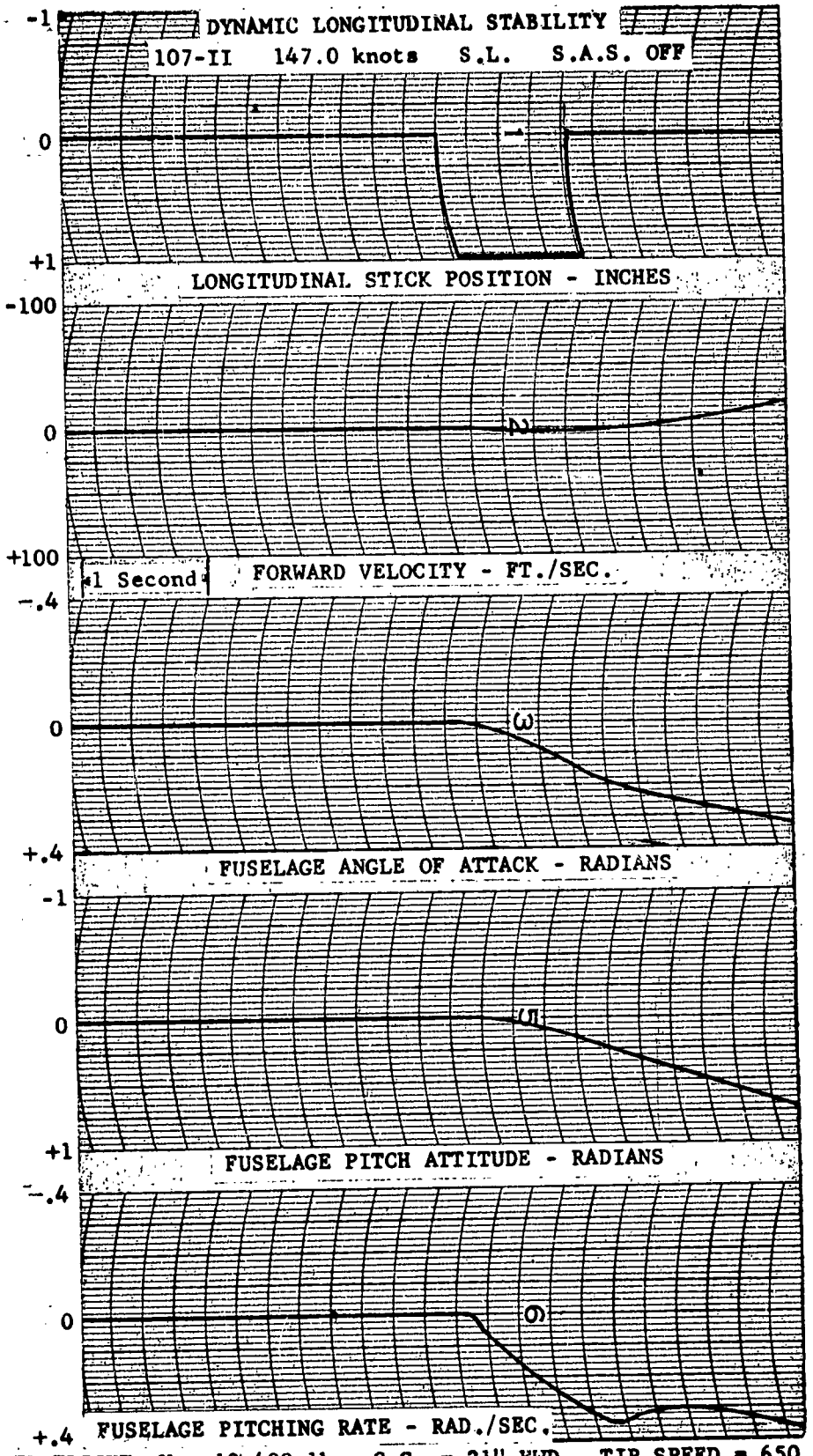
The traces also indicate that a moderate increase of pitch attitude and pitching velocity is experienced in response to a pulse input as the gross weight and altitude are increased. This condition can be readily controlled and is not considered to be of such a magnitude as to constitute a deficiency. A more detailed design of the configuration, undertaken in the development of a prototype would undoubtedly lead to a complete elimination of this mild divergence.

The behavior exhibited by the High Performance 107-II when a lateral stick input is fed into the dynamic system tends to indicate that the Stability Augmentation System exerts considerable damping on the system. No discontinuities in initial direction or rate are indicated for the stick input shown. The absence of sideslip associated with the lateral stick input shown indicates that this aircraft can execute an excellent coordinated turn.

The dynamic characteristics shown herein, can be altered by an optimization of the SAS for the particular aircraft. For purposes of evaluation, however, no deficiencies are incurred with the increase of speed capability of the High Performance 107-II over the other aircraft of the 107 series.

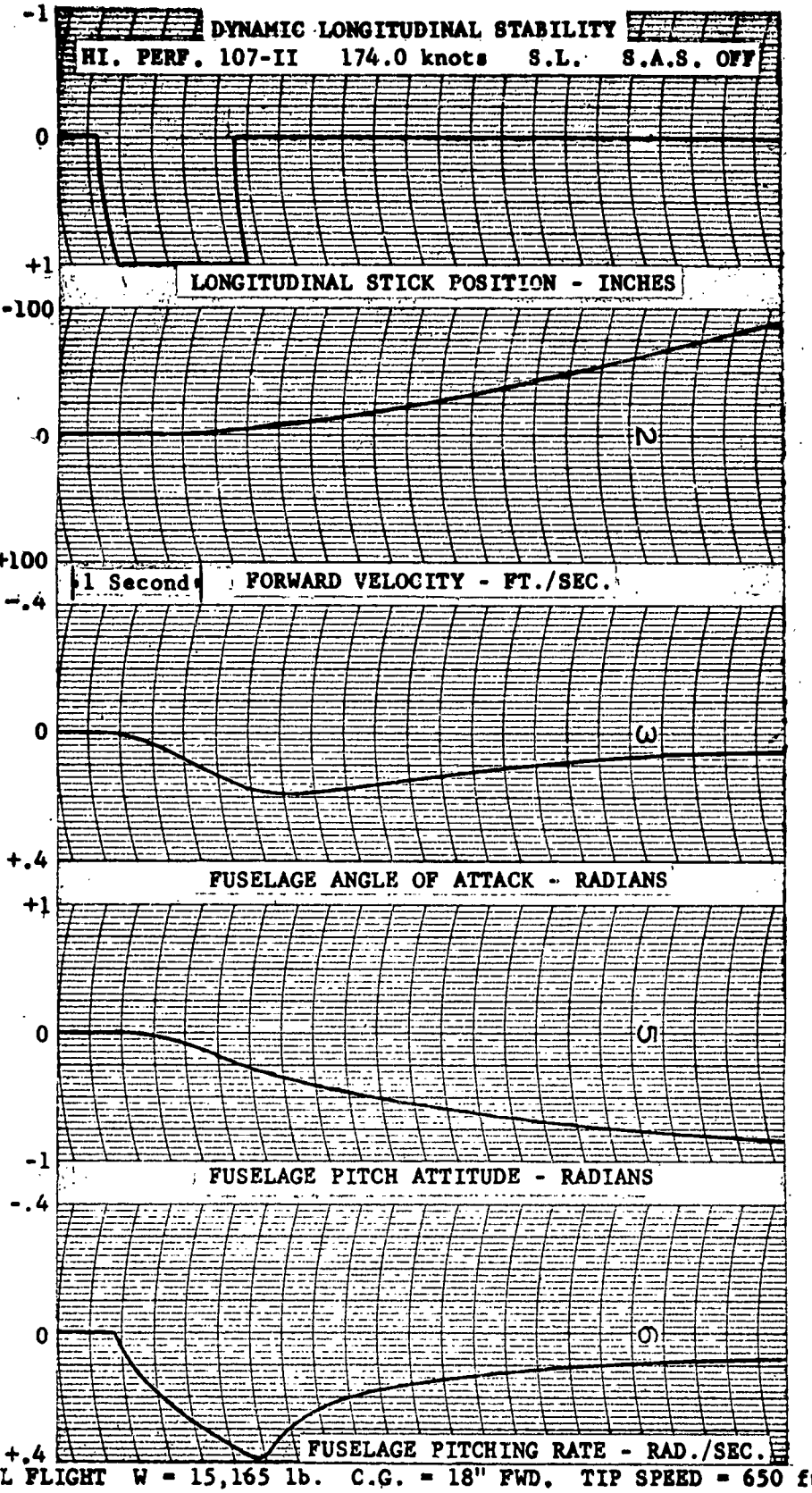
The cases investigated indicate that the increased performance capability of the High Performance 107-II does not influence the excellent flying qualities inherent in the 107 series aircraft.

FIGURE 93a



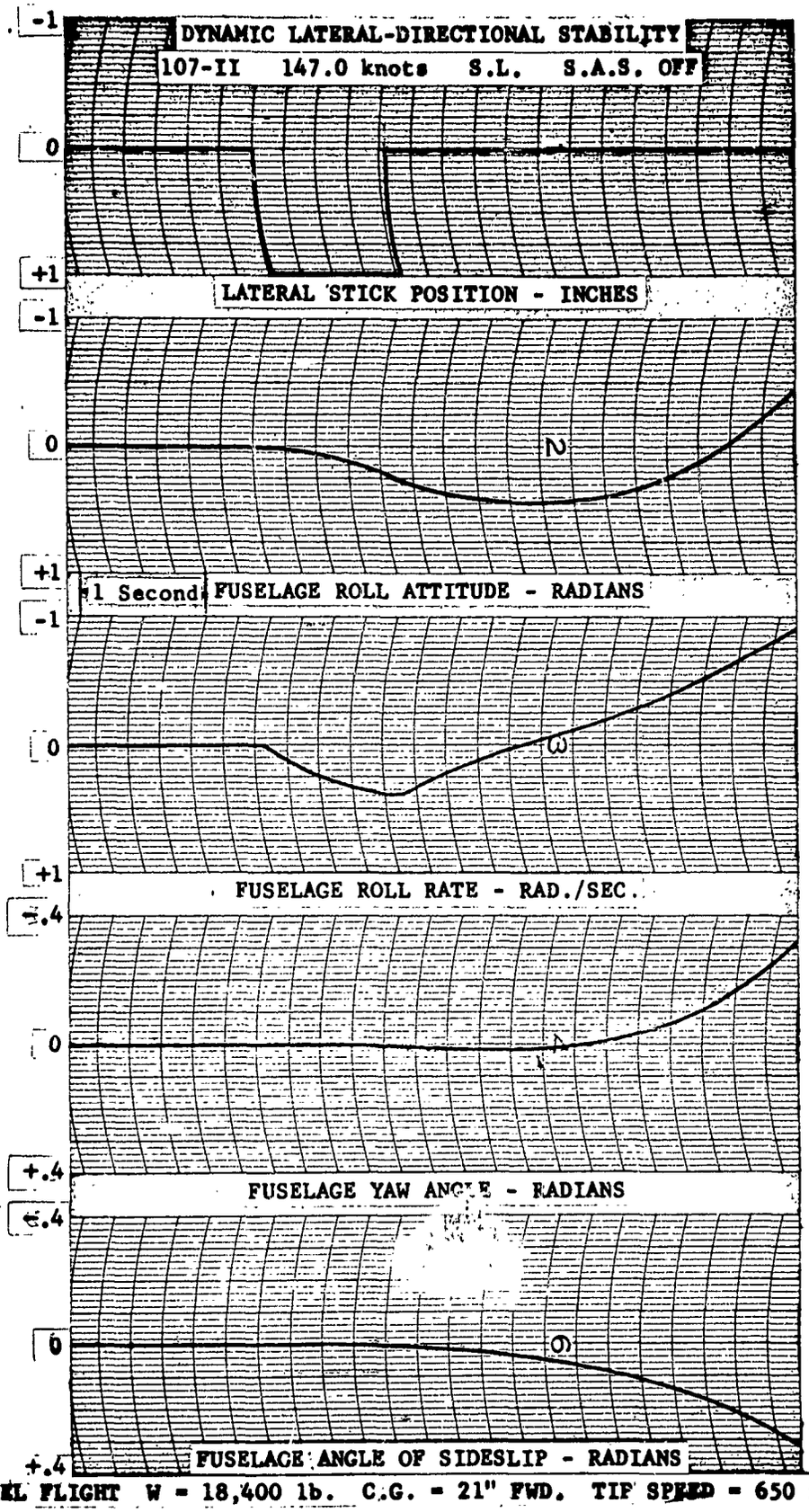
LEVEL FLIGHT W = 18,400 lb. C.G. = 21" FWD. TIP SPEED = 650 ft./sec.

FIGURE 93b



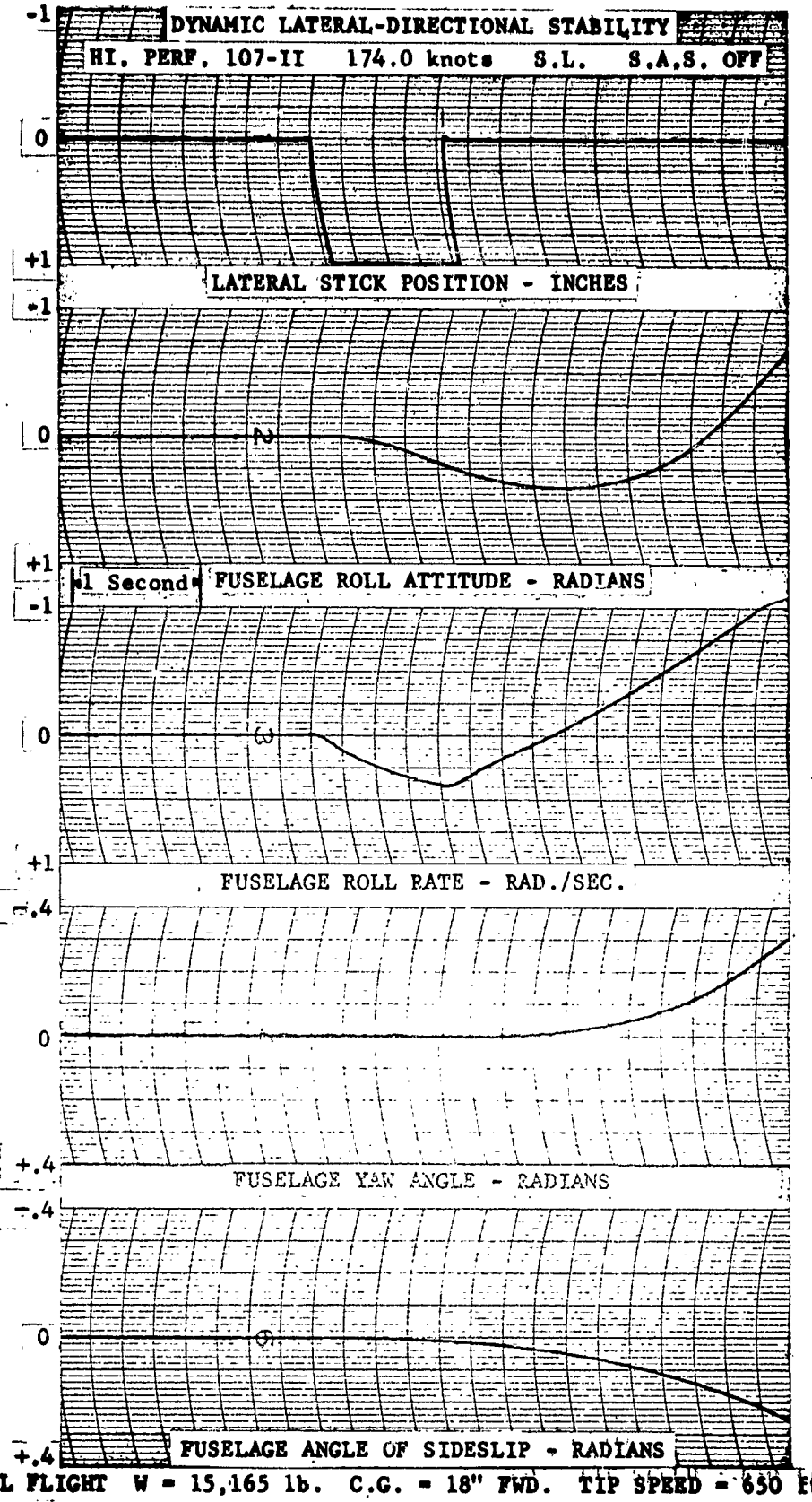
LEVEL FLIGHT W = 15,165 lb. C.G. = 18" FWD. TIP SPEED = 650 ft./sec.

FIGURE 93c



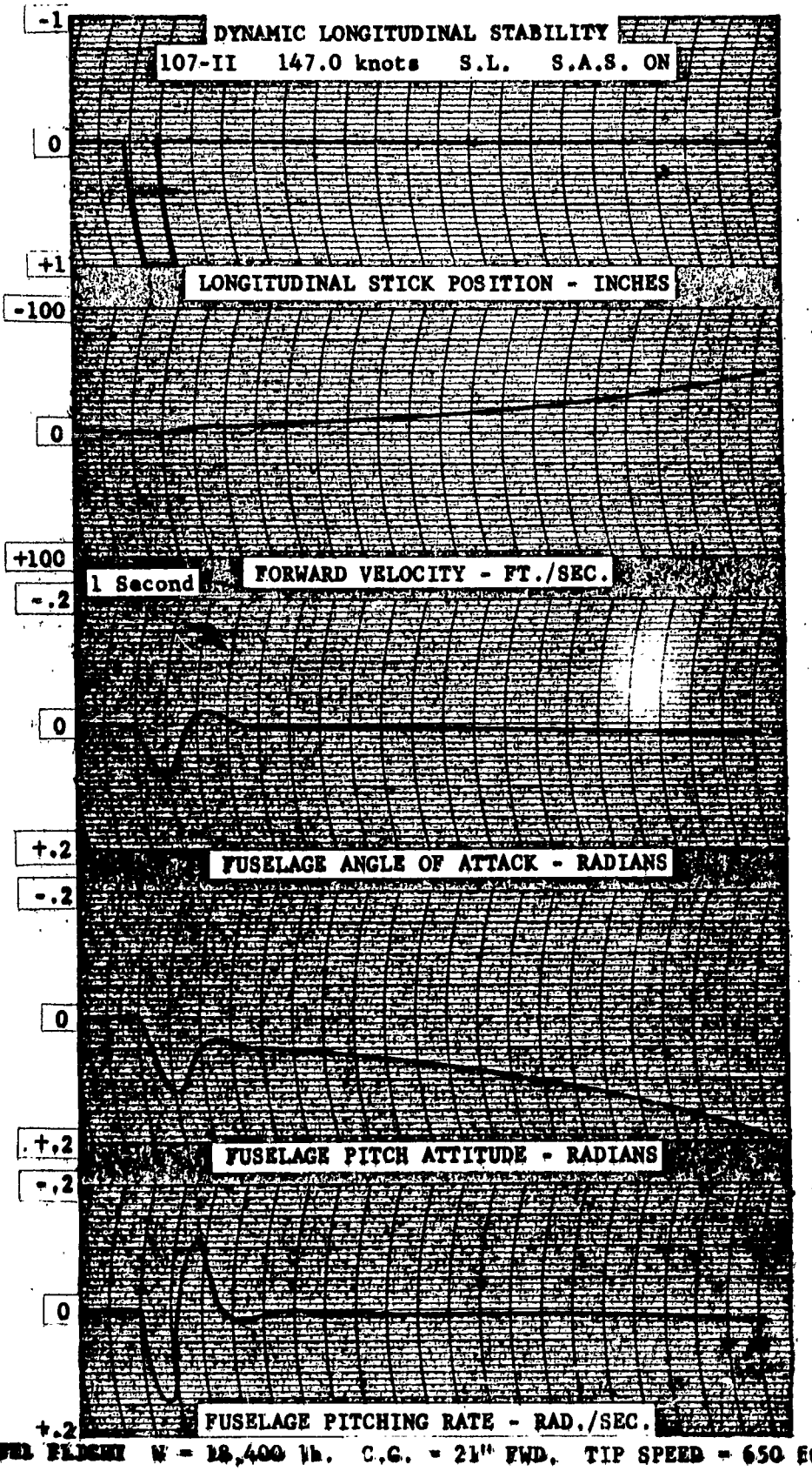
LEVEL FLIGHT W = 18,400 lb. C.G. = 21" FWD. TIP SPEED = 650 ft./sec.

FIGURE 93d



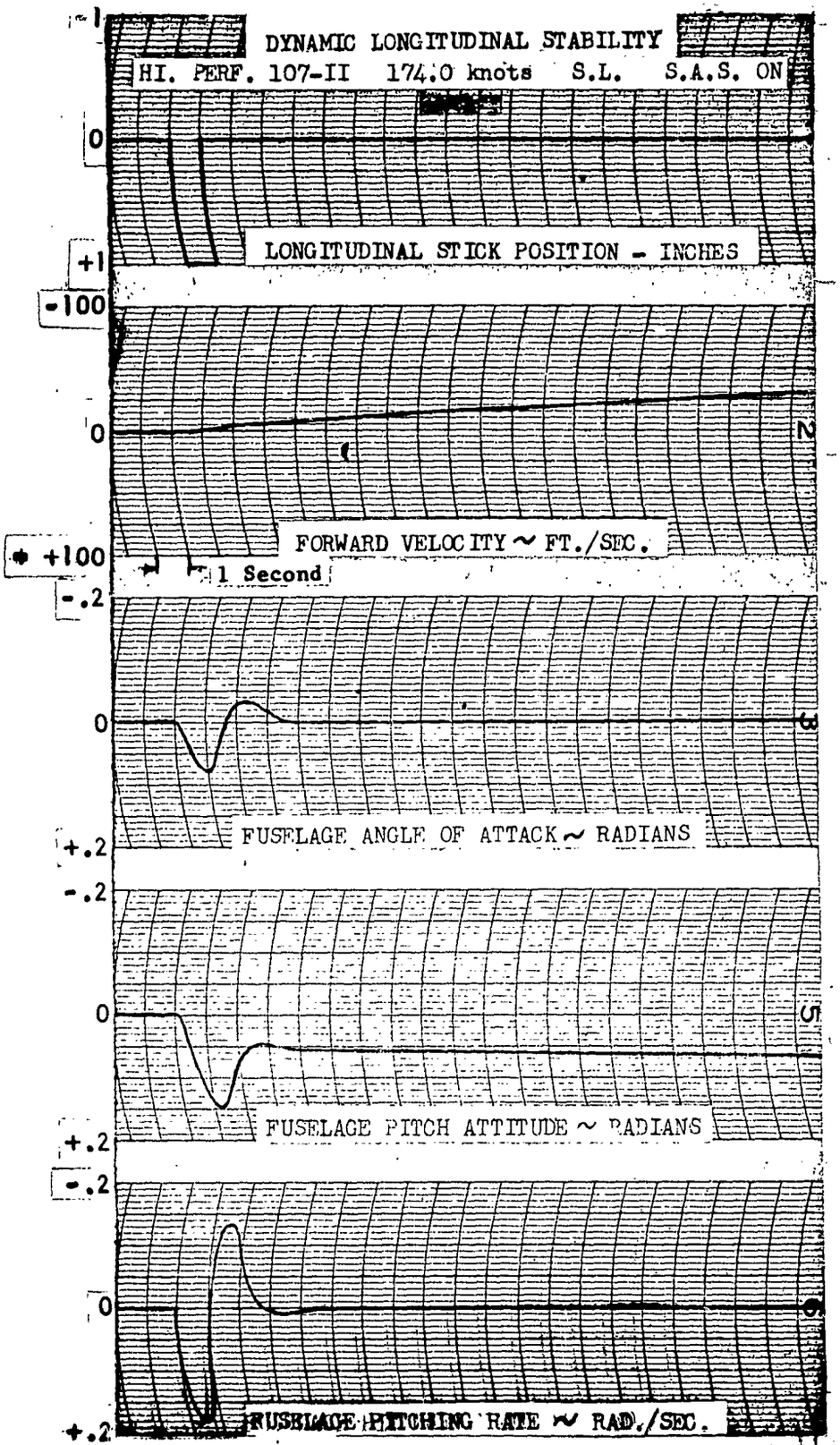
LEVEL FLIGHT W = 15,165 lb. C.G. = 18" FWD. TIP SPEED = 650 ft./sec

FIGURE 94a



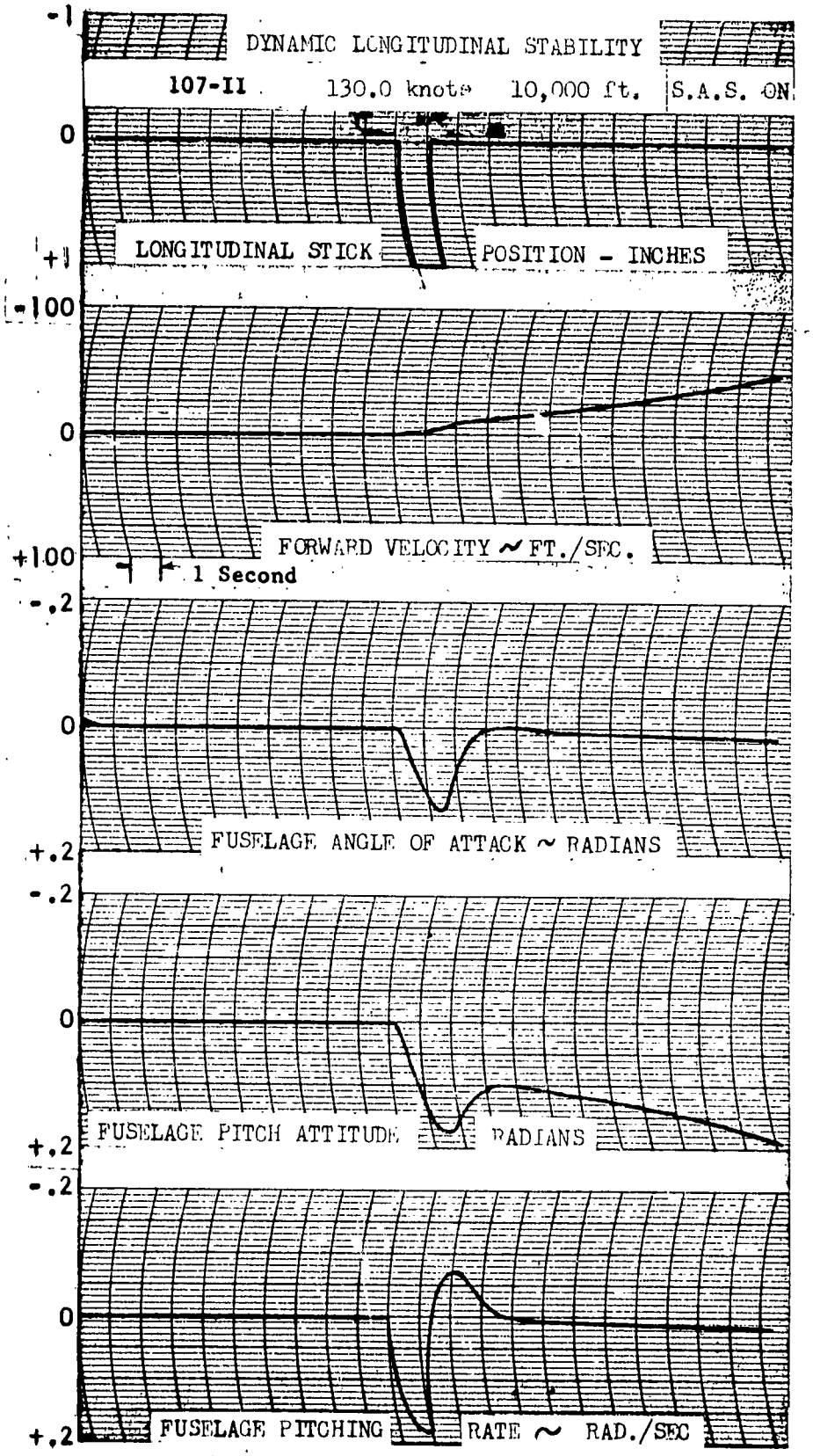
LEVEL FLIGHT W = 18,400 lb. C.G. = 21" FWD. TIP SPEED = 650 ft./sec.

FIGURE 94b



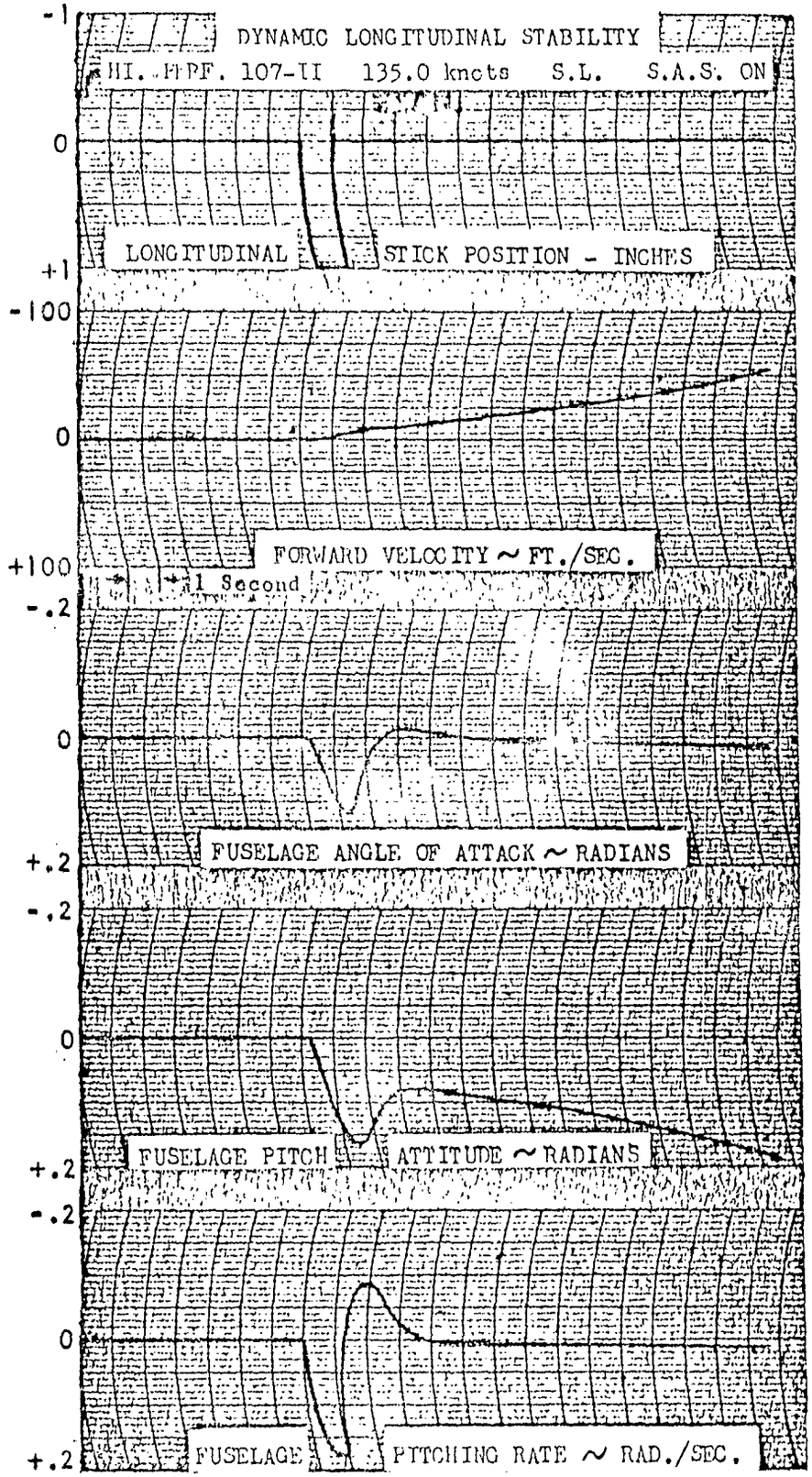
LEVEL FLIGHT W = 15,165 lb. C.G. = 18" FWD. TIP SPEED = 650 ft./sec.

FIGURE 94c



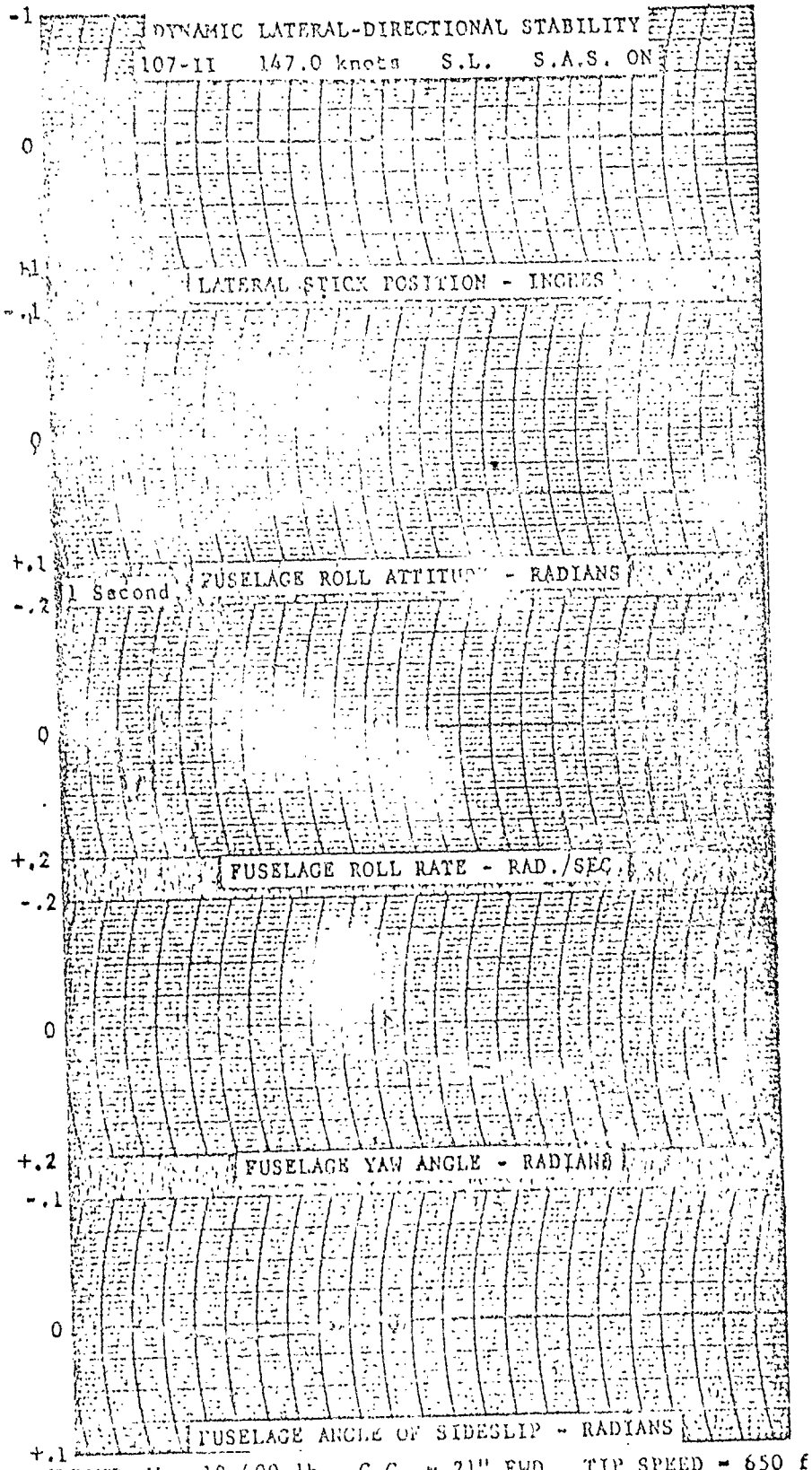
LEVEL FLIGHT W = 26,250 lb. C.G. = 18" FWD. TIP SPEED = 700 ft./sec.

FIGURE 94d



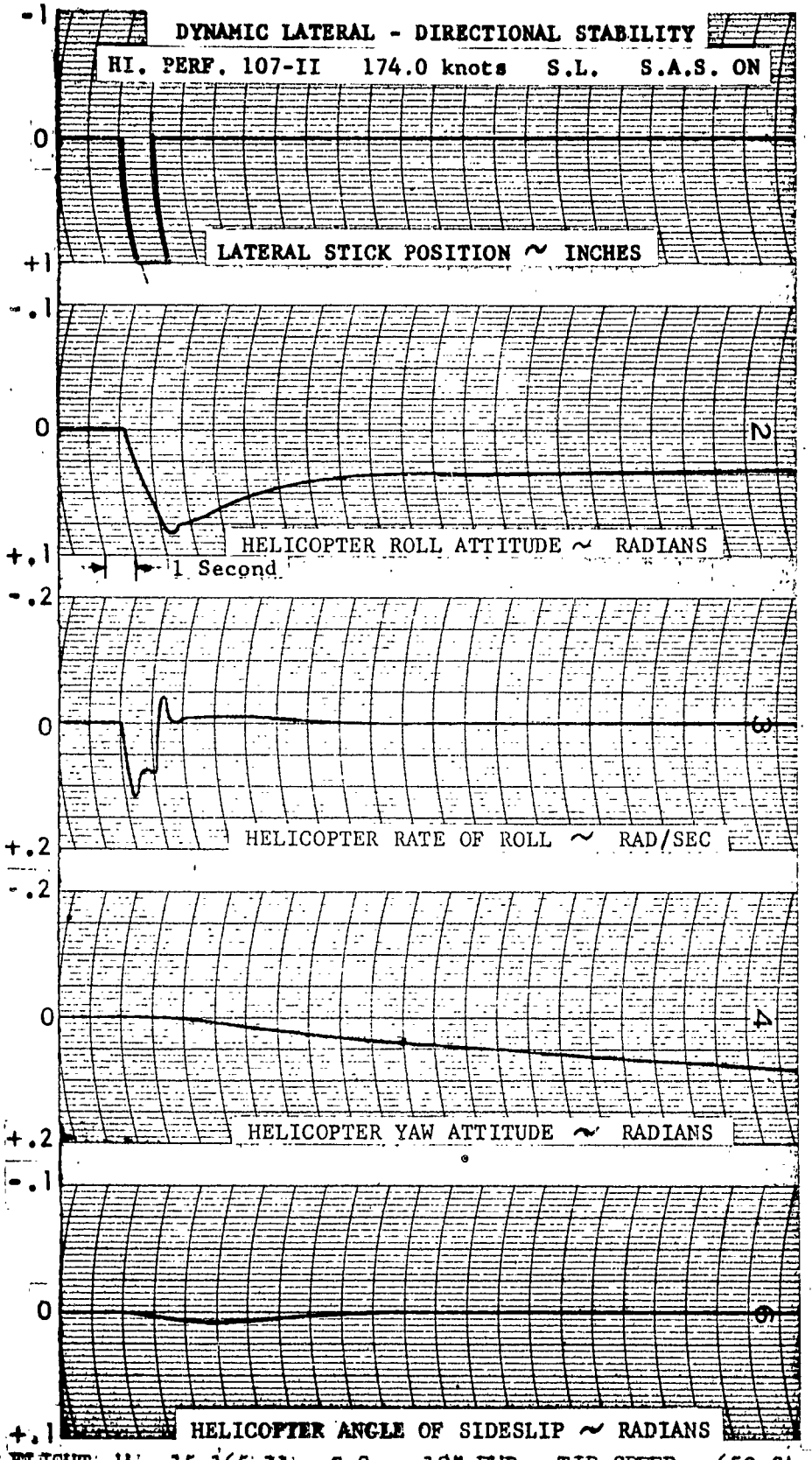
LEVEL FLIGHT W = 26,250 lb. C.G. = 18" FWD. TIP SPEED = 650 ft./sec.

FIGURE 94e



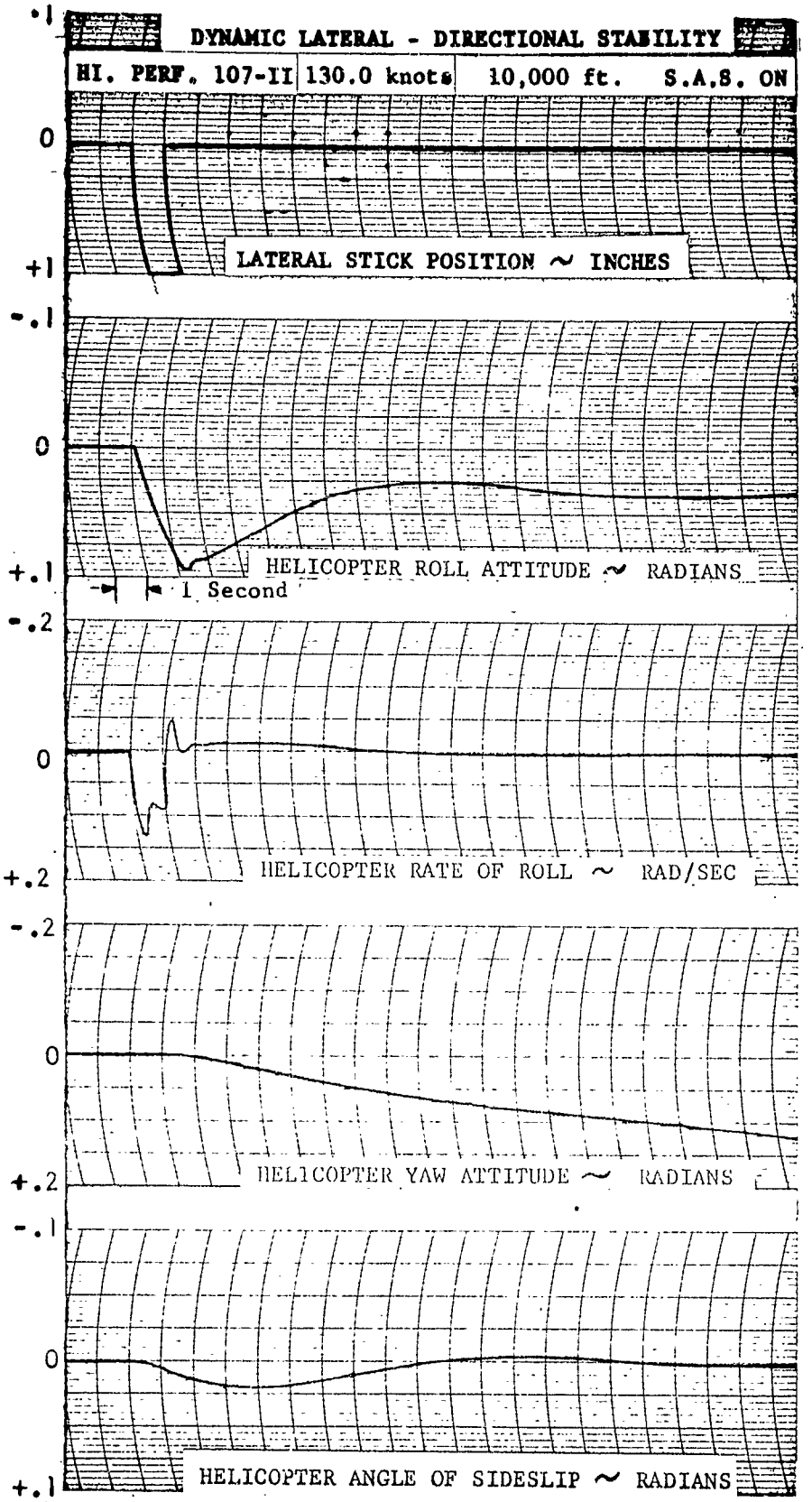
LEVEL FLIGHT W = 18,400 lb. C.G. = 21" FWD. TIP SPEED = 650 ft./sec.

FIGURE 94f



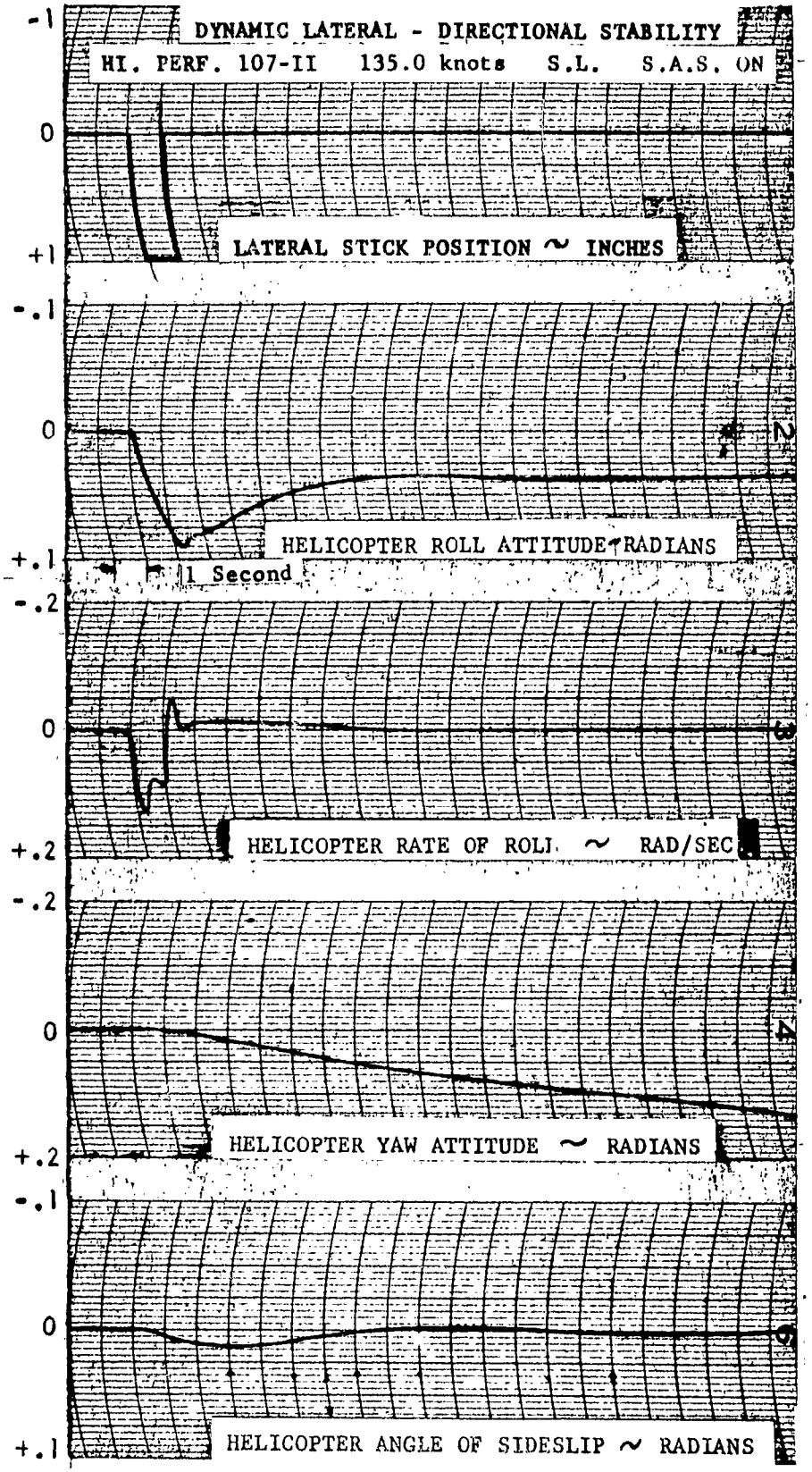
LEVEL FLIGHT W = 15,165 lb. C.G. = 18" FWD. TIP SPEED = 650 ft./sec.

FIGURE 94g



LEVEL FLIGHT W = 26,250 lb. C.G. = 18" FWD. TIP SPEED = 700 ft./sec.

FIGURE 94h



LEVEL FLIGHT W = 26,250 lb. C.G. = 18" FWD. TIP SPEED = 650 ft./sec.

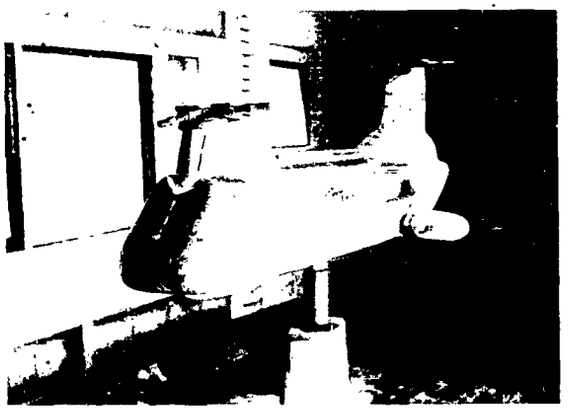
WIND TUNNEL TESTS

Wind tunnel tests were conducted on a 1/8 scale model of the Boeing-Vertol High Performance 107-II at the University of Maryland during the period November 13 through November 18, 1960. The configuration tested included: (1) removal of the landing gear (for all runs), (2) modifications to the fuselage after body, (3) an extended chord aft pylon, (4) aft pylon fairing, (5) a rudder on the aft pylon, (6) nose gear fairing for the retracted gear, (7) and two locations of the stub tanks at 8.5° of incidence. All tests were conducted at a tunnel velocity of approximately 200 mph. The effective Reynolds Number, based on model length was 10.9×10^6. The primary purpose of the tests was to minimize the drag of the model in the high speed configuration.

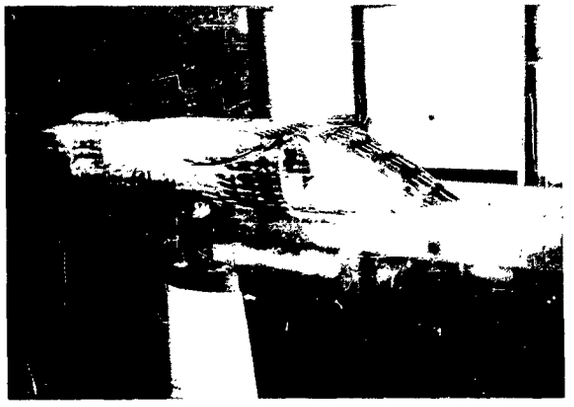
In addition to obtaining force and moment data on the six component balance systems in pitch and yaw, luminescent oil runs, tuft studies, and rudder deflection runs were made. (As illustrated below). Promising configurations were tested in yaw.

FIGURE 95

WIND TUNNEL TEST OF THE HIGH PERFORMANCE 107-II



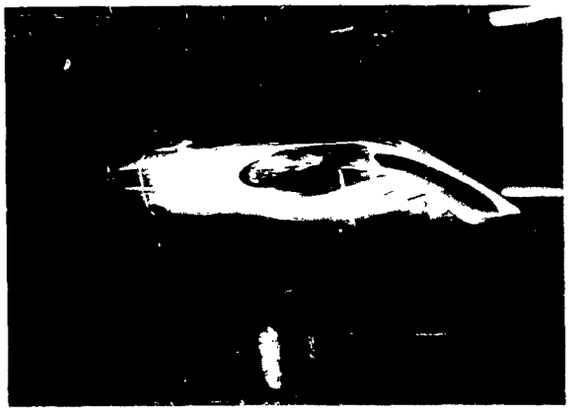
3/4 FRONT VIEW



TUFT STUDY



LUMINESCENT OIL STUDY



LUMINESCENT OIL STUDY

FUSELAGE

The standard nose and constant cross section portion of the model was tested throughout the entire series of tests. However, three afterbodies were tested in pitch and are summarized in the following table:

TABLE XVI

COMPARISON OF AFTERBODIES

Afterbody	α @D/q min	D/q min	L/q@$\alpha=0^o$	D/q@$\alpha=0^o$
Model II	7.5^o	5.78	-8.4	6.54
Flattened Rear Ramp	7.7^o	5.56	-9.1	6.51
Hi-Perf.	5.6^o	5.42	-6.3	5.66

It may be noted from the above table that the High Performance 107-II afterbody produces less negative lift than the other two configurations at the design angle of attack of zero degrees, indicating that some of the drag attributed to the other afterbodies may be induced drag. This is further substantiated by the fact that minimum drag occurs near zero L/q for all afterbody configurations. The High Performance 107-II afterbody characteristics are shown in Figure 97.

A determining factor in base fuselage minimum drag is the position of the apex of the tail cone in relation to the centerline of the fuselage. The present high position associated with rear ramp loading establishes large positive angles of attack for minimum drag and hence increases profile drag.

A comparison of the wetted area drag coefficient of the High Performance 107-II fuselage alone and empirical data from Reference 20 is shown below.

FIGURE 96

WETTED AREA DRAG COEFFICIENT
VS
REYNOLD'S NUMBER

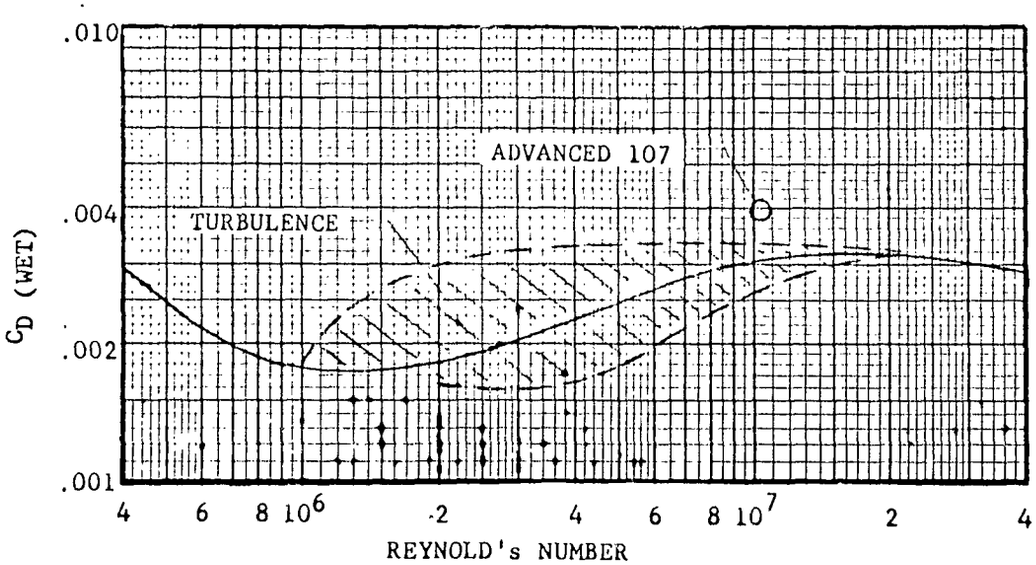
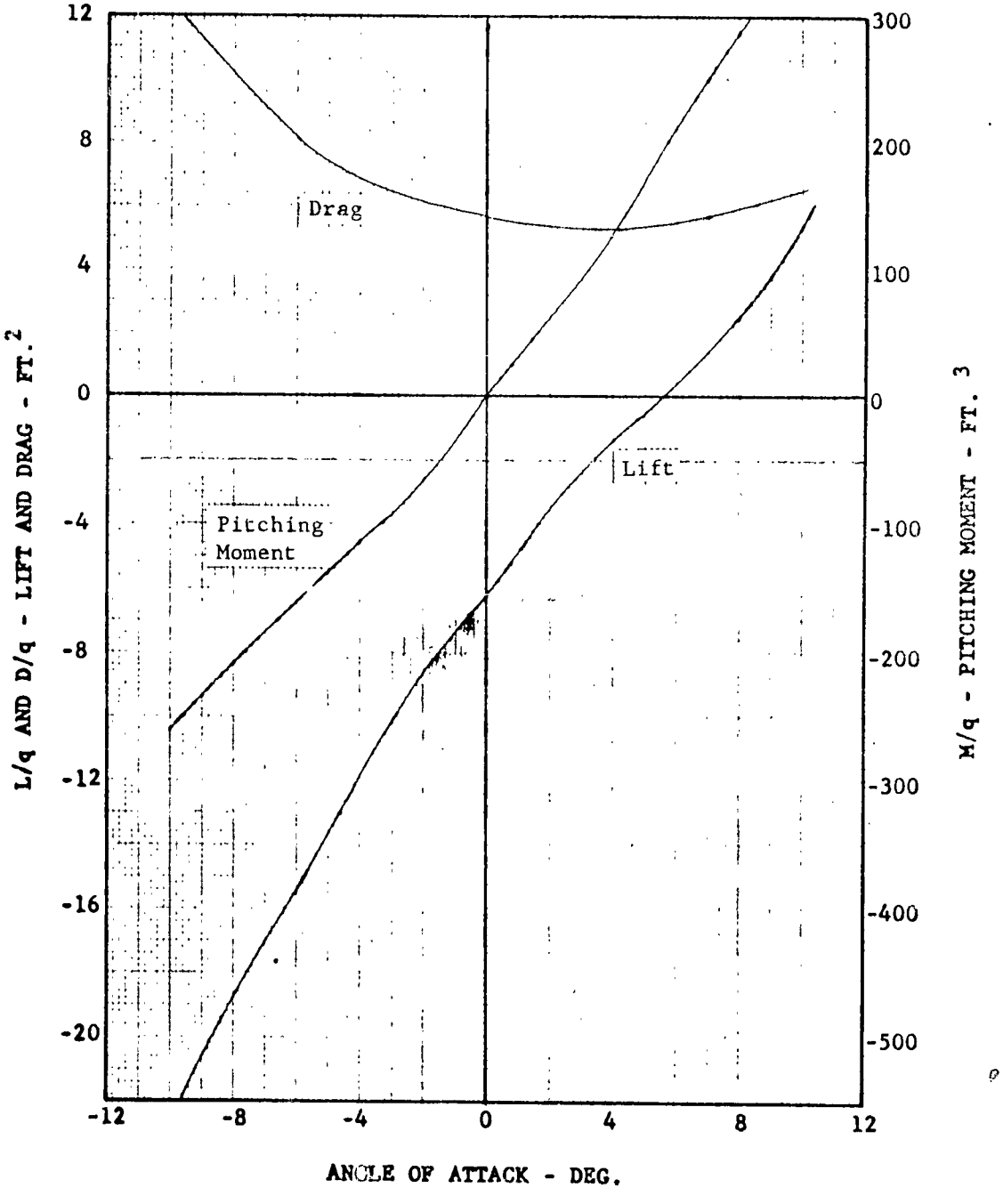


FIGURE 97

LIFT, DRAG, AND PITCHING MOMENT VS ANGLE OF ATTACK
FUSELAGE ALONE
$R.N._e = 10,910,000$



Extensive wind tunnel testing during the development of the YHC-1B permits a comparison of the High Performance 107-II results with minimum drag data for the YHC-1B. Experimental data from other sources is also shown. Table XVII presents this comparison.

TABLE XVII COMPARISON OF FUSELAGE DRAG

REFERENCE	CONFIGURATION	R.N.*	L/D (Fineness)	Wetted Area Model	Frontal Area Model	C_D Wet	$C_{D_{ff}}$ Frontal Area	$\Delta D/q$ (Friction)	$\Delta D/q$ (Form)	F_e (Full Scale)	D/q Model
High Performance Model 107-II	HIGH SPEED	10.4×10^6 (M.S.) 81.5×10^6 (F.S.)	5.84	21.22	.721	.00404	.1190	3.98	1.52	5.50	.086
Perkins & Hage	Streamlined	25×10^6	5.84	-	.721	-	.067	-	-	3.10	0485
Horner	Streamlined	10.4×10^6	5.50	21.22	-	.0025	-	-	-	3.40	.0532
Horner	Streamline Stimulated Turbulence	10.4×10^6	5.50	21.22	-	0035	-	-	-	4.87	.0745
Horner	Streamline Stimulated Turbulence	87.5×10^6	5.50	21.22	-	.0024	-	-	-	3.27	.051
Chinook	Short Afterbody	8.26×10^6	4.97	20.98	1.095	.00591	.113	4.20	3.70	7.90	.1238
Chinook	Standard Afterbody	8.26×10^6	5.42	22.56	1.095	.00452	.093	4.50	2.00	6.50	.1018
Chinook	Long Afterbody	8.26×10^6	6.03	24.86	1.095	.00384	.087	4.90	1.20	6.10	.0955
Chinook	Short Beaver Tail Afterbody	8.26×10^6	4.97	21.07	1.095	.00602	.116	4.20	3.90	8.10	.1268
Chinook	Standard Beaver Tail Afterbody	8.26×10^6	5.42	22.63	1.095	.00397	.082	4.50	1.25	5.75	.090
Chinook	Long Beaver Tail Afterbody	8.26×10^6	6.03	24.98	1.095	.0032	.073	4.90	.20	5.10	.0798
Chinook	Tear-Drop Standard Afterbody	8.26×10^6	5.42	21.96	1.095	.0041	.082	4.45	1.30	5.75	.090
Landing Gear Drag Study Princeton Report No. 357	Simulated Fuselage	2.84×10^6 1.20×10^6	3.94 3.94	- -	1.70 1.70	- -	.103 .1015	- -	- -	- -	176 .174

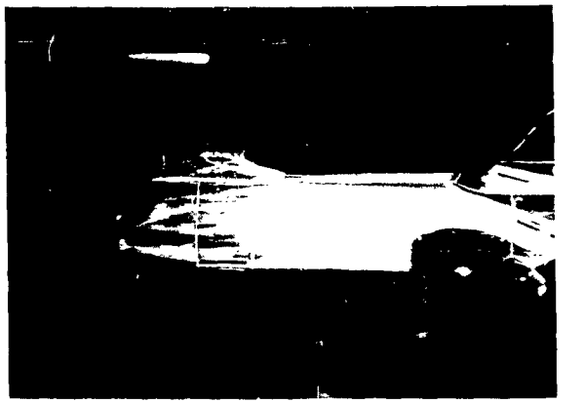
*(Not Corrected for Turbulence)

FORWARD PYLON

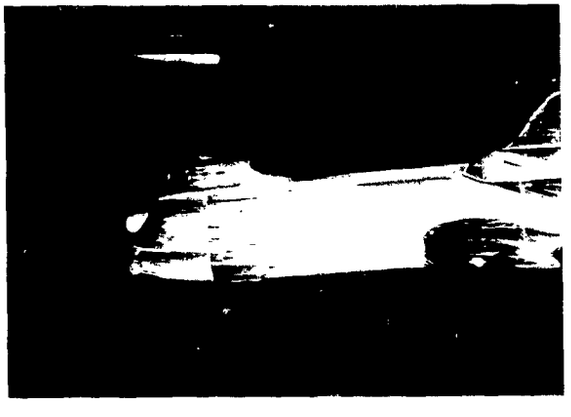
The forward pylon tested was the same pylon tested on the Model 107-II. Resulting increments of drag for this pylon were very small, even at higher or lower angles of attack.

FIGURE 98

LUMINESCENT OIL PHOTOGRAPHS - FORWARD PYLON



$\alpha = 0^\circ$



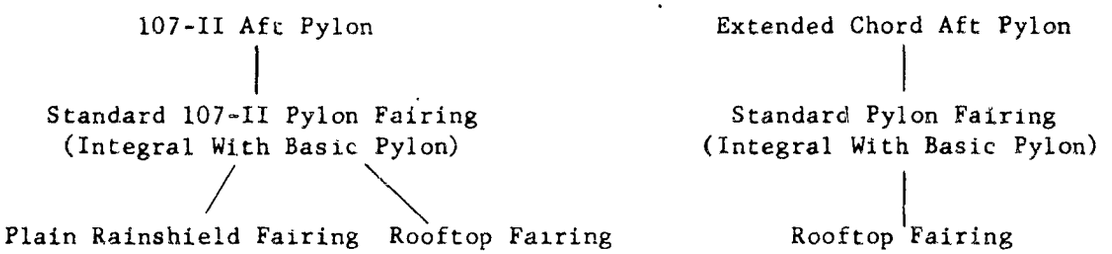
$\alpha = -5^\circ$

ROTOR HUBS

The forward and aft rotor hubs tested on this model were not of the same scale as the model or of the same configuration to be used on the final configuration. The primary function of these hubs was to simulate interference effects on the pylons.

AFT PYLONS AND FAIRINGS

Two aft pylons were tested. The first pylon was the basic 107-II with an attached rudder. The second pylon had an extended chord and an attached rudder. The schematic below diagrams which fairings were used with the pylons.



The standard fairings were present on all aft pylon configurations The rainshield and rooftop fairings were appendages near the top of the pylon to reduce interference effects from the rotor hubs With rotor hubs mounted, the configuration netting the least drag increment (6 18 ft ^{2}) was the extended chord pylon with a rooftop fairing and hub

NOSE GEAR FAIRINGS

Three different nose gear fairings were tested to enclose the partially retracted nose gear. None of the fairings had any appreciable effect on lift, drag, or moment In general, the fairings added from zero to .30 ft^2 of drag area.

STUB TANKS

The two stub tank configurations were identical except for location, one position being aft, the other position forward. Stub tanks were mounted with $8\frac{1}{2}^{o}$ positive incidence for all tests involving the tanks. The general configuration for the stub tanks forward and aft are shown in Figure 99.

The testing of the stub tanks in the forward position was deemed advisable to establish the tank drag with minimum interference effects. The minimum drag of the stub tanks is approximately .85 ft.^{2} with interference drag adding approximately .30 ft.^{2}. Figure 100 presents the lift, drag and pitching moment versus angle of attack with aft stub tanks.

FIGURE 99

LUMINESCENT OIL PHOTOGRAPHS - STUB TANKS



FORWARD POSITION



AFT POSITION

FINAL CONFIGURATION

The best configuration to emerge from this series of wind tunnel tests incorporated the High Performance 107-II afterbody, the extended chord pylon and rooftop fairing, a Vertol Design nose gear fairing, and stub tanks in the aft position.

This configuration was thoroughly tested in pitch at zero yaw angle, and in yaw at constant angles of attack from -10^{o} through $+15^{o}$. Figure 101 presents the lift, drag and pitching moment characteristics in pitch. Figure 102 gives the yawing moment characteristics in yaw and Figure 103 gives a yawing moment comparison of the present 107-II aft pylon with the extended chord pylon with a rooftop rainshield fairing.

The characteristics of the finalized aircraft in pitch show a minimum drag value of 20.5 $ft.^2$ occurring at approximately -2.5^{o}. This value of drag compares to 30.2 $ft.^2$ for the Boeing-Vertol 107-II.

The extended chord pylon with the larger rudder is the most effective in yaw and deflection. The yawing moment is more effective with positive deflections than with negative deflections because of the cambered aft pylon. The yawing moment data versus angle of yaw appear erratic because of the saw-tooth pattern. This is merely due to slots in the forward pylon relieving the pressure on the forward pylon as it progresses through yaw angle. Oil studies, and the static directional stability characteristics are presented in Figures 104 and 105.

FIGURE 100

LIFT, DRAG, AND PITCHING MOMENT VS. ANGLE OF ATTACK
FUSELAGE WITH AFT STUB TANKS
R.N.$_e$ = 10,910,000

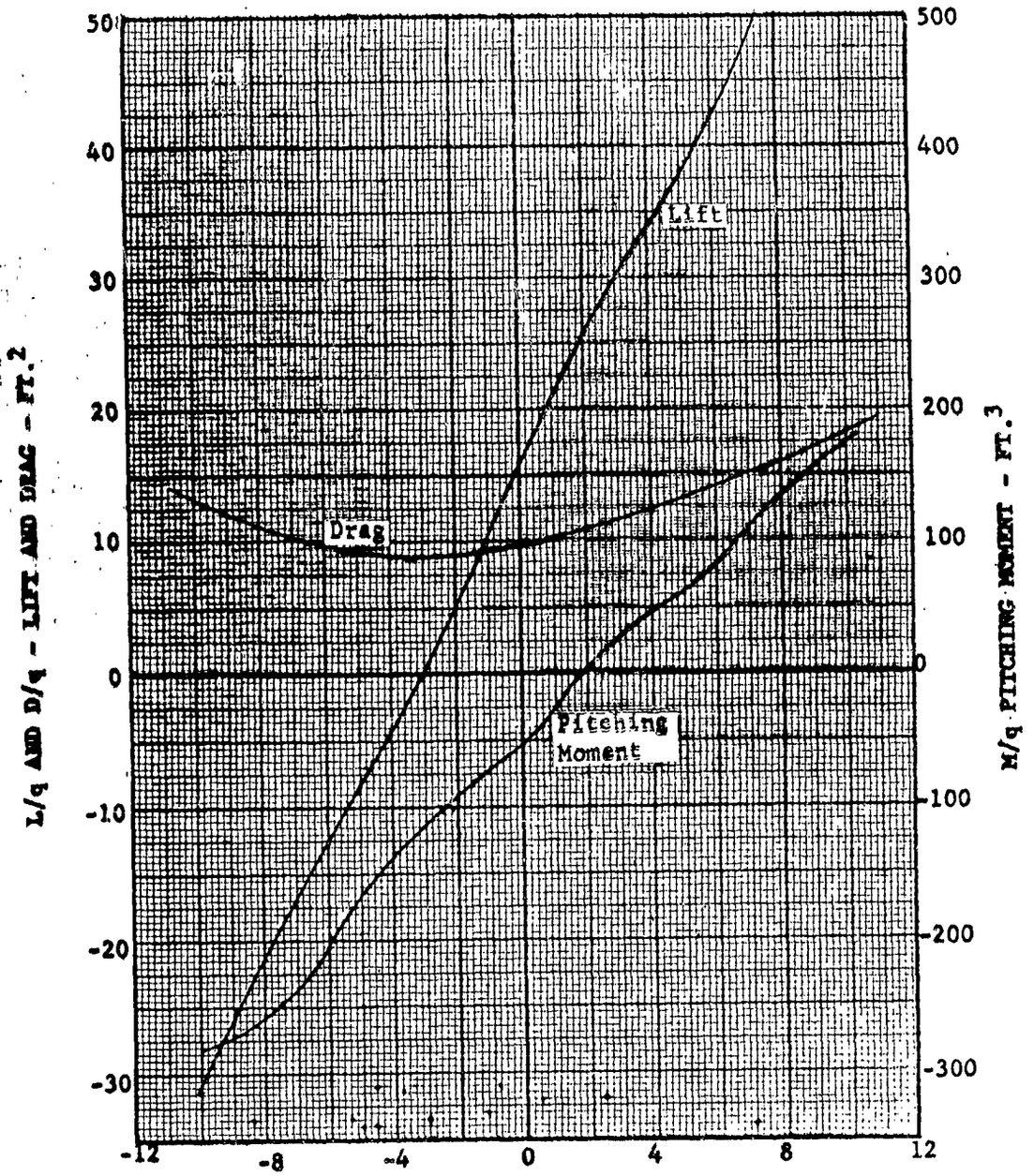


FIGURE 101

LIFT, DRAG, AND PITCHING MOMENT VS. ANGLE OF ATTACK
FINAL CONFIGURATION
$R.N._e = 10,910,000$

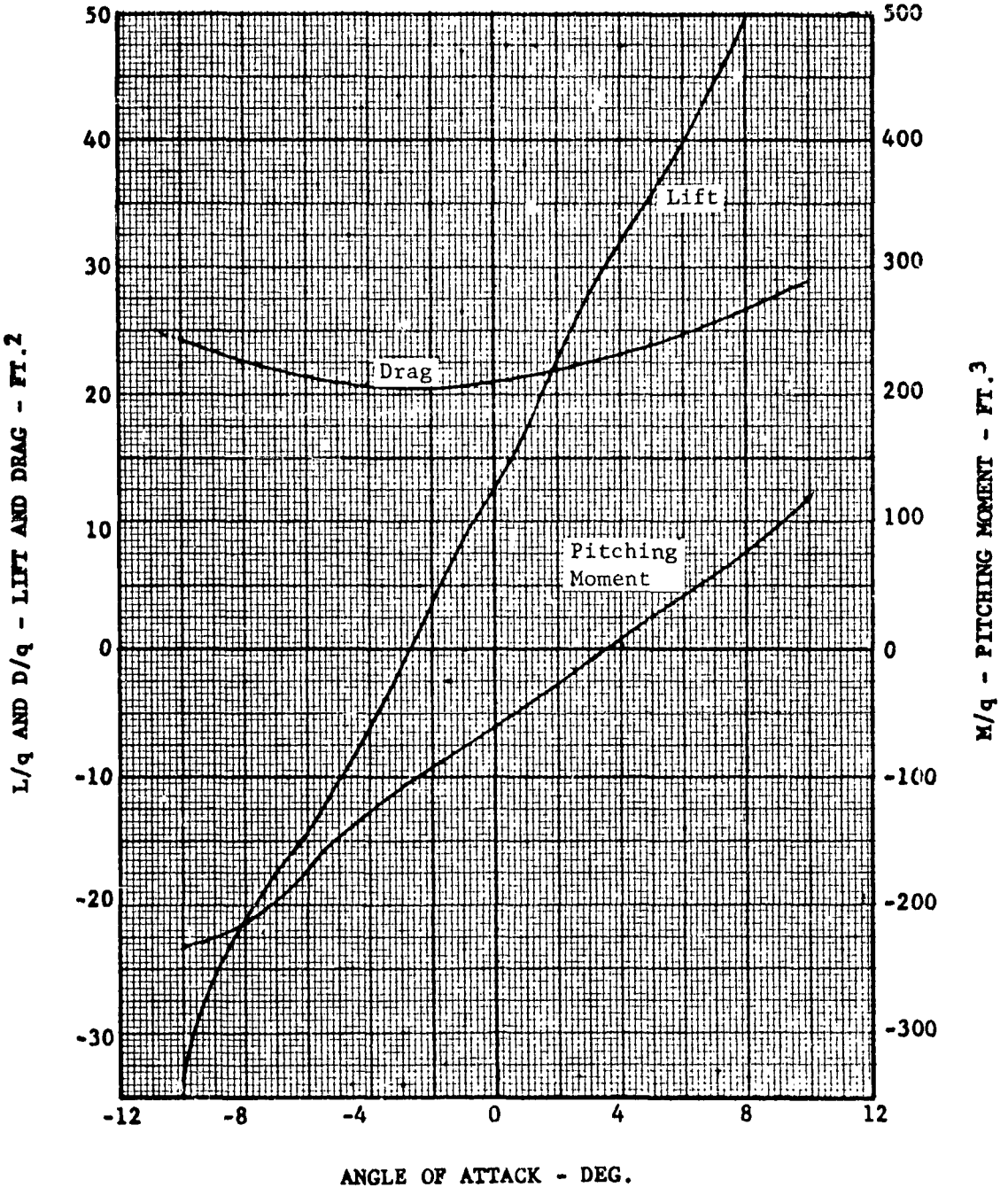


FIGURE 102
YAWING MOMENT, ROLLING MOMENT, AND SIDE FORCE VS. ANGLE OF YAW
FINAL CONFIGURATION
$R.N._e = 10,910,000$
BODY AXIS

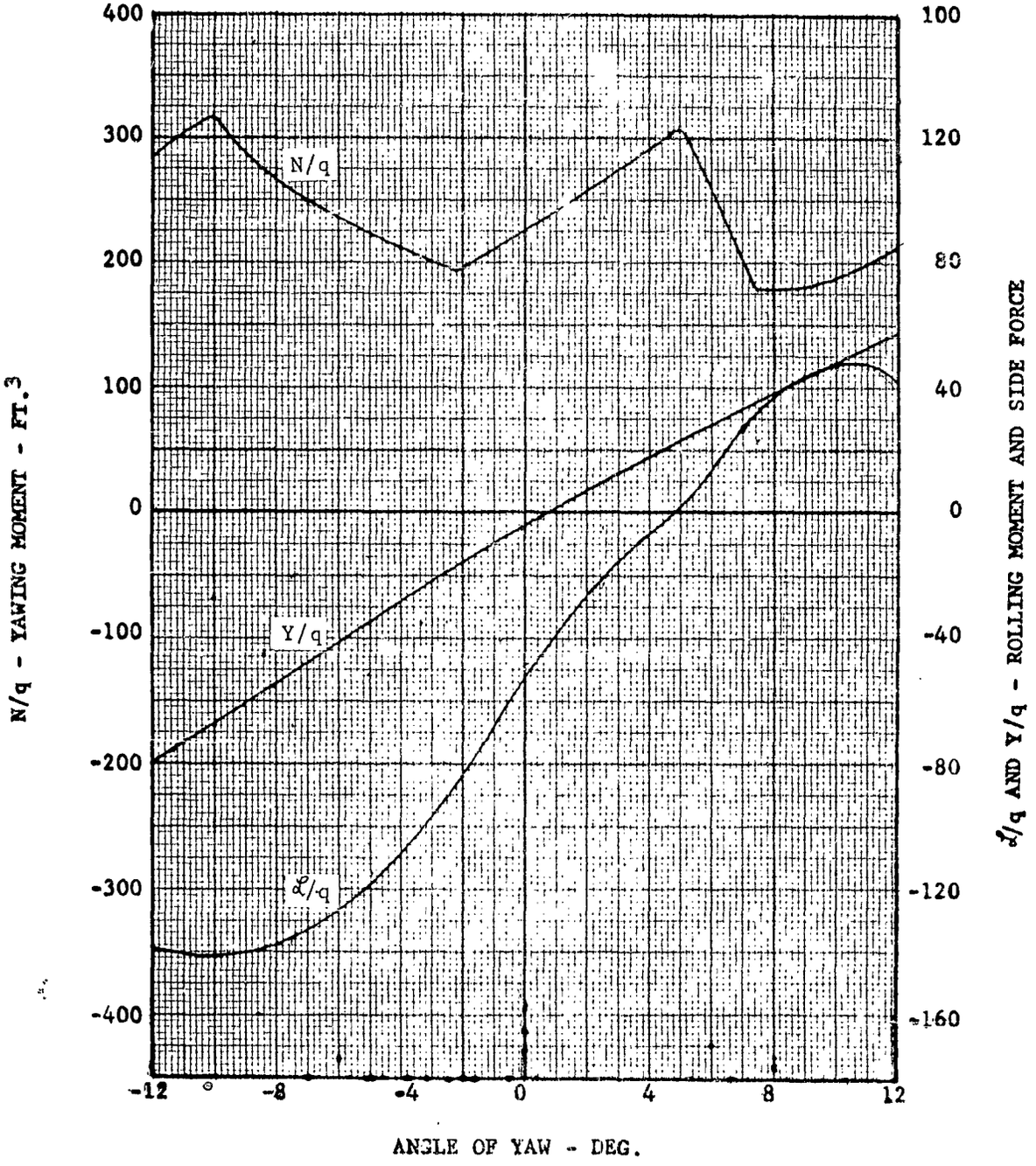


FIGURE 10?
YAWING MOMENT VS. ANGLE OF YAW
COMPARISON OF 107-II AFT PYLON AND EXTENDED CHORD PYLON
$R.N._e$ = 10,910,000

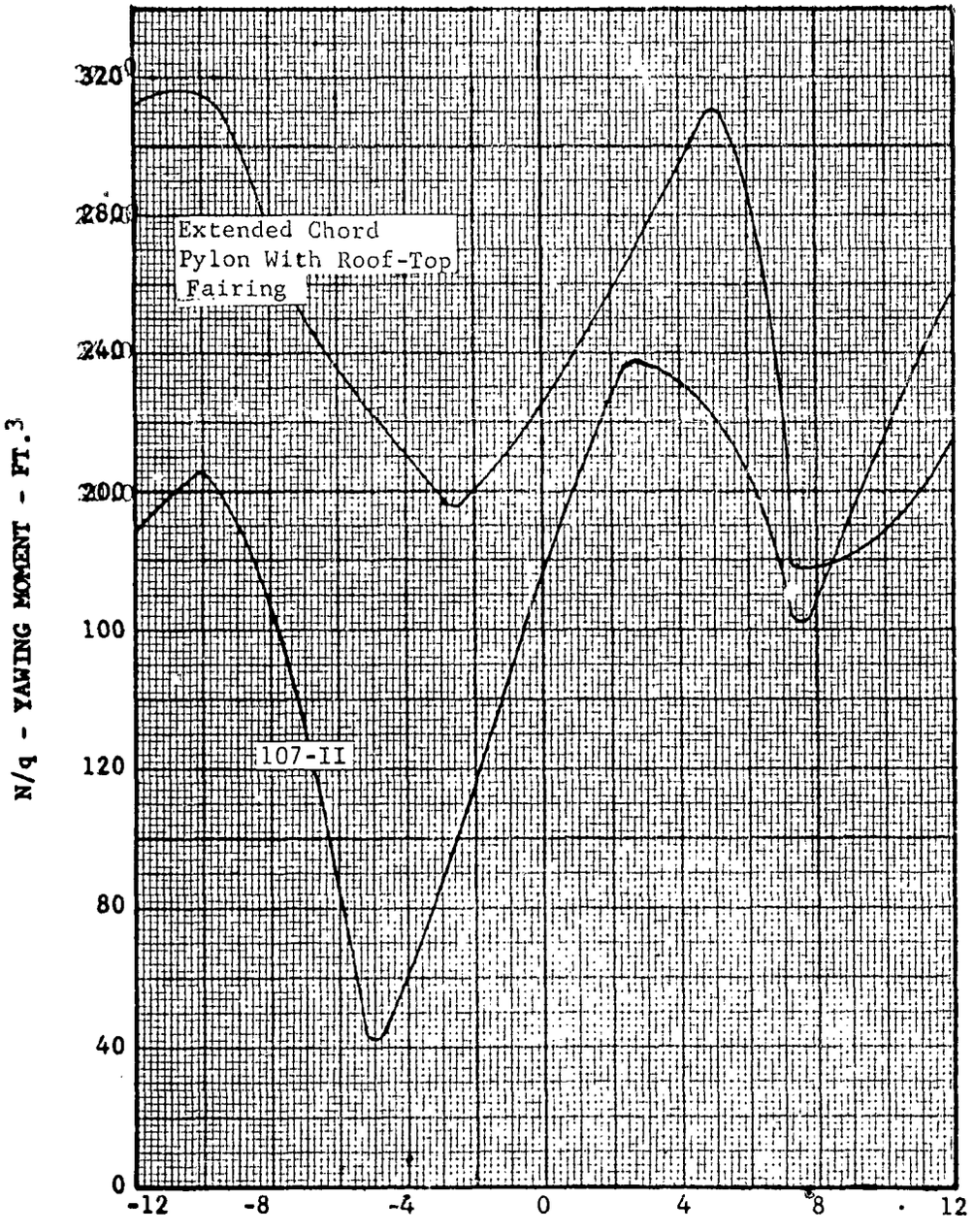
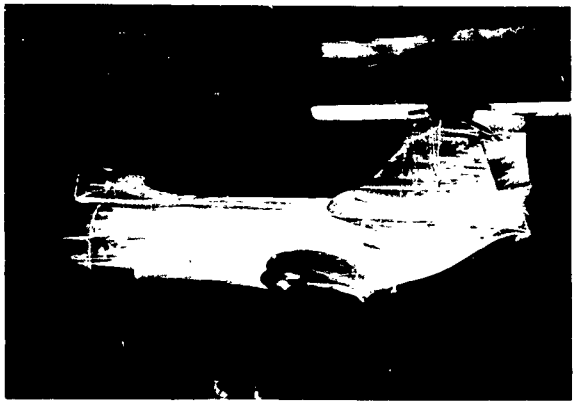


FIGURE 104

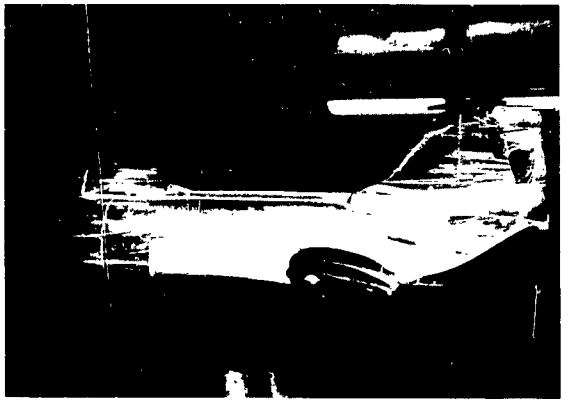
FINAL CONFIGURATION IN YAW
OIL STUDY



$\psi = 0^\circ$



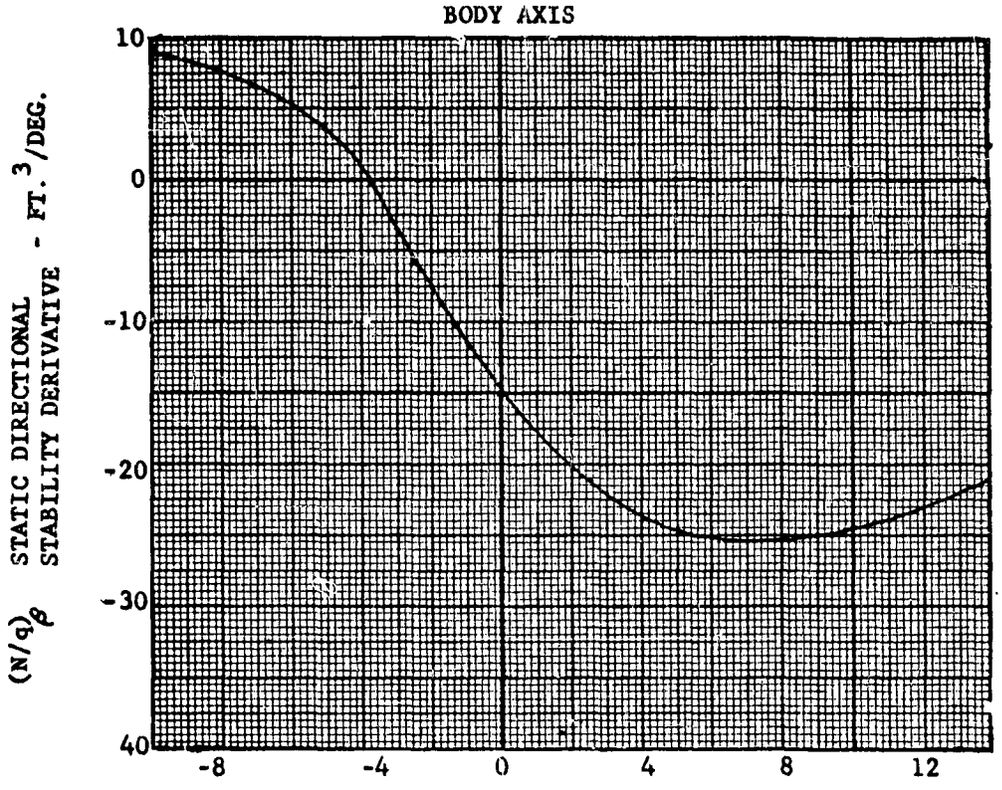
$\psi = -5^\circ$



$\psi = -10^\circ$

FIGURE 105

STATIC DIRECTIONAL STABILITY DERIVATIVE VS ANGLE OF ATTACK
FINAL CONFIGURATION - RN_e = 10,910,000



CONCLUSIONS

Significant reductions in drag have been realized from this program. The High Performance 107-II final configuration yielded a minimum drag area of 20.5 ft.^{2} which compares with 30.2 ft.^{2} for the Boeing-Vertol 107-II. Reduction in drag resulted from refairing of the fuselage afterbody, landing gear retraction, and reducing hub-pylon interference.

Further reductions in drag are desirable and appear attainable by refairing the afterbody i.e. lowering the tail cone apex, fairing the rotor hubs, and optimizing stub tank incidence.

Static-directional stability was improved on the High Performance 107-II model with the extended chord pylon.

SUMMARY

The basic concept of this design study has been to obtain high performance using the maximum possible proportion of existing components. This concept contributed to the initial decision to modify the YHC-1A rather than develop the Vertol Model 127, since more useable components exist for the current helicopter.

The major fuselage changes to obtain high performance do not compromise the operational qualities of the present YHC-1A helicopter. Rear ramp loading is retained. Aft pylon size is increased to insure adequate directional stability. The main gear retracts into the stub wing fuel tanks, while the nose gear is partially retracted into the fuselage and the exposed portion faired.

The ground instability analysis indicates instability bands above normal rotor speed except at the high percent airborne. The damping ratio is greater than unity at all conditions investigated, however, which insures a safe convergent oscillation.

Design of the rotor blade for the High Performance 107-II was accomplished in two phases. First, the blade having the most desirable dynamic properties was found; then, this blade was used in an investigation to determine the effects of total aircraft drag, solidity, gross weight, speed, tip speed, twist and chordwise center of gravity on blade moments and stresses. The final blade adapts the 107 Model II spar to the 23 inch chord of the High Performance 107-II which produces an NACA 0009.5 airfoil section. An intermediate blade having a twist of -8.33 degrees twist has been designed.

The rotor hub followed the YHC-1B and HUP design with the lag hinge outboard of the flapping hinge. The use of a "wire-ply" pack instead of tension-torsion straps allows movement of the lag-hinge closer to the centerline of rotation. An increase in pitch arm radius to alleviate interferences was found necessary. Conventional methods of stress analysis were used and fatigue stresses in critical areas were limited to allowables used in similar applications on the 107 Model II.

The rotor controls for the High Performance 107-II are essentially those of the 107 Model II. Recent flight testing has indicated the desirability of increased stiffness as a deterent to helicopter vibration and these stiffness modifications have been designed in to this control system.

The rotor hub fairing for the High Performance 107-II has been designed to further reduce the drag of the rotor system to a minimum. The light-weight fiber glass construction permits full kinematic freedom of the rotor for flight and also has the capability for possible folding requirements.

The present 107 Model II transmissions, drive shafting, and rotor shafting have adequate ultimate and fatigue strength to withstand high performance helicopter loadings.

The increased flight control loads in the high performance helicopter necessitate changes in the bellcranks at the rotor end of the system to insure adequate strength and stiffness. This is achieved by the use of steel bellcranks. The hydraulic system pressure in the control boost is increased from 1500 to 2000 pounds per square inch with no change in the existing actuators. Minor bellcranks changes are made in the lower system to adjust the control travels to the required values.

All weight studies were performed using Boeing-Vertol developed trend data. The weight estimate for the High Performance 107-II, was obtained from actual 107 Model II components and study of design layouts. An increase in weight empty of 390 lbs. resulted from the changes required. The weight empty is 9988 lbs., fixed useful load is 459 lbs. and provision for 2275 lbs. of fuel exist.

Fuselage Changes

The structural design criteria utilized in the configuration studies pursued in this contract are in agreement with Specification MIL-S-8698 (ASG) "Structural Design Requirements - Helicopters" with minor deviations based on past experience of the contractor with tandem rotor turbine helicopters. Allowable loads and stresses are in accordance with MIL-HDBK-5 "Strength of Metal Aircraft Elements."

All dynamic components have been designed to have unlimited fatigue life for the most critical unaccelerated flight conditions up to the 200 mph (174 knots) design maximum level flight speed. The only exception to this philosophy of unlimited life is in transmission and rotor hub bearings which have finite lives.

Those components of the airframe which are critical for dynamic pressure loads such as cowling, nose enclosure, pylon fairing, etc., are being redesigned to improve the drag characteristics of the aircraft. Appropriate strength increases will be incorporated in the detail design to provide for the higher pressures.

The basic airframe of the Boeing-Vertol 107-II is designed for 2.67g limit load factors at the aircraft c.g. at 18,450 pounds Basic Design Gross Weight. The alighting gear will be redesigned to accommodate the retraction mechanism and will be re-drop tested to ensure adequacy of the design.

The major fuselage changes are discussed below.

Main Landing Gear (SK 10249)

The wheels, tires and oleos of the 107 are retained on the high performance version but their attachments are modified to permit retraction.

On the main gear, this requires provision for new attachments to the stub wing and the installation of an electrical actuator to permit forward retraction of the gear. The fuel tank is modified to provide retraction space, and hinged doors close all gaps when the gear is in the retracted position. The system is arranged so that all sequencing is mechanical. The main gear retraction system utilizes the existing structural support points on the BL74 face of the stub wing torque box.

A forward rotation reduces fuel tank volume; however, this is remedied by moving the gear outboard. Frame loads at Station 382 and Station 410 are increased. The structure will be made adequate for the increased loads.

An aft rotation would require a duster to house the wheel assembly.

Nose Gear (SK 10333)

With regard to the nose gear, a different mounting has been incorporated in order to permit swiveling as required, with an electrical actuator for rearward retraction. Cutouts and doors are provided in the fuselage to accommodate and enclose the retracted gear. The nose gear retraction system utilizes the existing structural support points on the fuselage former at Station 101 and the auxiliary structure above and forward. The

exterior fairing lends itself to a one-piece integral fiberglass construction.

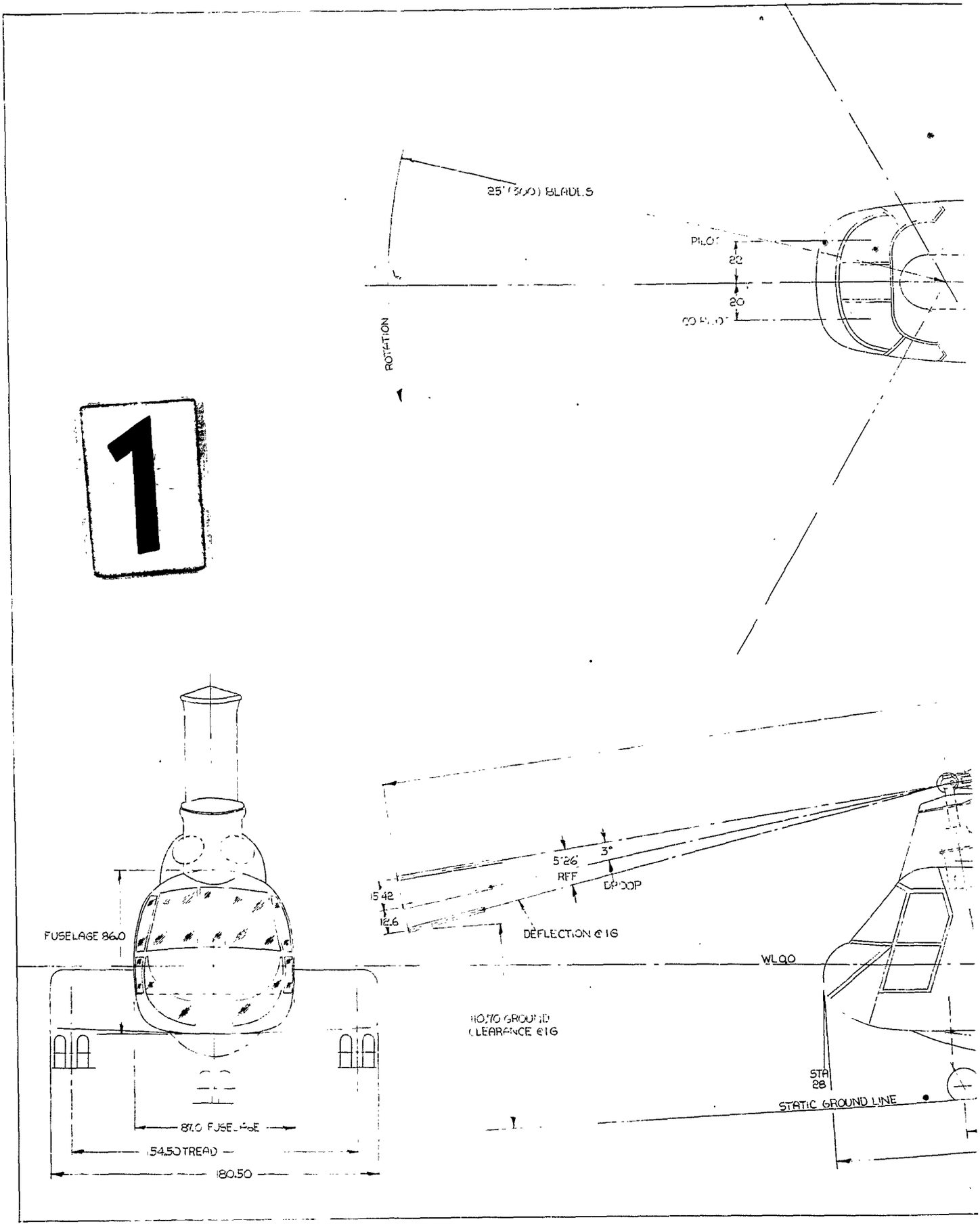
Changes to Afterbody Pylon (SK 10340)

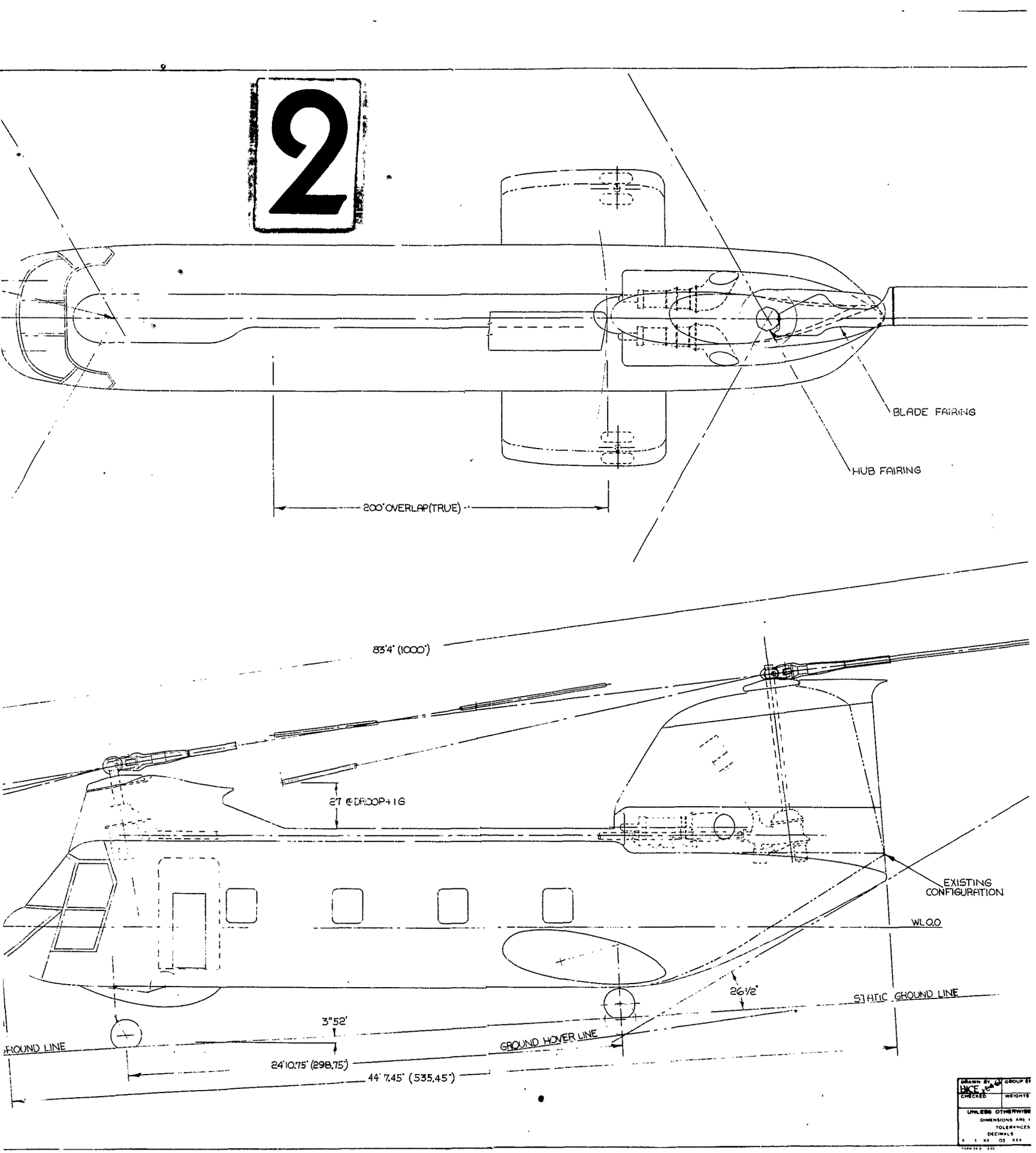
In order to reduce drag, the lines of the rear portion of the pylon have been refaired. The enclosed drawing illustrates the configuration changes for the afterbody as compared with the lines of the basic Model 107. The revised fairing structure will be designed for the aerodynamic loading consistent with the high forward speeds.

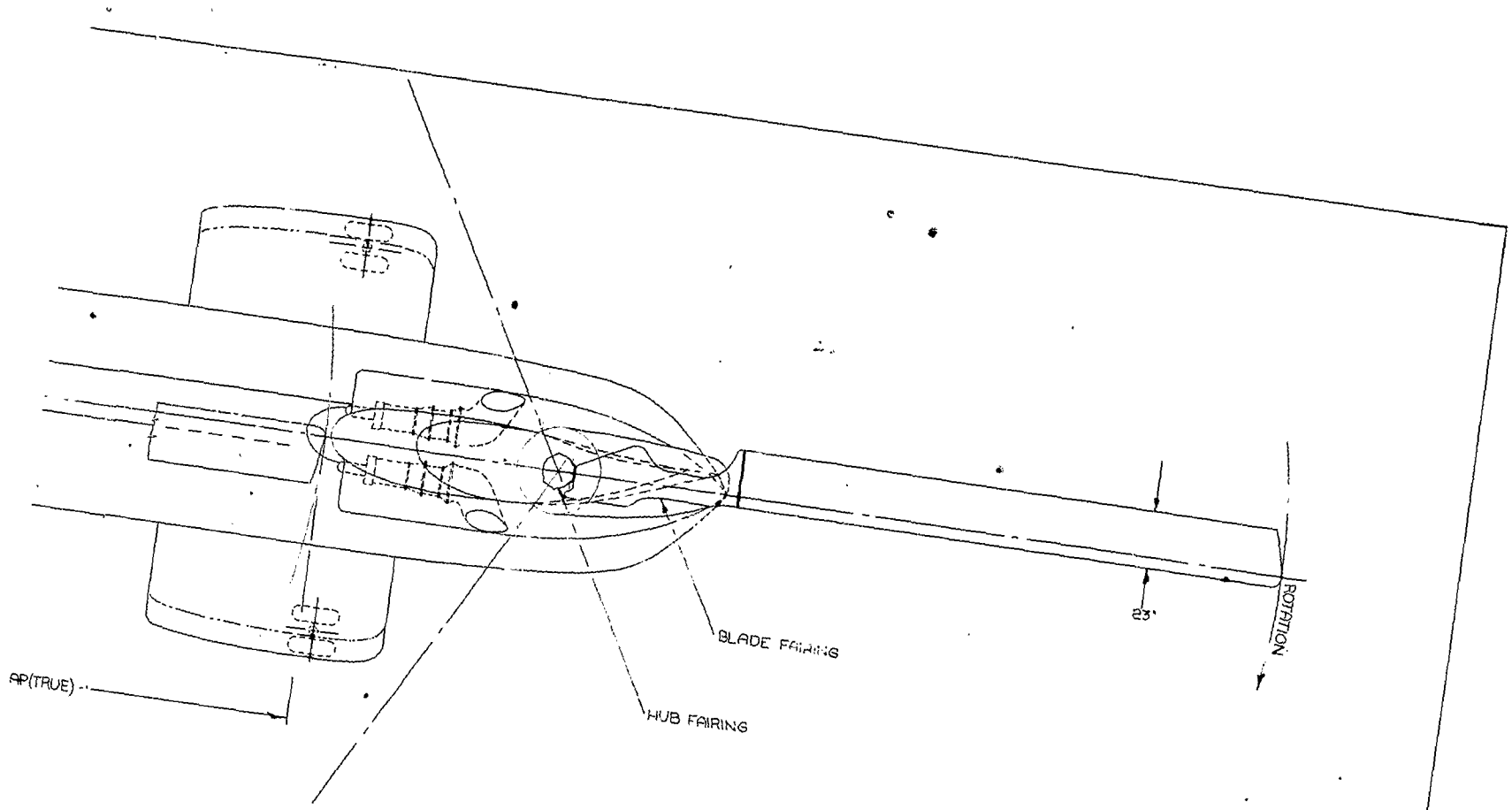
Changes to the Nose Enclosure (SK 10327)

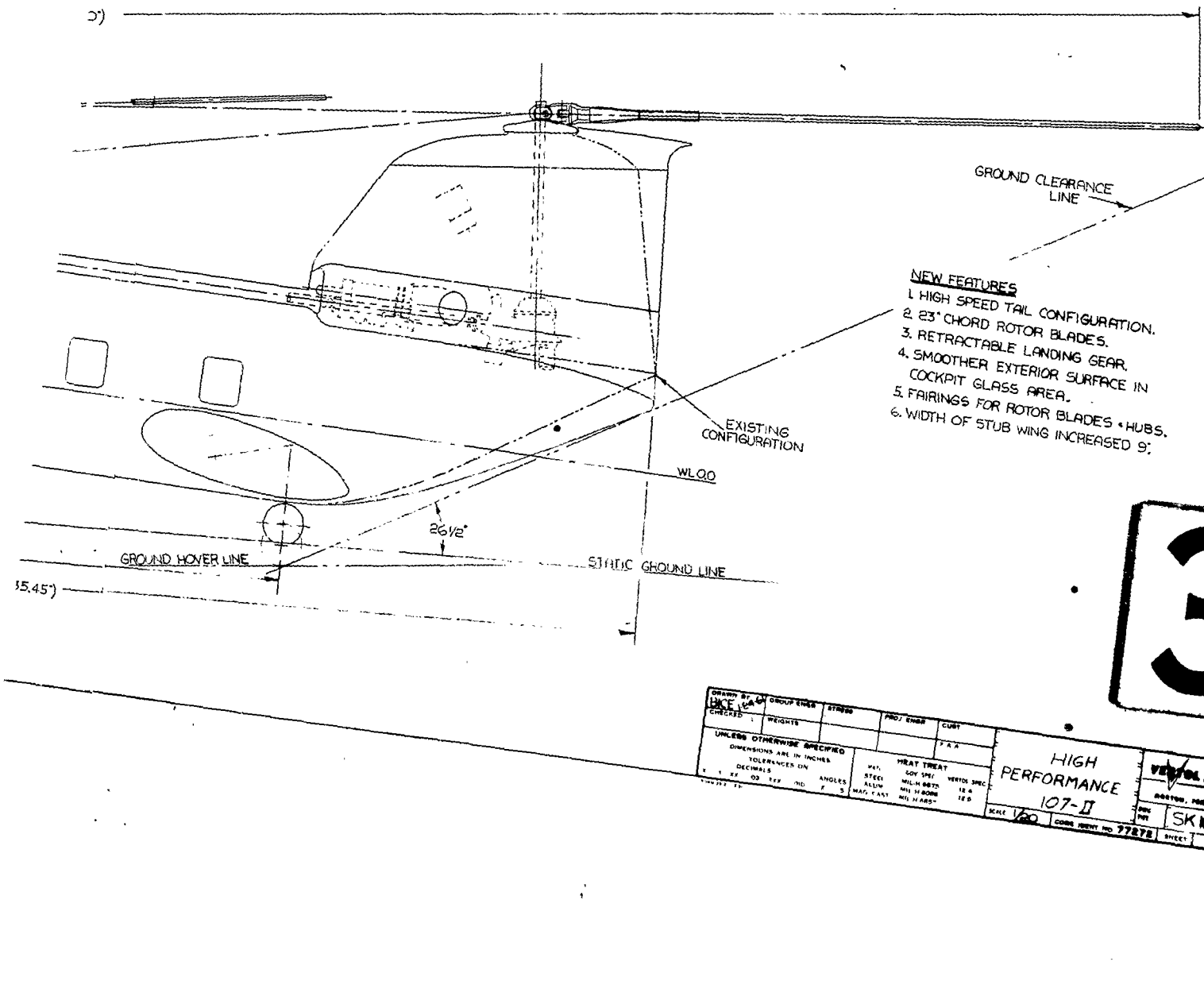
Minor changes are made in the cockpit enclosure to provide flush windows and increase strength in the glass enclosure areas. A drawing of the proposed approach is SK 10327. This method of passing a screw fastener through an oversize hole in the cockpit glass not only produces greater exterior smoothness but also provides greater "end fixity" for the glass mounting which aids in handling the increased in-flight airloads. This method has been adapted for all the cockpit glass installation on the YHC-1B helicopter.

Miscellaneous minor fairing will also be used in areas such as heater intake, vents, drains, etc., and minor strengthening in some cowling areas to sustain the increased airloads.


25' (300) BLADES
ROTATION
PILOT
22
20
20 PILOT
1
FUSELAGE 86.0
87.0 FUSELAGE
154.50 TREAD
180.50
5°26'
REF
3°
DROOP
15.42
12.6
DEFLECTION @ 16
WL 90
110.70 GROUND
CLEARANCE @ 16
STA
28
STATIC GROUND LINE

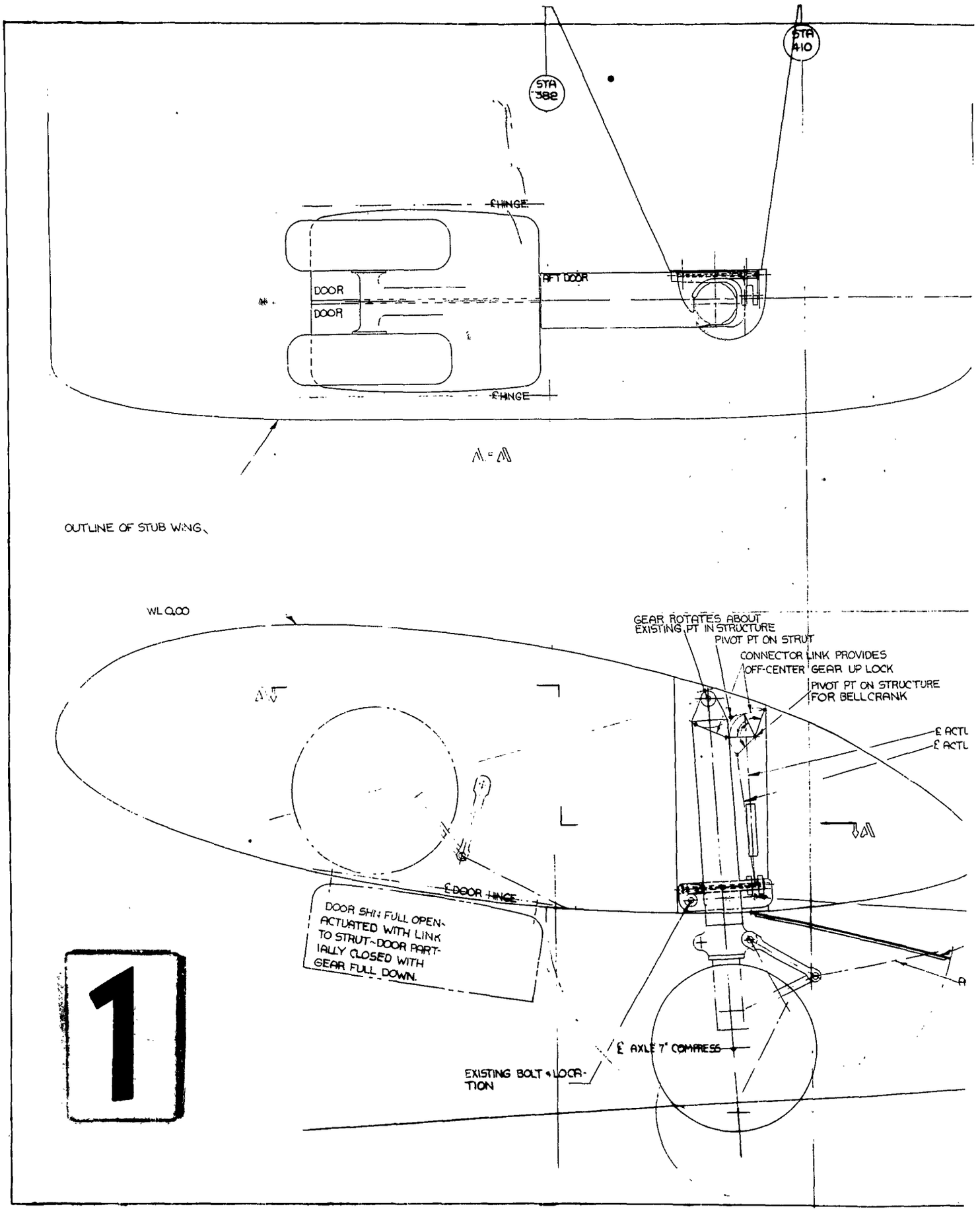

2
BLADE FAIRING
HUB FAIRING
200" OVERLAP (TRUE)
85'4" (1000")
27 @ DROOP + 16
EXISTING CONFIGURATION
WL 0.0
26½°
STATIC GROUND LINE
3°52'
GROUND HOVER LINE
24'10.75" (298.75")
44' 7.45" (535.45")





3

DRAWN BY LHCE	GROUP ENGR	STRESS	PROJ ENGR	CUST
CHECKED	WEIGHTS			
UNLESS OTHERWISE SPECIFIED DIMENSIONS ARE IN INCHES TOLERANCES ON DECIMALS		HEAT TREAT	HIGH PERFORMANCE 107-II	VERTOL
			SCALE 1/20	DRG NO SK 10321


STA 382
STA 410
℄HINGE
DOOR
DOOR
AFT DOOR
℄HINGE
A - A
OUTLINE OF STUB WING
WL 0.00
GEAR ROTATES ABOUT EXISTING PT IN STRUCTURE
PIVOT PT ON STRUT
CONNECTOR LINK PROVIDES OFF-CENTER GEAR UP LOCK
PIVOT PT ON STRUCTURE FOR BELLCRANK
℄ ACTL
℄ ACTL
A
A
℄ DOOR HINGE
DOOR SHN FULL OPEN- ACTUATED WITH LINK TO STRUT-DOOR PART- IALLY CLOSED WITH GEAR FULL DOWN.
℄ AXLE 7" COMPRESS
EXISTING BOLT LOCA- TION
1

BL 77.25

WL 0.00

VIDES
P LOCK
ON STRUCTURE
LCRANK

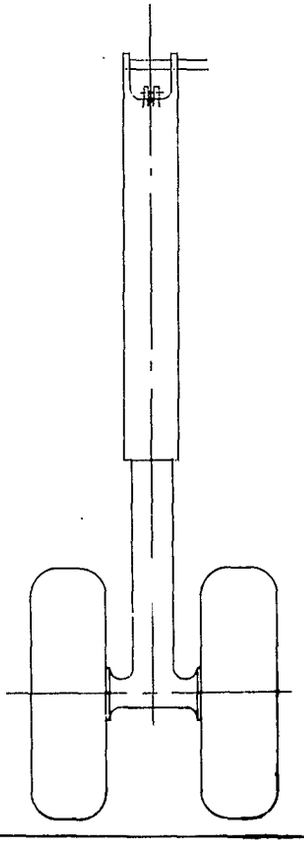
℄ ACTUATOR GEAR DN
℄ ACTUATOR GEAR UP

EXISTING LOCATION
WITH BARREL NUT IN FORGING

AFT DOOR OPEN

AFT DOOR ACTUATING LINK

STATIC GROUND LINE



2

NOTES
1. TORQUE BOX & STRUCT AFT OF TORQUE BOX HAS NO BASIC CHANGES.
2 GEAR UP POSITION VIOLATES FUEL TANK AREA
~VOLUME MAY BE REGAINED BY ROTATING GEAR IN PLANE 8° OUTBD & ADDING 14" TO WIDTH OF STUB
3. WIDTH OF STUB INCREASED 9".
4. FUEL TANK ASSY STILL EASY TO REMOVE

MAIN GEAR RETRACTION

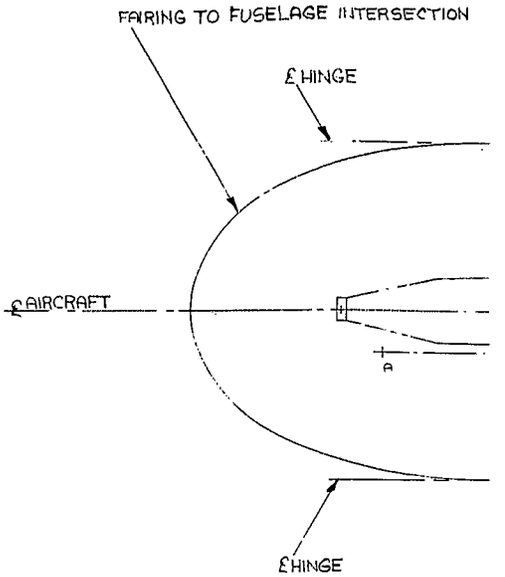
SK 10869

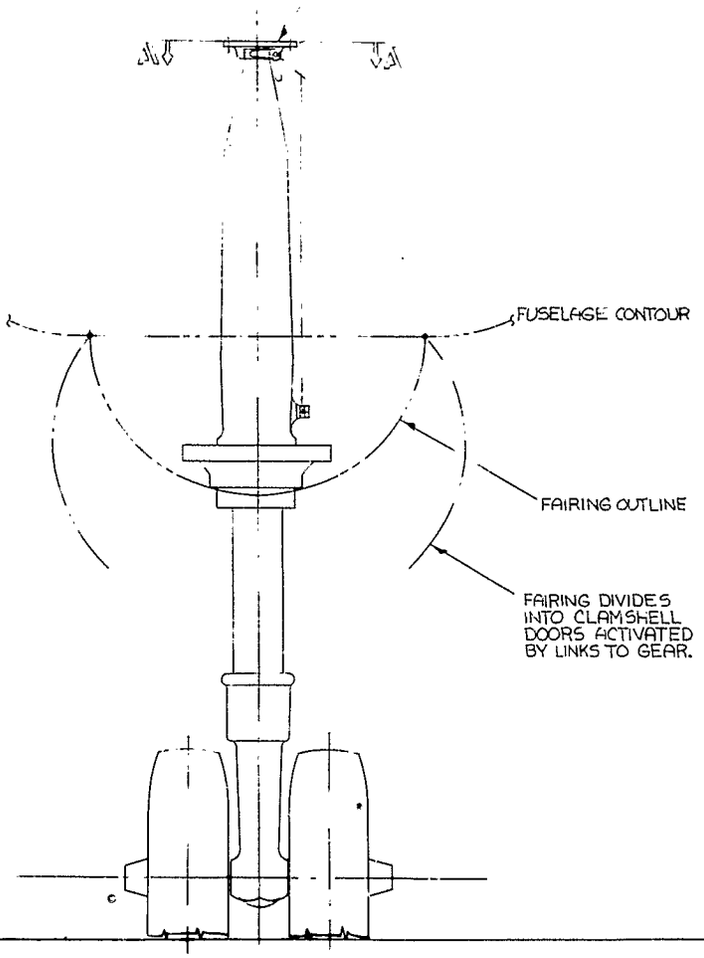


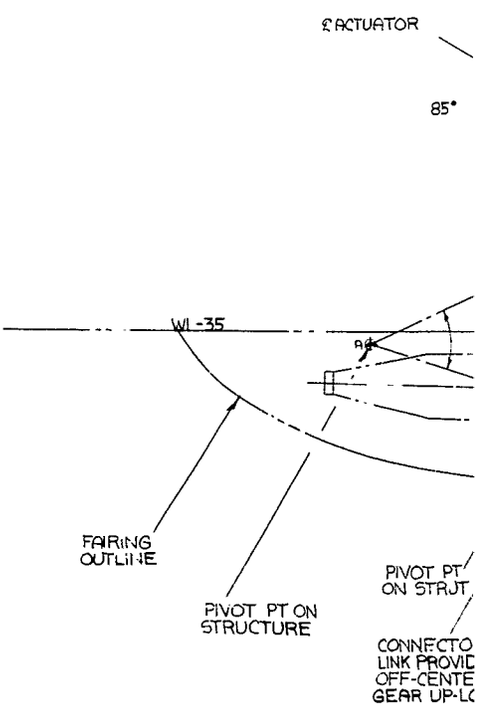


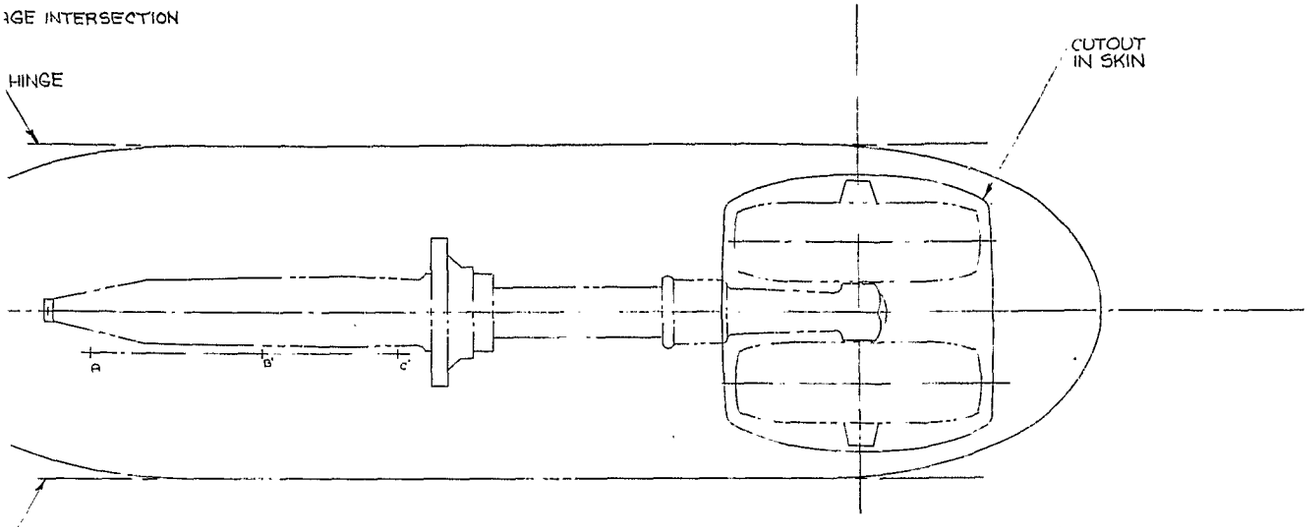
℄ AIRCRAFT

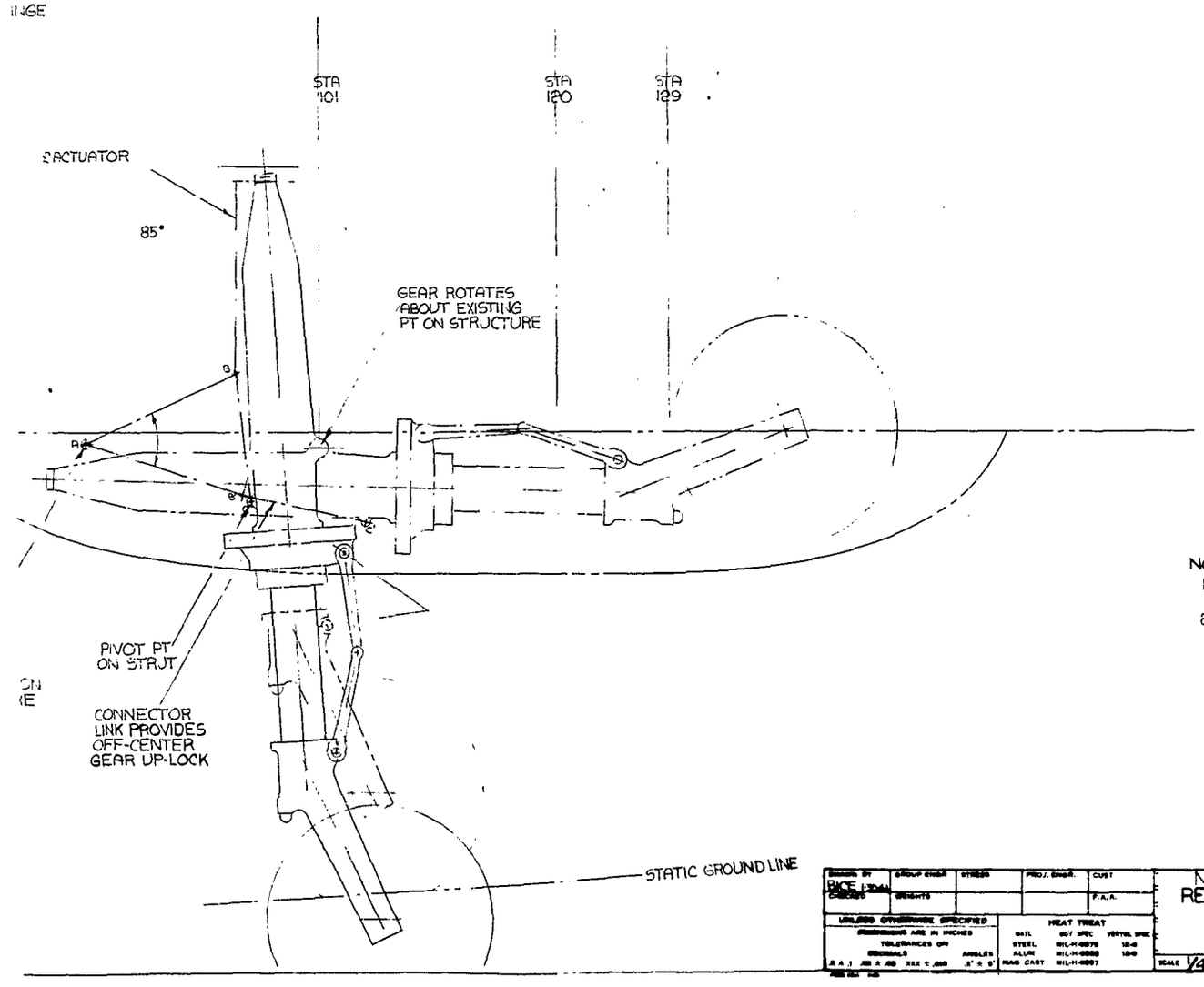
YOKE FITTING FOR SIDE LOADS • MOVEABLE JAW ACTUATED WITH GEAR FOR FWD • AFT LOADS.









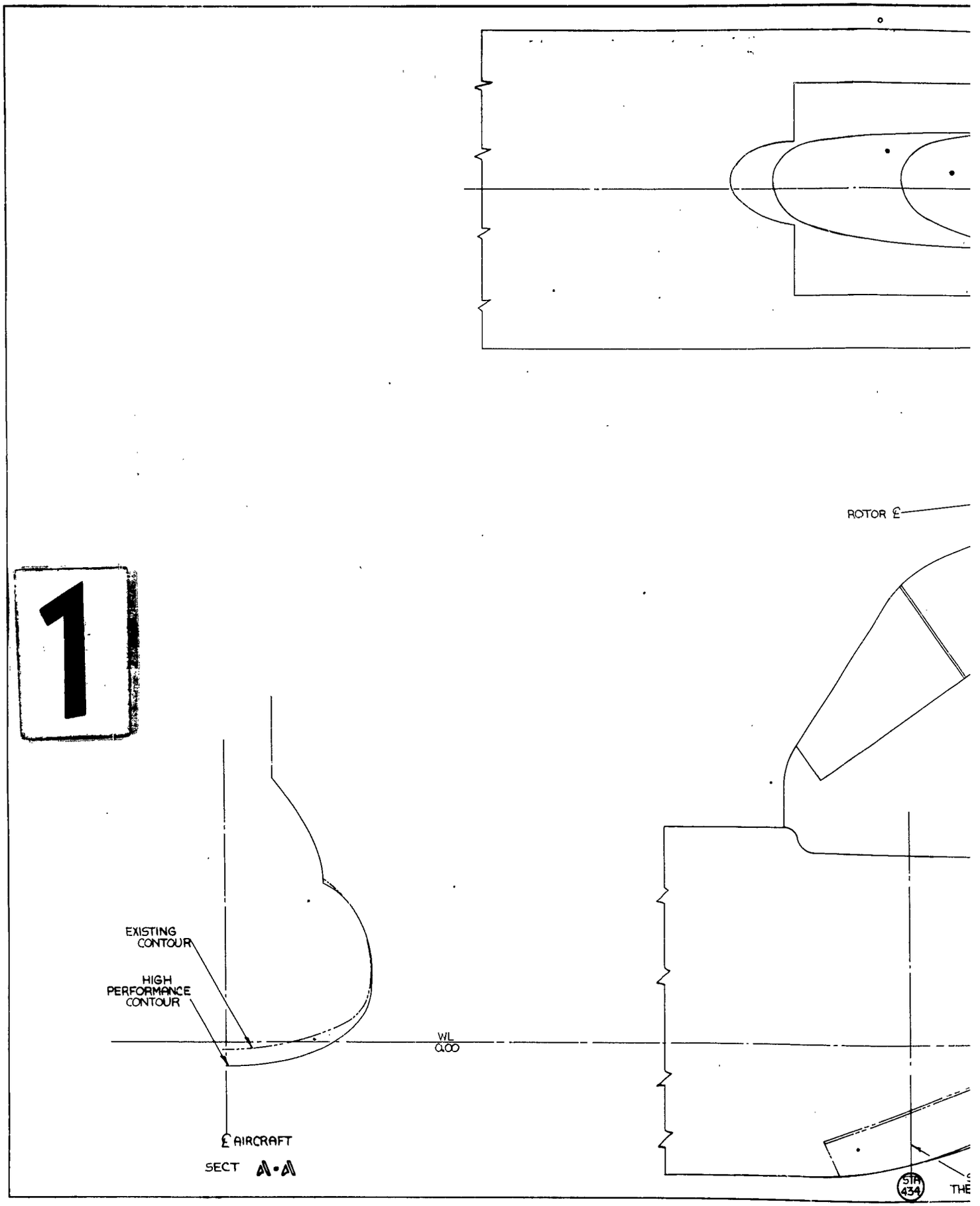


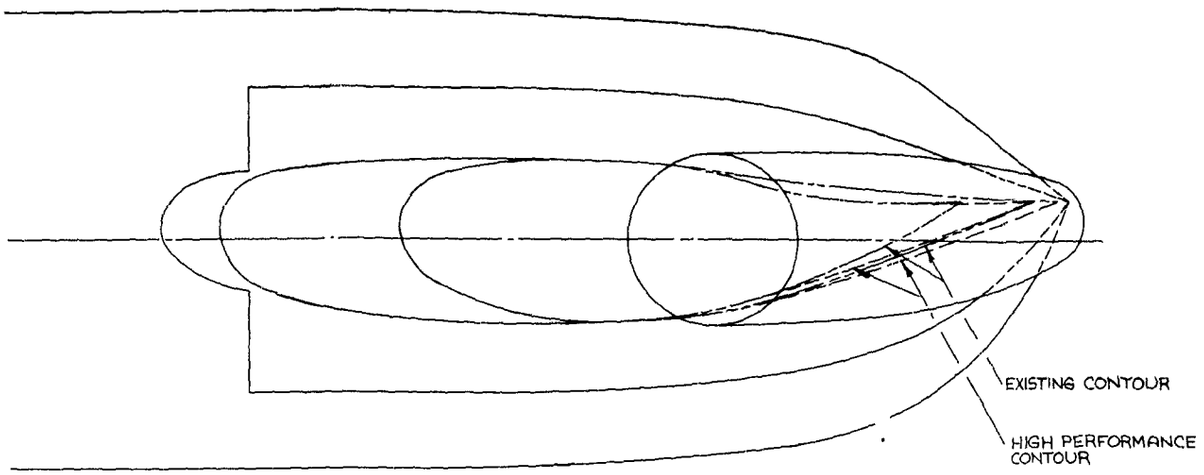
2

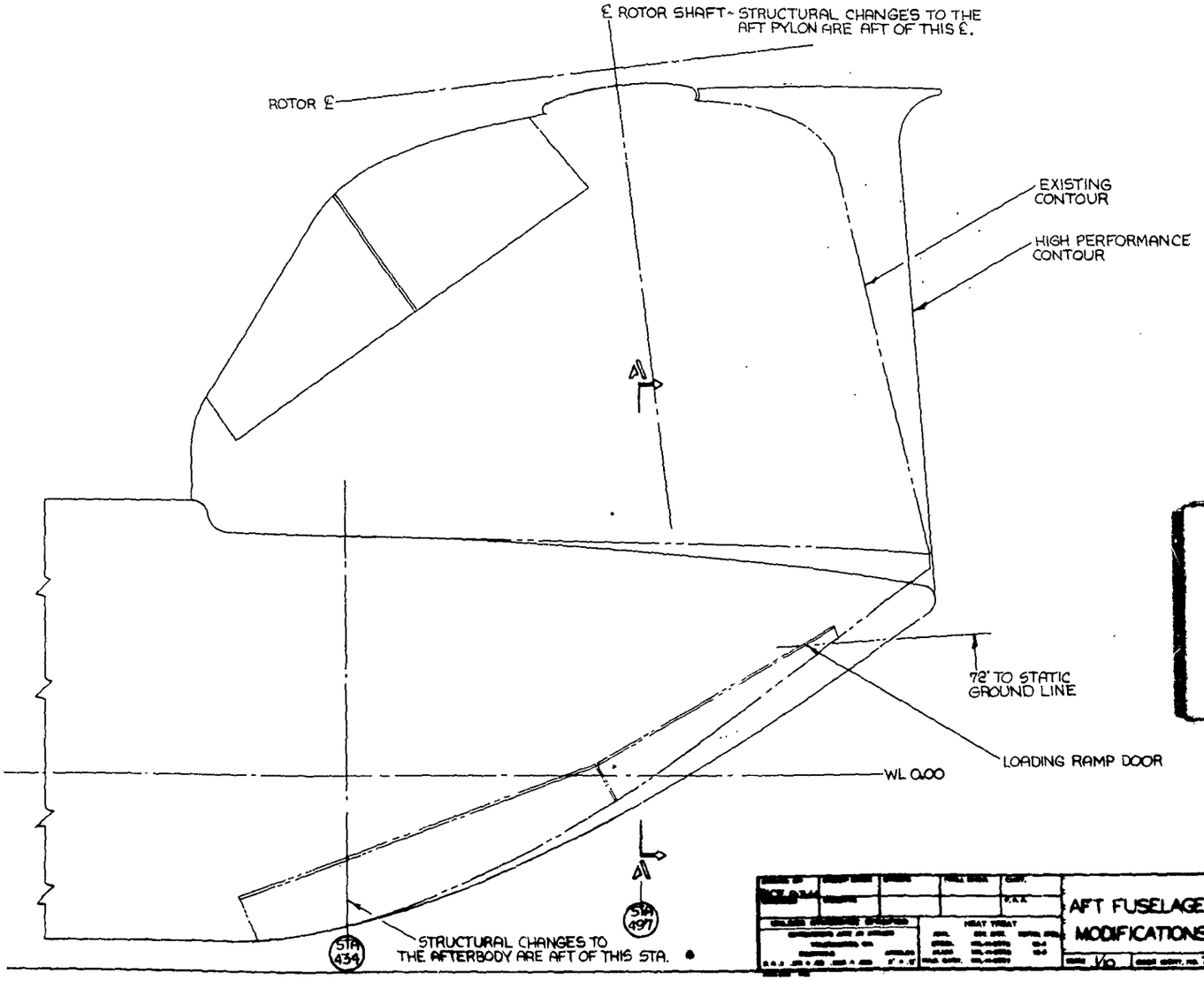
NOTES:

1. GEAR DOES NOT COMPRESS DURING RETRACTION
2. ARRANGEMENT UTILIZES EXISTING STRUCTURAL SUPPORT POINTS.

Drawn BY BICE	GROUP ENGR	STRESS	PROJ. ENGR.	CUST F.A.A.	NOSE GEAR RETRACTION
CHECKED	WEIGHTS				
UNLESS OTHERWISE SPECIFIED: DIMENSIONS ARE IN INCHES; TOLERANCES ON DECIMALS .X ± .1, .XX ± .03, .XXX ± .010, ANGLES .5° ± 0°		HEAT TREAT: DATE / SPEC / VERTOL SPEC; STEEL MIL-H-6875 125-0; ALUM MIL-H-6088 160; MAG CAST MIL-H-6857			VERTOL DIVISION, BOEING, PHILADELPHIA, PENNSYLVANIA
					SCALE 1/4 — CODE IDENT NO. 77272 — DWG NO. SK10333 — SHEET — OF


ROTOR ℄
EXISTING CONTOUR
HIGH PERFORMANCE CONTOUR
WL 0.00
℄ AIRCRAFT
SECT A-A
STA 434



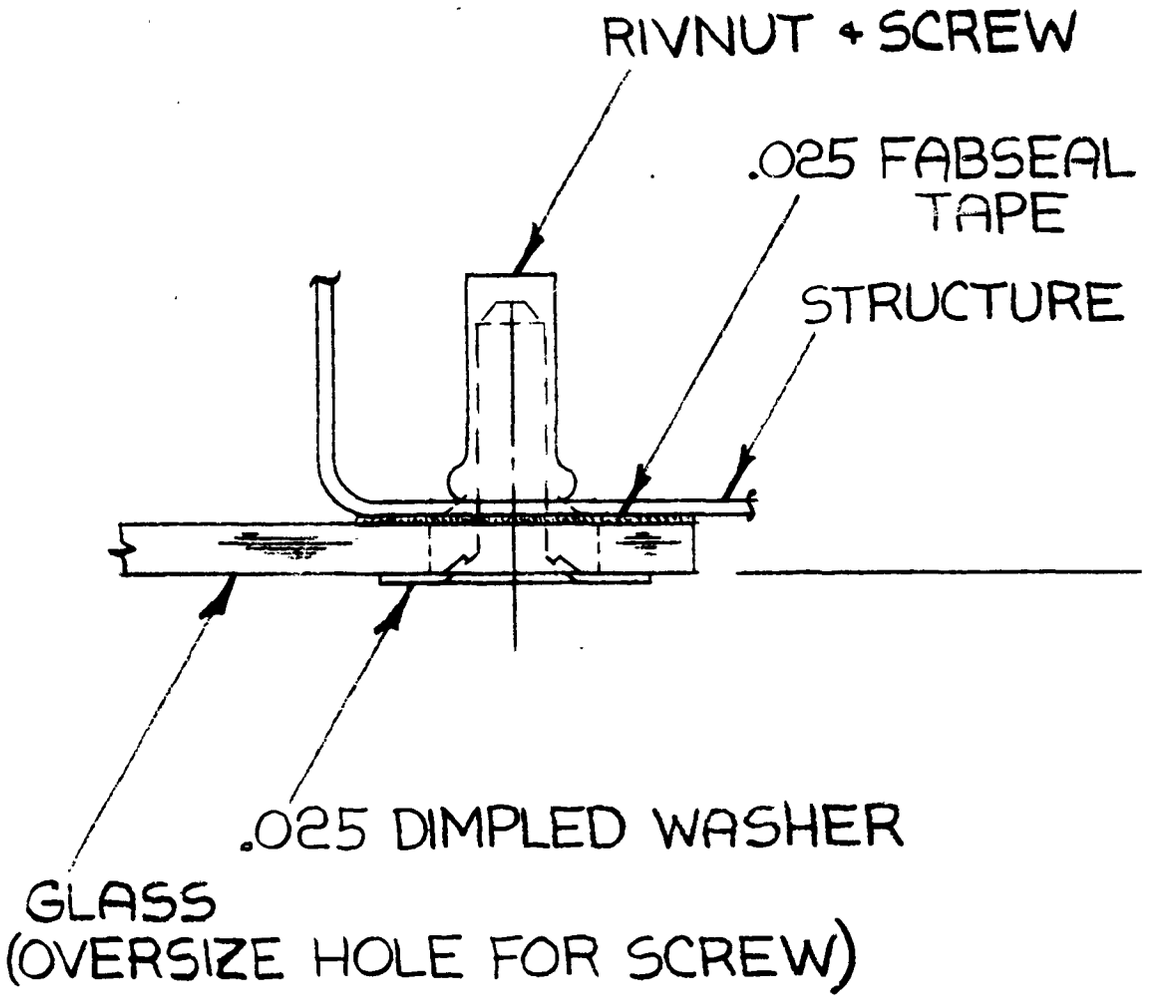


2

AFT FUSELAGE MODIFICATIONS

SK1034D

PROPOSED


RIVNUT + SCREW
.025 FABSEAL TAPE
STRUCTURE
.025 DIMPLED WASHER
GLASS
(OVERSIZE HOLE FOR SCREW)

1

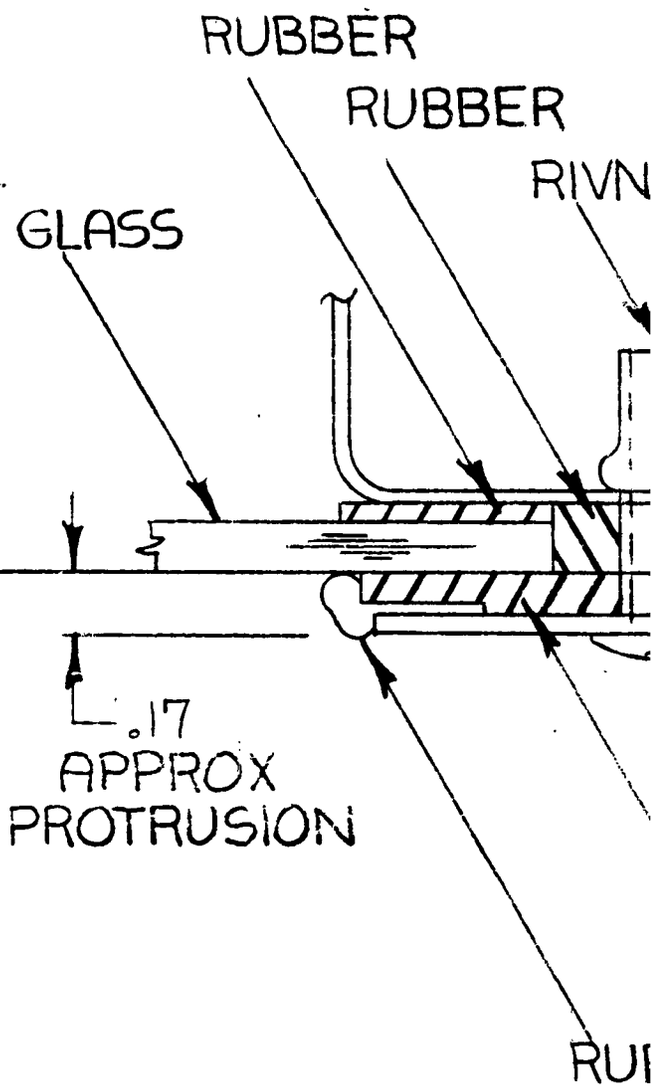
PRESENT

SCREW

FABSEAL
TAPE

RUCTURE

2



DRAWN BY BICE 1-27-61	GROUP ENGR.	STRESS	PROJ. ENGR.	CUST.
CHECKED	WEIGHTS			F. A. A.

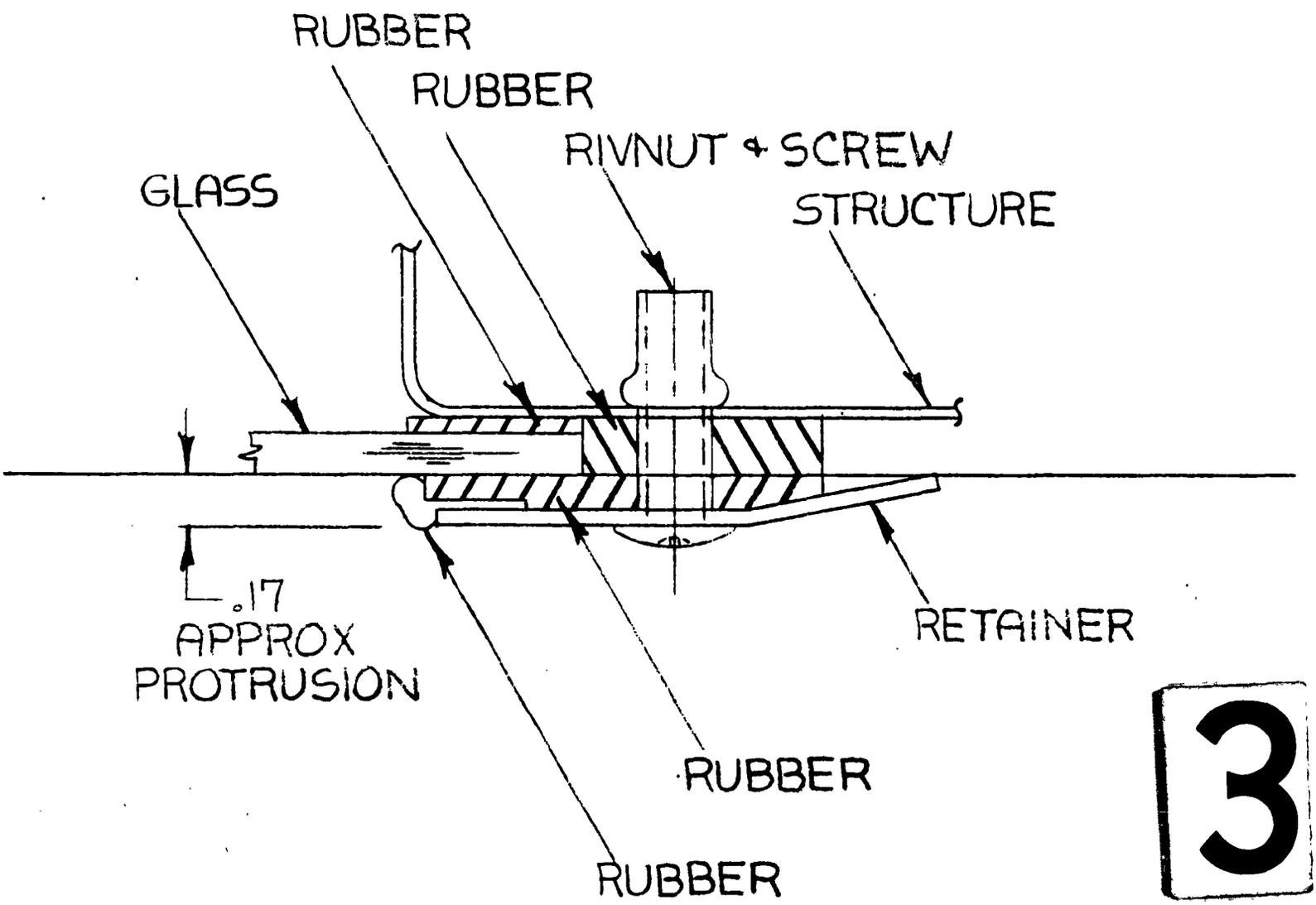
UNLESS OTHERWISE SPECIFIED			HEAT TREAT		
DIMENSIONS ARE IN INCHES			MATL.	GOV. SPEC.	VERTOL SPEC.
TOLERANCES ON			STEEL	MIL-H-6875	12-4
DECIMALS		ANGLES	ALUM.	MIL-H-6088	12-9
.X ± .1	.XX ± .03 .XXX ± .010	.X° ± .5°	MAG. CAST.	MIL-H-6857	

CO
GLASS

SCALE DOUBLE

FORM 2812 3-60

PRESENT



3

	PROJ. ENGR.	CUST.
		F. A. A.

HEAT TREAT

MATL.	GOV. SPEC.	VERTOL SPEC.
STEEL	MIL-H-6875	12-4
ALUM.	MIL-H-6088	12-9
G. CAST.	MIL-H-6857	

COCKPIT GLASS INSTL

VERTOL DIVISION BOEING
MORTON, PENNSYLVANIA

DWG. SIZE | SK 10327 | REV.

SCALE DOUBLE | CODE IDENT. NO. 77272 | SHEET | OF

MECHANICAL INSTABILITY

INTRODUCTION

The present section reviews the problem of ground instability control for the Vertol 107 High Performance Aircraft. Since this aircraft differs from the basic Model 107 in regard to landing gear and blades, a ground instability analysis is performed to determine the influence of these changes, and to recommend specification criteria for detail design. Three gross weights are considered, (1) 14,300 lbs., (2) 19,130 lbs., and (3) 23,000 lbs.

The following sections review the helicopter design with particular regard to those areas which most affect the ground instability characteristics, describe the general problem of instability and the method of analysis employed, present the numerical results, and contain the conclusions.

DESCRIPTION OF THE HELICOPTER AND LANDING GEAR

The High Performance 107-II is similar to the basic 107 Model II except for blades, retractable landing gear, and revised fuselage contours and rotor hubs for drag reduction. Drawings SK 10321, 10333, and 10249 show the helicopter and landing gear and retraction arrangements. The forward gear is retracted upward and back into a fuselage fairing and the aft gear is rotated forward into the stub wings.

When the helicopter is on the ground, the rotors are tilted forward with respect to the ground. If the rotors were accelerated up to normal speed with uniform collective pitch applied, the helicopter would move forward along the ground. To prevent this motion, the customary take-off procedure is to lift the forward gear off the ground by differential collective rotor control, rotating the helicopter about the aft gear, so that the rotors take an attitude parallel to the ground. Then, further collective control is applied and the aft gear is lifted off the ground.

Since ground instability involves lateral and roll motion of the helicopter on its landing gear, and the forward gear is off the ground during much of the take-off cycle, the aft gear properties are most important in establishing the ground instability characteristics. The aft gear has an 11 inch stroke oleo with twin 18 x 5.5 tires operated normally at 150 psi. Vertical and lateral stiffness of the oleo strut and the tires, and the oscillatory damping available in the oleo, are important parameters in the ground instability problem. The aft gear tire tread is also a significant item, and this has been increased to 85.35 inches from the 77.25 inch tread of the V-107 Model II. Numerical stiffness data for the oleo and tires are used from the Model II since these values were found to be satisfactory for that aircraft, and these will be used as tentative specification requirements in this analysis.

EXPLANATION OF GROUND INSTABILITY AND METHOD OF ANALYSIS

There exists in all rotary wing aircraft the possibility of encountering a condition of instability commonly called "ground resonance" if certain design criteria are not met. Under these circumstances, the vast kinetic

energy of rotation is transferred into producing divergent oscillation of the fuselage on its landing gear, and may become so violent as to damage or destroy the aircraft. This unstable condition involves blade depatterning in which the individual rotor blades oscillate in the plane of rotation in such a manner that the combined center of gravity of all the blades does not coincide with the shaft center, but whirls about it in some eccentric locus. This motion couples with the motion in a natural mode of the helicopter on its landing gear in such a phase relation that the motion becomes divergent. Fundamental analytical work on the ground instability problem was performed by Coleman and recently compiled in Reference 15.

All modern helicopters employ some device or design feature aimed at preventing or controlling this destructive phenomenon. One means is to use rotor blades with the lowest natural frequency of blade lag motion higher than the maximum operating rotor speed. While this is effective from the ground instability standpoint, it penalizes the blade root design by requiring blade structure heavy enough to carry the root moments, instead of the zero root moments existent with hinged blades. A common means of instability prevention for hinged blades is the use of lag dampers at the hinges, and hydraulic damping in the landing gear shock struts. Both are necessary and their combined energy dissipation capacity must be sufficient to prevent divergence of any oscillation. An alternate approach is to design the landing gear stiffnesses to place the natural frequencies of the helicopter on its landing gear high enough that the related instability range is clear of the normal rotor speed and will, therefore, not be encountered in normal operations.

Present design practice at Boeing-Vertol aims at a combination of the last two procedures, that is, to place natural frequencies so as to remove instabilities from the normal rotor speed range, under all normal operating conditions and to also provide damping adequate to prevent the growth of any instability encountered under all conditions.

With conventional helicopters, two regions of instability are generally considered; the first is a predominantly lateral helicopter motion accompanied by blade depatterning whose frequency is located well below normal rotor speed, usually about 100 CPM; the second is a predominantly roll helicopter motion about a mode line close to the center of gravity, also accompanied by blade depatterning, and usually located close to or in the normal rotor operating speed range. It is this roll motion which test experience has shown to be of major concern.

Each instability frequency region is located at a rotor speed some 10% to 60% above a "reference frequency". This reference frequency is merely one of the two coupled roll-lateral natural frequencies of the helicopter mass and inertia on its landing gear oleo shock strut and tire springs. The springs whose rates are paramount in setting the reference natural frequencies are the oleo air spring, a widely varying parameter dependent on strut extension and air pressure, the lateral structural rate of the landing gear, the radial tire spring rate, and the lateral tire spring rate.

For the important roll mode, these springs may be thought of as forming an equivalent roll spring about a horizontal line running fore and aft through the helicopter center of gravity. The oleo vertical air spring rate and the tire radial rate add in series to form an equivalent rate, K_v, which is lower than either spring taken singly. This spring on the left landing gear, and its equal counterpart on the right landing gear act through the wheel tread distance 2e to form a rotational spring with rate $2K_{ve}^2$ about the c.g. Similarly, the tire lateral spring rate add in series with the lateral structural spring to form an equivalent lateral spring K_L, which acts through a vertical arm h reaching from the ground up to the c.g. to form a rotational spring with rate $2K_Lh^2$. The total rotational roll spring $2K_{ve}^2 + 2K_{Lh}2$, together with the roll inertia of the helicopter essentially determine the roll mode reference frequency.

Thus for conventional gear, at low percents airborne, all the spring elements - oleo and tire, contribute to a high reference frequency; at high percents airborne, the oleo and tire vertical spring combination are negligible, and the lateral springs are principally responsible for the reference frequency.

If spring rate limitations render the placement of the instability band above the normal rotor speed impractical, or if conservative design is practical, sufficient damping in the oleo strut and lag damper are provided so that the growth of any instability can be prevented. The quantity of damping present in a given condition is generally measured by a damping ratio μ, a ratio of available to required damping:

$$\mu = \frac{C_r \, C_\zeta}{B_y \, B_\zeta}$$

where C_r = effective damping at the rotor hub in the rth mode of the helicopter, produced by the oleo struts

C_ζ = damping produced by each blade lag damper

B_yB_ζ = damping product required for neutral stability from reference 15

When the ratio μ, is greater than unity, there is more damping available to control the instability than is actually required, and μ may be viewed as a sort of margin of safety. The term C_r, effective damping at the hub, is obtained through equating the damping energy produced by the oleos in a given mode to an equivalent mathematical damper at the rotor hub operating in the lateral hub direction. Thus for $\dot{y}$ and $\dot{q}_{hub}$ and oleo velocities respectively,

$$\text{Damping Energy} = 1/2 \, (C_r) \, (\dot{o}2_{y\,hub}) = 1/2 \sum_{oleo} C_{oqoleo} \dot{o}2$$

or

$$C_r = \sum_{oleo} C_{oqoleo} \dot{o}2 / \dot{o}2_{yhub}$$

Occasionally, the mode shape of the reference natural frequency is such that

motion and hence the velocity at the oleo is much larger than that of the hub, so that $(\dot{\zeta}/\dot{y})^2$ becomes large, and the damper C_r and finally the damping ratio turn out to be large numbers. This means that the damping available is well above that required, and the helicopter is in a very safe position. This will be found to be true in a number of the numerical cases presented herein.

The actual method employed in the present analysis is based on Coleman and Feingold's theory of mechanical instability in Reference (15). The application of this theory to the solution of helicopter mechanical instability is contained in Reference (16) and programmed on an IBM 650 computer.

DISCUSSION OF RESULTS

Results of the ground instability analysis are presented as plots of frequency in CPM vs. percent airborne (Figures 106a, 106b, 106c). In these figures the wide cross-hatched band is the instability band and the center curve is the center of instability; finally, the dashed curve shows the variation of the ratio of available-to-required-damping with the percent airborne. The line on which a discontinuity occurs denotes the percent airborne at which each aft oleo piston engages its bottoming spring. This spring is a Vertol innovation which prevents metal-to-metal bottoming of the oleo struts at high percents airborne, and always allows oscillatory motion of the oleo so as to provide damping control at all times. This spring engagement is reflected in the discontinuity of the instability plot between 70 and 80% airborne.

From experience, the critical mode of ground instability is the helicopter roll mode which consists of roll oscillations of the helicopter on its oleo and tire springs about a line passing through its c.g. This is accompanied by blade depatterning and is usually located close to or in the normal rotor operating speed range where the instability band is above the rotor speed where the aircraft is inherently stable. If the instability band intersects the rotor speed, sufficient damping must be available in the oleo and the blade lag dampers to suppress the instability. A measure of control of this instability is the damping ratio curve, mentioned earlier and labeled as μ. If μ is greater than unity the aircraft will be stable on the ground.

Most of the physical data used in the analysis are taken from the Model II; this approach is convenient since the advanced version is a modification of that aircraft. Each rotor has 3 blades having a 25 feet radius and a 23 inch chord. The lag hinge is situated 24 inches outboard of the hub which is greater than the 13.9 inches used with the Model II blades. The aft tire tread has been increased from the standard 77.25 inches to 85.35 inches. Except for hub and aft fin fairing, the underside blister for the retractable landing gear, and the increased stub tank span, the High Performance 107-II has the same dimensions as the Model II.

The results of the analysis at a gross weight of 14,300 lb. are plotted in Figure 106a. From 0% to about 70% airborne the instability band is well above the normal rotor speed. This means that in this interval mechanical instability of the helicopter is highly unlikely. Further, any oscillation that may occur would be controlled by the damping in the blade damper and oleo, which is indicated by the greater than unity value of the damping ratio μ. After the engagement of the bottoming spring at 71%, the instability band at 340 cpm decreases rapidly with increasing percentage airborne, following the decreasing lateral tire spring rate, until the lower instability boundary crosses the normal rotor speed line at 92% airborne. Because the center of instability remains above the 258 rpm normal rotor speed and the damping ratio is still greater than unity, the normal-rotor speed-crossing of the lower instability boundary should not cause any uncontrolled oscillation. The available damping in the system is adequate to control or dissipate any oscillation in the helicopter.

Figure 106b is a plot of the results for the 19,130 lb. gross weight. Between 0% and about 70% airborne, a slightly lower instability band, but still above normal rotor speed, is a result of the increased gross weight. Only the lower boundary of the instability band crosses the normal rotor speed line from above to below 258 rpm at two points: 78% and 92.5% airborne. However, the damping ratio is quite high so that there is adequate margin for controlling and dissipating any oscillation.

Usually, the critical configuration of a helicopter with regard to ground instability is at the maximum gross weight. Examination of Figure 106c, which is the result of the analysis for the 23,000 lb. ferry or overload version of the Vertol 107 Research Vehicle supports this observation. From a high of 300 rpm at 0% airborne, the lower instability boundary gradually decreases until it crosses the normal rotor speed line at 68% airborne. After engagement of the bottoming spring at 78% airborne, the lower instability band again decreases from a high of 270 rpm until it crosses the normal rotor speed line at 92% airborne. In this configuration the most critical percent airborne is at 78% when the center of instability is almost on the rotor speed. However, the damping ratio is very large, which may be seen also in Figure 106c, so that there is more than ample damping in the blade damper and oleo to control and dissipate any oscillation that may arise during operation of the helicopter.

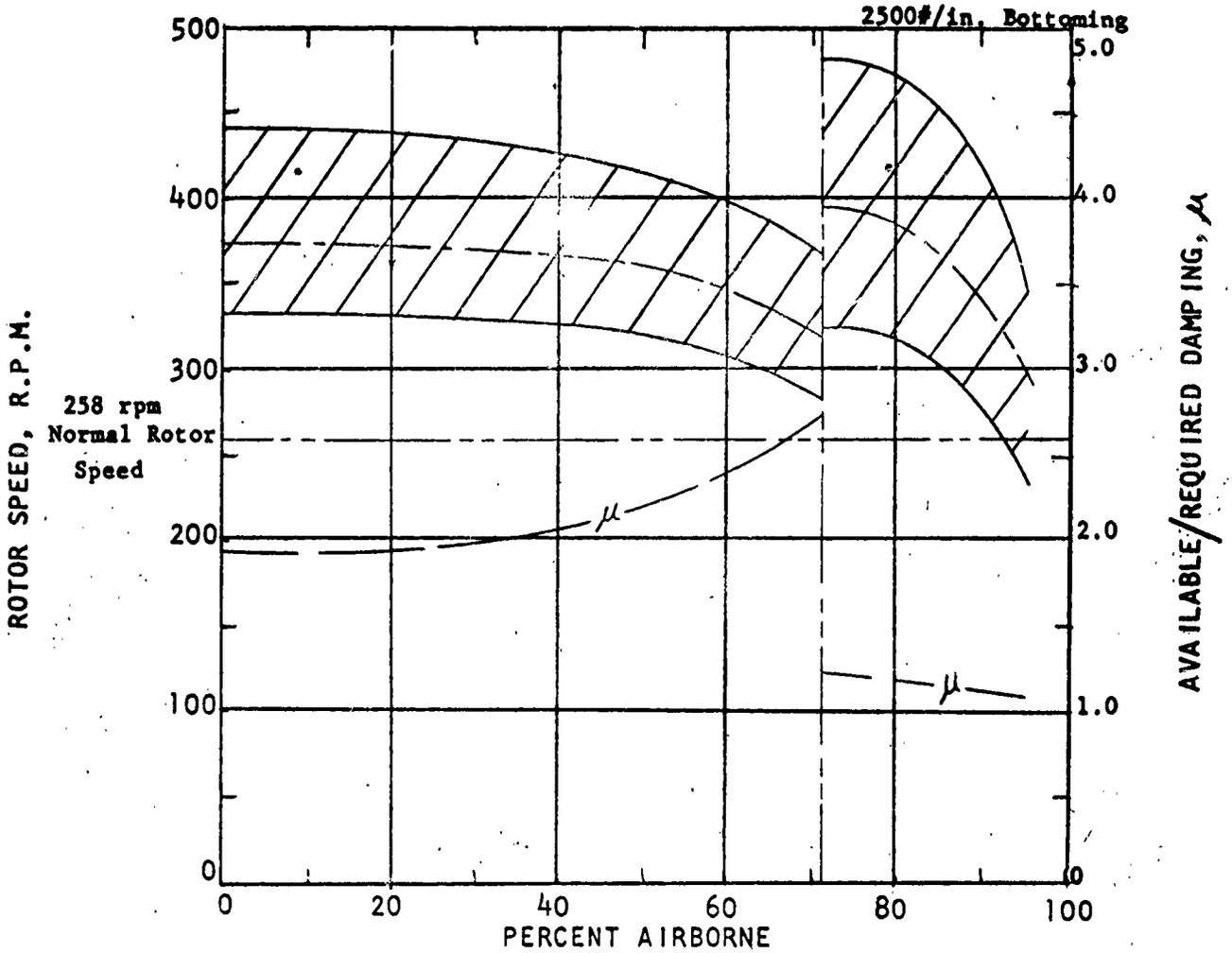
CONCLUSIONS

The ground instability analysis at the three gross weights of the High Performance 107-II show that the instability bands are located above normal rotor speed except at certain high percent airborne conditions where the lower boundaries of the instability bands cross the normal rotor speed line. However, the damping ratio is greater than unity in all versions for all percents airborne such that any oscillation will always be convergent as energy is dissipated by the damping in the blade-damper-oleo system of the helicopter.

Figure 106a

GROUND INSTABILITY ANALYSIS

18 x 5.5 Aft Tires 14,300# G.W. Oleo: 4000#/in. Extended
150 psi 9000#/in. Static
2500#/in. Bottoming



A/C Weight:* 14,300# Roll Inertia: 90,250 CG to Grnd, Static: 75.0 CG to Fwd Rotor: 73.8 CG to Aft Rotor: 126.5 * I.P.S. Units	Blade: 25 Ft. Weight: Lag Moment: 53.73 Lag Inertia: 9912	Lag Damper:— YHC-1B Preload: 1100# Damping Rate: 98#/in./sec. Oleo Damping Rate:— Fwd: Aft: 625#/in./sec.

Fwd Tire Size:
No. Tires/Oleo:
Fwd Tire Pressure:

Aft Tire Size: 18 x 5.5
No. Tires/Oleo: 2
Aft Tire Pressure: 150 psi

Spring Rates Per Gear

% Airborne	0%	50%	-71%	71%	78%	95%
Fwd Oleo Vert.						
Fwd Oleo Lat.						
Aft Oleo Vert.	890	557	190	2690	2690	2690
Aft Oleo Lat.	9000	6500	4000	4000	4000	4000
Fwd Tire Vert.						
Fwd Tire Lat.						
Aft Tire Vert.	8560	8000	6800	6800	6260	1750
Aft Tire Lat.	4450	4420	4050	4050	3950	1240

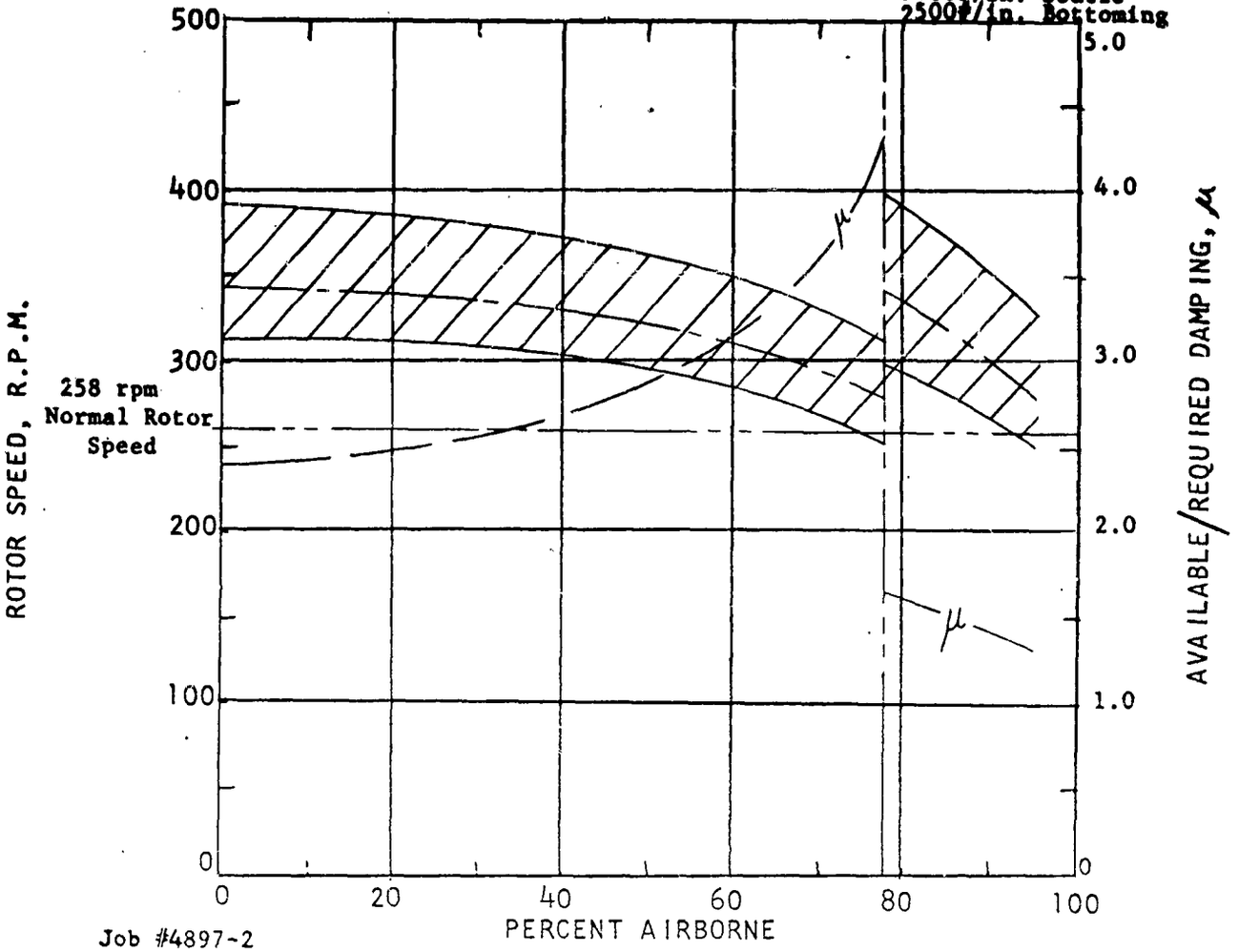
Figure 1068

GROUND INSTABILITY ANALYSIS

18 x 5.5 Aft Tires
150 psi

19130# G.W.

Oleo: 4000#/in. Extended
9000#/in. Static
2500#/in. Bottoming



Job #4897-2

A/C Weight: * 19,130#	Blade: 25 Ft.	Lag Damper: — YHC-1B
Roll Inertia: 120,600		Preload: 1100#
CG to Grnd, Static: 75.0	Weight:	Damping Rate: 98#/in./sec.
CG to Fwd Rotor: 73.8	Lag Moment: 53.73	Oleo Damping Rate: —
CG to Aft Rotor: 126.5	Lag Inertia: 9912	Fwd:
* I.P.S. Units		Aft: 625#/in./sec.

Fwd Tire Size:	Aft Tire Size: 18 x 5.5
No. Tires/Oleo:	No. Tires/Oleo: 2
Fwd Tire Pressure:	Aft Tire Pressure: 150 psi

Spring Rates Per Gear

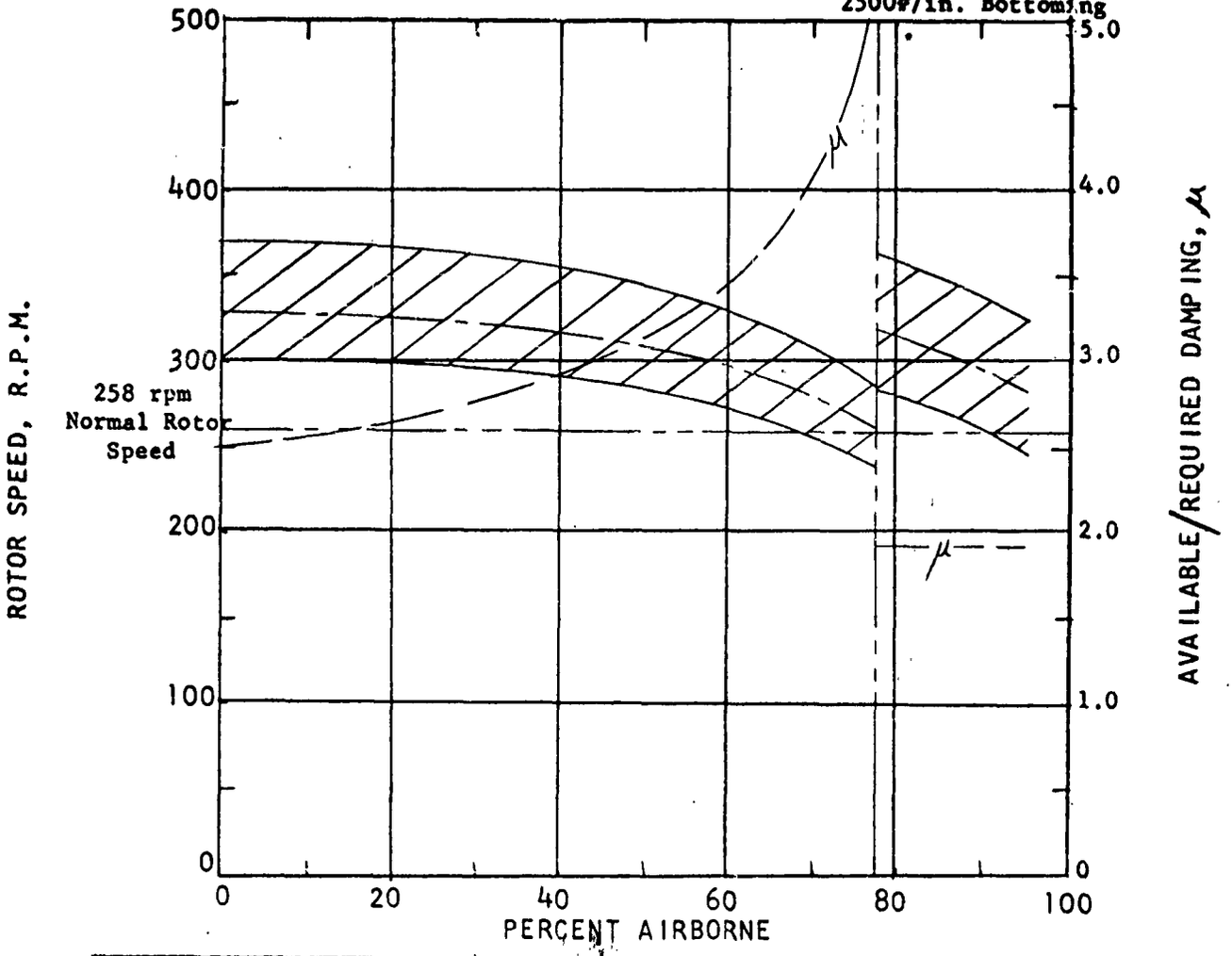
% Airborne	0%	50%	-78%	78%	95%
Fwd Oleo Vert.					
Fwd Oleo Lat.					
Aft Oleo Vert.	1610	1002	195	2695	2695
Aft Oleo Lat.	9000	6500	4000	4000	4000
Fwd Tire Vert.					
Fwd Tire Lat.					
Aft Tire Vert.	9260	8780	6860	6860	2500
Aft Tire Lat.	4500	4450	4080	4080	1850

Figure 106c

GROUND INSTABILITY ANALYSIS

18 x 5.5 Aft Tires 23,000# G.W.
150 psi

Oleo: 4000#/in. Extended
9000#/in. Static
2500#/in. Bottoming



A/C Weight: * 23,000# Roll Inertia: 145,000 CG to Grnd, Static: 75.0 CG to Fwd Rotor: 73.8 CG to Aft Rotor: 126.5 * I.P.S. Units	Blade: 25 Ft. Weight: Lag Moment: 53.73 Lag Inertia: 9912	Lag Damper: YHC-1B Preload: 1100# Damping Rate: 98#/in./sec. Oleo Damping Rate: — Fwd: Aft: 625#/in./sec.

Fwd Tire Size:	Aft Tire Size: 18 x 5.5
No. Tires/Oleo:	No. Tires/Oleo: 2
Fwd Tire Pressure:	Aft Tire Pressure: 150 psi

Spring Rates Per Gear

% Airborne	0%	50%	-78%	78%	95%
Fwd Oleo Vert.					
Fwd Oleo Lat.					
Aft Oleo Vert.	2300	1450	280	2780	2780
Aft Oleo Lat.	9000	6500	4000	4000	4000
Fwd Tire Vert.					
Fwd Tire Lat.					
Aft Tire Vert.	9750	9140	7250	7250	4700
Aft Tire Lat.	4550	4500	4240	4240	2240

ROTOR BLADE

INTRODUCTION

The rotor blade proposed for the high performance helicopter design is the result of a rigorous design effort to achieve greater rotor solidity without accepting an excessive weight penalty with its accompanying centrifugal forces, and without sacrificing dynamic acceptability which plays an important role in reducing helicopter vibration level.

A blade design was selected for purposes of detailed structural study after achieving acceptable centrifugal force levels and dynamic characteristics.

Continued aerodynamic study resulted in an optimized blade configuration differing somewhat from the blade design for which details of structural analysis are presented.

Further study will be necessary to obtain optimum structural characteristics for the final blade design. This study presents a detailed examination of an intermediate blade design, and is typical of the study which will be performed on the final blade. A comparison of the intermediate and final blade designs follows:

	Intermediate Blade	Final Blade
Blade Radius	25'	26.25'
Blade Chord	21.5" Airfoil + 1.5" Cusp	19.5" Airfoil + 1.5" Cusp
Airfoil	NACA 0009.5	NACA 0009.5
Twist (Root to Tip)	-8.33°	-14°

PHASE I

Initial studies centered around a reduced span version of the NACA 0012 airfoil 23 inch chord Boeing-Vertol YHC-1B Chinook blade, thus taking advantage of existing blade tooling. This blade would have weighed 60 pounds per blade more than the final blade design, plus the addition of 20 pounds of natural frequency weight to each blade, for a total weight penalty of approximately 500 pounds per helicopter in blade weight alone. This would, of course, require a larger hub and greater capacity retention system.

Further studies were directed toward reducing weight by modifying the spar on the YHC-1B, still preserving most of the tooling built for this blade. Three such blade configurations were designed and analyzed, resulting in the reduction of blade weight by 50 pounds per blade; however, acceptable dynamic characteristics were not provided. The basic problem lies in the fact that, while mass reductions were possible at the cost of expensive manufacturing methods, the stiffness of the blade could not be reduced in the same ratio, hence the first mode flapwise natural frequency preferably around 2.9, increased toward 3.0 which is dynamically undesirable for three-bladed rotors.

A YHC-1B blade was analyzed, using an aluminum spar. For the same weight, stiffness was again too great because of spar thickness, and both natural frequency and blade stresses were excessively high.

Hopes to salvage most of existing tooling were then abandoned, and a change to a thinner airfoil section investigated. The first such blade configuration, based on a 0009.5 airfoil, used a 5.1 inch diameter spar. Because of manufacturing limitations, the outboard wall thickness of this blade could not be reduced below .060. The resulting stiffness-to-mass ratio was very low and resulted in a blade which was very limber outboard, causing excessive static droop and subject to centrifugal stiffening due to tip weights, thus producing an unacceptably high rotating natural frequency.

The studies discussed above are summarized briefly in the following table:

TABLE XVIII

SUMMARY OF BLADES EXAMINED FOR DYNAMIC PROPERTIES

Blade Configuration	Weight W/O Nat'l. Freq. Weight	First Flapwise Nat'l. Freq.	Comments
Reduced Span YHC-1B	227	2.578	Saves existing tooling Short development time Costs 500 lbs/helicopter
Modified YHC-1B Steel Spar A	187.5	2.685	Use much of existing tooling
B	179.0	2.665	Requires difficult manufacturing techniques to reduce spar weight.
C	172.00	2.612	Requires excessive weight to reduce natural frequency
Reduced Span YHC-1B Alum. Spar	159.0	2.629	New spar development Excessive natural frequency. Weight required. High spar stresses, poor erosion and corrosion characteristics
0009.5 Airfoil 5.1 Dia. Steel Spar	170.0	2.558	New spar tube, complete blade tooling, long lead time, natural frequency too high, requires additional weight.

The rotor blade design studies reviewed above, led to a decision to adapt the Boeing-Vertol 107 Model II spar to the longer chord 23 inch high performance design. This permits matching the dynamic characteristics of the desired blade to the Boeing-Vertol 107-II blade which is presently in production.

The design configuration is as follows:

Blade Weight	168 lb. (does not include 18 lb. of tuning weight assembly in forward blades)
First Flapwise Natural Frequency - Forward Blades	2.43
Airfoil Section	NACA 0009.5
Blade Radius	25 feet
Blade Chord	21.5" Airfoil + 1.5" Cusp = 23' total
Spar	4340" Rockrited" single piece steel spar, rolled, using same tools as Model II with positions of steps changed.
Airfoil, Aft of Spar	Fiberglass reinforced epoxy laminated skins bonded over aluminum ribs are structurally bonded to the heel of the 4340 steel spar to comprise the NACA 0009.5 airfoil.

While the actual components are completely new, extensive testing on similar Boeing-Vertol 107-II and YHC-1B blade box construction indicates excellent serviceability.

Balance Provisions	As with Boeing-Vertol 107-II, blades are made individually interchangeable by means of close manufacturing control and addition of balance weights in the nose of the spar and in the tip.
Root Fitting	The blade is attached to the hub components with a single pin which serves as the lag hinge. The blade is threaded and clamped to a forged 4340 socket through which the vertical pin is secured. This is the same principle used on the YHC-1B.
Natural Frequency - Weight	Fixed 10 pound weights are housed within, but isolated from, the forward blade spars at 40% radius as evaluated on Boeing-Vertol 107-II.

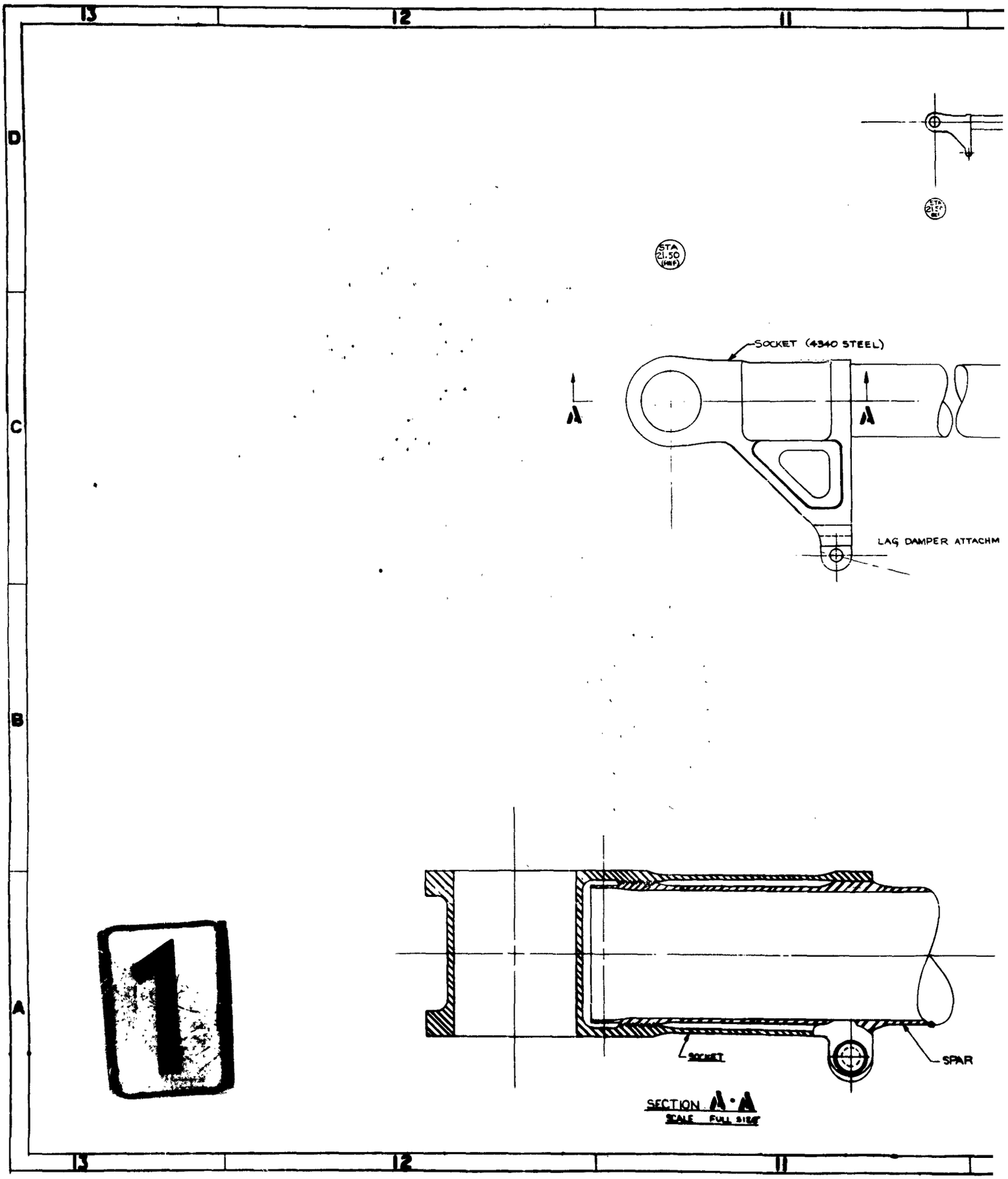
The dynamic characteristics of the high performance helicopter design blade match those of the Boeing-Vertol Model 107-II closely.

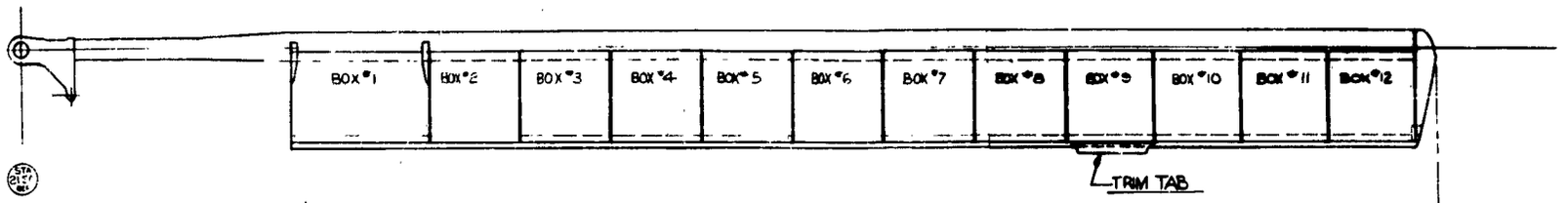
TABLE XIX

COMPARISON OF BOEING-VERTOL 107 AND HIGH PERFORMANCE 107 BLADE DYNAMIC PROPERTIES

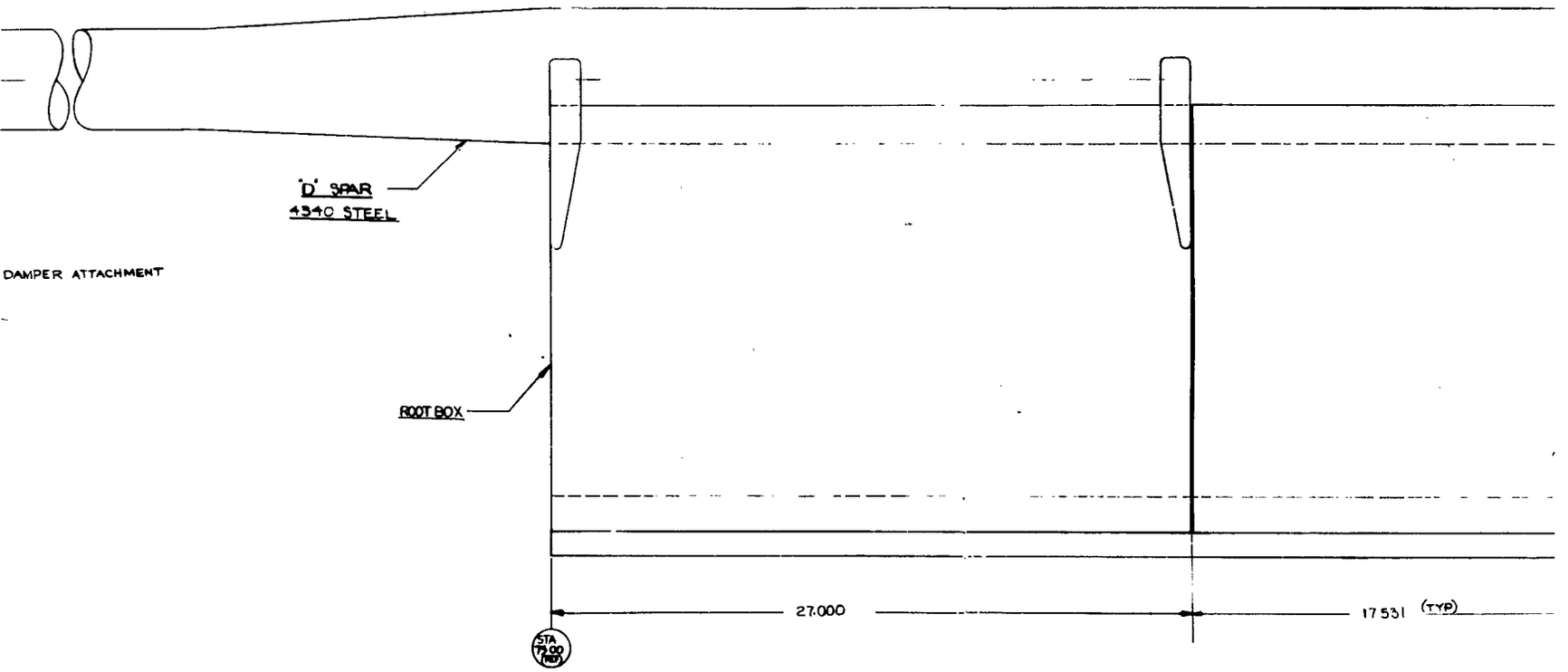
	Boeing-Vertol 107-II	High Performance Helicopter
1f First flapwise mode rotating natural frequency	2.49	2.43
13f Damped amplification factor, first flapwise mode, third harmonic (measure of 3/rev response)	1.812	1.602
2f Second flapwise mode rotating natural frequency	4.618	4.632
25f Damped amplification factor, second flapwise mode, fifth harmonic (measure of flapwise moment response)	4.065	3.963
1c First chordwise mode rotating natural frequency	4.80	4.774
15c Undamped amplification factor first chordwise mode, fifth harmonic	12.00	10.33

The High Performance 107-II blade physical properties of weight and stiffness distribution, centrifugal force, and chordwise neutral axis and center of gravity location are presented on the following pages. All data shown are for the intermediate design selected for detailed structural study.


13
12
11
D
C
B
A
STA 21.50 (MIR)
SOCKET (4340 STEEL)
LAG DAMPER ATTACHM
SOCKET
SPAR
SECTION A-A
SCALE FULL SIZE



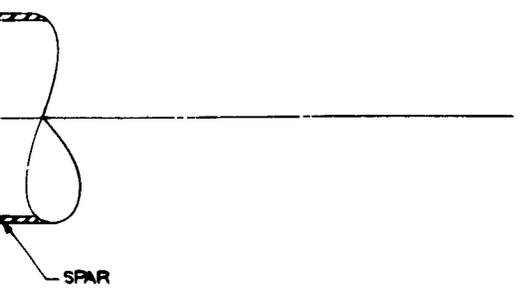
PLAN VIEW SCALE 1/10 SIZE



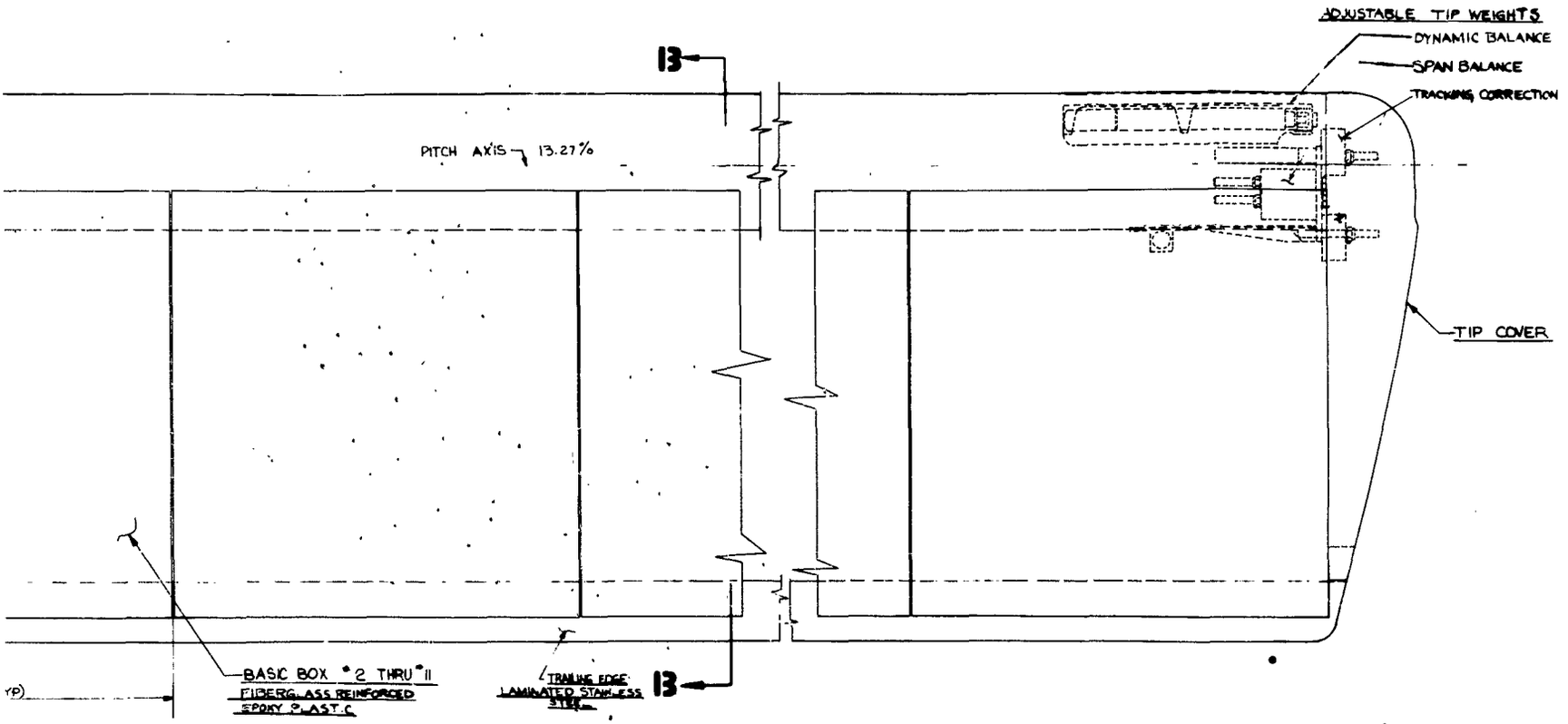
(-1) BLADE ASSY SHN (FW

(-2) BLADE ASSY OPP (AF

SCALE = 1/2 SIZE



2



Y SHN (FWD)

OPP (AFT)

3E

3

VERTOL FINISH SPEC

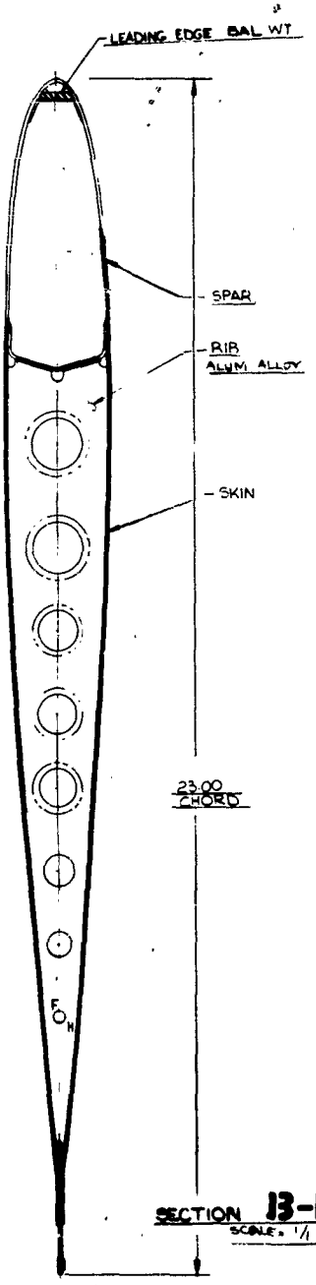
FINISH				FINISH		

* FOR VERTOL AND VERTOL VENDOR USE ONLY

THE DRAWING RELEASE DESIGNATION PREFIXED TO VERTOL DRAWING [illegible] SHALL NOT WARRANT RELEASED OF VERTOL DRAWING ISSUED IS USED OR [illegible] BY AGENCIES OTHER THAN AGENCIES OF THE U. S. GOVERNMENT ACTING [illegible] CONTRACTUAL OR TREATMENT AGREEMENTS.

ADJUSTABLE TIP WEIGHTS
DYNAMIC BALANCE
SPAN BALANCE
TRACKING CORRECTION

TIP COVER



SECTION 13-13
SCALE, 1/1

4

VENDOR STATUS
C - CATALOGUED ITEM — NO VENDOR DRAWING REQUIRED.
D - NON-CATALOGUED ITEM — VENDOR DRAWING REQUIRED.
S - FOR [illegible] ONLY, NOT KNOWN TO BE [illegible] OR STOCK [illegible]
T - FOR [illegible] OR THIS VENDOR, TO BECOME [illegible]
[illegible] FROM A CATALOG ITEM.
D* - INSPECTION REQUIRED PER TO VENDOR

FORM 8A1(A) (5-62)

VERTOL FINISH SPEC N

FINISH	MIL SPEC	COLOR NO.	FINISH	MIL SPEC	COLOR NO.

* FOR VERTOL AND VERTOL VERSIONS USE ONLY

THIS DRAWING RELEASE INFORMATION PERTINENT TO VERTOL DESIGN NEEDS AND SHALL NOT WITHOUT PUBLICATION OF VERTOL DESIGN DETAIL IS USED OR DUPLICATED BY AGENCIES OTHER THAN AGENCIES OF THE U. S. GOVERNMENT ACTING PURSUANT TO CONTRACTUAL OR STATUTORY AUTHORIZATION.

ZONE	REVISION NO.	BY	CHKD	APP'D	DESCRIPTION	DATE	APPROVAL

ZONE	REVISION NO.	BY	CHKD	APP'D	DESCRIPTION	DATE	APPROVAL

5

SK9892 REV.

SK9892 REV.

ITEM DESIG. NO.	QUANTITY	DESCRIPTION	STOCK SIZE	MATL	MATL SPEC.	WEIGHT UNIT	WEIGHT TOTAL	PART NO. DASH	PART NO. SYMB	MFG. CODE	SOURCE CODE	DRAWING NO. OR PART ASSY BLOCK	ZONE	NOMENCLATURE	REV. STATUS

LIST OF MATERIAL

SECURITY CLASSIFICATION

MODEL	FOR USE ON	NEXT ASSEMBLY

TORQUE VALUES
C—CHANGING ITEM—NO TORQUE VALUES REQUIRED.
D—NON-CHANGING ITEM—TORQUE VALUES REQUIRED.
S—FOR [illegible] SEE SPECIFICATION [illegible]
T—FOR [illegible] SEE SPECIFICATION [illegible]
▶ DIMENSION REQUIRED FOR VS SPEC

F—MOD HEAD PART NO.
H—MOD HEAD NOMI SIZE
DASH NO. FOR SPA—
I—SERIES AT SHEL—
SHEL CODE—
S—SHAPE—
NO. OF SHEETS SHOWN—
C—CODE

DRAWN	CHECKED	ENGR APPR	MFG APPR	QUAL	CODE
					N.A.

UNLESS OTHERWISE SPECIFIED
ENGINEERING ACE IN INCHES
TOLERANCES ON
FRACTIONS ANGLES
.X ± .1 .XX ± .02 .XXX ± .010 .X° ± .5°

HEAT TREAT	CONDITION	TENSILE STRENGTH
STEEL	MIL-H-6875	154
ALUM.	MIL-H-6088	150
MAGN. CAST.	MIL-H-6857	

25 FT METAL ROTOR BLADE 00095 AIRFOIL

VERTOL DIVISION
THE BOEING COMPANY
MORTON, PENNSYLVANIA

SIZE A | DRAWING NO. SK9892 | REV. J

SCALE 1/2 & 1/4 FULL | CODE IDENT. NO. 77272 | SHEET 1 OF 1

PHASE II

Having established a dynamically satisfactory blade, a theoretical study was made to determine the effects of various flight parameters on blade moments and stresses. This study was performed by making step-by-step changes from the present Boeing-Vertol 107 Model II flight and blade parameters to the High Performance 107-II.

The Leone-Myklestad Method of Rotor Blade Aeroelastic Vibration Analysis with basic trim data provided by aerodynamics yielded the theoretical bending moments. Except for the vibratory moments, agreement between the theoretically calculated data and presently available flight test data is excellent. The vibratory moments are semiempirically adjusted through past data to insure flight test agreement.

Eight cases were investigated and tabulated below:

TABLE XX

CASES CONSIDERED IN BLADE MOMENT AND STRESS STUDY

Case	Gross Weight	f_e	Chord Inches	Twist Degrees	V_t	μ	C_T/σ	Knots	Effect of
1	18,400	30.2	18	-8 1/3	670	.355	.0827	141	Base Case 107-II
2	18,400	20.5	18	-8 1/3	670	.355	.0768	141	Drag
3	18,400	20.5	23	-8 1/3	670	.355	.0597	141	Solidity
4	15,000	20.5	23	-8 1/3	670	.355	.0489	141	Gross Weight
5	15,000	20.5	23	-8 1/3	670	.438	.0505	174	Forward Speed
6	15,000	20.5	23	-8 1/3	650	.452	.0544	174	Tip Speed
7	15,000	20.5	23	-14	650	.452	.0537	174	Twist
8*	15,000	20.5	23	-8 1/3	670	.438	.0505	174	Chordwise C.G.

* Same as Case 5 except that the chordwise C.G. of outboard blade section moved from .26c to .24c

The theoretical bending moment data - both flap and chordwise results - are presented, for the above eight cases in Figures 115 through 118. These curves formed the basis of a detailed stress study of the rotor blade with satisfactory dynamic characteristics as established from the Phase I study.

The table below summarizes the results of this stress study. An interpretation of the results follows the table.

TABLE XXI

SUMMARY OF BLADE MOMENT AND STRESS STUDY

Case	Flap Bending Stresses (psi) 090 Wall	072 Wall	050 Wall	Trailing Edge Stresses (psi) (50% Blade Radius)
1	26,700 ± 13,300	32,000 ± 15,100	37,500 ± 24,500	32,670 ± 15,000
2	26,200 ± 13,300	30,900 ± 14,800	36,100 ± 18,800	32,670 ± 16,000
3	25,600 ± 12,600	30,700 ± 13,500	39,800 ± 15,000	50,400 ± 12,600
4	25,900 ± 12,000	30,600 ± 12,900	37,500 ± 18,000	50,400 ± 14,000
5	26,100 ± 19,000	30,800 ± 19,100	41,800 ± 30,600	47,400 ± 18,100
6	25,900 ± 21,000	31,100 ± 21,000	41,800 ± 30,600	45,600 ± 22,200
7	29,500 ± 25,600	35,300 ± 27,300	41,800 ± 28,200	47,400 ± 23,800
8	26,200 ± 19,600	30,900 ± 20,600	43,400 ± 23,500	41,600 ± 17,400

1. Effect of Helicopter Drag - Case 1 and 2

   Steady flap stresses are reduced. Chordwise stresses are not affected. Flap vibratory stresses are reduced for the low drag version in the 072 wall and 050 wall section.

2. Effect of Gross Weight - Case 3 and 4

   Steady flap stresses are slightly lower for the 090 wall and higher for the 072 and 050 wall for the higher G.W., Case 3. Steady chord stresses are not affected. Vibratory flap stresses increase slightly for the higher gross weight version in the 072 and 090 wall sections but lower in the 050 wall section. Vibratory chord stresses are reduced slightly for the higher gross weight version.

3. Effect of Increased Forward Speed - Case 4 and 5

   This condition had the most significant effect on blade vibratory bending moments. Flap vibratory stresses increased by approximately 50% to 70%. The stress level of 30,600 psi in the 050 outboard section would be unacceptable for unlimited life. Chord vibratory stresses increased considerably but stress levels are still reasonable. The effect of steady stresses is insignificant.

4. Effect of Twist Angle - Case 6 and 7

   The change of steady stresses is significant. The higher twist increases the flap vibratory stresses on the inboard sections, 072 and 090 wall, by a factor of 1.3. The stresses thus produced on the spar in the intermediate design studied herein are considered too high. Thus, modification to the spar configuration will be required to reduce stresses to an acceptable level on the final blade design chosen for optimum performance.

5. Effect of Chordwise C.G. Location - Case 5 and 8

Condition 5 initially looked satisfactory except for the high outboard flap vibratory stresses. It was realized that the outboard hump on the flap curves is due to the steady chord moment as affected by the large amount of blade cyclic. The steady chord loads were reduced by balancing the outboard portion of the blade as far forward as considered satisfactory. The chordwise C.G. was thereby shifted from 26% to 24% chord. The distance from the C.G. to the neutral axis was considerably affected. The reduction in steady chord moment can be seen in Figure 117. The reduction of flap vibratory stresses in the outboard 050 wall section from 30,600 psi to 23,500 psi was a significant improvement. The effect on steady flap stresses are reduced slightly.

The study performed has resulted in an understanding of the effects of reduced drag, increased solidity, increased speed, twist angle, blade chordwise C.G. change, blade loading, and tip speed ratio in the high forward level flight speed regimes. By careful evaluation of the flight parameters, it is possible to arrive at an optimum blade structural configuration.

HIGH SPEED LEVEL FLIGHT STRESS EVALUATION

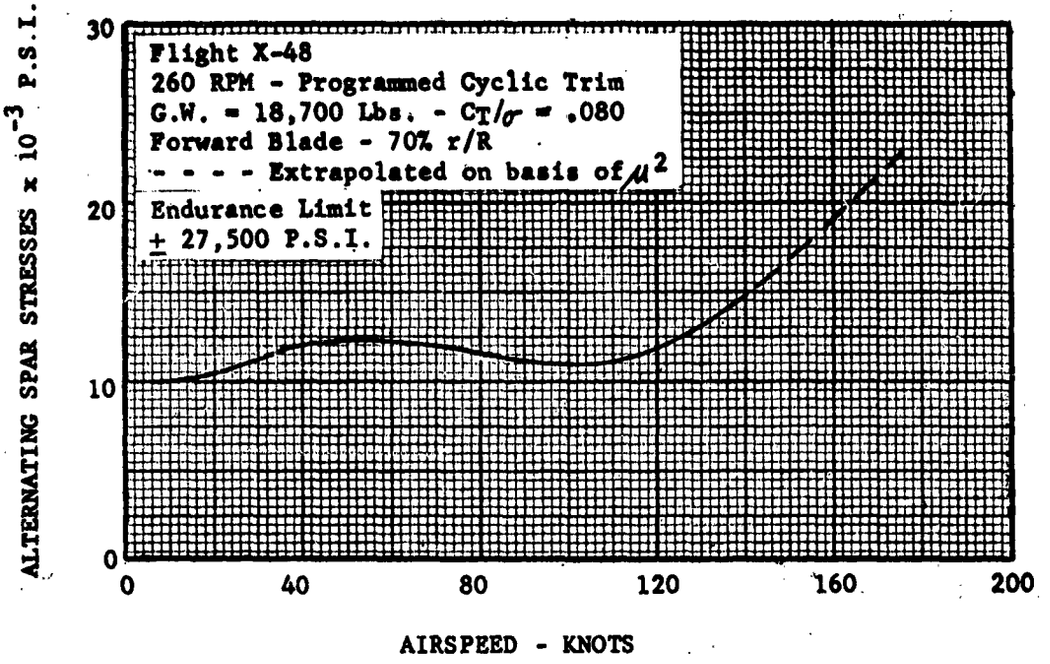
The evaluation of the study conducted on the intermediate blade design indicates that the conditions of a Case 8 satisfy the design requirements. The critical flap bending stresses for Case 8 are in the outboard section at 80% blade radius. The stress is $\pm$ 23,500 psi. Test endurance limits for rockrited 4340 steel spar tubes have been shown to be 27,000 psi. The endurance limit of the laminated stainless steel training edge strip based on recent full scale tests is 22,000 psi. Stresses predicted for a 200 MPH speed do not exceed these stress levels, therefore no life restrictions would be imposed upon the blade for unaccelerated high speed level flight. Additional analysis of a similar nature is required to optimize the structural design of the final blade configuration selected for performance.

FLIGHT STRESSES

A plot is presented of blade stresses measured on the Boeing-Vertol 107-II, showing the trend of the upper scatterband of data. The extrapolation shown indicates an increase in blade stresses proportional to μ^2. Based on this, the maximum expected stress level at r/R = .70 is 23,000 psi. This would be a conservative estimate since C_T/σ for the high performance vehicle is lower than for the Boeing-Vertol 107-II. It should be noted that this value compares favorably with the stress of 23,500 psi computed from semiempirical considerations.

FIGURE 107

FLIGHT STRESSES



STRESS ANALYSIS

Blade moments are determined by a semiempirical method developed at Vertol Division during the past few years. A study was made (SMR-172) to determine the relationship between measured blade moments and theoretically calculated moments.* It was evident that if calculated flap moments had more second mode bending and calculated chord moments more first mode bending there would be a much better agreement.

It is felt that if the theoretical analysis could be programmed to include the higher harmonics (4th harmonics and above) there would also be a much better agreement. The only limitation is computer capacity.

The theoretical blade bending data are presented for the eight cases in Figure 115 through 118.

The vibratory bending moments are semiempirically adjusted to insure flight test agreement.

The present method is to determine the appropriate factor based on past experience for the various flight regimes such as transition, high speed flight, and maneuvers. Applying these factors to the theoretically calculated moments results in a good estimate of expected in-flight blade moments.

* Calculated using Leone-Myklestad Method

BLADE ANALYSIS

TABLE XXII

BLADE SECOND MODE AMPLIFICATION FACTORS

Forward Blade Inboard @ $\frac{r}{R}$ = .12	Flap Peak Meas. / Peak Calc.	Chord Peak Meas. / Peak Calc.
High Speed	1.695	3.0
Transition	1.960	3.0
Maneuver	3.480	4.0
Outboard $\frac{r}{R}$ = .70		
High Speed	2.89	3.0
Transition	2.89	3.0
Maneuver	3.88	4.0

The semiempirically corrected average vibratory flap bending moments are presented on Figures 119a through 119f.

An abbreviated summary of the stress work leading to Table XXI follows on Page 13-10 through 13-12

STRESS ANALYSIS

The following data are presented:

1. Section properties of the blade at various sections
2. Steady flapwise stresses at critical station for vibratory moments
3. Vibratory flapwise moments and stresses
4. Steady chordwise stresses at critical station for vibratory moments
5. Vibratory chordwise moments and stresses
6. Summary table of stresses

TABLE XXIII

1. SECTION PROPERTIES OF BLADE AT VARIOUS SECTIONS

Stations	182 to 300	128 to 174	73 to 119
Flapwise	050 Wall	070 Wall	090 Wall
	$\frac{r}{R}$ = .610 to 1.00 I/C = .425 in.^{3}	$\frac{r}{R}$ = .43 to .58 I/C = .608 in.^{3}	$\frac{r}{R}$ = .24 to .40 I/C = .715 in.^{3}
Chordwise (for T.E. stresses)	050 Wall $\frac{r}{R}$ = .610 to 1.00 I/C = 1.13 in.^{3}	070 Wall $\frac{r}{R}$ = .43 to .58 I/C = 1.24 in.^{3}	090 Wall $\frac{r}{R}$ = .24 to .40 I/C = 1.33 in.^{3}

TABLE XXIV

2. STEADY FLAPWISE STRESSES

Case	80% Moment (Outbd.) 050	40% Moment (Inbd.) 070	f_b outboard*	f_b inboard*
1	8,800	4,300	20,700	7,050
2	8,200	3,800	19,300	6,240
3	9,800	3,000	24,000	4,940
4	8,800	3,400	20,700	5,600
5	10,600	3,600	25,000	5,900
6	10,600	3,400	25,000	5,600
7	11,300	7,600	26,000	12,500
8	9,000	2,000	21,200	3,200

<u>CF Stresses @ 256 RPM</u>

Outboard 80% 17,500 x $\left(\frac{256}{262}\right)^2$ = 16,800 psi 050

Inboard 40% 29,000 x $\left(\frac{256}{262}\right)^2$ = 27,700 psi 072

26,000 x $\left(\frac{256}{262}\right)^2$ = 23,000 psi 090

* I/C = .425 outboard
.608 inboard

TABLE XXV

3. VIBRATORY FLAPWISE STRESSES AND MOMENTS
(HIGH SPEED LEVEL FLIGHT)

Case	Maximum Moment 050 Wall	Maximum Moment 072 Wall	Maximum Moment 050 Wall
1	9,600	9,200	10,400
2	9,300	9,000	8,000
3	9,000	9,200	6,400
4	8,560	7,600	7,600
5	13,600	11,600	13,000
6	15,000	12,800	13,000
7	18,300	16,600	12,400
8	14,000	12,000	10,000

Case	Maximum Stress 090	Maximum Stress 072	Maximum Stress 050
1	13,300	15,100	24,500
2	13,000	14,800	18,800
3	12,600	13,500	15,000
4	12,000	12,900	18,000
5	19,000	19,100	30,600
6	21,000	21,000	30,600
7	25,600	27,300	28,200
8	19,600	20,600	23,500

Proposed Blade Configuration, Intermediate Design

Plots of the moments listed above are given on the following pages.

TABLE XXVI ·

4. STEADY CHORDWISE STRESSES

Critical Station is $\frac{r}{R}$ = .50 or Station 150 I/C = 1.24

Case	Moment	f_t
1	11,000	8,870
2	11,000	8,870
3	33,000	26,600
4	33,000	26,600
5	29,000	23,600
6	27,000	21,800
7	29,000	23,600
8	22,000	17,800

Proposed Blade Configuration - Intermediate Design

CF Stress @ $\frac{r}{R}$ = .5 = 27,500 x $\frac{26}{29}$ x $\left(\frac{256}{262}\right)^2$ x = 23,800 psi

TABLE XXVII

5. VIBRATORY CHORDWISE STRESSES (INCLUDING FIRST MODE CORRECT)

Critical Station $\frac{r}{R}$ = .50 or Station 150

Case	Moment*	psi
1	± 19,800	± 16,000
2	± 19,800	± 16,000
3	± 15,600	± 12,600
4	± 17,400	± 14,000
5	± 22,500	± 18,100
6	± 27,500	± 22,200
7	± 29,600	± 23,800
8	± 21,600	± 17,400

Proposed Blade Configuration, Intermediate Design

I/C = 1.24

FIGURE 108
HIGH PERFORMANCE HELICOPTER METAL ROTOR BLADE
SPANWISE WEIGHT DISTRIBUTION

AFT BLADE - 25 FT. RADIUS, 23 IN. CHORD
NACA 0009.5 AIRFOIL

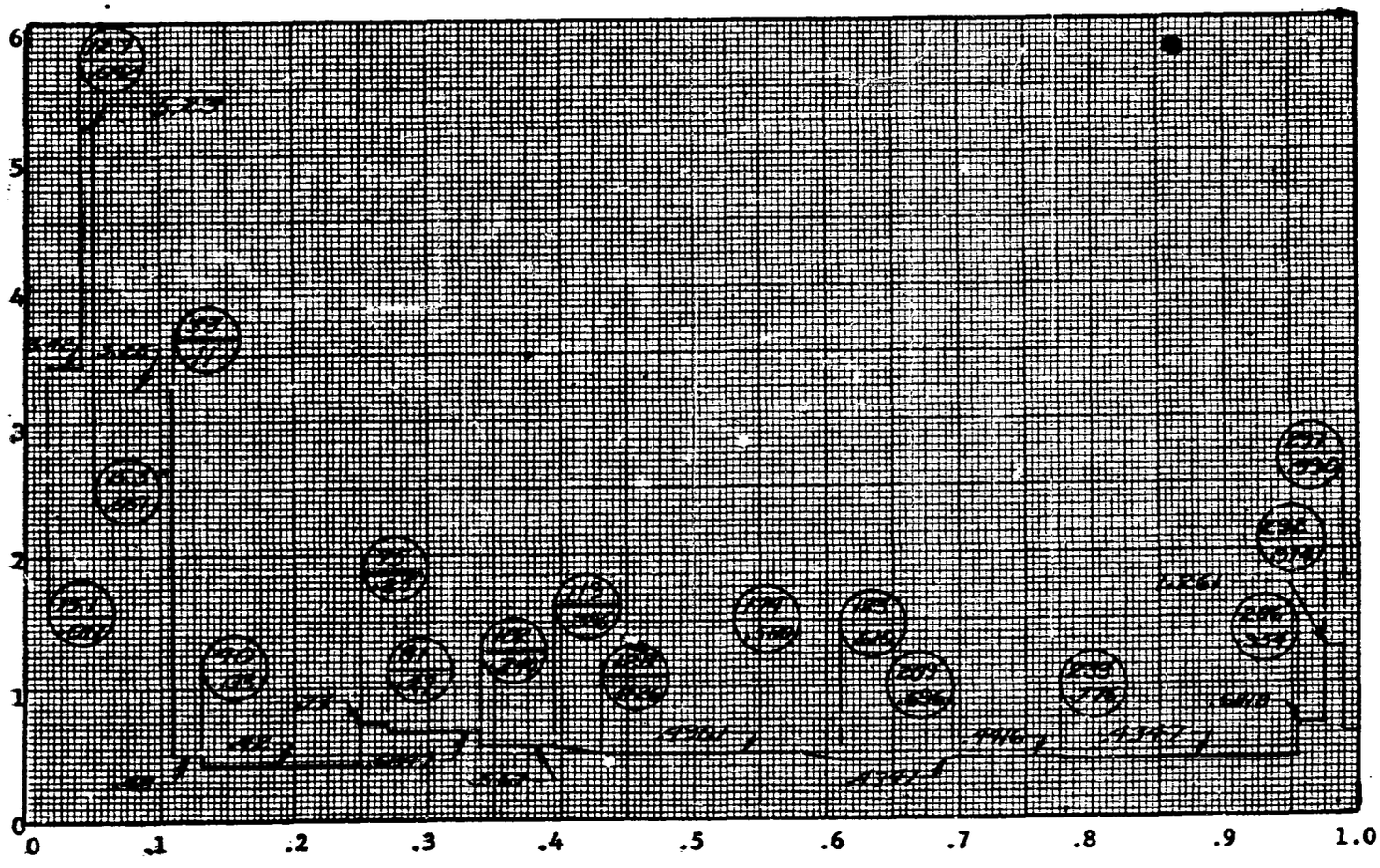


FIGURE 109

HIGH PERFORMANCE HELICOPTER
RADIAL DISTRIBUTION OF FLAPWISE STIFFNESS

FORWARD AND AFT BLADES - 23 FT. RADIUS, 23 IN. CHORD
NACA 0009.5 AIRFOIL

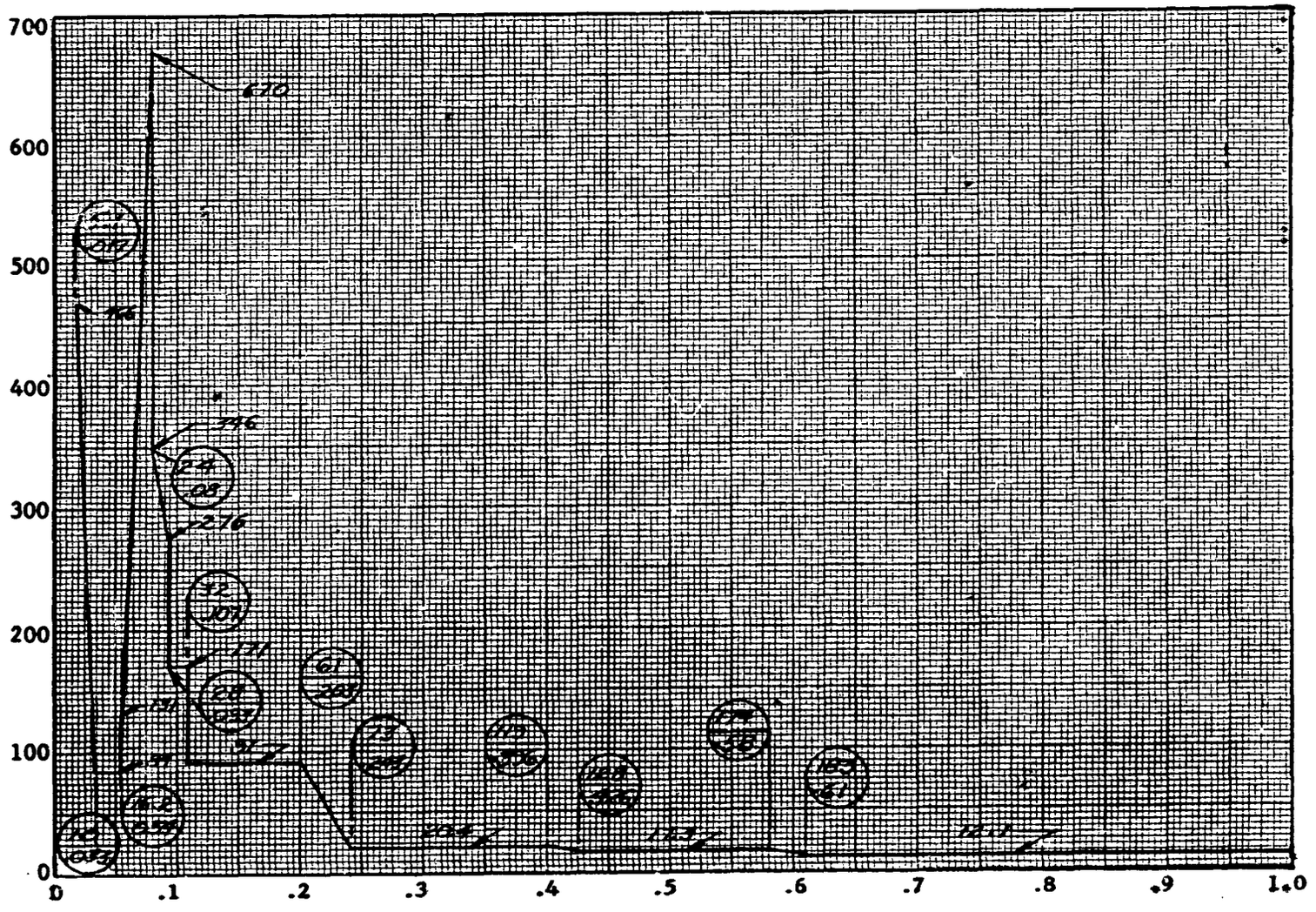


FIGURE 110

HIGH PERFORMANCE HELICOPTER
RADIAL DISTRIBUTION OF CHORDWISE STIFFNESS

AFT BLADE - 25 FT. RADIUS, 23 IN. CHORD
NACA 0009.5 AIRFOIL

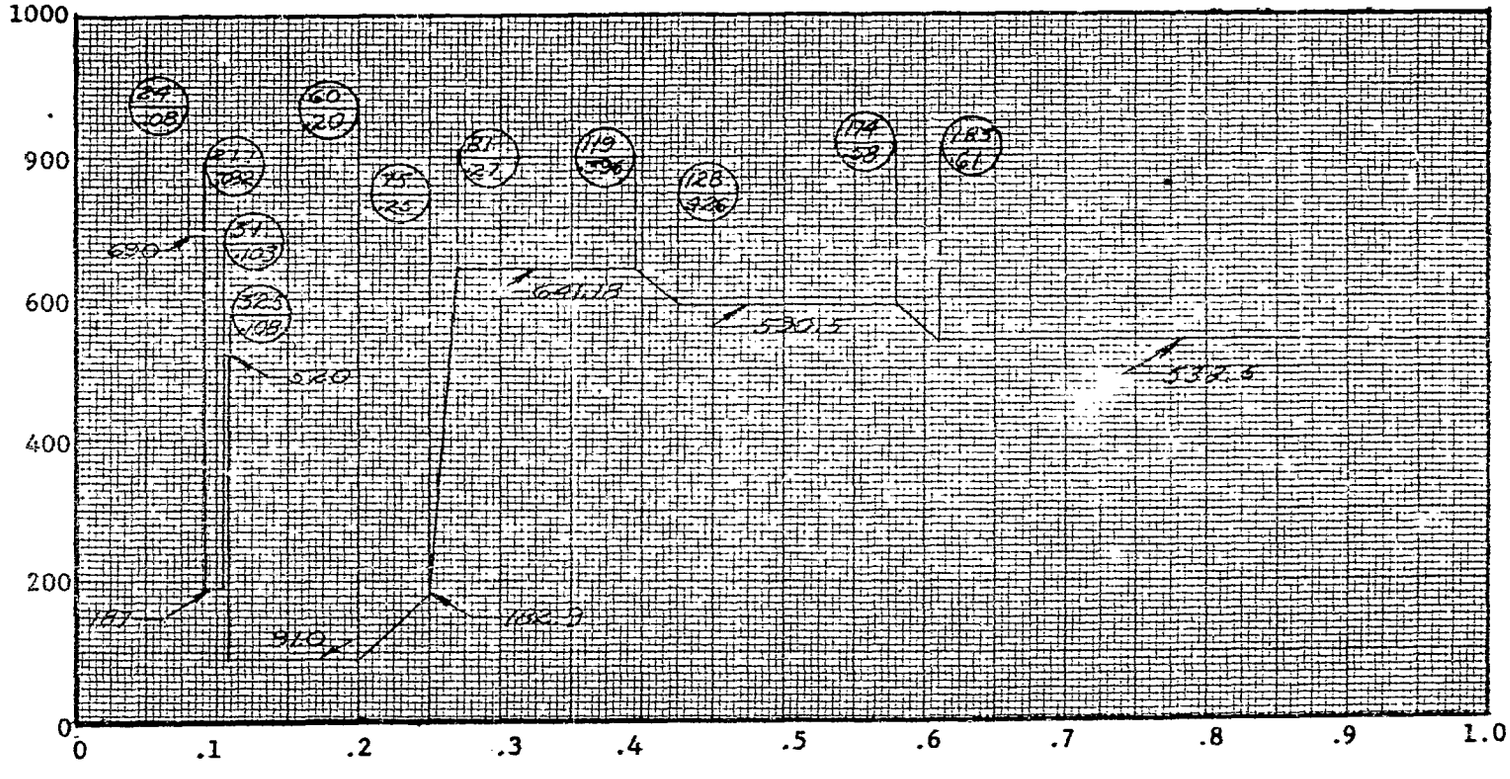


FIGURE 111
HIGH PERFORMANCE HELICOPTER
25 FT. RADIUS - 0009.5 AIRFOIL - AFT BLADE

CHORDWISE NEUTRAL AXIS LOCATION _____

CHORDWISE CG LOCATION - - - - - -

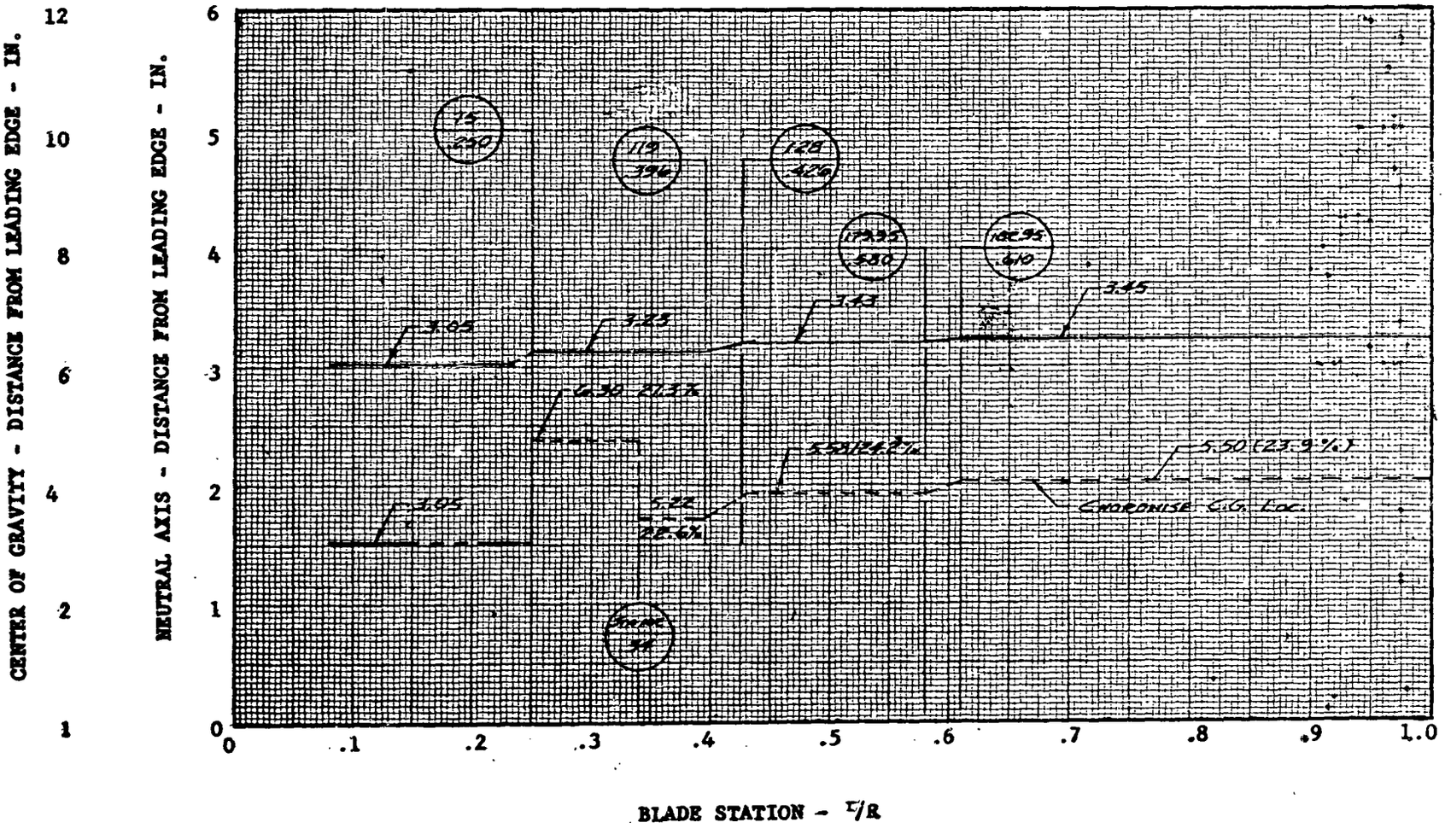


FIGURE 112
HIGH PERFORMANCE HELICOPTER
STATIC MOMENT DIAGRAM
NACA 0009.5 AIRFOIL

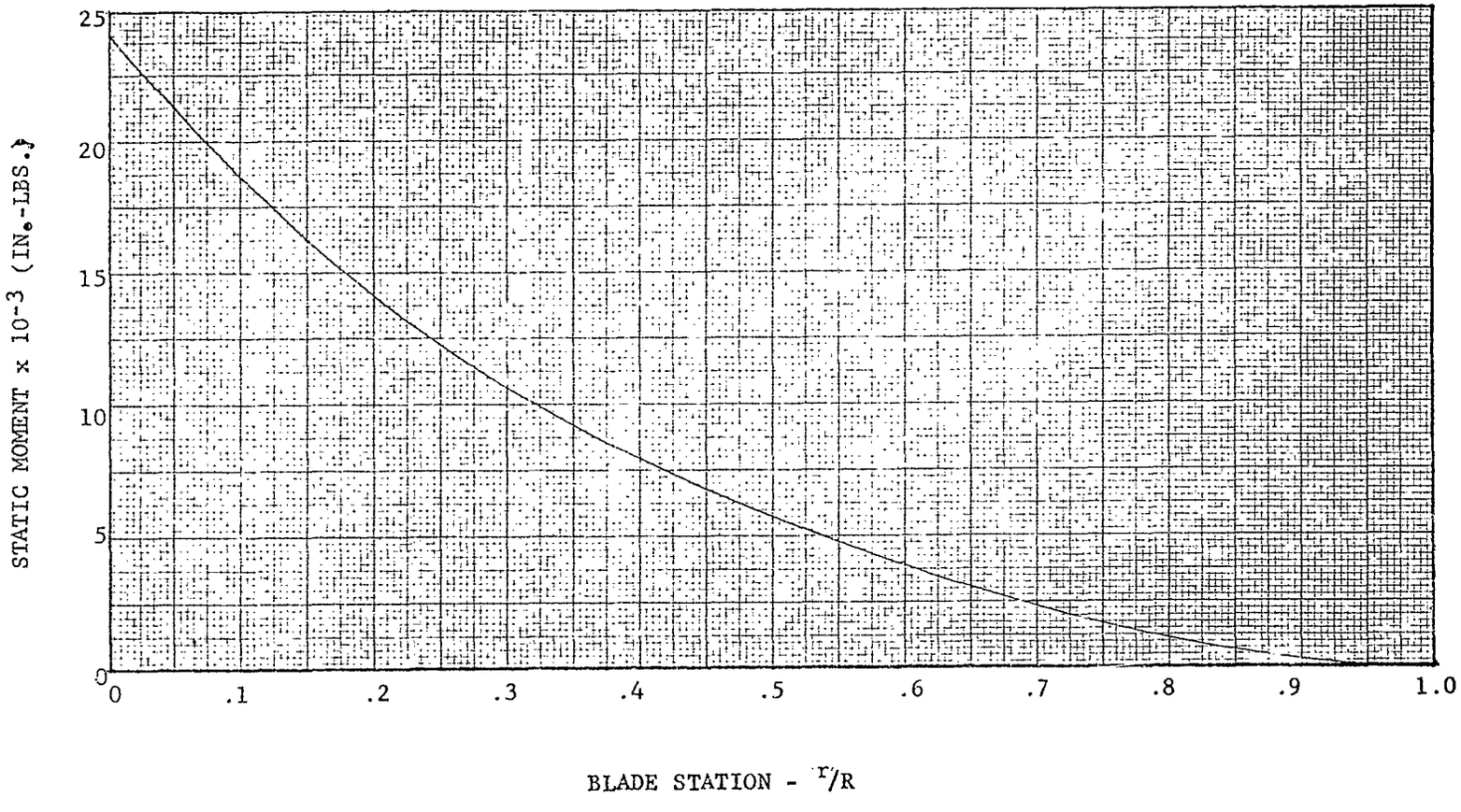
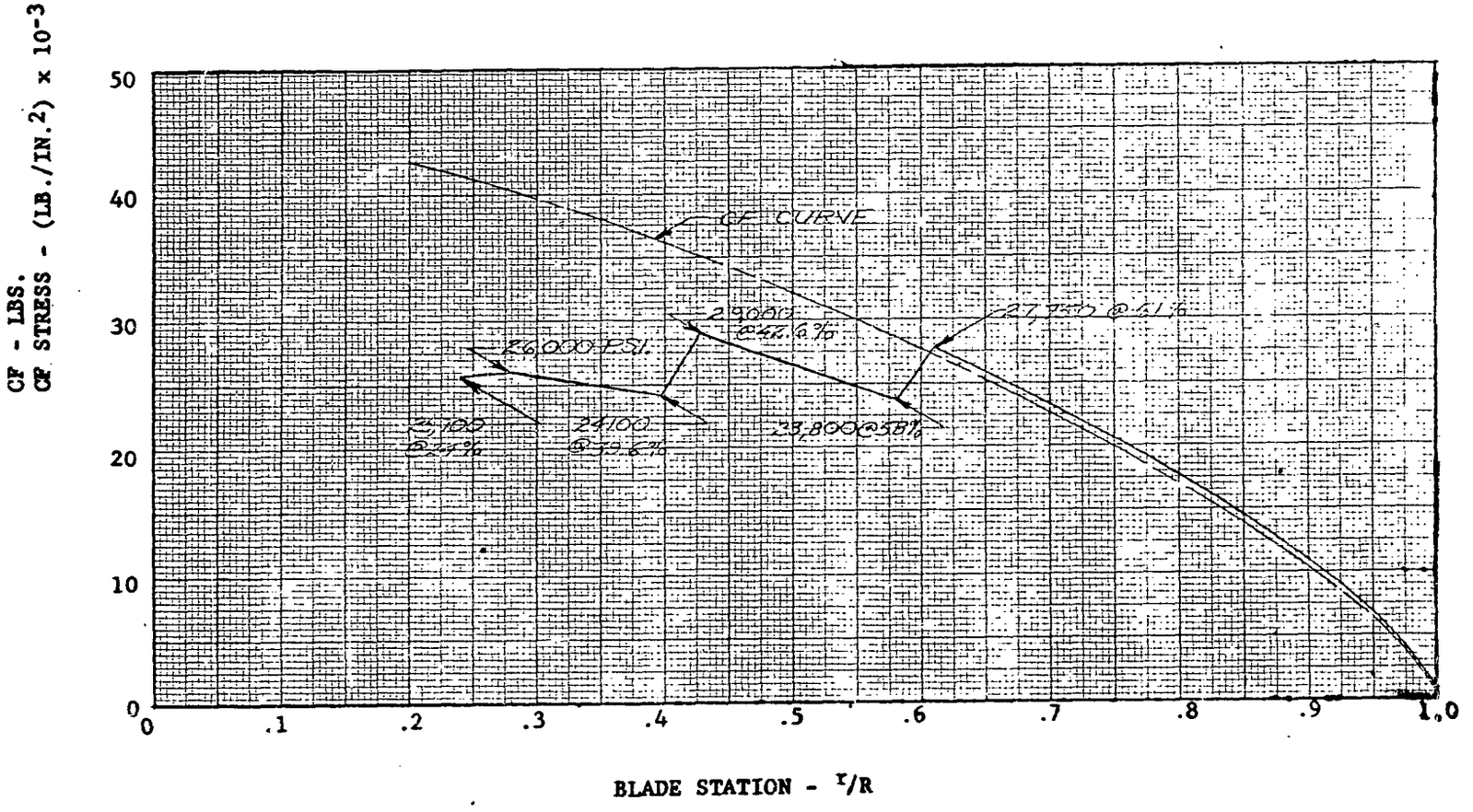
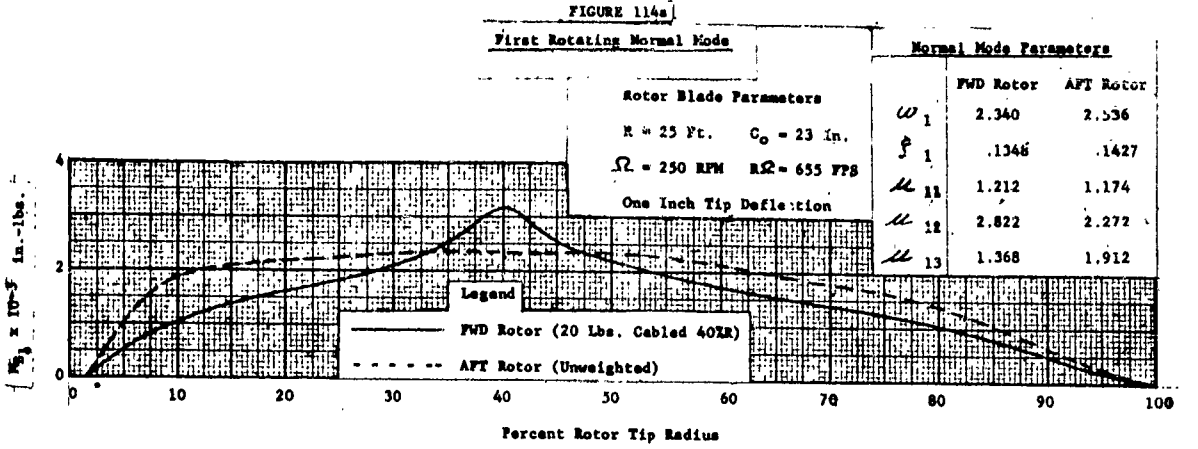


FIGURE 113
HIGH PERFORMANCE HELICOPTER
CENTRIFUGAL LOAD AND STRESS @ 262 ROTOR RPM



HIGH PERFORMANCE HELICOPTER METAL ROTOR BLADE
RADIAL DISTRIBUTION OF FLAP BENDING MOMENT IN A VACUUM
LEONE-MYKLESTAD METHOD

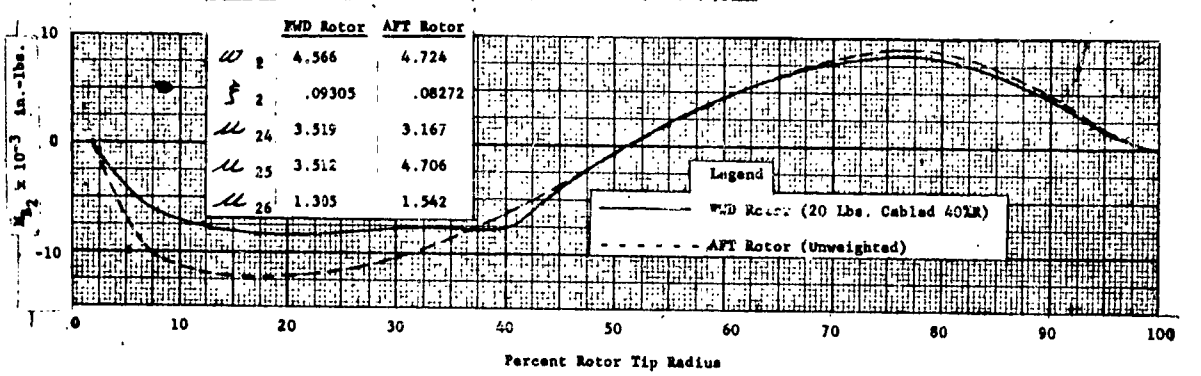
FIGURE 114a
First Rotating Normal Mode



Normal Mode Parameters

	FWD Rotor	AFT Rotor
ω_1	2.340	2.536
f_1	.1348	.1427
μ_{11}	1.212	1.174
μ_{12}	2.822	2.272
μ_{13}	1.368	1.912

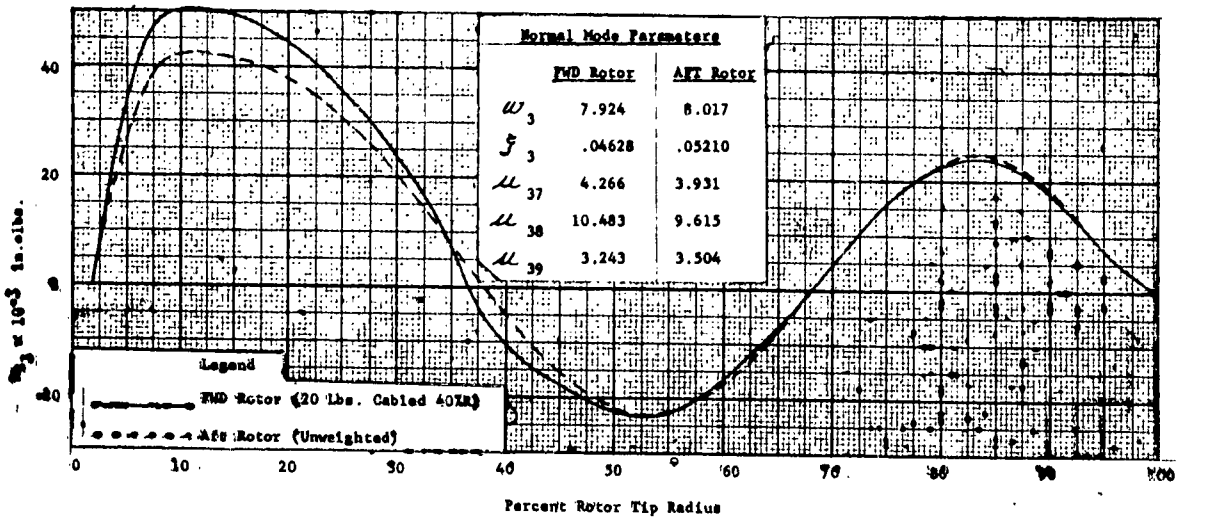
FIGURE 114b
Second Rotating Normal Mode



Normal Mode Parameters

	FWD Rotor	AFT Rotor
ω_2	4.566	4.724
f_2	.09305	.08272
μ_{24}	3.519	3.167
μ_{25}	3.512	4.706
μ_{26}	1.303	1.542

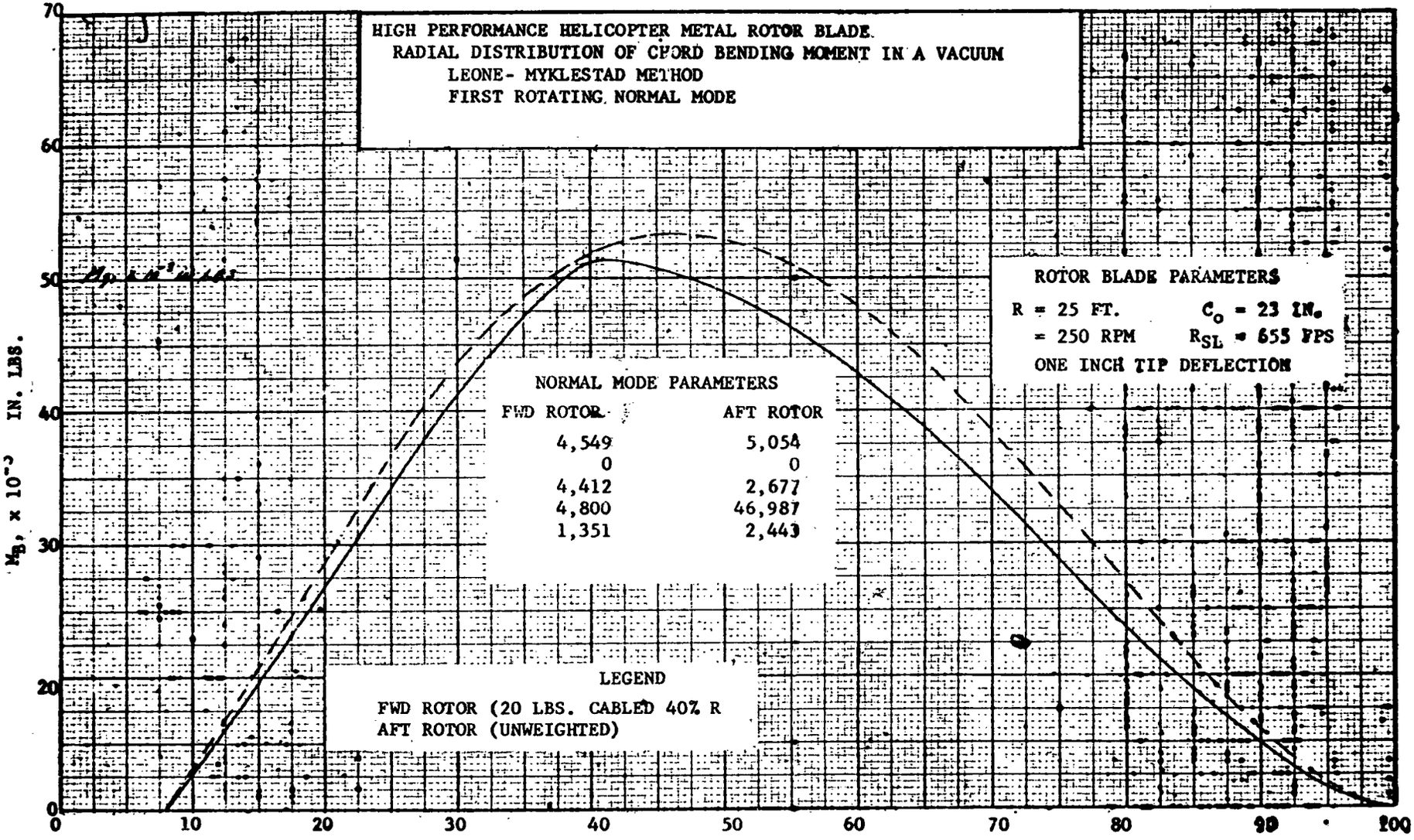
FIGURE 114c
Third Rotating Normal Mode



Normal Mode Parameters

	FWD Rotor	AFT Rotor
ω_3	7.924	8.017
f_3	.04628	.05210
μ_{37}	4.266	3.931
μ_{38}	10.483	9.615
μ_{39}	3.243	3.504

FIGURE 115


HIGH PERFORMANCE HELICOPTER METAL ROTOR BLADE
RADIAL DISTRIBUTION OF CHORD BENDING MOMENT IN A VACUUM
LEONE- MYKLESTAD METHOD
FIRST ROTATING NORMAL MODE
ROTOR BLADE PARAMETERS
R = 25 FT. C_o = 23 IN.
= 250 RPM R_{SL} = 655 FPS
ONE INCH TIP DEFLECTION
NORMAL MODE PARAMETERS
FWD ROTOR AFT ROTOR
4,549 5,054
0 0
4,412 2,677
4,800 46,987
1,351 2,443
LEGEND
FWD ROTOR (20 LBS. CABLED 40% R
AFT ROTOR (UNWEIGHTED)
M_B, x 10^{-3} IN. LBS.
0
20
30
40
50
60
70
0
10
20
30
40
50
60
70
80
90
100
PERCENT ROTOR TIP RADIUS

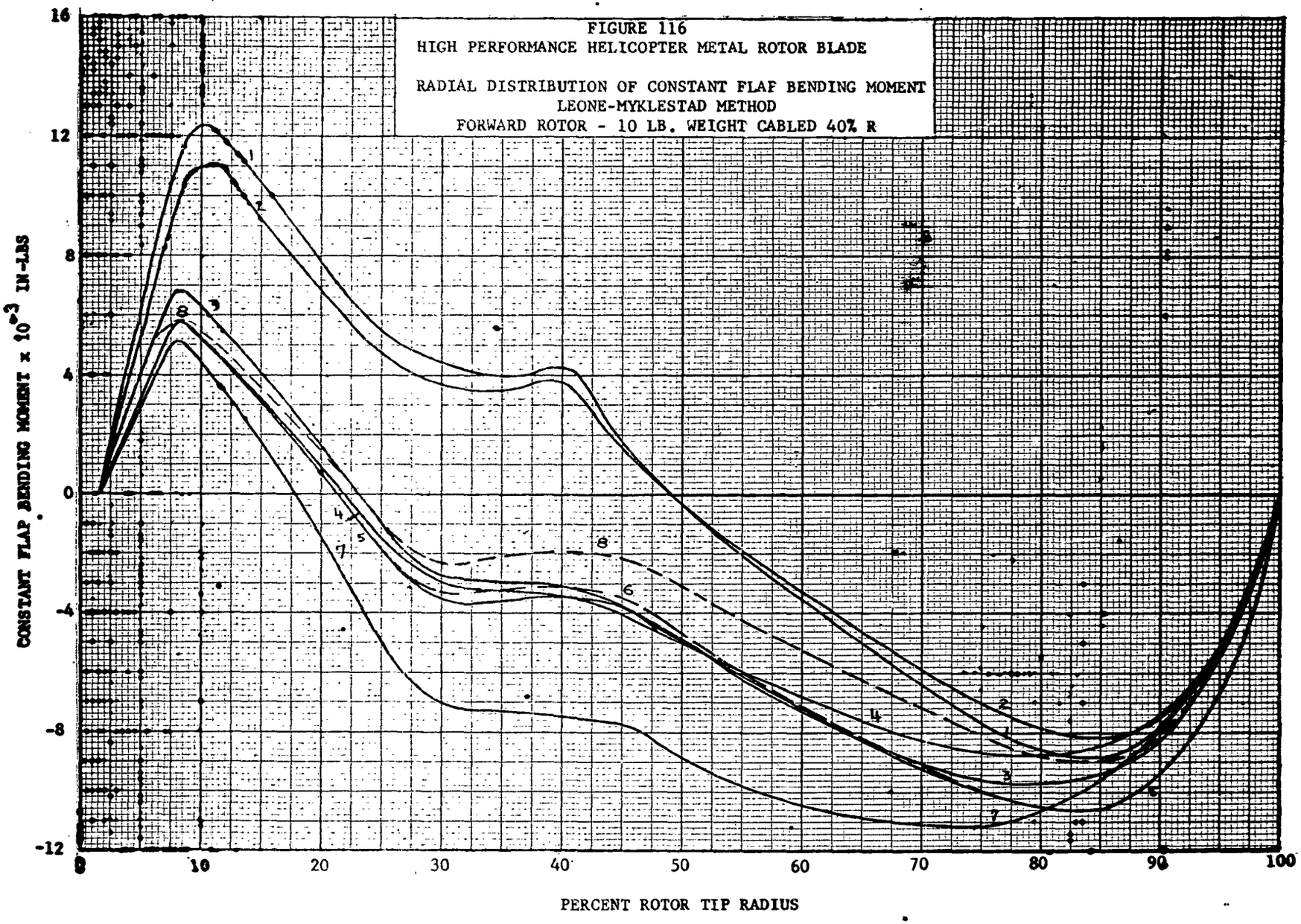
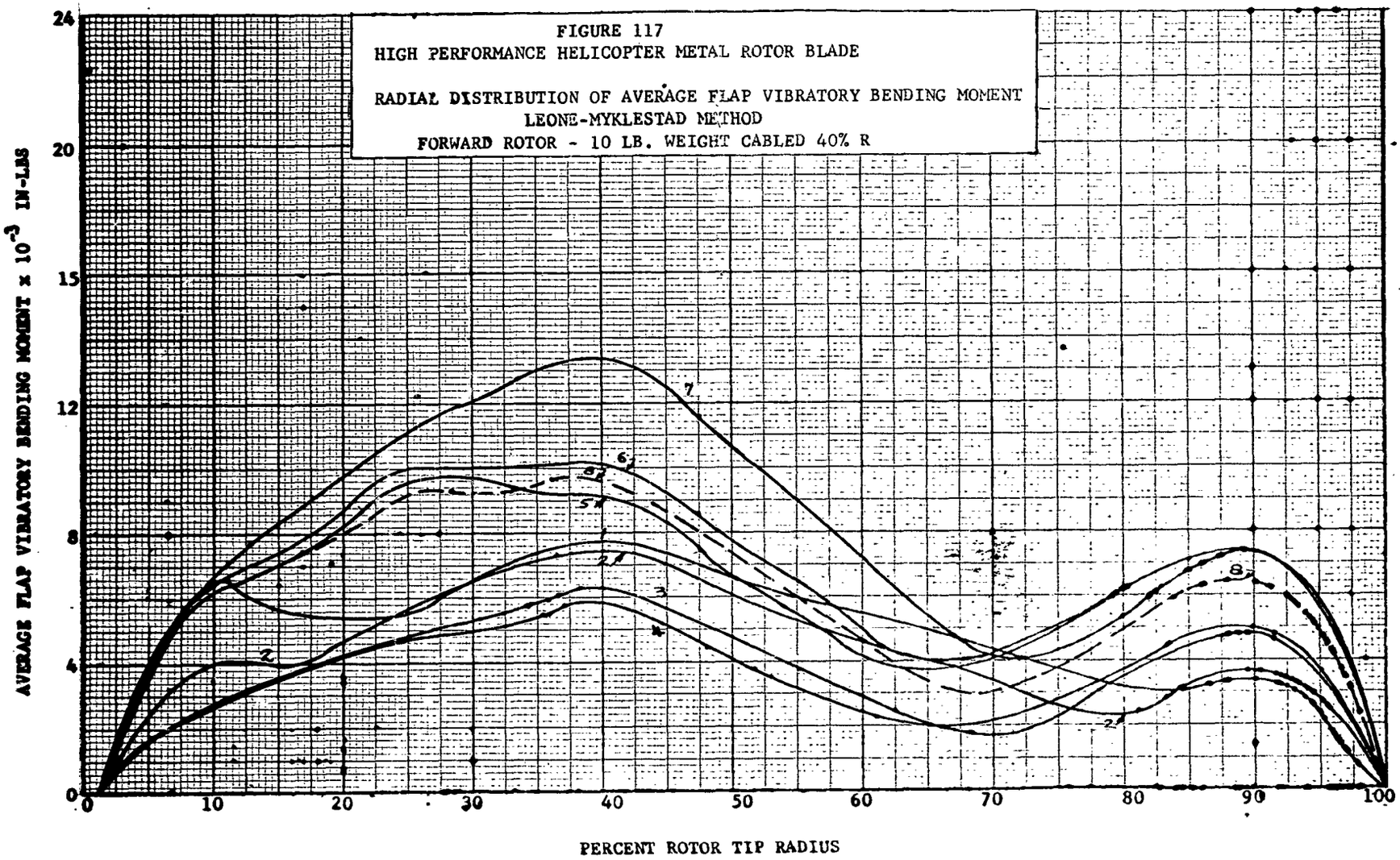

FIGURE 116
HIGH PERFORMANCE HELICOPTER METAL ROTOR BLADE
RADIAL DISTRIBUTION OF CONSTANT FLAP BENDING MOMENT
LEONE-MYKLESTAD METHOD
FORWARD ROTOR - 10 LB. WEIGHT CABLED 40% R
CONSTANT FLAP BENDING MOMENT x 10^-3 IN-LBS
16
12
8
4
0
-4
-8
-12
0
10
20
30
40
50
60
70
80
90
100
PERCENT ROTOR TIP RADIUS

FIGURE 117
HIGH PERFORMANCE HELICOPTER METAL ROTOR BLADE

RADIAL DISTRIBUTION OF AVERAGE FLAP VIBRATORY BENDING MOMENT
LEONE-MYKLESTAD METHOD
FORWARD ROTOR - 10 LB. WEIGHT CABLED 40% R



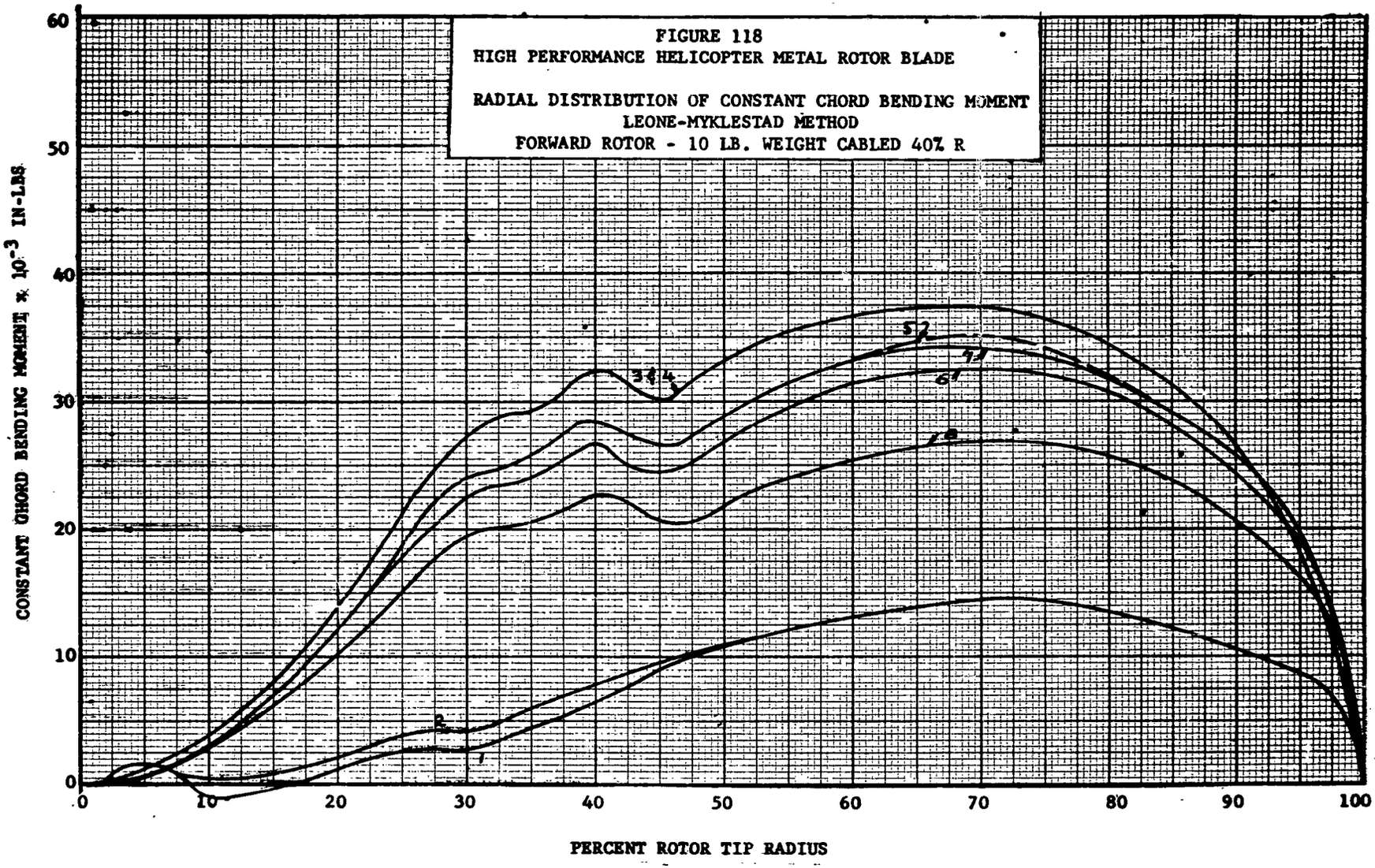
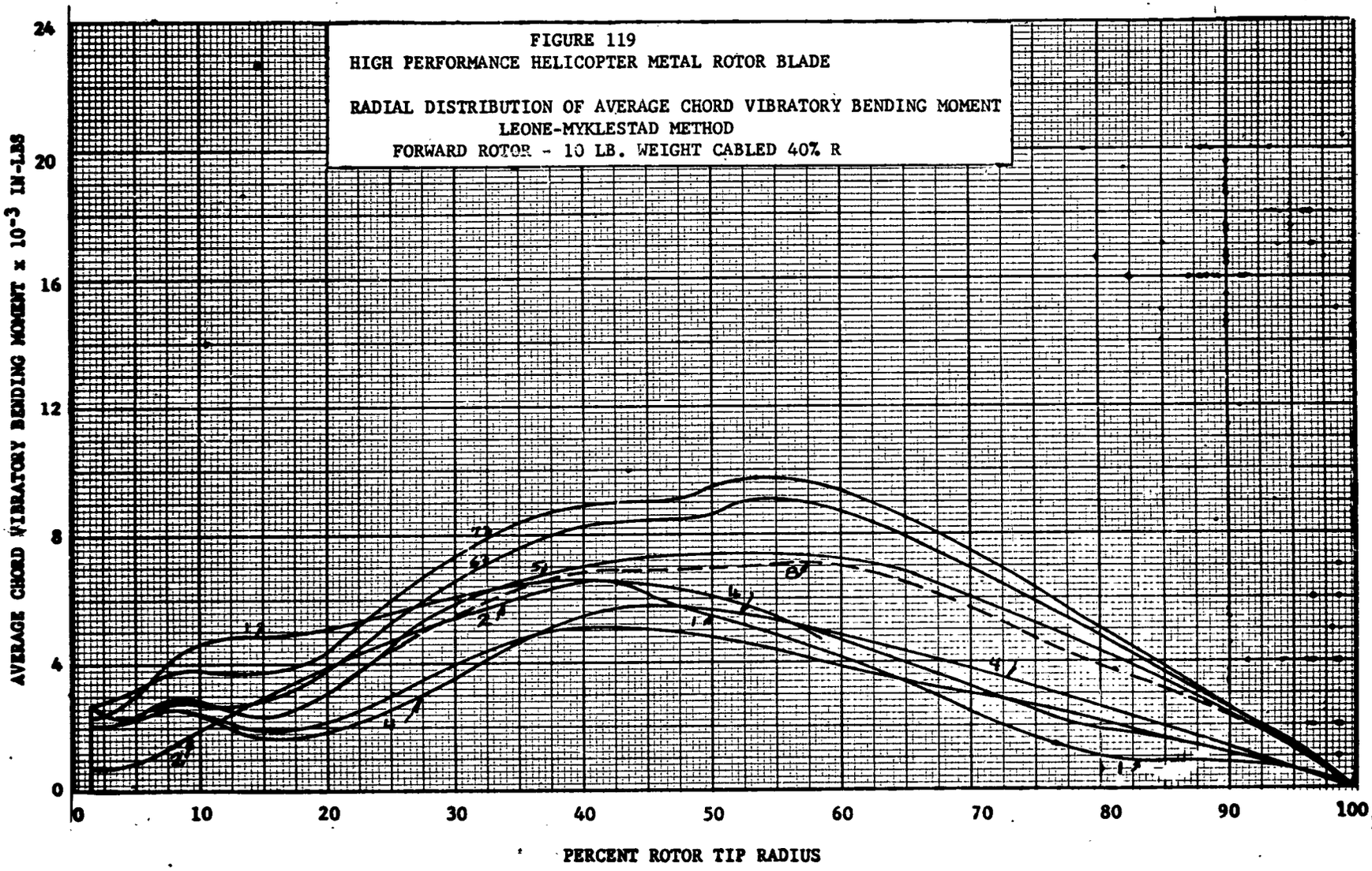
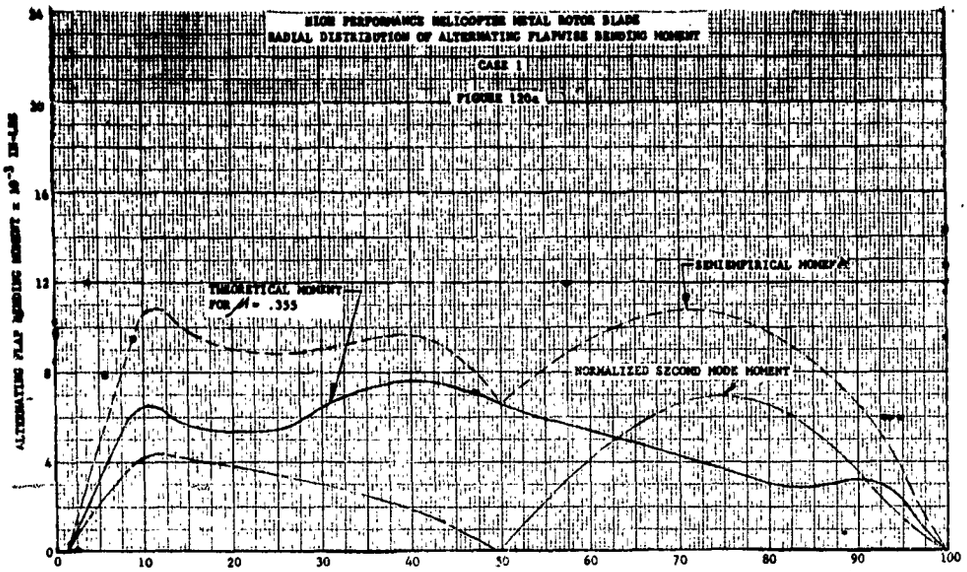
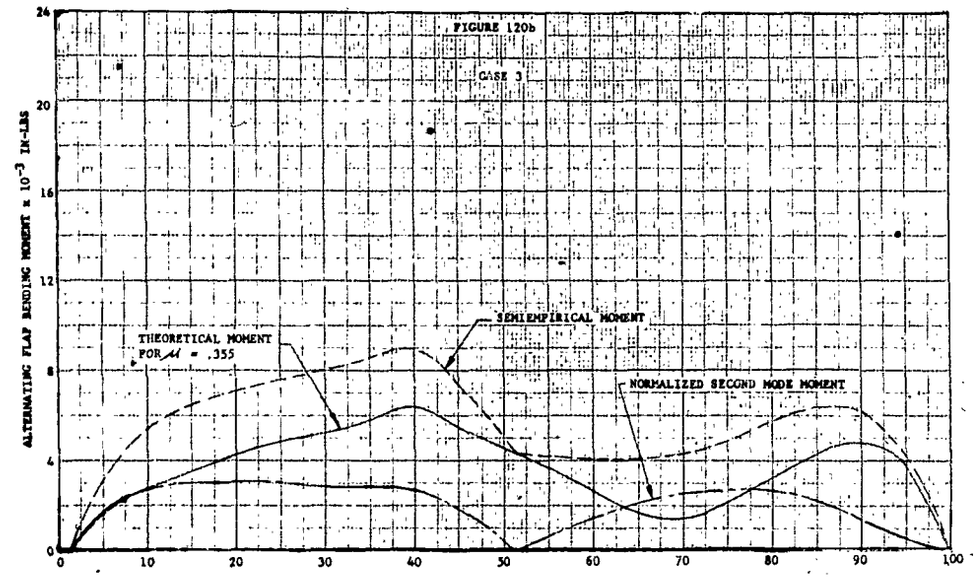

FIGURE 118
HIGH PERFORMANCE HELICOPTER METAL ROTOR BLADE
RADIAL DISTRIBUTION OF CONSTANT CHORD BENDING MOMENT
LEONE-MYKLESTAD METHOD
FORWARD ROTOR - 10 LB. WEIGHT CABLED 40% R
CONSTANT CHORD BENDING MOMENT x 10^-3 IN-LBS
PERCENT ROTOR TIP RADIUS
0
10
20
30
40
50
60
70
80
90
100
5-2
4-1
6-1
1-0
3-4
2
1

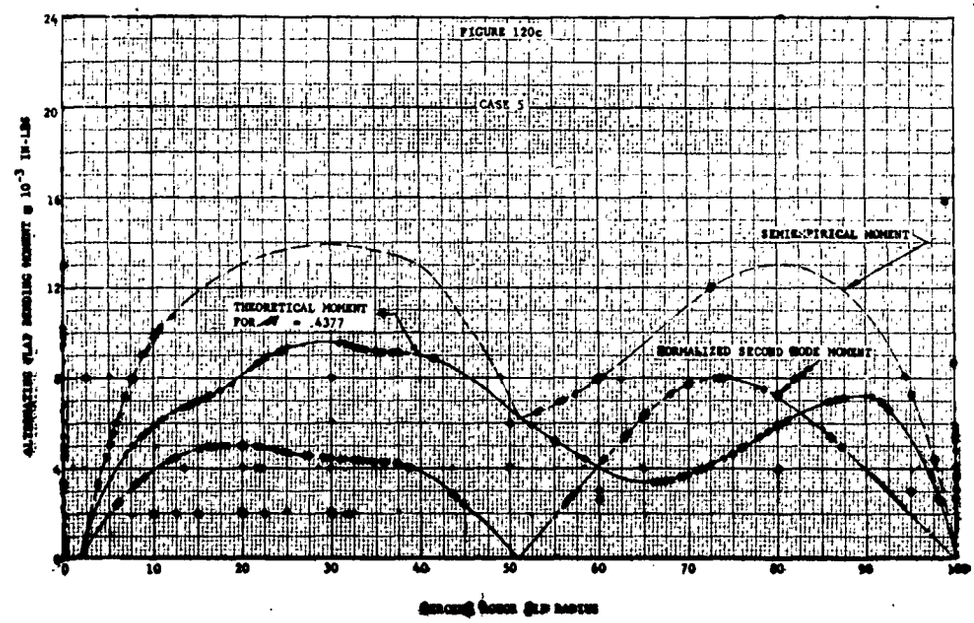
FIGURE 119
HIGH PERFORMANCE HELICOPTER METAL ROTOR BLADE

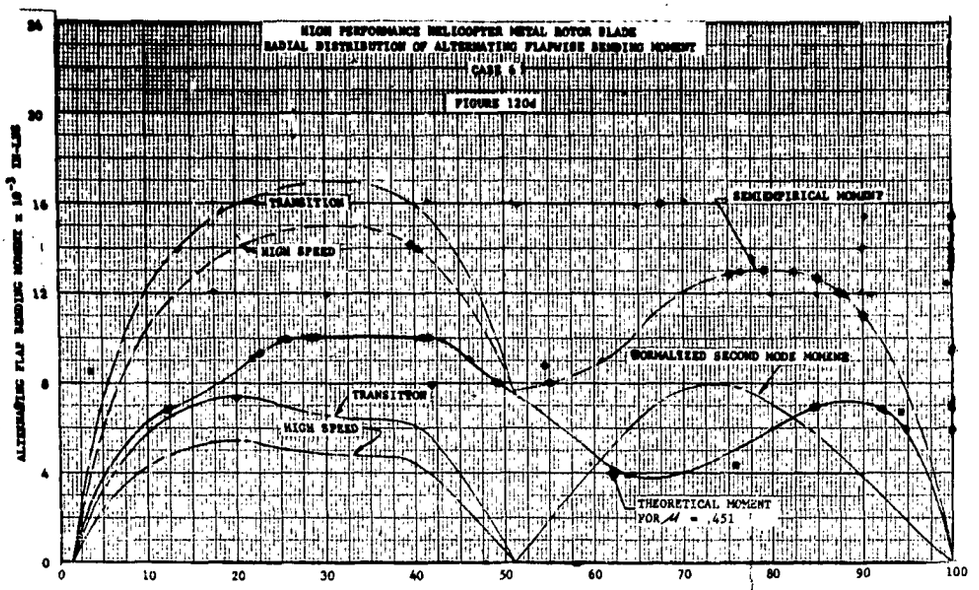
RADIAL DISTRIBUTION OF AVERAGE CHORD VIBRATORY BENDING MOMENT
LEONE-MYKLESTAD METHOD
FORWARD ROTOR - 10 LB. WEIGHT CABLED 40% R

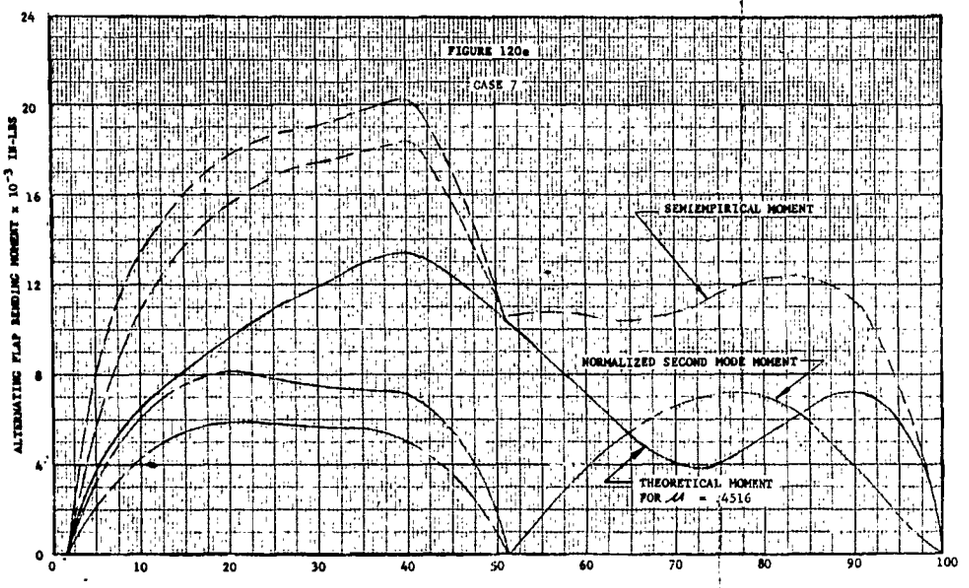


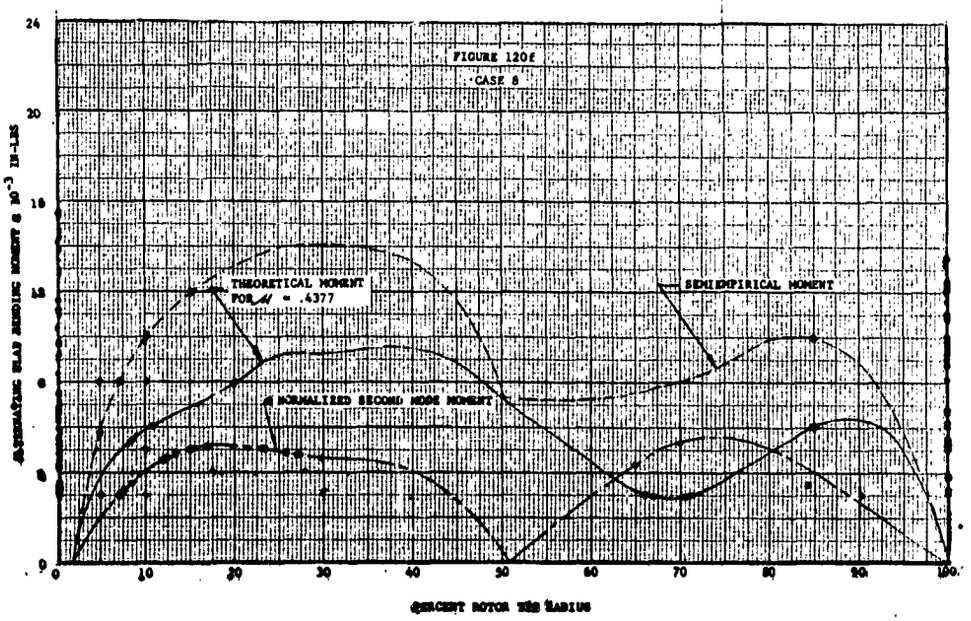

HIGH PERFORMANCE HELICOPTER METAL ROTOR BLADE
RADIAL DISTRIBUTION OF ALTERNATING FLAPWISE BENDING MOMENT
CASE 1
FIGURE 120a
ALTERNATING FLAP BENDING MOMENT x 10^-3 IN-LBS
THEORETICAL MOMENT FOR μ = .355
SEMIEMPIRICAL MOMENT
NORMALIZED SECOND MODE MOMENT
0
4
8
12
16
20
24
0
10
20
30
40
50
60
70
80
90
100


FIGURE 120b
CASE 3
ALTERNATING FLAP BENDING MOMENT x 10^-3 IN-LBS
THEORETICAL MOMENT FOR μ = .355
SEMIEMPIRICAL MOMENT
NORMALIZED SECOND MODE MOMENT
0
4
8
12
16
20
24
0
10
20
30
40
50
60
70
80
90
100


FIGURE 120c
CASE 5
ALTERNATING FLAP BENDING MOMENT x 10^-3 IN-LBS
THEORETICAL MOMENT FOR μ = .4377
SEMIEMPIRICAL MOMENT
NORMALIZED SECOND MODE MOMENT
0
4
8
12
16
20
24
0
10
20
30
40
50
60
70
80
90
100


HIGH PERFORMANCE HELICOPTER METAL ROTOR BLADE
RADIAL DISTRIBUTION OF ALTERNATING FLAPWISE BENDING MOMENT
CASE 6
FIGURE 120d
ALTERNATING FLAP BENDING MOMENT x 10⁻³ IN-LBS
TRANSITION
HIGH SPEED
SEMIEMPIRICAL MOMENT
NORMALIZED SECOND MODE MOMENT
TRANSITION
HIGH SPEED
THEORETICAL MOMENT FOR μ = .451
0
4
8
12
16
20
24
0
10
20
30
40
50
60
70
80
90
100


FIGURE 120e
CASE 7
ALTERNATING FLAP BENDING MOMENT x 10⁻³ IN-LBS
SEMIEMPIRICAL MOMENT
NORMALIZED SECOND MODE MOMENT
THEORETICAL MOMENT FOR μ = .4516
0
4
8
12
16
20
24
0
10
20
30
40
50
60
70
80
90
100


FIGURE 120f
CASE 8
ALTERNATING FLAP BENDING MOMENT x 10⁻³ IN-LBS
THEORETICAL MOMENT FOR μ = .4377
SEMIEMPIRICAL MOMENT
NORMALIZED SECOND MODE MOMENT
0
4
8
12
16
20
24
0
10
20
30
40
50
60
70
80
90
100
PERCENT ROTOR TIP RADIUS

ROTOR HUB

DISCUSSION

The choice of configuration was evolved from the following affecting factors and sequence of events.

1. The increased total blade pitch required for the high performance helicopter caused interference in the basic Boeing-Vertol 107-II hub and control linkage due to lead-lag and flap effects.

2. An increase in pitch arm radius to alleviate interferences resulted in increase of total control motions of swashplate.

3. Any increase in existing Boeing-Vertol 107-II total control motions of swashplate was impractical for this research vehicle as it required new rotor shafts and a raising of the rotor plane.

4. To effect the sizeable increase in control required, it was necessary to change the control ratios by shortening the pitch arm radius. This was only possible by eliminating the lead-lag effect on pitch.

Consideration of other configurations on a size comparison basis showed that for the lowest inherent drag, the lightest weight rotor and the smallest in size would be the YHC-1B "Chinook" style (also HUP series) rotor with certain modifications.

A new hub utilizing Boeing-Vertol 107-II bearings required larger root attachment for the pitch shaft to the horizontal pin because of larger chord moments resulting from the vertical pin being further outboard. The increase in moment required an increase in the horizontal pin joint strength. This was obtained by increasing the distance between bearings and resulting in a slight increase in the horizontal pin location.

The increased centrifugal force for the High Performance 107-II resulted in reduced horizontal pin bearing life (Boeing-Vertol 107-II bearings). Since bearing life can be greatly affected by pin slopes, the pin stiffness was increased to duplicate Boeing-Vertol 107-II slopes. Calculated bearing lives are reduced to 985 hours requiring no development program as the expected initial lives are considered reasonable for the High Performance 107-II.

The location of the vertical pin, while being further outboard than Model II vertical pin, is none the less closer in than normal for this configuration because of the use of new type tension-torsion system.

Recent studies at Vertol utilizing a "wire-ply" pack consisting of 550,000 UTS steel wire wound continuously around specially designed end fittings has indicated that considerably shorter packs can be designed to operate satisfactorily under the same oscillatory conditions as the strap pack on the Model II. Usually, the tension-torsion system and its required twist limitations dictate its length and, thereby, the location of the vertical pin. As this is no longer true, for a wire-ply tension-torsion system, the governing factor for vertical pin location becomes critical as a function of the pitch bearing (also from Boeing-Vertol 107-II) spacing for the flap moments.

The use of Teflon bearings in the vertical pin also contributed favorably to the vertical pin location and to the reduction of the vertical pin joint height, thereby reducing drag. The projected use of Teflon in the horizontal pin and pitch bearings does not appear practical at this time.

The integral pitch arm and pitch housing with a much reduced frontal area has resulted in lower drag.

The blade socket with its Teflon vertical pin bearings and conventional Boeing-Vertol blade attachment is compatible with possible folding requirements.

A YHC-1B lag damper (with modified attaching ends) was used in preference to either a completely new design or the Model II damper which was not adequate from a ground instability viewpoint. This unit has been designed to handle higher loads than encountered on the research vehicle.

Conventional methods of stress analysis were used and fatigue stresses in critical areas were limited to allowables used in similar applications on the Boeing-Vertol 107 Model II.

ANALYSIS

The following pages contain the rotor hub loads derivation and analysis. Because of increased centrifugal force loads (higher than the Boeing-Vertol 107-II) and because of new hub components, a complete analysis is required. Fatigue loadings are more critical than ultimate loadings, and for this reason only a fatigue analysis is presented. Only the results of the analysis are presented, i.e., loads and stresses are summarized.

Analysis methods are conventional and allowables are consistent with all other Boeing-Vertol designs. Stress levels for this design shown on SK 10307 are low enough so that an unlimited life can be expected for unaccelerated high speed level flight conditions.

Appendix III contains a summary of stresses and "life" on critical components.

1. Loads
2. Pitch housing analysis summary
3. Pitch shaft analysis summary
4. Tie rod analysis - "wire-ply" strap
5. Rotary wing socket analysis summary
6. Vertical pin analysis summary
7. Horizontal pin bearing lives and slopes

(a) Loads

The following data was obtained from Aerodynamics:

TABLE XXVIII

FLIGHT CONDITIONS FOR ROTOR HUB ANALYSIS

Flight Conditions	V Kts.	V_t ft/sec.	RPM	Fwd Rotor HP	Aft Rotor HP
V_{max}	172	680	260	1,390	940
Cruise	141	640	244	840	725
Max. Power Climb	80	660	252	1,360	970
Transition	30	650	248	1,100	900
Hover O.G.E.	0	650	248	1,300	1,100
Autorotation	65	650 (est)	248	0	0

G.W. = 19,400 lbs. R = 25' C = 23" $\theta_c = 14^\circ$

Airfoil Section, NACA 0009.5

V_t = tip speed

$$RPM = \text{tip speed} \frac{\times 60}{25' \times 2\pi}$$

$$= 0.382 \times \text{tip speed}$$

TABLE XXIX

CENTRIFUGAL FORCE LOADS

Flight Condition	RPM	$(CF)_{VP}$ Fwd(lb)	$(CF)_{VP}$ Aft(lb)	$(CF)_{HP}$ Fwd(lb)	$(CF)_{HP}$ Aft(lb)
V_{max}	260	49,000	44,600	52,450	46,500
Cruise	244	43,200	39,280	46,040	40,920
Max. Power Climb	252	46,000	41,900	49,200	43,700
Transition	248	44,550	40,500	47,600	42,300
Hover O.G.E.	248	44,550	40,500	47,600	42,300
Autorotation	248	44,550	40,500	47,600	42,300

Aft Blade:

@ 262 RPM $(CF)_{VP}$ = 45,300 lb.

$(CF)_{HP}$ = 47,200 lb.

$\left(\frac{260}{262}\right)^2 = 0.985$

$\left(\frac{252}{262}\right)^2 = 0.925$

Forward Blade:

$(CF)_{VP}$ = 49,820 lb.

$(CF)_{HP}$ = 53,100 lb.

$\left(\frac{248}{262}\right)^2 = 0.895$

$\left(\frac{244}{262}\right)^2 = 0.867$

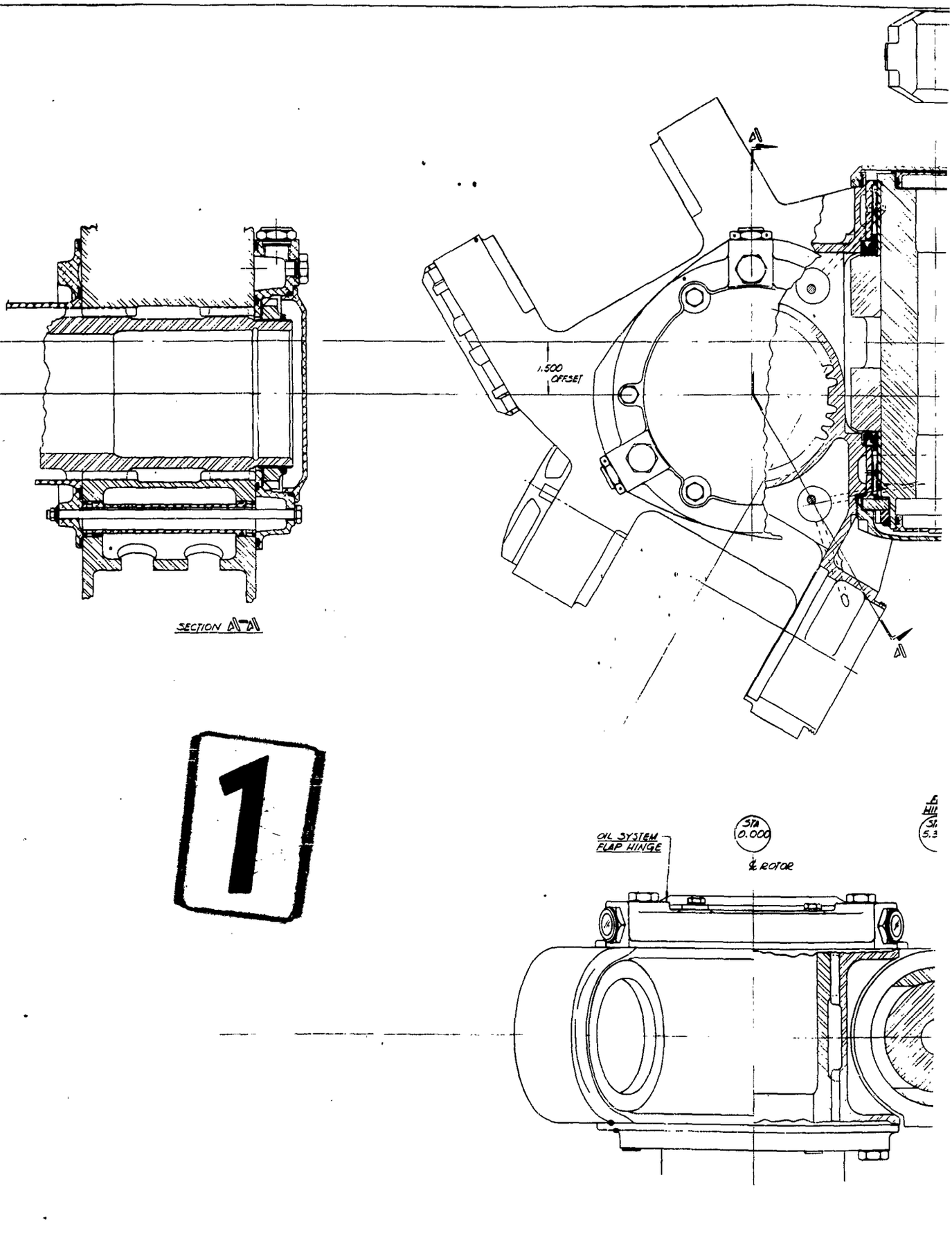
TABLE XXX

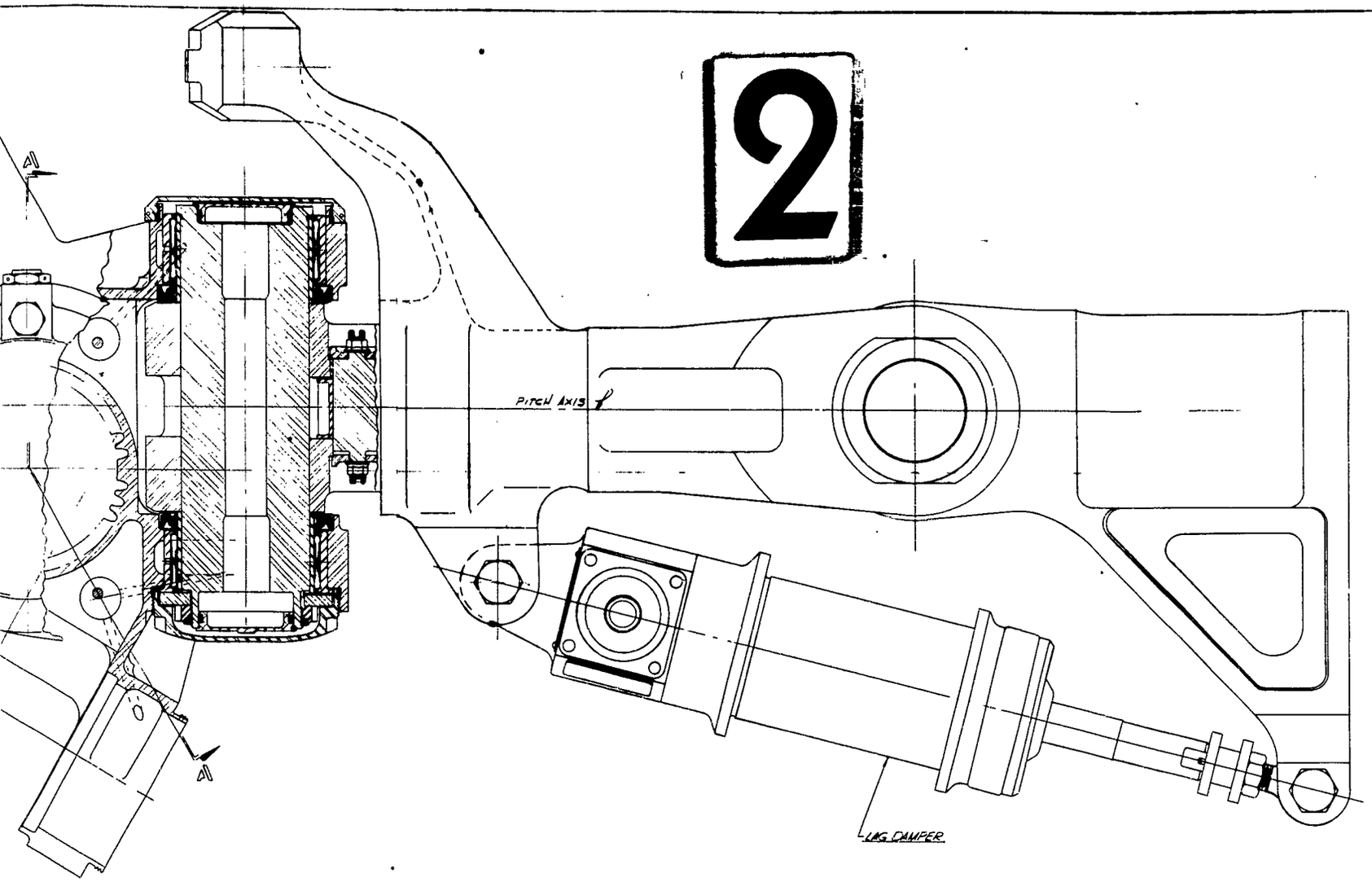
IN PLANE HUB LOADS

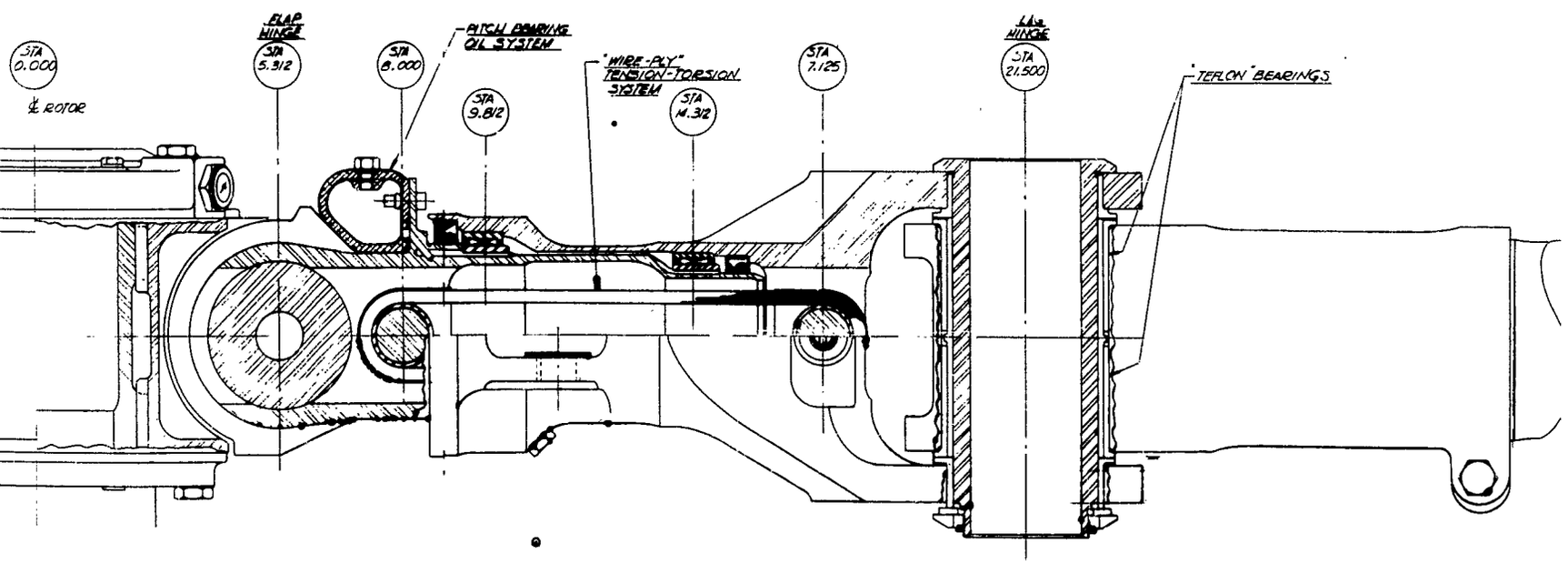
Flight Condition	RPM	F_b* damper force	Torque/Blade	
			Fwd Rotor	Aft Rotor
V_{max}	260	±1800 lb.	112,200	75,900
Cruise	244	±1770 lb.	72,300	62,400
Max. Power Climb	252	±1790 lb.	113,300	80,900
Transition	248	±1780 lb.	93,100	76,200
Hover O.G.E.	248	±1780 lb.	110,000	93,000
Autorotation	248	±1780 lb.	0	0

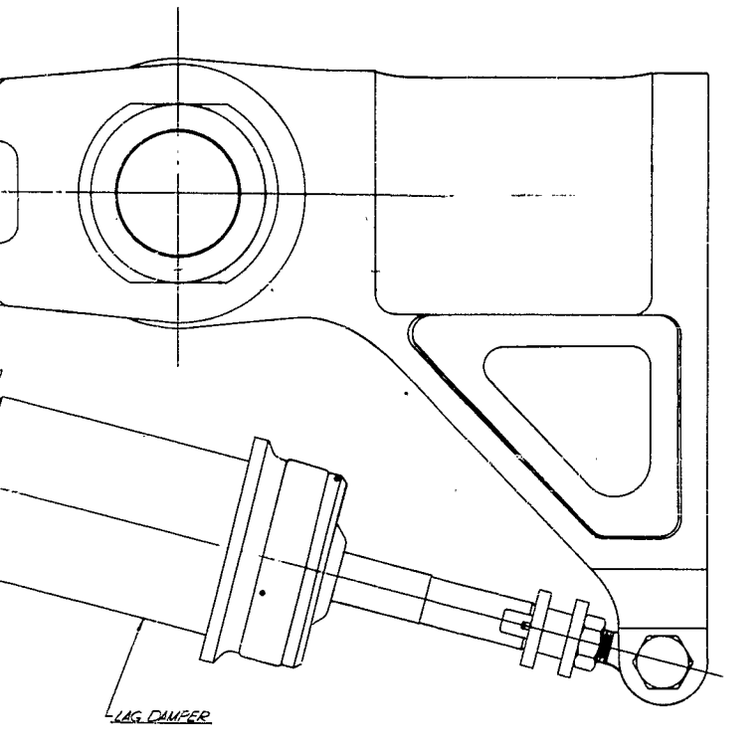
$$Q/b = 21{,}000 \times \frac{HP}{RPM}$$

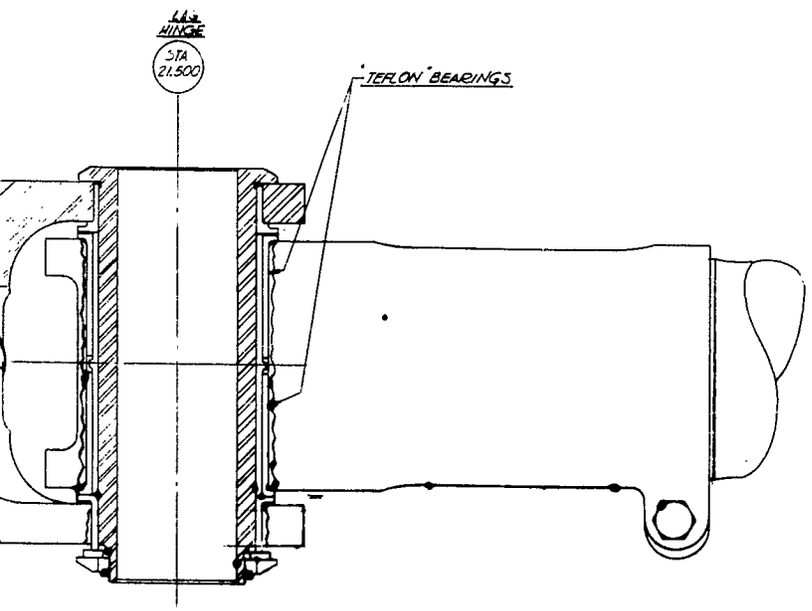
* Based on YHC-1B Damper Characteristics


1.500
OFFSET
SECTION
OIL SYSTEM
FLAP HINGE
STA
0.000
℄ ROTOR


2
PITCH AXIS
LAG DAMPER


STA 0.000
℄ ROTOR
FLAP HINGE
STA 5.312
STA 8.000
PITCH BEARING OIL SYSTEM
STA 9.812
"WIRE-PLY" TENSION-TORSION SYSTEM
STA 14.312
STA 17.125
LAG HINGE
STA 21.500
TEFLON BEARINGS





3

DRAWN BY	CHECKED BY	STRESS	PROJ ENGR	ENGR	
				P.A.A.	
UNLESS OTHERWISE SPECIFIED			HEAT TREAT		ROTOR HUB
DIMENSIONS ARE IN INCHES			MATL	SPEC	
TOLERANCES ON			STEEL	MIL-H-6875	
DECIMALS	ANGLES		ALUM	MIL-H-6088	
			MISC CAST	MIL-H-8851	
					SCALE FULL
					CODE IDENT NO 77278
					SK0307

ROTOR CONTROLS

Discussion

Essentially, the Boeing-Vertol Model II rotor controls are used with some modification for the increased control loads. The increased total control motions were acceptable to the available space by the choice of rotor system configuration permitting a change in control ratios.

A method of estimating pitch link loads for the effect of μ and C_T/σ has been developed at Boeing-Vertol during the past few years. The approach is semiempirical but has resulted in a remarkable agreement of data. This approach has been utilized as shown on the following pages to evaluate pitch link loads.

The extrapolation required to obtain loads for the High Performance 107-II is not too great. Therefore, we are confident that the loads calculated are of the proper order of magnitude.

It was necessary to consider one other factor for estimation of loads. The increase in blade chord, utilizing the spar from the Boeing-Vertol Model II, resulted in a shift of the blade pitch axis from 18.4% chord to 13% chord. A study of measured data on different blade designs with different pitch axis locations indicated that the effect on vibratory pitching moments is small but steady pitching moments are considerably affected. The results of this study are shown on the following pages.

Recent flight tests performed on the Boeing-Vertol Model II with a control system with an increased stiffness has definitely proven the importance of a stiff control system in reducing helicopter vibration level. For this reason the control system for the High Performance 107-II has been designed for control stiffness requirements.

The Boeing-Vertol Model II swashplate bearing internal design with new attaching flanges is used. The increase in control loads would result in a reduction of calculated bearing life from 1425 hours (Model II) to 900 hours which is considered acceptable.

Another feature which has been continued from the Model II is the use of Teflon bearings in the control system with their "no maintenance requirements."

The control system, where critical for an increase in loads of 16% over the Boeing-Vertol 107-II, has been improved upon with minor modification to existing components. A modified drawing of these components is shown on SK 10242.

Ultimate analysis of 107-II rotor control components is given in Vertol Report 107-S-207-2-3. All items with margins of safety less than .6 have been improved upon accordingly.

It may be concluded that the control components shown on drawing, SK 10242, are capable of withstanding the imposed loads due to unaccelerated level flight at 174 knots.

Pitch Axis Effect on Pitching Moments

A review of pitching moment data on helicopter Models H-21, HUP-2 wood BL, HUP-2 metal, HUP-4, H-16, V-107, YHC-1A has indicated the following:

1. A semiempirical approach for determination of pitching moments on blades such as described in Vertol Report RDM 019 can be used for predicting or estimating vibratory pitching moments on blades such as those mentioned above with a few exceptions.

2. Given the above method, the characteristics could have been predicted for a range of $\mu = 0$ to $\mu = .36$ and $C_T/\sigma = .070$ to $C_T/\sigma = .124$.

3. The exceptions to the rule are:

   a. HUP-2 Prewitt Metal Blade - ϵ (dist. from pitch axis to A.C.) is smaller than other blades but if the same were used as for others, the data would agree.

   b. H-16 Metal Blade - ϵ is very small, A.C. is almost on P.A. The effect is in the right direction but not as effective as indicated. A slight shift in est. A.C. would make data agree with the rest of the blades.

4. There does not appear to be an effect of hub configuration in pitching moments, i.e., HUP data falls in line with all the other data.

High Performance Helicopter Control Loads

High Performance 107 loads will be compared to Boeing-Vertol 107 Model II loads because of its close similarity.

Pitch link loads may be estimated using a semiempirical method such as described below.

The family of curves in Figure 121 represents a nondimensionalized pitching moment coefficient plotted vs μ for different values of C_T/σ

$$\frac{C_T}{\sigma} = \frac{T_o}{b \rho C_o R (R\Omega)^2}$$

$$\mu = \frac{1.689 \times V}{R\Omega}$$

$$\lambda_v = \frac{(M_{\theta_v} \times 10^3}{(\tfrac{1}{2} \rho a_o C_o^2 R)(R\Omega)^2}$$

T_o = Thrust on rotor (lb)
b = Number of blades/rotor
ρ = .002242 for 2,000 ft
a_o = 5.75 (lift curve slope)
C_o = Blade chord (ft)
R = Blade radius (ft)
$R\Omega$ = Tip speed (ft/sec)
V = Forward velocity
ϵ = A.C. to pitch axis (% chord)
M_{θ_v} = Pitching Mom. (ft lb)

107-II

$$\frac{C_T}{\sigma} = \frac{10,300}{3 \times .002242 \times 1.5 \times 25 \times 670^2} = .091 \text{ (based on 162 knots)}$$

$$= \frac{1.689 \times 162}{670} = .408$$

$$= 55.6 \text{ from curve} = \frac{(M_{\theta_v}) \times 10^3}{.067 \times \frac{1}{2} \times .002242 \times 5.75 \times 1.5^2 \times 25 \times 670^2}$$

Therefore M_{θ_v} = 605 ft. lb. or 7280 in. lb.

Pitch Link Load = $\frac{7280}{8.5} = \pm 855$ lb.

GW = 19,400 T_o = .55 x 19,400 = 10,600 lb. MFCG HSLF

R = 25' C_o = 23" or 1.91 ft θ_o - 14° NACA 0009.5

V = 172 knots = 260 RPM or 27.3 rad/sec

V_t = 25 x 27.3 = 680 ft/sec

$$C_T/\sigma = \frac{10,600}{3 \times .002242 \times 1.91 \times 25 \times (680)^2} = .071$$

$$\mu = \frac{1.69 \times 172}{680} = .426$$

$$\lambda_v = 37.2 \text{ (from curve)} = \frac{M_{\theta_v} \times 10^3}{.067 \times \frac{1}{2} \times .002242 \times 5.75 \times (1.91)^2 \times 25 \times (680)^2}$$

M_{θ_v} = 680 ft. lb. or 8160 in. lb.

Pitch Link Load = $\frac{8160}{8.18} = \pm 998$ lb.

Ratio $\frac{\text{HPHD Loads}}{\text{107-II Loads}} = \frac{\pm 998}{\pm 855} = 1.16$

Steady Loads

Model II = 250 lb. pitch link load

High Performance 107 = 798 lb. (Higher than 107-II because of different hub configuration)

Total Pitch Link Load 107-II = 250 ± 885 = 1105 lb.

HPHD = 798 ± 998 = 1796 lb.

Since maneuver loads may be related to total load

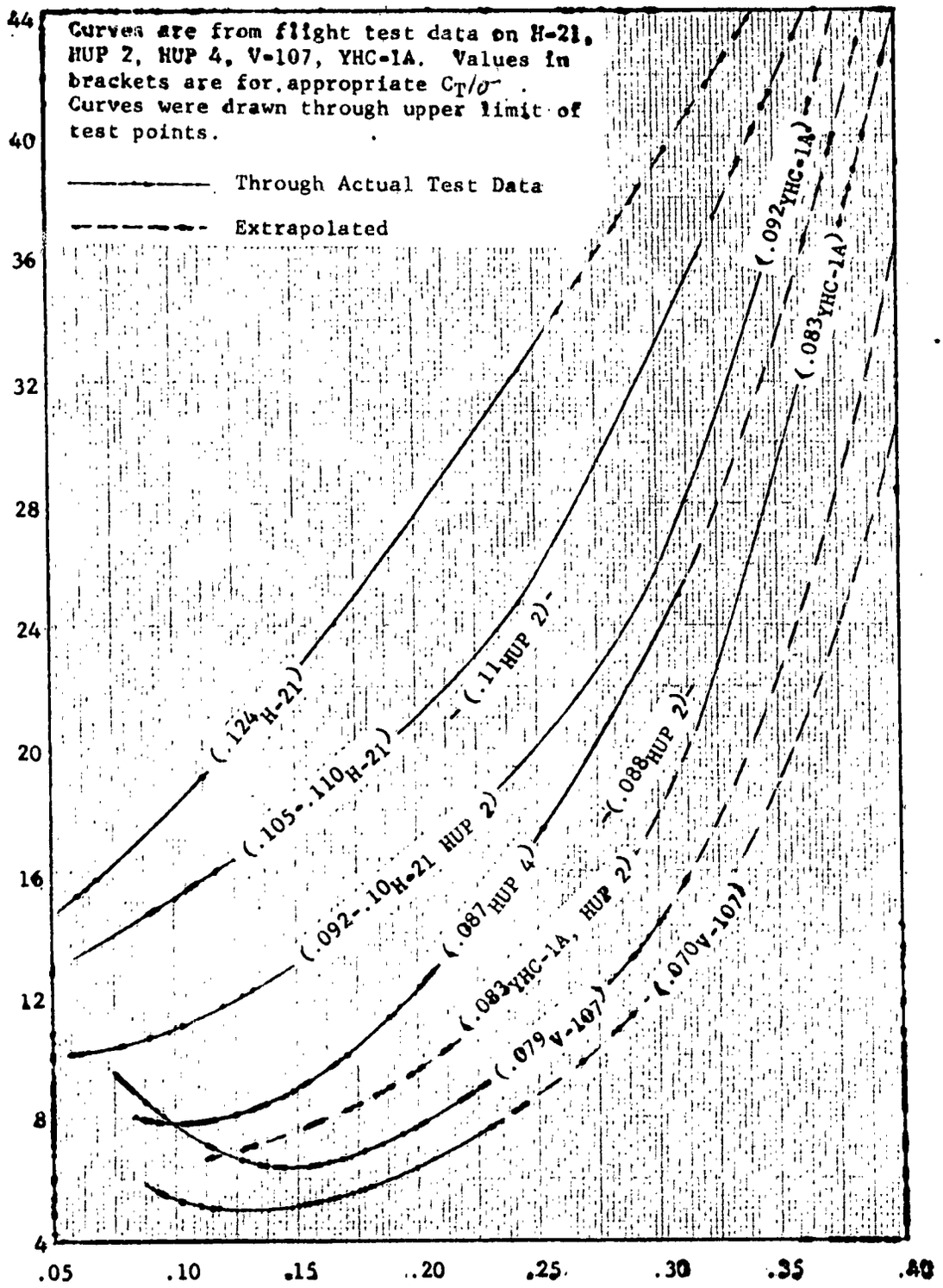
$$\text{Ratio } \frac{\text{ULT HPHD Loads}}{\text{ULT 107-II Loads}} = \frac{1796}{1105} = 1.6$$

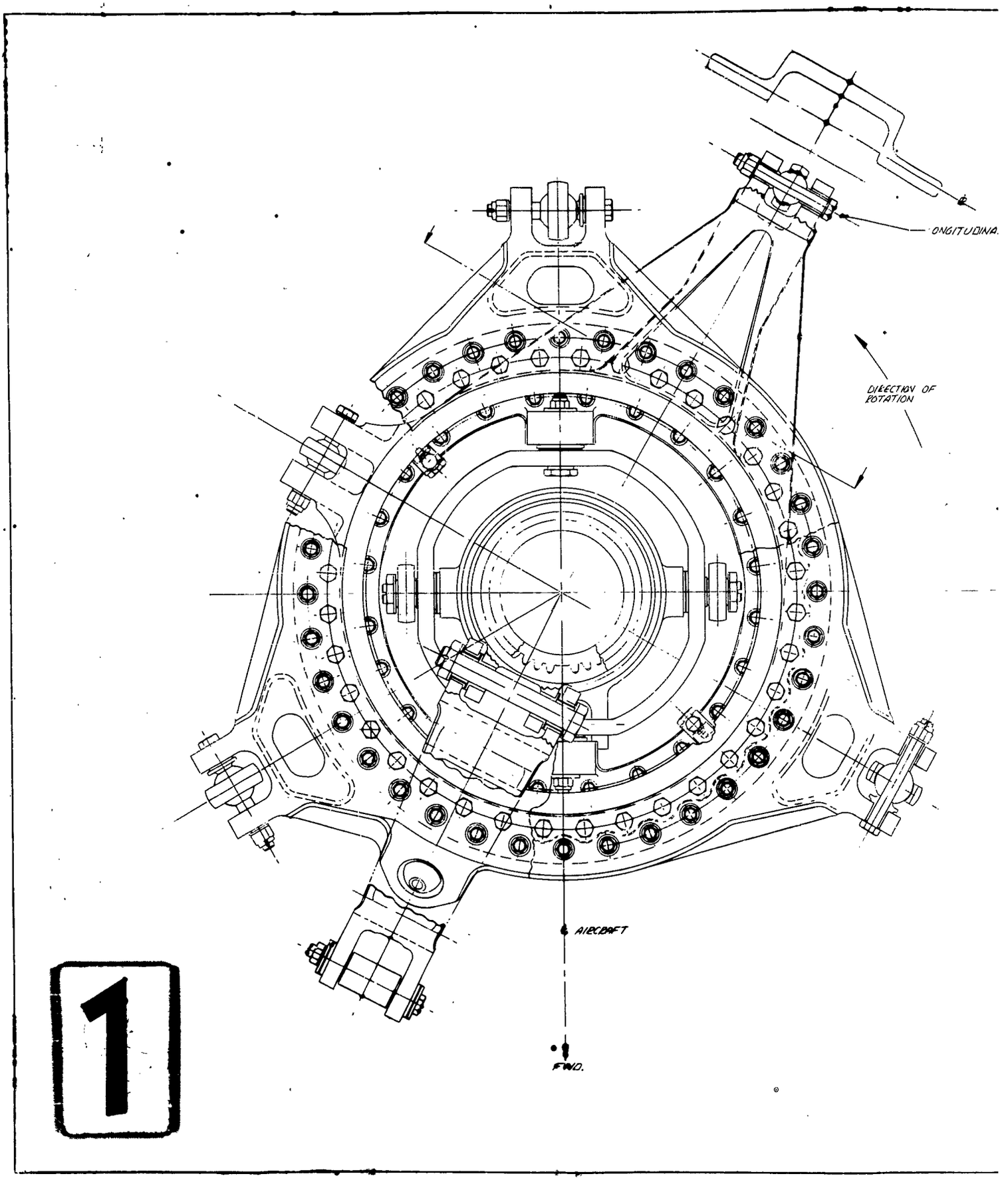
FIGURE 121

NON-DIMENSIONAL PITCHING MOMENT COEFFICIENT

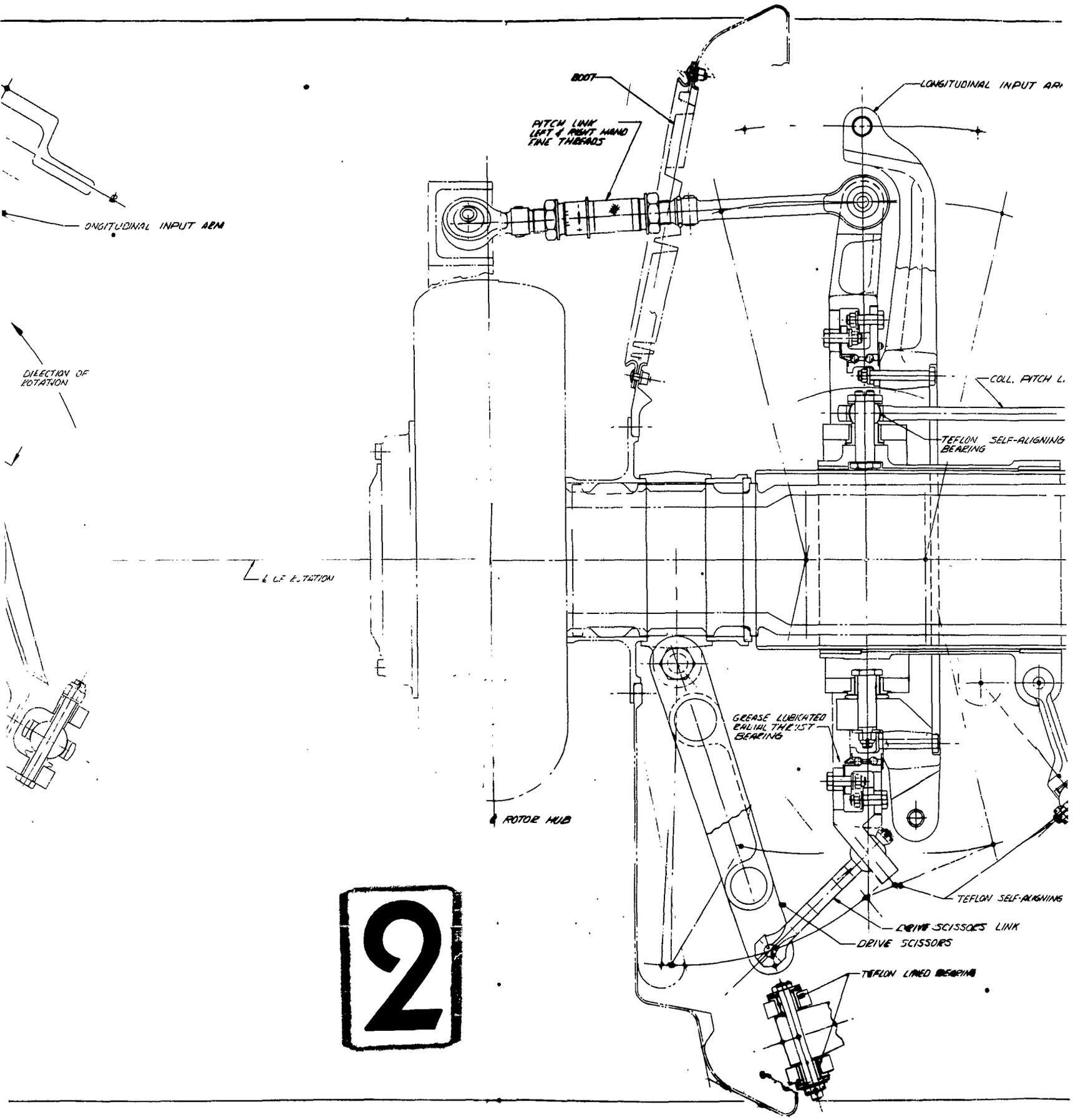
VS

ROTOR ADVANCE RATIO

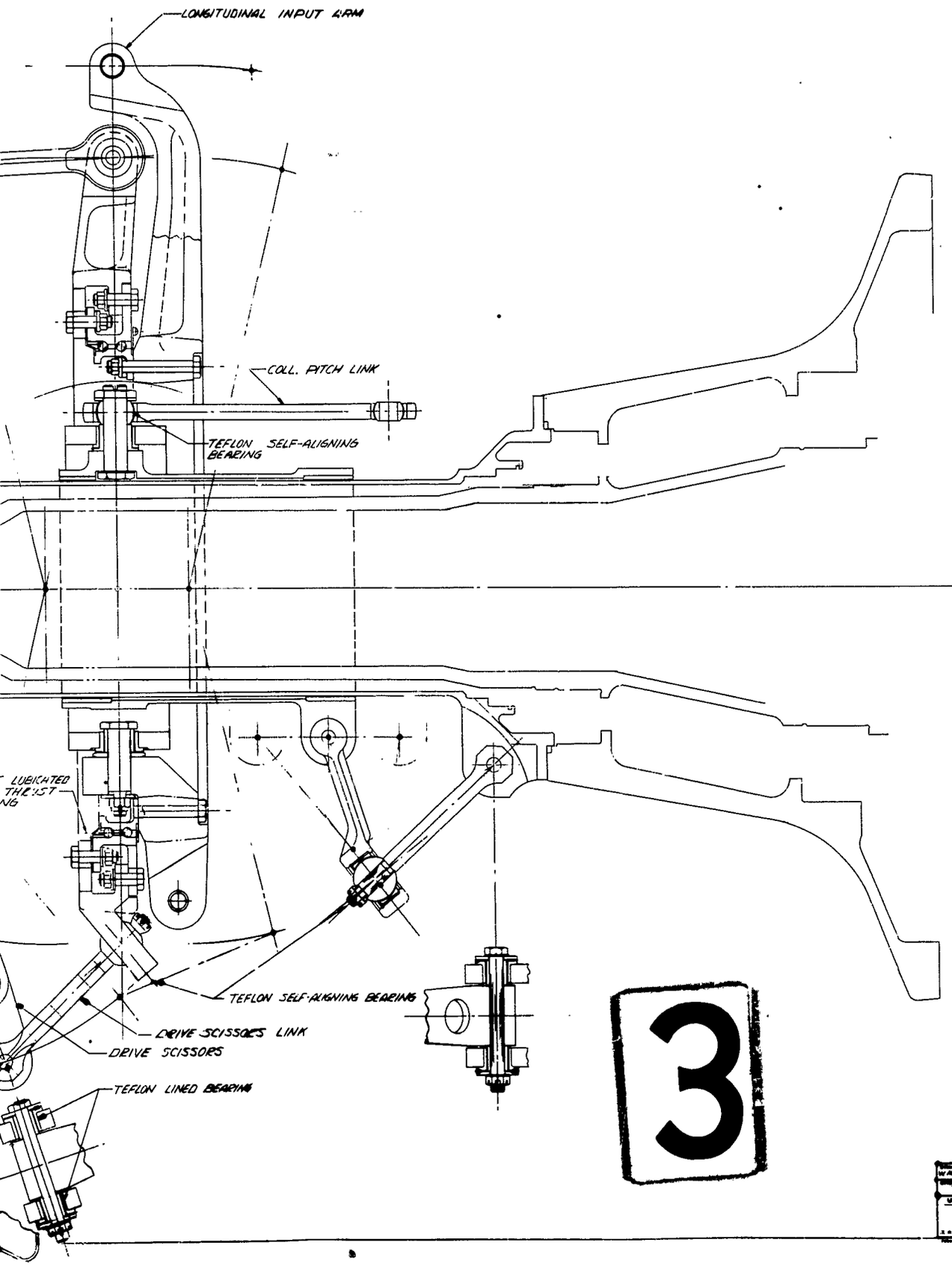




1


BOOT
PITCH LINK LEFT & RIGHT HAND FINE THREADS
LONGITUDINAL INPUT ARM
LONGITUDINAL INPUT ARM
DIRECTION OF ROTATION
COLL. PITCH L
TEFLON SELF-ALIGNING BEARING
GREASE LUBICATED RADIAL THRUST BEARING
ROTOR HUB
TEFLON SELF-ALIGNING
DRIVE SCISSORS LINK
DRIVE SCISSORS
TEFLON LINED BEARING

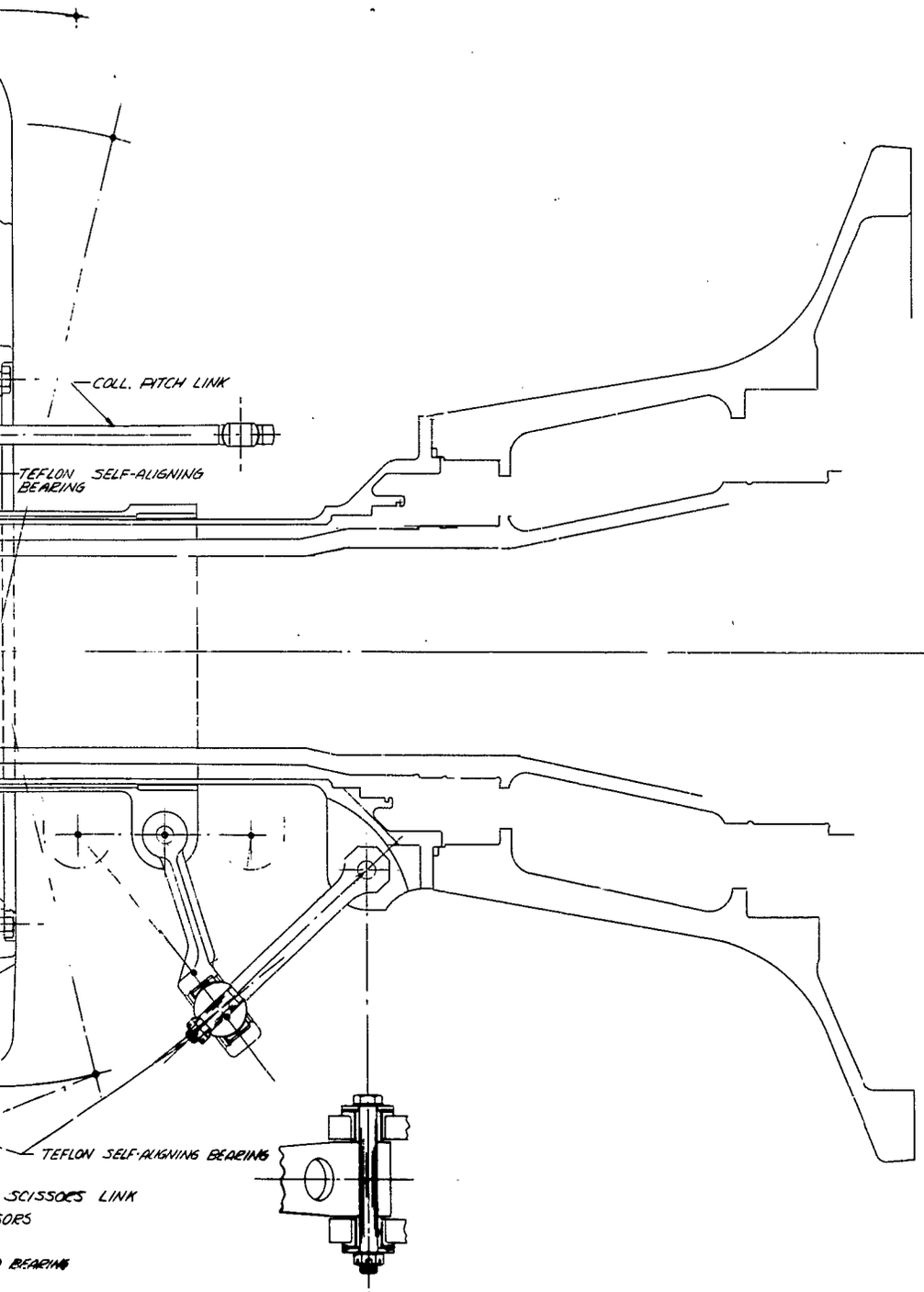
2



3

ROTOR CONTROLS

ONGITUDINAL INPUT ARM



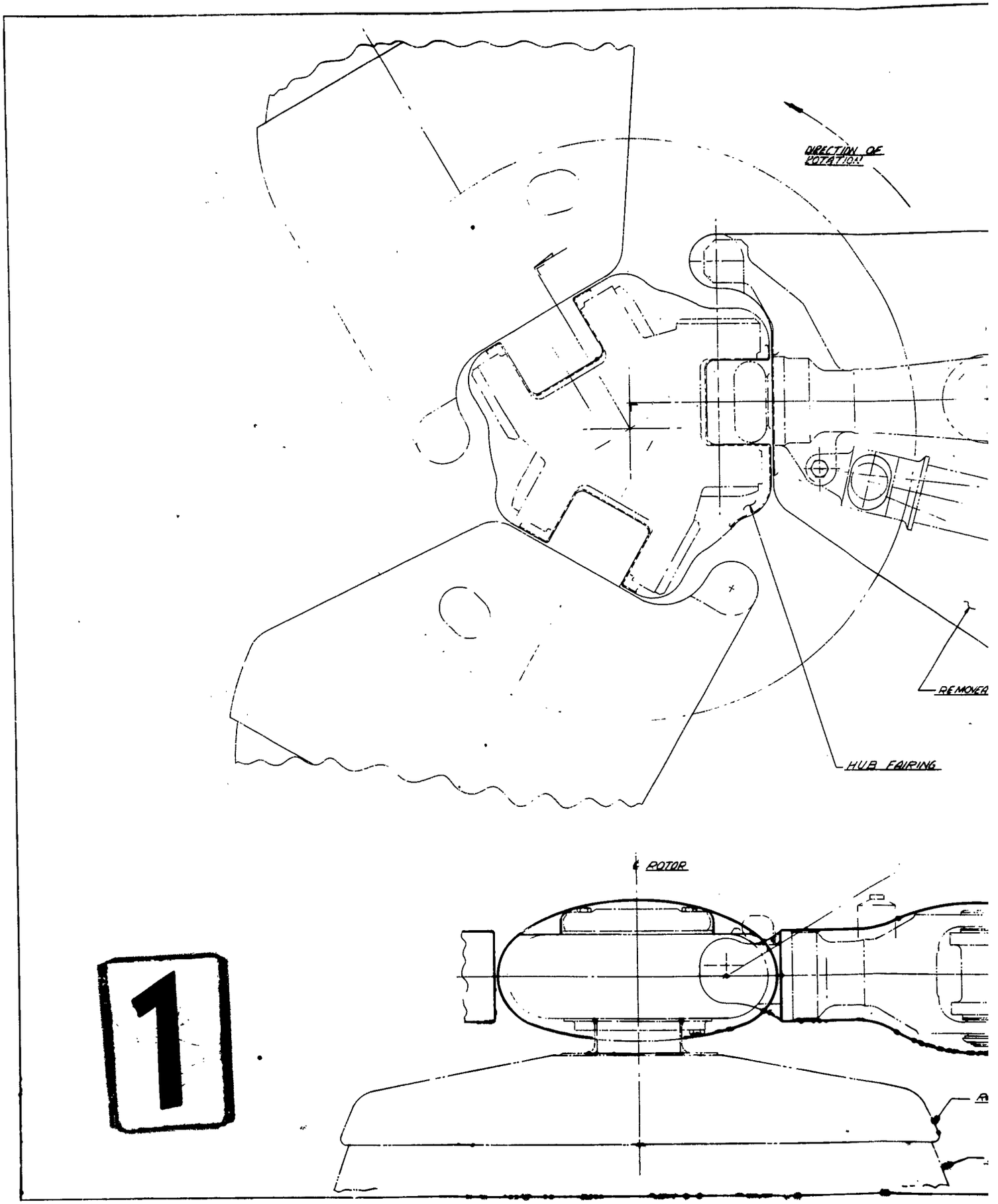
4

ROTOR CONTROLS

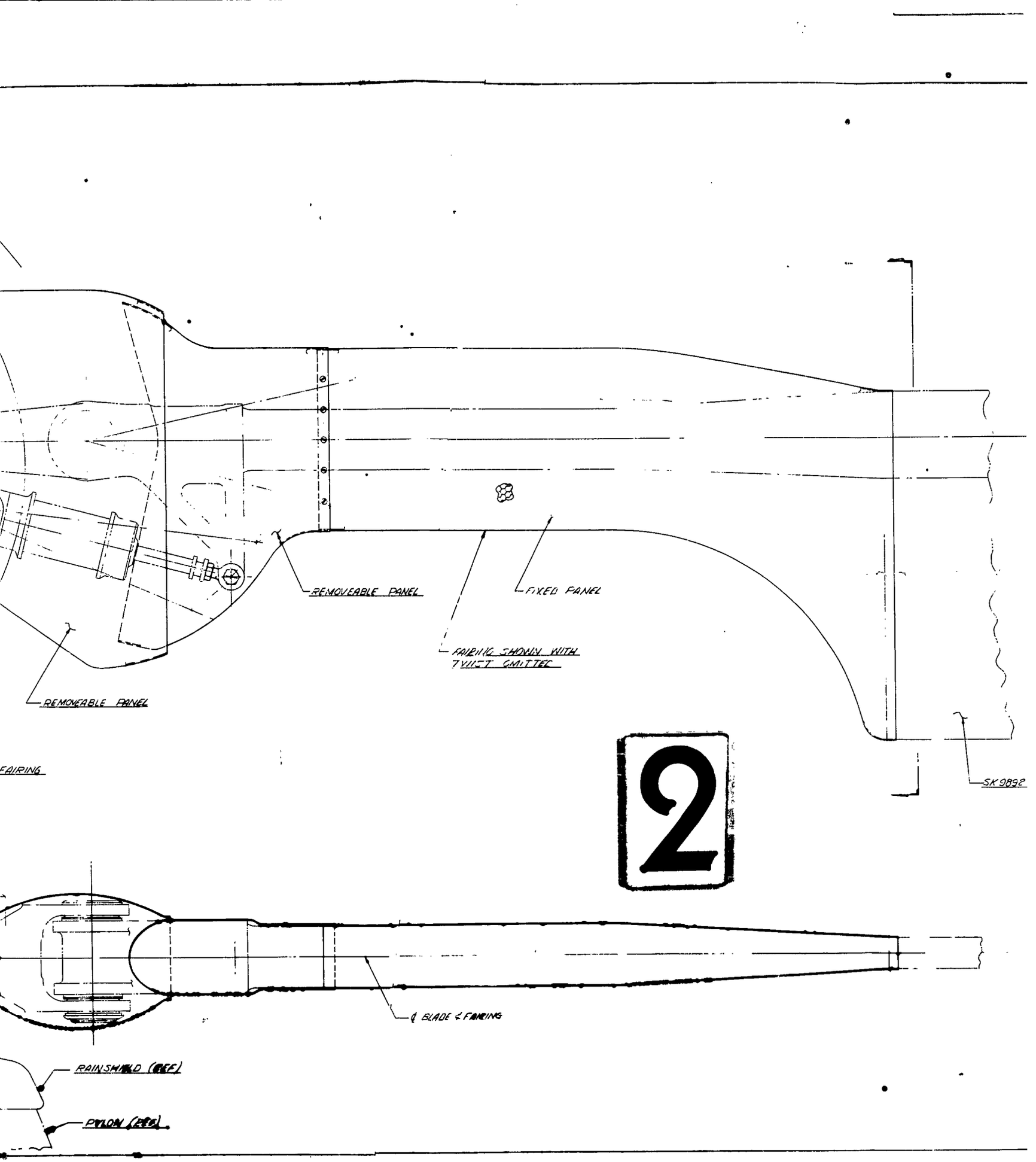
SK10242

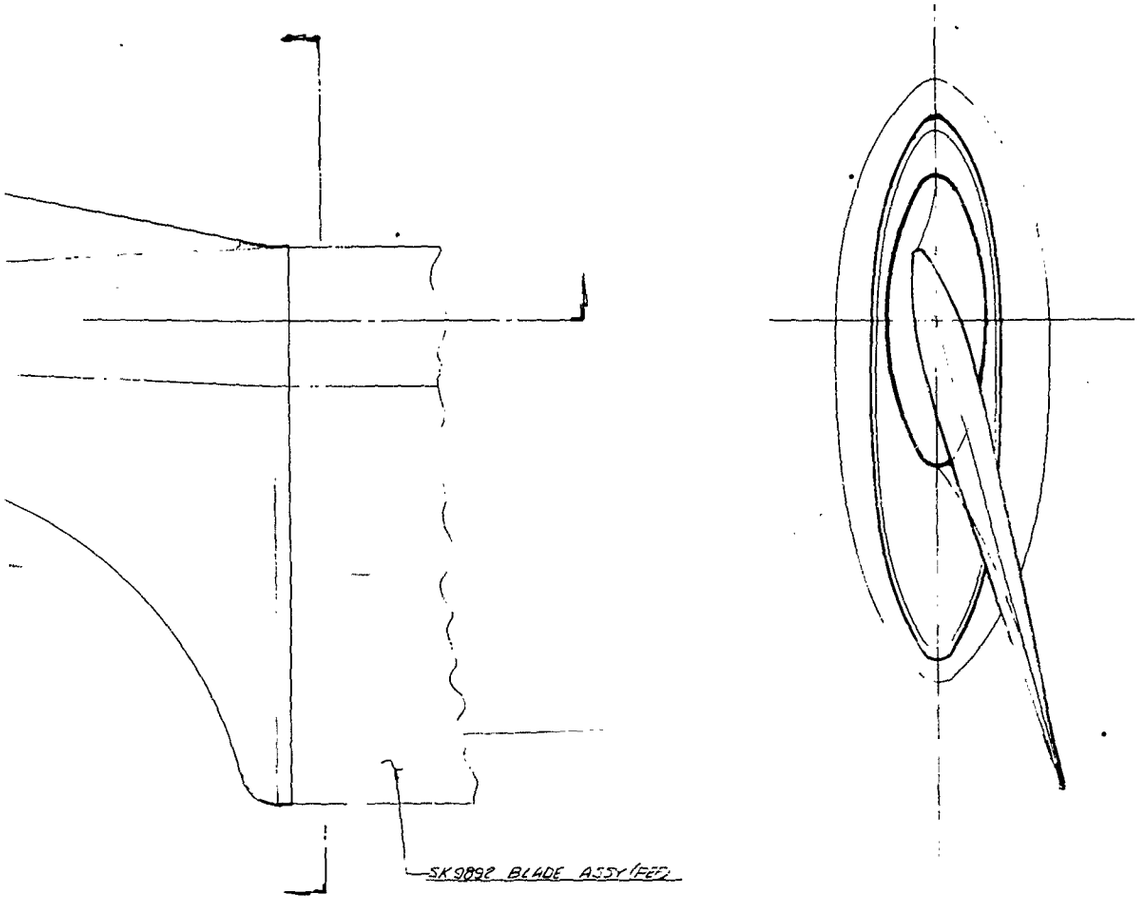
ROTOR HUB FAIRING

The fairing for the High Performance 107-II has been designed to reduce the drag of the rotor system to a minimum. The light-weight fiber glass construction permits full kinematic freedom of the rotor for flight and also has the capability for possible folding requirements. Drawing SK 10319 shows the details of this fairing.



1


REMOVEABLE PANEL
FIXED PANEL
FAIRING SHOWN WITH TWIST OMITTED
REMOVEABLE PANEL
FAIRING
SK 9892
2
℄ BLADE & FAIRING
RAINSHIELD (REF)
PYLON (REF)



SCALE - 1000 INCHE.

3

ROTOR HUB FAIRING

SK10319

DRIVE SYSTEM

The high performance helicopter will utilize the 107 Model II transmissions. These transmissions have been designed for a torque equivalent of 2300 HP @ 18,370 RPM and a growth potential (based on Vertol experience on the 107 prototype, YHC-1A, 105 and H-21D helicopters) to 2500 HP @ 18,370 RPM. No change in components of the 107 Model II transmissions are contemplated when used in the high performance helicopter at 2500 HP and 18,370 RPM.

Drive Shafting

The drive shafting in the 107 Model II helicopter was designed for 2500 HP @ 18,370 RPM and, therefore, no change is necessary for the High Performance 107-II.

Rotor Shafting

The rotor shafts of the 107 Model II helicopter have adequate ultimate and fatigue strength, based on MIL HDBK 5 and Vertol bench fatigue tests, to withstand high performance helicopter loading.

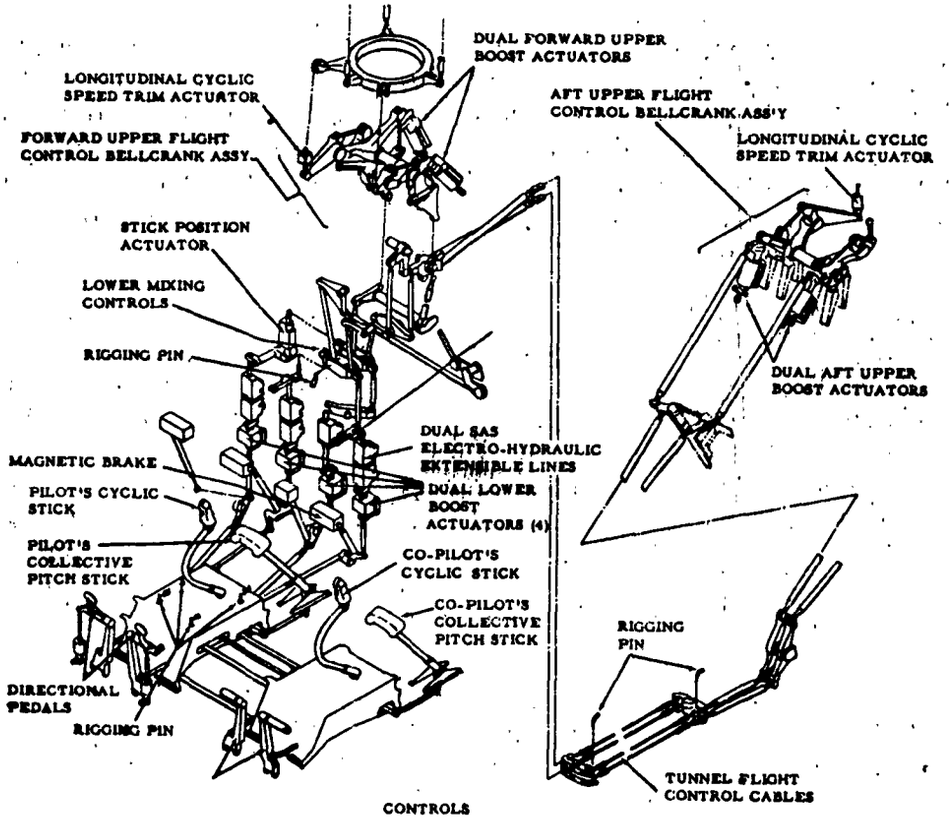
FLIGHT CONTROLS

The increased control loads in the high performance helicopter necessitate changes in the bellcranks at the rotor end of the control system to increase their strength and stiffness. This is achieved mainly by making them out of steel. The system pressure in the control boost is increased from 1500 to 2000 psi in order to deal with the higher control loads. Ample strength is available in the existing actuators for the increased system pressure.

Minor bellcrank changes are made in the lower system to adjust the control travels to the required values. A more detailed discussion of the above modifications follows:

FIGURE 12.2

MODIFICATIONS TO THE FLIGHT CONTROL SYSTEM OF THE BOEING-VERTOL 107 MODEL II FOR THE HIGH PERFORMANCE HELICOPTER DESIGN



Kinematics

Basically, the kinematics of the Boeing-Vertol 107 Model II are the same as the High Performance 107 except for the following:

Roll-Yaw Mechanical Coupling - Eliminated from the lower mixing area.

Changes to meet the required blade angle travels and a decrease in the swashplate motion factor (inches of travel per blade angle degree - Reference Table XXXI).

Collective Pitch - Motion of swashplate is increased by opening up the system stops below the lower mixing area thereby causing the collective pitch lever to increase its motion by 2.5%.

Longitudinal DCP - Motion to swashplate is decreased by closing up the lower system stops below the lower mixing area thereby causing the longitudinal stick to decrease its motion by 3.3%.

Combined Collective Pitch and Longitudinal DCP - Approximately the same total motion to the swashplate due to paragraph 1 and 2 above.

Longitudinal "q" Cyclic - Increased motion to swashplate.

Changes in the Parts of the Control System

Lateral System - Revision to lateral bellcrank in the lower mixing area (equal radius on output arms). Note increase in ultimate lateral output load does not affect upper parts as it is still below directional loads that designed the upper system.

"q" DCP Actuator - Separation of "q" DCP function from the longitudinal stick positioner actuator because of inability to provide additional 1° "Nose Down" recovery in the event of a malfunction of a combined actuator. Therefore, the "q" DCP actuator to be placed below the stick boost actuator so as to be below the "pure" longitudinal stops.

Upper Controls - An increase in the alternating fatigue loads is expected which will result in the following changes to be made above the dual upper boost actuators (includes actuator supports).

Control bellcranks, C.P. yoke and supports to be made from steel. (Steel parts to be four times the stiffness of the present parts.) Clearance check with the present system shows adequate clearances in most areas but will not allow growth of parts required for increase in fatigue loads. A delta weight increase of 147 pounds would result.

Longitudinal "q" Cyclic Actuator - New actuators required for forward and aft controls due to increase in swashplate motion required. Aft actuator to "fail safe" to the aft cyclic (zero speed) position. A dual-motor, diff. geared actuator is proposed with two power sources. Normal operation would have both motors energized, fail safe operation would have either motor driving the actuator at half speed.

Description of the Hydraulic Flight Control Boost System

Because of the anticipated increase in flight loads, the operating pressure of the hydraulic system shall be increased from 1500 psi to 2000 psi. This will require the following changes to be made.

Flexible Hose - Change to hose rated higher, also fittings.

Seals and Packings in Components - Change where required.

Hydraulic Pump - Resetting of compensator.

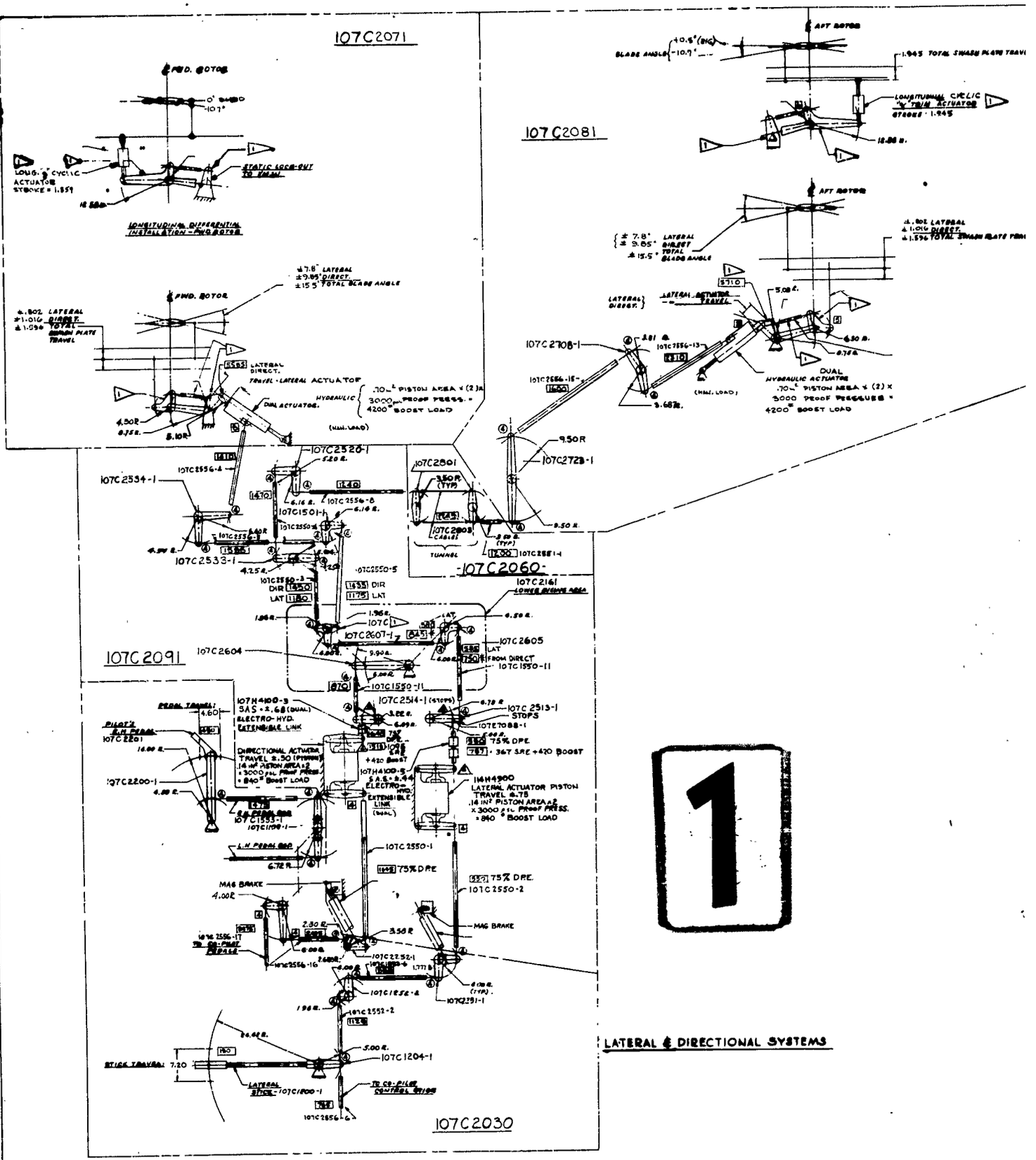
System Pressure Relief Valve - Reset.

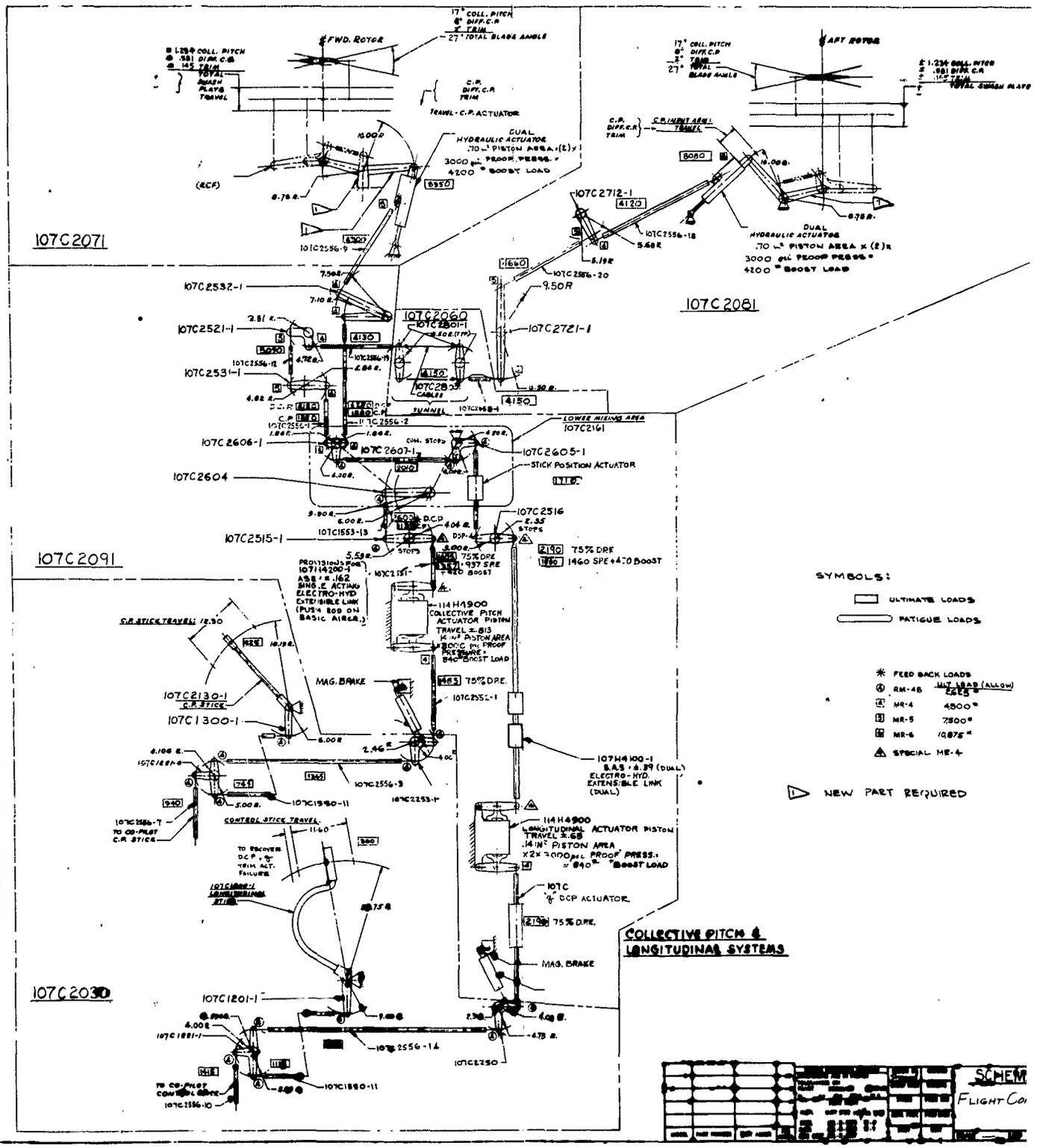
Miscellaneous Equipment - The following parts would require changing - pressure switch, gauges, indicators, pressure transmitters, check valves, etc.

TABLE XXXI

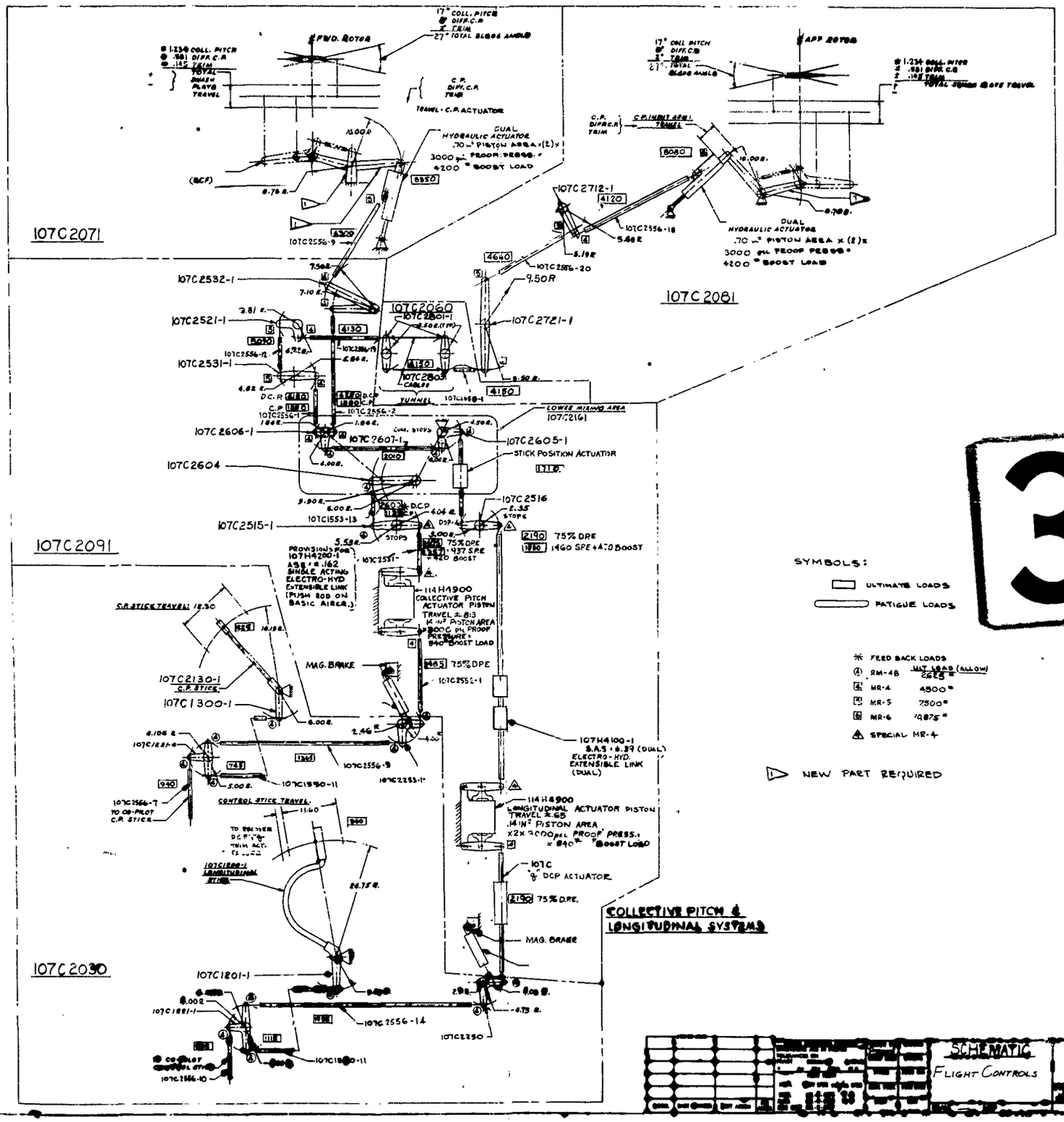
TABLE OF CONTROL RANGES

SYSTEM		107-II	HIGH PERFORMANCE HELICOPTER DESIGN
Collective Pitch:	Lever Travel	0 to 12.00"	0 to 12.30"
	Blade Travel(@..75R)	1° to 17°	1° to 18°
Longitudinal:	Stick Travel	± 6.00"	± 5.8"
	DCP Blade Travel	± 4.00°	± 4.00°
	Cyclic Trim ("q" Sensor)		
	Front Rotor	0° to -5°	0° to -10.7°
	Aft Rotor	+.5° to 7.7°	+.5° to -10.7°
	DCP Trim ("q" Sensor)		
	Front Rotor	0° to 1.91°	0° to 3°
	Aft Rotor	0° to -1.91°	0° to -3°
	Stick Positioner		
	Stick Range	± 1.5"	± 1.45"
	Blade Travel	± 1°	± 1°
Lateral:	Stick Travel	± 3.4"	± 3.6"
	Cyclic Blade Travel		
	Front Rotor	± 8.5°*	± 7.8°
	Rear Rotor	± 7.09°*	± 7.8°
* Mechanical Roll-Yaw Coupling			
Directional:	Rudder Pedal Travel	± 2.18"	± 2.3"
	Diff. Lat. Cyclic Blade Travel	± 9.0°	± 9.5°
Lateral - Directional Design Total			
	Front Rotor	±14.5°	±15.5°
	Aft Rotor	±14.0°	±15.5°
Swashplate Link Travel to Give 1° Blade Angle Change:			
Longitudinal Cyclic		.1805	.1737
Collective Pitch		.1505	.1452
Lateral Cyclic		.1070	.1030


107C2071
FWD. ROTOR
LONG. 'S' CYCLIC ACTUATOR STROKE = 1.859
STATIC LOCK-OUT TO SWASH
LONGITUDINAL DIFFERENTIAL INSTALLATION - FWD ROTOR
±7.8° LATERAL
±9.85° DIRECT.
±15.5° TOTAL BLADE ANGLE
±.802 LATERAL
±1.016 DIRECT.
±1.596 TOTAL SWASH PLATE TRAVEL
LATERAL DIRECT. TRAVEL - LATERAL ACTUATOR
DUAL ACTUATOR.
HYDRAULIC
.70 SQ. IN. PISTON AREA x (2)
3000 PSI PROOF PRESS. =
4200 LB BOOST LOAD
(MAX. LOAD)
107C2081
AFT ROTOR
BLADE ANGLE +10.5° (BIG) -10.7°
1.945 TOTAL SWASH PLATE TRAVEL
LONGITUDINAL CYCLIC 'S' TRIM ACTUATOR
STROKE = 1.945
18.86 R.
±7.8° LATERAL
±9.85° DIRECT.
±15.5° TOTAL BLADE ANGLE
±.802 LATERAL
±1.016 DIRECT.
±1.596 TOTAL SWASH PLATE TRAVEL
LATERAL DIRECT.
LATERAL ACTUATOR TRAVEL
DUAL HYDRAULIC ACTUATOR
.70 SQ. IN. PISTON AREA x (2) x
3000 PROOF PRESSURE =
4200 LB BOOST LOAD
(MAX. LOAD)
107C2060-
107C2161
LOWER BUSHING AREA
107C2091
107C2604
107C2605
107C2513-1
STOPS
107E7088-1
75% DPE
367 SRE +420 BOOST
PEDAL TRAVEL
PILOT'S L.H PEDAL
107C2201
107C2200-1
DIRECTIONAL ACTUATOR TRAVEL 2.50 (PISTON) .14 in² PISTON AREA x 3000 PSI PROOF PRESS. = 840 LB BOOST LOAD
107H4100-3 SAS = ±.68 (DUAL) ELECTRO-HYD. EXTENSIBLE LINK
107H4100-5 SAS = ±.44 ELECTRO-HYD. EXTENSIBLE LINK (DUAL)
+420 BOOST
114H4900 LATERAL ACTUATOR PISTON TRAVEL 6.75 .14 in² PISTON AREA x 3000 PSI PROOF PRESS. = 840 LB BOOST LOAD
L.H PEDAL ASS'Y
107C2550-1
75% DPE
MAG BRAKE
107C2550-2
TO CO-PILOT PEDALS
107C2291-1
107C1204-1
STICK TRAVEL 7.20
LATERAL STICK - 107C1200-1
TO CO-PILOT CONTROL STICK
107C2030
1
LATERAL & DIRECTIONAL SYSTEMS


FWD. ROTOR
AFT ROTOR
17° COLL. PITCH
6° DIFF. C.P.
2° TRIM
27° TOTAL BLADE ANGLE
DUAL HYDRAULIC ACTUATOR .70 L² PISTON AREA x (2) x 3000 psi PROOF PRESS. x 4200 " BOOST LOAD
107C2071
107C2081
107C2532-1
107C2521-1
107C2531-1
107C2606-1
107C2604
107C2515-1
107C2060
107C2801-1
107C2803 CABLES
107C2721-1
107C2712-1
107C2556-18
107C2556-20
107C2556-9
107C2556-12
107C2556-19
107C2556-2
107C2556-1
107C2607-1
107C2605-1
STICK POSITION ACTUATOR
LOWER MIXING AREA 107C2161
107C2516
107C1553-13
107C2091
PR9113100-3 FOR 107H4200-1 ASS'Y. ELECTRO-HYD EXTENSIBLE LINK (PUSH ROD ON BASIC AIRCR.)
114H4900 COLLECTIVE PITCH ACTUATOR PISTON TRAVEL ±.813 .14 IN² PISTON AREA 3000 psi PROOF PRESSURE 840 " BOOST LOAD
C.P. STICK TRAVEL: 12.30
107C2130-1 C.P. STICK
MAG. BRAKE
107C1300-1
107C2552-1
107C1880-1
107C1880-11
107C2556-3
107C2253-1
107C2556-7 TO CO-PILOT C.P. STICK
CONTROL STICK TRAVEL: 11.60
TO RECOVER D.C.P. & TRIM ACT. FAILURE
107C2250
107C2556-14
107C2556-10
107H4100-1 S.A.S. ±.89 (DUAL) ELECTRO-HYD. EXTENSIBLE LINK (DUAL)
114H4900 LONGITUDINAL ACTUATOR PISTON TRAVEL ±.65 .14 IN² PISTON AREA x2x 3000 psi PROOF PRESS. = 840 lbs. BOOST LOAD
107C DCP ACTUATOR
75% D.R.E.
1460 SPE + 420 Boost
SYMBOLS:
ULTIMATE LOADS
FATIGUE LOADS
FEED BACK LOADS
RM-4B
MR-4 4800#
MR-5 7500#
MR-6 10875#
SPECIAL ME-4
NEW PART REQUIRED
COLLECTIVE PITCH & LONGITUDINAL SYSTEMS
SCHEM
FLIGHT CO

2


107C2071
107C2081
107C2091
107C2090
107C2021
FWD. ROTOR
AFT ROTOR
C.P. DIFF. C.R TRIM
TRAVEL - C.P. ACTUATOR
DUAL HYDRAULIC ACTUATOR .70 in² PISTON AREA x (2)x 3000 psi PROOF PRESS.* 4200 * BOOST LOAD
107C2556-9
107C2556-18
107C2712-1
107C2532-1
107C2521-1
107C2531-1
107C2606-1
107C2604
107C2515-1
107C2060
107C2801-1
107C2803 CABLES
107C2721-1
107C2586-20
107C2556-12
107C2556-19
107C2556-1
107C2556-2
107C2607-1
107C2605-1
STICK POSITION ACTUATOR
107C2516
107C1553-13
LOWER MIXING AREA 107C2161
TUNNEL
107C2586-1
DCP
DC.P
C.P
75% DPE
1460 SPE + 420 Boost
937 SPE + 420 BOOST
PROVISIONS FOR 107H4200-1 ASS'Y ± .162 SINGLE ACTING ELECTRO-HYD EXTENSIBLE LINK (PUSH ROD ON BASIC AIRCR.)
114H4900 COLLECTIVE PITCH ACTUATOR PISTON TRAVEL ± .813 .14 in² PISTON AREA 3000 psi PROOF PRESS.* 840 BOOST LOAD
MAG. BRAKE
107C2130-1 C.P. STICK
107C1300-1
C.P. STICK TRAVEL: 12.30
107C2556-7 TO CO-PILOT C.P. STICK
CONTROL STICK TRAVEL: 11.60
107C1801-1
107C2556-14
107C2556-11
107C2250
107H4100-1 S.A.S ± .89 (DUAL) ELECTRO-HYD. EXTENSIBLE LINK (DUAL)
114H4900 LONGITUDINAL ACTUATOR PISTON TRAVEL ± .65 .14 in² PISTON AREA X2 X 3000 psi PROOF PRESS.* 840 * BOOST LOAD
107C DCP ACTUATOR
2190 75% DPE
MAG. BRAKE
SYMBOLS:
ULTIMATE LOADS
FATIGUE LOADS
FEED BACK LOADS
RM-4B LIMIT LOAD (ALLOW) 2625 #
MR-4 4500 #
MR-5 7500 #
MR-6 19875 #
SPECIAL MR-4
NEW PART REQUIRED
3
COLLECTIVE PITCH & LONGITUDINAL SYSTEMS
SCHEMATIC
FLIGHT CONTROLS
107C2021

WEIGHT STUDIES

CONFIGURATION STUDY - PHASE I

The gross weights for the parametric selection of the optimum high performance helicopter were obtained from Boeing-Vertol developed weight trends, constant weights for engines, equipment and fixed useful load weight plus fuel for a one and one half hour mission. Trend curve equations were utilized for the rotor group, body group, and drive system weights, while the alighting gear and flight controls were expressed as a function of gross weight only. Boeing-Vertol experience in the design and manufacture of helicopters encompasses the size and weight range of the helicopters investigated. This experience has enabled Vertol to develop weight trends which reliably predict the variation of weight for various combinations of basic design parameters. The parameters that were varied in this study were:

1. GW Gross weight - in pounds
2. R Rotor radius - in feet
3. c Blade chord - in feet
4. b Number of blades per rotor
5. W_e Engine(s) installation weight-pounds
6. C Fuselage Circumference - at the constant section - in feet
7. L Distance between rotor centerlines - in feet

Some simplifying assumptions were adopted to expedite the study, they were:

1. Engine installation limited to either one or two General Electric T-58-8 engines.
2. The maximum design rotor blade tip speed is 1.25 times the normal tip speed.
3. The fuselage circumference varies linearly between 15.18 feet for a gross weight of 6,250 pounds to 24.6 feet for a gross weight of 18,400. These dimensions are based on previously designed operational helicopters.
4. The distance between rotors is determined from a percent rotor overlap that varies linearly from 38% at gross weight 6,250 pounds to 33-1/3% at gross weight equals 18,400 pounds.

The rotor group weight has been calculated from the following expression:

$$W = (33.6)\, r^{.239} \left(\frac{1.25\, V_t}{10^2}\right)^{1.024} \left(\frac{R \times HP \times b \times c}{10^4}\right)^{.555}$$

where

r = distance from $\mathcal{L}$ rotation to blade attaching bolt (assumed to equal 0.1R)
V_t = Aerodynamic design tip speed - feet per second (assumed to be a constant 641 feet per second)
R = rotor radius - feet
HP = horsepower per rotor - 0.6 take-off horsepower
b = number of blades per rotor
c = blade chord - feet

Body group weight was obtained from this expression:

$$W_b = 710 \left[L \times C \frac{GW^2}{10^5} \right]^{.388}$$

where

GW = design gross weight - pounds
L = distance between rotor centerlines - feet
C = fuselage circumference at constant section - feet

The weight of the alighting gear is assumed to be 4% of design gross weight. Experience and design studies have indicated that a retractable helicopter alighting gear can be built for this percentage of gross weight.

Flight control weight is expressed as a non-linear function of gross weight, based on an examination of Boeing-Vertol tandem helicopter flight control systems including stability augmentation and dual hydraulic boost system.

$$W_{fc} = \text{weight of flight controls} = 500 \left[\frac{GW}{10^4} \right]^{.77}$$

Engine installation weights were determined from actual installation of the General Electric T-58 engines and include, the engine section, engine(s), air induction system, exhaust system, cooling system, lubrication system, fuel system (less tanks which are included with fuel weight), engine controls and starting system.

Engine installation weight = W_e
W_e for (1) T58-8 = 540 pounds
W_e for (2) T58-8 = 1080 pounds

The entire drive system including all shafting and transmission lubrication systems has been expressed as a function representing rotor shaft torque at take-off.

$$W_d = \text{weight of drive system} = 336 \left[\frac{HP}{N_r} \right]^{.763}$$

where

HP = total take off horsepower
N_r = rotor RPM at take-off

A minimum of fixed equipment has been assumed, weighing 613 pounds. Fixed useful load, including a crew of two and trapped liquids equal -

for (1) T58 engines 429 pounds
(2) T58 engines 459 pounds

The fuel required for 1-1/2 hours endurance at normal rated power at S.L. std day plus 0.5 pound per gallon for fuel tanks was calculated for each engine installed.

$W_{fuel\ \&\ tankage}$ = 1,336 for (1) T58 Engine

$W_{fuel\ \&\ tankage}$ = 2,672 for (2) T58 Engines

Assuming a minimum payload of 800 pounds the gross weight becomes:

(1) T58-8 Engine
GW = Weight Empty + 1336 + 800

(2) T58-8 Engines
GW = Weight Empty + 2672 + 800

Approximately 84 different combinations of design parameters were placed in the weight equation yielding 84 different gross weights. The results were incorporated into the aerodynamic parametric studies, Section 3, Configuration Study.

DETAILED STUDY OF ROTOR PARAMETER FOR HIGH PERFORMANCE 107-II - PHASE I

A second parametric study was conducted, with the purpose of selecting an optimum rotor for a helicopter similar to the Boeing-Vertol Model 107-II. Rotor radii of 25, 27, and 29 feet, blade chords of 18, 20.5, and 23 inches, and tip speeds ranging from 881 to 1043 feet per second, depending on the radius and chord were investigated. The effect of varying these parameters on the weight of the fuselage and drive system was also included. The primary difference in this particular study compared to the first was the use of a fixed design gross weight of 19,200 pounds and the specific equipment and general configuration of Boeing-Vertol 107-II utility helicopter. Weight trend relationships were again used to predict the change of component weights.

The basic 107-II utility configuration was modified to include the high performance requirements of increased gross weight (18,000 to 19,200 pounds), drag cleanup of fuselage (rear ramp area extended and refaired), the addition of retractable alighting gear, and redesign of flight controls for the increased loads associated with higher speeds.

PHASE II HIGH PERFORMANCE 107-II

A weight estimate was conducted for converting an existing Boeing-Vertol 107-II utility helicopter into a high performance helicopter, retaining the same blade radius and distance between rotors. The hub and hinge and hub fairing are a new design. The only change to the body group is a short extension and refairing at the aft end of the fuselage. A retraction system has been added to the basic alighting gear and the upper controls in the flight control system have been redesigned for the higher flight control loads associated with the increase in forward speed. The weight penalties associated with these changes have been estimated from design layouts. All other items of equipment and the engine installation are unchanged from the 107-II utility except for the addition of an allowance of 300 pounds for electronics.

A summary weight statement for this helicopter is shown below.

TABLE XXXII

SUMMARY WEIGHT STATEMENT

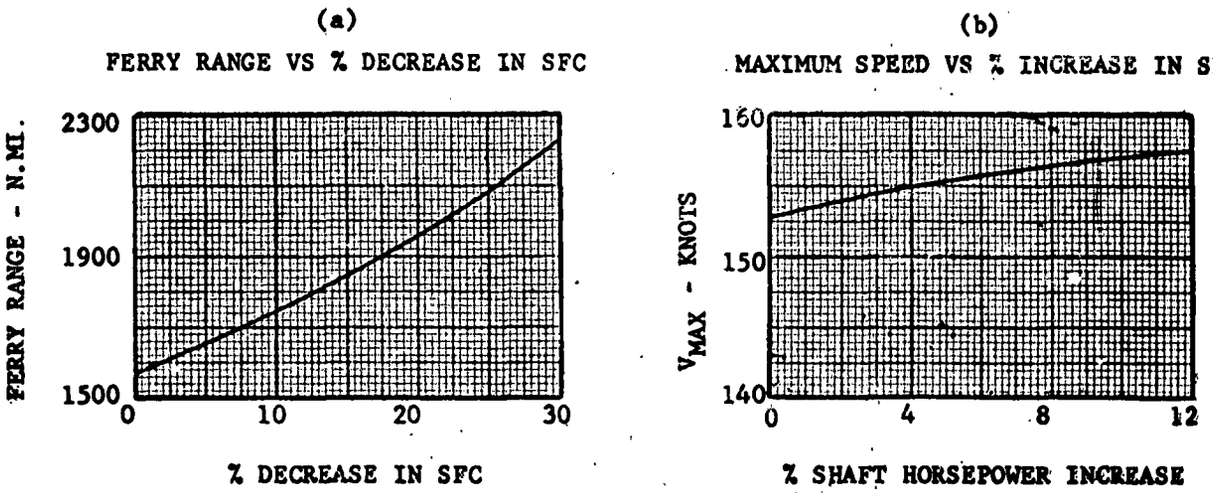
	High Performance 107-II	
Rotor Group	1964 lbs.	
Body Group	2366	
Alighting Gear	667	
Flight Controls	758	
Engine Section	68	
Propulsion Group	2807	
Engine(s)		566 lbs.
Air Induction		17
Exhaust System		6
Cooling System		17
Lubricating System		55
Fuel System		285
Engine Controls		41
Starting System		73
Drive System		1747
Aux. Power Plant	135 lbs.	
Instr. and Nav.	436	
Electronics Group	300	
Furn. & Equip. Group	266	
Air Cond. & Deicing	164	
Auxiliary Gear	44	
Mfg. Variation	13	
Weight Empty	9988	
Fixed Useful Load	459	
Crew		400 lbs.
Trapped Liquids		28
Engine Oil		31

Fundamentals of Performance Increases

The most important parameters for obtaining range improvement are engine specific fuel consumption and aerodynamic cleanliness of the aircraft. The most important parameters for increased speed are power loading, blade loading, and again, aerodynamic cleanliness.

Possible improvements in engine characteristics, i.e., specific fuel consumption and available power are insufficient in themselves, however, to achieve the desired gains in range and speed. The effects of improved specific fuel consumption on ferry range and the effect of power available increase on maximum speed for the present Vertol 107 helicopter are shown below in Figures 123(a) and 123(b).

FIGURE 123



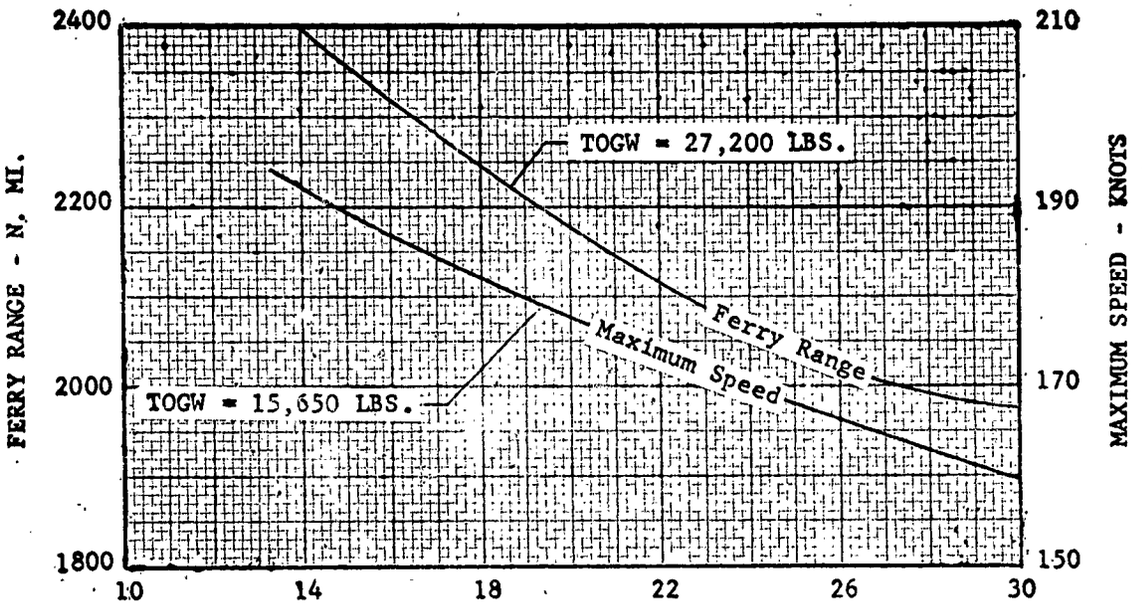
An increase of 25% in ferry range would require a decrease of 21% in S.F.C. An increase in speed of 5 knots would require a 12% power available increase.

The effects of aerodynamic cleanliness are shown below for the extended radius version of the Vertol 107.

The 25% increase in ferry range can be obtained with a 54% decrease in equivalent flat plate area. An increase of 5 miles per hour in speed results from a 10% decrease in equivalent flat plate area.

FIGURE 124

FERRY RANGE AND MAXIMUM SPEED VS. EQUIVALENT FLAT PLATE AREA



GROWTH VERSIONS

Using the present Vertol 107 as a base point for comparison, a review of two other configurations derived from the basic Vertol 107 is presented, along with the prototype research vehicle under design in this contract.

Despite the fact that the prototype research vehicle meets the primary requirements of performance outlined in Contract No. DA44-177-TC-686, High Performance Helicopter, it fails to substantially improve overall productivity, i.e., mission efficiency. To establish what performance might be expected from the next generation of helicopters, in the Vertol 107 class, the performance of the following two aircraft has been evaluated and compared with the present Vertol 107 and High Performance 107-II.

1. Increased Power Available Version - No change from prototype in rotor size.

   The basic ratings of the GE T-58-8 were raised from 1250 SHP to 1450 SHP Mil Power at S.L. and 1050 SHP to 1250 NRP at S.L. Equivalent flat plate area reduced to 13 sq. ft.

2. Increased Radius Version - No change in installed power. The rotor was resized to recoup the useful load of the present Vertol 107 in hover.

Table XXXIII summarizes the weights and performance for the three derivatives of the present Vertol 107. The normal gross weight is defined from a hover ceiling criteria of 6000 feet at 95°F day. The ferry range overload gross weight is found from a 500 FPM rate of climb, NRP at S.L.

The Army's primary need at this time is a large improvement in ferry range capability to enable self-transport-ability of tactical and logistics helicopters to the combat zone in the event of hostilities. The bar chart below, illustrates at zero headwind, the payload-range characteristics for sea level and 10,000 feet, maximum altitude without oxygen equipment.

FIGURE 125

FERRY RANGE, 107 SERIES

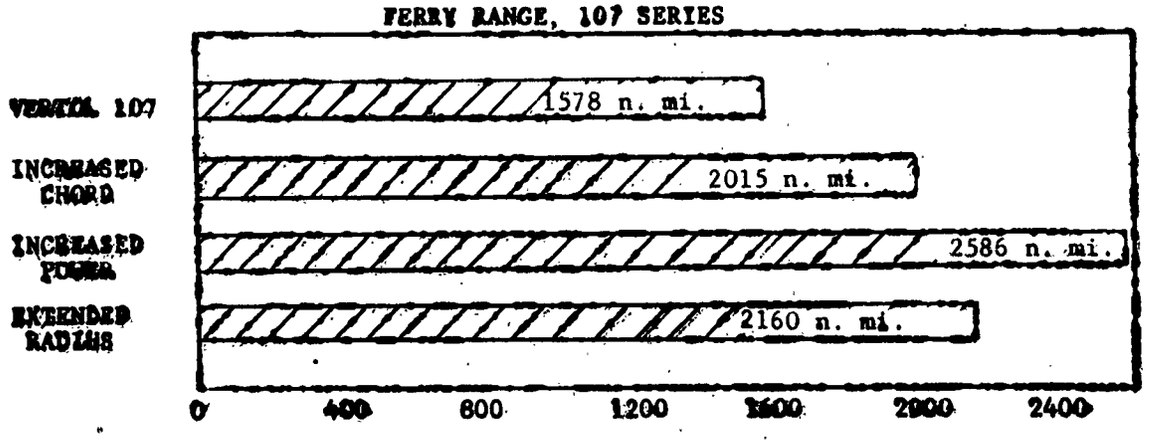


TABLE XXXIII

SUMMARY - WEIGHTS AND PERFORMANCE

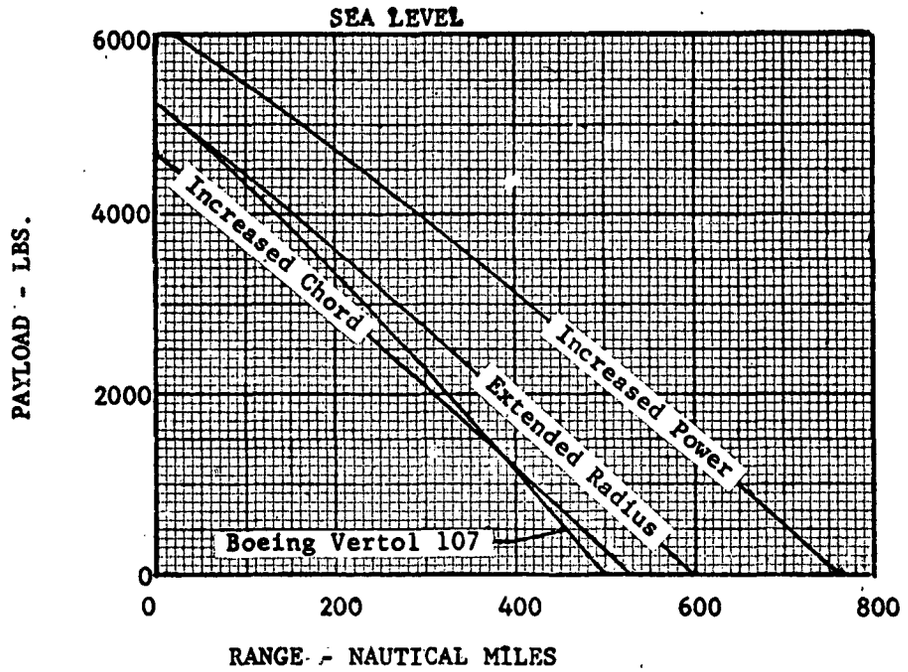
				V-107 SERIES		
		Unit	V-107-II	Increased Chord	Increased Power	Advanced V-107-II
DESCRIPTION	Rotor Radius/Rotor Solidity	ft/-	25/.0573	25/.07321	25/.07321	26.25/.0636
	Rotor Chord/No. of Blades	in/-	18/3	23/3	23/3	21/3
	Rotor Twist/Rotor Tip Speed	deg/fps	-8.33/690	-14/655	-14/675	-14/655
	Rotor Airfoil Section	-	0012	0009.5	0009.5	0009.5
	Equivalent Flat Plate Area	ft^2	30.2	20.5	13.0	20.5
	No. of Eng/Eng Designation	-	(2)T-58-8	(2)T-58-8	(2)T-58-8 Adv.	(2)T-58-8
	Military Power Per Eng.	SHP	1250	1250	1450	1250
	Normal Rated Power Per Eng.	SHP	1050	1050	1250	1050
WEIGHTS	Rotor Group	lbs	1749	1964	2104	1937
	Body Group	lbs	2336	2356	2356	2403
	Alighting Group	lbs	557	667	667	667
	Flight Controls	lbs	723	758	778	758
	Propulsion Group	lbs	2875	2875	2995	2875
	Instr., Nav., & Aux. Power Plt.	lbs	135	135	135	135
	Hydr. Elect. & Electronics Group	lbs	736	736	736	736
	Furn. & Equip. Group	lbs	487	487	487	487
	Weight Empty	lbs	9598	9988	10248	9998
	Useful Load	lbs	5652	5177	6652	5652
	Fixed Useful Load	lbs	459	459	459	459
	Fuel (100n.mi. radius)	lbs	2036	1842	1710	1850
	Payload (outbound only)	lbs	3157	2876	4483	3343
	Gross Weight*	lbs	15250	15165	16900	15650
PERFORMANCE	Hover Ceiling @95°F, OGE	ft	6000	6000	6000	6000
	Max. Speed. Mil. Pow. S.L.	knots	153	174	200	176
	Max. Speed, NRP, S.L.	knots	147	168	192	170
	Speed for Best Range, S.L.	knots	130	158	176	161
	Fwd, R/C, NRP, S.L.	fpm	2460	2200	2620	2175
	Ferry Range	n.mi	1578	2015	2586	2160
	Assoc. G.W. for Ferry Range**	lbs	25740	26250	30400	27200

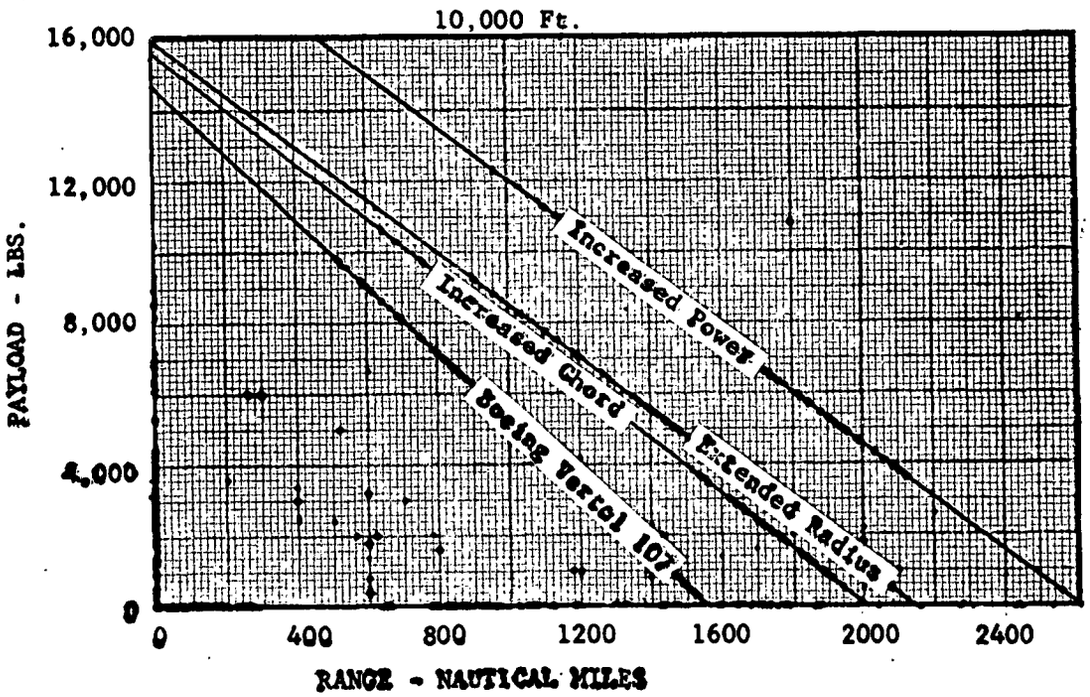
* Normal gross weight defined by hover @ 6000 ft., 95°F day

** Gross weight defined by 500 fpm rate of climb, NRP at S.L.

Figure 126 illustrates, at zero headwind, the payload-range characteristics for sea level and 10,000 feet.

FIGURE 126
RANGE-PAYLOAD



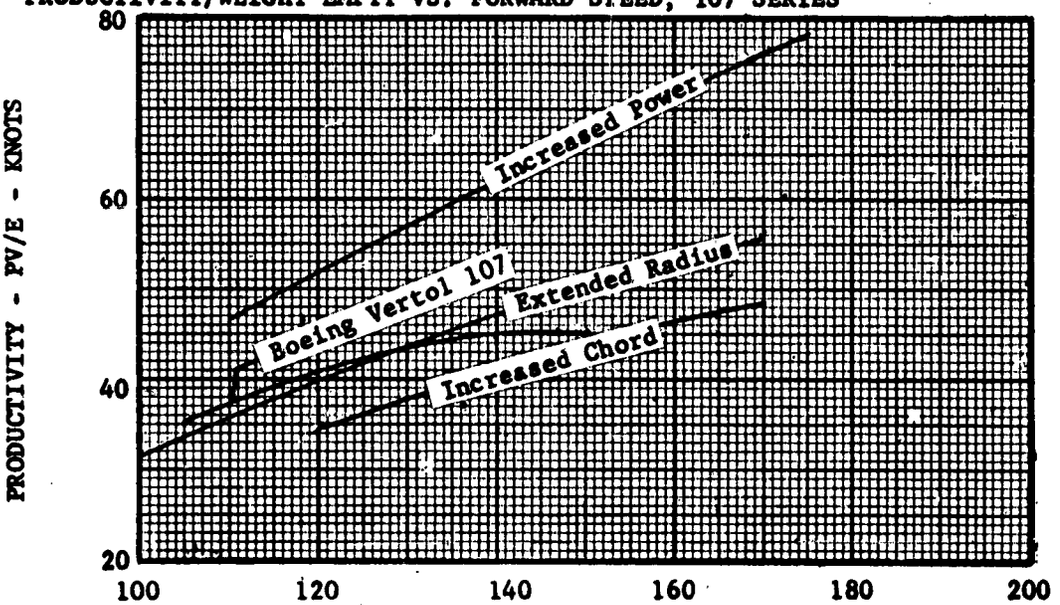


Productivity (PV, payload times forward speed) is often employed as a criterion to compare aircraft efficiency in transport applications. A more meaningful parameter, however, has been found to be the ratio of the productivity to empty weight (PV/E) as this is proportional to ultimate economic criterion, ton/nautical miles per dollar.

The parameter, PV/E, plotted against forward speed, is shown in Figure 127 below.

FIGURE 127

PRODUCTIVITY/WEIGHT EMPTY VS. FORWARD SPEED, 107 SERIES

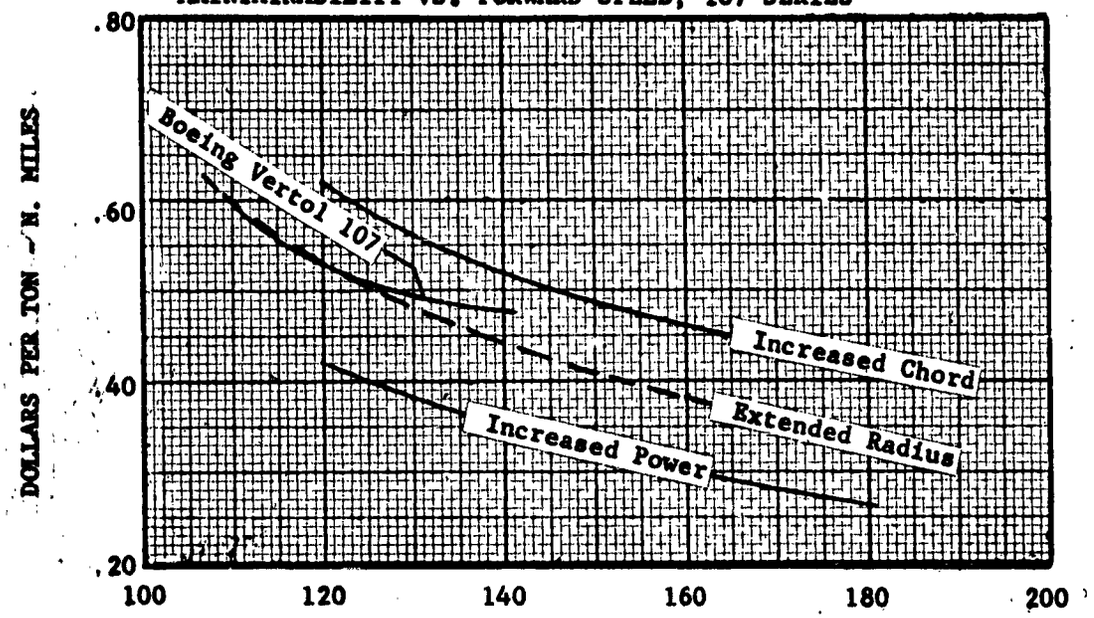


PV/E optimizes at speeds close to maximum forward speed rather than best range speed which means that best overall economy is attained by consuming more fuel and flying as fast as possible.

The maintainability, expressed in dollars of maintenance cost per ton nautical mile, is shown in Figure 128 below.

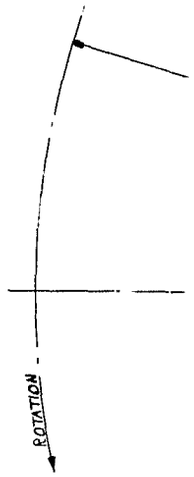
FIGURE 128

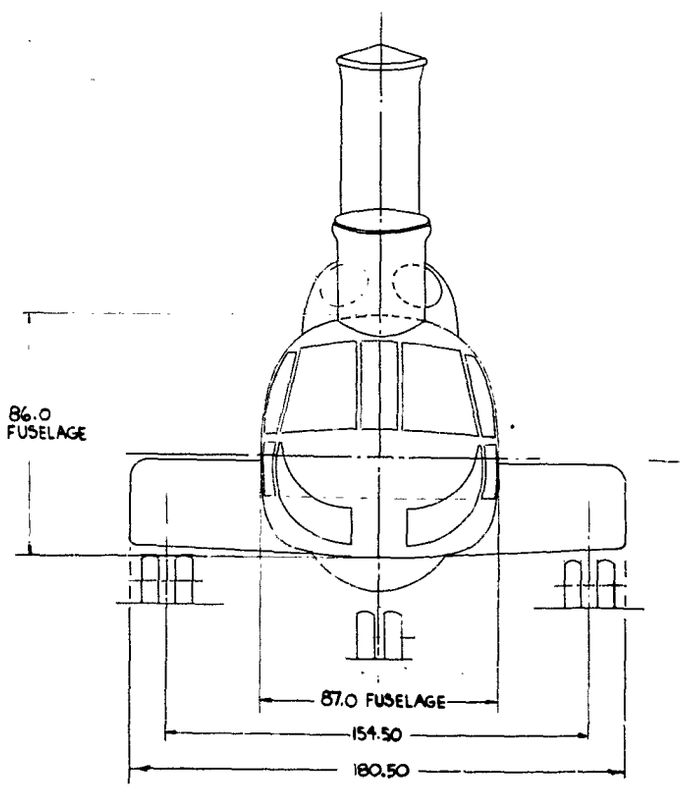
MAINTAINABILITY VS. FORWARD SPEED, 107 SERIES

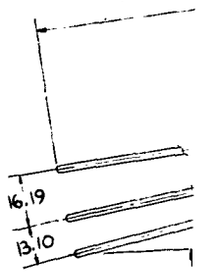


The maintenance dollars per flight hour was derived from studies of present helicopter operation extrapolated to turbine powered versions as a function of weight empty and installed power. These costs are summarized below:

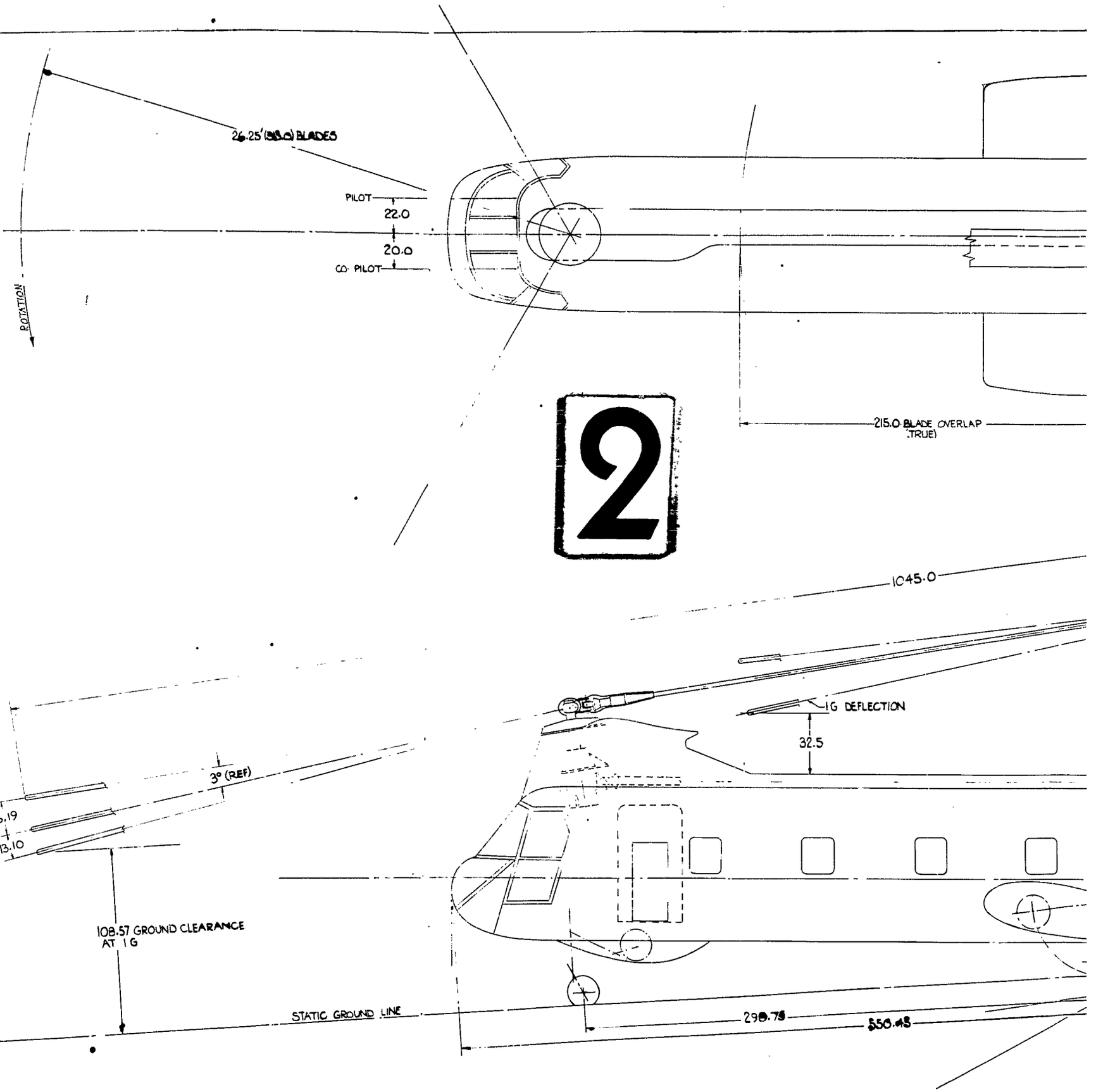
Present Vertol 107	$104.30/flight-hour
Increased Chord	$106.43/flight-hour
Increased Power Version	$111.84/flight-hour
Extended Radius Version	$106.64/flight-hour

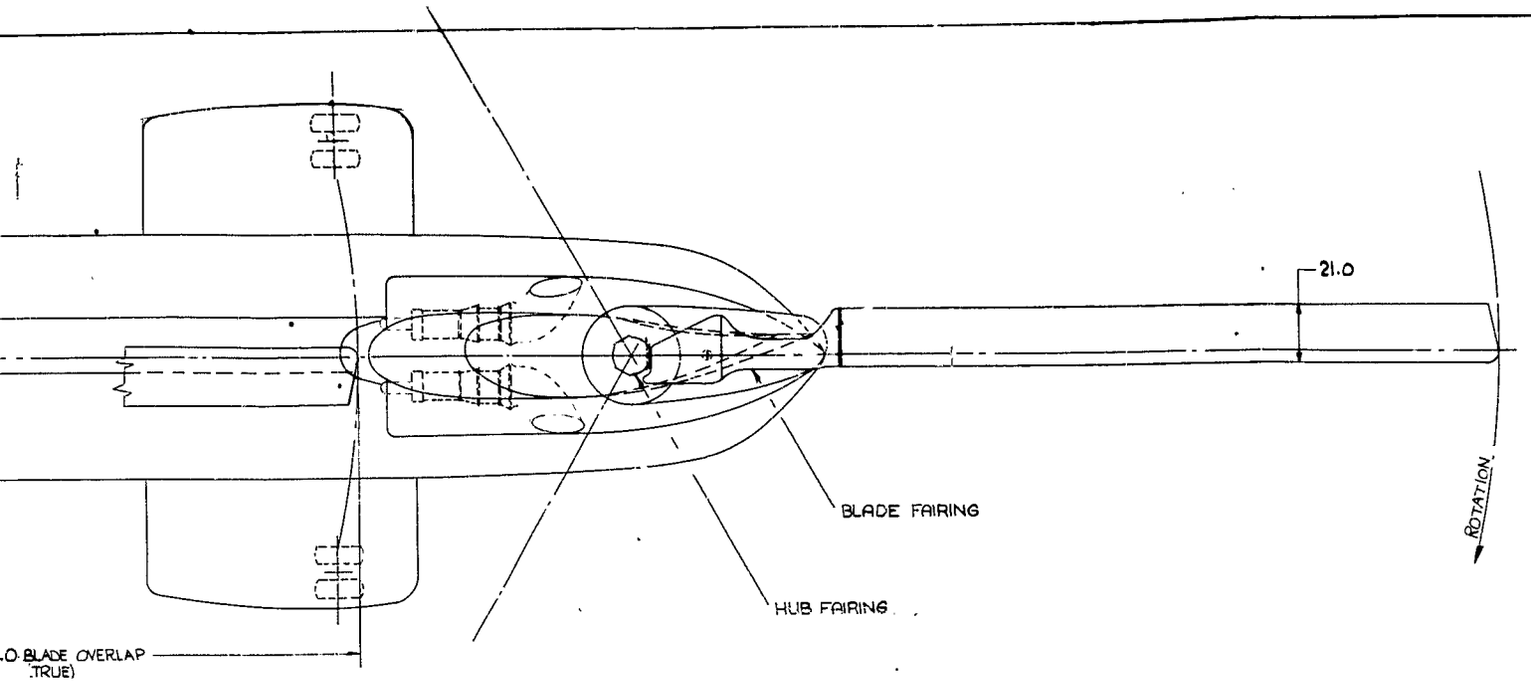


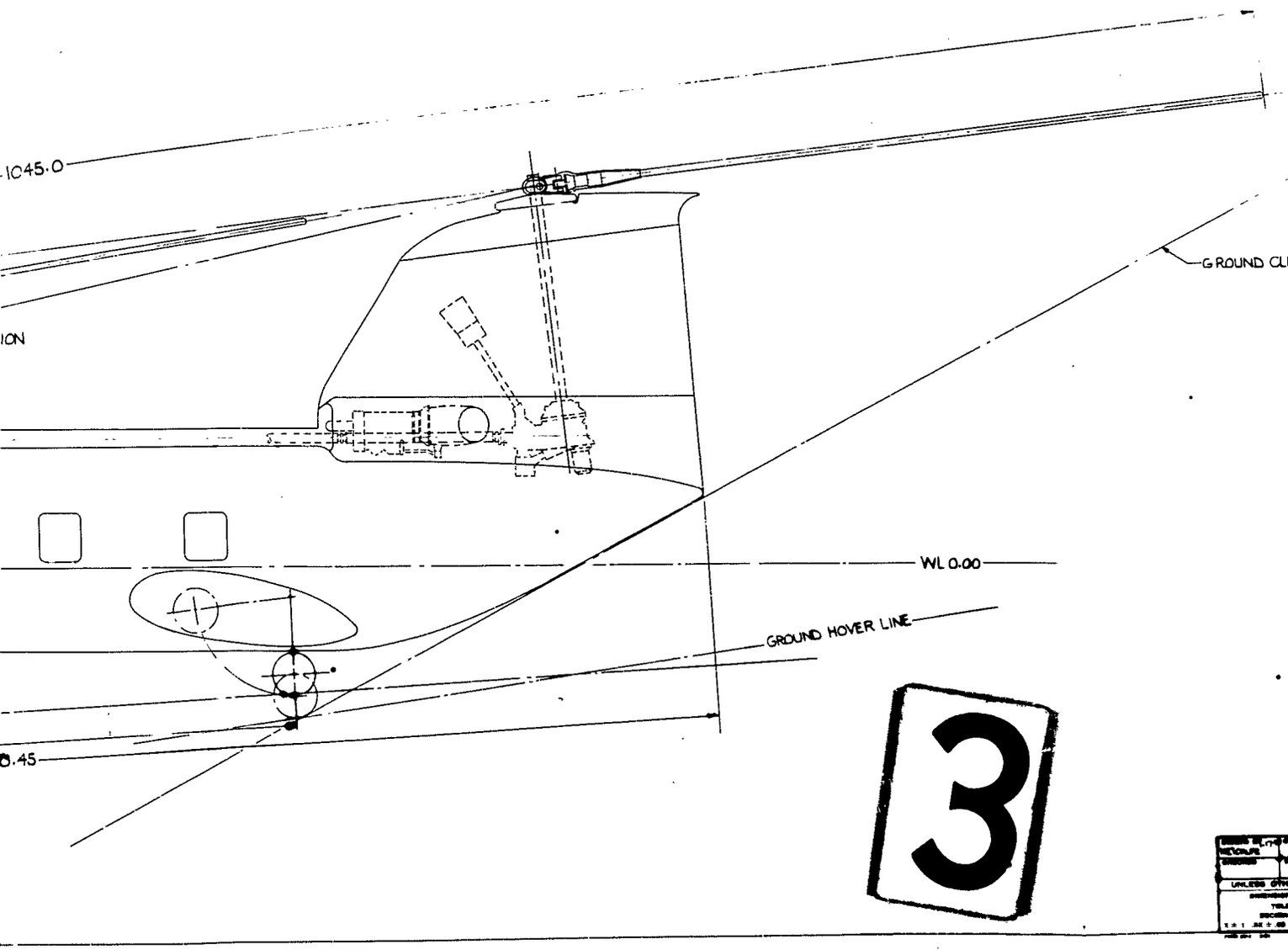




1


26.25' (315.0) BLADES
PILOT
22.0
20.0
CO- PILOT
ROTATION
215.0 BLADE OVERLAP (TRUE)
2
1045.0
1G DEFLECTION
32.5
3° (REF)
108.57 GROUND CLEARANCE AT 1G
STATIC GROUND LINE
298.75
550.45



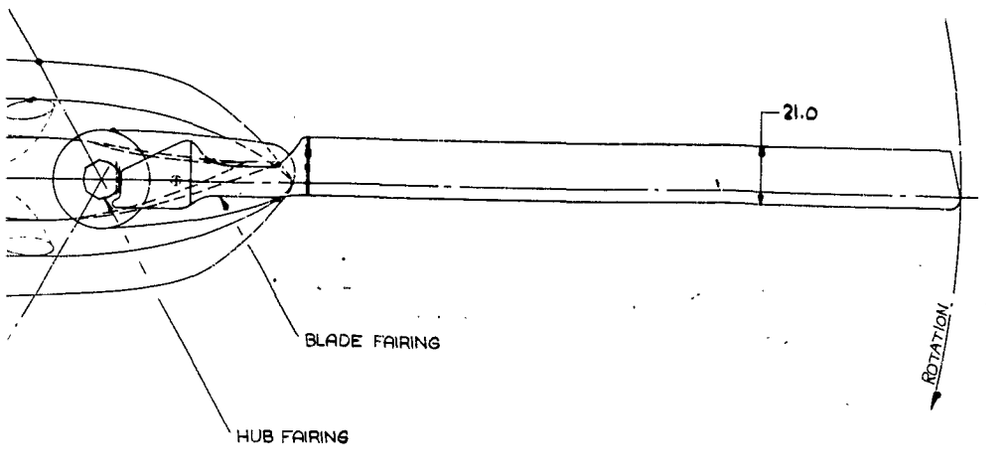


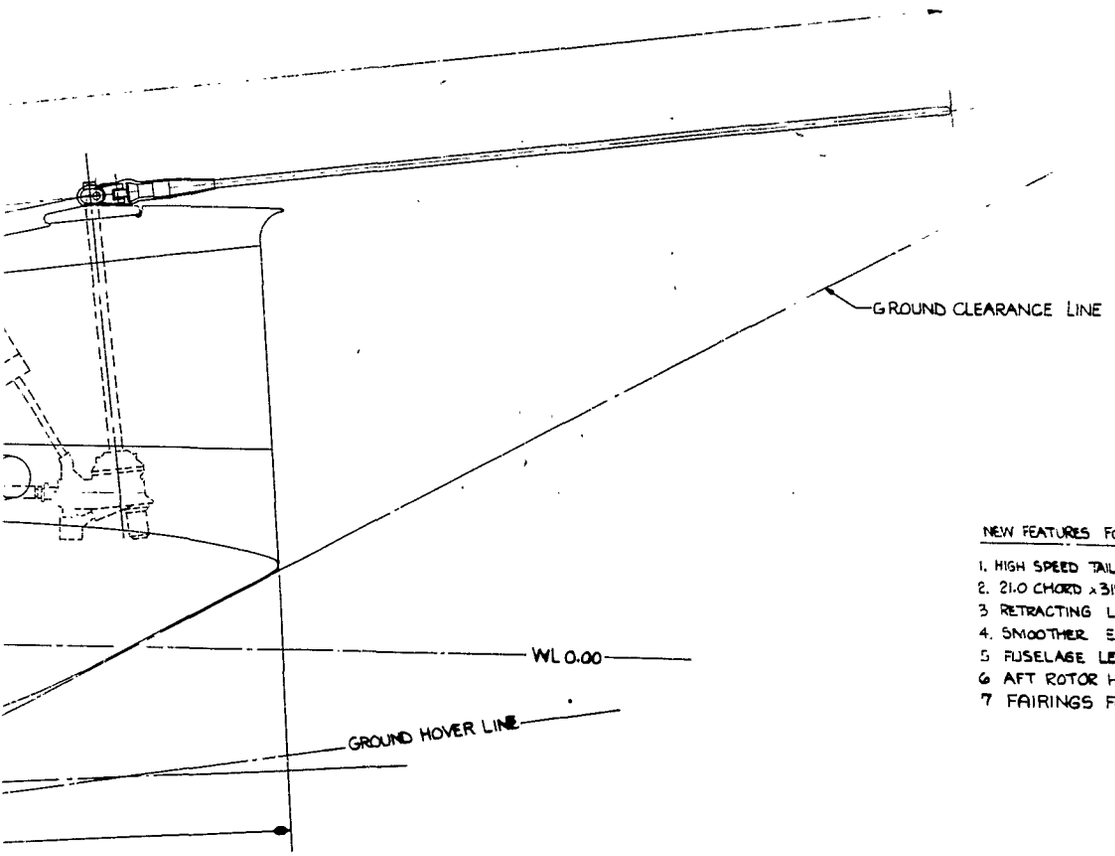
NEW FEATURES FOR T

1. HIGH SPEED TAIL CO
2. 21.0 CHORD x 315.0 (
3 RETRACTING LAND
4. SMOOTHER EXTER
5 FUSELAGE LENGTH
6 AFT ROTOR HEIG
7 FAIRINGS FOR

3

UNLESS OTHERWISE SPECIFIED





4

NEW FEATURES FOR THE ADVANCED 107-II

1. HIGH SPEED TAIL CONFIGURATION
2. 21.0 CHORD x 315.0 (26'-3") LONG ROTOR BLADES
3. RETRACTING LANDING GEAR.
4. SMOOTHER EXTERIOR SURFACE IN COCKPIT GLASS AREA
5. FUSELAGE LENGTH INCREASED 15.0
6. AFT ROTOR HEIGHT INCREASED 10.0
7. FAIRINGS FOR ROTOR BLADES & HUB.

REVISIONS	GROUP MASS	SYMBOL	PART/ASSY.	COST	
CHECKED	WEIGHTS				
UNLESS OTHERWISE SPECIFIED DIMENSIONS ARE IN INCHES TOLERANCES ON DECIMALS .X ± .1 .XX ± .02 XXX ± .010 ANGLES .X° ± 0°					
MATL. STEEL ALUM. MAG. CAST	HEAT TREAT SPEC. NO. MIL-H-6875 MIL-H-6088 MIL-H-6857				

ADVANCED 107-II

SCALE 1/20 DRAWING NO. 97272 SHEET 1 OF 1

SK 10315

UNLOADED ROTOR VERSIONS

The use of auxiliary lifting and/or propulsive devices to the basic helicopter is often suggested as a means of increasing both range and speed potential.

To more fully determine the potential of these compound helicopter versions, two configurations derived from the advanced 107 were considered:

1. Unloading of propulsive force to an auxiliary pusher propeller. No auxiliary lifting surface.

2. Unloading of both propulsive force and lift to the pusher propeller and auxiliary wing.

In both configurations it was found necessary to add a third T58-GE-8 turbine engine so that the loss in useful load due to empty weight increase could be recovered in hover.

UNLOADED PROPULSIVE FORCE VERSION

The total propulsive force of this configuration, including a slight percentage of rotor drag, is carried by a pusher propeller having an aerodynamic efficiency of .90 and a propeller transmission efficiency of .95. The advanced107 rotors of 26.25 foot radius, 21 inch chord carried the total gross weight of the configuration. The equivalent flat plate area of 20.5 square feet remains constant.

UNLOADED PROPULSIVE FORCE AND LIFT VERSION

To the unloaded propulsive force configuration described above, a wing of L/D_{max} equal to 22 at lift coefficient, C_L, of .5 and aspect ratio, of 6 was designed to unload the rotor in lift and thus permit lowering of rotor RPM.

The wing area of 200 square feet was determined from minimum download considerations in hover and L/D_{max} operation at NRP and sea level. The tip speed was fixed at 300 fps for sea level operation and 350 fps tip speed during the ferry range mission.

Table XXXIV presents a summary of weights and performance for the two compound versions compared to the advanced 107. Figure 129 and 130 illustrate comparisons of ferry range and maximum speed between the three configurations.

TABLE XXXIV

SUMMARY OF WEIGHTS AND PERFORMANCE
UNLOADED ROTOR VERSIONS

		UNIT	ADVANCED 107	AUX. PROPELLER	AUX. PROP. AND WING
DESCRIPTION	Rotor Radius/Solidity	ft/	26.25/.0636	26.25/.0636	26.25/.0636
	Rotor Chord/No. of Blades	in/	21/3	21/3	21/3
	Rotor Twist/Tip Speed	deg/fps	-14/655	-14/655	-14/655
	Rotor Airfoil Section		0009.5	0009.5	0009.5
	Equiv. Flat Plate Area	ft^2	20.5	20.5	20.5
	No. of Eng./Eng. Designation		(2)T-58-8	3/T-58-8	3/T-58-8
	Mil. Power Per Eng.	SHP	1250	1250	1250
	Normal Rated Power Per Eng.	SHP	1050	1050	1050
	Wing Area	ft^2			200.0
	Wing Span	ft.			35.1
	Wing Chord	ft.			5.7
	Prop. Dia./Tip Speed	ft/fps		8/950	8/950
	No. of Blades/Activity Factor			4/200	4/200
WEIGHTS	Rotor Group	lbs.	1937	2030	2030
	Body Group	lbs.	2403	2480	2480
	Wing Group	lbs.			780
	Prop. Group	lbs.		390	390
	Alighting Group	lbs.	667	707	707
	Flight Controls	lbs.	758	788	788
	Propulsion Group	lbs.	2875	4070	4070
	Instr., Nav., & Aux. Power	lbs.	135	167	167
	Hydr. Elect. & Electronic	lbs.	736	736	736
	Furn. & Equip. Group	lbs.	487	487	487
	WEIGHT EMPTY	lbs.	9998	11855	12635
	Useful Load	lbs.	5652	8885	7665
	Fixed Useful Load	lbs.	459	480	480
	Fuel (100 N.Mi. Radius)	lbs.	1850	1760	1670
	Payload (Outbound Only)	lbs.	3343	6645	5515
	GROSS WEIGHT	lbs.	15650	20740	20300
PERFORMANCE	Hover Ceiling @ 95°F, OGE	ft.	6000	6000	6000
	Max. Speed Mil. Power, S.L.	kts.	176	199	227
	Max. Speed NRP, S.L.	kts.	170	189	210
	Speed for Best Range, S.L.	kts.	161	174	197
	Ferry Range	n.mi.	2160	2210	2770
	Assoc. G.W. for Ferry Range	lbs.	27200	31000	38200

FIGURE 129

COMPARISON OF FERRY RANGE

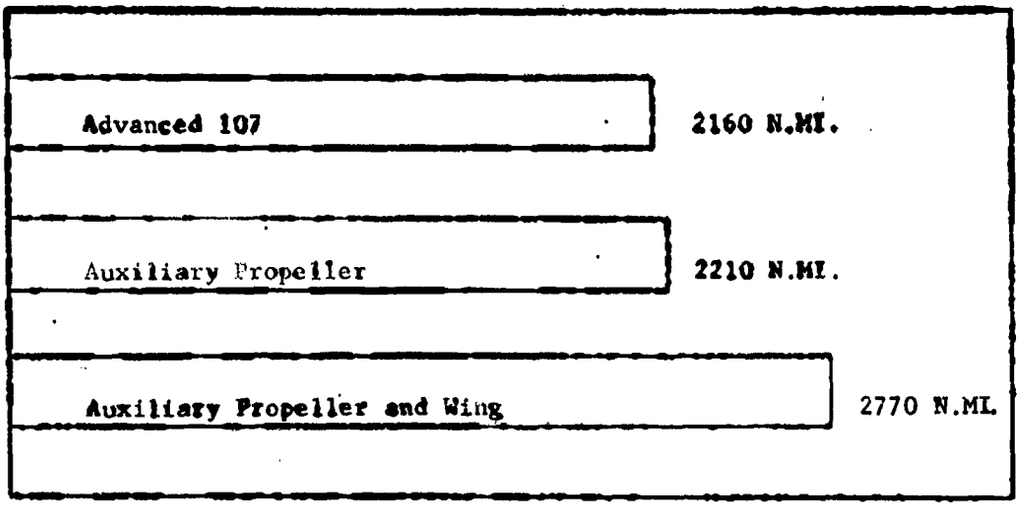
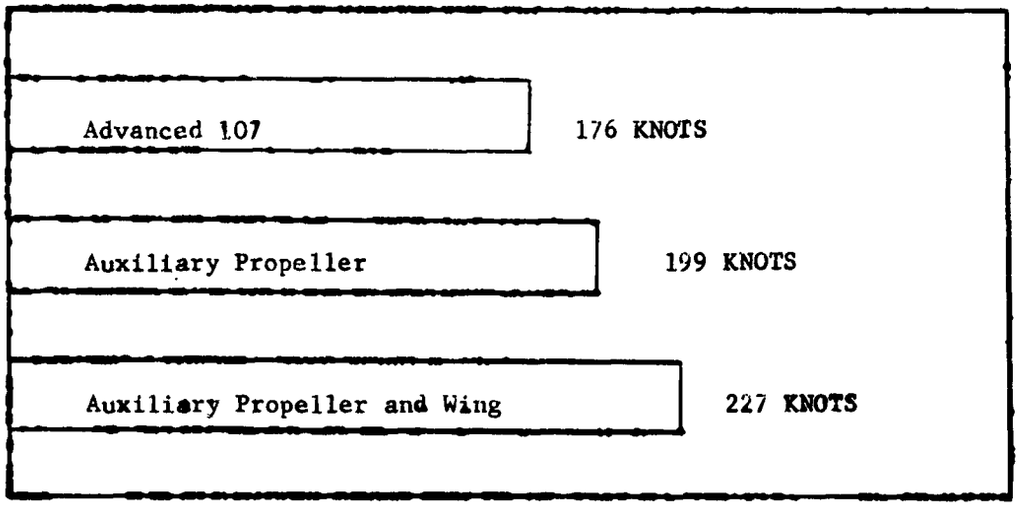


FIGURE 130

COMPARISON OF MAX. FWD. SPEED @ MIL. POWER



REFERENCES

1. Vertol Division, The Boeing Company, Preliminary Design Proposal for a High Performance Research Helicopter. PR-343, April 15, 1960.

2. Phase I Report, High Performance Helicopter. Boeing-Vertol Report R-212.

3. A. Gessow and A. D. Crim, A Method for Studying the Transient Blade-Flapping Behaviour of Lifting Rotors at Extreme Operating Conditions. NACA Technical Note 3366, January 1955.

4. A. Gessow, Equations and Procedures for Numerically Calculating the Aerodynamic Characteristics of Lifting Rotors. NACA Technical Note 3747, October 1956.

5. General Electric Company, Model Specification Engine, Aircraft, Turboshaft. T-58-GE-8 engine. Specification No. E-1025, May 1960.

6. Lycoming Specification No. 124.18-B, Model Specification T-55-L-5. Shaft Turbine Engine, 22 January 1960.

7. D. C. Hazen and R. F. Lehnert, An Investigation of Aerodynamic Forces and Moments Acting Upon a 1/12 Scale Model of the Vertol 107 Helicopter. Princeton University Report No. 400, September 1957.

8. E. L. Davenport and K. E. Smith, Wind Tunnel Tests, Vertol 107B Part I and Part II. University of Detroit, Project 2671, June 1958.

9. F. Harris, Wind Tunnel Tests Report for 1/8 Scale Model YHC-1A Helicopter. Vertol Report No. 107-A-06, January 21, 1958.

10. R. Stroub, Summary Wind Tunnel Test Report for 1/8 Scale Model of the Vertol 107-II. Vertol Report No. 107-A-10, December 2, 1960.

11. F. Harris and G. Holcombe, Wind Tunnel Report, High Performance Helicopter. Vertol Report No. 222, December 2, 1960, Contract No. DA44-177-TC-686.

12. M. Kahn and R. Stroub, Wind Tunnel Tests of a 1/8 Scale Model of the YHC-1B Helicopter. Boeing-Vertol Report 114-A-04.2, June 1960.

13. D. Julian, Wind Tunnel Tests of the Advanced Chinook Helicopter. Boeing-Vertol Report R-235, February 1961.

14. D. Julian, Wind Tunnel Tests of a Chinook 1/3 Scale Powered Hub Model. Boeing-Vertol Report R-236, February 1961.

15. R. P. Coleman, A. M. Feingold, Theory of Self-Excited Mechanical Oscillations of Helicopter Rotors with Hinged Blades. NACA Technical Note 3844, February 1957.

16. Wing Tunnel Tests and Further Analysis of the Floating Wing Fuel Tanks for Helicopter Range Extension, Volume 2, Ground and Air Mechanical Instability Analysis. TREC 60-65, Vertol-Boeing Report No. R-197, October 1960.

17. P. F. Leone, Theory of Rotor Blade Uncoupled Flap Bending Aeroelastic Vibrations. Proceedings Tenth Annual AHS Forum, May 1954, Washington, D. C.

18. P. F. Leone, Theory of Rotor Blade Uncoupled Lag Bending Aeroelastic Vibrations. Proceedings Eleventh Annual AHS Forum, April 1955, Washington, D. C.

19. Army Study Requirement No. 3-60.

20. Horner, Dr. -Ing. Sighard F., Fluid Dynamic Drag.

21. Summary Report, High Performance Helicopter Study. Boeing-Vertol Report R-233. (TREC-TR 61-42)

GROWTH VERSIONS

The introduction into this contract of the YHC-1B series was based upon the realization that a satisfactory High Performance Helicopter would require the development of a new blade. Since the development of a new blade for the Chinook is as feasible as for the Boeing-Vertol 107, a brief study of performance potential with aircraft derived from the YHC-1B Helicopter was completed and is presented in this Appendix.

Three configurations are compared to the present YHC-1B:

1. Same power, same blade radius, but increased chord to 32.2 inches. Drag reduction yields an equivalent flat plate area of 25.0 square feet. This aircraft will permit feasibility testing for ferry range and 200 mile per hour speed, but exhibits poor short range payload and productivity characteristics. This is a consequence of decrease in useful load at basically constant gross weight.

2. A growth version of the preceeding helicopter is shown which uses advanced ratings for the T-55-L-5 engine. The radius remains at 29.5 feet and 32.2 inch chord. The engine development period would allow a further reduction of equivalent flap plate area to 18 square feet.

3. An increased radius version with no change in the engine characteristics. The rotor was resized to recoup the useful load of the present YHC-1B. The rotor radius becomes 30.8 feet with a chord of 26 inches. The equivalent flat plate area is 25.0 square feet.

Table XXXV summarizes the weights and performance for the three derivations of the present YHC-1B. The normal gross weight is defined from a hover ceiling criteria of 6,000 feet at 95°F day. The ferry range overload gross weight is found from a 500 FPM rate of climb, NRP at S.L.

The Army's primary need at this time is a large improvement in ferry range capability to enable self-transportability of tactical and logistics helicopters to the combat zone in the event of hostilities. The bar chart below, Figure 131, illustrates at zero headwind, the payload-range characteristics for sea level and 10,000 feet, maximum altitude without oxygen equipment.

FIGURE 131

FERRY RANGE, CHINOOK SERIES

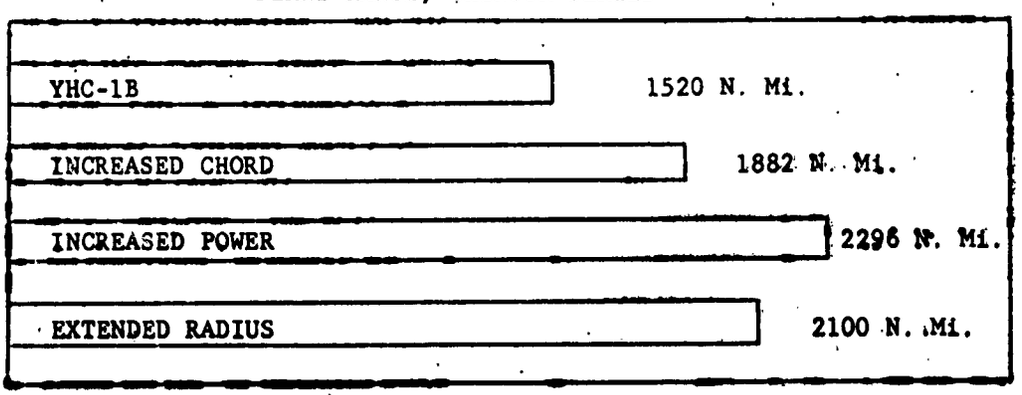


TABLE XXXV

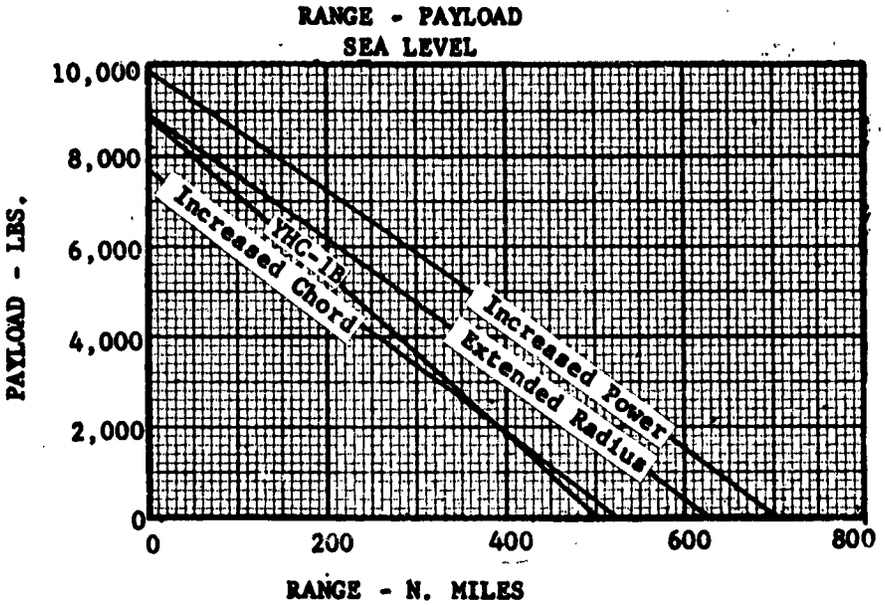
SUMMARY OF WEIGHTS AND PERFORMANCE

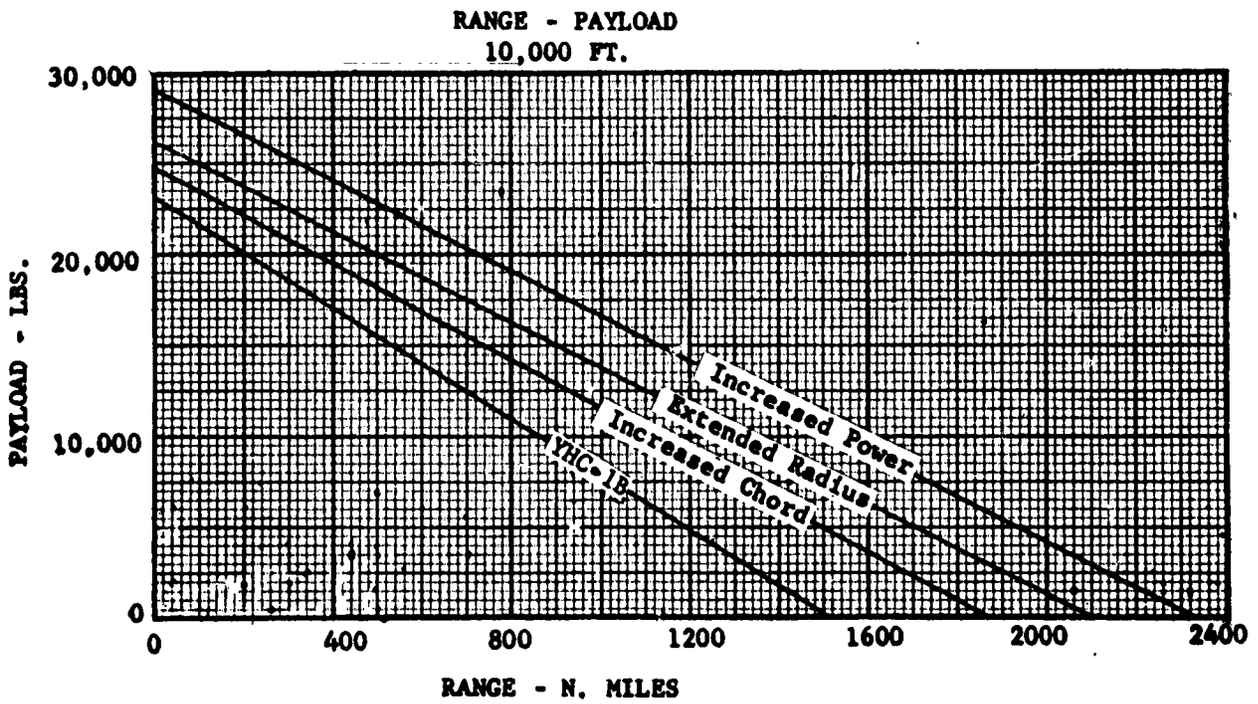
			CHINOOK SERIES			
		Unit	YHC-1B	Increased Chord	Increased Power	Increased R Advanced YHC-1B
DESCRIPTION	Rotor Radius/Rotor Solidity	ft./-	29.5/.0620	29.5/.0861	29.5/.0861	30.8/.0672
	Rotor Chord/No. of Blades	in./-	23/3	32.2/3	32.2/3	26/3
	Rotor Twist/Rotor Tip Speed	deg./fps	-9/710	-14/675	-14/685	-14/675
	Rotor Airfoil Section	--	0012	0009.5	0009.5	0009.5
	Equiv. Flat Plate Area	$ft.^2$	43.0	25.2	18.0	25.2
	No. of Eng./Eng. Designation	--	(2)T-55-L-5	(2)T-55-L-5	(2)T55ADV.	(2)T-55-L-5
	Military Power Per Eng.	SHP	2200	2200	2500	2200
	Normal Rated Power Per Eng.	SHP	1850	1850	2200	1850
WEIGHTS	Rotor Group	lbs.	3030	3655	3735	3430
	Body Group	lbs.	3662	3787	3987	3890
	Landing Gear Group	lbs.	938	1138	1138	1220
	Flight Controls	lbs.	1021	1021	1061	1046
	Propulsion Group	lbs.	5218	5218	5368	5218
	Instr., Nav., & Aux. Power Plant	lbs.	282	282	282	282
	Hydr. Elect. & Electronics Group	lbs.	942	942	942	942
	Furn. & Equip. Group	lbs.	1015	1015	1015	1015
	Weight Empty	lbs.	16138	17058	17528	17043
	Useful Load	lbs.	9512	8492	10777	9512
	Fixed Useful Load	lbs.	662	662	662	662
	Fuel (100 N. Mi. Radius)	lbs.	3453	3040	2880	3069
	Payload (Outbound only)	lbs.	5397	4790	7235	5781
	Gross Weight	lbs.	25650	25550	28305	26555
PERFORMANCE	Hover Ceiling @ 95°F, O.G.E.	ft.	6000	6000	6000	6000
	Max. Speed, Mil. Pow., S.L.	Knots	159	185	202	183
	Max. Speed, N.R.P., S.L.	Knots	152	177	195	176
	Speed For Best Range, S.L.	Knots	130	168	181	167
	Fwd R/C, NRP, S.L.	fpm	2440	2355	2790	2330
	Ferry Range	n.mi.	1520	1882	2296	2100
	Assoc. G.W. For Ferry Range*	lbs.	41300	43925	50200	45300

* 500 FPM R/C @ S.L. NRP

Figure 132 illustrates, at zero headwind, the payload-range characteristics for sea level and 10,000 feet.

FIGURE 132

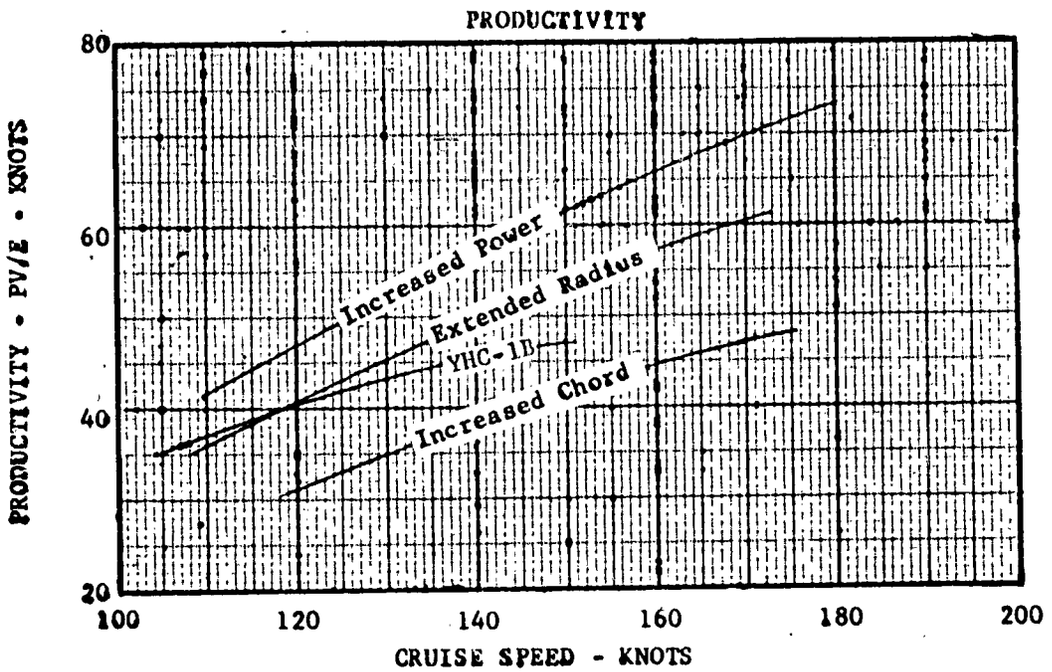




Productivity (PV, payload times forward speed) is often employed as a criterion to compare aircraft efficiency in transport applications. A more meaningful parameter, however, has been found to be the ratio of the productivity to empty weight (PV/E) as this is proportional to ultimate economic criterion, ton/nautical miles per dollar.

The parameter, PV/E, plotted against forward speed is shown in Figure 133 below.

FIGURE 133

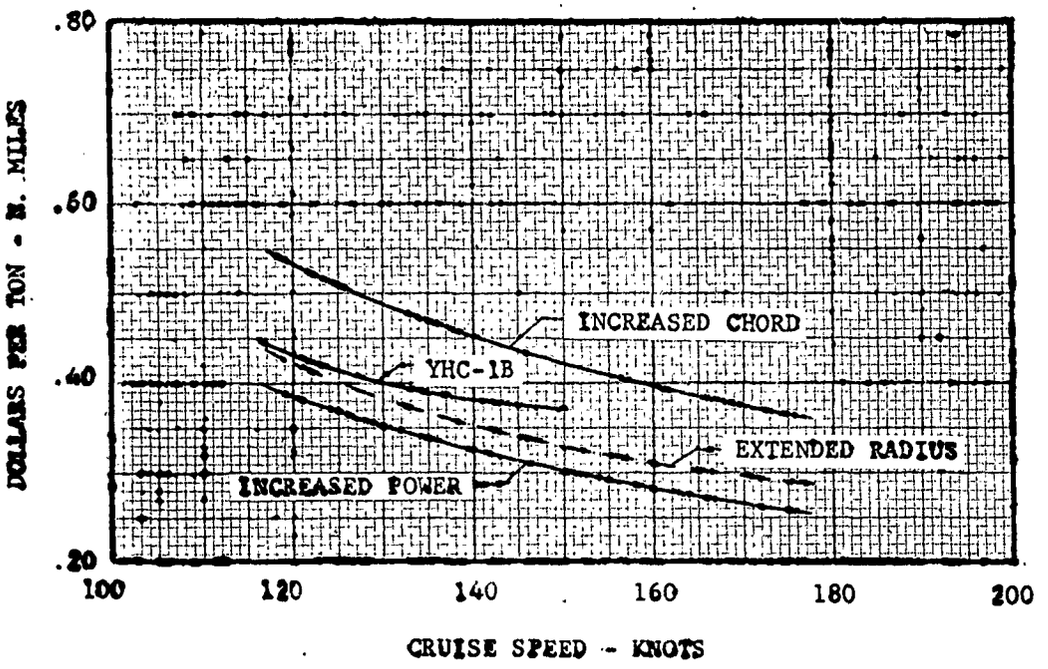


PV/E optimizes at speeds close to maximum forward speed rather than best range speed which means that best overall economy is attained by consuming more fuel and flying as fast as possible.

The maintainability, expressed in dollars of maintenance cost per ton nautical mile, is shown in Figure 134.

FIGURE 134

MAINTAINABILITY



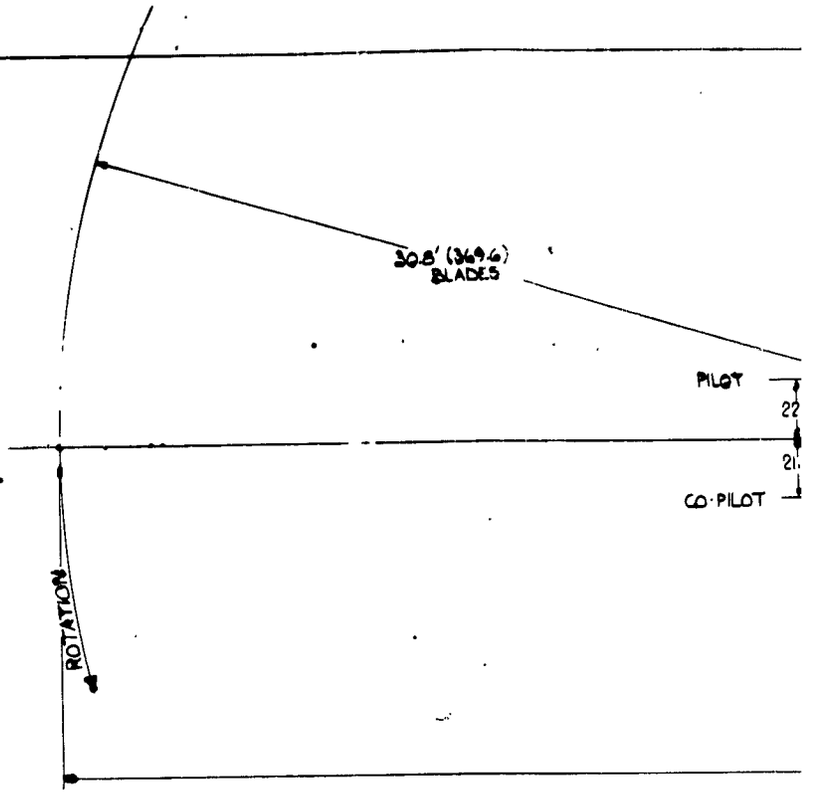
The maintenance dollars per flight hour was derived from studies of present helicopter operation extrapolated to turbine powered versions as a function of weight empty and installed power.

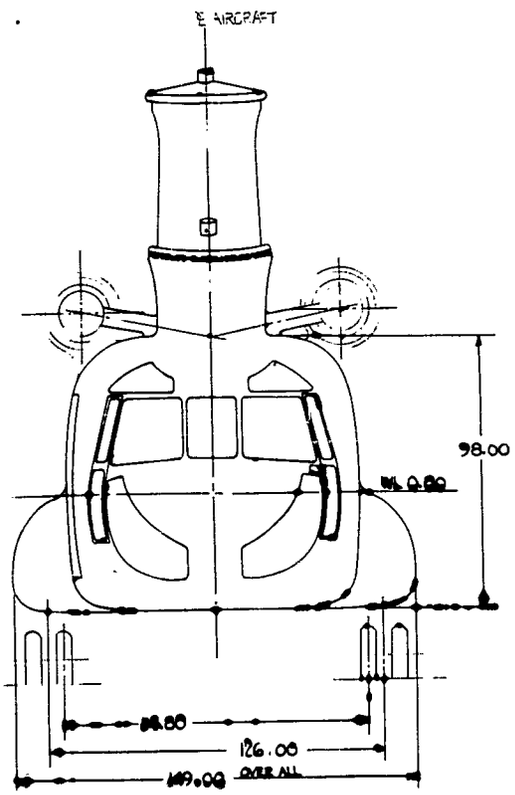
SUMMARY OF GROWTH VERSIONS

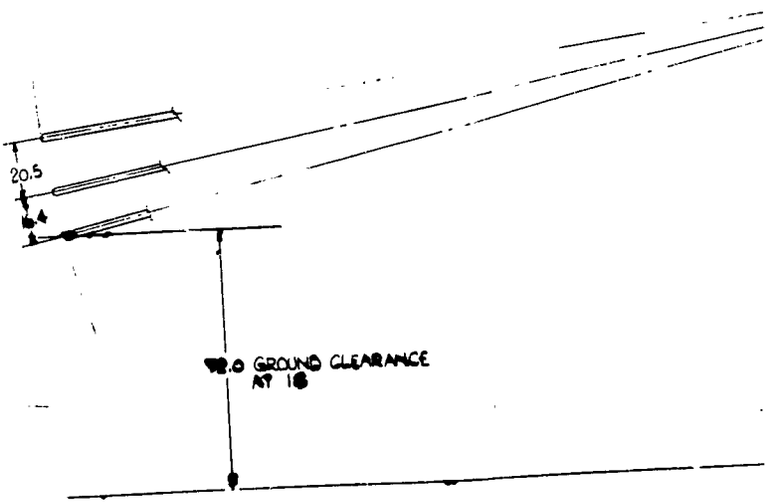
A review of the various means for achieving increased performance with configurations derived from the present YHC-1B has been made. The performance potential can be realized using an operational aircraft by either an increase in power available or decrease in power required by extended radius, the more efficient method being the latter.

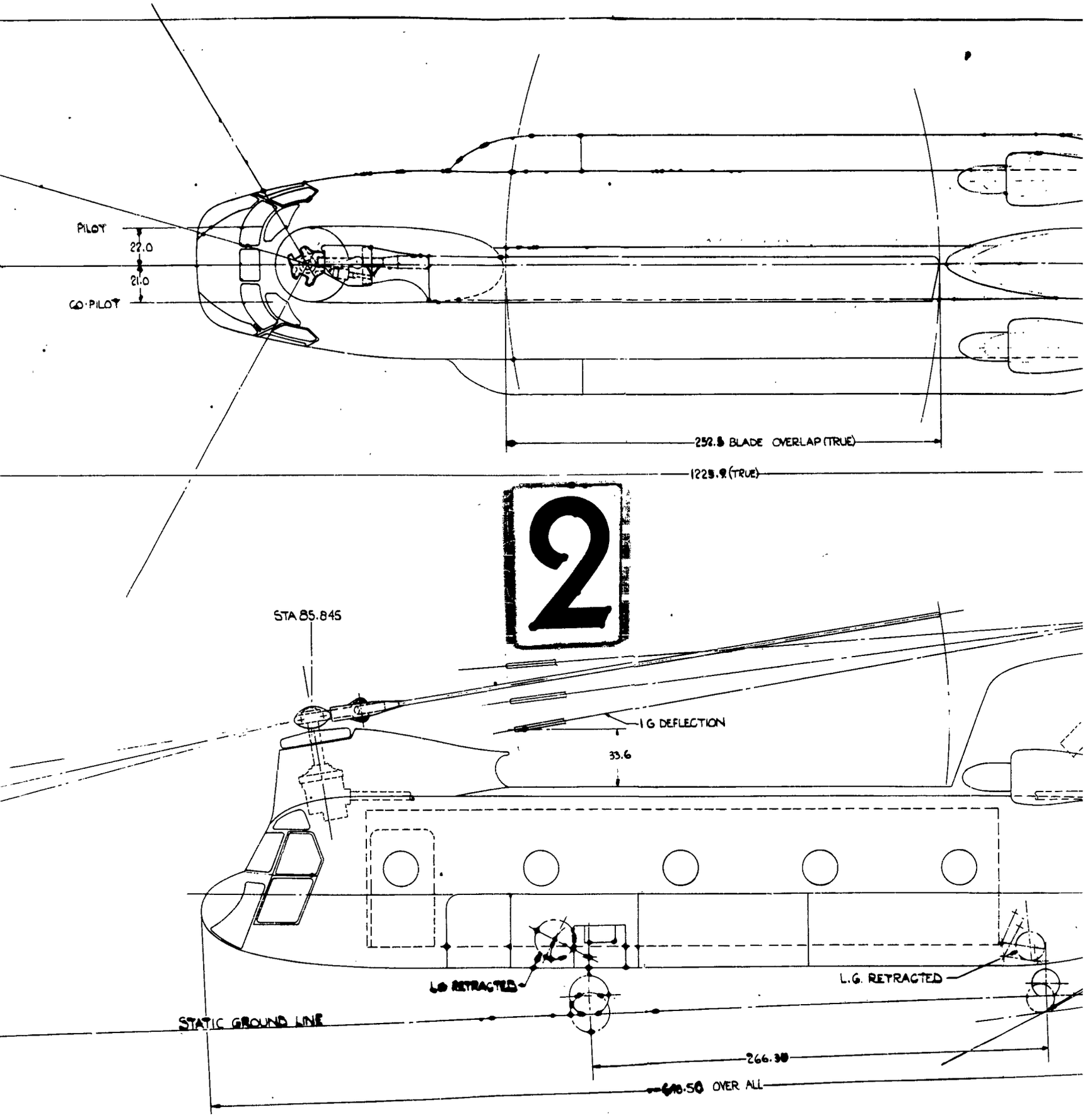
To establish an operational helicopter the loss in payload due to a weight empty increase, required by drag reduction, must be recouped. If not, both productivity and maintainability suffer. Excellent increases in range and maximum and cruise speeds will still result, however, as shown by the performance of the prototype research vehicle.

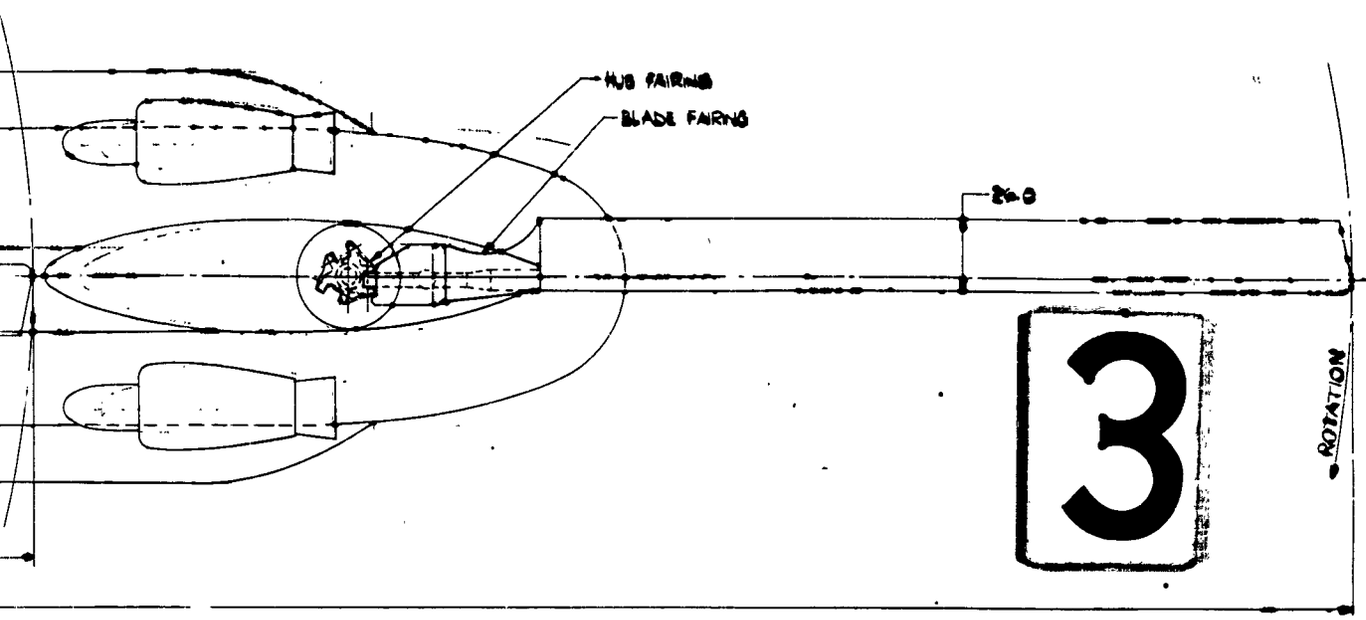

1

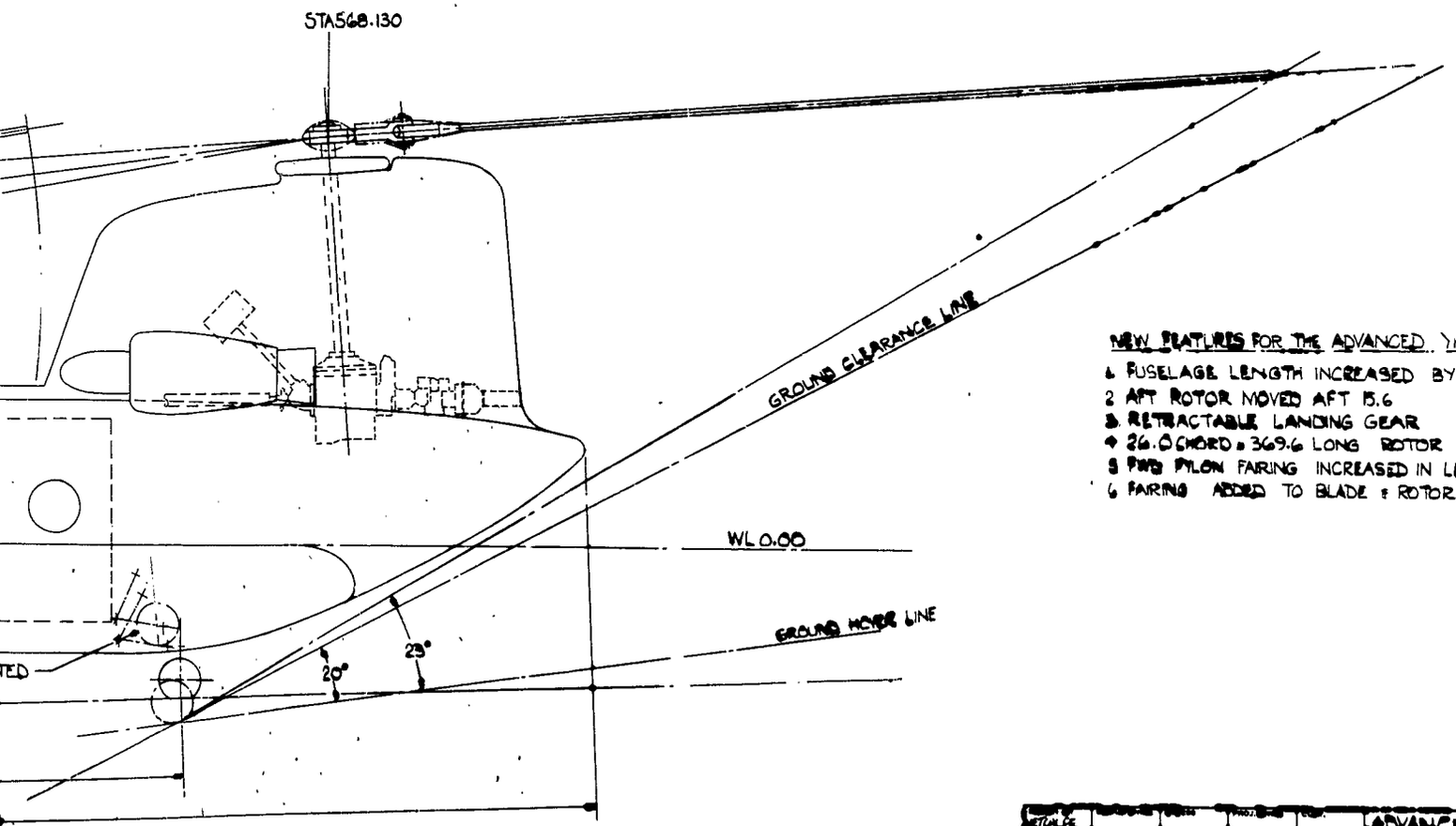

30.8' (369.6)
BLADES
PILOT
CO-PILOT
ROTATION


E AIRCRAFT
98.00
88.80
126.00
149.00 OVER ALL


20.5
GROUND CLEARANCE
AT 18


PILOT
22.0
21.0
CO-PILOT
252.5 BLADE OVERLAP (TRUE)
1229.9 (TRUE)
2
STA 85.845
1 G DEFLECTION
33.6
L.G. RETRACTED
L.G. RETRACTED
STATIC GROUND LINE
266.38
OVER ALL

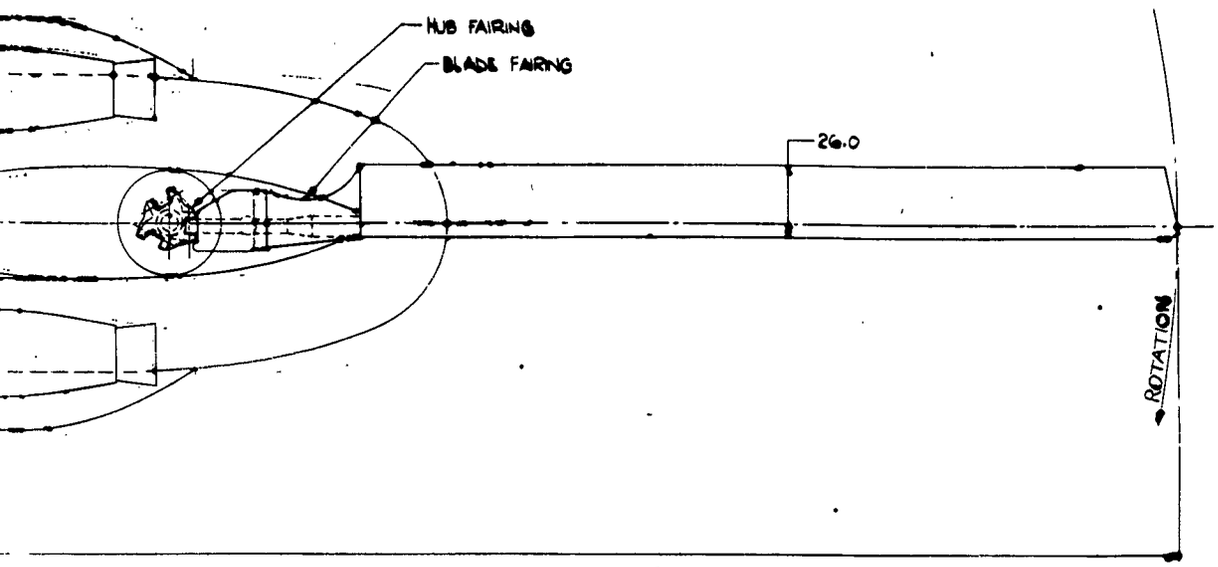




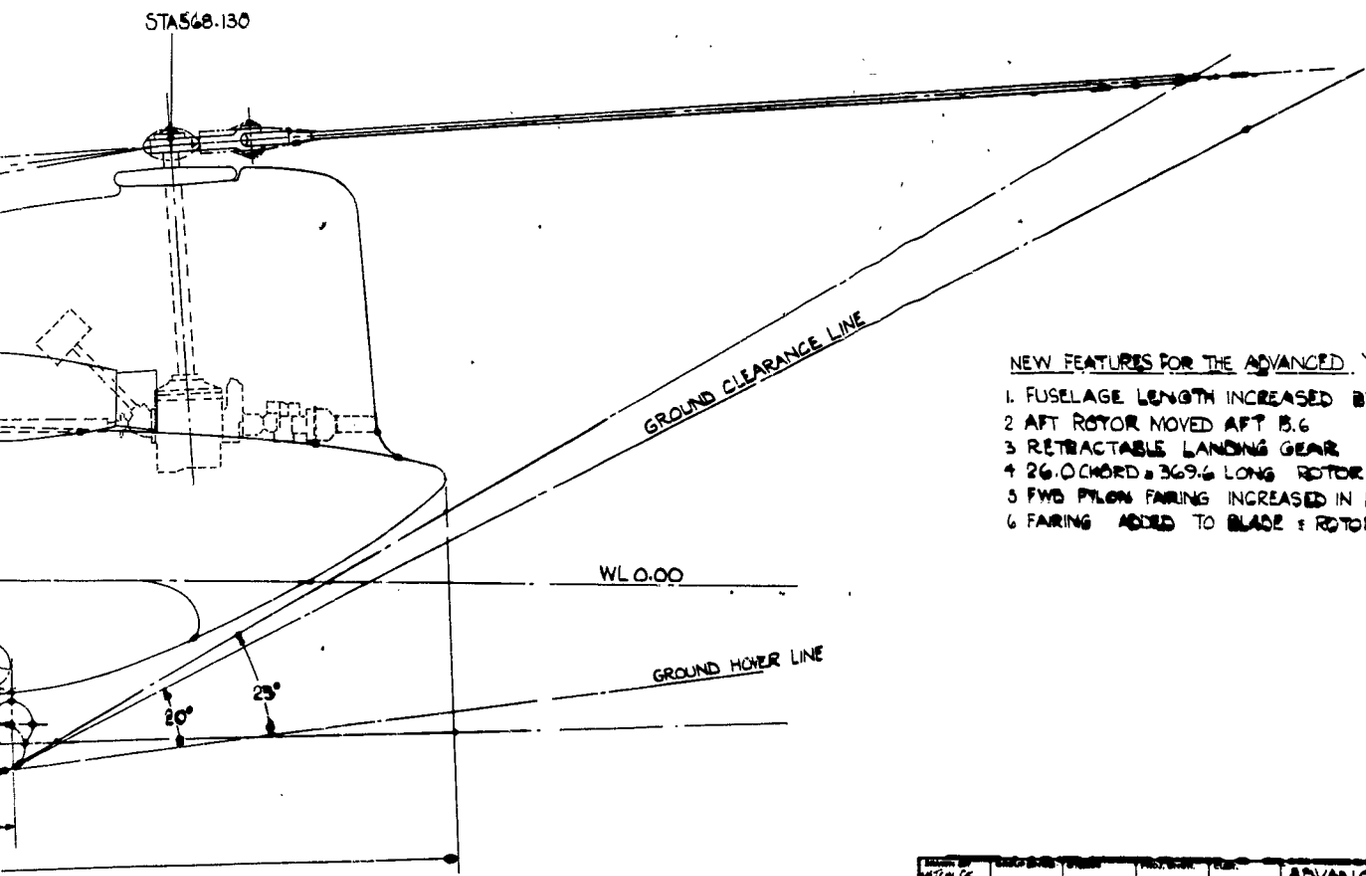
NEW FEATURES FOR THE ADVANCED YHC-1B

1. FUSELAGE LENGTH INCREASED BY 39.5
2. AFT ROTOR MOVED AFT 15.6
3. RETRACTABLE LANDING GEAR
4. 26.0 CHORD x 369.6 LONG ROTOR BLADES
5. FWD PYLON FAIRING INCREASED IN LENGTH
6. FAIRING ADDED TO BLADE & ROTOR HUB

ADVANCED YHC-1B



4



NEW FEATURES FOR THE ADVANCED VHC-1B

1. FUSELAGE LENGTH INCREASED BY 39.5
2. AFT ROTOR MOVED AFT 15.6
3. RETRACTABLE LANDING GEAR
4. 26.0 CHORD x 369.6 LONG ROTOR BLADES
5. FWD PYLON FAIRING INCREASED IN LENGTH
6. FAIRING ADDED TO BLADE ℄ ROTOR HUB

ADVANCED VHC-1B

VERTOL

SK10314

Logistics Support

The requirements for U. S. Army transport aircraft for the 1965-70 time period were the subject of recent industry-wide studies (ASR-3-60). Vertol's contribution, as reported in Reference 19, visualized the Vertol 107 as applicable to the following missions in the combat zone:

a. Combat group tactical missions of 25 nautical mile radius, or less, within the combat zone from battle group area to FEBA.

b. Logistical resupply missions of 75-100 nautical mile radius from division rear to battle group area.

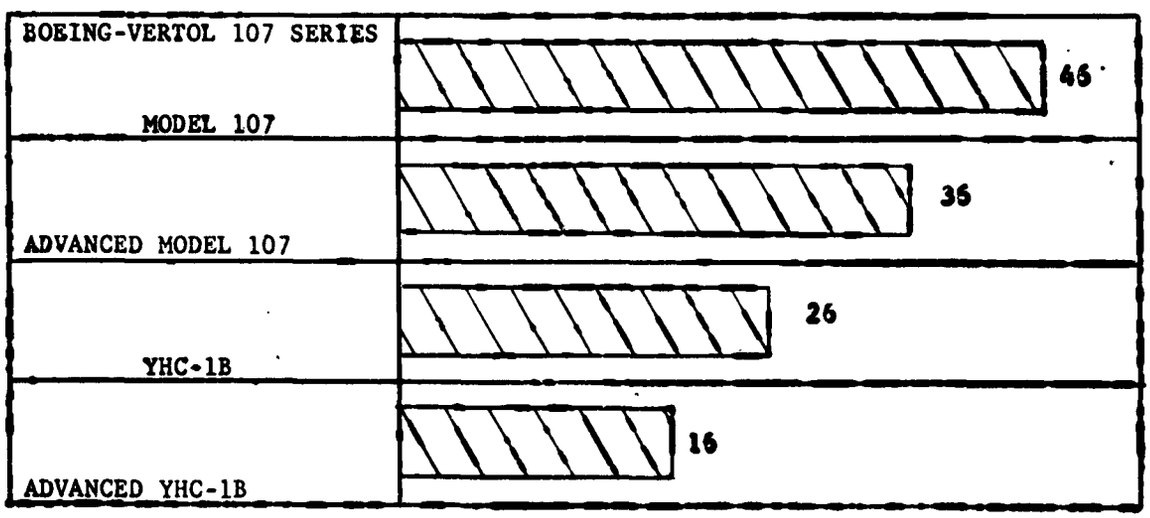
The YHC-1B capability was found relevant to these missions, plus longer range logistical resupply missions of 300 to 400 nautical mile radius.

The effect of performance improvements in these two aircraft on the numbers of aircraft required per Army division is shown in the following chart for the short range logistical mission. As in ASR-3, a logistical resupply for the five battle groups of the division is assumed to be 40 tons per group, or a total of 200 tons per division. Results of mission calculations assume an average usage of 4 hours per day for each aircraft in the total complement, based upon an availability of 67% of total aircraft and average usage of available aircraft of 6 hours per day.

The utilization of advanced Vertol 107 helicopters is seen to reduce the required number of aircraft from 46 to 36, or 21.8%. The advanced YHC-1B 26 to 19 would permit a 27.0% reduction. These gains, which are presented as a measure of procurement requirements and hence lower cost, are a direct result of the improvement in speed capability. The bar graph below summarizes the results of this comparison.

FIGURE 135

NUMBER OF AIRCRAFT REQUIRED



APPENDIX OF STRESS CALCULATIONS FOR ROTOR HUB SECTION

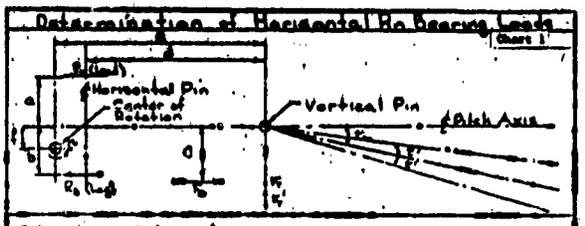
ROTOR HUB ANALYSIS

Horizontal Pin Bearing Lives and Slopes

The following pages contain a derivation of horizontal pin bearing loads for various flight conditions, cubic mean bearing loads and bearing lives. The critical pin slope at the bearings is calculated also.

Determination of Horizontal Pin Bearing Loads

Chart 1



P_o steady $= \frac{b}{a+b}(C.F.)_{FR} + \frac{d}{a+b} F_T$

R_o steady $= \frac{a}{a+b}(C.F.)_{FR} - \frac{d}{a+b} F_T$

$R_{all_o} = \pm\left(\frac{1}{a+b}\right)\sqrt{[c(F_T)]^2 + c^2[F_T - F_T']^2}$

$F_T' = \frac{(C.F.)_{FR}(f')}{1+f'/r}\left[2 - \left(\frac{1-\frac{MF_R}{T_{FR}}}{10\frac{MF_R}{T_{FR}}}\right)(10+f')\right]$

a =	3.771 inches
b =	3.600 inches
c =	6.662 inches
d =	16.188 inches
e =	21.50 inches
f =	20.85 inches
a+b =	7.460 inches
$\frac{b}{a+b}$ =	0.506
$\frac{a}{a+b}$ =	0.494
$\frac{d}{a+b}$ =	2.17
$1+f'/r$ =	1.244
f' =	0.0349 Radians

Forward Rotor

$\frac{f'}{10+f'}$ =	0.02806
$10+f'$ =	10.0349
M_F =	64.0
M_{FR} =	17.28
M_{FA} =	2.72
I_{FR} =	10,240
$\frac{MF_R}{I_{FR}}$ =	0.1262
$\frac{MF_A}{I_{FR}}$ =	0.02656
$1-\frac{MF_R}{I_{FR}}$ =	0.8738
$1+\frac{MF_A}{I_{FR}}$ =	1.0266
$\frac{1-\frac{MF_R}{I_{FR}}}{10\frac{MF_A}{I_{FR}}}$ =	0.798
$\left(1+\frac{MF_R}{10\frac{MF_A}{I_{FR}}}\right)(10+f')$ =	0.946
$\frac{f'}{10+f'}\left[2-\left(\frac{1-\frac{MF_R}{I_{FR}}}{10\frac{MF_A}{I_{FR}}}\right)(10+f')\right]$ =	0.0256

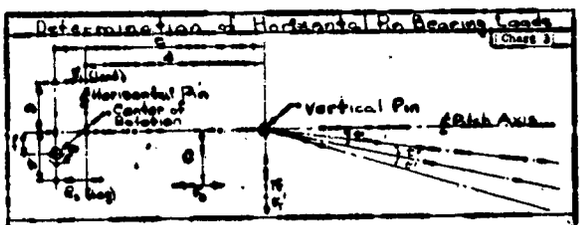
Determination of Horizontal Pin Bearing Loads

Chart 2

Forward Rotor	Flight Conditions	Static	Cruise	Max Power Climb	Transition	Hover O.G.E.	Autorotation
①	$(C.F.)_{FR}$	52,150#	46,040#	48,200#	47,600#	47,600#	47,600#
②	F_T	1815	357	2070	1734	2023	-3110
③	$\frac{a}{a+b}$ · ①	26,500#	23,300#	24,900#	24,100#	24,100#	24,100#
④	$\frac{b}{a+b}$ · ①	25,950#	22,740#	24,300#	23,500#	23,500#	23,500#
⑤	$\frac{d}{a+b}$ · ②	3940	780	4800	2680	4400	-6750
⑥	P_o steady ③ + ⑤	29,890#	23,520#	28,800#	26,180#	27,900#	16,750#
⑦	R_o steady ④ − ⑤	22,560#	22,310#	20,400#	21,420#	18,780#	30,850#
⑧	$(C.F.)_{AR}$	49,000	43,200	46,000	44,550	44,550	44,550
⑨	F_T'	±1450#	±1280#	±1361#	±1320#	±1826#	±1926#
⑩	F_T	1150	1150	1150	1150	1150	1150
⑪	d · ⑧	23,500	20,700	22,100	21,400	21,400	21,400
⑫	c · ⑨	7,630	7,630	7,630	7,630	7,630	7,630
⑬	⑪ + ⑫	31,130	28,330	29,730	29,030	29,030	29,030
⑭	Θ'	9.65 ×10⁻⁶	8.00 ×10⁻⁶	8.41 ×10⁻⁶	8.41 ×10⁻⁶	8.41 ×10⁻⁶	8.41 ×10⁻⁶
⑮	F_o	1800	1770	1790	1780	1780	1790
⑯	⑩ − ⑨	650	620	640	630	630	630
⑰	Θ'	0.00421 ×10⁻⁶	0.00384 ×10⁻⁶	0.00405 ×10⁻⁶	0.00396 ×10⁻⁶	0.00396 ×10⁻⁶	0.00396 ×10⁻⁶
⑱	C^2 · ⑰	0.1842 ×10⁻⁶	0.1675 ×10⁻⁶	0.1768 ×10⁻⁶	0.1730 ×10⁻⁶	0.1730 ×10⁻⁶	0.1730 ×10⁻⁶
⑲	⑭ + ⑱	9.8042 ×10⁻⁶	8.1675 ×10⁻⁶	8.5768 ×10⁻⁶	8.5730 ×10⁻⁶	8.5730 ×10⁻⁶	8.5730 ×10⁻⁶
⑳	$\sqrt{⑲}$	31,400	28,600	30,000	29,800	29,800	29,800
㉑	$\cos^{-1}\frac{⑯}{⑳}$	±8210#	±8030#	±8020#	±8010#	±8010#	±8010#

Determination of Horizontal Pin Bearing Loads

Chart 3



P_i steady $= \frac{b}{a+b}(C.F.)_{AR} + \frac{d}{a+b} F_T$

R_i steady $= \frac{a}{a+b}(C.F.)_{AR} - \frac{d}{a+b} F_T$

$R_{all_i} = \pm\left(\frac{1}{a+b}\right)\sqrt{[c(F_T')]^2 + c^2[F_T - F_T']^2}$

$F_T' = \frac{(C.F.)_{AR}(f')}{1+f'/r}\left[2 - \left(\frac{1-\frac{MF_R}{I_{AR}}}{10\frac{MF_A}{I_{AR}}}\right)(10+f')\right]$

a =	3.771 inches
b =	3.682 inches
c =	6.662 inches
d =	16.188 inches
e =	21.50 inches
f =	20.85 inches
a+b =	7.452 inches
$\frac{b}{a+b}$ =	0.506
$\frac{a}{a+b}$ =	0.494
$\frac{d}{a+b}$ =	2.19
$1+f'/r$ =	1.245
f' =	0.0349 Radians

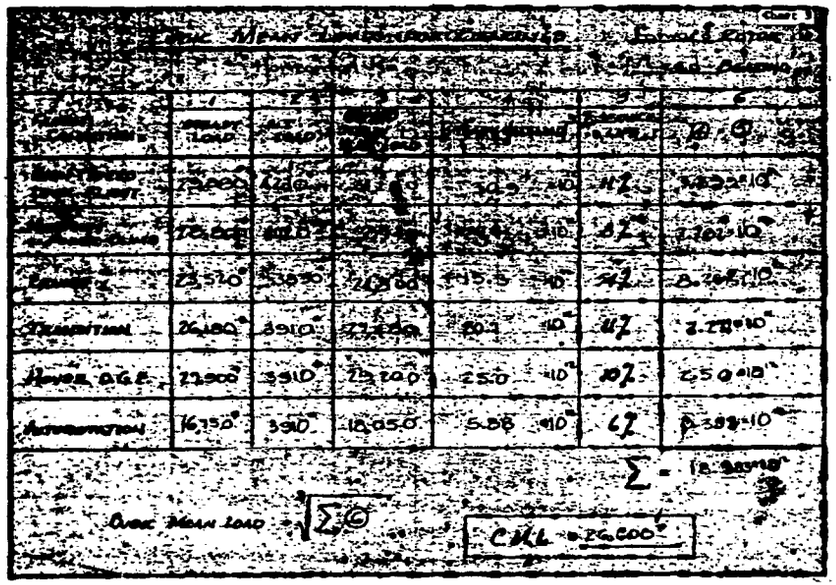
Aft Rotor

$\frac{f'}{10+f'}$ =	0.0220
$10+f'$ =	10.124
M_F =	51.2
M_{FR} =	11.17
M_{FA} =	8.29
I_{AR} =	9,690
$\frac{MF_R}{I_{AR}}$ =	0.1152
$\frac{MF_A}{I_{AR}}$ =	0.0856
$1-\frac{MF_R}{I_{AR}}$ =	0.8848
$1+\frac{MF_A}{I_{AR}}$ =	1.0856
$\frac{1-\frac{MF_R}{I_{AR}}}{10\frac{MF_A}{I_{AR}}}$ =	0.814
$\left(1+\frac{MF_R}{10\frac{MF_A}{I_{AR}}}\right)(10+f')$ =	0.965
$\frac{f'}{10+f'}\left[2-\left(\frac{1-\frac{MF_R}{I_{AR}}}{10\frac{MF_A}{I_{AR}}}\right)(10+f')\right]$ =	0.0220

Determination of Horizontal Pin Bearing Loads

Chart 4

Aft Rotor	Flight Conditions	Static	Cruise	Max Power Climb	Transition	Hover O.G.E.	Autorotation
①	$(C.F.)_{AR}$	46,800#	40,920#	43,780#	42,300#	42,300#	42,300#
②	F_T	429	170	852	728	1518	-2830
③	$\frac{a}{a+b}$ · ①	28,550#	25,700#	27,100#	26,400#	26,400#	26,400#
④	$\frac{b}{a+b}$ · ①	27,350#	24,620#	26,000#	25,300#	25,300#	25,300#
⑤	$\frac{d}{a+b}$ · ②	930	370	1850	1580	3300	-6180
⑥	P_i steady ③ + ⑤	29,480#	26,070#	28,950#	27,980#	29,700#	19,220#
⑦	R_i steady ④ − ⑤	26,420#	24,250#	24,150#	25,020#	22,600#	31,480#
⑧	$(C.F.)_{AR}$	44,600	39,280	41,900	40,500	40,500	40,500
⑨	F_T'	1295	1140	1213	1177	1177	1177
⑩	F_T	1150	1150	1150	1150	1150	1150
⑪	d · ⑧	20,900	18,450	19,700	19,000	19,000	19,000
⑫	c · ⑨	7,630	7,630	7,630	7,630	7,630	7,630
⑬	⑪ + ⑫	30,530	26,080	27,330	26,630	26,630	26,630
⑭	Θ'	8.8 ×10⁻⁶	6.8 ×10⁻⁶	7.43 ×10⁻⁶	7.1 ×10⁻⁶	7.1 ×10⁻⁶	11 ×10⁻⁶
⑮	F_o	1800	1790	1790	1780	1780	1780
⑯	⑩ − ⑨	650	620	640	630	630	630
⑰	Θ'	0.00423 ×10⁻⁶	0.00384 ×10⁻⁶	0.00405 ×10⁻⁶	0.00396 ×10⁻⁶	0.00396 ×10⁻⁶	0.00396 ×10⁻⁶
⑱	C^2 · ⑰	0.1842 ×10⁻⁶	0.1675 ×10⁻⁶	0.1768 ×10⁻⁶	0.1730 ×10⁻⁶	0.1730 ×10⁻⁶	0.1730 ×10⁻⁶
⑲	⑭ + ⑱	9.0842 ×10⁻⁶	6.8675 ×10⁻⁶	7.6068 ×10⁻⁶	7.2730 ×10⁻⁶	7.2730 ×10⁻⁶	7.2730 ×10⁻⁶
⑳	$\sqrt{⑲}$	30,800	26,400	27,600	27,000	27,000	27,000
㉑	$\cos^{-1}\frac{⑯}{⑳}$	±4190#	±3840#	±3700#	±3620#	±3620#	±3620#

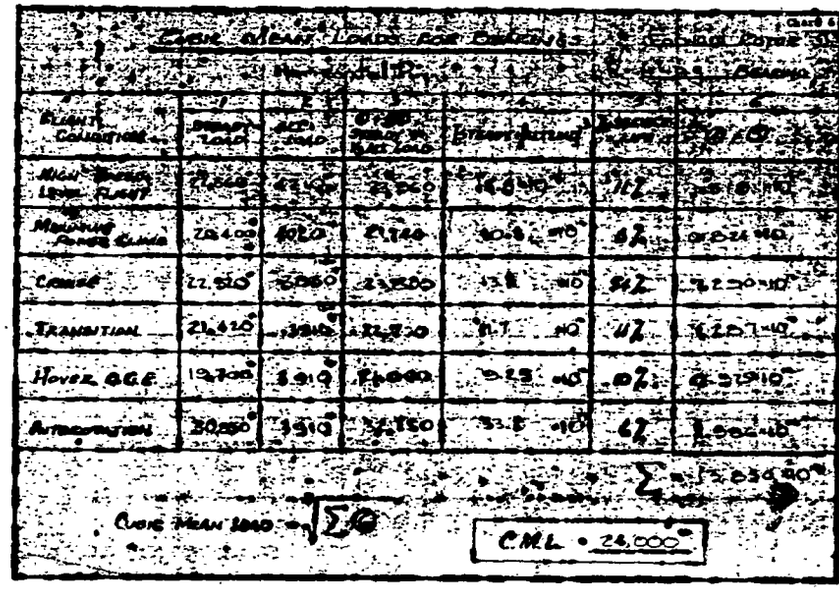


CUBIC MEAN LOADS FOR CONDITIONS

FLIGHT CONDITION	1 STEADY LOAD	2 ALT. LOAD	3 (1)+(2) STEADY + ½ ALT. LOAD	4 FREQUENCY FACTOR	5 EXPONENT FACTOR	6 (3)^n × (4)
HIGH SPEED LEVEL FLIGHT	23,000	4,000	25,000	1.0 ×10^0	3	1.563×10^13
MANEUVER PULL-UP	23,450	3,900	25,400	1.0 ×10^0	3	1.638×10^13
CRUISE	23,510	3,980	25,500	1.5 ×10^0	3	2.668×10^13
TRANSITION	21,480	3,910	23,400	1.0 ×10^0	3	1.278×10^13
HOVER OGE	21,900	3,910	23,800	2.5 ×10^0	3	3.500×10^13
AUTOROTATION	16,350	3,910	18,305	5.0 ×10^0	3	5.109×10^13

$\Sigma = 15.856 \times 10^{13}$

CUBIC MEAN LOAD $= \sqrt[3]{\Sigma \textcircled{6}}$ CML = 24,000

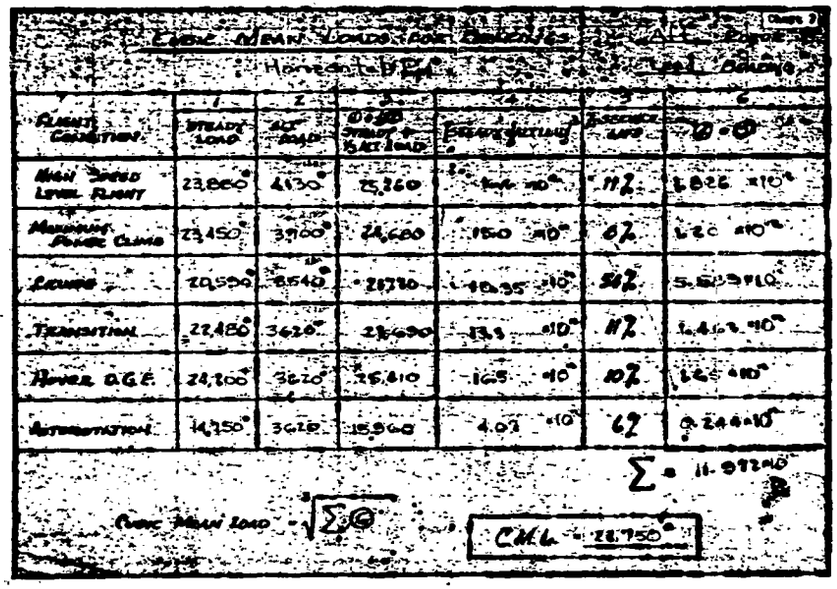


CUBIC MEAN LOADS FOR CONDITIONS

FLIGHT CONDITION	1 STEADY LOAD	2 ALT. LOAD	3 (1)+(2) STEADY + ½ ALT. LOAD	4 FREQUENCY FACTOR	5 EXPONENT FACTOR	6 (3)^n × (4)
HIGH SPEED LEVEL FLIGHT	23,000	4,000	25,000	1.0 ×10^0	3	1.563×10^13
MANEUVER PULL-UP	23,450	3,900	25,400	1.0 ×10^0	3	1.638×10^13
CRUISE	22,510	3,980	24,500	1.5 ×10^0	3	2.295×10^13
TRANSITION	21,480	3,910	23,400	1.0 ×10^0	3	1.278×10^13
HOVER OGE	19,900	3,910	21,800	2.5 ×10^0	3	2.315×10^13
AUTOROTATION	16,350	3,910	18,305	5.0 ×10^0	3	5.109×10^13

$\Sigma = 14.198 \times 10^{13}$

CUBIC MEAN LOAD $= \sqrt[3]{\Sigma \textcircled{6}}$ CML = 24,000

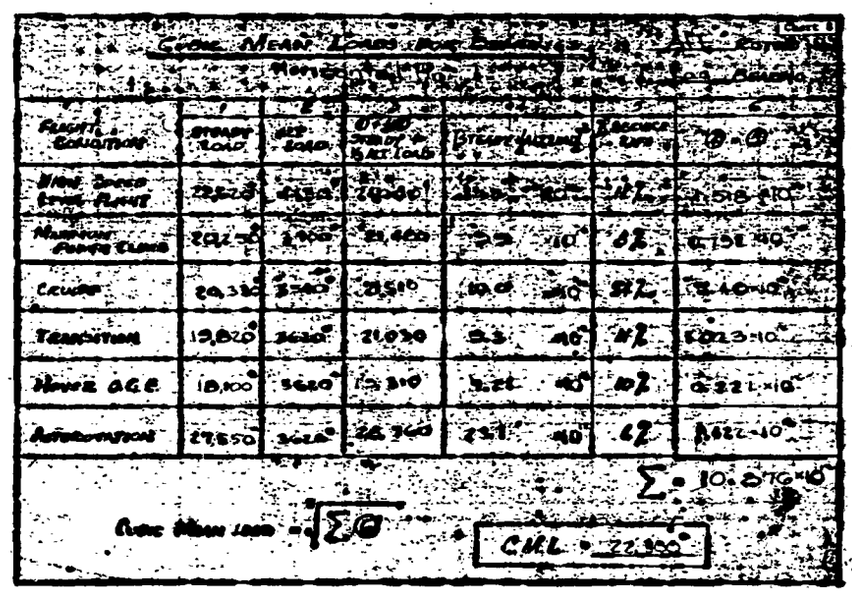


CUBIC MEAN LOADS FOR CONDITIONS

FLIGHT CONDITION	1 STEADY LOAD	2 ALT. LOAD	3 (1)+(2) STEADY + ½ ALT. LOAD	4 FREQUENCY FACTOR	5 EXPONENT FACTOR	6 (3)^n × (4)
HIGH SPEED LEVEL FLIGHT	23,850	4,150	25,360	1.0 ×10^0	3	1.632×10^13
MANEUVER PULL-UP	23,450	3,900	24,600	1.50 ×10^0	3	1.26 ×10^13
CRUISE	20,590	3,540	22,730	10.35 ×10^0	3	5.963×10^13
TRANSITION	22,480	3,620	24,690	13.3 ×10^0	3	1.463×10^13
HOVER OGE	24,100	3,620	25,910	1.65 ×10^0	3	1.46 ×10^13
AUTOROTATION	14,750	3,620	15,960	4.01 ×10^0	3	0.244×10^13

$\Sigma = 11.972 \times 10^{13}$

CUBIC MEAN LOAD $= \sqrt[3]{\Sigma \textcircled{6}}$ CML = 22,750



CUBIC MEAN LOADS FOR CONDITIONS

FLIGHT CONDITION	1 STEADY LOAD	2 ALT. LOAD	3 (1)+(2) STEADY + ½ ALT. LOAD	4 FREQUENCY FACTOR	5 EXPONENT FACTOR	6 (3)^n × (4)
HIGH SPEED LEVEL FLIGHT	23,850	4,150	25,960	1.0 ×10^0	3	1.750×10^13
MANEUVER PULL-UP	23,450	3,900	25,400	1.0 ×10^0	3	1.638×10^13
CRUISE	20,590	3,540	22,360	10.35 ×10^0	3	5.963×10^13
TRANSITION	19,820	3,620	21,630	5.3 ×10^0	3	1.603×10^13
HOVER OGE	18,100	3,620	19,910	5.21 ×10^0	3	0.321×10^13
AUTOROTATION	27,850	3,620	29,660	29.1 ×10^0	3	5.622×10^13

$\Sigma = 10.076 \times 10^{13}$

CUBIC MEAN LOAD $= \sqrt[3]{\Sigma \textcircled{6}}$ CML = 22,000

Chart 9

Bearing Lives

BV107-II

Forward Rotors — Life (cycles)

(CML) load = 22,600# — 1750 hrs.

(CML) lag = 20,250# — 1620 hrs.

Aft Rotors

(CML) load = 21,880#

(CML) lag = 19,810#

RV-BV107

Forward Rotors

(CML) load = 26,600#

(CML) lag = 24,000#

Aft Rotors

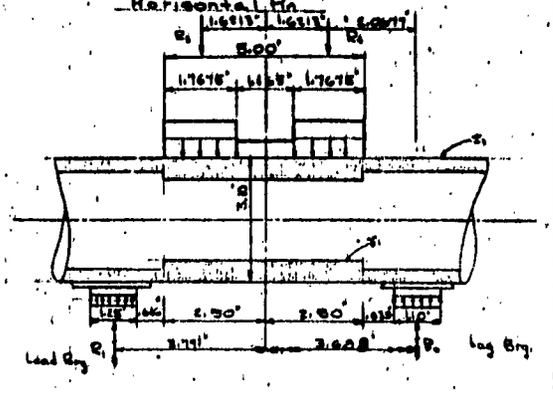
(CML) load = 22,780#

(CML) lag = 22,380#

Change in Life from BV107-II			to BV107 Life (cycles)
Fwd. Rotors	Load Brg. = $(\frac{22.6}{26.6})^3$ =	0.616	1070 hrs
	Lag Brg. = $(\frac{20.25}{24.0})^3$ =	0.600	965 hrs
Aft Rotors	Load Brg. = $(\frac{21.88}{22.78})^3$ =	0.885	1538 hrs
	Lag Brg. = $(\frac{19.81}{22.38})^3$ =	0.781	1373 hrs

Chart 10

Horizontal Pin



R_1 = 23,850# R_2 = 22,650#

(Vmax - Fwd Rotor - steady landing)

$R_1 = 9.000 + 2.0877 R_1 + 2.5000 R_2$

$R_2 = -0.8387 R_1 + 42,000$

$53,450 = R_1 + R_2$

$42,000 - 0.1613 R_1 = 53,450 - R_1$

$0.6613 R_1 = 12,450$

$R_1 = 17,100\#$

$R_2 = 35,350\#$

Chart 11

Horizontal Pin

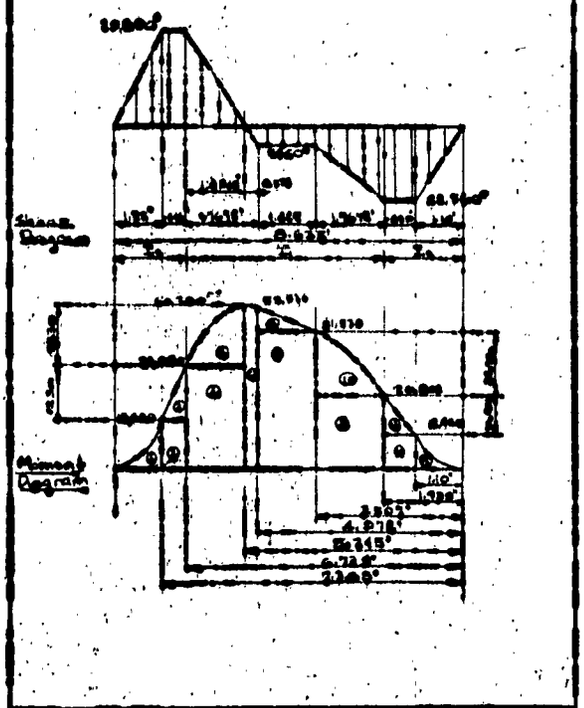


Chart 12

Horizontal Pin

Section	Area	Arm	Moment
①	$\frac{2780}{I_2}$	7.625	$\frac{59,000}{I_2}$
②	$\frac{13,100}{I_2}$	9.062	$\frac{265,500}{I_2}$
③	$\frac{6,240}{I_2}$	6.956	$\frac{43,300}{I_2}$
④	$\frac{56700}{I_1}$	5.552	$\frac{330,500}{I_1}$
⑤	$\frac{22,200}{I_1}$	5.615	$\frac{124,500}{I_1}$
⑥	$\frac{16,830}{I_1}$	5.108	$\frac{85,500}{I_1}$
⑦	$\frac{75,500}{I_1}$	4.240	$\frac{320,000}{I_1}$
⑧	$\frac{5,954}{I_1}$	4.408	$\frac{26,250}{I_1}$
⑨	$\frac{47,300}{I_1}$	2.623	$\frac{124,200}{I_1}$
⑩	$\frac{22,100}{I_1}$	3.062	$\frac{68,100}{I_1}$
⑪	$\frac{7,220}{I_2}$	1.438	$\frac{1,700}{I_2}$
⑫	$\frac{4,600}{I_2}$	1.313	$\frac{6,040}{I_2}$
⑬	$\frac{4,550}{I_2}$	0.275	$\frac{1250}{I_2}$

$\frac{282,800}{I_1} + \frac{43,150}{I_2}$ $\qquad$ $\frac{1,107,450}{I_1} + \frac{207,250}{I_2}$

load $Q_1' = \frac{1107.450}{I_1} + \frac{207.250}{I_2} \div \left[\frac{1422.4787}{I_1} + \frac{0.0276463}{I_2}\right]$

lag $R_1' = \left[\frac{832.3488}{I_1} + \frac{1489.3103}{I_2}\right] \times 10^{-3} R_2'$

$R_2' = \left[\frac{4.3900282}{I_1} + \frac{9.4616850}{I_2}\right] \times 10^{-3}$

Horizontal Pin

Lead Brg. $(\text{Slope})_{mom} = R_2 \cdot \frac{7.780}{2} \cdot \frac{1}{I_2} - \left[\frac{\text{[illegible]}}{I_2}\right] \times 10^{-6}$

$= \left[\frac{\text{[illegible]}}{I_1} + \frac{\text{[illegible]}}{I_2}\right] \times 10^{-6}$

Lag Brg. $(\text{Slope})_{mom} = R_2' \cdot \frac{4.220}{2 I_2} \cdot \frac{1}{2} \cdot R_2 \cdot \left[\frac{0.823916}{I_1}\right]$

$= \left[\frac{1.390888}{I_1} + \frac{0.623466}{I_2}\right] \times 10^{-6}$

Lead Brg. $(\text{Slope})_V = \frac{K_2 R_1 \omega_2 \times \text{Leff}}{33 \times 10^6}$

$= K_2(\omega_2 \text{Leff}) = \frac{20.850}{33 \times 10^6}$

$= K_2(\omega_2 \text{Leff}) = 0.509716 \times 10^{-3}$

$\omega_2 = 1'' \times \frac{0.833}{7.460} = \frac{1}{\text{Leff}}$

$(\text{Slope})_V = \underline{K_2 = 0.823988 \times 10^{-3}}$

Lag Brg. $(\text{Slope})_V = \frac{K_3 R_1 \omega_3 \times \text{Leff}}{33 \times 10^6}$

$= K_3(\omega_3 \text{Leff}) = \frac{22.360}{33 \times 10^6}$

$\omega_3 = 1'' \times \frac{0.833}{7.460} = \frac{1}{\text{Leff}}$

$(\text{Slope})_V = \underline{K_3 = 0.677816 \times 10^{-3}}$

Horizontal Pin

I_1 :

$0.D_1 = 5.16'' \quad I.D = 4.60''$

$I_1 = 4.0858\text{cm}^4$

Lead Brg. $(\text{Slope})_{mom} = 0.000,000,0891 \times \left[\frac{\text{illegible}}{I_2}\right]$

I_2 :

$0.D_2 = 5.16'' \quad I.D = 4.125''$

$I_2 = 4.0858\text{cm}^4$

$(\text{Slope})_{mom} = 0.000,000,0891 \times 0.000,190,68$

$= 0.000,116,066 \text{ in/in}$

$(\text{Slope})_{shear} = K_2 = 0.823988 \times 10^{-3}$

$\frac{a_i}{D_o} = 0.3683$

$K = 1.1685$

$K_2 = \frac{1.1685}{3.10 \times 1.375} = 0.274868$

$(\text{Slope})_{shear} = 0.000,227,857 \text{ in/in}$

Max. Total Slope - Lead Brg. = $0.000,343,924$ in/in

@ 104°F - II : $0.000,137,7$ in/in

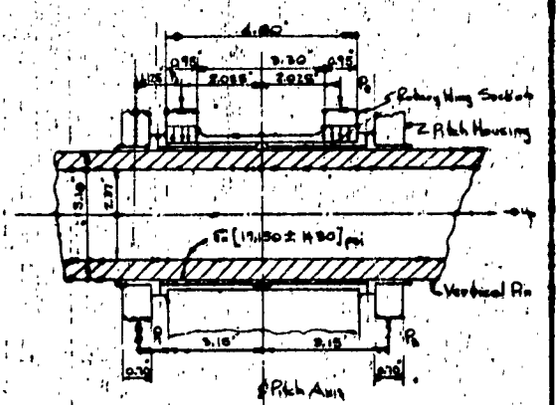
M-31 : $0.000,206,2$ in/in

Rotor Hub Analysis

Vertical Pin

The following charts contain a derivation of the fatigue loading on the vertical pin, and the critical stress is shown on the sketch of the pin.

Vertical Pin



R_2 : Chordwise Loads

R_1 : Vertical Loads

R_3 : Flapwise Loads

$R_2 = 5.60 R = 4.60 R_3$

$R_1 R_2 = R_1 R_3$

$3.60 R_1 = 4.60 R_1 = R_3$

$R_1 = 1.28 R = 0.278 R$

$R_3 = 1.28 R - 0.278 R$

Chart 16

V_{max} ~ Forward Rotor

Vertical Pin Loads

Loading	Value	P_{Ra}	P_{Rb}	P_{Lx}	P_{Ln}	P_{Sa}	P_{Sb}	P_{Sx}	P_{Sz}
$(C.F)_{A.R}$	49,000#	24,500#	24,500#	~	~	24,500#	24,500#	~	~
Flap. Moment	[34,600 ± 9,000]#	[5,810 ± 1,438]#	-[5,810 ± 1,438]#	~	~	[8580 ± 2280]#	-[8580 ± 2280]#	~	~
Pitching Moment	[9,820 ± 11,250]#	~	~	[1906 ± 1,998]#	-[1,606 ± 1,966]#	~	~	[2470 ± 3040]#	-[2470 ± 3040]#
F_T	1815#	~	~	907#	907#	~	~	907#	907#
F_T'	±1450#	~	~	± 725#	± 725#	~	~	± 725#	± 725#
Damper Load	± 600#	± 300#	± 300#	~	~	± 300#	± 300#	~	~
Total		[30,010 ± 2,938]#	[18,990 ± 538]#	[2410 ± 2280]#	-[660 ± 1230]#	[33,080 ± 3180]#	[15,920 ± 1380]#	[3380 ± 3760]#	-[1840 ± 2815]#

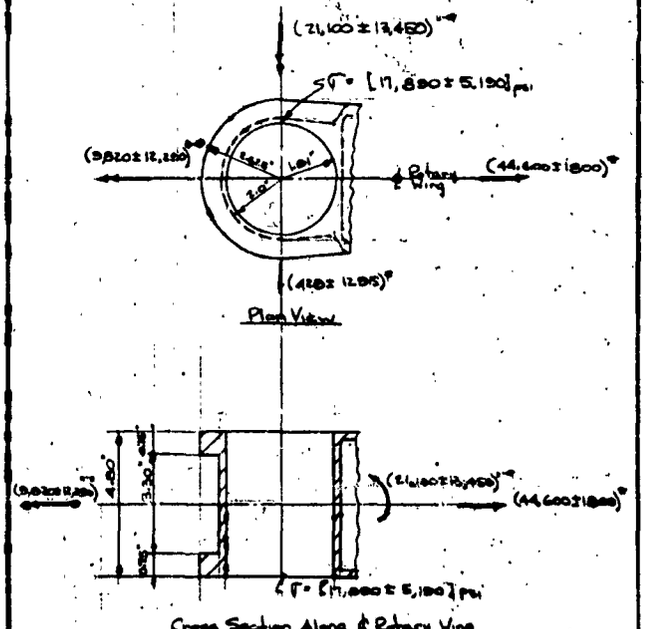
Rotor Hub Analysis

Rotary Wing Socket

The following chart shows the fatigue loading on the rotary wing socket. This loading is for the Aft Rotor, and is the critical condition. The critical stress is given also.

Chart 17

Rotary Wing Socket



Cross Section Along ℄ Rotary Wing

Rotor Hub Analysis

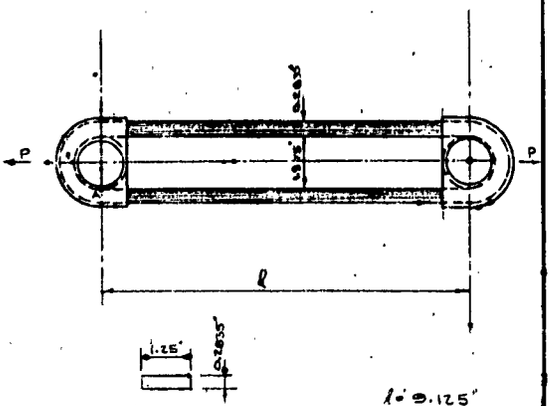
Wire Ply Tie Bar (Tension-Torsion Strap)

The following charts contain an analysis of the wire ply tie bar for both fatigue and limit maneuver conditions.

The tie bar is made by winding 250 rectangular wires (U.T.S. = 550,000 psi) around two end bushings. The wires are wound into a belt, 81 layers thick and 250 wires per layer. Each wire is coated with an elastomer, which binds the belt together and prevents fretting between individual wires.

Chart 18

Wire Ply Tie Bar



Belt Cross Section

ℓ = 9.125"

Θ = Twist Angle

Case I:

P = 49,000# (220 R.P.M.) Θ = 10.2° Fatigue

Case II:

P = 79,000# (330 R.P.M.) Θ = 22° Limit Maneuver

Chart 19

Wire Ply Tie Bar

Belt Width	= 1.25"
Belt Thickness	= 0.2835"
Belt Length	= 9.125" (Between Centers)
Dia. End	= 1.375"
Wire Size	= 0.003" × 0.0045"
Wire Coating	= 0.00025"
Finished Wire Size	= 0.0035" × 0.005"
Wires per Layer	= 250
Layers	= 81
Total Wires	= 20,250
Area per Wire	= 0.000012 in²

$$\frac{1}{\rho} = \frac{M}{EI}$$

$$M = \frac{EI}{\rho}$$

$$S = \frac{Mc}{I} = \frac{EI}{\rho} \times \frac{c}{I} = \frac{Ec}{\rho}$$

Chart 20

Wire Ply Tie Bar

Case I

Point C:

Tensile Stress

$$S_t = \frac{24{,}500\#}{0.000012 \times 20{,}250 \text{ wires}} = 101{,}000 \text{ psi}$$

Bending Stress

$$S = 29 \times 10^6 \times \frac{0.0015"}{0.6875"} = 63{,}300 \text{ psi}$$

Bearing Stress

$$S_b = -\frac{49{,}000\#}{1.25 \times 1.375"} \times \frac{.0045}{.00226 \text{ wire net}} = -49{,}300 \text{ psi}$$

Combined Stress

$S_t = 101{,}000 + 63{,}300 = 164{,}300$ psi

$S_r = -49{,}300$ psi Compression

$$S = \sqrt{S_t^2 + S_r^2 - S_t S_r}$$ ..... Constant Energy of Distortion Theory

$$= \sqrt{\frac{29{,}420 + 8100}{39{,}520}} \times 10^3$$

$S = 194{,}000$ psi

Chart 21

Wire Ply Tie Bar

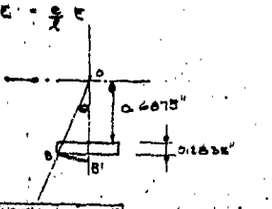
Point A:

Tensile Stress

S_t = 101,000 psi

Tensile stress due to Twisting

$S = \epsilon E = \frac{c}{\ell} E$



$OB = \sqrt{(.375)^2 + (0.9710)^2} = 1.1548"$

$BB' = Chord = OB - \Theta = 1.1548 - 0.1780$

$BB' = 0.20555"$



$AB = \ell = 5.125"$

$AB' = \sqrt{AB^2 + BB'^2}$

$\theta = AB' - AB$

$S = \left[\frac{AB'}{AB} - 1\right] E$

Chart 22

Wire Ply Tie Bar

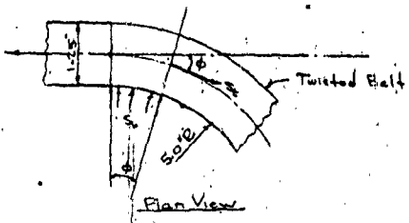
$AB' = \sqrt{\quad} = 5.1275"$

$S = [1.000025208 - 1]\,29 \times 10^6$

S = 7,310 psi

Bearing Stress

Assume that the wire next to the relieved exit flange of the end bushing is subject to the highest bearing stress.



$\phi = \frac{0.9710" \times 0.1780 \text{ Radians}}{5.125"} = 0.01695$ Radians

$= 1.085°$

Chart 23

Wire Ply Tie Bar

$S_b = R \cdot \phi \cdot \frac{0.003"}{2} = S_t \times \phi \times 0.0000012" \times 250$ Wire Length

$S_b = \frac{S_t \times 0.0000214 \times 250}{0.0032" \text{ 5" Radius}} = S_t \times 0.40$

$S_b = [7,310 + 101,000] \times 0.40$

S_b = 43,320 psi

Steady Stress = 101,000 psi

Oscillating Stresses:

Twisting ±10.2° = 7,310 psi

Bending (5"R) = $\frac{Ec}{R} = \frac{29 \times 10^6 \times 0.0025}{5"}$ = 13,000 psi

Bearing (5"R) = −43,320 psi

Combined Oscillating Stress

$= \sqrt{(20,310)^2 + (43,320)^2 + 20,310 \times 43,320}$

$= 10^3 \sqrt{411 + 1870 + 872 \cdot 3160}$

= 56,300 psi peak to peak

= ± 28,150 psi

Stress Level = [129,150 ± 28,150] psi

[MHC-18 Wire Ply · (130,800 ± 28,400) psi]

Chart 24

Wire Ply Tie Bar

Case II

Point C:

Tensile Stress

$S_t = \frac{P}{A} = \frac{\frac{1}{4} \cdot 79,000}{0.0000012" \times 29 \times 250 \text{ Wires}}$ = 162,500 psi

Bending Stress

$S = \frac{c}{\ell} \cdot E$ = 63,300 psi

Bearing Stress

$S_b = -\frac{79,000}{1.25 \times 1.375} \cdot \frac{.0045}{.0026} = -79,750$ psi

Combined Stress

$\sigma = \sqrt{S_r^2 + S_t^2 - S_r \cdot S_t}$

S_r = −79,750 psi

S_t = 225,800 psi

$\sigma = 10^3 \sqrt{63.30 + 50,800 + 18,000}$ −79,750

σ = 274,500 psi Limit

[MHC-18 Wire Ply σ = 296,600 psi]

M.S. = $\frac{550,600}{1.8 \times 274,500} - 1 =$ 0.833

Chart 25

Wire Ply Tie Bar

Point A:

Tensile Stress

$S_t = 162,500$ psi

Tensile Stress due to Twisting

$OB = 1.1545"$

$\theta = 22° = 0.3840$ Radians

$BB' = 1.1545 \times 0.3840 = 0.4434$

$AB_1' = \sqrt{63.2653 + 0.1966} = 7.9599"$

$AB' = 7.9599"$

$S = \left[\frac{AB'}{AB} - 1\right] E = [0.00118 \times 29] = 34,230$ psi

$S_s = 34,230$ psi

Bending (5° Rad.)

$S = \frac{c}{\rho} E = 13,000$ psi

Bearing Stress

$S_b = 0.40 S_t$

$S_b = 0.40\ [162,500 + 34,230]$

$S_b = 78,692$ psi

Chart 26

Wire Ply Tie Bar

Combined Stress

$S_t = 162,500$ psi

$S_{bb} = 78,692$ psi

$S = 10^3 \sqrt{(13,000 + 61,804 + 13,800)^2 + (78,692)^2}$

$S = 238,000$ psi

[Wire Ply $S = 244,000$ psi]

M.S. $= \frac{250}{238} - 1 = 0.42$

Chart 27

Rotor Hub Analysis

Pitch Shaft

The following charts show the flapping and chord moment distribution on the pitch shaft, and a sketch of the pitch shaft showing the critical fatigue stresses.

Chart 28

Pitch Shaft

Fatigue Condition

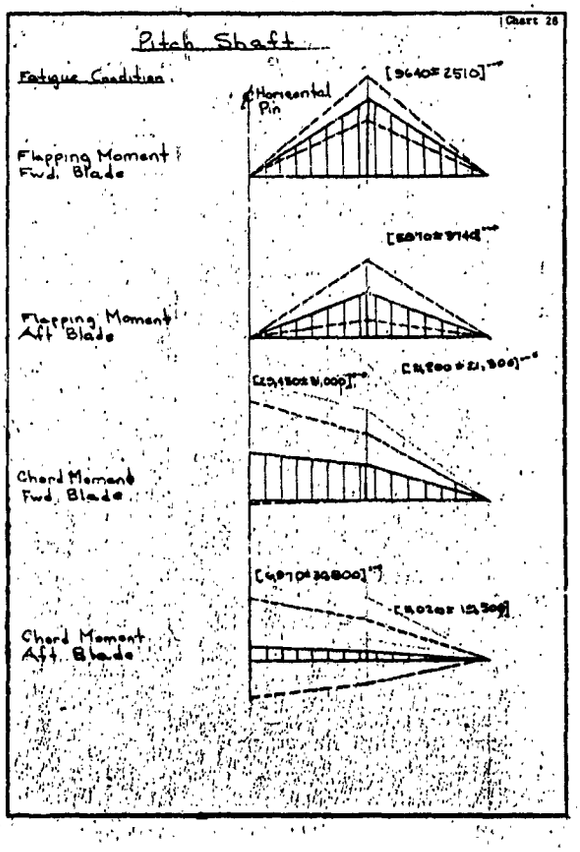
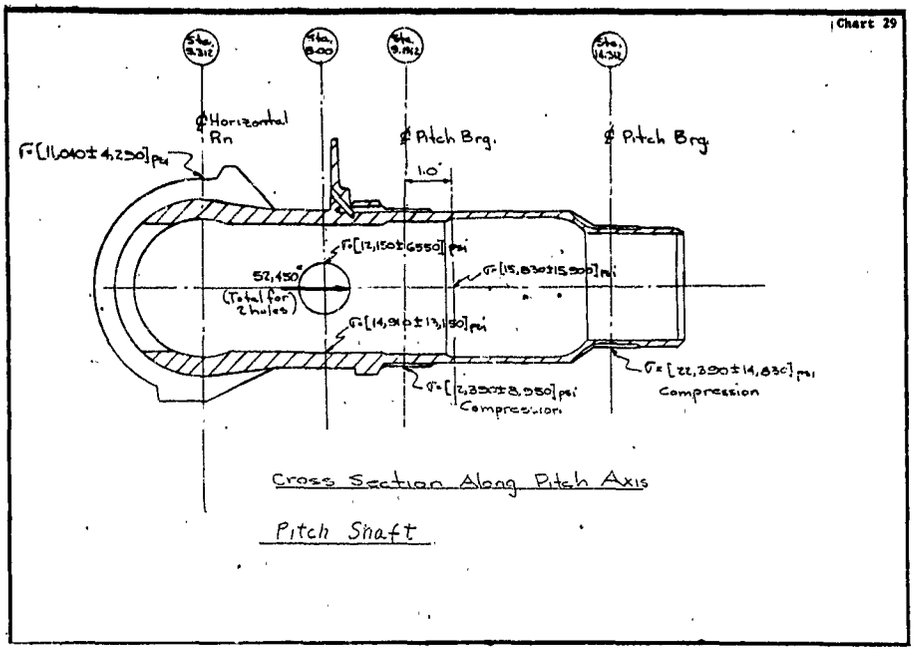


Chart 29



Cross Section Along Pitch Axis

Pitch Shaft

Rotor Hub Analysis

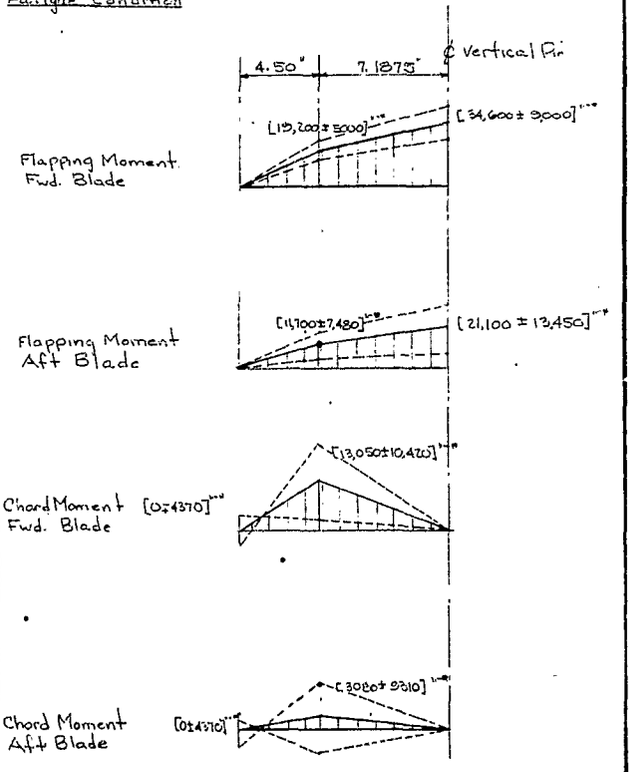
Pitch Housing

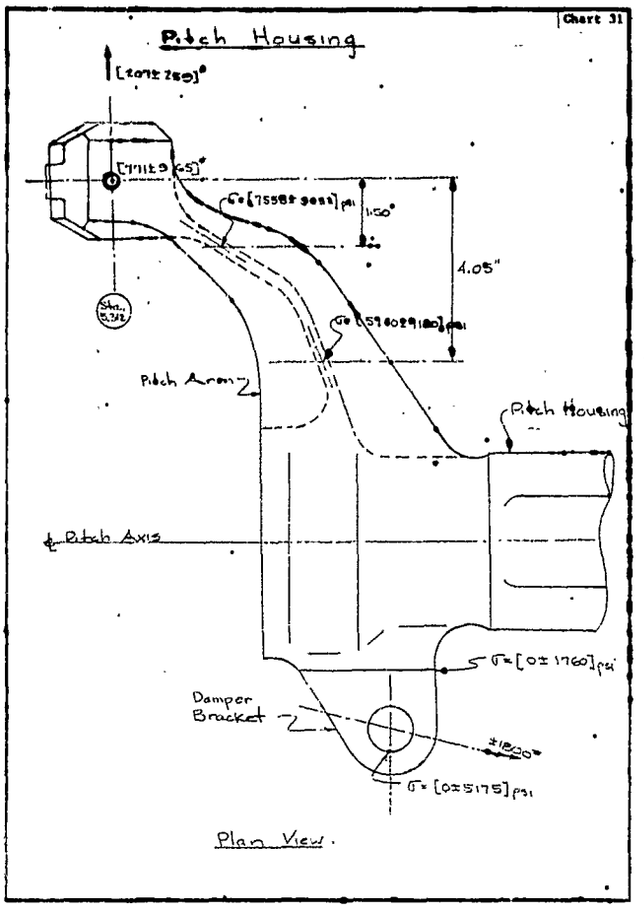
The following charts show the flapping and chord moment distribution on the pitch housing, and sketches of the pitch housing showing the critical fatigue stresses.

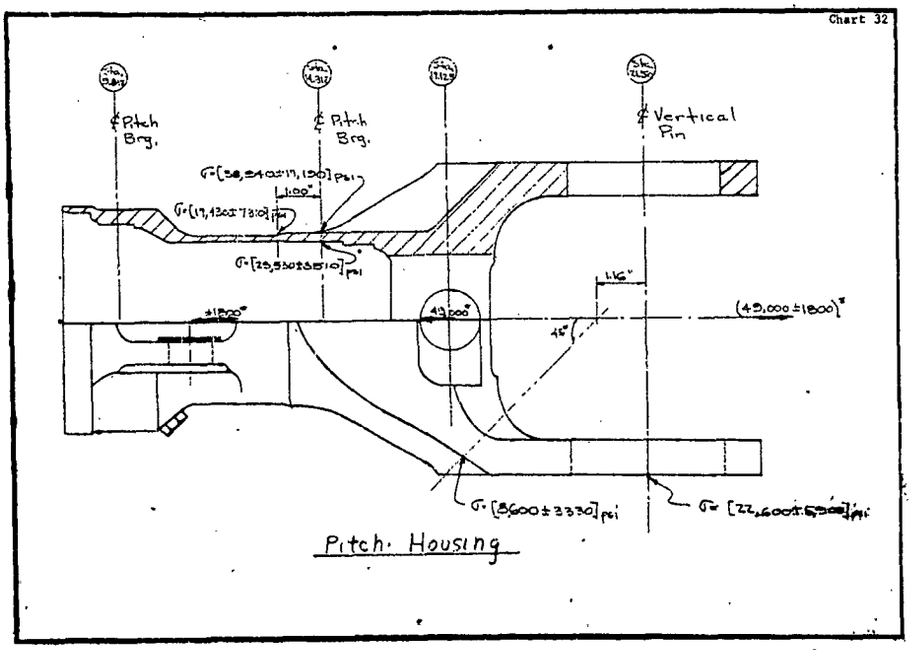
Chart 30

Pitch Housing

Fatigue Condition




Chart 31
Pitch Housing
4.05"
Pitch Arm
Pitch Housing
℄ Pitch Axis
Damper Bracket
Plan View.


Chart 32
℄ Pitch Brg.
℄ Pitch Brg.
℄ Vertical Pin
1.00"
1.16"
45°
Pitch Housing

Rotor Hub Analysis

Loads

The following charts contain the basic Loads on the Rotor Hub structure:

Chart 33

Loads

High Performance Helicopter
Ref. AVO of 12-30-60 to J. Mallen & W. Gittens

Flight Conditions	V	V_t ft/sec.	R.P.M.	Fwd. Rotor HP	Aft Rotor HP
Vmax	112 Kts.	680	260	1300	840
Cruise	141 Kts	640	244	840	725
Max. Power Climb	80 Kts.	660	252	1860	970
Transition	30 Kts.	650	248	1100	900
Hover O.G.E.	0	650	248	1300	1100
Autorotation	65 Kts.	600 estimated	248	0.	0

G.W. = 13,400# R = 25' c = 2.3" θ_{tw} = 14°
NASA 00098

V_t = Tip Speed
R.P.M. = Tip Speed $\frac{60}{25' \times 2\pi}$
= 0.382 × Tip Speed

Chart 34

Loads

Flight Condition	R.P.M.	$(CF)_{H.P.}$ Fwd.	$(CF)_{H.P.}$ Aft	$(C.F.)_{H.P.}$ Fwd.	$(CF)_{H.P.}$ Aft
Vmax	260	49,000#	44,600#	52,450#	46,500#
Cruise	244	43,200#	39,280#	46,040#	40,920#
Max. Power Climb	252	46,000#	41,800#	49,200#	43,700#
Transition	248	44,550#	40,500#	47,600#	42,300#
Hover O.G.E.	248	44,550#	40,500#	47,600#	42,300#
Autorotation	240	44,550#	40,500#	47,600#	42,300#

Aft Blade:
@ 248 R.P.M. $(CF)_{H.P.}$ = 45,200#
$(CF)_{H.P.}$ = 42,280#

Forward Blade:
$(CF)_{H.P.}$ = 49,820#
$(CF)_{H.P.}$ = 53,100#

$\left(\frac{260}{262}\right)^2$ = 0.985 $\left(\frac{248}{262}\right)^2$ = 0.855
$\left(\frac{252}{262}\right)^2$ = 0.925 $\left(\frac{244}{262}\right)^2$ = 0.867

Chart 35

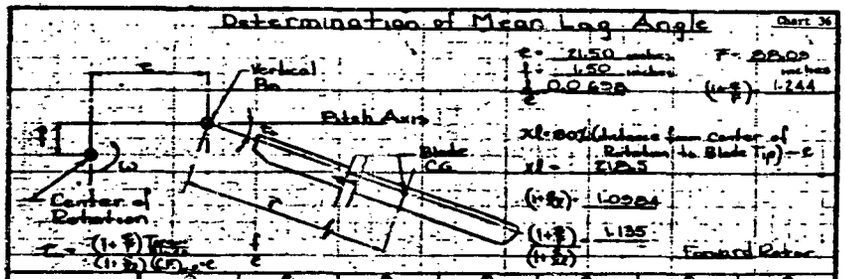
Loads

Flight Condition	R.P.M.	F_b damper force	Torque/Blade Fwd. Rotor	Torque/Blade Aft Rotor
Vmax	260	±1800#	112,200	95,800
Cruise	244	±1770#	72,300	62,400
Max. Power Climb	252	±1790#	118,300	80,900
Transition	248	±1780#	98,100	76,200
Hover O.G.E.	248	±1780#	110,000	93,000
Autorotation	248	±1780#	0	0

θ_{tw} = 2600 $\frac{\text{in}^\#}{\text{R.P.M.}}$
based on YHO-6B Damper Characteristics.

Determination of Mean Lag Angle

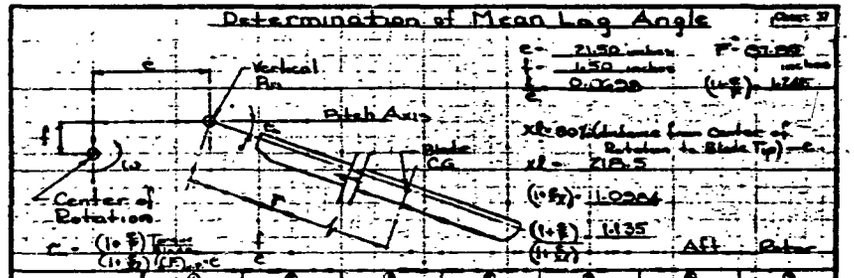
Chart 36



Flight Condition	① Torque / Blade	② (C.F.)$_{xl}$	③ (1+f/e) Torque / (1+f/xl)	④ ③/②×e	⑤ ④ − f/e×e (radians)	⑥ τ_m Degrees	⑦ Flattening from Column
Vmax	112,200	43,000	121,500	0.1210	0.0512	2.933°	2.2°
Cruise	72,300	43,200	82,200	0.0885	0.0187	1.071°	
Max Power Climb	113,300	46,000	128,700	0.1300	0.0602	3.450°	
Transition	93,100	44,550	106,000	0.1105	0.0407	2.333°	
Hover O.G.E.	110,000	44,550	125,000	0.1305	0.0607	3.478°	

Determination of Mean Lag Angle

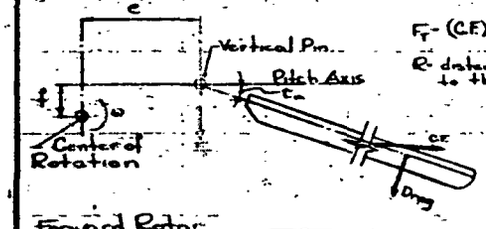
Chart 37



Flight Condition	① Torque / Blade	② (C.F.)$_{xl}$	③ (1+f/e) Torque / (1+f/xl)	④ ③/②×e	⑤ ④ − f/e×e (radians)	⑥ τ_m Degrees	⑦ Flattening from Column
Vmax	75,900	44,600	86,400	0.0900	0.0202	1.159°	.22°
Cruise	62,400	39,280	71,000	0.0840	0.0142	0.821°	
Max Power Climb	80,900	41,900	92,000	0.1022	0.0324	1.856°	
Transition	76,200	40,500	86,700	0.0955	0.0257	1.475°	
Hover O.G.E.	93,000	40,500	105,900	0.1215	0.0517	2.961°	

Determination of Drag Force - F_r

Chart 38



$F_r = (C.F.)_{xl}\left[\sin\tau_m - \frac{e}{(e+f)}\sin\left(\frac{f}{e}+\tau_m\right)\right] + \frac{\text{Torque}_{\text{Blade}}}{80\%\,R}$

R = distance from the center of rotation to the blade tip.

e = 21.50 inches. F = 88.09 inches

CF = 102.59 inches $\frac{e}{e+f}$ = 0.1962

R = 300 inches; 80%R = 240 inches

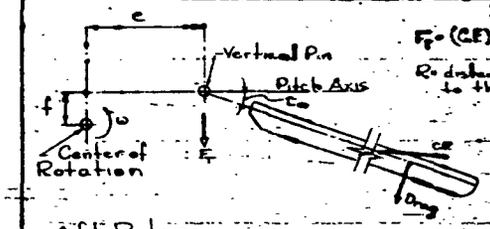
$\frac{f}{e}$ = 0.0698 = 4.00°

Forward Rotor

Flight Condition	① Torque / Blade / 80%R	② (C.F.)$_{xl}$	③ Sin τ_m	④ Sin($\frac{f}{e}+\tau_m$)	⑤ $\frac{e}{e+f}$ × ④	⑥ ① − ⑤	⑦ τ_m	⑧ Fr = ① + ⑥
Vmax	468°	43,000°	0.0512	0.1207	0.0237	0.0275	1347°	1815°
Cruise	301°	43,200°	0.0187	0.0884	0.0174	0.0013	56°	357°
Max Power Climb	472°	46,000°	0.0602	0.1297	0.0255	0.0347	1598°	2070°
Transition	388°	44,550°	0.0407	0.1103	0.0217	0.0190	846°	1234°
Hover O.G.E.	458°	44,550°	0.0607	0.1301	0.0256	0.0351	1565°	2023°
Autorotation	0	44,550°	−0.0698	0	0	−0.0698	−3110°	−3110°

Determination of Drag Force - F_r

Chart 39



$F_r = (C.F.)_{xl}\left[\sin\tau_m - \frac{e}{(e+f)}\sin\left(\frac{f}{e}+\tau_m\right)\right] + \frac{\text{Torque}_{\text{Blade}}}{80\%\,R}$

R = distance from the center of rotation to the blade tip.

e = 21.50 inches. F = 87.88 inches

CF = 102.35 inches $\frac{e}{e+f}$ = 0.1958

R = 300 inches; 80%R = 240 inches

$\frac{f}{e}$ = 0.0698 = 4.00°

Aft Rotor

Flight Condition	① Torque / Blade / 80%R	② (C.F.)$_{xl}$	③ Sin τ_m	④ Sin($\frac{f}{e}+\tau_m$)	⑤ $\frac{e}{e+f}$ × ④	⑥ ① − ⑤	⑦ τ_m	⑧ Fr = ① + ⑥
Vmax	316°	44,600	0.0202	0.0899	0.0177	0.0025	112°	428°
Cruise	260°	39,280	0.0142	0.0839	0.0165	−0.0023	−80°	170°
Max Power Climb	337°	41,900	0.0324	0.1021	0.0201	0.0123	515°	852°
Transition	317°	40,500	0.0257	0.0953	0.01955	0.01015	411°	728°
Hover O.G.E.	388°	40,500	0.0517	0.1211	0.0238	0.0279	1130°	1518°
Autorotation	0	40,500	−0.0698	0	0	−0.0698	−2830°	−2830°

Chart 40

Loads

Flapping Moment At Vertical Pin

BV107-II Gross Weight = 18,400#

Fwd. Blade - $M = [31,300 \pm 7,500]^{\#-ft}$

Aft Blade - $M = [20,000 \pm 11,200]^{\#-ft}$

RV-BV107 Gross Weight = 19,400#

The steady moments will increase by the ratio of rotor thrust of the RV-BV107 to the BV107-II, (i.e. will increase by the ratio of the gross weights of the two aircraft). It is estimated that the thrust on the forward rotor will be 5% higher due to the higher forward speed of the RV-BV107. The alternating moments are estimated to be 20% higher than the BV107-II.

Fwd Blade $M = [1.05 \times \frac{19.4}{18.4} \times 31,300 \pm 1.20 \times 7500]$

$M = [34,600 \pm 9,000]^{\#-ft}$

Aft Blade $M = [\frac{19.4}{18.4} \times 20,000 \pm 1.20 \times 11,200]$

$M = [21,100 \pm 13,450]^{\#-ft}$

Chart 41

Loads

Pitching Moment & Pitch Link Loads

$P = (1200 \pm 1500)^{\#}$ preliminary estimate

$M_P = 0.185 \times P = [8,820 \pm 12,250]^{\#-ft}$

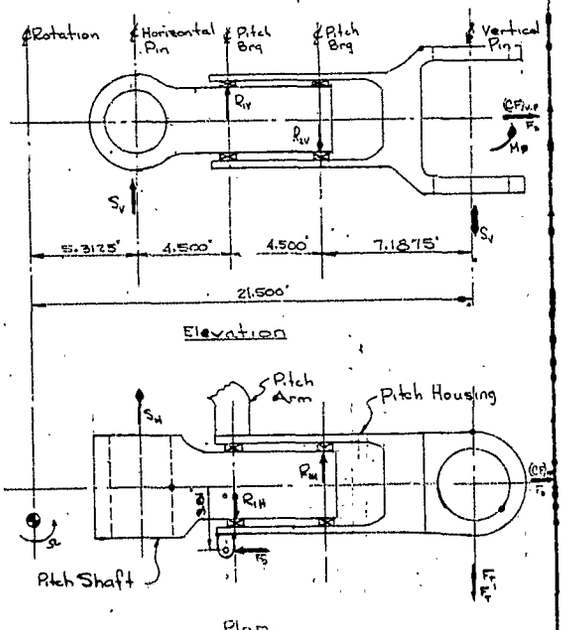
The estimated pitch link load is

$P = (795 \pm 995)^{\#}$

The above preliminary estimate was used in the analysis of the hub components, and is conservative.

Chart 42

Pitch Bearing Loads



Elevation

Plan

Chart 43

Pitch Bearing Loads

$S_V = [21.50 - 5.3125] \cdot M_P$

$S_V = \frac{M_P}{16.1875'}$

$R_{IV} \times 4.50' = M_P + 11.6875 S_V$

$= M_P - 0.722 M_P$

$= 0.278 M_P$

$R_{IV} = 0.06175 M_P$

$R_{IV} - R_{IV} = S_V$

$R_{IV} = S_V + R_{IV}$

$= \frac{M_P}{16.1875} + 0.06175 M_P$

$R_{IV} = 0.1235 M_P$

F_T & F_T' the damper preload (F_P) are in phase

$S_H = F_T \pm F_T'$

$4.50 R_{IH} - 11.6875 [F_T \pm F_T'] \mp 3.81 F_P = 0$

$R_{IH} = 2.60 [F_T \pm F_T'] \pm 0.845 F_P$

Chart 44

Pitch Bearing Loads

$$-R_{iH} + R_{vH} - [F_T \pm F_T'] \cdot 0$$

$$R_{iH} = 1.60[F_T \pm F_T'] \pm 0.845 F_p$$

Chart 45

Pitch Bearing Loads (V_{max})

Fwd. Blade. M_p = [34,600 ± 21000]*

Aft Blade M_p = [21,100 ± 13,450]*

Fwd. Blade S_V = [2,140 ± 556]*

Aft Blade S_V = [1,305 ± 831]*

Fwd. Blade R_{vV} = [2,140 ± 556]*

Aft Blade R_{vV} = [1,305 ± 831]*

Fwd. Blade R_V = [4,280 ± 1112]*

Aft Blade R_{iV} = [2,610 ± 1662]*

F_p = 1,150*

Fwd. Blade F_T = 1,815* F_T' = 1450* } ε's ± 2*

Aft Blade F_T = 428* F_T' = 1295* }

Fwd. Blade S_H = [1,815 ± 1450]*

Aft Blade S_H = [428 ± 1295]*

Fwd Blade R_{iH} = 4720 ± 3770 ± 975 = [4720 ± 4745]*

Aft Blade R_{iH} = 1115 ± 3360 ± 975 = [1115 ± 4335]*

Fwd. Blade R_{iH} = 2900 ± 2320 ± 975 = [2900 ± 3295]*

Aft Blade R_{iH} = 685 ± 2070 ± 975 = [685 ± 3045]*

DISTRIBUTION LIST

Vertol Report

"High Performance Tandem Helicopter Study"

Volume 2 - Design Analysis

Commanding General
United States Continental Army Command
ATTN: Materiel Developments
Fort Monroe, Virginia (1)

Headquarters
U. S. Army Aviation Test Office
ATTN: FTZAT
Edwards Air Force Base, California (1)

Chief of R&D
ATTN: Air Mobility Division
Department of the Army
Washington 25, D. C. (1)

Commander
Naval Air Test Center
ATTN: U. S. Army Liaison Officer
Patuxent River, Maryland (1)

Chief of Transportation
ATTN: TCDRD (1)
ATTN: TCAFO-R (1)
Department of the Army
Washington 25, D. C.

Commanding Officer
U. S. Army Transportation Combat Development Group (1)
Fort Eustis, Virginia

Commanding General
U. S. Army Transportation Materiel Command
ATTN: TCMAC-APU (2)
P. O. Box 209, Main Office
St. Louis 66, Missouri

Commandant
U. S. Army Transportation School
ATTN: Adjutant
Fort Eustis, Virginia (1)

Commanding Officer
U. S. Army Transportation Research Command
ATTN: DCO for Aviation (1)
ATTN: Long Range Technical Forecast Office (1)
ATTN: Executive for Programs (1)
ATTN: Research Reference Center (4)
ATTN: Aviation Directorate (5)
ATTN: Military Liaison & Advisory Office (4)
Fort Eustis, Virginia

Commanding Officer
U. S. Army Transportation Research Command Liaison Office
ATTN: MCLATS (2)
Wright Patterson AFB, Ohio

Chief
U. S. Army Research & Development Liaison Group (9851 DU)
ATTN: USATRECOM LO (1)
APO 757
New York, New York

Commander
Air Research & Development Command
ATTN: RDR-LA (1)
Andrews Air Force Base
Washington 25, D. C.

WADD (WWAD-Library)
Wright-Patterson AFB, Ohio (1)

Chief, Bureau of Naval Weapons (R-38)
Department of the Navy
ATTN: RA-4 (2)
Washington 25, D. C.

Commanding Officer and Director
David Taylor Model Basin
Aerodynamics Laboratory Library
Washington 7, D. C. (1)

Commandant
U. S. Army Transportation School
ATTN: Marine Corps Liaison Officer (1)
Fort Eustis, Virginia

National Aviation Facilities Experimental Center
ATTN: Library (2)
Atlantic City, New Jersey

Librarian
Langley Research Center
National Aeronautics & Space Administration
Langley Field, Virginia (2)

National Aeronautics and Space Administration
ATTN: Bertram A. Mulcahy
Assistant Director for Technical Information (2)
1520 H Street, N. W.
Washington 25, D. C.

Ames Research Center
National Aeronautics and Space Agency
ATTN: Library (2)
Moffett Field, California

National Aeronautics & Space Administration
Lewis Research Center
ATTN: Library
21000 Brookpark Road (1)
Cleveland 35, Ohio

U. S. Army Standardization Group, U. K.
Box 65, U. S. Navy 100
FPO New York, New York (1)

Office of the Senior Standardization Representative
U. S. Army Standardization Group, Canada
c/o Director of Equipment Policy
Canadian Army Headquarters
Ottawa, Canada (1)

Canadian Army Liaison Officer
Liaison Group, Room 208
U. S. Army Transportation School
Fort Eustis, Virginia (3)

British Joint Services Mission (Army Staff)
ATTN: Lt. Col. R. J. Wade, RE
DAQMG (Mov & Tn)
3100 Massachusetts Avenue, N. W.
Washington 8, D. C. (3)

Commander
Armed Services Technical Information Agency
ATTN: TIPCR
Arlington Hall Station
Arlington 12, Virginia (10)

Bell Helicopter Company
Division of Bell Aerospace Corporation
P. O. Box 482
Fort Worth 1, Texas
ATTN: Mr. Robert R. Lynn
Chief Research Engineer (1)

Hughes Tool Company
Aircraft Division
Culver City, California
ATTN: Library (1)

Kaman Aircraft Corporation
Bloomfield, Connecticut
ATTN: Library (1)

Kellett Aircraft Corporation
P. O. Box 35
Willow Grove, Pennsylvania
ATTN: Library (1)

McDonnell Aircraft Corporation
St. Louis, Missouri
ATTN: Library (1)

Lockheed Aircraft Corporation
Burbank, California
ATTN: Library (1)

Sikorsky Aircraft
Division of United Aircraft Corporation
Stratford, Connecticut
ATTN: Mr. Evan Fradenburgh
Head, Rotor and Aerodynamic Research Section (1)

Hiller Aircraft Corporation
Palo Alto, California
ATTN: Library (1)

Doman Helicopters, Incorporated
Danbury Municipal Airport
P. O. Box 603
Danbury, Connecticut (1)

Republic Aviation Corporation
Farmingdale, Long Island, New York
ATTN: Library (1)

Piasecki Aircraft Corporation
Island Road, International Airport
Philadelphia, Pennsylvania (1)

Office of Technical Services
Acquisition Section
Department of Commerce
Washington 25, D. C. (2)

ROTOR AERODYNAMIC ENVIRONMENT

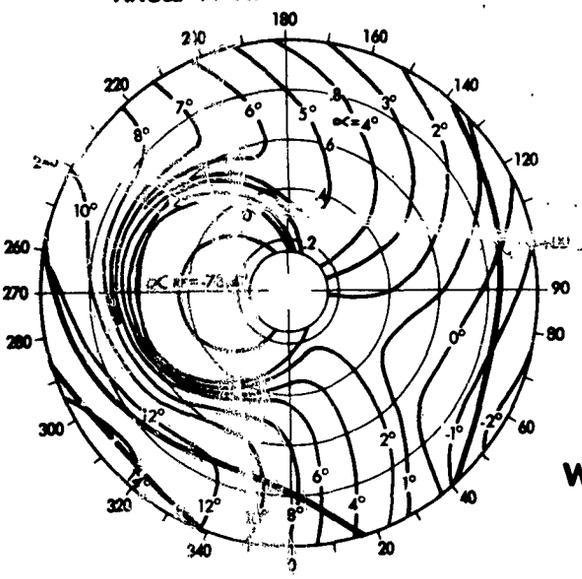
CASE 1.—NACA 0012 : BASE REFERENCE CASE

μ=0.45 λ=−0.15 M_t=0.85 θ_1=−9° θ_o=19.255° σ=0.10

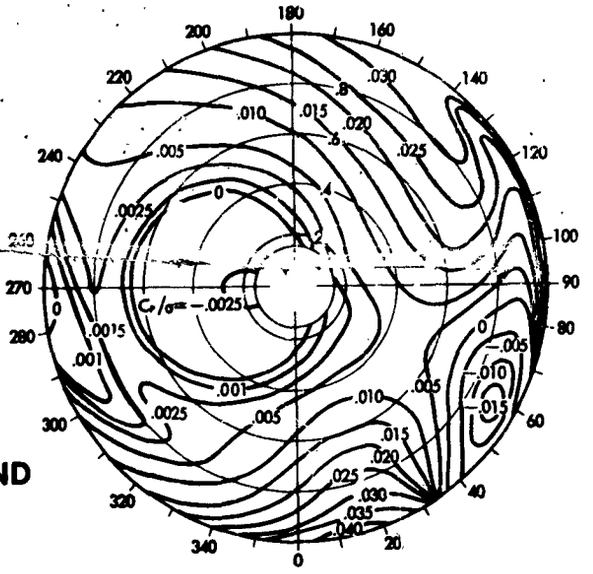
COMPRESSIBILITY ——————

STALL —— —— ——

ANGLE OF ATTACK DISTRIBUTION



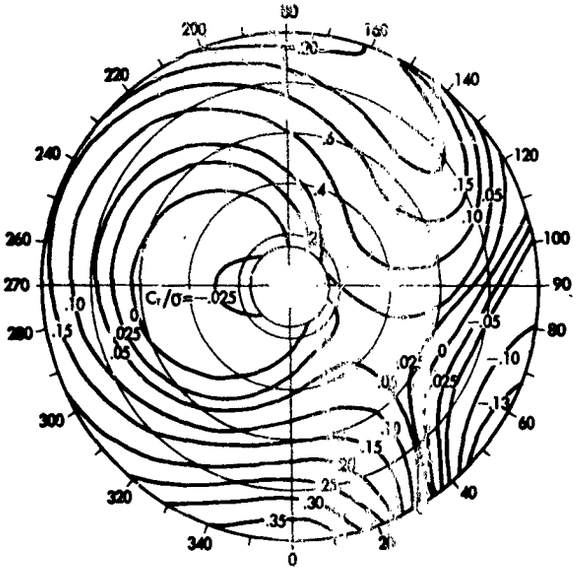
TOTAL POWER DISTRIBUTION



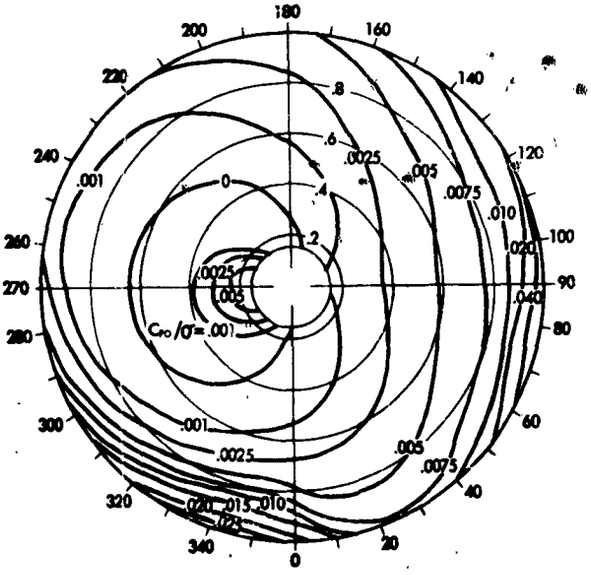
WIND

L/D_t=8.93
C_t/σ=0.0561
X/L=0.1185

THRUST DISTRIBUTION



PROFILE POWER DISTRIBUTION



ROTOR AERODYNAMIC ENVIRONMENT

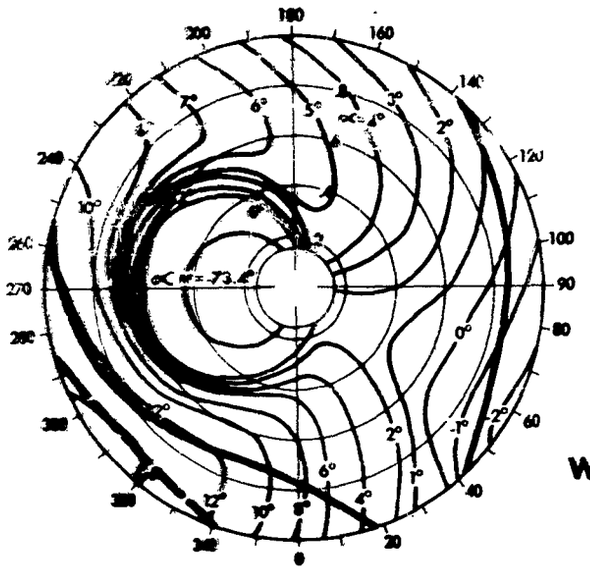
CASE 1.—NACA 0012: BASE REFERENCE CASE

μ=0.45 λ=−0.15 M_t=0.85 θ_1=−9° θ_o=19.255° σ=0.10

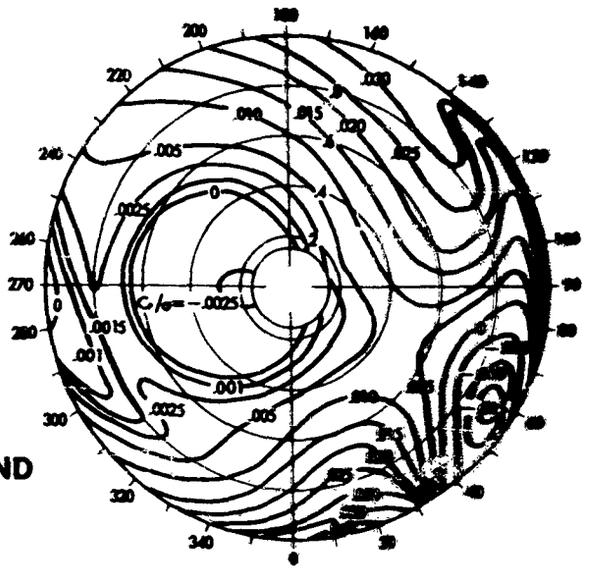
COMPRESSIBILITY ——————

STALL — — — —

ANGLE OF ATTACK DISTRIBUTION



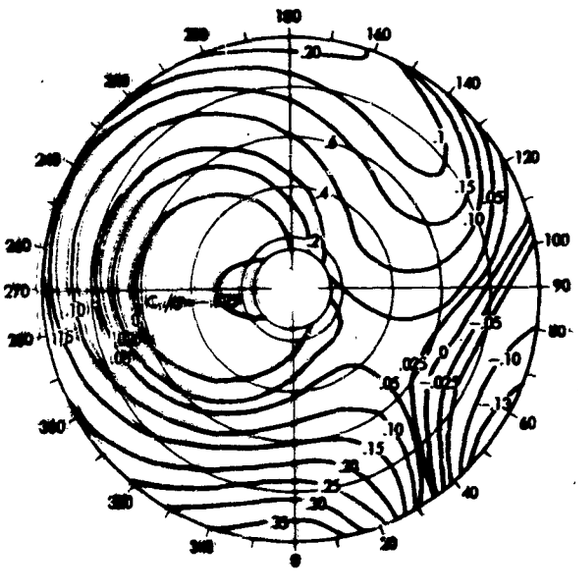
TOTAL POWER DISTRIBUTION



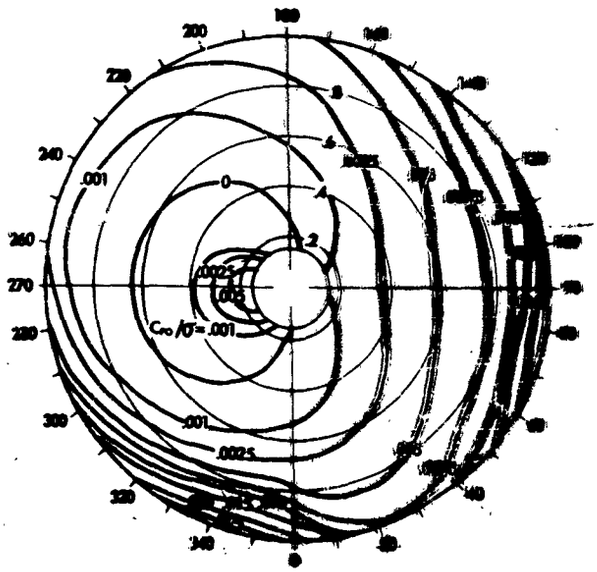
WIND

L/D_t=8.93
C_t/σ=0.0561
X/L=0.1185

THRUST DISTRIBUTION



PROFILE POWER DISTRIBUTION



ROTOR AERODYNAMIC ENVIRONMENT

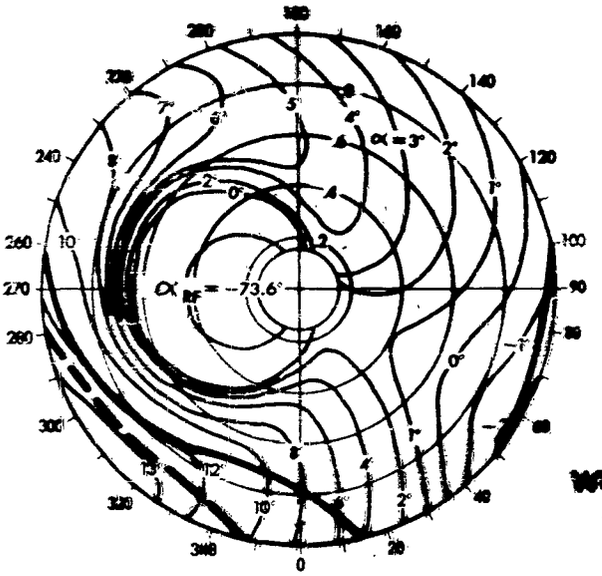
CASE 9 NACA 0009.5 REFERENCE CASE

μ =0.45 λ=−0.15 M_t=0.85 θ_t=−9° $\theta_{.75}$=19.37° σ=0.09

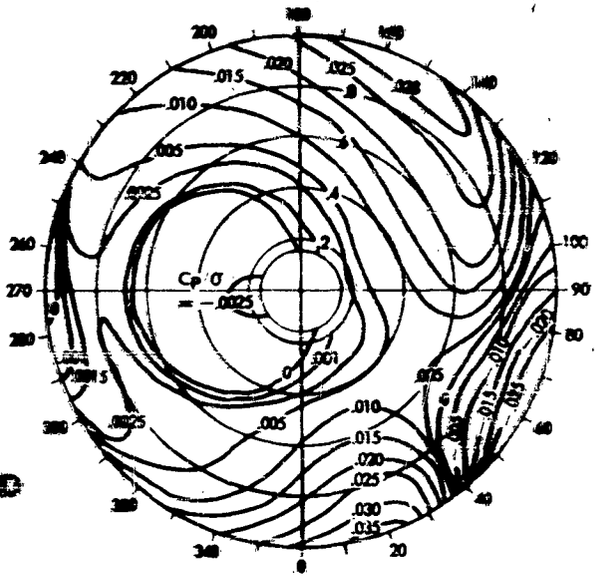
INCOMPRESSIBILITY ——————

STALL — — — —

ANGLE OF ATTACK DISTRIBUTION



TOTAL POWER DISTRIBUTION



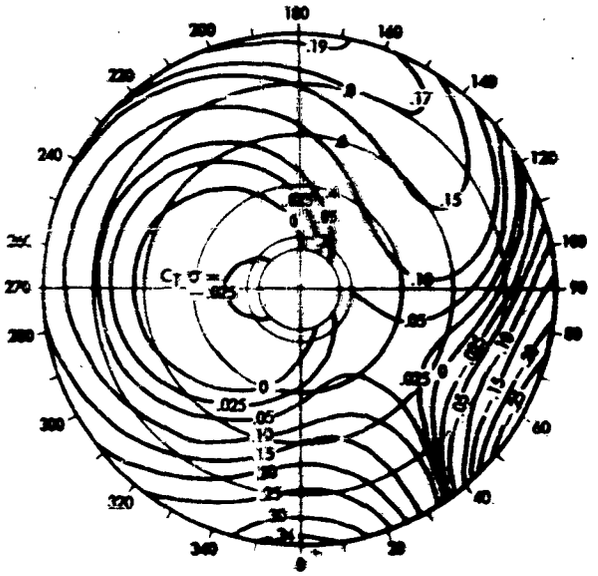
WIND

L/B_L =11.13

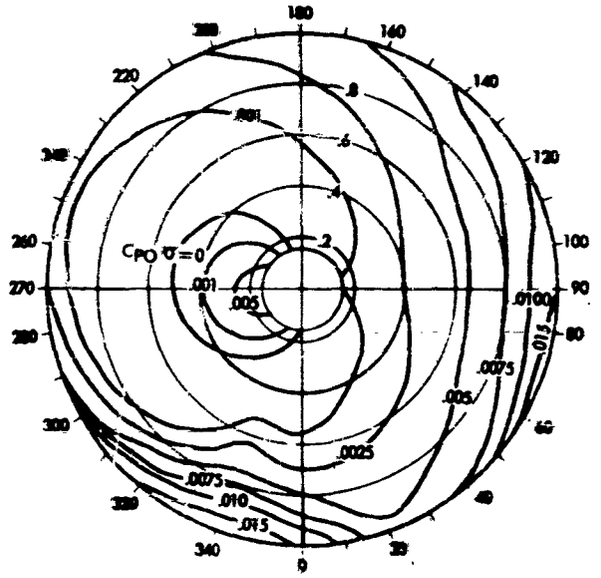
C_T/σ =0.05497

$\bar{x}/L$ =0.72264

THRUST DISTRIBUTION



PROFILE POWER DISTRIBUTION



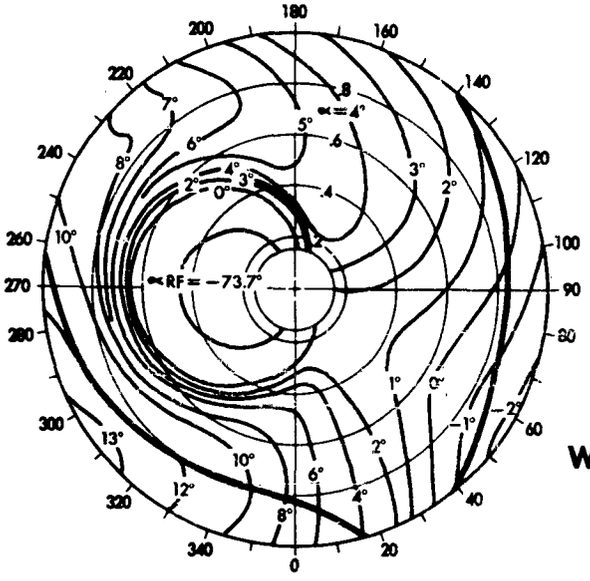
ROTOR AERODYNAMIC ENVIRONMENT

CASE 2 NACA 0012: EFFECT OF CHANGING COLLECTIVE PITCH

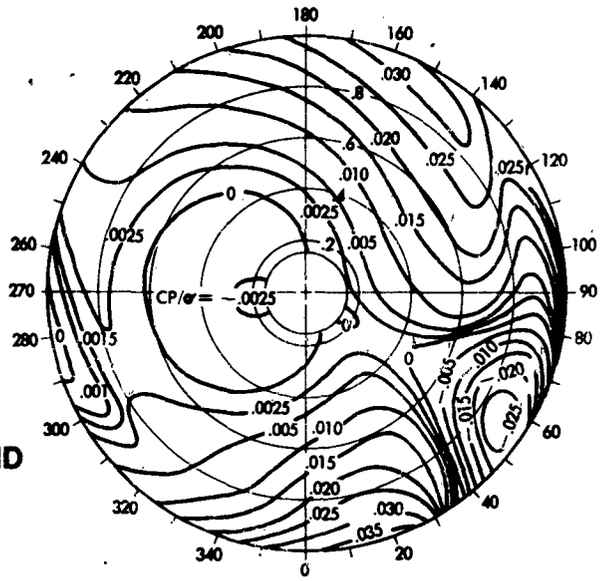
μ =0.45 λ =−0.15 M_t =0.85 θ_t =−9° θ_o =19.0° σ =0.10

COMPRESSIBILITY

ANGLE OF ATTACK DISTRIBUTION



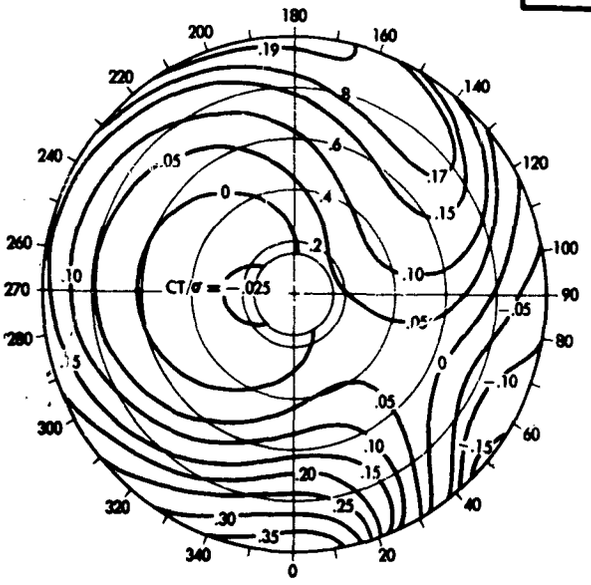
TOTAL POWER DISTRIBUTION



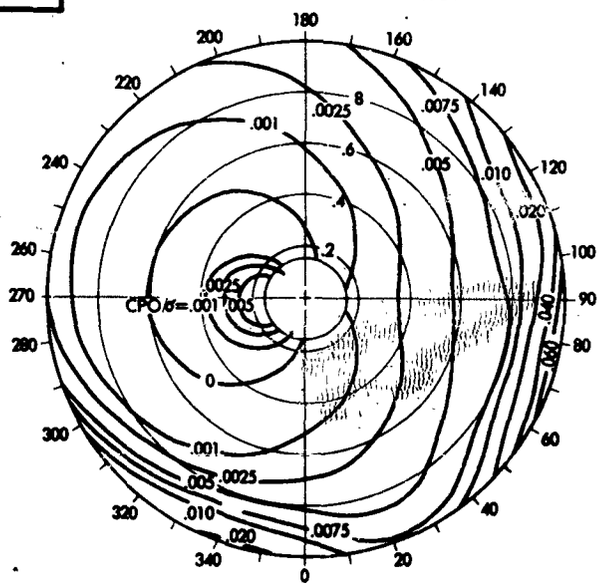
WIND

L/D_e = 8.86
C_T/σ = 0.0513
X/L = 0.1215

THRUST DISTRIBUTION



PROFILE POWER DISTRIBUTION



ROTOR AERODYNAMIC ENVIRONMENT

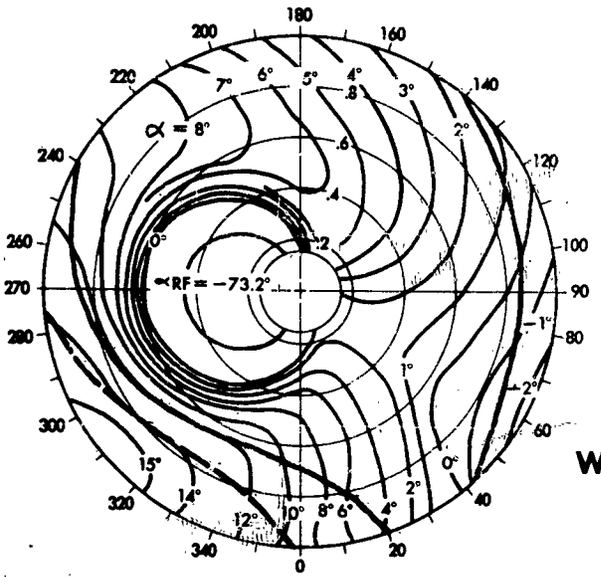
CASE 3 NACA 0012: EFFECT OF CHANGING COLLECTIVE PITCH

$\mu = 0.45$ $\lambda = -0.15$ $M_t = 0.85$ $\theta_t = -9°$ $\theta_o = 19.5°$ $\sigma = 0.10$

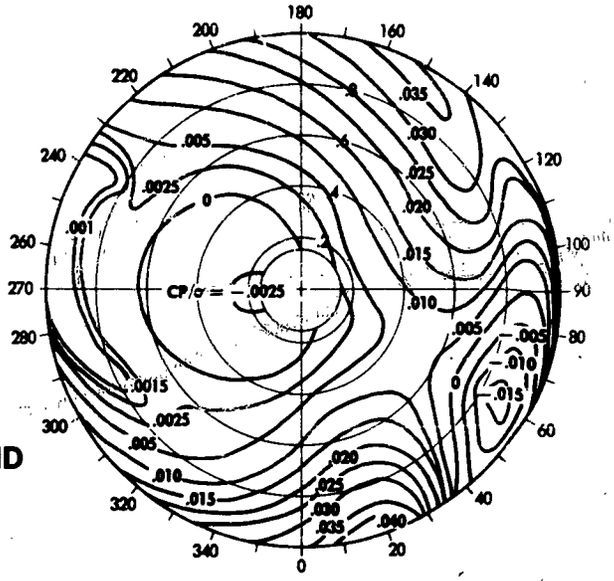
COMPRESSIBILITY ——————

STALL — — —

ANGLE OF ATTACK DISTRIBUTION



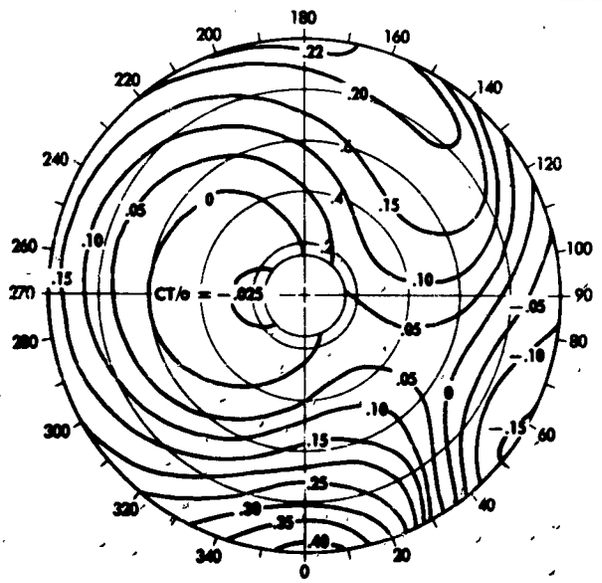
TOTAL POWER DISTRIBUTION



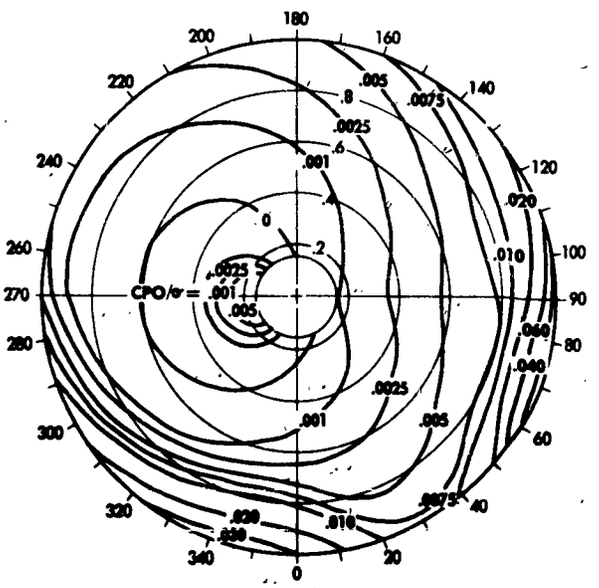
WIND

$L/D_e = 8.73$
$C_T/\sigma = 0.0601$
$X/L = 0.1145$

THRUST DISTRIBUTION



PROFILE POWER DISTRIBUTION



ROTOR AERODYNAMIC ENVIRONMENT

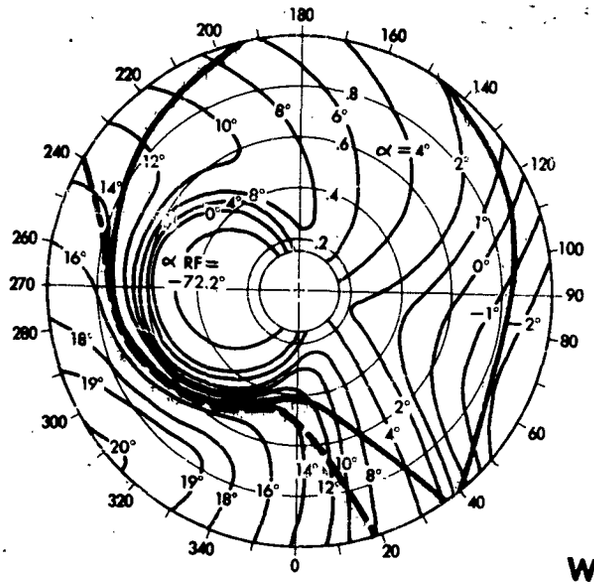
CASE 4 NACA 0012: EFFECT OF CHANGING COLLECTIVE PITCH

$\mu = 0.45$ $\lambda = -0.15$ $M_t = 0.85$ $\theta_t = -9°$ **$\theta_o = 20.5°$** $\sigma = 0.10$

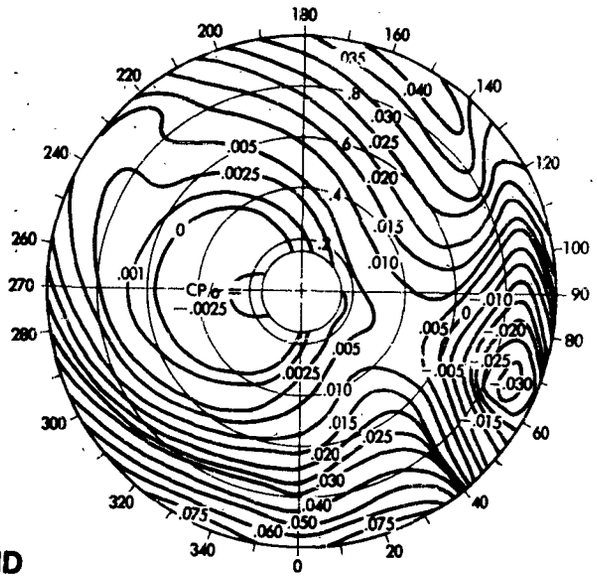
COMPRESSIBILITY ——————

STALL — — — —

ANGLE OF ATTACK DISTRIBUTION

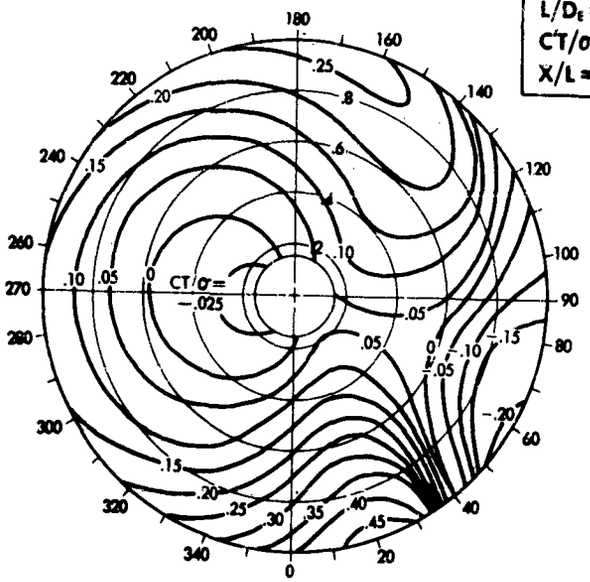


TOTAL POWER DISTRIBUTION



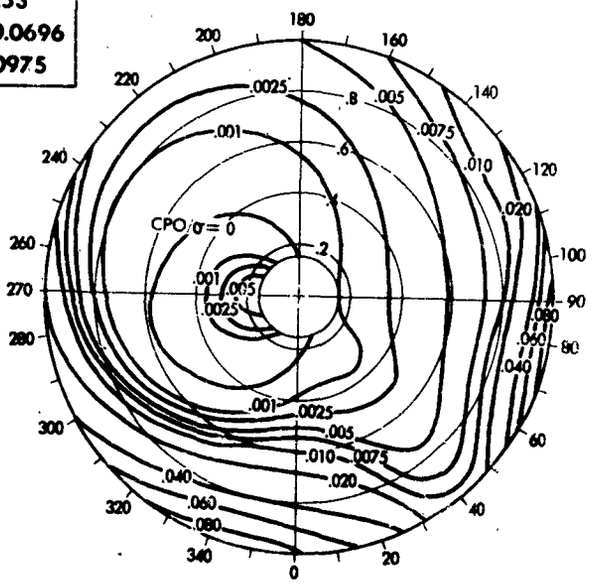
WIND

THRUST DISTRIBUTION



$L/D_e = 5.53$
$CT/\sigma = 0.0696$
$X/L = 0.0975$

PROFILE POWER DISTRIBUTION



ROTOR AERODYNAMIC ENVIRONMENT

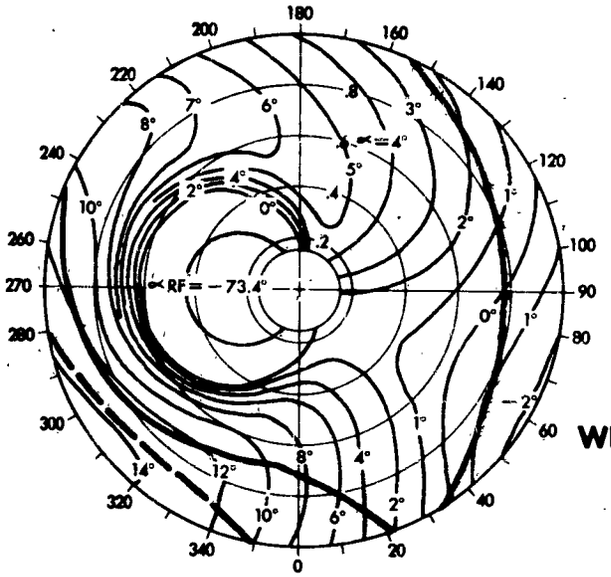
CASE 5 NACA 0012: EFFECT OF MACH NUMBER

$\mu = 0.45$ $\lambda = -0.15$ $M_t = 0.90$ $\theta_t = -9°$ $\theta_o = 19.23°$ $\sigma = 0.10$

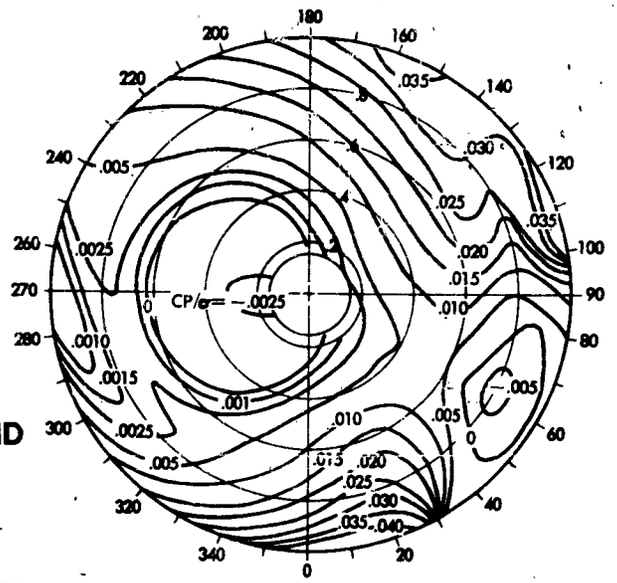
COMPRESSIBILITY ———————

STALL — — — —

ANGLE OF ATTACK DISTRIBUTION



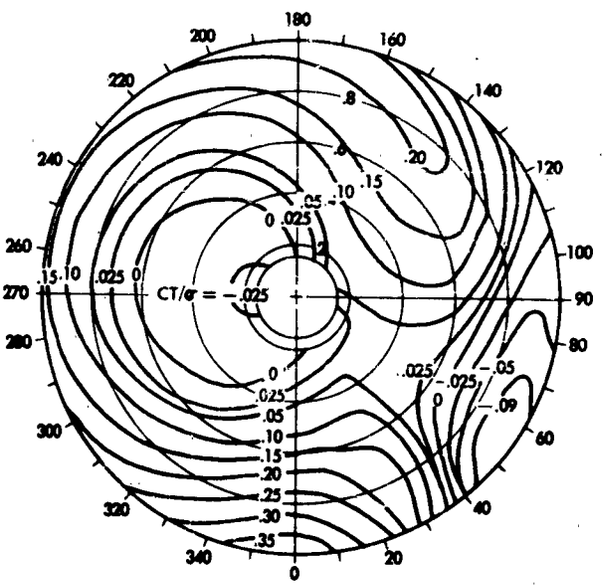
TOTAL POWER DISTRIBUTION



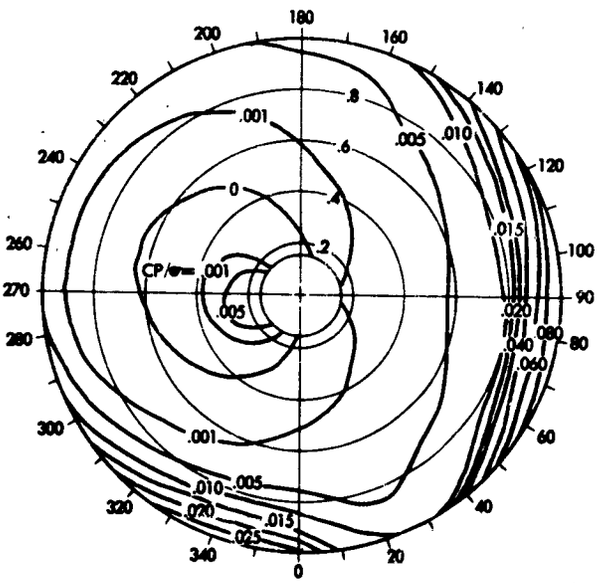
WIND

$L/D_e = 6.40$
$C_T/\sigma = 0.0564$
$X/L = 0.1058$

THRUST DISTRIBUTION



PROFILE POWER DISTRIBUTION



ROTOR AERODYNAMIC ENVIRONMENT

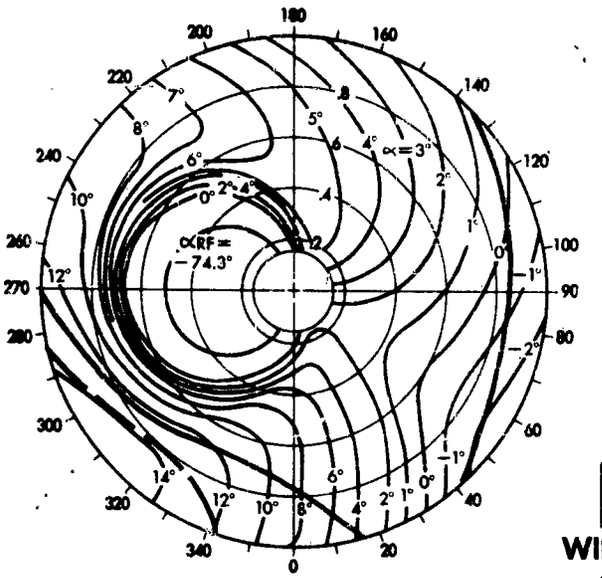
CASE 6 NACA 0012: EFFECT OF ADVANCE RATIO

$\mu = 0.50$ $\lambda = -0.15$ $M_t = 0.85$ $\theta_t = -9°$ $\theta_o = 18.55°$ $\sigma = 0.10$

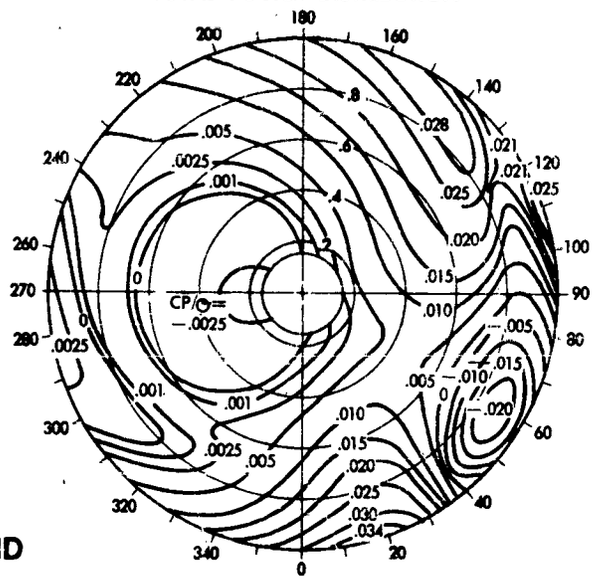
COMPRESSIBILITY ——————————

STALL —— — —— ——

ANGLE OF ATTACK DISTRIBUTION

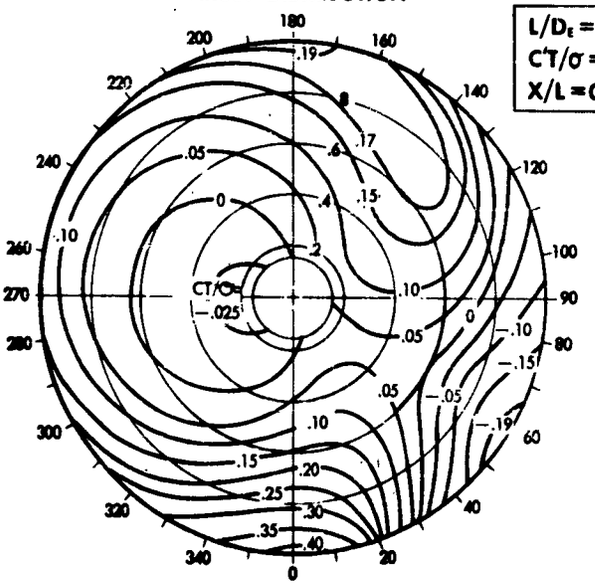


TOTAL POWER DISTRIBUTION



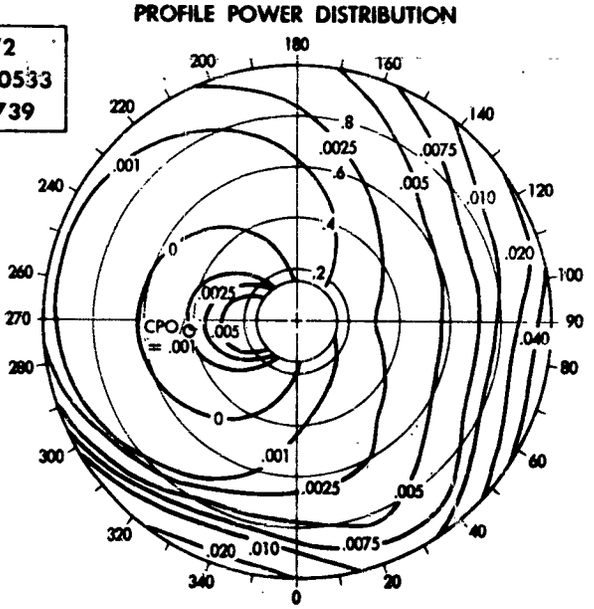
WIND

THRUST DISTRIBUTION



$L/D_E = 8.72$
$C_T/\sigma = 0.0533$
$X/L = 0.0739$

PROFILE POWER DISTRIBUTION



ROTOR AERODYNAMIC ENVIRONMENT

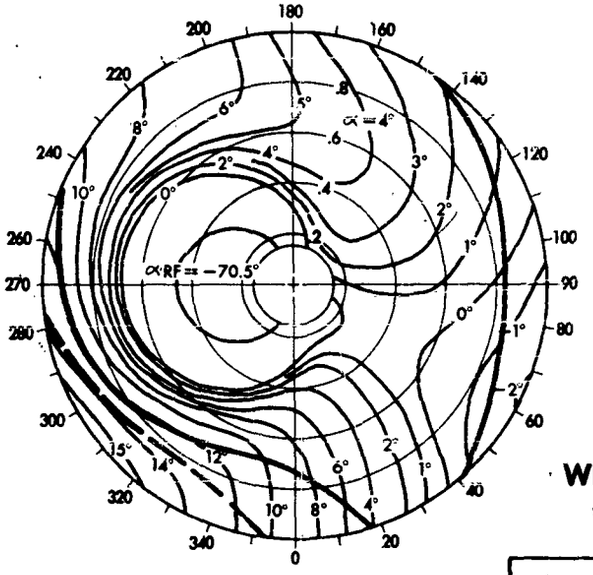
CASE 7 NACA 0012: EFFECT OF INFLOW RATIO

$\mu = 0.45$ $\boxed{\lambda = -0.20}$ $M_t = 0.85$ $\theta_t = -9°$ $\theta_o = 22.23°$ $\sigma = 0.10$

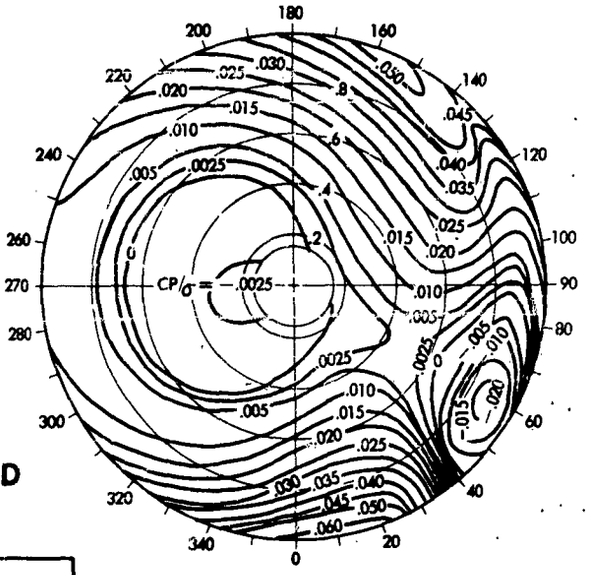
COMPRESSIBILITY ————————————

STALL ———— ———— ————

ANGLE OF ATTACK DISTRIBUTION



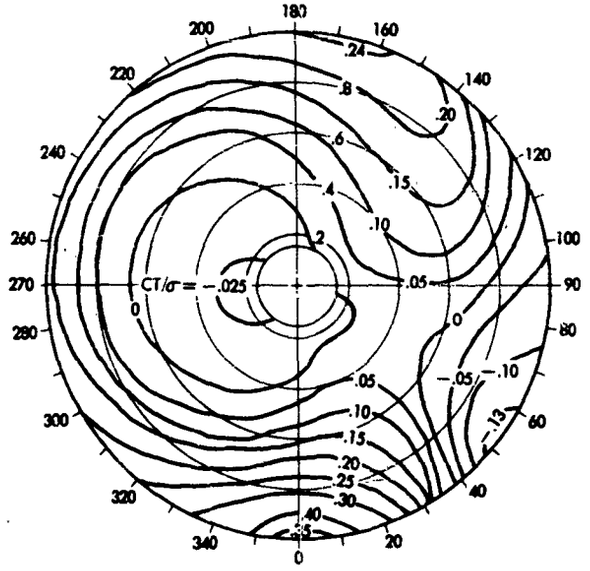
TOTAL POWER DISTRIBUTION



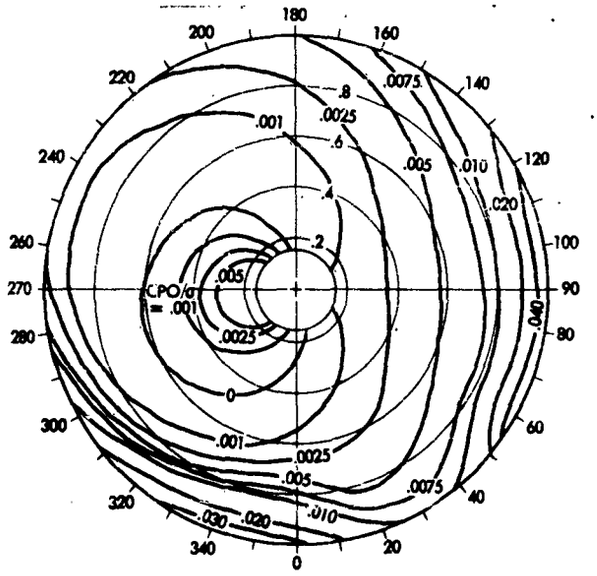
WIND

$L/D_E = 6.90$
$C_T/\sigma = 0.0489$
$X/L = 0.1813$

THRUST DISTRIBUTION



PROFILE POWER DISTRIBUTION



ROTOR AERODYNAMIC ENVIRONMENT

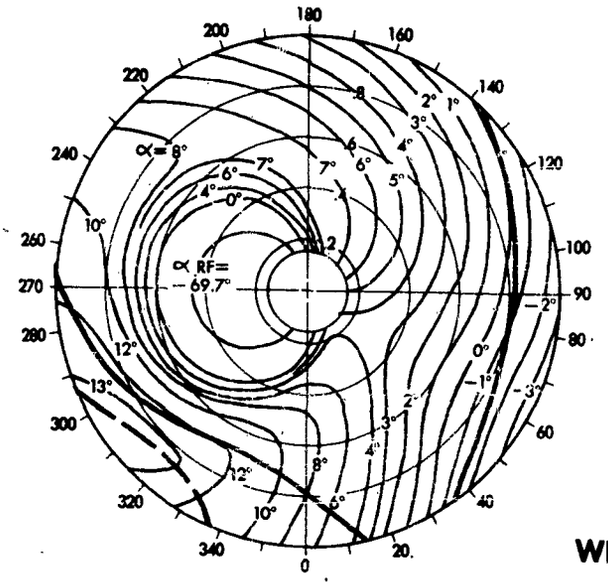
CASE 8 NACA 0012: EFFECT OF BLADE TWIST

$\mu = 0.45$ $\lambda = -0.15$ $M_t = 0.85$ $\theta_t = -14°$ $\theta_o = 23.00$ $\sigma = 0.10$

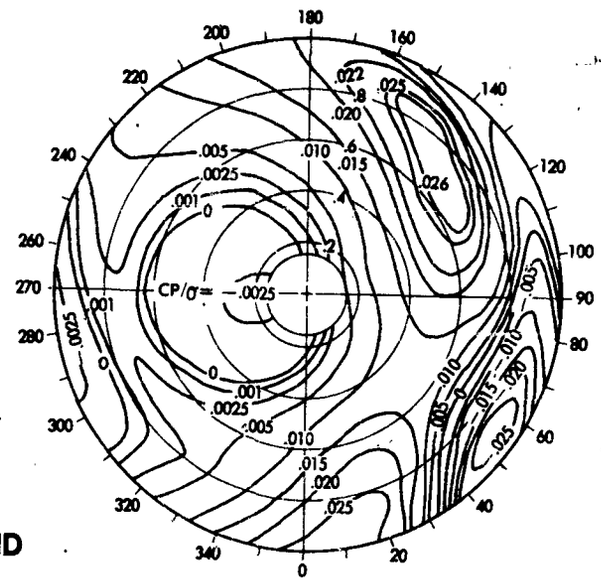
COMPRESSIBILITY ————————

STALL — — — — —

ANGLE OF ATTACK DISTRIBUTION

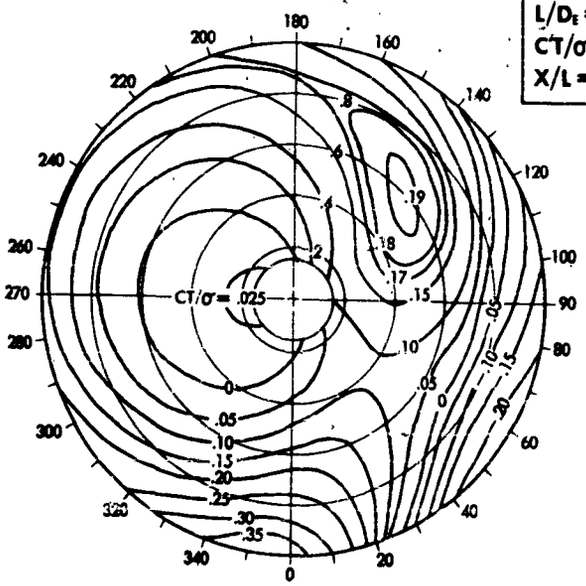


TOTAL POWER DISTRIBUTION



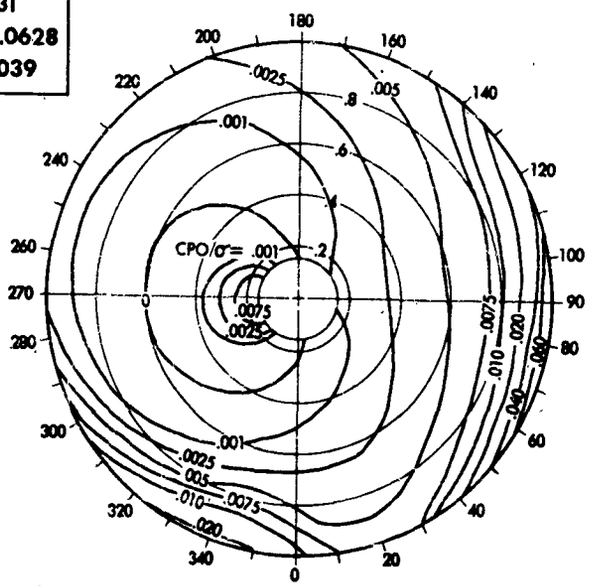
WIND

THRUST DISTRIBUTION



$L/D_E = 9.31$
$C_T/\sigma = 0.0628$
$X/L = 0.1039$

PROFILE POWER DISTRIBUTION



ROTOR AERODYNAMIC ENVIRONMENT

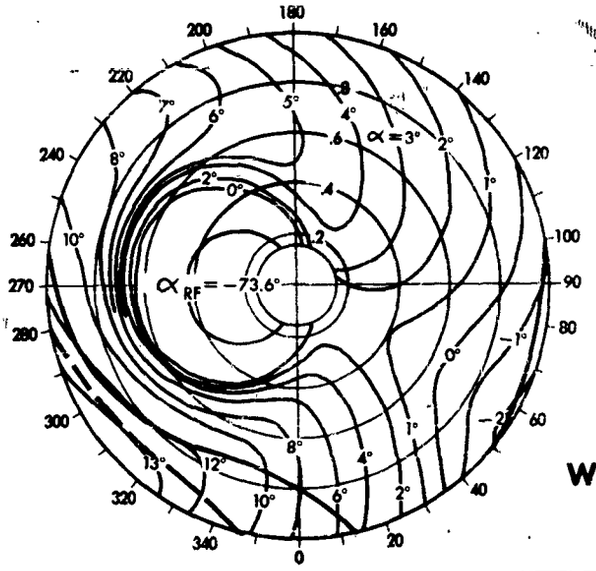
CASE 9 NACA 0009.5 REFERENCE CASE

$\mu = 0.45$ $\lambda = -0.15$ $M_t = 0.85$ $\theta_t = -9°$ $\theta_o = 19.07°$ $\sigma = 0.10$

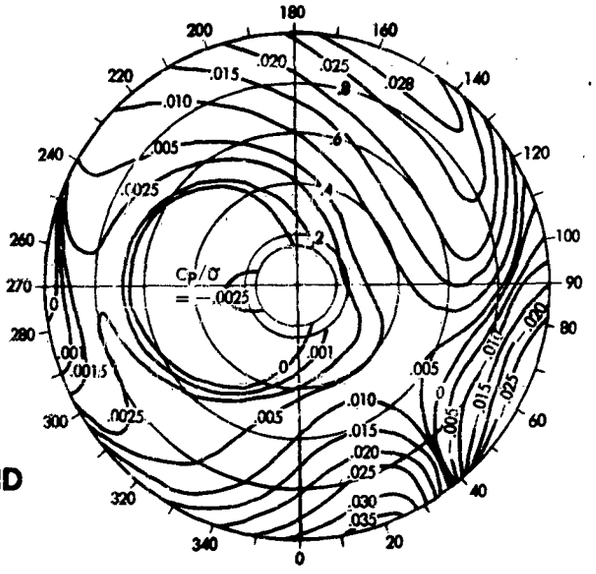
COMPRESSIBILITY ——————

STALL — — — — —

ANGLE OF ATTACK DISTRIBUTION



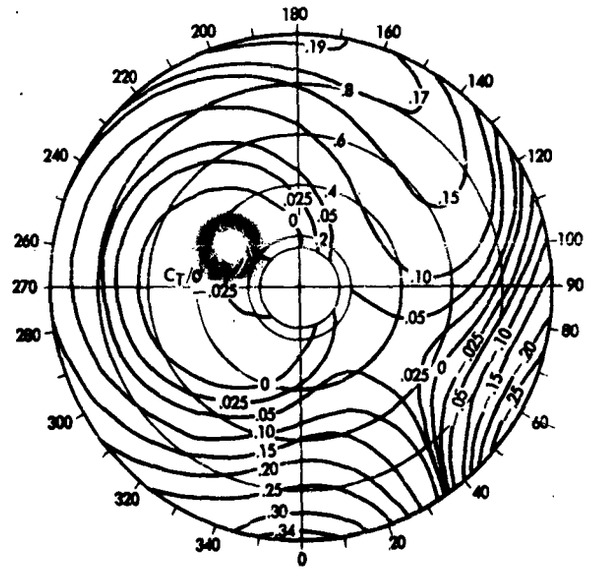
TOTAL POWER DISTRIBUTION



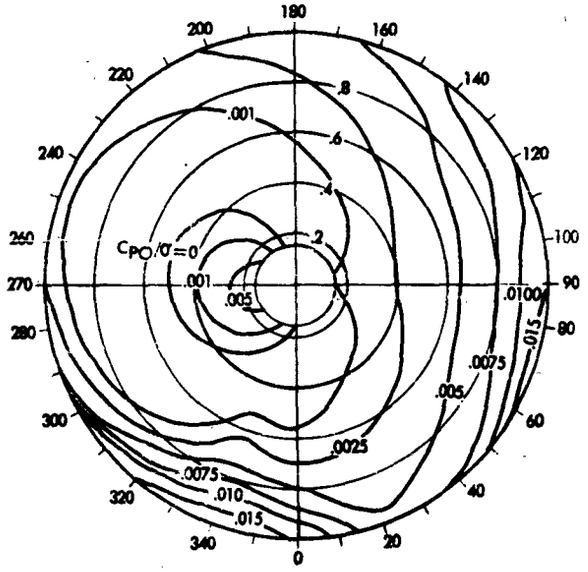
WIND

$L/D_E = 11.13$
$C_T/\sigma = 0.0507$
$X/L = 0.1284$

THRUST DISTRIBUTION



PROFILE POWER DISTRIBUTION



ROTOR AERODYNAMIC ENVIRONMENT

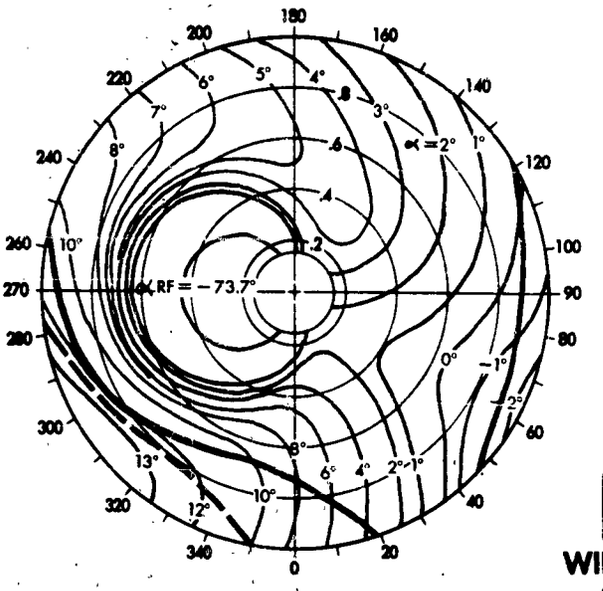
CASE 10 NACA 0009.5 EFFECT OF MACH NUMBER

$\mu = 0.45$ $\lambda = -0.15$ $M_t = 0.90$ $\theta_t = -9°$ $\theta_o = 19.03°$ $\sigma = 0.10$

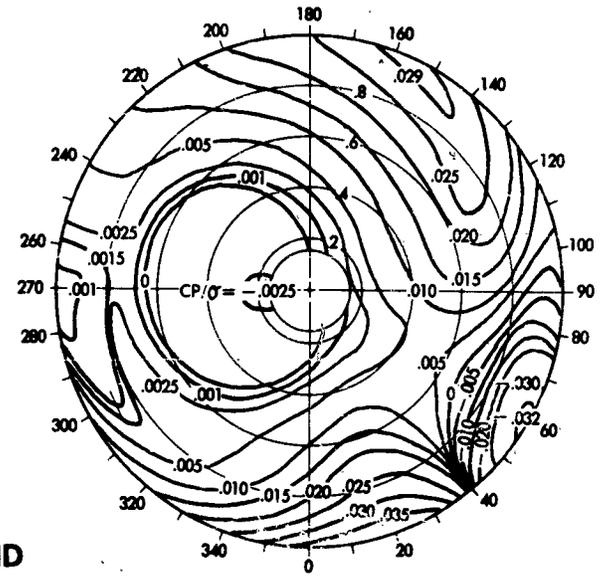
COMPRESSIBILITY _____

STALL — — — —

ANGLE OF ATTACK DISTRIBUTION

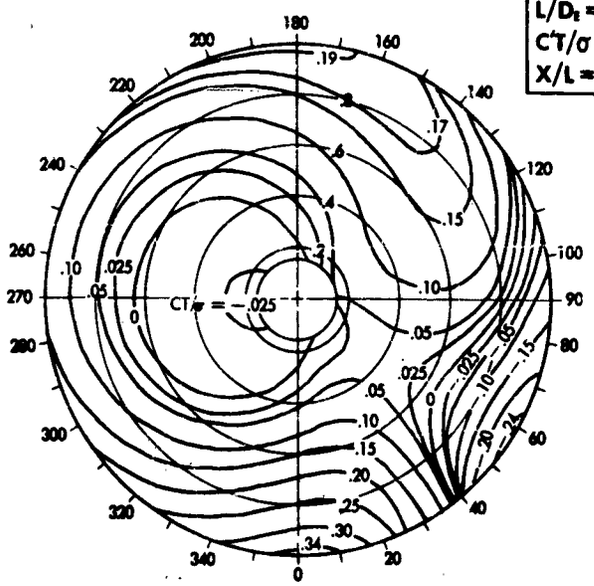


TOTAL POWER DISTRIBUTION



WIND

THRUST DISTRIBUTION

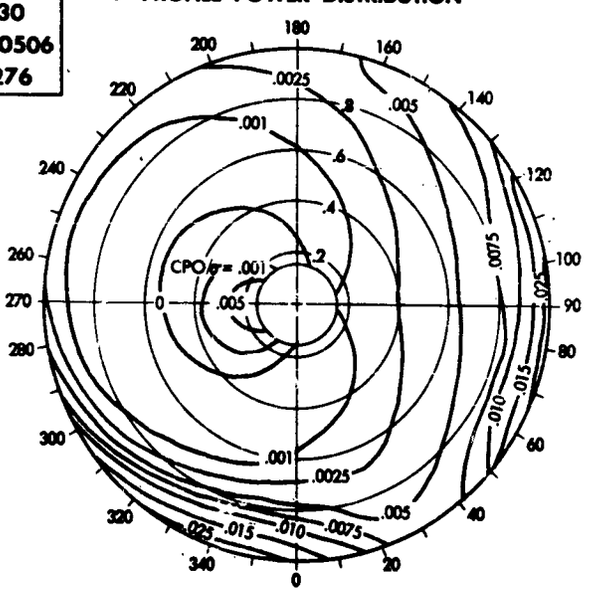


$L/D_t = 10.30$

$C_T/\sigma = 0.0506$

$X/L = 0.1276$

PROFILE POWER DISTRIBUTION



TREC 61-43

Vertol Division, The Boeing Company, Morton, Pennsylvania, High Performance Tandem Helicopter Study, Volume II - Design Analysis, January 1961. 316 pp. including illustrations, tables. Contract DA44-177-TC-686..

Unclassified Report

A preliminary design study has been conducted to establish a tandem helicopter configuration capable of the following minimum performance: (1) 1600 nautical miles ferry range at zero headwind with 1 hour fuel reserve. (2) 200 miles per hour speed with a minimum payload of 800 pounds.. (3) Flying qualities to meet MIL-H-8501. Detailed aerodynamic and design layout studies are presented for the High Performance 107-11. The (over)

Unclassified

Unclassified

major design areas covered are rotor blades, hub, and controls; mechanical instability, drive system, fuselage changes, flight controls, and weight. Both performance and flying qualities are thoroughly investigated. Overall feasibility of a high performance helicopter is assured. Studies of an Advanced 107 and Advanced YHC-1B (Chinook) indicate that operational high performance helicopters are obtained if the ratio of payload to empty weight is maintained in going to the high performance configuration

Unclassified

Unclassified

TREC 61-43

Vertol Division, The Boeing Company, Morton, Pennsylvania, High Performance Tandem Helicopter Study, Volume II - Design Analysis, January 1961. 316 pp. including illustrations, tables. Contract DA44-177-TC-686.

Unclassified Report

A preliminary design study has been conducted to establish a tandem helicopter configuration capable of the following minimum performance: (1) 1600 nautical miles ferry range at zero headwind with 1 hour fuel reserve. (2) 200 miles per hour speed with a minimum payload of 800 pounds. (3) Flying qualities to meet MIL-H-8501. Detailed aerodynamic and design layout studies are presented for the High Performance 107-11. The (over)

Unclassified

Unclassified

major design areas covered are rotor blades, hub, and controls; mechanical instability, drive system, fuselage changes, flight controls, and weight. Both performance and flying qualities are thoroughly investigated. Overall feasibility of a high performance helicopter is assured. Studies of an Advanced 107 and Advanced YHC-1B (Chinook) indicate that operational high performance helicopters are obtained if the ratio of payload to empty weight is maintained in going to the high performance configuration

Unclassified

Unclassified

TREC 61-43

Vertol Division, The Boeing Company, Morton, Pennsylvania, High Performance Tandem Helicopter Study, Volume II - Design Analysis, January 1961. 316 pp. including illustrations, tables. Contract DA44-177-TC-686.

Unclassified Report

A preliminary design study has been conducted to establish a tandem helicopter configuration capable of the following minimum performance: (1) 1600 nautical miles ferry range at zero headwind with 1 hour fuel reserve. (2) 200 miles per hour speed with a minimum payload of 800 pounds. (3) Flying qualities to meet MIL-H-8501. Detailed aerodynamic and design layout studies are presented for the High Performance 107-II. The

(over)

Unclassified

Unclassified

major design areas covered are rotor blades, hub, and controls; mechanical instability, drive system, fuselage changes, flight controls, and weight. Both performance and flying qualities are thoroughly investigated. Overall feasibility of a high performance helicopter is assured. Studies of an Advanced 107 and Advanced YHC-1B (Chinook) indicate that operational high performance helicopters are obtained if the ratio of payload to empty weight is maintained in going to the high performance configuration

Unclassified

TREC 61-43

Vertol Division, The Boeing Company, Morton, Pennsylvania, High Performance Tandem Helicopter Study, Volume II - Design Analysis, January 1961. 316 pp. including illustrations, tables. Contract DA44-177-TC-686.

Unclassified Report

A preliminary design study has been conducted to establish a tandem helicopter configuration capable of the following minimum performance: (1) 1600 nautical miles ferry range at zero headwind with 1 hour fuel reserve. (2) 200 miles per hour speed with a minimum payload of 800 pounds. (3) Flying qualities to meet MIL-H-8501. Detailed aerodynamic and design layout studies are presented for the High Performance 107-II. The

(over)

Unclassified

Unclassified

major design areas covered are rotor blades, hub, and controls; mechanical instability, drive system, fuselage changes, flight controls, and weight. Both performance and flying qualities are thoroughly investigated. Overall feasibility of a high performance helicopter is assured. Studies of an Advanced 107 and Advanced YHC-1B (Chinook) indicate that operational high performance helicopters are obtained if the ratio of payload to empty weight is maintained in going to the high performance configuration

Unclassified

TREC 61-43

Vertol Division, The Boeing Company, Morton, Pennsylvania, High Performance Tandem Helicopter Study, Volume II - Design Analysis, January 1961. 316 pp. including illustrations, tables. Contract DA44-177-TC-686..

Unclassified Report

A preliminary design study has been conducted to establish a tandem helicopter configuration capable of the following minimum performance: (1) 1600 nautical miles ferry range at zero headwind with 1 hour fuel reserve. (2) 200 miles per hour speed with a minimum payload of 800 pounds.. (3) Flying qualities to meet MIL-H-8501. Detailed aerodynamic and design layout studies are presented for the High Performance 107-II. The

(over)

Unclassified

major design areas covered are rotor blades, hub, and controls; mechanical instability, drive system, fuselage changes, flight controls, and weight. Both performance and flying qualities are thoroughly investigated. Overall feasibility of a high performance helicopter is assured. Studies of an Advanced 107 and Advanced YHC-18 (Chinook) indicate that operational high performance helicopters are obtained if the ratio of payload to empty weight is maintained in going to the high performance configuration

Unclassified

TREC 61-43

Vertol Division, The Boeing Company, Morton, Pennsylvania, High Performance Tandem Helicopter Study, Volume II - Design Analysis, January 1961. 316 pp. including illustrations, tables. Contract DA44-177-TC-686.

Unclassified Report

A preliminary design study has been conducted to establish a tandem helicopter configuration capable of the following minimum performance: (1) 1600 nautical miles ferry range at zero headwind with 1 hour fuel reserve. (2) 200 miles per hour speed with a minimum payload of 800 pounds. (3) Flying qualities to meet MIL-H-8501. Detailed aerodynamic and design layout studies are presented for the High Performance 107-II. The

(over)

Unclassified

major design areas covered are rotor blades, hub, and controls; mechanical instability, drive system, fuselage changes, flight controls, and weight. Both performance and flying qualities are thoroughly investigated. Overall feasibility of a high performance helicopter is assured. Studies of an Advanced 107 and Advanced YHC-18 (Chinook) indicate that operational high performance helicopters are obtained if the ratio of payload to empty weight is maintained in going to the high performance configuration

Unclassified

TREC 61-43

Vertol Division, The Boeing Company, Morton, Pennsylvania, High Performance Tandem Helicopter Study, Volume II - Design Analysis, January 1961. 316 pp. including illustrations, tables. Contract DA44-177-TC-686.

Unclassified Report

A preliminary design study has been conducted to establish a tandem helicopter configuration capable of the following minimum performance: (1) 1600 nautical miles ferry range at zero headwind with 1 hour fuel reserve. (2) 200 miles per hour speed with a minimum payload of 800 pounds. (3) Flying qualities to meet MIL-H-8501. Detailed aerodynamic and design layout studies are presented for the High Performance 107-II. The

(over)

Unclassified

Unclassified

major design areas covered are rotor blades, hub, and controls; mechanical instability, drive system, fuselage changes, flight controls, and weight. Both performance and flying qualities are thoroughly investigated. Overall feasibility of a high performance helicopter is assured. Studies of an Advanced 107 and Advanced YHC-18 (Chinook) indicate that operational high performance helicopters are obtained if the ratio of payload to empty weight is maintained in going to the high performance configuration

Unclassified

Unclassified

TREC 61-43

Vertol Division, The Boeing Company, Morton, Pennsylvania, High Performance Tandem Helicopter Study, Volume II - Design Analysis, January 1961. 316 pp. including illustrations, tables. Contract DA44-177-TC-686.

Unclassified Report

A preliminary design study has been conducted to establish a tandem helicopter configuration capable of the following minimum performance: (1) 1600 nautical miles ferry range at zero headwind with 1 hour fuel reserve. (2) 200 miles per hour speed with a minimum payload of 800 pounds. (3) Flying qualities to meet MIL-H-8501. Detailed aerodynamic and design layout studies are presented for the High Performance 107-II. The

(over)

Unclassified

Unclassified

major design areas covered are rotor blades, hub, and controls; mechanical instability, drive system, fuselage changes, flight controls, and weight. Both performance and flying qualities are thoroughly investigated. Overall feasibility of a high performance helicopter is assured. Studies of an Advanced 107 and Advanced YHC-18 (Chinook) indicate that operational high performance helicopters are obtained if the ratio of payload to empty weight is maintained in going to the high performance configuration

Unclassified

Unclassified

TREC 61-43

Vertol Division, The Boeing Company, Morton, Pennsylvania, High Performance Tandem Helicopter Study, Volume II - Design Analysis, January 1961. 316 pp. including illustrations, tables. Contract DA44-177-TC-686..

Unclassified Report

A preliminary design study has been conducted to establish a tandem helicopter configuration capable of the following minimum performance: (1) 1600 nautical miles ferry range at zero headwind with 1 hour fuel reserve. (2) 200 miles per hour speed with a minimum payload of 800 pounds.. (3) Flying qualities to meet MIL-H-8501. Detailed aerodynamic and design layout studies are presented for the High Performance 107-II. The

(over)

Unclassified

Unclassified

major design areas covered are rotor blades, hub, and controls; mechanical instability, drive system, fuselage changes, flight controls, and weight. Both performance and flying qualities are thoroughly investigated. Overall feasibility of a high performance helicopter is assured. Studies of an Advanced 107 and Advanced YHC-18 (Chinook) indicate that operational high performance helicopters are obtained if the ratio of payload to empty weight is maintained in going to the high performance configuration

Unclassified

Unclassified

TREC 61-43

Vertol Division, The Boeing Company, Morton, Pennsylvania, High Performance Tandem Helicopter Study, Volume II - Design Analysis, January 1961. 316 pp. including illustrations, tables. Contract DA44-177-TC-686.

Unclassified Report

A preliminary design study has been conducted to establish a tandem helicopter configuration capable of the following minimum performance: (1) 1600 nautical miles ferry range at zero headwind with 1 hour fuel reserve. (2) 200 miles per hour speed with a minimum payload of 800 pounds. (3) Flying qualities to meet MIL-H-8501. Detailed aerodynamic and design layout studies are presented for the High Performance 107-II. The

(over)

Unclassified

Unclassified

major design areas covered are rotor blades, hub, and controls; mechanical instability, drive system, fuselage changes, flight controls, and weight. Both performance and flying qualities are thoroughly investigated. Overall feasibility of a high performance helicopter is assured. Studies of an Advanced 107 and Advanced YHC-18 (Chinook) indicate that operational high performance helicopters are obtained if the ratio of payload to empty weight is maintained in going to the high performance configuration

Unclassified

Unclassified

TREC 61-43

Vertol Division, The Boeing Company, Morton, Pennsylvania, High Performance Tandem Helicopter Study, Volume II - Design Analysis, January 1961. 316 pp. including illustrations, tables. Contract DA44-177-TC-686.

Unclassified Report

A preliminary design study has been conducted to establish a tandem helicopter configuration capable of the following minimum performance: (1) 1600 nautical miles ferry range at zero headwind with 1 hour fuel reserve. (2) 200 miles per hour speed with a minimum payload of 800 pounds. (3) Flying qualities to meet MIL-H-8501. Detailed aerodynamic and design layout studies are presented for the High Performance 107-II. The

(over)

Unclassified

Unclassified

major design areas covered are rotor blades, hub, and controls; mechanical instability, drive system, fuselage changes, flight controls, and weight. Both performance and flying qualities are thoroughly investigated. Overall feasibility of a high performance helicopter is assured. Studies of an Advanced 107 and Advanced YHC-1B (Chinook) indicate that operational high performance helicopters are obtained if the ratio of payload to empty weight is maintained in going to the high performance configuration

Unclassified

Unclassified

TREC 61-43

Vertol Division, The Boeing Company, Morton, Pennsylvania, High Performance Tandem Helicopter Study, Volume II - Design Analysis, January 1961. 316 pp. including illustrations, tables. Contract DA44-177-TC-686.

Unclassified Report

A preliminary design study has been conducted to establish a tandem helicopter configuration capable of the following minimum performance: (1) 1600 nautical miles ferry range at zero headwind with 1 hour fuel reserve. (2) 200 miles per hour speed with a minimum payload of 800 pounds. (3) Flying qualities to meet MIL-H-8501. Detailed aerodynamic and design layout studies are presented for the High Performance 107-II. The

(over)

Unclassified

Unclassified

major design areas covered are rotor blades, hub, and controls; mechanical instability, drive system, fuselage changes, flight controls, and weight. Both performance and flying qualities are thoroughly investigated. Overall feasibility of a high performance helicopter is assured. Studies of an Advanced 107 and Advanced YHC-1B (Chinook) indicate that operational high performance helicopters are obtained if the ratio of payload to empty weight is maintained in going to the high performance configuration

Unclassified

Unclassified

UNCLASSIFIED

UNCLASSIFIED